REACTIONS OF NITRIC OXIDE WITH CARBONS : THE KINETICS OF NO CHEMISORPTION ON CARBON

Hsisheng Teng, E. M. Suuberg and J. M. Calo

Division of Engineering
Brown University
Providence, Rhode Island 02912

Keywords: Nitric Oxide, Carbon, Chemisorption

INTRODUCTION

The fact that NO formed during a combustion process can be heterogeneously reduced by carbonaceous solids is well known[1]. There have been a modest number of studies of various aspects of NO-char studies in the last 30 years(e.g. ref. 2~6). In general, the overall reaction has been reported to actually include the following stoichiometric reactions :

$$C + 2\,NO \rightarrow CO_2 + N_2$$
$$C + NO \rightarrow CO + 1/2\,N_2$$
$$CO + NO \rightarrow CO_2 + 1/2\,N_2$$

It has been noted that the reaction of NO with char parallels in some respects the reaction of O_2 with chars, in that surface oxide intermediates play a role in the mechanism. For example, it has been reported[2] that at temperatures betwen 123 and 473 K, there are carbon-oxygen complexes formed on the char surface, with the release of N_2 as a gaseous product. The NO-char reaction studies reported by previous workers focus mainly on the investigation of the global kinetics during the pseudo steady state gasification. From the global kinetic results, one group[4] proposed a mechanism for the reaction of carbon with NO as follows :

$$NO + C^* \rightarrow C(O) + 1/2\,N_2 \quad (R1)$$
$$CO + C(O) \rightarrow CO_2 + C^* \quad (R2)$$
$$C(O) \rightarrow CO \quad (R3)$$

This reaction scheme was used to derive a Langmuir-Hinshelwood type rate expression for the rate of NO consumption. The authors of this model noted its shortcoming in terms of failing to correctly predict an overall first order rate with respect to NO pressure. An alternative mechanism [2] is somewhat more elaborate :

$$2\,NO + 2\,C^* \rightarrow 2\,C(O) + N_2 \quad (R4)$$
$$NO + C + C(O) \leftrightarrow C(O..ON)C \quad (R5)$$
$$NO + C(O..ON)C \rightarrow CO_2 + N_2 + C(O) \quad (R6)$$
$$NO + C(O..ON)C \rightarrow CO_2 + N_2 + CO \quad (R7)$$
$$2\,NO + 2\,CO \rightarrow 2\,CO_2 + N_2 \quad (R8)$$

The original presentation of this model included two reversible steps of form (R5), representing the formation of the two different types of C(O..ON)C complexes that react according to (R6) and (R7). There is general agreement that the first step is chemisorption of NO at almost any temperature of relevance. It probably involves addition of NO in an N-down configuration[7], followed by release of N_2 and formation of carbon oxide surface complexes , as suggested in (R4). In our recent study[6], we found that N_2 is a significant product during desorption from NO oxidized char even at high temperatures(> 1000 K). Although (R5) of the above mechanism represents the existence of long-lived N containing complexes on the surface, the C(O..ON)C complex with the weak physical bonding suggested by the authors[2] still most likely cannot represent the long-lived N containing complexes we have observed. It might then be possible that the C(O..ON)C complex is actually a chemisorbed complex, and that the desorption of N_2 we have observed involves the reverse of reaction (R5) followed by (R6), (R7) or (R8). We however see no evidence of desorption of NO as

such, except at low temperatures(see below). Thus we feel it most likely that the reaction (R4) does not proceed as indicated in a single step, and that there is some way of forming N containing surface species that can desorb as N_2 even in the absence of NO. Furthermore, the above model is deficient in not including a straight desorption route for formation of CO[6].

The validity of (R1) or (R4) as the route for NO sorption is thus in doubt. A more sophisticated sorption model should be constructed to explain the observations.This paper presents some results of NO-char sorption at low temperatures(< 523 K), at which the gasification of char is negligible.

EXPERIMENTAL

A standard thermogravimatric device(TGA) was used for the present study. Experiments were performed in a static system, in He/NO mixtures at 101 kPa total pressure. The volume of the vessel was large enough to ensure that under any reaction conditions, the consumption of NO was not significant. Pulverized char samples(50~100 mg) were held in a quartz bucket suspended in the heated zone of a quartz tube. A thermocouple placed within a few millimeters of the bucket served to indicate the temperature of the sample. The vessel could be purged following an experiment, and the contents analyzed by gas chromatography.

The chars used in present study were derived from phenol-formaldehyde resins. These resin have structure features similar to those in coals, but contain few catalytic impurities. These can be controlled to very low levels in synthesis. The resin char was prepared by pyrolysis of the phenol-formaldehyde resin in a nitrogen environment at 1323 K for 2 hours, then ground and sieved to give the desired particle size. The surface of the char was cleaned of oxides prior to NO sorption experiments by heating the sample to 1223 K in high purity helium for at least 2 hours.

NO sorption experiments were performed after surface cleaning by lowering the temperature of the sample from 1223 K to the desired sorption temperature, and then quickly introducing the desired NO/He mixture. Three sequences(I, II and III) were used to monitor the NO uptake. Sequence I started with a continuous monitoring of NO uptake for at least 24 hours until the mass gain is undetectable(i.e. $\pm$ 10 μg). Sequence II involved performing sorption, as in sequence I, to a constant mass uptake, followed by a series of changes in temperature, which affected the mass on the surface. Each temperature step lasted for 10 hours until there was no longer any detectable variation of the sample mass. Sequence III also involved performing sequence I, followed by an abrupt replacement of NO atmosphere by pure helium. After a period of monitoring the sample mass in helium, until there was no detectable mass variation, the original mixture of NO/He was reintroduced to the system, and the mass was monitored. Sequence III was performed under isothermal conditions.

RESULTS AND DISCUSSION

The NO uptake curves and the final mass uptake in sequence I sorption at different experimental conditions are shown in Fig. 1 and Table 1, respectively. The shape of the NO uptake curve is similar to that of O_2 chemisorption[8] on char. However it was found that the amount of NO uptake decreases with the increase of the temperature of char sample, while there was always an increase of the amount of O_2 uptake with increase in temperaure[8]. These results suggested that gasification of the char by NO might be occuring in this temperature range, and that the increase in the rate of sorption with increasing temperature might have been counterbalanced by an increase in the rate of a gasification step. However, no mass decline was observed after four days of sorption in an NO atmosphere, unlike the case in O_2 chemisorption when the rate of gasification ultimately overtakes the rate of chemisorption, as all the surface sites are filled. Furthermore, only small amount of CO_2 were formed (no CO was found) after the long period of chemisorption. These amount of CO_2 were negligible in comparison to the large decreases in mass seen with increasing temperature. Finally, according to our previous studies, the steady state gasification of char by NO proceeds at an undetectable level at temperatures lower than 673K. Therefore, we rule out gasification of char by NO in this temperature range. Combining the above results with the claim that there exist long-lived N containing complexes on the NO oxidized char surface, as shown in our recent studies[6], one can conclude that NO sorption on char with the simultaneous release of N_2, as described by (R1), is not the route for NO sorption on char. A better model to describe this chemisorption might be as follows

$$C + NO \rightarrow C(NO) \qquad (R9)$$
$$C(NO) \rightarrow C(O) + 1/2\,N_2 \qquad (R10)$$

In this model, both C(O) and C(NO) exist on the char surface. The C(NO) complex above can represent the N containing complex on NO oxidized char, and N_2 can be released through (R10) during desorption.The release of N_2 in (R10) would be activated by raising the temperature of the char sample, therefore the mass uptake during NO chemisorption on char would be less at higher temperature owing to the the N_2 release. The possibility of the backward reaction of (R9) to release NO should be also considered, and will be discussed later in this paper.

The results of sequence II sorption are given in Table 2. It shows that the mass of the sample decreased when the temperature was raised, and mass was regained on the sample when the temperature was lowered to the original value. The sequence is shown in Table 2. Mass is always lost with an increase in sample temperature. Returning to the same temperature results in a significant regain of mass (e.g. compare 5 and 6), but does not always restore the mass on the surface to the original values - compare steps 1 and 6, 4 and 8, 3 and 9, 2 and 10. The process appears to reach a measure of reversibility with continued cycling, however (compare 6 and 11). Experimental work on this this point continues. Thus the mass loss or gain of the sample was found to be somewhat reversible with respect to the temperature of the sample. It appears from these experiments that there may be a reversible pathway for NO chemisorption. This will be further supported below. Since there are some complexes that cannot be removed by these procedures, there must be an essentially irreversible pathway for sorption as well (recall that there are N-complexes stable up to > 1000 K). As mentioned above in discussing sequence I, no significant amounts of carbon oxides were found during sorption in this temperature range. Therefore, reaction (R10) is the candidate for the irreversible loss of mass during heating in this temperature range.

The results of sequence III are shown in Fig. 2 and Table 3. The mass variation was reversible with respect to the partial pressure of NO, and, therefore, contributed to by NO uptake or release.The results in Fig. 2 can be well described by the low pressure limit of Langmuir sorption isotherm and a temperature dependent equilibrium constant :

$$w = k_0 \cdot \exp[-Q/RT] \cdot P_{NO} \ ,$$

where k_0 is the preexponential factor in $g/(m^2 \cdot kPa)$, w is the NO uptake in g/m^2, P_{NO} is NO partial pressure in kPa, and Q is the heat of reversible sorption in kJ/mole. From a plot of ln(w) vs. 1/T, the value $7.63 \cdot 10^{-13}$ $g/(m^2 \cdot kPa)$for k_0 and -41.7 kJ/mol (i.e. exothermic) for Q were determined. The temperature dependence of the data of Table 3 is ,incidentally, entirely consistent with that of the data of Table 2 considering only the reversible part of the chemisorption. The conclusion is that the reversible sorbate in sequence II is NO. Therefore, there must exist a reversible chemisorption pathway in addition to the irreversible (R9) :

$$C' + NO \leftrightarrow C'(NO) \qquad (R11)$$

with a value of 41.7 kJ/mol as the heat of exothermic sorption, as described above. The heat of sorption of this value is much higher than that of usual physisorption which is usually less than 20 kJ/mol. This might be attributable to the free radical nature of NO molecules and thus an ability to form bonds stronger than physical bonds.

Similar to the O_2 chemisorption[9], the chemisorption behavior of NO can also be well described by the Elovich equation :

$$dq/dt = b \cdot \exp[-a \cdot q]$$

where a and b are fitting parameters, and q is the amount of mass uptake normalized by the total amount of mass uptake at the end of the run. The results given in Table 4 were determined by subtracting the contribution of the reversible step (R11), assuming it to occur instantaneously at time zero. It is unclear whether this is strictly speaking justified, but the rate of the reversible step appears to be quite high, compared to the overall rate for sorption, so the approximation may not be bad. Table 4 clearly shows that the b value, the extrapolated sorption rate at zero coverage, is roughly

proportional to NO pressure in the case of 423 K sorption temperature. This suggests that the rate of irreversible NO chemisorption (R9) is proportional to NO pressure. The value of a is not a function of NO pressure in the case of 423 K sorption, suggesting that the variation of kinetics of irreversible sorption with coverage is unaffected by the changing of NO pressure. It is of interest to note that the b value decreases with the sorption temperatures, which would imply a negative activation energy for the initial chemisorption. There is no physical significance to this result, because the role of N_2 release through (R10) has been neglected in the calculation.This aspect of the process will receive further attention.

The apparent activation energies of chemisorption (including both irreversible and reversible routes) at different extents of surface coverage, determined from the rates of mass uptake at several sorption temperautres, are shown in Fig. 3. The increase of the apparent activation energy, as shown in Fig. 3, from negative to positive values in the course of site filling suggests that the rate of N_2 release slows down compared to that of NO uptake when there are more complexes accumulated on the char surface. The reasons for this are not yet fully understood, and experiments are under way to verify the role of the N_2 release processes.

CONCLUSIONS

The chemisorption of NO on char surface is not always immediately followed by the release of N_2 from the dissociation of the NO molecule. The complexes C(NO) as well as C(O), derived from NO chemisorption, can both exist on char surface. The rate of NO chemisorption on clean char surface is roughly proportional to NO pressure. There are both irreversible and reversible routes for chemisorption of NO on carbon.

ACKNOWLEDGEMENT

We gratefully acknowledge the support of the USDOE through grant DEFG22-87PC79929 and the experimental assistant of Mr. William D. Lilly.

REFERENCES

1. Pereira, F. J., Beer, J. M., Gibbs, B. and Hedley, A. B., 15th Symposium(International) on Combustion, The Combustion Institute, Pittsburgh, 1149(1974)
2. Smith, R. N.,Swinehart, J. and Lesnini, D., Journal of Physical Chemistry, 63, 544(1959)
3. Furusawa, T., Kunil, D., Oguma, A. and Yamada, N., International Chemical Engineering, 20, No. 2,239(1980)
4. Chan, L. K., Sarofim, A. F. and Beer, J. M., Combustion and Flame, 52, 37/45(1983)
5. Teng, H., Suuberg, E. M., Calo, J. M. and Hall, P. J., Proc. 19th Conf. on Carbon, 574 (1989)
6. Suuberg, E. M., Teng H. and Calo, J. M., 23rd Symposium(International) on Combustion, The Combustion Institute, in press(1990)
7. Zarifyanz, Y. A., Kiselev, V. F., Lezhnev, N. N., and Nikitina, O. V., Carbon, 5, 127(1967)
8. Suuberg, E. M., Calo, J. M. and Wojtowicz, M., ACS, Division of Fuel Chemistry, Preprint, 31(3), 186(1986)
9. Suuberg, E. M., Wojtowicz, M. and Calo, J. M., Carbon, 27(3), 431(1989)

Table 1. Total amount of mass uptake(q_f) for NO adsorption on char in sequence I

P_{NO}	10.1 kPa				4.04 kPa
Temperature(K)	523	473	423	423	423
q_f $(g/m^2)\cdot 10^5$	1.59	2.20	2.71	2.48	2.08

Table 2. Variation in mass of sorbed species (m) for the reaction sequence II at constant NO partial pressure of 10.1 kPa

Step	1	2	3	4	5	6	7	8	9	10	11
Temp.(K)	$m(g/m^2)\cdot 10^6$										
373	34.20					30.88					30.86
398		30.75								28.26	
423			28.73						27.30		
448				27.48				26.93			
473					26.90		26.90				

Table 3. Amount of reversible NO uptake(w) at different temperatures and NO pressures in sequence III

	$w\ (g/m^2)\cdot 10^6$		
P_{NO}(kPa)	10.1	4.04	2.02
Temperature(K)			
373	4.29	1.72	0.889
398	1.80	0.693	0.320
423	0.849	0.319	0.182
448	0.512		
473	0.297		

Table 4. The Elovich parameters for NO chemisorption on char

P_{NO}	10.1 kPa			4.04 kPa
Temperature(K)	523	473	423	423
* a	4.55	5.59	5.70	5.78
** $b\cdot 100$	3.06	3.70	4.17	1.73

* a is a non-dimensional quantity. ** b is in units of min^{-1}

Fig. 1 The monitoring of NO chemisorption on char

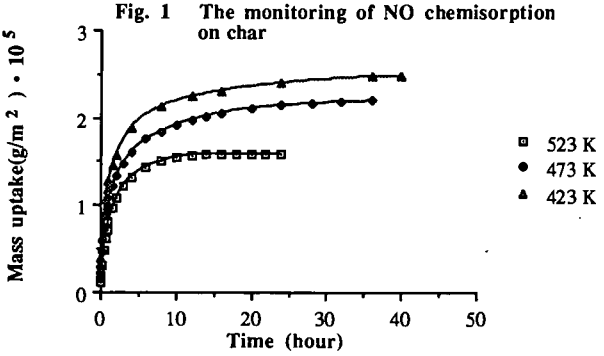

Fig. 2 Reversible NO uptake in sequence III

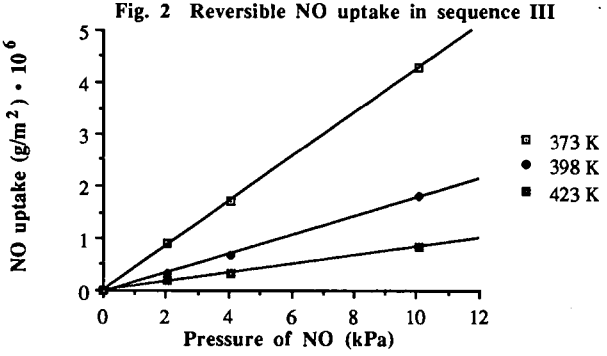

Fig. 3 Apparent activation energy of NO chemisorption on char at different surface coverages

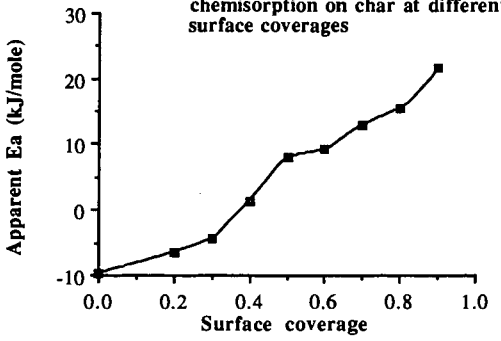

THE PREDICTION/CORRELATION OF CHAR REACTIVITY FROM DISTRIBUTIONS OF DESORPTION ACTIVATION ENERGIES

P.J. Hall and J.M. Calo
Chemical Engineering Program
Division of Engineering
Brown University
Providence, Rhode Island 02912

Keywords: Char gasification; carbon-oxygen surface complex energetics; temperature programmed desorption.

INTRODUCTION

Recently, in our laboratory, we have been concerned with the determination of distributions of desorption activation energies of oxygen surface complexes on carbons and chars from temperature programmed desorption (TPD) spectra. In the current communication we report on the application of probability density functions of desorption activation energies to the prediction/correlation of CO_2 gasification reactivities for chars produced from Wyodak coal and phenol-formaldehyde resin, which are desorption rate-controlled under the experimental conditions examined here. The resultant technique represents what we believe to be the first truly *a priori* prediction of CO_2 gasification reactivity as a function of temperature.

EXPERIMENTAL

Chars were prepared from Wyodak coal obtained from the Argonne Premium Coal Sample Bank, and phenol formaldehyde resin *via* pyrolysis in ultrahigh purity helium at 1273K with a soak time of 1 hour. The resin was synthesized in our laboratory according to a previously described procedure [1]. Care was taken to insure that contamination by any potentially catalytic impurities was kept to a minimum. Subsequent analysis by atomic absorption spectrometry revealed only nominal levels of alkali metal impurities.

The TPD apparatus and methods have been described elsewhere [2]. The most salient experimental details are as follows. Char gasification was performed in a TGA apparatus in 0.1 MPa CO_2 at the temperatures noted. Following cooling to room temperature in the TGA apparatus, the samples were transferred to a TPD reactor. Tests involving comparisons of TPD spectra obtained using this procedure with those following *in situ* oxidation in the TPD reactor have shown that transfer of the sample in this manner does not affect the resultant spectra.

The TPD reactor was constructed from a high-purity silica tube, 1-cm inside diameter, within which a close-fitting, circular silica sinter is used to support the sample. Ultrahigh purity helium

carrier gas is passed over the sample in downflow. Heating is accomplished electrically via nichrome wire wrapped around the outside of the silica tube, powered by a high current variable transformer. The heating regimen is controlled by a microcomputer. The resultant TPD reactor has a low thermal capacitance which allows linear heating rates of up to 500K/min.

Detection of desorbed species is accomplished with a quadrupole mass spectrometer (MS) which samples a small portion of the carrier flow. The MS output is fed to a microcomputer which also provides for multiple species detection via mass programming.

Typical sample sizes for the TPD measurements were ~10 mg. This size resulted in less than a monolayer coverage on the silica frit that was used as the sample holder in the TPD reactor. This, when combined with high helium carrier gas sweep rates, insured the absence of secondary interactions between the bulk gas species and the char samples.

Repeated experiments with char samples obtained from the same batch indicate that the reproducibility of gas desorption rates is approximately $\pm$10%. This error is attributable to a combination of effects arising primarily from sample inhomogeneity, sample size and MS calibration. For this reason, the spectra reported are representative, rather than averages.

THE APPROACH

The specific gasification reactivity, W, is given by:

$$W = -(1/C)\, dC/dt = k_d\, C_t\, \theta, \qquad [1]$$

where C is the amount of carbon, k_d is the desorption rate constant of oxygen surface complexes, C_t represents the total moles of active sites per mole of carbon, and θ is the fraction of the active carbon sites that are occupied by oxygen complex. For conditions where the surface is saturated with oxygen complex, θ =1 and Eq. [1] indicates that the specific gasification rate becomes desorption rate-controlled.

Eq. [1] applies explicitly to a homogeneous surface; i.e., one discrete surface complex with a single desorption activation energy. Actual char surfaces, however, are known to be distinctly heterogeneous, with a distribution of desorption energies. In a companion paper in this symposium [3], we present a method, based on the original work of Redhead [4], by which the the probability density function of desorption activation energies of oxygen surface complexes can be obtained by analysis of TPD spectra following gasification. The resultant transformation is given by:

$$d[CO]/dt = [C\text{-}O]_o\, S(E^*)\, dE^*/dt, \qquad [2]$$

where d[CO]/dt is the desorption rate of oxygen surface complexes as CO, $[C\text{-}O]_0$ is the total amount of oxygen surface complex initially on the char surface, S(E*) is the probability density function of desorption activation energies, and dE*/dt is the time derivative of the desorption activation energy during the TPD heating regimen. Since a TPD experiment yields the instantaneous d[CO]/dt directly, then knowledge of E* and dE*/dt defines the initial energetic distribution of surface complex, $[C\text{-}O]_0 S(E^*)$. The expression for E* and dE*/dt are given by [3]:

$$E^*/RT = [\ln (\nu_0 T/\beta) - 3.64], \qquad [3]$$

$$dE^*/dt = R\beta\,[E^*/RT] = R\beta\,[\ln (\nu_0 T/\beta) - 3.64], \qquad [4]$$

where ν_0 is the pre-exponential frequency factor for the desorption rate constant (assumed to be constant with energy and temperature), T is the temperature during desorption, and β is the local heating rate (constant for linear TPD).

The resultant energetic distribution can then be applied in a desorption rate-controlled reactivity expression similar to Eq. [1], with the exception that k_d must be energy-averaged over all surface complexes. In this case, the corresponding expression for W becomes:

$$W = \int_0^\infty \nu_0 \exp(-E^*/RT)\,[C\text{-}O]_0\,S(E^*)\,dE^*. \qquad [5]$$

RESULTS AND DISCUSSION

TPD spectra of oxygen complexes formed during burn-off of Wyodak and resin char samples at 850°C in 0.1 MPa CO_2 were compared after rapid quenching in helium, and after slow cooling in an atmosphere of CO_2. These experiments were performed in order to ascertain whether or not the surface was saturated with oxygen surface complex (i.e., θ=1) under these gasification conditions. It was reasoned that if θ is indeed a function of temperature, by cooling in CO_2 the resultant surface coverage would also change and differ from that obtained upon rapid quenching in helium. However, all the resultant spectra were virtually identical. This result implies that CO_2 gasification for these chars under these conditions is indeed desorption rate-controlled. This has also been concluded by other workers under similar conditions (e.g., see [5,6]).

Wyodak Coal Char. TPD spectra for a Wyodak subbituminous coal char sample are presented in Figure 1. In this figure, the rates of evolution of CO and CO_2 upon heating a Wyodak sample that has been gasified to 20% burn-off in CO_2 are presented as a function of temperature. As can be seen, the evolved gas is mostly CO, and its evolution is essentially continuous above a threshold temperature. The temperatures attained are quite high, indicating that the oxygen surface complexes from which the gases derive are quite thermally stable. The CO_2 evolved in

this case has been attributed to secondary reaction of desorbed CO with other surface complexes during TPD [2].

The energetic distribution, $[C\text{-}O]_o S(E^*)$, was obtained directly from these data using Eq. [2]. The result is presented in Figure 2. The prominent "bulge" on the leading edge of the distribution is also evident in the TPD spectra *ca.* 1000K. This feature has been attributed to catalytic mineral matter in the Wyodak char (most probably calcium oxide) in some of our work using demineralized samples. As is shown below, this feature accounts for practically all the reactivity of the char over the temperature range examined.

Since all the complex was not recovered in this experiment, due to the very high temperatures required, the entire distribution was also not determined. However, this could have been accomplished in principle by holding the sample at a final elevated temperature, T_f, until all the complex had desorbed. In any event, in order to predict the reactivity in the current temperature range of interest, knowledge of the entire distribution is not necessary, as explained below.

Predicted reactivities for the Wyodak coal char were determined from the preceding experimentally determined energetic distribution using Eq. [5]. The resultant parity plot of predicted versus measured reactivities (taken at 5% burn-off in other experiments in a TGA microbalance) is presented in Figure 3. As shown, the agreement between predicted and measured values is almost perfect for this char. It is noted that over the temperature range explored (i.e., 650-800°C), the gasification reactivity increased by three orders of magnitude, and Eq. [5] predicts the exact same behavior.

The reason for the large change in reactivity is clearly evident in Figure 4 which presents the differential reactivity over the distribution (i.e., the kernel of the integral in Eq. [5], along with the energetic distribution from Figure 2. As shown, as the temperature increases, an increasing number of surface complexes become involved in a highly nonlinear manner *via* the Arrhenius-dependent exponential term. It is also quite evident that gasification reactivity is controlled by only a very small fraction of the oxygen surface complexes located in the vicinity of the 1000K desorption feature; most of the complexes once formed are stable under these gasification conditions. Thus, this formulation shows in a very simple and graphic manner precisely why CO_2 gasification reactivity is so low at the lower temperatures and why it increases so precipitously with temperature.

Phenol-Formaldehyde Resin Char. In view of the suspected control of reactivity by mineral matter in the Wyodak coal char, we undertook some experiments with a "model compound" char produced from phenol-formaldehyde resin. A CO TPD from this char gasified to 11.7% in 0.1 MPa CO_2 at 1173K is presented in Figure 5. For this particular char, the amount of secondary CO_2 was negligible. As shown, the absolute amount of surface oxygen complex on this char is significantly less than for the Wyodak coal char gasified at even lower temperatures. In addition,

the CO spectrum is shifted significantly to higher temperatures than for the Wyodak char, and the low temperature "bulge," which controls the CO_2 reactivity for the Wyodak coal char, is noticeably absent.

The resultant energetic distribution of oxygen surface complexes, determined from Eq. [2], is shifted to higher energies than the Wyodak coal char. This fact should be directly reflected in significantly reduced predicted CO_2 gasification reactivity; and, indeed this is the case, as shown in the parity plot of predicted versus measured reactivities (taken at 5% burn-off in other experiments in a microbalance) presented in Figure 6. As shown, the agreement between predicted and measured values is quite good (to within a factor of two), although not as good as for the Wyodak reactivity predictions presented in Figure 3. It is noted that the CO_2 reactivity of the resin char is three orders of magnitude less than that of the Wyodak coal char at 1073K, and the current formulation predicts this considerable difference quite well.

It is also important to note that the oxygen reactivities measured for these same two chars at 623K in 0.1 MPa of oxygen are almost exactly the same on a total active surface area (ASA) basis, as measured by oxygen chemisorption. Therefore, it seems apparent that oxygen reactivity is not a good indicator of CO_2 reactivity, at least for these two chars. Therefore, it appears that correlations of char CO_2 reactivities according to ASA, as determined by low temperature oxygen chemisorption, can fail quite dramatically for certain chars.

CONCLUSIONS

We believe that this work represents the first truly *a priori* prediction of the CO_2 gasification reactivity of chars. With this method the reactivity of a char as a function of temperature can be predicted from a single TPD experiment following mild gasification at a single temperature. Currently, this prediction can be made for the case where gasification reactivity is controlled by the thermal desorption of oxygen surface complexes formed during gasification; however, the approach may be extended to arbitrary conditions as well. The implications of this work potentially affect all aspects of coal char behavior. It represents a foundation for the development of techniques for coal char characterization and reactivity prediction/correlation based upon knowledge of the energetic heterogeneity of the coal char surface as described by the appropriate probability density function.

Acknowledgement. This work was supported by the Morgantown Energy Technology Center of the Department of Energy under Contract No. DE-AC21-MC23284.

REFERENCES

1. Suuberg, E.M.; Wojtowicz, M.; Calo, J.M. *Carbon* **1989**, *27*, 431.
2. Hall, P.J.; J.M. Calo *Energy & Fuels* **1989**, *3*, 370.

3. Hall, P.J.; Calo, J.M. *ACS Div. Fuel Chem. Prepr.* **1990,** "Energetic distributions of oxygen surface complexes on porous carbons and chars," this symposium.
4. Redhead, P.A. *Vacuum* **1962,** *12*, 203.
5. Mentser, M., and S. Ergun, *A Study of the Carbon Dioxide-Carbon Reaction by Oxygen Exchange, 1973,* U.S.Bur.Mines Bull. 664.
6. Yang, R.T., in *Chemistry and Physics of Carbon,* **1984,** Volume 19, P.A. Thrower, ed., pp. 203-263, Marcel Dekker, NY.

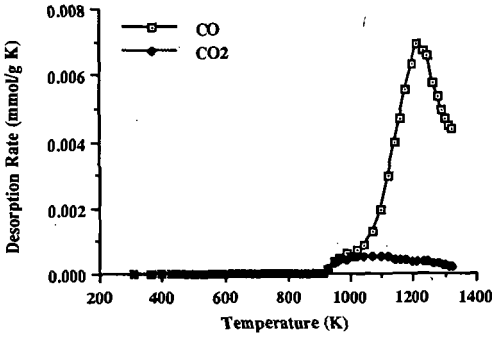

Figure 1. 100K/min CO and CO_2 TPD spectra from Wyodak coal char gasified to 20% burn-off in 0.1MPa CO_2 at 1173K, and cooled in ultrahigh purity helium.

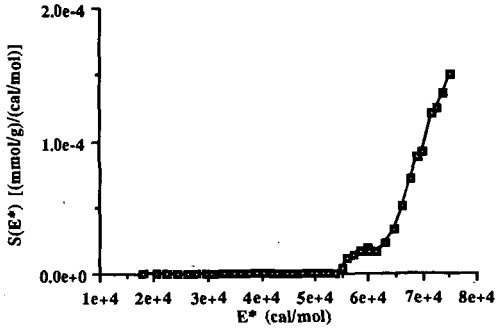

Figure 2. Probability density function of desorption activation energies, S(E*), for Wyodak coal char burned-off to 20% in 0.1MPa CO_2 at 1173K, and cooled in ultrahigh purity helium.

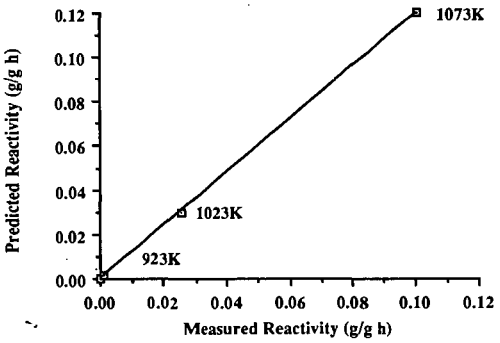

Figure 3. Parity plot of predicted *vs.* measured reactivities for Wyodak coal char in 0.1MPa CO_2 as a function of temperature.

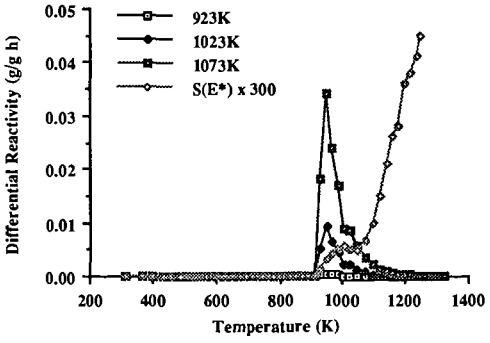

Figure 4. Differential reactivities as a function of temperature, and S(E*) for Wyodak coal char in 0.1MPa CO_2.

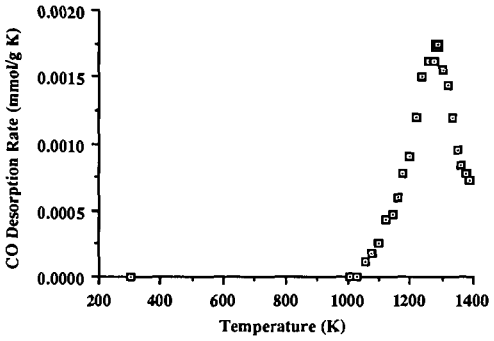

Figure 5. 100K/min CO TPD spectrum for resin char gasified to 11.7% burn-off in 0.1MPa CO_2 at 1173K, and cooled in ultrahigh purity helium.

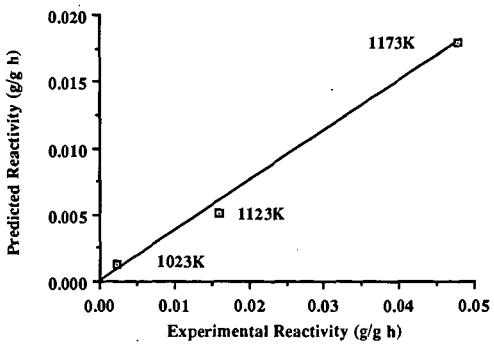

Figure 6. Parity plot of predicted *vs.*measured reactivities of resin char in 0.1MPa CO_2 as a function of temperature.

THE INFLUENCE OF COAL SURFACE CHEMISTRY ON THE ADSORPTION OF COAL CONVERSION CATALYSTS

Godfried M. K. Abotsi, Kofi B. Bota and Gautam Saha

Research Center for Science and Technology
Clark Atlanta University
Atlanta, GA 30314

Keywords: Adsorption, catalysts, coal surface charge.

INTRODUCTION

Prior to its gasification, coal is generally loaded with catalytic materials by mechanically mixing the coal with a solid catalyst precursor, by impregnation with a solution containing the catalyst precursor (incipient wetness technique), or by ion-exchange of the catalyst precursor metal ions with protons on the coal (1-3). For the same catalytic material, the various techniques typically produce different coal char reactivities under identical reaction conditions. The disparities in catalyst performance has been attributed to differences in catalyst dispersion, induced by differences in coal-catalyst contact.

Despite their significant influence on catalyst activity, the effects of interfacial phenomena on the adsorption of coal gasification metal catalysts has not been previously investigated. This paper describes the effects of coal surface charge on the adsorption of calcium and potassium ions from solution.

EXPERIMENTAL

The coals used in the study are a lignite (PSOC 1482) and a subbituminous coal (PSOC 1485), both of which were sealed in argon and supplied by the Penn State Coal Sample Bank. The ultimate and proximate analyses of the coals are provided in Table 1.

The surface charge properties of the coals were measured at room temperature using a Pen Kem Model 501 Lazer Zee Meter zeta potential instrument. Slurries were prepared by dispersing 300mg samples of each coal (equal proportions of -20 and -80 U.S. mesh sizes) in a liter of deionized water containing 10^{-3} moles l^{-1} $AgNO_3$ for ionic strength control. After the coal particles have been well-dispersed by

agitation in an ultrasonic bath, the sediments were separated from the suspended particles, the latter fraction was divided into 50.0 cm^3 portions, and the pH's of the dispersions were varied with nitric acid or ammonium hydroxide solutions. After 4h equilibration (by mechanical agitation), each sample was transferred to the zetameter and the zeta potential of the coal particles were measured.

The effect of coal surface charge on the adsorption of potassium and calcium ions was determined by dispersing 1.0g samples of coal in 10^{-2} or 10^{-3} moles l^{-1} of K^+ or Ca^{2+}. The samples were conditioned by shaking for 24h after which they were filtered and the filtrates analyzed for potassium or calcium with atomic absorption spectrophometry. Metals uptake were calculated as the difference in Ca or K content of the solutions prior to and after adsorption.

RESULTS AND DISCUSSION

The zeta potential results given in Figure 1 show that the surfaces of the lignite coal particles are negatively charged over a wide range of pH and that the isoelectric point (iep) occurs at about pH 1.9, the surfaces of the coal particles being positively and negatively charged, respectively, below and above this pH value. A review of the iep's of coals shows that the iep of coals occurs in the acidic range (4).

A striking feature of Figure 1 is that the negative charge density increases with increase in pH. A similar trend was observed for the subbituminous coal. These observations can be explained in terms of the surface functional groups on coal. It is well known that the surfaces of low-rank coals are dominated by oxygenated surface groups. Several studies [5-7] have shown that the surface chemistry of these coals is determined by these groups, although inorganic species also play a role [6]. In aqueous and basic environments, these acidic groups dissociate and the coal particles acquire negative charges, whereas the surface groups are protonated in acidic medium, reducing the negative charge density, and the surface may become positively charged in strongly acidic media [5,6]. The formation of surface charge on coals is depicted by equations (1)-(4) for carboxyl (COOH) and hydroxyl (OH) functional groups:

$$-COOH_{(s)} + OH^- \longrightarrow -COO^-_{(s)} + H_2O \quad (1)$$

$$-COH_{(s)} + OH^- \longrightarrow -CO^-_{(s)} + H_2O \quad (2)$$

$$-COOH_{(s)} + H^+ \longrightarrow -COOH_2^+{}_{(s)} \quad (3)$$

$$-COH_{(s)} + H^+ \longrightarrow -COH_2^+{}_{(s)} \quad (4)$$

where the subscript(s) designates the coal surface. Such reactions have also been reported for carbon surface oxygen functionality (8-10).

Figure 2 shows the quantities of calcium adsorbed by the lignite as a function of pH. It is observed that calcium uptake is not only inhibited in strongly acidic media (pH < 4), but calcium is actually extracted from the coal into solution, as indicated by the negative calcium values. However, calcium adsorption progressively increased as the pH's of the coal slurries increase. These trends are consistent with the surface charge properties of the coals. As the coal particles become more negatively charged, coal-Ca^{2+} interactions become more pronounced as a result of electrostatic interaction between the metal ions (Ca^{2+}) and the anionic coal surface. A similar trend was obtained for potassium adsorption onto the coals.

In synopsis, for the first time, it has been shown from the current study that coal surface charge exerts a predominant influence on the adsorption of coal gasification metal ions from solution. Metal ion adsorption is favored in highly alkaline solution, while it is suppressed in strongly acidic environments. Thus, efficient catalyst impregnation and improved catalyst dispersion and activity may be obtained by controlling the pH and the surface charge on coals.

REFERENCES

1. Wood, B. J., Sancier, K. M., Catal. Rev. - Sci. Eng. 1984, 26 (2), 233.

2. Radovic, L. R., Walker, Jr., P. L., Jenkins, R. G., *Fuel* 1983, 62, 209.

3. Johnson, J. L. *In Fundamentals of Coal Utilization: 2nd Supplementary Volume*, Elliot, M. A., Ed.; John Wiley: New York, 1981.

4. Quast, K. B., Readett, D. J. *Adv. Coll. Int. Sci.* 1987, 27(3-4), 169.

5. Kelebek, S. Salman, T.: Smith, G. W. *Canad. Metal. Quart.* 1982, 21, 205.

6. Fuerstenau, D. W.; Rosenbaum, J. M.; Laskowski, J. *Coll. Surf.* 1983, 8, 137.

7. Laskowski, J. s., Parfitt, G. D., In "Interfacial Phenomena in Coal Technology," Botsaris, G. D. Glazman, Y. M., Eds., Marcel Dekker, New York, 1988 p. 279.

8. Abotsi, G. M. K.; Scaroni, A. W. *Carbon '88 Proceedings* of Soc. Chem. Ind. (London), 1988, 422.

9. Abotsi, G. M. K.; Scaroni, A. W. *Carbon 1990*, 28, 000.

10. Abotsi, G. M. K., Osseo-Asare, K., Int. J. Miner. Process. 1986, 18, 217.

ACKNOWLEDGEMENT

Financial support for this work is provided by the U.S. Department of Energy Under Grant Number DE-FG22-89PC89760.

Table 1. Properties of Coals Used

Penn State Sample Number	PS0C-1482	PS0C-1485
Seam	Hagel	Rosebud
State	N. Dakota	Montana
Rank	Lignite	Subbit. B
Ultimate Analysis (daf, %)		
Carbon	71.34	75.78
Hydrogen	4.5	5.30
Nitrogen	1.14	1.19
Total Sulfur	0.79	0.99
Oxygen (by diff.)	22.24	16.75
Proximate Analysis (As Rec'd, %)		
Moisture	34.45	25.37
Volatile Matter	28.18	27.43
Fixed Carbon	31.80	38.67
Ash	5.57	8.54

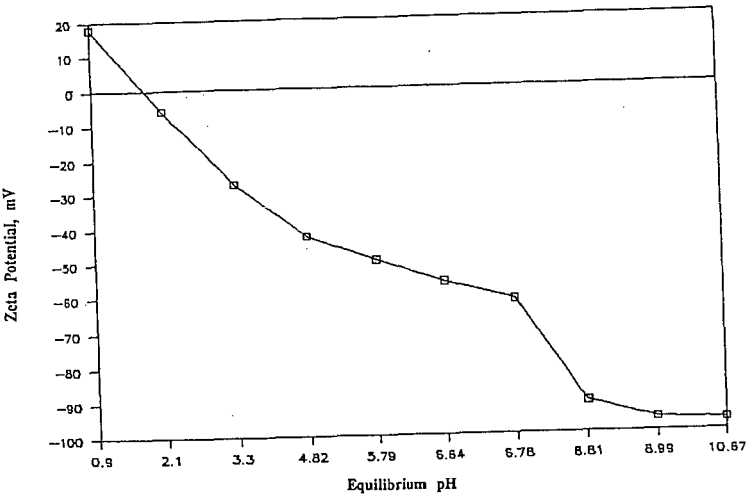

Figure 1: Dependence of Zeta Potential on pH for North Dakota (Hagel) Lignite (PSOC 1482). Ionic strength was controlled with 10^{-3} moles l^{-1} $AgNO_3$.

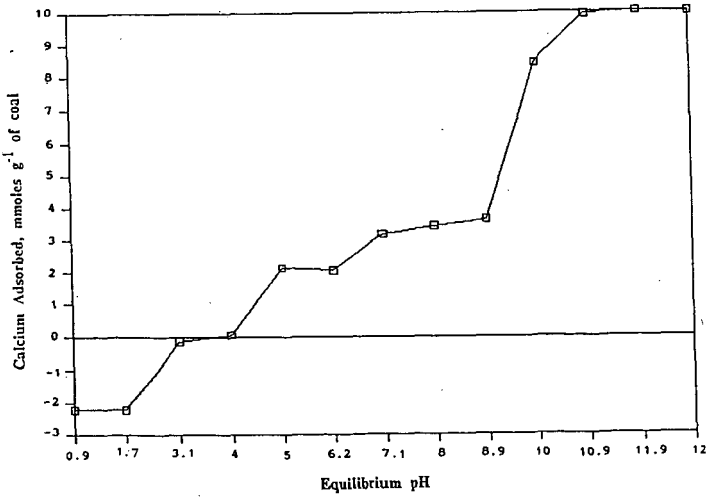

Figure 2: Calcium Adsorption as a Function of pH by Hagel Lignite (PSOC 1482).

HYDROTREATMENT OF COAL GASIFICATION LIQUID BY-PRODUCTS WITH A SOLID ACID CATALYST

Edwin S. Olson, Ramesh K. Sharma, and John W. Diehl
University of North Dakota Energy and Environmental Research Center
Box 8213 University Station, Grand Forks, ND 58202

KEY WORDS: hydrotreating, gasification, coal tar

INTRODUCTION

The production of transportation fuels by hydrotreatment of coal tars has been practiced for many years. Coal tars represent an important part of the products of coal gasification units, and as more of these units become operational, a large source of hydrocarbon fuels will be available. Three liquid by-products are produced at the Great Plains Gasification Plant. These include tar oil, crude phenol, and a light naphtha from the rectisol desulfurization unit. Mild gasification processes currently under study produce a liquid product in addition to the char and gas. Conversion of these tars to a transportation fuel requires removal of heteroatoms (nitrogen, sulfur, and oxygen) as well as hydrogenation and cracking of the larger aromatic and aliphatic components.

The production of a high density jet fuel from the Great Plains tar-oil by-product was investigated by hydrogenation with commercial supported bimetallic catalysts (1). The products contained large amounts of cyclohexane components from hydrogenation of the aromatics. For conversion to a gasoline fuel, hydrocracking of polynuclear aromatics in the tars is desired, but addition of hydrogen to single ring aromatics is not required. A new solid acid catalyst has been developed in our laboratory appropriate for the type of hydrotreating needed to produce a gasoline-type fuel with high single ring aromatic content. This catalyst consists of zinc chloride supported on and complexed with silica gel. Coal liquefaction and hydrodesulfurization with this new solid acid catalyst have been recently reported (2,3,4), and its effectiveness for hydrotreating tar samples is discussed in this paper.

EXPERIMENTAL

A tar oil sample resulting from the gasification of North Dakota lignite (Beulah) had the elemental analysis (5) shown in Table 1. The sample was hydrotreated at 400°C with 1000 psi hydrogen, as previously described (2) for hydrotreatment of liquefaction samples. The product slurry from the reaction of Great Plains tar oil with silica gel-zinc chloride catalyst was transferred into a centrifugation tube and separated into solid and liquid products.

The liquid product was analyzed by GC/FID and GC/MS analyses. Carbon and sulfur emission spectroscopy (GC/MS/AES) was used for the qualitative analyses of the reaction products. The solid product was washed with dichloromethane, vacuum dried, and weighed. Sulfur was analyzed with the Leco instrument, chlorine by the method in Vogel (2).

The second sample was a tar sample produced several years ago in the Grand Forks Energy Technology Center's slagging fixed-bed gasifier from a North Dakota lignite (Indian Head) This sample consisted of the residue after distillation of the light oil components shortly after collection of the tar. The sample was stored in a glass jar without any special precautions against oxidation. The elemental analysis of the sample is given in Table 1.

Hydrotreatment was carried out as described above, and the product distilled under vacuum (2 torr) to 250°C. The distillate was mixed with the appropriate internal standard and analyzed by GC/FID and GC/FTIR/MS/AED, as above. The solid residue was extracted with dichloromethane, and the soluble and insoluble fractions were weighed and analyzed by elemental analysis and infrared spectroscopy.

RESULTS AND DISCUSSIONS

The reactions of tar oil with a silica gel-zinc chloride catalyst were carried out at 400°C for 3 hours and in the presence of 1000 psig (repressurizations at 1-hour intervals) of molecular hydrogen. The product consisted entirely of distillable material (Table 2). Elemental analysis and mass balance indicated that the dichloromethane-insoluble product was essentially the recovered catalyst. No coke formation was observed.

The original tar oil contained 8% aliphatics, 48% aromatics, and 36% polar compounds (5). Aromatic components consisted of mostly alkylbenzenes and alkylnaphthalenes, but ranged from toluene to pyrene. Polar components consisted of phenolics, as well as dihydroxybenzenes and nitrogen bases. The hydrotreated product contained much fewer polar compounds, with no dihydroxybenzene and no nitrogen bases. The aromatic fraction of the hydrotreated product contained benzene, tetralins, and indanes and their alkyl substituted derivatives as the major components.

Major sulfur components of the original tar oil were alkylthiophenes, benzothiophenes, and a small amount of dibenzothiophene. The very sensitive sulfur emission determination of components by GC/AED showed that all thiophenes and benzothiophenes were removed and only a trace of dibenzothiophene remained in the hydrotreated product.

The dry tar sample was hydrotreated with the silica-gel-supported zinc chloride to give a similar slate of products (Table 2), but with higher average molecular weight. The distillate yield for the dry tar reaction product (82%) represented a substantial improvement over that obtained for the original dry tar.

The distribution of compound types in the original dry tar was 11% aliphatic compounds (alkanes/alkenes), 25% aromatic compounds, and 63% polar compounds. The major aromatic components of the original tar were three- and four-ring compounds. The polar components included a considerable amount of dihydroxybenzene and nitrogen bases.

The aliphatic fraction of the hydrotreated product distillate contained some cycloalkanes, and the distribution of larger alkanes (C_{14} to C_{33}) was essentially unchanged. The distillate still contained small amounts of aromatics such as phenanthrene and pyrene, however the majority of the product components were hydroaromatics, such as tetralin, and alkylbenzenes. The phenolic components consisted of phenol, cresols, and other alkylphenols, but no dihydroxybenzenes were present. No nitrogen components were observed in the distillate.

The major sulfur compound in the original dry tar was dibenzothiophene. The reconstructed sulfur emission chromatogram of the distillate indicated that only a trace of dibenzothiophene remained in the hydrotreated product, and no other organosulfur components were present.

The dichloromethane-soluble fraction of the residue represented 8 wt% of the starting material. This product was analyzed by elemental analysis (C, 77.4; H, 7.9; N, 0.31; S, <0.01; and O, 14.4). The dichloromethane-insoluble fraction was mainly recovered catalyst along with a small amount (6%) of organic material. Approximately 4% of starting material was converted to gas.

CONCLUSIONS

The silica gel-zinc chloride catalyst was effective in removing heteroatoms form the coal tars. Dihydroxybenzenes were converted to phenols and aromatics. Polynuclear aromatic components were hydrogenated to hydroaromatics, which were further cracked to smaller compounds, but hydrogenation of single ring aromatics was minimal. Retrograde coking reactions were also minimal. The products obtained were too heavy for gasoline; however, a distillate cut of the hydrotreated products containing components in the benzene to xylene range could be a gasoline additive. Further hydrocracking is need to convert the multi-ring components.

REFERENCES

1. Knudson, C.L. "Production of Jet Fuels from Coal-Derived Liquids"; Vol. XIV, Oxygenates Content of Coal-Derived Jet Fuels, AFWAL-TR-87-2042, 1990.

2. Sharma, R.K.; Diehl, J.W.; Olson, E.S. Prepr. Pap. - Am. Chem. Soc., Div. Fuel Chem., 1990, 35, 414-422.

3. Olson, E.S.; Diehl, J.W.; Sharma, R.K. Prepr. Pap. - Am. Chem. Soc., Div. of Fuel Chem., Preprints, 1990, 35, 563-569.

4. Sharma, R.K.; Diehl, J.W.; Olson, E.S. 3rd Int. Conf. on Proc. and Util. of High-Sulfur Coals; Ames, Iowa, Nov. 14-16, 1989.

5. Knudson, C.L. "Production of Jet Fuels from Coal-Derived Liquids"; Vol. II, Characterization of Liquid By-Products from the Great Plains Gasification Plant, AFWAL-TR-87-2042, 1988.

TABLE 1

ELEMENTAL ANALYTICAL DATA, WT%

Element	Tar Oil	Tar Residue
Carbon	83.76	83.12
Hydrogen	8.86	7.96
Nitrogen	0.52	0.88
Sulfur	0.39	0.32

TABLE 2

CATALYTIC HYDROTREATING REACTIONS

Reactants (g)			React. Cond.		Products (%)		
Sample	Cat.	Hydrog. (psi)	Temp. (°C)	Time (hr)	CH_2Cl_2-I	CH_2Cl_2-S	Dist.
Dry Tar 1.01	SZC 0.5	3 x 1000	400	3	6.0	8.0	82
Tar Oil 2.0	SZC 1.0	3 x 1000	400	3	0	0	98

BENCH-SCALE TEST RESULTS AND CALCULATION PROCEDURE FOR IN-SITU SULFUR CAPTURE VIA SORBENT ADDITION TO COAL SLAGS UNDER PARTIAL OXIDATION CONDITIONS

Mitri S. Najjar and Dick Y. Jung
Texaco Inc.
P. O. Box 509
Beacon, NY 12508

Keywords: in-situ desulfurization; coal gasification; optical basicity

SUMMARY

The addition of sorbents with the coal feed is being examined as a means to capture sulfur in-situ during the partial oxidation of coal in a Texaco gasifier operated in the slagging mode. To rapidly screen candidate sorbents for sulfur capture prior to their being tested in an experimental bench scale unit, a calculation scheme based on an extended use of the concept of optical basicity is being tested for estimating the solubility of sulfur in a given coal slag with and without added potential sorbents. This calculation method identified iron, calcium and sodium based compounds as well as combinations of these additives as potentially good sulfur-capturing sorbents for a coal slag. Experimental EDX data from bench-scale drop tube furnace runs with coal slag using these additive packages under simulated Texaco coal gasifier syngas conditions are presented which verify the predicted higher sulfur solubility in the resultant slag-additive mixtures.

INTRODUCTION

One of the most promising approaches for utilizing coal in an environmentally safe manner that has been recently demonstrated is the generation of electric power via partial oxidation of coal in an integrated gasification-combined cycle (IGCC) plant. To minimize emission of sulfur compounds, these processes typically separate the reaction step (where coal is converted to raw syngas under reducing conditions at high temperatures) from the acid gas removal step (where physical solvents are generally used to scrub hydrogen sulfide and carbonyl sulfide from the crude syngas). Currently, this approach requires cooling of the hot syngas to the low temperatures commonly needed for physical solvents and subsequent reheating of this cleaned syngas prior to its introduction into the gas turbine. Consequently, these heating and cooling cycles require significant capital investments as well as operating costs.

A potentially more efficient alternative is to combine coal combustion with the sulfur removal step in the same vessel. However, the total solubility of sulfur in coal slags is typically quite low (between 0.01 and 0.5 weight percent). One possible approach to enhance sulfur solubility in coal slags is the addition of sulfur-capturing sorbents along with the coal feed to the gasifier. The ideal sorbent would be an inexpensive additive that chemically reacts with the gas phase sulfur compounds (primarily hydrogen sulfide with smaller amounts of carbonyl sulfide) to form sulfide(s) that are encapsulated in a disposable slag-additive mixture but the addition

of this additive should not cause any complications for slag flow from the gasifier.

To rapidly screen candidate sorbents, a method to estimate the amount of sulfur captured by the mixture of coal slag with these potential additives would be quite useful to reduce the number of required experimental tests. Consequently, we have been exploring the use of an extended concept of optical basicity to estimate the sulfide capacity for mixtures of coal slag with various additives. This proposed calculation scheme estimates the sulfide capacity at a given temperature based solely on the elemental composition of the slag-additive mixture. With an estimate of the sulfur and oxygen partial pressures as well as the weight percentage of sulfur in the coal, the sulfur content in the slag mixture can then be approximated.

METHODS

Calculations

Slag basicity may be defined as being directly proportional to its free oxygen ion activity. Wagner[1] defined the basicity of a slag with respect to its "capacity" to absorb various constituents. For example, the main reaction that describes the sulfur-oxygen exchange behavior between slag and gas under reducing conditions is represented by the following reaction which has an equilibrium constant K_1:

$$[O^{-2}] + \tfrac{1}{2} S_2(g) = [S^{-2}] + \tfrac{1}{2} O_2(g) \quad (1)$$

where the brackets indicate that ions are present in the slag. Since the oxygen ion activity as well as the sulfide activity coefficient are difficult to measure in ionic melts, Fincham and Richardson[2] expressed the potential of a silicate slag to absorb sulfur in terms of a measured quantity called the sulfide capacity (C_s) that is related to the oxygen and sulfur partial pressures in the gas phase by:

$$C_s = [\%S] (P_{O2}/P_{S2})^{\frac{1}{2}} \quad (2)$$

where [%S] represents the concentration of sulfur as sulfide (sulfur solubility) in the slag mixture while P_{O2} and P_{S2} represent the oxygen and sulfur partial pressures in the gas phase, respectively. Utilizing the equilibrium constant expression for the reaction in Equation (1) and solving for the sulfide capacity:

$$C_s = K_1 (a_{O-2}/\gamma_{S-2}) = [\%S] (P_{O2}/P_{S2})^{\frac{1}{2}} \quad (3)$$

This equation ties the equilibrium constant and the sulfide capacity with the gas phase oxygen and sulfur partial pressures inside the gasifier. The sulfide capacity for a number of slag compositions has been measured[3] by classical physicochemical methods. However, the available literature data on sulfide capacity for slags are insufficient to cover the entire range of compositions that are of interest for in-situ sulfur capture.

An alternative approach is to estimate the slag's sulfide capacity using the concept of "optical basicity". Optical basicity (denoted by Λ) refers to a measure of basicity determined by spectroscopic methods that has been shown to be predictable from Pauling's electronegativity of the individual elements in a slag. For a large number of slag compositions at 1500°C, the relationship[4] between the optical basicity of a slag and its sulfide capacity is:

$$\log C_s = 12.6 \Lambda - 12.3 \quad (4)$$

To account for the effect of temperature on the equilibrium reaction, consider the calcium sulfide-oxide equilibrium reaction:

$$CaS(s) + \tfrac{1}{2} O_2(g) = CaO(s) + \tfrac{1}{2} S_2(g) \quad (5)$$

Based on this chemical equilibrium, a temperature-dependent correction

term (B) is introduced which gives the following temperature-corrected expression[5] for the sulfide capacity:

$$\log C_s = \log C_s^* + B \quad (6)$$

$$B = -4534\ (1773 - T)/\ (1773\ T) \quad (7)$$

where T is the temperature of interest in degrees Kelvin. The advantage of using optical basicity lies in the observation that it is simply extended to multicomponent systems by:

$$\Lambda = N_A\Lambda_A + N_B\Lambda_B + \ldots + N_Z\Lambda_Z \quad (8)$$

where N_i is the normalized "equivalent cation fraction" of the ith oxide in the solution based on the formula MO_y, i. e. the number of atoms of oxygen per metal in the oxide. Values of optical basicities[3,4] for several oxides commonly found in coal slags are available in the literature. Hence, it is possible to estimate the optical basicity for a slag-sorbent mixture knowing just its chemical composition.

It should be noted that these correlations were empirically developed based primarily on experimental data for metallurgical slags and have not been tested for coal slag mixtures with sulfur sorbents. Consequently, equilibrium drop tube furnace experiments using coal slags with selected additives were performed to check if the potential sorbent systems identified by this proposed calculation procedure would indeed capture sulfur.

Experiments

Bench scale tests were conducted at atmospheric pressure using temperatures and gas compositions selected to simulate gasifier conditions using the apparatus shown schematically in Figure 1. The principal units for high temperature testing are two identical LeMont Scientific quench furnaces capable of reaching 3000°F. Slag and sorbent samples (50-100 mg) were placed in a crucible that is suspended in the furnace by a thin platinum wire which is then equilibrated by exposure to a flowing gas mixture for at least 18 hours. Gaseous mixtures of CO, CO_2 and 1 vol %SO_2 in Argon were selected to simulate the S_2 and O_2 partial pressures at the desired temperatures and ambient pressure based on equilibrium calculations using a multiphase free energy minimization computer program, an in-house version of SOLGASMIX[6]. The suspended slag-sorbent sample was then rapidly quenched by dropping the crucible into a pool of water or simulated syngas. This was accomplished by passing an electrical current through the suspending platinum wire which causes the wire to break.

The quenched sample was recovered and characterized by petrographic examination using a Leitz Orthoplan microscope and electron microprobe analysis. An Amray 1645 scanning electron microscope equipped with secondary and backscattered electron detectors for imaging as well as a Tracor Northern TN-5500 energy dispersive X-ray microanalysis system with 40 MByte data storage capacity and color display were used to obtain SEM photomicrographs to show phase morphologies as well as EDX multielement semiquant chemical analysis to confirm phase identifications.

RESULTS

Calculations based on this extended use of the concept of optical basicity identified additive systems based on iron, calcium, and sodium compounds along with combinations of these compounds as potential sulfur-capturing sorbent systems under oxygen and sulfur

partial pressures found in Texaco coal gasifiers. For these additive packages, the sulfur solubility in the resultant mixture for these slag-additive systems are estimated to be substantially increased. A summary of several calculation results for Pittsburgh No. 8 coal slag with and without several additive packages are listed in Table 1. Note the increase in the predicted sulfur solubility in the resultant slag-additive mixtures depends on the chemical composition of the additive package.

The effects of gas composition and temperature on equilibrium in-situ sulfur capture were considered. For constant temperatures, calculations predict that a more reducing gas atmosphere (i. e. lower oxygen partial pressure) increases the sulfur solubility in the slag-additive mixture. Also, for constant sorbent composition, the sulfur solubility in the slag-additive mixture increases as the temperature decreases. Hence, the most favorable Texaco coal gasifier conditions for in-situ sulfur capture by these sorbents are expected to be at lower temperatures with a highly reducing gas atmosphere. However, several practical considerations (e.g. coal conversion and slag viscosity) place limits on the achievable operating conditions in Texaco coal gasifiers.

In addition, the effect of sorbent composition was also examined. The calculations indicate that sodium is incrementally more effective than either iron or calcium as a sulfur sorbent. Among the additive mixtures considered, calculations indicate that the iron-sodium package is expected to be the most effective with possible synergistic effects between the two components while the iron-calcium package is expected to be marginally better than a physical mixture of the two components.

To validate these predictions, experimental bench scale data using coal slag equilibrated with several of these proposed sorbent packages under simulated Texaco coal gasifier syngas environments were performed. Experimental sulfur solubilities in the slag's silicate phase as measured by EDX are shown as a function of temperature for bench scale runs for Pittsburgh No. 8 slag with a sodium additive are shown in Fig. 2. These experimental results qualitatively confirm the predicted increase in sulfur solubility for these resultant slag-additive mixtures as a function of temperature under simulated syngas conditions for a Texaco coal gasifier operated in a slagging mode with a coal-water slurry feed. In addition, several sorbent mixtures were tested that qualitatively confirm the estimated greater incremental effect of sodium-based sorbents versus either iron- or calcium-based sorbents as well as the synergistic interactions for a combined iron-sodium sorbent package. Hence, the extended use of the concept of optical basicity shows promise as a means to identify additive packages which can enhance the sulfur solubility in coal slag-additive mixtures under simulated Texaco coal gasifier syngas conditions.

CONCLUSIONS

A proposed calculation scheme based on an extended use of the concept of optical basicity was found to qualitatively identify several possible sorbent packages that could potentially capture sulfur in-situ under simulated Texaco coal gasifier syngas conditions. Experimental bench scale data confirm that addition of several of these additive packages enhance sulfur solubility in the resultant coal slag-additive mixtures. Consequently, this proposed calculation

scheme shows promise as a rapid method to identify potential sorbent packages which can enhance in-situ sulfur capture by the slag.

ACKNOWLEDGEMENTS

The authors gratefully acknowledge financial support for this work under the five year Texaco/Department of Energy Cooperative Program (Contract No. DE-FC21-87MC23277) on "Integration and Testing of Hot Desulfurization and Entrained Flow Gasification for Power Generation Systems" with METC's Dr. J. Beeson as Contract Manager. Mitri Najjar would like to thank Prof. John F. Elliot for several helpful discussions. Ron McKeon performed most of the experimental runs while Tris Laurion provided EDX analyses of the slag samples.

REFERENCES

1. C. Wagner, Met. Trans., 6B (1975) 405-409.
2. C. J. B. Fincham and F. D. Richardson, "The behavior of sulfur in silicate and aluminate melts", Proc. Roy. Soc. London, A223 (1954) 40-62.
3. J. A. Duffy and M. D. Ingram, "The Behavior of Optical Basicity Indicator Ions in Relation to the Ideal Optical Basicity of Glasses", Physics and Chemistry of Glasses, 16 (1975) 119-23.
4. I. D. Sommerville and D. J. Sosinski, "The Application of Optical Basicity Concept to Metallurgical Slags", in A. H. Fine and D. R. Gastell (Ed.), Second International Symposium on Metallurgical Slags and Fluxes, The Metallurgical Society, AIME, Warrendale, PA, (1984) 1015.
5. J. F. Elliot, Private communication.
6. G. Eriksson, Acta Chem. Scand., 25 (1971) 2651.

TABLE 1
Calculation results for Pittsburgh No. 8 coal slag with various additive packages based on extended use of optical basicity

Pittsburgh No. 8 slag Chemical Analysis (wt%)		Syngas Conditions
Na_2O	1.42	Temperature = 2200°F
CaO	5.04	Total Sulfur = 2.14 wt%
MgO	1.00	$P_{S2} = 4.09 \times 10^{-5}$ atm
Al_2O_3	22.33	
SiO_2	44.57	$P_{O2} = 2.59 \times 10^{-12}$ atm
FeO	24.17	Coal-water slurry feed
TiO_2	1.05	Air Gasification
P_2O_5	0.42	Slagging Mode

	Case I	Case II	Case III	Case IV
Additive, wt% slag	None	22wt% CaO	12wt% Na_2O 10wt% FeO	22% Na_2O
Optical basicity	0.61	0.65	0.68	0.71
log(Sulfide Capacity)	-5.10	-4.47	-4.20	-3.92
Sulfur Solubility in slag	0.03	0.14	0.25	0.47

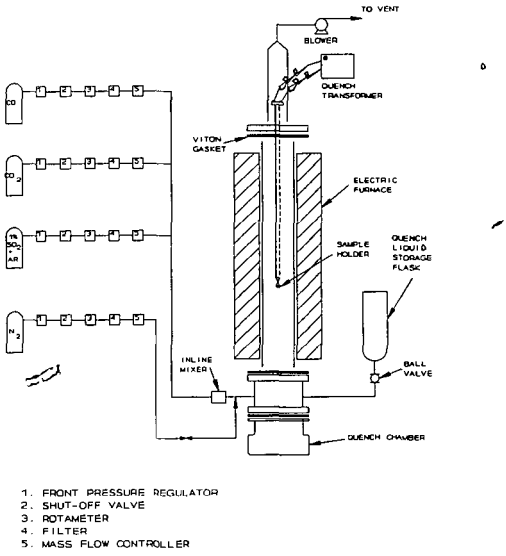

FIGURE 1 Schematic for Equilibrium Furnace

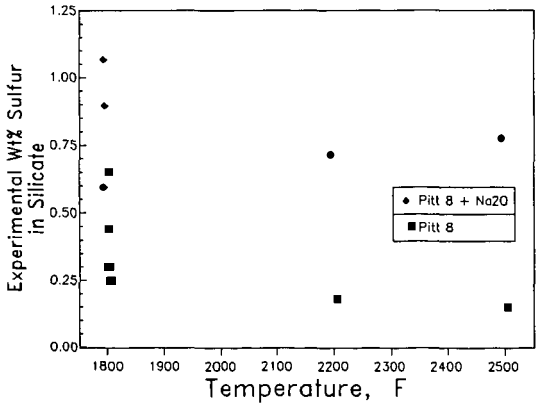

FIGURE 2 Effect of temperature and sodium addition on sulfur capture for Pittsburgh No. 8 slag under simulated Texaco coal gasifier slagging mode conditions

TRENDS IN THE EVOLUTION OF FLY ASH SIZE DURING COMBUSTION

Chris J. Zygarlicke, Donald L. Toman, and Steven A. Benson
Combustion and Environmental Research Center
University of North Dakota Energy and Environmental Research Center
Box 8213 University Station, Grand Forks, ND 58202

KEYWORDS Fly Ash, Particle-Size Distribution, Coalescence

ABSTRACT

Processes governing the evolution of the intermediate ash (inorganic gases, liquids, and solids) during pulverized coal combustion were examined in detail by combusting carefully sized fractions of Beulah lignite and Upper Freeport bituminous coals in a laminar flow drop-tube furnace. Char (partially combusted coal) and fly ash produced at various temperatures and residence times were analyzed using advanced scanning electron microprobe techniques. Fly ash was collected and sized in multicyclone and impactor devices. Work was focused on determining the relationship between the sizes of the original coal and coal minerals and the size of the resulting fly ash. Time-resolved size distributions of inorganic phases associated with chars show that Beulah and Upper Freeport phases exhibit some coalescence of inorganic phases with time. The Upper Freeport shows an initial increase in the amount of particles in the lower size ranges possibly due to fragmentation of minerals or the formation of smaller inorganic ash droplets from submicron minerals or organically associated inorganic constituents. The level of ash and coal minerals in size ranges greater than 3 microns is nearly equal for Upper Freeport, possibly indicating the influence of fragmentation. Size distributions of both the Upper Freeport coal minerals and resulting fly ash were larger than similar distributions for the Beulah. Both coals gave slightly smaller fly ash sizes for higher gas temperatures. In support of this observation, calculations revealed that both coals produced more fly ash particles per coal particle for higher combustion temperatures. The mechanism of fly ash formation for the Beulah was the result of partial coalescence of minerals and organically bound constituents. Upper Freeport ash revealed coalescence for the smaller (<3.0 μm) minerals. Using different coal sized fractions and the same gas temperature of 1500°C, larger fly ash particle size distributions were observed for the smaller-sized coal fractions.

INTRODUCTION

Today's coal energy technologies are being severely challenged by tighter pollution control regulations and demands to obtain higher yields from lower quality coals. Research on the chemical and physical transformations of inorganic components during combustion is a relevant branch of coal energy research geared to meet the challenge of today's demands because the results obtained pertain not only to emissions, but also to boiler efficiency. Intermediate inorganic components in combustion systems consist of inorganic gas, liquid, and solid phases produced during the combustion of coal. These inorganic components can cause significant problems in utility boilers, including:

fireside ash deposition on heat transfer surfaces, erosion and corrosion of boiler parts, and production of fly ash that is difficult to collect. The goal is to develop a means to predict the particle-size distribution and chemistry of the fly ash for a given coal, based on the character of the initial coal inorganic constituents and combustion conditions. In order to attain this goal, quantitative data is needed to describe the transformation of coal inorganic components to fly ash particulate, so that realistic predictive models can be devised. Carefully controlled laboratory-scale combustion regimes are being used, such as the laminar flow drop-tube furnace, which can simulate gas temperatures, particle residence times, and particulate stream flow rates in larger scale combustors. Also, more sophisticated analytical tools are now available which provide a more comprehensive means of quantifying inorganic constituents in coals, fly ash, and ash deposits (1,2).

Studies of fly ash particle sizes indicate a bimodal size distribution (3,4,5,6). The submicron size particles have an average diameter of about 0.1 micrometer. These small particles form as a result of the homogeneous condensation of flame-volatilized species. Flame-volatilized species may also condense heterogeneously on the surfaces of larger particles. Larger-sized particles are sometimes referred to as residual ash, which is largely derived from discrete mineral grains. The composition and size distribution of the larger particles are a result of the transformations and interactions between discrete mineral grains and organically bound inorganic components in the coal. Processes such as coalescence, fragmentation of minerals and char, and shedding of inorganic components all play a role in the final fly ash produced. Loehden et al., (7) indicate that three potential models for fly ash generation can be used to describe fly ash particle size and composition evolution. The first, "fine limit," assumes that each mineral grain forms a fly ash particle and that the organically associated elements form fly ash particles less than 2 μm. The second, total coalescence assumes one fly ash particle forms per coal particle. The third limit, partial coalescence, suggests that the fly ash composition and particle size evolves due to partial coalescence.

The focus of work presented in this paper was to observe trends of fly ash particle size evolution during combustion of low-rank Beulah lignite and higher-rank Upper Freeport bituminous coals. The approach was to carefully quantify the association and size of the inorganic constituents in the original coal and examine the combustion products quenched at successively longer residence times in an entrained laminar flow drop-tube furnace. In this way the stages of fly ash development can be discerned for coals of varying rank and composition. Accurate information of how ash particle sizes and compositions change with time and how specific coal inorganics and minerals are transformed and other new high-temperature products formed may lead to recognizing trends in fly ash evolution.

EXPERIMENTAL

Coal and Char Characterization

Sonically sieved fractions of Beulah and Upper Freeport coals (38-53-μm, 53-74-μm, and 74-106-μm fractions) were prepared. Extensive testing of these coal fractions and their combustion by-products were performed as part of a Department of Energy contract to study inorganic transformations during combustion. Computer-controlled scanning electron microscopy (CCSEM) (1,2) was

used to ascertain abundance and size distribution of minerals or inorganic phases in the coals and chars. Standard ash determination and bulk coal ash analyses were also performed on the coal fractions. Chemical fractionation analysis (8) of the Beulah lignite gave 92% of the sodium and 46% of the calcium as being organically bound in the coal matrix. Table 1 summarizes the initial coal characterization data for Beulah and Upper Freeport.

Production and Characterization of Ash Constituents

Time-resolved studies of the evolution of fly ash particle size were accomplished for the Beulah and Upper Freeport coals by tracking particle-size transformations beginning with the original coal minerals, progressing through short residence time chars, and ending in the near 100% carbon burnout. Fly ash and char were produced using an entrained flow-tube furnace, also known as a drop-tube furnace. The drop-tube furnace is a laboratory-scale furnace system that can simulate conditions in commercial combustors without the high cost associated with pilot-scale combustion testing. Figure 1 shows the drop-tube furnace used at the EERC. The combustion temperature, residence time, and gas cooling rate can be closely controlled and monitored (9).

Fly ash was collected using a Southern Research Institute Five-Stage Cyclone, equipped with a final filter, and a University of Washington Mark 5 Source Test Cascade Impactor. The multicyclone aerodynamically separates the fly ash into six stages or aerodynamic categories, while the impactor segregates the ash into twelve stages.

A short residence time probe was used to collect char samples at five residence time intervals: 0.05, 0.1, 0.2, 0.5, and 0.8 seconds. Particle-size distributions of original coal minerals and char phases were determined using CCSEM, and fly ash was sized using multicyclone and impactor collection devices attached to the drop-tube furnace. The effects of combustion temperature and coal particle size on the final fly ash size distribution were investigated as well.

Fly ash was produced at 1300, 1400, and 1500°C using 53-74 μm fractions of Beulah and Upper Freeport coals. The combustion parameters are given in Table 2. Near 100% carbon burnout was achieved under these conditions. The fly ash was cooled by means of a fly ash quenching probe and collected using the multicyclone. In addition, three size fractions of each coal were combusted at 1500°C and collected in the impactor to note changes in fly ash particle-size distribution with varying coal size (Table 3). Table 4 gives the combustion parameters used to produce chars from Upper Freeport and Beulah (53-74 μm) coals, respectively, at various residence times. Based on thermal gravimetric analysis, a steady decrease in carbon content was noted with increasing residence time for both coals, and by 0.8 seconds, near 100% burnout was achieved. The chars were analyzed using CCSEM to determine the size and composition of inorganic ash particles.

RESULTS AND DISCUSSION

Fly Ash Particle-Size Evolution

Detailed analysis was made of the Beulah and Upper Freeport inorganic components associated with the coal, char, and fly ash by observing area, weight, and number percent concentrations of inorganic components in different size categories. Number percent data refers to the number of particles in a particular size category, whereas weight percent data is a weighted average of the ash in different size categories which approximate a mass distribution. In effect, this gives a time-resolved look at the development of fly ash particle size which is helpful input into models which attempt to predict fly ash size and composition.

The analysis of Beulah char phases revealed that greater quantities of larger-sized particles were formed during char formation as compared to the original mineral size distribution (Figure 2). This may be evidence for coalescence of smaller inorganic particles to form larger ones.

The particle-size distribution for mineral phases in the Upper Freeport chars (Figure 3) shows an initial increase in the number of particles in the smaller size categories. By 0.8 seconds, however, larger quantities of phases are found in the >11.0 μm fraction than in the coal. This trend may indicate that, initially, fragmentation of mineral grains may be occurring with subsequent coalescence of ash particles as time in the hot zone progresses. Another trend noted for these coals is that the Upper Freeport, which had an overall larger mineral particle-size distribution than did the Beulah (Figure 4a), also produced a larger fly ash size distribution (Figure 4b). This may help answer the question as to whether the fly ash size distribution is heavily dependent on the size of the original discrete mineral phases.

The degree of coalescence in Beulah and Upper Freeport was examined by comparing the measured ash particle size-distributions with particle-size distributions at the extremes for total coalescence or no coalescence. The hypothesis is that the true fly ash size distribution should fall somewhere between ideal coalescence, where one ash particle is produced per coal particle, and no coalescence where each coal mineral grain remains intact as a separate particle. The predicted mean diameter (D_a) of an ash particle was derived using the ash % of the coal and the diameter (D_c) of the coal grains from Malvern (Equation 1). Assumptions made were that the coal particles were spheres

$$D_a = D_c \sqrt[3]{\%Ash} \qquad (1)$$

and that percent ash was evenly distributed throughout all the coal particles. The discrete minerals and the fly ash were sized using CCSEM. The size distribution curve for Beulah 0.8 second char, which closely approximates fly ash, falls between the mineral and predicted ash curves (Figure 5a). This is an indication of partial coalescence. Upper Freeport ash, on the other hand, follows very closely to the original coal size distribution for particles greater than approximately 3 microns (Figure 5b).

Both the Beulah and Upper Freeport showed some evidence of smaller fly ash particle size distributions at higher temperatures (Figure 6 a and b). Although the overall fly ash particle size was partially the result of coalescing mineral and organically bound constituents, early combustion stage char fragmentation may have occurred at higher temperatures resulting in finer-sized fly ash. To check the validity of smaller fly ash at higher temperatures, the number of fly ash grains produced per coal grain (F/C) was calculated for the fly ash size fractions in each multicyclone (Equation 2). The input variables needed to make the calculations were the mass of ash (m_n) in each multicyclone stage (n), total mass collected in the multicyclones (m_{tot}), density of the coal and ash (ρ_c and ρ_f), percent ash in the coal, and the diameters of the coal and fly ash grains (d_c and d_f). For simplicity, it was assumed that the coal and fly ash grains were spherical and had uniform densities of 1.4 and 2.7, respectively. Mean coal particle sizes (d_c) were obtained from Malvern sizing analysis, and the mean fly ash sizes (d_f) were calculated from the percent mass in each of the multicyclones. The same calculations apply for impactor data. The results

$$F/C = \frac{m_n \rho_c}{m_{tot} \rho_f} \left(\frac{\%Ash}{100}\right) \left(\frac{d_c}{d_f}\right)^3 \qquad (2)$$

of the calculations, given in Table 5a, are reported for fly ash grains greater than 1 μm. These very basic calculations verify the PSD data from the multicyclones that larger quantities of smaller fly ash particles are generated at higher temperatures. This may indicate that larger coal particles are reverting to the smaller-sized ash distributions dictated by the original coal mineral sizes as carbon matrix burns away.

Fly ash produced at 1500°C, using different Beulah coal size fractions and collected in the impactor, was larger for the smaller-sized coal fractions (Figure 7a). A similar result was achieved for Upper Freeport coal size fractions, especially for ash particles greater than 2.8 microns (Figure 7b). Calculations of fly ash particles generated per coal particle for the different coal size fractions showed more fly ash grains for the larger coal fractions, for both Beulah and Upper Freeport (Table 5b). Smaller minerals were observed earlier to experience a greater degree of coalescence. It may be that the smaller coal size fractions contain more smaller-sized minerals more apt to coalesce to form a larger ash particle.

CONCLUSIONS

Particle-size distributions of discrete mineral or amorphous phases in intermediates produced in the DTF for two coals were examined. Coal minerals and char inorganic phases approximately <3.0μm in the Beulah and Upper Freeport tend to coalesce with time. Upon combustion, the Upper Freeport shows an initial increase in the amount of particles in the lower size ranges, possibly due to fragmentation of minerals or the formation of smaller inorganic ash droplets from submicron minerals or inorganics. The Upper Freeport coal minerals PSD and resulting fly ash PSD are distributed over larger size ranges than the same PSDs for the Beulah.

The size distribution curve for Beulah ash falls between the mineral and predicted coalescence ash curves. This is an indication of partial coalescence.

Upper Freeport ash, on the other hand, follows very closely to the original coal size distribution for particles greater than approximately 3 microns. The mechanism may not necessarily be fragmentation of coal particles, but rather that as carbon matrix burns away, larger coal particles are reverting to the smaller-sized ash distributions as dictated by the original coal mineral sizes. Beulah, on the other hand, shows more coalescence influence, possibly due to the Na-Ca-rich phases from the organic bonding sites that envelop and react with aluminosilicates, resulting during combustion.

Particle-size distributions of the fly ash at three different temperatures showed slightly smaller fly ash sizes at the higher temperature for both coals. In support of this observation, both coals produced more fly ash particles per coal particle for higher combustion temperatures. Although the fly ash overall was a result of coalescing mineral and organically bound constituents, the early stage chars may have experienced more initial fragmentation at higher temperatures. Fly ash produced at 1500°C, using different coal size fractions and collected in the impactor, was larger for the smaller sized coal fraction.

The trends in fly ash formation observed here using empirical data are in agreement with various models of fly ash evolution and provide a good framework for verifying and testing future models.

ACKNOWLEDGEMENTS

This work was performed under contract to the Department of Energy under Cooperative Agreement No. DE-FC21-86MC10637. The authors thank the Contracting Officers Technical Representative, Mr. Philip M. Goldberg, for his support and permission to publish the results of this work.

REFERENCES

1. Jones, M.L., Kalmanovitch, D.P., Steadman, E.N., Zygarlicke, C.J., and Benson, S.A. "Application of SEM Techniques to the Characterization of Coal and Coal Ash Products", Advances in Coal Spectroscopy, in press, 1990.

2. Steadman, E.N., Zygarlicke, C.J., Benson, S.A., and Jones, M.L. "A Microanalytical Approach to the Characterization of Coal, Ash, and Deposits", ASME Seminar on Fireside Fouling Problems, Brigham Young University, Provo, Utah, April 1990.

3. Sarofim, A.F., Howard, J.B., and Padia, A.S. Combustion Science and Technology, Vol. 16, 1977, p. 187.

4. Flagan, R.C., and Friedlander, S.K. "Particle Formation in Pulverized Coal Combustion", Recent Developments in Aerosol Science, Ed. D.T. Shaw, Wiley, New York, 1978, Chapter 2.

5. Damle, A.S., Ensor, D.S., and Ranada, M.B. Aerosol Science and Technology, 1982, Vol. 1, p. 119.

6. Wall, T.F., Bailey, J.G., and Wibberley, L.J. "The Influence of Coal Properties and Combustion Conditions on the Size Distribution of Fly Ash", In Mineral Matter and Ash Deposition From Coal, Eds. Richard W. Bryers, Karl S. Vorres, Engineering Foundation Conferences Proceedings, Feb. 22-26, 1988, Santa Barbara, California, p. 249, 1990.

7. Loehden, D., Walsh, P.M., Sayre, A.N., Beer, J.M., and Sarofim, A.F. "Fly Ash Generation and Deposition in Pulverized Coal Combustion", In Mineral Matter and Ash Deposition From Coal, Eds. Richard W. Bryers, Karl S. Vorres, Engineering Foundation Conferences Proceedings, Feb. 22-26, 1988, Santa Barbara, California, p. 279, 1990.

8. Benson, S.A., and Holm, P.L. Ind. Eng. Chem. Prod. Res. Dev., 24, 145, 1985.

9. Zygarlicke, C.J., Steadman, E.N., and Benson, S.A. "Studies of the Transformations of Inorganic Constituents in a Texas Lignite During Combustion", Progress in Energy and Combustion Science: Special Issue on Ash Deposition, Pergamum Press, 1990, in press.

TABLE 1

INORGANIC CHARACTERIZATION OF BEULAH AND UPPER FREEPORT COALS

Coal Ash Analysis	Beulah	Upper Freeport
SiO_2	21.5	50.5
Al_2O_3	13.5	24.2
Fe_2O_3	10.8	12.8
TiO_2	1.0	1.3
P_2O_5	0.9	0.1
CaO	16.1	3.1
MgO	4.0	1.5
Na_2O	6.2	0.0
K_2O	0.2	3.7
SO_3	25.7	2.7
% Ash (Dry Basis)	6.9	19.6
CCSEM Mineral Analysis		
Quartz	17.5	12.6
Iron Oxide	1.6	1.9
Aluminosilicate	40.8	24.3
Ca-aluminosilicate	0.2	0.6
Fe-aluminosilicate	0.1	3.6
K-aluminosilicate	0.9	31.6
Pyrite	27.5	13.8
Gypsum	1.6	0.5
Barite	0.9	0.0
Calcite	0.1	1.1
Rutile	0.3	0.9
Pyrrhotite	0.7	1.3
Si-Rich	0.4	0.3
Unknown	6.7	6.9
Total Minerals (Coal Basis)	4.8	22.1

TABLE 2

DROP-TUBE FURNACE RUN CONDITIONS FOR MULTICYCLONE COLLECTION OF FLY ASH FOR BEULAH AND UPPER FREEPORT 53-74 μm COALS

	UPPER FREEPORT			BEULAH		
Run #	1	2	3	1	2	3
Gas Flow Rates (L\min):						
Primary air	1	1	1	1	1	1
Secondary air	4	4	4	3	3	3
Quench Gas (N_2)	4	4	4	3	3	3
Vacuum	10	10	10	10	10	10
Temperatures (°C):						
Secondary air	1000	1000	1000	933	930	930
Furnace Upper Wall	1298	1406	1498	1300	1400	1500
Furnace Lower Wall	--	1429	--	--	--	--
Coal Feed Rate (g/min)	0.13	0.09	0.06	0.29	0.45	0.31
Residence Time (sec)	2.5	2.4	2.3	2.5	2.4	2.3

TABLE 3

DROP-TUBE FURNACE RUN CONDITIONS FOR THE FORMATION OF FLY ASH FROM BEULAH AND UPPER FREEPORT COAL SIZE FRACTIONS

Coal Size, μm	38-53	53-74	74-106
Gas Flow Rates (L\min):			
Primary air	1	1	1
Secondary air	3-4	3-4	3-4
Quench Gas (N_2)	3-4	3-4	3-4
Vacuum	10	10	10
Temperatures (°C):			
Secondary air	980	990	980
Furnace 1 Upper Wall	1498	1500	1500
Furnace 1 Lower Wall	1530	1530	1510
Coal Feed Rate (g/min)	0.03-0.24	0.03-0.2	0.03-0.2
Residence Time (sec)	2.5	2.3	2.0

TABLE 4

DROP-TUBE FURNACE RUN CONDITIONS FOR CHAR COLLECTION
OF BEULAH AND UPPER FREEPORT 53-74 μm COALS

	Beulah				Upper Freeport				
Run #	1	2	3	4	1	2	3	4	5
Gas Flow Rates (L\min):									
Primary air	1	1	1	1	1.2	1.2	1.2	2	1.2
Secondary air	4	4	4	4	3	3	3	2.5	3
Quench Gas (N_2)	3	3	3	3	5	5	5	5	5
Vacuum	10	10	10	10	10	10	10	10	10
Temperatures (°C):									
Secondary air	1000	1000	1000	1000	982	982	983	982	992
Furnace 1 Upper Wall	1467	1470	1475	1442	1502	1498	1497	1503	1499
Furnace 1 Lower Wall	1487	1480	1478	1434	1572	1570	1563	1552	1545
Coal Feed Rate (g/min)	0.08	0.08	0.29	0.34	0.06	0.06	0.06	0.05	0.06
Residence Time (sec)	0.1	0.2	0.5	0.8	0.05	0.1	0.2	0.5	0.8

TABLE 5

CALCULATED FLY ASH GRAINS PER COAL GRAIN
(PARTICLES > 1 MICRON)

(a) Varied Temperature and 53-75 μm Coal

	Temperature °C		
	1300	1400	1500
Beulah	6.3	5.9	9.0
Upper Freeport	16.5	21.6	26.3

(b) Varied Coal Size

	Coal Size (μm)		
	38-53	53-74	74-106
Beulah	14	66	147
Upper Freeport	159	134	316

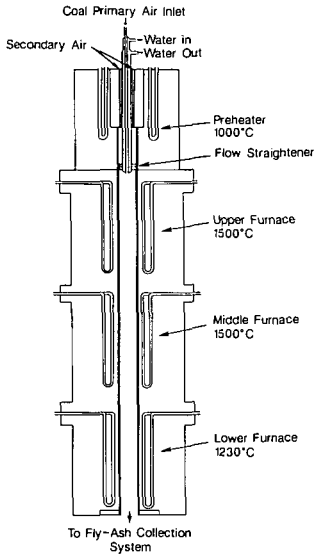

Figure 1. Schematic drawing of the EERC drop-tube furnace.

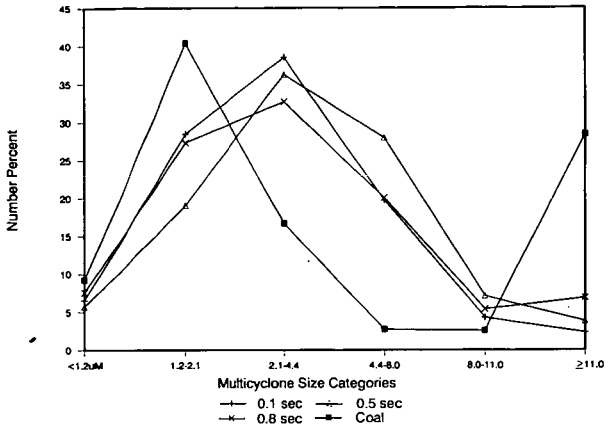

Figure 2. Particle-size distribution of inorganic particles in Beulah chars based on the numbers of particles in each size category determined using CCSEM of whole grain mounts.

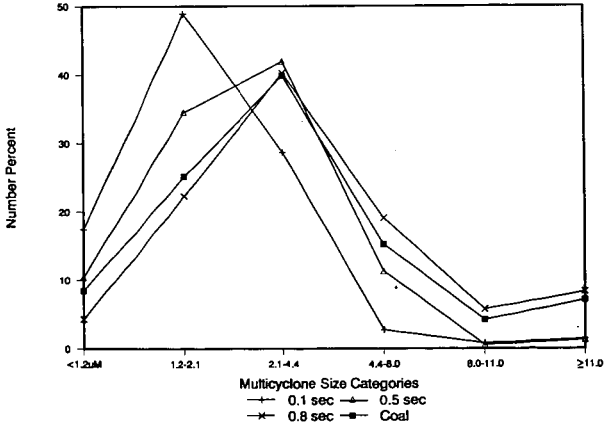

Figure 3. Particle-size distribution of inorganic particles in Upper Freeport chars based on the number of particles in each size category determined using CCSEM of whole grain mounts.

(a)

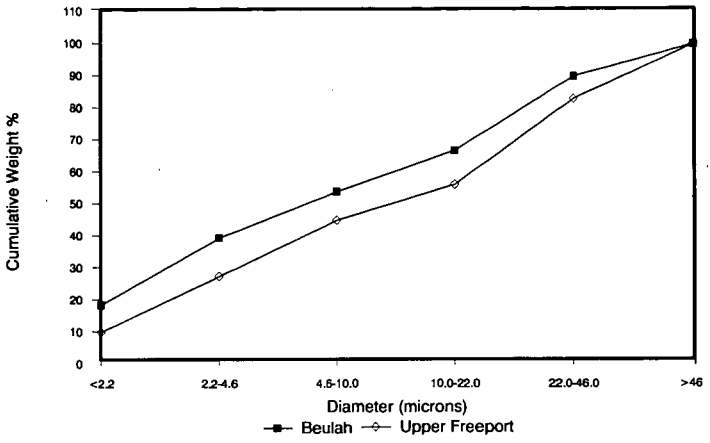

(b)

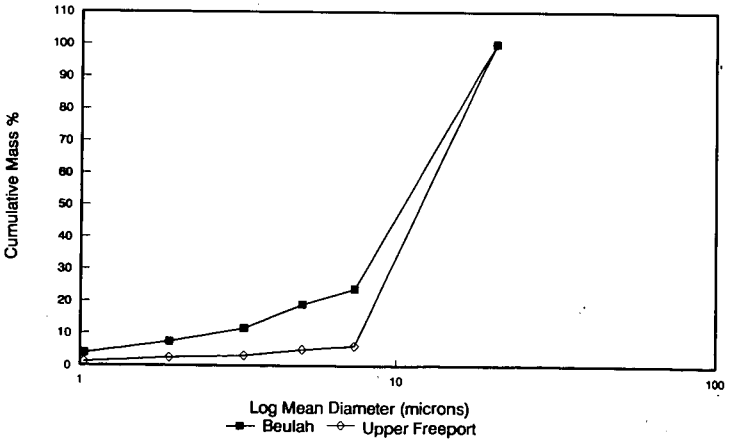

Figure 4. (a) Size distribution of minerals in Beulah and Upper Freeport 53-75 μm.
(b) Size distribution of fly ash in Beulah and Upper Freeport generated at 1500°C on the 53-74 μm fraction.

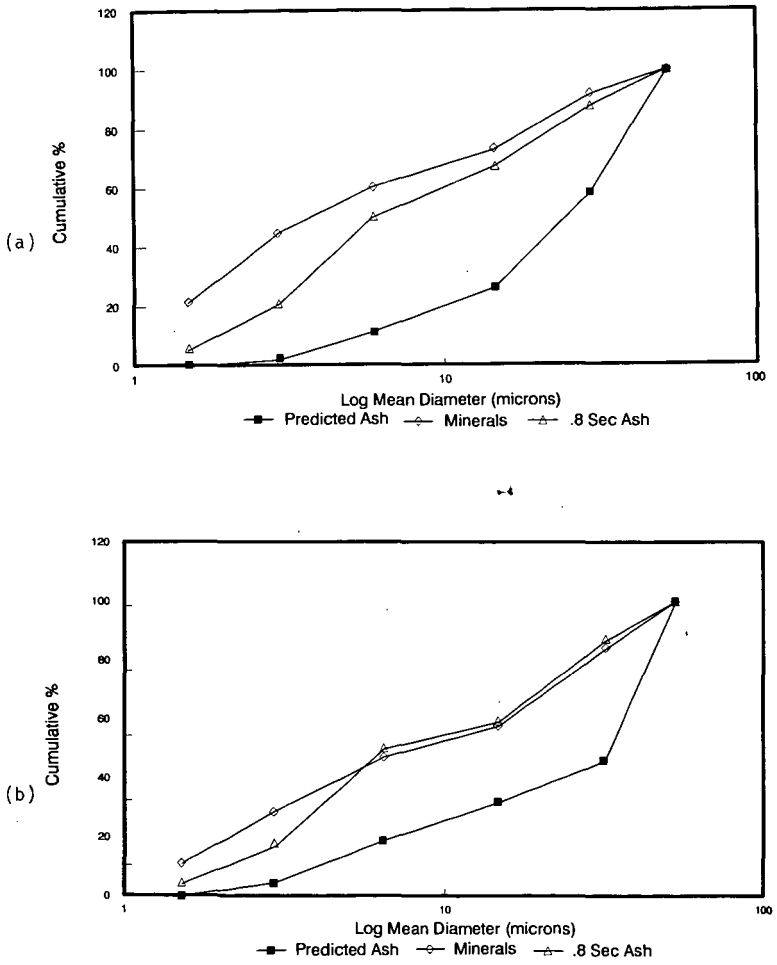

Figure 5. Cumulative particle-size distribution of predicted ash from total inorganic coalescence of each coal particle, coal minerals, and 0.8 fly ash, using CCSEM and Malvern data, for (a) Beulah and (b) Upper Freeport.

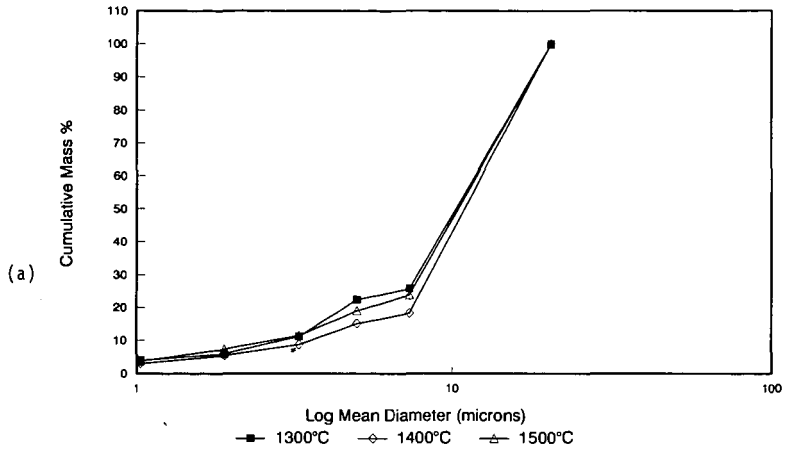

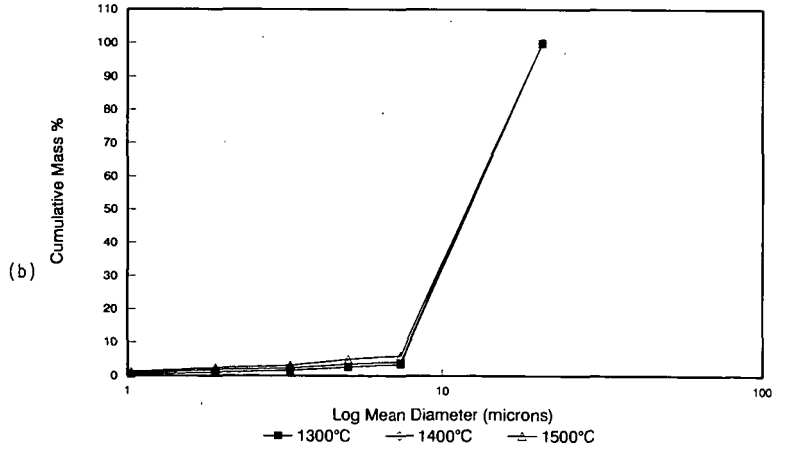

Figure 6. Fly ash particle-size distributions observed at 1300, 1400, and 1500°C after combustion of (a) Beulah and (b) Upper Freeport 53-74 μm coals.

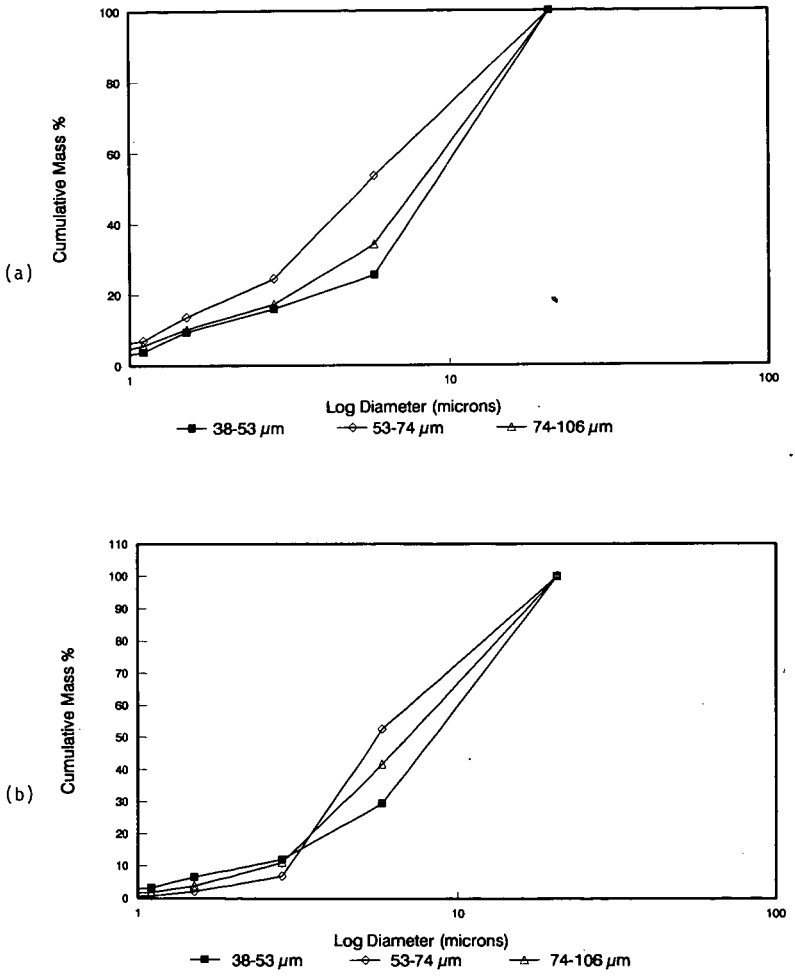

Figure 7. Fly ash particle-size distribution observed after combustion of 38-53, 53-74, and 74-106 μm coal size fractions of (a) Beulah and (b) Upper Freeport.

A Study of Ash Formation During the Combustion of Pulverized Coal

Sharon.F. Miller, Harold.H. Schobert, and Alan.W.Scaroni
The Pennsylvania State University
Fuel Science Program
University Park, PA 16802

Keywords: ash formation, particle size distribution, pulverized coal combustion.

INTRODUCTION

In order to predict the potential problems caused by ash in a pulverized coal in comparison to a coal-water fuel fired systems, it is necessary to understand the mechanism by which an ash particle acquires its particular size and compositional character. The particle size distribution (PSD) of an ash and its composition are determined by the following: the mineral matter composition and size distribution in the coal, the coal composition and particle size, the morphology of the char produced upon devolatilization of the coal particle, the local atmosphere surrounding the mineral particles, and the phase transformations of the mineral matter during combustion. When one or more of the above characteristics or conditions varies, the resulting ash size and composition may also change. In the process of preparing and burning a coal-water fuel, several or all of the above characteristics or conditions are different from those of the pulverized coal. It is the objective of this research to understand the effect that the form in which a coal is fired, pulverized versus coal-water fuel, has on the mechanisms responsible for the size and composition of the char and ash produced during combustion. Two coals, the Elk Creek bituminous and Beulah lignite, are being studied. Each coal is being fired in a pulverized form and as a coal-water fuel.

The following discussion concentrates on the preliminary results of the combustion tests on the Elk Creek and Beulah pulverized coals. The results presented show that the two pulverized coals produce distinctly different char-ash morphologies and sizes. The discussion provides comparisons between the coal PSD, the PSD of the mineral matter in the coal, and the PSDs of the char-ash samples collected at various locations down the combustor representing various degrees of burnout. The conclusions are based primarily on size data and observations of the morphologies of the various char-ash samples.

COMBUSTION SYSTEM AND ANALYTICAL TECHNIQUES

The combustion experiments were conducted in the down-fired combustor shown in Figure 1. The main radiant section of the combustor is modular and consists of four 0.46 m (18 inch) tall and 0.41 m (16 inch) diameter refractory sections. A divergent refractory cone, commonly termed a quarl, is positioned on top of the circular refractory sections. The quarl is 0.83 m (32.5 inches) high. The burner is located on top of the quarl as shown in the Figure 1. The divergent cone top has a half-angle of approximately ten degrees and was used to minimize recirculation and swirl in the combustor. Swirl was not introduced in order to minimize ash deposition on the combustor walls and to ensure an even distribution of ash flow for sampling. Below the four circular refractory sections is a constrictor segment and a flue gas exit section. The flue gas passes through the convective section and enters a spray chamber to decrease the gas temperature prior to exiting the system via the induced draft fan and the stack. The overall length of the combustor is 3.05 m (10 feet). For more detail see Hurley (1990).

A series of 7.62 cm (3 inch) sampling ports extend the length of the combustor. Sample ports are numbered 1 through 10 starting at the top of the combustor. During this study, particulate and gas sampling were conducted in Ports 1, 2, and 10. Wall temperatures were monitored using thermocouples at eight locations along the length of the combustor. The temperature profile was considered stable when the temperature in the top four ports changed at a rate of less than 0.5°C/min. The combustor was preheated using natural gas at a firing rate of 0.26 GJ/h. The preheat period typically lasted approximately three hours after which the natural gas was shut off and the pulverized coal introduced. The fuels were fed at a rate of 0.32 GJ/h corresponding to a volumetric heat release rate of 1.14 GJ/m^3-h. The Beulah lignite and Elk Creek bituminous pulverized coals were fed using an open helix dry feeder at a rate of 19.1 kg/h and 10.0 kg/h, respectively. The coal was entrained from the dry feeder and transported to the burner by the primary air which accounted for 18% of the total air required for combustion. The fuels were fired at 20% excess air. Total particle residence times within the radiant section of the combustor for the Beulah and Elk Creek coals were 2.09 and 2.13 seconds, respectively. Particle residence times for the samples collected at Ports 1, 2, and 10 are listed in Table 1. Overall carbon conversion levels of 99.4% and 99.9% were obtained at Port 10 for the Elk Creek coal and the Beulah pulverized coal, respectively.

During combustion, particulates were sampled isokinetically at a constant volumetric rate using a water-cooled sampling probe. A three-stage Anderson multicyclone and filter assembly was used to

classify the particulates during sampling. The cyclone aerodynamic diameter 50% cutpoints were 15 μm (cyclone 1), 2.7 μm (cyclone 2), and 0.46 μm (cyclone 3). The final filter was a polypropylene fiber filter which collected particles greater than 0.3 μm in diameter. Sampling isokinetically and at a constant volumetric rate ensured collecting representative samples of different sized char and ash particles by the probe and that the 50% cut sizes of the cyclones were consistent at each port. Gas sampling was conducted using a second water-cooled probe. The gas sample was withdrawn at each port and passed through a refrigeration unit to remove moisture from the gas prior to entering O_2, CO, CO_2, SO_2, and NO_x analyzers.

The ultimate analysis of each coal was determined using a Leco Corporation CHN-600 and a Leco Corporation SC-132 Sulfur Determinator. Sulfur forms of the coals were determined using ASTM D 2492. Calorific values of the coals were determined using a Parr Adiabatic Calorimeter. Proximate analysis of the coals was determined using a Leco Corporation MAC-400 proximate analyzer. Proximate analysis, ultimate analysis, and calorific value for both coals are presented in Table 2. The proximate analysis of the cyclone samples was determined thermogravimetrically with a Perkin Elmer 10 Series Thermal Analysis System. The thermogravimetric analyzer (TGA) was used for the proximate analysis of the cyclone samples because the TGA requires only 10 milligrams of sample for each analysis as compared to 1 gram for the MAC-400. TGA data was also used to determine the percent burnout, or carbon conversion, of the samples collected in the cyclones. Fuel burnout was calculated using ash as a tracer. Bulk inorganic compositional analysis for each coal ASTM ash was determined by a Spectrometrics Spectrospan 3 direct plasma spectrometer (DCP) (Table 2). The inorganic elements analyzed included silicon, aluminum, calcium, sodium, potassium, iron, magnesium, manganese, titanium, phosphorous, barium, sulfur, and strontium. Elemental analyses are reported on an oxide basis.

Computer-controlled scanning electron microscopy (CCSEM) was used to identify and quantify the size and composition of the mineral matter in the raw coal. The system is operated in conjunction with energy dispersive X-ray analysis provided by a Tracor Northern Electron Probe Microanalyzer EDS system at the University of North Dakota Energy and Environmental Center. The compositional analysis of each particle was compared with known compositional ranges of different mineral species. The computer then categorized each particle as a specific mineral phase. Mineral size data are presented in graphical form in the results section. Actual mineralogical analysis for each coal is not presented at this time. For a more detailed description of the sample preparation and procedure refer to Hurley (1990) and DeHoff and Rhines (1968). Photomicrographs were taken with a ISI ABT SX-40A SEM to study the morphology associated with the various cyclone sized fractions sampled at the different ports.

Size analysis of the coals and ash samples was conducted with a Malvern 2600 Particle Size Analyzer. The Malvern Particle Size Analyzer is an optical, nonimaging technique used to make *in situ* particle size measurements (Meyer, 1986) Composite samples from each sample port (i.e. Ports 1, 2, and 10) were used for size analysis. The particle size data are presented as cumulative volume percent as a function of the log size in microns. The data are presented in this manner in order to compare with the Malvern results which are reported on a volume distribution basis for each size category.

RESULTS AND DISCUSSION

Relation Between Coal, Mineral Matter, and Char-Ash Particle Size Distributions

Elk Creek Coal

In the case of the Elk Creek coal the data suggest that the individual mineral particles in the original coal do not form individual ash particles but rather that several mineral particles form an individual ash particle either by coalescence or agglomeration. The PSDs of the Elk Creek coal, mineral matter, and char-ash samples are shown in Figure 2. The d_{50} of the char-ash samples collected from Ports 1, 2, and 10 are 28.1, 21.1 and 8.6 μm while d_{50} of the coal is 19.4 μm. The increase in particle size at Port 1 is seen throughout the entire size range. A possible explanation for the increase in PSD is that the Elk Creek coal has a Free Swelling Index (FSI) of 6 and exhibits swelling during heating. Such coal will typically pass through a fluid or plastic phase at approximately 350 to 400°C (Scaroni et al., 1986). During the fluid phase, volatiles are evolved which result in swelling of the coal particle.

Examination of SEM micrographs indicates that samples collected at Port 1 are composed of spherical char particles which have gone through a melt phase and experienced swelling. Holes due to the release of volatiles are visible on the char surfaces. The extent of carbon conversion is approximately 59.8%. Char cenospheres are present and fragmented, suggesting rapid heating rates. According to Solomon and Hamblen (1985), char particles melt and gas is evolved into the internal micropores forming small gas pockets. With continued heating, the size of the gas pockets increases and in some cases they may coalesce. At this point, significant swelling is not usually observed. According to Solomon and Hamblen (1985), the particle changes which subsequently occur are determined by the heating rate. With

rapid heating (10^5 °C/s), the cell walls rupture, blowing multiple holes in the surface of the char. At an intermediate heating rate, some coalescence of the bubbles occurs before rupturing. At lower heating rates (i.e. 10^3 °C/s), the gas pockets expand and coalesce, eventually forming large cenospheres. In the second cyclone, ruptured char cenospheres containing individual and coalesced ash spheres are present which suggests the particles experienced rapid heating rates. The heating rate of the d_{50} (19.4 μm) Elk Creek coal particle in the combustor is estimated to be approximately 3.0×10^5 °C/s. Based on the particle size data and the char morphologies, it is reasonable to suggest that the coarser size distribution of the samples collected at Port 1 is due to the swollen char particles found in the first cyclone.

At Port 2, the char particles are 88.9% burned out. The char cenospheres are lacy in appearance and numerous ash spheres are present on the larger char surfaces. The ash spheres appear on the char surface as the surface recedes during combustion. As the char surface recedes, mineral matter particles in the char are exposed at the char surface and melt forming slag beads on the char surface. However, individual slag beads do not coalesce or spread upon the char surface due to their inability to wet a carbon surface. Eventually, as the char surface continues to recede, the ash particles will coalesce forming larger solid ash particles. Some char cenospheres are fragmented either due to impact or rupture during gas evolution.

At Port 10, the overall carbon conversion level is 99.4%. The PSD distribution of the sample collected at Port 10 approaches the PSD of the original mineral matter (Figure 3). In fact, the curves meet at approximately 48 μm, however, the mineral matter PSD consists of much finer particles than the final ash sample. The data suggest that the individual mineral particles in the original coal do not form individual ash particles but rather that several mineral particles form an individual ash particle either by coalescence or agglomeration. If each individual mineral particle were responsible for forming an individual ash particle, the PSD curves of the ash and mineral matter would be nearly identical in shape. Evidence for the coalescence of mineral matter is based on the morphology of the char and ash during combustion and the composition and size of the mineral matter in the raw coal. The individual ash particles are composed of small ash spheres which are coalesced and highly agglomerated. The char only occurs as highly fragmented lacy structures (Figure 4).

The SEM evidence supports the premise that individual mineral particles do not form individual ash particles but rather several mineral particles in the form of coalesced ash spheres comprise an individual ash particle. The result is that the ash PSD at Port 10 consists of larger particles than the mineral matter PSD in the raw coal.

Beulah Lignite

The PSDs of the Beulah coal, mineral matter, and char-ash samples are shown in Figure 4. The interpretation of the PSD data is that the char and the larger mineral matter particles in the coal undergo shedding and fragmentation during combustion. The d_{50} of samples collected from Ports 1, 2, and 10 decreases from 67.0 to 46.8 to 8.2 μm as carbon conversion increases. However, the sample collected at Port 1 has a larger volume mean diameter than the original coal mean volume diameter of 46.4 μm. The shift to a coarser PSD can be attributed to burning of the smaller coal particles thereby removing then from the total PSD. Unlike the Elk Creek coal, the Beulah coal has a FSI of 0. Therefore, the possibility of swelling as the mechanism responsible for the larger particle sizes is not reasonable. The carbon conversion at Port 1 is approximately 20%.

The samples collected from Port 2 show more extensive recession of the char surface. The surface of the char is sharply convoluted with ash cenospheres located between the ridges. The ash spheres are approximately 5 μm in diameter and are fairly uniform in size. The ash spheres represent mineral matter that has melted on the char surface as it is exposed by the receding char surface. The Beulah lignite does not pass through a fluid phase during heat up as does the Elk Creek coal and this may explain the difference in the surface appearance of the Beulah char as compared with the smooth surface of the Elk Creek char. As the char continues to burn and the char surface recedes, the char surface becomes even more jagged. Some fractured lacy carbonaceous particles and ash spheres are present in the smaller size fraction of the second cyclone where burnout is approximately 95.4%.

As with the Elk Creek coal, the size distributions for the Beulah samples collected from Port 1 through Port 10 shift to a finer overall PSD as would be expected with increasing burnout. However, unlike the Elk Creek ash PSD at Port 10, the Beulah ash PSD at Port 10 is characterized as finer than the mineral matter PSD in the original coal. The greatest difference between the PSD of the original mineral matter and the sample collected at Port 10 occurs at the coarser end of the cumulative volume percent curve. The curves actually superimpose in the size range of 4.6 μm and smaller. The interpretation of the PSD data is that the char and the larger mineral matter particles in the coal undergo shedding and fragmentation during combustion which results in the finer PSD of the ash relative to the mineral matter.

Therefore, individual large mineral particles and coal particles are actually forming several ash particles. Evidence for this is based on the morphology of the char and ash and the size and composition of the mineral matter in the pulverized coal. The mineral matter which is finely dispersed throughout the coal particle would normally form small, molten spheres on the char surface and eventually coalesce forming larger ash spheres. However, if char fragmentation occurs, the small mineral particles are unable to coalesce. The molten ash particles are released on smaller fragments of char and may coalesce but the overall increase in ash sphere size is minimized. The ash spheres may also be released into the gas stream as individual particles and retain their original size contributing to the finer size fraction of the ash. Fragmentation of ash agglomerates and cenospheres can also occur contributing to an increase in the smaller size fractions of ash. Fragmentation by either the ash particles separating from the char prior to char burnout or the fragmentation of ash cenospheres during and after char burnout are probably both occurring in the Beulah coal char and ash.

At Port 10, the overall carbon conversion is 99.88%. Micrographs of the composite sample show the ash to be composed of mostly separate individual angular ash and char particles, fragmented cenospheres, solid ash cenospheres (1.5 to 6.0 μm in diameter), and sintered spheres joined by neck structures (Figure 5). In general, there is no agglomeration of the larger ash particles suggesting that, as ash spheres are formed on the char surface they do not coalesce to form larger ash spheres or perhaps the char fragments prior to the ash spheres coalescing.

The mineral matter composition and its PSD in the Beulah coal also provide an additional explanation for the finer PSD of the ash as compared to the coal mineral matter. Thirty-four percent of the mineral matter by weight is pyrite. Ninety-seven percent of the pyrite by weight is greater than 4.6 μm in diameter and 60% is greater than 48 μm in diameter. In addition, of the 32% of the total mineral matter in the Beulah coal that is greater than 48 μm, 14.2% is pyrite. The pyrite can be considered to be mostly extraneous based on its large size when compared to the pulverized coal PSD. Large particles of pyrite are known to fracture and disintegrate when rapidly heated (Helble et al., 1989a, 1989b; Baxter and Mitchell, 1989). Some of the pyrite fragments will agglomerate upon melting; however, the resulting particle sizes of the iron-containing species are generally still smaller than the original pyrite particles. Helble et al. (1989a, 1989b) investigated the effects of oxygen levels on pyrite oxidation and subsequent fragmentation during combustion of the Beulah lignite in a drop-tube furnace. Their results showed that the ash PSD was less than the mineral matter PSD in the presence of 21% oxygen. The results from this study are in direct agreement with Helble's results in that the Port 10 sample has a finer PSD than the coal mineral matter PSD. The fragmentation of larger sized mineral particles has also been noted by Srinivasachar et al. (1989) and Bryers (1985). The fragmentation occurs primarily in pyrite particles greater than 4.6 μm based on the experimental PSD of the ash and mineral matter. Pyrite rapidly decomposes to pyrrhotite ($Fe_{1-x}S$) at 1027°C. In the presence of oxygen, pyrrhotite is converted to magnetite (Fe_3O_4). The final step in the oxidation process is the oxidation of magnetite to hematite (Fe_2O_3) (Helble et al., 1989a). Based on the evidence available at this time, the fragmentation of pyrite appears to contribute to the finer PSD of the final ash sample collected at Port 10 relative to the mineral matter in the original pulverized coal. Therefore, one larger mineral particle is actually forming several ash particles.

It should also be noted that 30% of the mineral matter in the Beulah coal was classified as unknown by the CCSEM. This mineral matter tends to be less than 2 μm in size and is composed of iron sulfur compounds and aluminosilicates. These particles are most likely finely disseminated throughout the coal particle and are therefore referred to as inherent. These mineral particles are not included in the PSD of the mineral matter shown in Figure 7. It is possible that these mineral particles may coalesce during combustion of the coal and appear as larger, although still relatively small ash particles in the PSD of the Port 10 sample. The result is an increase in the small particle portion of the PSD curve for the samples collected at Port 10 compared to the original mineral matter PSD. The fragmentation of the char and the larger extraneous mineral particles, and possible coalescence of disseminated mineral matter are the predominating mechanisms determining the PSD of the final Beulah ash sample.

CONCLUSIONS

Based on the evidence, the different mechanisms responsible for the char-ash PSDs for the Elk Creek and Beulah coals are agglomeration and fragmentation, respectively. The chars and ash particles produced during the combustion of the Beulah and Elk Creek pulverized coals exhibit very different morphologies and PSDs relative to the original coal and mineral matter PSDs. For instance, the initial Elk Creek coal char samples collected at Port 1 were coarser than the original coal PSD due to swelling of char particles. The explanation for the increase in char PSD is based on the increased internal pressure generated by volatiles released during devolatilization while the coal is fluid causing increased swelling and

the formation of large cenospheres. The result is a coarser PSD of the char samples collected at Port 1 than the original coal PSD.

The final Elk Creek ash PSD (Port 10) was coarser than that of the original mineral matter. Evidence based on particle sizing and SEM photomicrographs suggests that the individual mineral particles in the original coal do not form individual ash particles, but rather several mineral particles form an individual ash particle. The Elk Creek char passes through a fluid phase forming numerous carbonaceous cenospheres. Individual mineral matter particles form individual molten ash spheres on the exterior surface of the char as the char surface recedes during burning. The ash spheres gradually coalesce as the char surface continues to recede forming larger ash spheres. The end result is a coarser PSD for the final ash than the original PSD of the mineral matter.

A final ash PSD finer than the original mineral matter in the coal was observed during the Beulah testing. The particle size data and the SEM photomicrographs suggest that the char and the larger mineral matter particles in the coal undergo shedding and fragmentation during combustion which results in the finer PSD of the ash relative to the mineral matter. Therefore, individual large mineral particles and coal particles are actually forming several ash particles. Char samples collected from Port 1 have a fragmented appearance and the surface of the char particles tends to be very jagged. As the char surface recedes, mineral matter becomes exposed on the surface forming small ash spheres. Unlike the Elk Creek chars, the Beulah char often fragments prior to coalescing of the ash spheres. This char fragmentation results in smaller ash particle sizes.

A second source of smaller ash particles is the pyrite in the coal. The larger pyrite fragments are not present within the coal particle but rather occur as extraneous particles. These pyrite particles often fragment when heated rapidly and oxidized during combustion and form numerous smaller iron-rich particles in the final ash (Srinivasachar et al., 1989 and Bryers, 1989). In addition, finely disseminated iron-rich particles and aluminosilicate particles are present throughout the coal particle. It is possible that these mineral particles may coalesce during combustion of the coal prior to char fragmentation and appear as larger, although still relatively small, ash particles in the ash PSD. The end result of both early char fragmentation and pyrite fragmentation, as well as the agglomeration of extremely fine mineral particles, is a finer ash PSD than mineral matter PSD in the original coal.

Based on the evidence, the different mechanisms responsible for the char-ash PSDs for the Elk Creek and Beulah coals are agglomeration and fragmentation, respectively. The d_{50} values of the Beulah and Elk Creek coals are quite different being 46.4 μm and 19.4 μm, respectively and the mineral matter in the Beulah coal is coarser than that in the Elk Creek coal. However, the d_{50} values of the samples collected at Port 10 during the Beulah and Elk Creek tests are very similiar being 8.2 μm and 8.6 μm, respectively. The process of fragmentation results in the finer PSD of the Beulah ash relative to the coal mineral matter PSD. The process of coalescence and agglomeration of the Elk Creek char and ash results in a coarser ash PSD relative to the Elk Creek mineral matter PSD. The result is that the final PSDs of the two samples have similiar d_{50} values.

REFERENCES

Baxter, L.L. and R.E. Mitchell, Sixth Annual International Pittsburgh Coal Conference, v.1, pp.64-73 1989.

Bryers, R.W., Symposium on Slagging and Fouling in Steam Generators, Brigham Young University, 63 pp., January, 1987.

DeHoff, R.T. and F.N. Rhines, Materials Science and Engineering Series, McGraw Hill Book Company: New York, 422pp., 1968.

Helble, J.J., S. Srinivasachar, A.A. Boni, S.G. Kang, A.F. Sarofim, J.M. Beer, N. Gallagher, L. Bool, T.W. Peterson, J.O.L. Wendt, N. Shah, F.E. Huggins, and G.P. Huffman, Sixth Annual International Pittsburgh Coal Conference, v.1, pp.81-89, 1989a

Helble, J.J., S. Srinivasachar, C.B. Katz. and A.A. Boni, Proceedings of the 15th Biennial Low-Rank Fuels Symposium, St. Paul, MN., 15 pp., May 1989b.

Hurley, J.P., Ph.D. Dissertation, Pennsylvania State University, 247 pp., 1990.

Meyer, P. L., Ph.D. Dissertation, Carnegie-Mellon University, 219 pp., 1986.

Scaroni, A. W., M. R. Khan, S. Eser, and L. R. Radovic, "Coal Pyrolysis" in: Ullmann's Encylopedia of Industrial Chemistry, VCH Verlagsgesellschaft: Weinheim, Germany, pp. 245-280, 1986.

Solomon, P.R. and D.G. Hamblen, "Pyrolysis" in: Chemistry of Coal Conversion, R.H. Schlosberg, ed., Plenum: New York, pp. 121-252, 1985.

Srinivasachar, S., J.J. Helble, C.B. Katz, and A.A. Boni, Proceedings of the Engineering Foundation Conference on Mineral Matter and Ash in Coal, R.W. Bryers and K.S. Vorres, eds., (in press), 1989.

TABLE 1. Particle Residence Times

Port	Residence Time in Combustor (sec)	
	Elk Creek Particle (d_{50} = 19.4 μm)	Beulah Particle (d_{50} = 46.4 μm)
1	0.160	0.157
2	0.417	0.410
10	1.820	1.790

TABLE 2. Elk Creek and Beulah Pulverized Coal Analysis

Coal :	Elk Creek		Beulah	
	A.R.[a]	Dry	A.R.	Dry
Proximate Analysis, %wt.				
Moisture	0.90	---	29.99	---
Volatile Matter	30.19	30.50	30.98	44.25
Fixed Carbon	62.85	63.40	33.02	47.10
Ash	6.06	6.12	6.01	8.57
Ultimate Analysis, %wt.				
Moisture	0.90	---	29.99	---
Carbon	80.95	81.69	45.71	65.29
Hydrogen	4.89	4.94	2.98	4.26
Nitrogen	1.58	1.59	0.68	0.97
Sulfur	0.68	0.69	0.66	0.94
Oxygen	5.84	5.89	13.97	19.96
Ash	6.06	6.12	6.01	8.57
Higher Heating Value, MJ/kg	31.0	33.6	16.5	25.2
(Btu/lb)	(13,350	(14,470)	(7,116)	(10,837)
Particle Size Distribution[b], μm				
D (v, 0.9)		58.9		129.4
D (v, 0.5)		19.4		46.4
D (v, 0.1)		5.3		8.7
Ash Composition, %wt.				
SiO_2		53.70		18.00
Al_2O_3		30.00		9.96
TiO_2		1.63		0.48
Fe_2O_3		6.95		9.96
MgO		0.90		6.05
CaO		1.23		20.90
MnO		0.02		0.07
Na_2O		0.67		9.55
K_2O		1.93		0.43
SO_3		0.90		20.60
P2O5		0.19		0.67
BaO		0.22		1.40
SrO		0.16		0.80
LOI		2.05		1.32
Total		100.55		99.19

[a]As Received

[b]The D(v,0.9), D(v,0.5), and D(v,0.1) values are the particle sizes where, respectively, 90%, 50%, and 10% of the particles, by volume, are less than the indicated particle size.

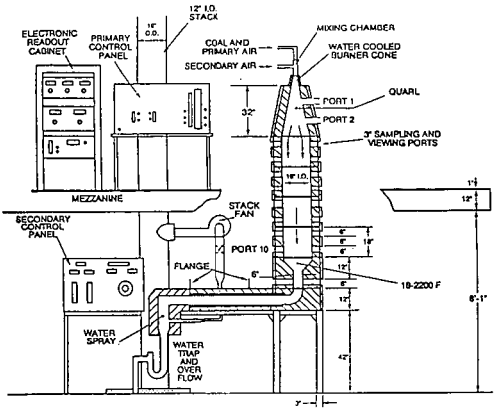

Figure 1. Down-fired Combustor

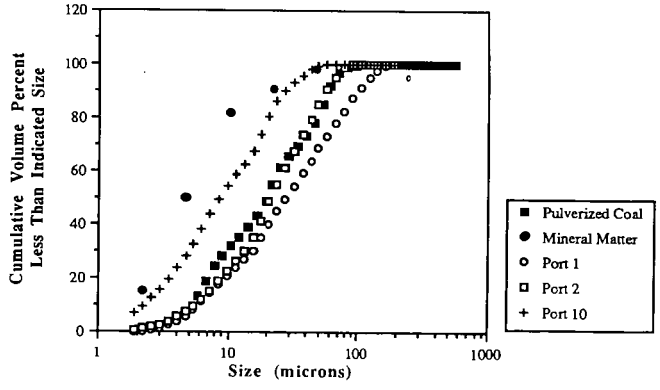

Figure 2. Comparison of PSDs of Elk Creek Coal, Mineral Matter, and Char-Ash Samples Collected from Ports 1, 2, and 10

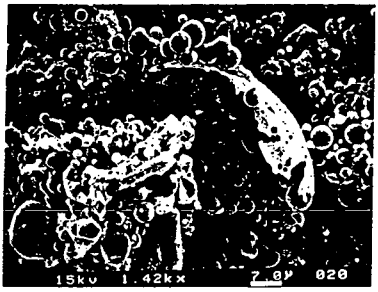

Figure 3. Elk Creek char-ash collected at Port 10.

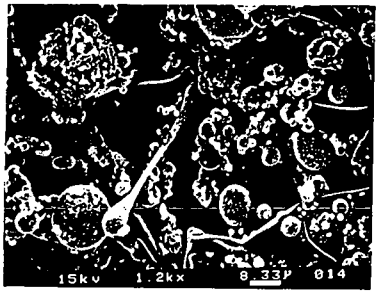

Figure 5. Beulah char-ash collected at Port 10.

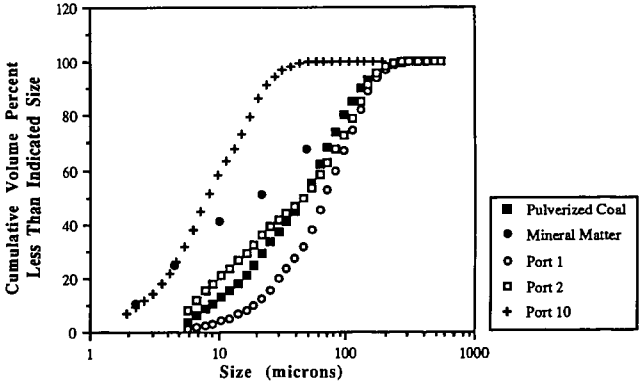

Figure 4. Comparison of PSDs of Beulah Coal, Mineral Matter, and Char-Ash Samples Collected from Ports 1, 2, and 10

A PILOT-SCALE STUDY OF THE FORMATION OF ASH DURING PULVERIZED LOW-RANK COAL COMBUSTION

John Hurley
University of North Dakota
Energy and Environmental Research Center
Grand Forks, North Dakota 58202

Keywords: char morphology, transmission electron microscopy, submicron ash

INTRODUCTION

In 1987 over 250 million tons of coal mined in the western-coal producing region of the United States was purchased by electric utilities (1,2). The goal of the utilities is to convert the chemical energy in the coal to electrical energy that can be sold at a profit. The most common conversion method involves pulverizing the coal and burning it in a boiler system. The steam produced is passed through a turbine which is used to turn an electrical generator. Unfortunately, because of the high temperatures present in a utility boiler, the ash formed during the combustion of the coal can cause a number of operational problems and can reduce the efficiency of the energy conversion process.

In an effort to delineate a portion of the process of ash formation during combustion of pulverized western U.S. low-rank coal, subbituminous coals from the Eagle Butte mine, WY, and the Sarpy Creek mine, MT, were burned in the Penn State down-fired combustor. Entrained particulate matter was collected at several stages of combustion. The particulates were analyzed by thermogravimetry, x-ray diffraction, computer-controlled scanning electron microscopy, and transmission electron microscopy (TEM) in order to discern changes in size and association of the inorganic matter during the combustion of the coal. Due to space limitations, the data and discussion presented here focus only on the TEM observations of the Eagle Butte coal as well as samples of the char and submicron ash particles produced during combustion.

EXPERIMENTAL

To properly understand the ash formation process, a knowledge of the time-temperature history and interactions of ash particles is required. Therefore, the Penn State down-fired combustor was designed for self-sustained combustion of pulverized coal in a nonrecirculating and nonswirling flame and to provide easy access for sampling at all stages of combustion. The combustor is described in depth elsewhere (3). It is illustrated in Figure 1.

Before firing with pulverized coal, the combustor was preheated on natural gas until the wall temperature profile approximated that encountered when firing the coal to be tested. During testing the coal feed rate was held at 200,000 Btu/hr which yielded a volumetric heat release rate of about 20,000 Btu/hr/ft^3. Particulate sampling commenced as soon as a stable temperature distribution occurred above the sampling point. Particulate samples were collected at three ports, the top (port 1), second

from the top (port 2), and from immediately above the accelerator at the bottom of the furnace (port 10). A four-stage multicyclone system, housed in a convective oven during sampling, was used to separate the particulates from the gas.

The morphologies of char and submicron inorganic particles were characterized by transmission electron microscopy (TEM). In order to allow analysis of particles that were included within a coal or char matrix, the samples were prepared by embedding them in LR White resin, then cutting ultrathin sections with the use of a Reichert Jung Ultracut E ultramicrotome. Only silver, gold, and violet sections were selected for analysis. The colors were an interference effect and indicated that the sections were between 0.08 to 0.2 μm thick (4). The TEM-STEM system used was a Phillips EM420 with a Link Systems 860 Series II x-ray analyzer.

RESULTS AND DISCUSSION

Coal Samples: TEM observations of ultrathin sections of the Eagle Butte coal showed that, in addition to larger irregularly shaped minerals, approximately one in four coal particles contained concentrations of small, high contrast inclusions with circular cross sections. A TEM photo of the edge of such a coal particle is shown in Figure 2. The inclusions occurred mainly in three distinct size ranges. The smallest particles had diameters of approximately 2 to 3 nanometers. They were evenly dispersed, although they were more easily visible in the thinner (lighter) portions of the coal section. A second size class of the inclusions had diameters between 20 and 30 nanometers. They did not appear to be as evenly dispersed across the coal particles as was the smallest size range. The largest size class was composed of particles with diameters greater than approximately 60 nanometers, although this size range was not completely distinct from the middle size range (i.e., there was some gradation between them).

The composition of the smallest high contrast inclusions was difficult to discern. Although the small inclusions strongly scattered the electron beam, electron diffraction was not practical because beam heating of the epoxy matrix caused the position of the particles to continually shift relative to the beam. Energy dispersive x-ray analysis of the smallest inclusions was also inconclusive because of the low signal to noise ratio in the EDS signal, although after counting times of several minutes, a signal did emerge in the EDS spectra of individual small particles or groupings. For the Eagle Butte coal the signal usually showed the presence of calcium, iron, and sulfur. Also, the source of the signals was obscured by the fact that calcium and sulfur, and possibly iron, are associated directly with the organic portion of the coal. Since the ultrathin section was approximately 100 nanometers thick, and the smallest particles were 2 nanometers in diameter, it was impossible to tell if the x-ray signal was emitted from organically associated elements or the particles. Although sodium and magnesium are also associated with the organic matrix, the detector may not have indicated the presence of those elements because they are present in lower concentrations, and the detector is not very sensitive to the K_α lines of those elements. In general, it was found that clear x-ray signals could only be obtained from particles that had diameters above several tens of nanometers, although some smaller particles gave strong x-ray signals if they were composed of high atomic number elements.

Because a strong x-ray signal from the small, high contrast inclusions was not clear, the possibility existed that the small inclusions were not inorganic. Friel and others have shown the formation of mesophase spheres upon heating of several

bituminous coals (5). The spheres they reported had the size and appearance of the medium size high contrast inclusions shown in Figure 2. However, several lines of evidence supported the conclusion that the small inclusions shown in Figure 2 were not similar to mesophase spheres. First, the coal had not been heated prior to analysis. Since mesophase usually forms on heating, one would not expect mesophase spheres to be present in the coal. However, some heating of the sample may have occurred in the TEM through absorption of energy from the electron beam. Second, the Eagle Butte and Robinson coals are subbituminous coals. Subbituminous coals do not usually form mesophase spheres upon heating. Third, and most convincing, a close examination of the boundary between the coal particles and the resin shows that some of the smallest particles have separated a small distance from the coal and reside in the resin. Mesophase spheres would not be expected to separate from the matrix.

Port 1 Samples: By the time the particulates reached the top port (port 1), the coal had undergone 50.8% burnout. The residence time of the particles in the radiant zone above that port was approximately 0.07 seconds. The maximum equilibrium temperature experienced by a nonreacting inorganic particle before sampling was approximately 1220°C.

Two main types of char particles were seen in the port 1 particulate samples: those that were highly vesicular and those that showed little internal structure. In general, the appearance of the char was essentially identical to the appearance of the char collected at port 2, so further discussion of char morphologies will be saved for the discussion of the port 2 chars.

Port 2 Samples: By the time the particulates reached port 2, the coal had undergone 96.3% burnout. The total residence time in the refractory lined portion of the combustor was approximately 0.2 seconds. The maximum equilibrium temperature reached by a nonreacting particle by the time it reached the sampling probe was approximately 1310°C. That temperature was reached immediately before the probe.

As in the case of the port 1 samples, two main types of char were evident in the ultrathin sections of the port 2 samples: highly vesicular particles and higher density particles that contained much less void space. Figure 3 is a 10,500x TEM photograph of a vesicular char particle. The thin walls of such particles suggest that they may fragment easily during combustion. The ash particles associated with such chars tend to be large globules lightly attached to either internal or external char surfaces. In addition to the large ash globules, the char particles contained high levels of the 3 and 30 nanometer particles seen in the coal. These particles are shown in Figure 4, which is a 82,000x TEM photograph of the char particle in Figure 3. The smallest inclusions underwent little change during the early stages of combustion.

The appearance of a high concentration of the small, high contrast inclusions shown in Figure 4 was an artifact of the difference in electron transmissivity of the char and the inclusions. In actuality, the thickness of the char surrounding the inclusions (the char is not obvious in the figure) was approximately 500 times the thickness of the smallest particles. Assuming that the particles had a density equal to that of quartz (2.6 g/cm^3), whereas the bulk char (i.e., carbonaceous and noncarbonaceous) had a density equal to the density of coal (1.3 g/cm^3), and that the average concentration of the particles in the char was equal to the concentration of particles shown in Figure 4 (a liberal assumption), the weight percent of the smallest inclusions can be, at most, 0.15% of the weight of the char. Assuming the concentration was the same in the coal and that the inclusions formed ash in a weight ratio of 1:1, then only about

2.5% of the weight of the ASTM ash was formed by the smallest inclusions. The mass concentration of the next larger class (30 nanometers) was approximately 0.5% of the char or 8.6% of the ash.

Figure 5 shows a TEM photograph (4,900x) of the second type of char particle, the type that showed much less void space than the highly vesicular char. Like the vesicular char, the two smallest size classes of high contrast inclusions were sometimes found in the more dense char particles. The inclusions in the higher density char collected at port 2, however, showed some coalescence which caused the distinctions between the size classes to become less pronounced. Unlike the smallest high contrast inclusions, the large globular particles of ash often associated with the highly vesicular chars were absent. This may have been because this type of char particle burned more slowly, so that particle coalescence was relatively slow and because the ash particles were shed from this type of char at a relatively high rate. Figure 5 is also interesting in that it shows two physical features of the ultrathin sections. First, grooves in the section, generally running right to left and sloping upwards slightly to the left, are caused by imperfections in the knife edge, most commonly remnants of previously cut sections. In addition, wrinkles in the ultrathin section can clearly be seen. The wrinkles generally run vertically or point toward the char section. The closeness of the wrinkles gives a visual indication of the ratio of length or width to thickness of the ultrathin sections. The typical dimensions of ultrathin sections are 0.7 mm long and 0.1 μm thick, so the length to thickness ratio is approximately 7000 to 1. The length to thickness ratio of writing paper is approximately 4000 to 1.

Port 10 Samples: By the time the particulates reached the sampling probe at port 10, the coal had undergone 99.8% burnout. The total residence time in the refractory lined portion of the combustor was approximately 2.4 seconds. The equilibrium temperature of a nonreacting particle at port 10 was approximately 1055°C.

Although uncommon, some char particles were still evident in the port 10 samples. Only the more dense char particles were seen however, indicating that the more vesicular char particles had burned out. Figure 6 is a TEM photograph (10,500x) of a portion of a char particle showing how the small, high contrast inclusions have melted. In some instances the particles coalesced to form particles with diameters in the 0.1 μm range. In other cases, the melted particles appeared to have flowed through pores within the char. The longer chain of flow regions running left to right across the photograph contained mostly iron. The large particle at the right edge of Figure 6 contained high concentrations of aluminum and silicon, with smaller amounts of nickel, chromium, and iron (possibly stainless steel). As was the case with the more dense char particles collected at port 2, no large globules of ash were seen at the surface of this type of char.

CONCLUSIONS

TEM observations of the coals indicated two main types of char form. One type was highly vesicular and burned out before the other more dense char. The thin walls of the highly vesicular char particles suggested that they may fragment easily, leading to the formation of several ash particles per char particle. However, the relatively few ash globules associated with the surfaces of the denser char particles indicated that less coalescence and more rapid shedding of ash particles occurred from the denser char than from the more vesicular char. Since the two chars most probably formed from different maceral types, a coal containing higher concentrations of the

maceral that forms the higher density char may produce more and smaller ash particles per coal grain than a coal having lower concentrations of the maceral type.

Approximately one in four coal particles contained concentrations of small, high contrast inclusions with circular cross sections. The inclusions fell into three size categories: 2 to 3 nanometers, 20 to 30 nanometers, and greater than 60 nanometers. EDS data indicated that the inclusions were composed primarily of calcium, sulfur, and iron, although the data was not conclusive. The inclusions were believed to be inorganic particles rather than organic regions such as mesophase. Calculations showed that, at most, 11% of the ash could be formed from the particles in the smallest two categories. The assumptions in the calculations were very liberal, so the actual weight was believed to be no more than 1%, within the range of the weight of fume produced during coal combustion. However, a great deal of coalescence of the inclusions occurred in later stages of particle combustion, so the importance of the inclusions in fume formation was not clear.

REFERENCES

1. U.S. Department of Energy, "Coal Production 1987", DOE/EIA0118, p 29 (1988).

2. U.S. Department of Energy, "Coal Distribution January/December 1987", DOE/EIA0125 (1988).

3. Hurley, J.P., "A Pilot-Scale Study of the Formation of Ash During Pulverized Low-Rank Coal Combustion", Ph.D. Thesis, The Pennsylvania State University (1990).

4. Peachey, L.D. "Thin Sections I. A Study of Section Thickness and Physical Distortion Produced During Microtomy", Journal of Biophysical and Biochemical Cytology, 4, 3, 233-245, 1958.

5. Friel, J.J., Mehta, S., Mitchell, G.D., Karpinski, J.M. "Direct Observation of the Mesophase in Coal", Fuel, 59, 610-616, 1980.

6. U.S. Department of Energy, "Combustion Inorganic Transformations", report for the period April 1988, to June 1989, DEFC2186MC10637 (1989).

ACKNOWLEDGEMENTS

Most of the funding for the research was provided by the U.S. Department of Energy under the Combustion Inorganic Transformations project, contract DEFC2186MC10637, Phillip Goldberg, COTR; and the Commonwealth of Pennsylvania under the Coal/Water Slurry Program. In addition, the author would like to thank Harold Schobert of Penn State and Steven Benson of the University of North Dakota Energy and Environmental Research Center for their support.

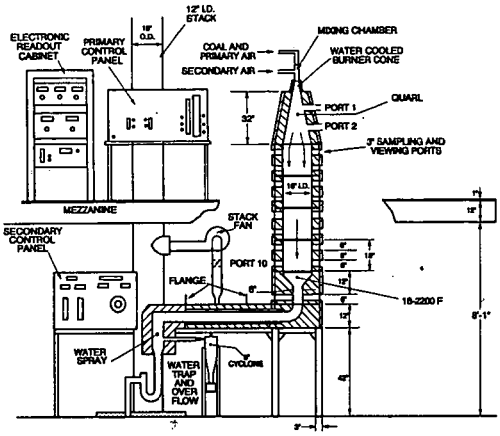

Figure 1. The Penn State down-fired combustor.

Figure 2. TEM photograph of an Eagle Butte coal particle containing high levels of high contrast inclusions.

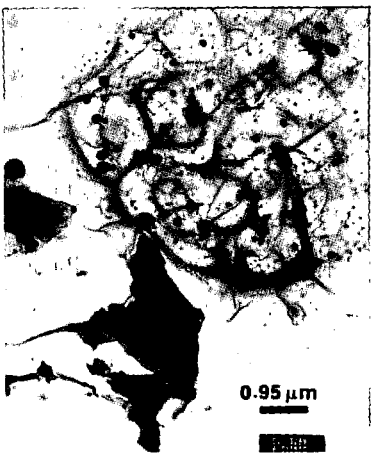

Figure 3. TEM photograph of vesicular Eagle Butte char particles showing large numbers of ash globules associated with both interior and exterior char surfaces.

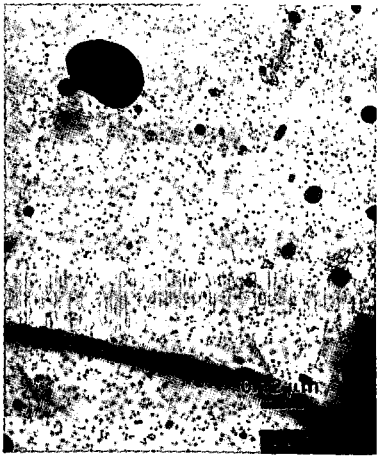

Figure 4. TEM photograph of the char particle shown in Figure 3 illustrating the unchanged nature of the 3- and 30-nanometer diameter contrast inclusions.

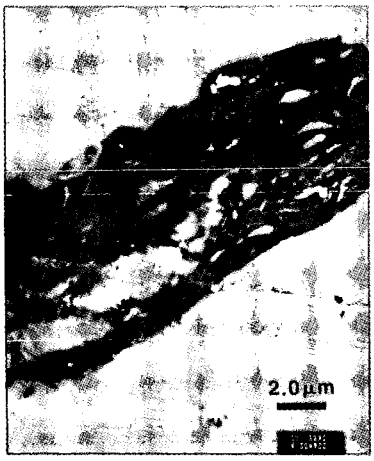

Figure 5. TEM photograph of a high density Eagle Butte char particle collected at port 2.

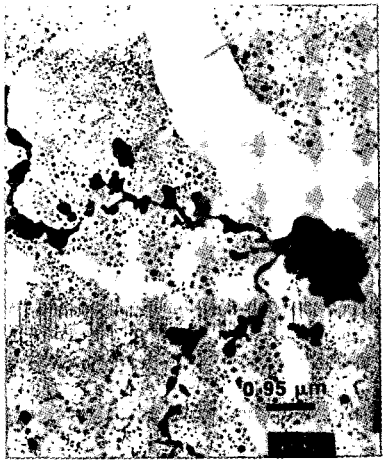

Figure 6. TEM photograph of a frozen flow of molten ash within pores in an Eagle Butte char particle collected at port 10.

THE FORM OF OCCURRENCE OF BASIC ELEMENTS IN COAL AND THEIR BEHAVIOUR DURING COMBUSTION

Anup Shah, F. E. Huggins, Naresh Shah, and G. P. Huffman
CFFLS, University of Kentucky
233 Mining & Mineral Resource Building
Lexington, KY 40506-0107

Keywords: Coal, Ash, Combustion

INTRODUCTION:

The basic elements in coal ash (alkalies,Ca,Fe) exhibit an interesting behaviour during combustion, which is closely related to the form of occurrence of these elements in the parent coal. The objective of this paper is to elucidate their evolution during combustion processes of variable time and temperature. Qualitative determinations are made from the data obtained from Computer Controlled Scanning Electron Microscopy (CCSEM), X-ray Absorption Fine Structure (XAFS) and Mössbauer spectroscopies.

Some of the data and the description of the techniques used in this paper are summarized in several publications (1-8). The main goal of this paper is to discuss some systematic trends in the behaviour of calcium, iron and the alkalies during high temperature coal combustion. It needs to be emphasized that our discussion deals only with high temperature (~1600 to 2000 K) pulverized coal combustion, and is not relevant to fluidized bed combustion.

EXPERIMENTAL PROCEDURES:

The CCSEM method measures the areas of cross-section and the energy-dispersive spectra for at least 1000 different particles in a random, polished section of the coal embedded in epoxy. The data is then reduced to derive the overall mineralogy and semi-quantitative size-distribution of individual mineral categories (9). CCSEM techniques for ash are similar to those for the coal, except that the particles are not embedded in epoxy but are mounted on Nucleopore (0.2 micrometer) filters by a process of filtration in triply-distilled acetone. The amount of material filtered is adjusted to give an optimum density of particles on the filter paper. The data reduction techniques for ash samples are similar to those used for coal minerals analysis (CMA) but the sorting program is based on the intensity of the energy-dispersive X-rays from the three most abundant elements, rather than on specific phases (9).

XAFS is used to examine specific elements and to obtain information on the bonding and structure of that element in the material at dilute concentrations (~0.1 to 1.0%). By comparing with standard materials, the phase in which the element exists is also identified.

Mössbauer spectroscopy complements the CCSEM technique by identifying the form of iron in a coal or ash. With this technique it is possible to measure the relative abundance of the major iron-bearing minerals in complex samples.

Furthermore the Mössbauer technique also provides a direct measure of the pyritic sulfur content.

RESULTS AND DISCUSSIONS:

The set of coals being investigated here are (low-rank coals) Beulah, Eagle Butte and San Miguel, (bituminous coals) Upper Freeport, Kentucky #9, Kentucky #11, Illinois #6 and (Australian brown coal) Loy Yang. These coals were combusted in different scale furnaces at Physical Sciences, Inc., M.I.T. and the University of Arizona (UA). The UA samples were collected on filter from different impactor plates of varying particle diameter.

Mössbauer data show that most of the iron in these coals is in the form of pyrite, except for Upper Freeport, in which 20% of the iron is contained in clay and siderite, and Loy Yang coals and that the pyrite contents of these coals are much higher than that of the bituminous coals. Unlike the U.S. coals, the iron in the Australian coal appeared to be present as iron oxyhydroxide (FeOOH).

If pyrite is contained in a burning coal particle that also contains clay minerals and/or quartz, it is likely to react with these minerals to form an aluminosilicate slag droplet. Isolated pyrite, either liberated or contained in a coal particle transforms into pyrrhotite by devolatilization which then undergoes exothermic oxidation, presumably to a molten Fe-O-S phase (6,7). Iron is found predominantly present as magnetite and as Fe^{+3} in glass in the ash samples of these coals. For these coals, the partitioning between iron oxide and glass appears to be simply related to amount of pyrite in the mineral matter. On this basis one would predict that the amount of iron as oxide should decrease in the order Illinois #6 > Beulah lignite > Kentucky #11 > Upper Freeport > Kentucky #9 > Eagle Butte, which is exactly the order in which iron is partitioned between iron oxide and glass in the ash samples. One would expect that how the pyrite is associated with other minerals would also play a role in determining this order, but for this particular sequence of coals, such association is apparently not an important factor or it is also dependent on the relative amount of pyrite in the sample to a first approximation (Table 1).

XANES spectra of calcium in Beulah lignite and Eagle Butte coals are very similar to the ones measured for other low-rank U.S. coals [10,11] and are characteristic of calcium bound through carboxyl groups to macerals (Fig. 1). XANES of calcium in San Miguel Texas lignite (Fig. I) also resembles that of the two low rank coals. XANES of calcium in Illinois #6 coal resembles the sum of XANES of calcite and that of a coal with carboxyl-bound calcium.

In the ash samples obtained from low rank coals, the predominant compositional classes are permutations of the three most abundant elements: Ca, Al and Si, except for the finest impactor plate where many Ca and Na sulfate particles are also present. Figures 2 show Ca-Si-Al triangular plots for each of the impactor plates of Beulah ash sample. Here each point represents an ash particle identified by the CCSEM analysis as containing > 80% Ca + Si + Al. The composition of each particle, normalized to three elements, is then plotted on the ternary diagram. The plots show a clear dependency of compositional clustering on size. These trends can be interpreted as indicating a size dependency for the reaction between CaO fume, derived from the carboxyl-bound calcium, and the kaolinite in the coal. The smaller the reactant particle, the

more probable is the formation of a Ca-Al-Si phase, and the less probable is the existence of separate Ca-rich or Al-Si particles. The fine particle compositions indicate the formation of calcium substituted glass phase. The XANES spectra (Fig. 3) are quite similar to that attributed to calcium in aluminosilicate glass [5] and indicate that the amount of CaO or $CaSO_4$ in ash is relatively minor (<10 vol%). Hence, the broader range in the Ca-Al-Si cluster observed for the coarser particles must represent the compositional range of Ca-Al-Si glass rather than mixed CaO-Al-Si particles. It should also be noted that there is a tendency for Ca enrichment near particle surfaces.

The principal alkali species in lignite is Na, believed to be molecularly dispersed through the maceral and bonded to the carboxyl group, like calcium. Sodium may also be present as hydrated Na^+ ions in the moisture associated with low-rank coals and this is probably the case with Loy Yang coal, even though appreciable NaCl was noted in the CCSEM analysis for the dried sample of this coal. Potassium is significant only for the four bituminous coals and San Miguel lignite. K in these coals is almost entirely present as illitic clays. Some KCl was noted in the CCSEM analysis of Loy Yang coal.

The behaviour of alkalies during combustion is strongly dependent on their form of occurrence in the parent coal. K, which is present as illite, is likely to remain with the aluminosilicate particle and form a molten slag droplet. Confirmed by potassium XANES (Fig.4) obtained from various ash samples, partial melting occurs because of eutectic regions in the K-Si-Al phase diagram [8,12]. The aluminosilicate glass produced by melting illite yields precisely this type of potassium XANES spectrum [8,13]. The composition of these molten particles is similar to that of the parent illite, as illustrated in Figure 5. Figure 4 shows the comparison of potassium XANES spectra of ash samples from different coals and all appear characteristic of potassium in glass. The subtle difference between the Eagle Butte spectra and the other spectra most likely reflects either its different bulk ash composition (richer in Ca, poorer in Fe) or a different mode of occurrence for potassium in the original coal.

The CCSEM analysis of Beulah lignite ash shows an abundance of sodium-aluminosilicate particles (Fig. 6). In contrast to the similar plot for calcium rich particles, the Na-rich particles cluster in the center of the Na-Al-Si ternary plot. The composition of this cluster of points corresponds to the phase nepheline ($NaAlSiO_4$). This phase must have been formed by reaction between kaolinite and Na cations volatilized in the combustion of the coal. This is an example of the efficiency of aluminosilicates derived from clays for the fixation of alkali elements in coal ash. This refutes the suggestion that alkali elements can be readily volatilized from clays or other aluminosilicates during combustion, at least to 1500 K under oxidizing conditions.

SUMMARY:

Iron (pyrite) either reacts with clay minerals to form aluminosilicate slag or devolatizes and undergoes oxidation to form oxides and sulfides, depending on whether it is associated with clay and quartz or isolated. Calcium is molecularly dispersed in coals and is bonded to carboxyl groups in the macerals. On combustion it forms CaO which may further react with clays to form aluminosilicate glass. Potassium in bituminous coals is contained in illite which melts and forms aluminosilicate glass. Finally, sodium which is believed to be molecularly dispersed in the macerals, volatilizes and reacts with clays

to form aluminosilicate glass with compositions corresponding to that of nepheline.

REFERENCES:

1. F. E. Huggins, N. Shah, G. P. Huffman, R. G. Jenkins, F. W. Lytle, and R. B. Greegor, Fuel, 67, 938-942 (1988).

2. G. P. Huffman, F. E. Huggins, and N. Shah, "EXAFS Spectroscopy: A New Technique for Investigating Impurity Elements in Coalthat Control Slagging and Fouling Behaviour", Engineering Foundation Conference on Mineral Matter and Ash in Coal, Santa Barbara, CA, 1988, Eds., K. S. Vorres and R. W. Bryers, to be published by Elsevier.

3. F. E. Huggins, G. P. Huffman, and A. A. Levasseur, "Ash Deposits from Raw and Washed Coals", ibid.

4. F. E. Huggins, G. P. Huffman, A. A. Levasseur, ACS Division of Fuel Chemistry Preprints, Vol. 33, No. 2, 73-80 (1988).

5. G. P. Huffman, F. E. Huggins, A. A. Levasseur, F. W. Lytle, R. B. Greegor, and A. Mehta, Fuel, 68, 238-242 (1989).

6. G. P. Huffman, F. E. Huggins, A. A. Levasseur, O. CHow, and S. Srinivasachar, Fuel, 68, 485-490 (1989).

7. S. Srinivasachar and A. Boni, Fuel, 68, 829 (1989).

8. G. P. Huffman, F. E. Huggins, R. W. Shoenberger, J. S. Walker, F. W. Lytle, and R. B. Greegor, Fuel, 65, 621-632 (1986).

9. G. P. Huffman, F. E. Huggins, N. Shah, and A. Shah, "Behaviour of Basic Elements During Coal Combustion", to be published in Progress in Energy and Combustion Science.

10. F. E. Huggins, G. P. Huffman, F. W. Lytle, and R. B. Greegor, "An EXAFS Investigation of Calcium in Coal", Proceedings of International Conference on Coal Science (Pittsburgh, PA), 679-682 (1983).

11. G. P Huffman, and F. E. Huggins, "Analysis of the Inorganic Constituents in low-rank Coals", ACS Division of Fuel Chemistry, Preprints, Vol. 264, 159-174 (1984).

12. E. M. Levin, H. F. McMurdie and H. P. Hall, Phase Diagrams for Ceramists, Amer. Ceramic Soc., Inc., Columbus, Ohio, 1964.

13. C. Spiro, J. Wong, F. W. Lytle, R. B. Greegor, D. H. Maylotte, S. Samson, and B. Glover, Fuel 65, 327 (1986).

TABLE 1. - Mössbauer data for ash samples from University of Arizona combustor

Coal	%Fe Distribution of Iron among Phases			
	Hematite	Magnetite	Ferric glass	Ferrous glass
Illinois #6	-	84	16	-
Beulah Lignite	-	71	24	5
Eagle Butte	-	46	54	-
Kentucky #11	8	67	12	14
Upper Freeport	3	67	18	13

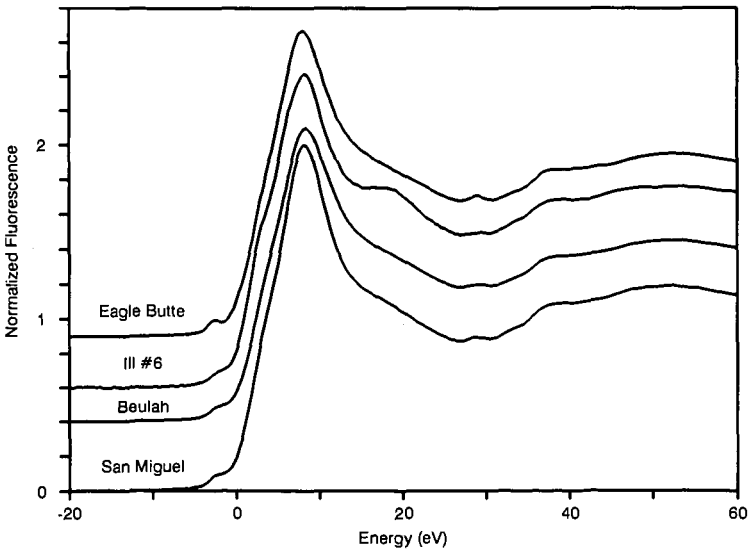

Figure 1. Ca XANES of high calcium PSI coals.

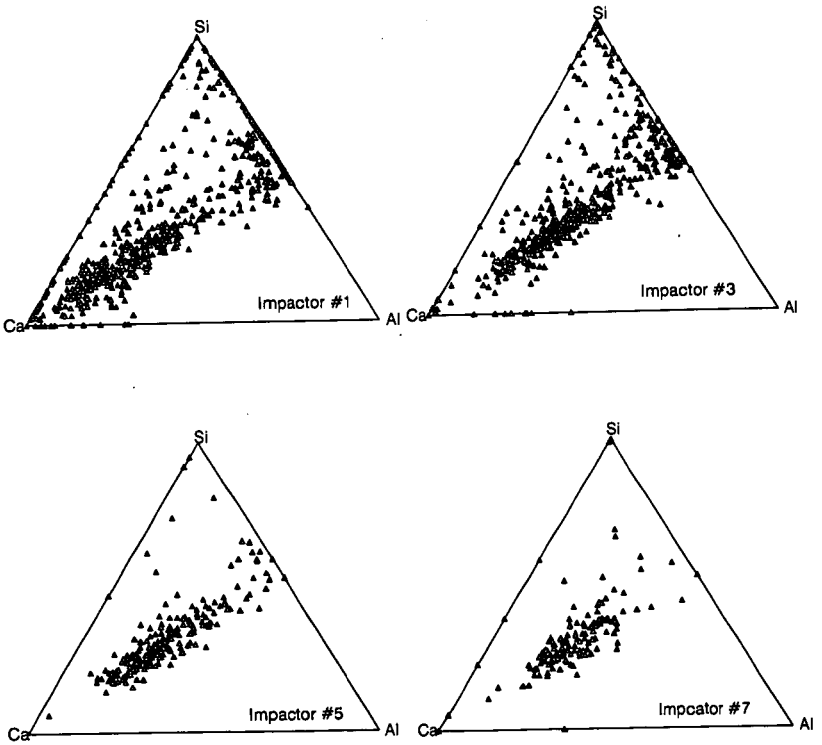

Figure 2. Ca-Al-Si triangular plots for Beulah lignite ash on different impactors in UA combustor. All particles contain Al+Si+Ca > 80%.

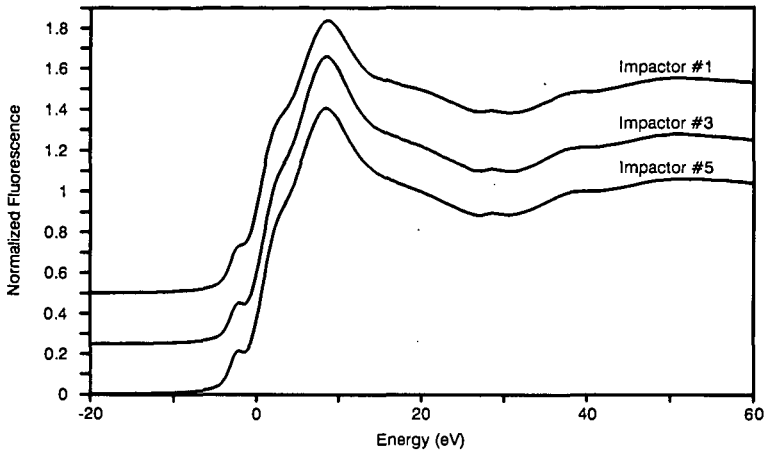

Figure 3. Ca XANES for Beulah ash from size segregated impactors of UA combustor

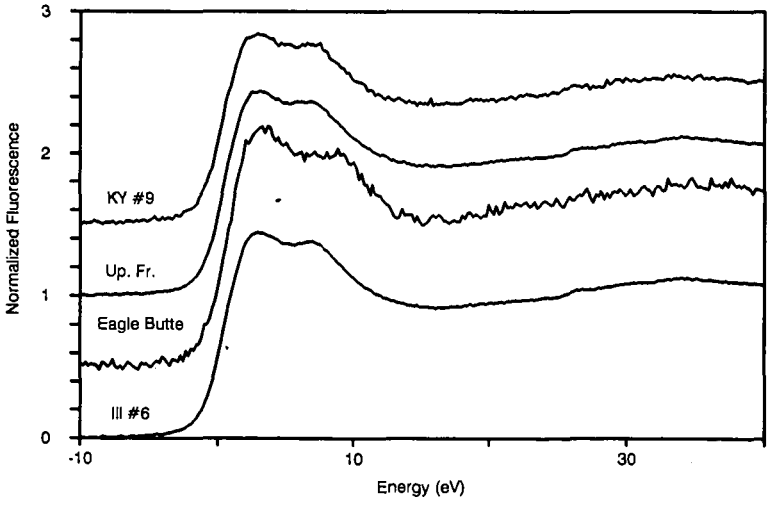

Figure 4. Potassium XANES of ash samples from MIT combustor.

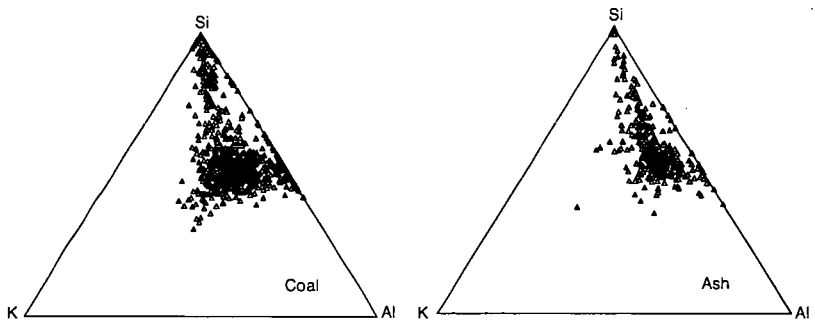

Figure 5. K-Si-Al triangular plots for Upper Freeport coal and ash

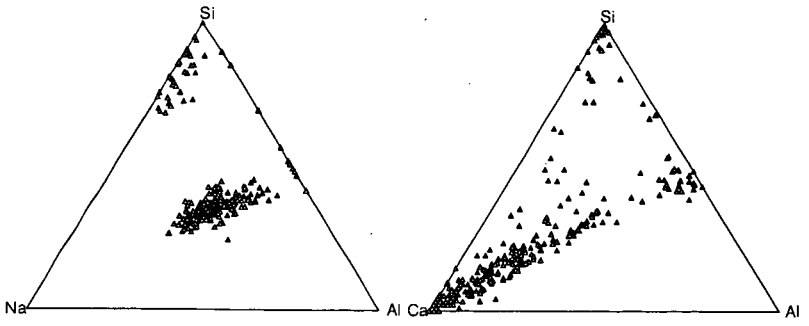

Figure 6. Triangular plots for Beulah ash from PSI drop tube furnace.
All particles contained Al+Si+Na/Ca > 80%.

FLY ASH DEVELOPMENT FROM SODIUM, SULFUR AND SILICA DURING COAL COMBUSTION

D.K. Ludlow and T.A. Erickson
Department of Chemical Engineering
University of North Dakota
Grand Forks, North Dakota 58203

S.A. Benson
Energy and Environmental Research Center
University of North Dakota

Introduction

The formation of ash during the combustion of coal is a very complex environmentally dependent reaction. Significant parameters include the combustion conditions and association and relative sizes of the inorganic constituents present. During pulverized coal combustion the inorganic constituents undergo chemical and physical transformations in the flame and during gas cooling to form inorganic vapors, liquids, and solids. These chemical and physical transformations dictate the size and composition distribution of the final ash product. Previous studies of the final ash product (fly ash) indicate that the size distribution is usually bimodal (Sarofim, 1977; Flagan and Friedlander, 1978; and Damle, 1982). The submicron size particles have an average diameter of about 0.1 microns. These small particles form as a result of the homogeneous condensation of flame volatilized species. These flame volatilized species may also condense heterogeneously on the surfaces of larger particles. The larger size fraction of the particles, referred to as the residual ash, are largely a result of the minerals present in the coal. The size and composition distributions of the larger particles are a result of the transformations and interactions of the minerals and other inorganic components in the coal. Physical processes such as coalescence, fragmentation of minerals and char, and shedding of inorganic components occur which effect the properties of the ash.

A furfuryl alcohol polymer containing Na, S, and SiO_2 was used to study the effect of combustion temperature on the formation of fly ash particles. Of specific interest to low-rank coal combustion systems is the interaction between sodium, sulfur and silica to form low melting point phases that can cause deposition problems (Jones, 1987). In order to identify key processes associated with the formation of ash in combustion systems carefully controlled combustion experiments using a laminar flow furnace system were performed. A precisely formulated synthetic coal/mineral mixture was produced, combusted in a laminar flow furnace, and the composition and size of the ash was examined. The synthetic coal was formulated to include only a specific composition of inorganic species in a specific form and size to facilitate the examination of the effects of combustion conditions on the final ash particles formed.

Experimental Approach

A furfuryl alcohol polymer was catalyzed with p-toluenesulfonic acid as outlined by Senior (1984) and modified by Erickson (1990). The coal was synthesized to include 10% by weight SiO_2 in the crystalline form of quartz. Computer Controlled Scanning Electron Microscopy (CCSEM) (Steadman et.al., 1990) and Inductively Coupled Plasma (ICP) analysis determined the synthetic coal to contain 9.3 and 11.3 % by weight

quartz, respectively. CCSEM analysis determined the quartz to range in diameter from 1 to 10 microns with the average size, based on a volume percent basis, to be 5.06 microns. Sodium (5% by weight) was added to the coal in the form of sodium benzoate in an alcohol solution. The solution was then allowed to evaporate off with the sodium remaining attached to the coal. This method gives a form of sodium which is easily volatilized (Mills, 1989) similar to the ease of the volatilization of sodium in low rank coals. Sublimed sulfur was added extraneously to comprise 1% by weight. The final coal was ground in a ball mill and sized to 46-106 microns with a sonic sieve.

The synthetic coal was combusted in a laminar flow furnace at 900, 1100, 1300, and 1500°C. The residence time of the coal was approximately 1.4 seconds with slight variations dependent upon temperature. After exiting the furnace the fly ash was cooled instantly with a quench probe and collected on a bulk filter.

After combustion the samples were mounted on a carbon plug with double stick tape, carbon coated and studied with the use of a JEOL Scanning Electron Microscope/Microprobe (SEM/EMPA). The SEM/EMPA is equipped with an ultra-thin window energy dispersive detector with a Tracor Northern 5600 processing system. The system also has the abilities of a Tracor Northern 8500 image analysis system. These three tools together create a flexible mechanism for determining the composition, size, and various characteristics of fly ash samples.

Results

Figures 1-4 show the fly ash formed at 900, 1100, 1300, and 1500°C, respectively (all four figures are at the same magnification). The particle size decreases with increasing combustion temperature. Virtually all of the particles are spherical in nature and were assumed to be for all subsequent calculations. Table 1 gives the average particle size of each of the samples. The particles were sized manually by randomly measuring 125 particles with the aid of the image analysis system. Figure 5 gives a graphical representation of the same data with the addition of: 1) the theoretical diameter of a fly ash particle assuming 100% coalescence of inorganics, and 2) the diameter of the original quartz prior to combustion. It should be noted that some of the particles at 900 and 1100°C show some evidence of either cenosphere formation or unburned carbon in the center. The combustion of the synthetic coal appears to be dominated by coalescence, i.e. formation of one fly ash particle per coal particle, at lower temperatures as shown in Figure 6, and by fragmentation followed by coalescence at higher temperatures, shown in Figure 7.

Figure 8 is a high magnification photo of the fly ash combusted at 900°C. On the surface of the larger grey particles are very small white moieties. The same phenomenon appears in all four samples but is most abundant and largest in size at the lower temperatures. Due to the small size of the moieties it is impossible to get an accurate chemical analysis of them with the SEM/EMPA (the excitation volume of the electron beam is 8 microns in diameter as compared to the submicron size of the moieties). Table 2 compares the grey area composition, moiety composition, and bulk area composition. It is important to note that SEM/EMPA analysis of the moieties includes analysis of a substantial amount of the fly ash behind and surrounding it. These analyses are averages of 3 to 5 samplings of each of the described areas. From these analyses it appears that the moieties are sodium sulfates which homogeneously condensed and impacted onto the Na-rich silicate particles.

SOLGASMIX (Erikkson and Rosen, 1973), a theoretical program based on minimization of Gibbs free energy, predicts that the abundance of sodium sulfates will decrease with increasing temperature. This corresponds to the observed results, with fewer and smaller sodium sulfate particles found at higher temperatures.

Conclusions

The formation of fly ash in the coal studied was dominated by coalescence at low temperatures (900 and 1100°C) and by fragmentation followed by coalescence at higher temperatures (1300 and 1500°C). The fragmentation during combustion may be caused by: 1) thermal breakup of the particle, 2) rapid combustion (explosion), 3) break up of pore structure, or 4) a number of other phenomena. There was increased formation of submicron sodium sulfates at lower temperatures while higher temperatures appeared to decrease both the size and abundance of the submicron sodium sulfate particles. At the higher temperatures, the sodium appears to interact with the silica to form sodium silicates.

References

Erickson, T.A., "The Fate of Flame Volatilized Sodium During the Combustion of Pulverized Coal in Reaction with Silica and Sulfur (Studied with the Aid of a Synthetic Coal)", Master Thesis, University of North Dakota, Grand Forks, N.D., 1990.

Erikkson, G., and Rosen, E., Chemica Scripta, 4, 193(1973).

Damle, A.S., Ensor, D.S. and Ranada, M.B., Aerosol Science and Technology, Vol. 1, p.119, 1982.

Flagan, R.C., and Friedlander, S.K., "Particle Formation in Pulverized Coal Combustion", Recent Developments in Aerosol Science, Ed. D.T. Shaw, Wiley, New York, Ch. 2, 1978.

Jones, M.L., and Benson, S.A., "An Overview of Fouling and Slagging in Low-Rank Coals", Conference on the Effects of Coal Quality on Power Plants, EPRI, Atlanta, Georgia, October 15-17, 1987.

Mills, M., "Sodium Release from Solids in Flames Studied using Laser Induced Fluorescence Spectroscopy", Chemistry Department, University of North Dakota, Grand Forks, N.D., 1989.

Sarofim, A.F., Howard, J.B., and Padia, A.S., Combustion Science and Technology, Vol. 16, p. 187, 1977.

Senior, C.L., "Submicron Aerosol Production During Combustion of Pulverized Coal", Ph.D. Thesis, California Institute of Technology, 1984.

Steadman, E.N., Zygarlicke, C.J., Benson, S.A., and Jones, M.L., "A Microanalytical Approach to the Characterization of Coal, Ash, and Deposit", Seminar on Fireside Fouling Problems, Brigham Young University, Provo, Utah, 1990.

Table 1

Average Particle Size of Fly Ash Formed From Synthetic Coal

Temperature(°C)	Diameter (microns)
900	27.0
1100	27.7
1300	17.6
1500	8.5

Table 2

Particle Surface Composition, Elemental %'s

Temperature	Bulk Composition			Grey Area Composition			White Moiety Composition		
(°C)	Na	S	Si	Na	S	Si	Na	S	Si
900	24	5	61	19	1	80	39	18	43
1500	80	1	19	5	0	95	6	1	93

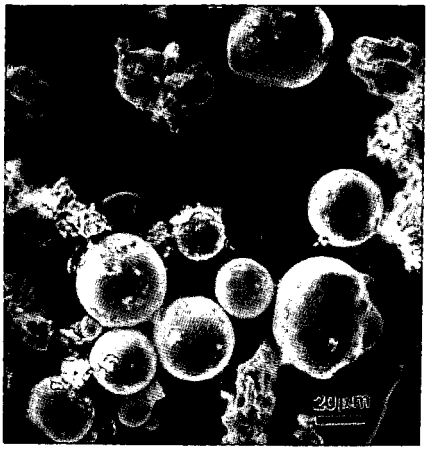

Figure 1 Fly Ash Particles Formed at 900°C, 500x.

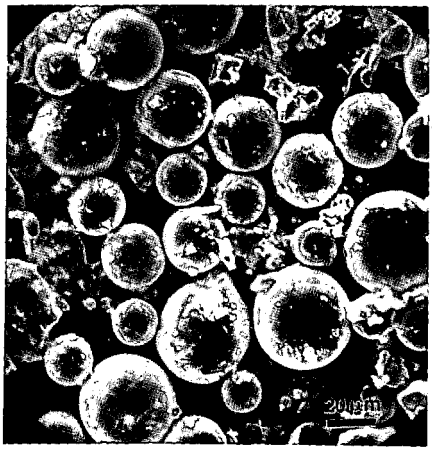

Figure 2 Fly Ash Particles Formed at 1100°C, 500x.

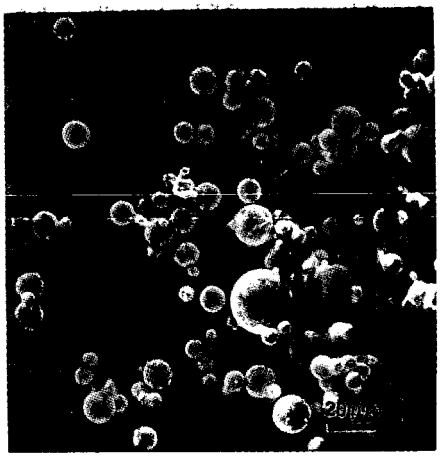

Figure 3 Fly Ash Particles Formed at 1300°C, 500x.

Figure 4 Fly Ash Particles Formed at 1500°C, 500x.

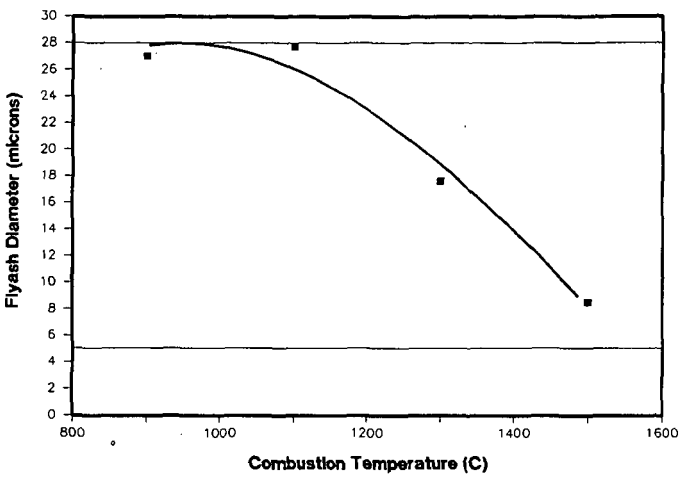

Figure 5 Particle Size versus Combustion Temperature. (upper line represents 100% coalescence and lower line represents original size of mineral grains)

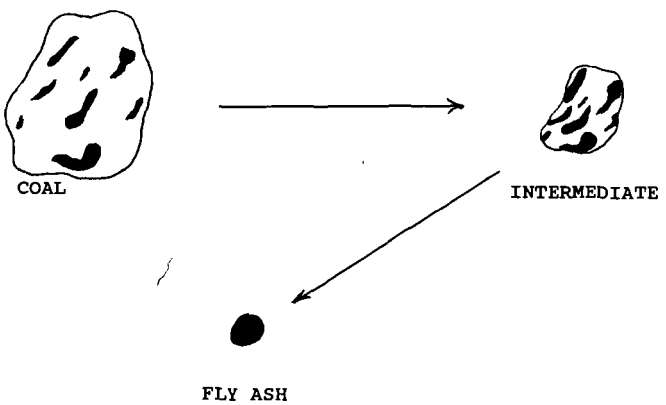

Figure 6 Diagram of the Formation of Fly Ash Particles Through Coalescence.

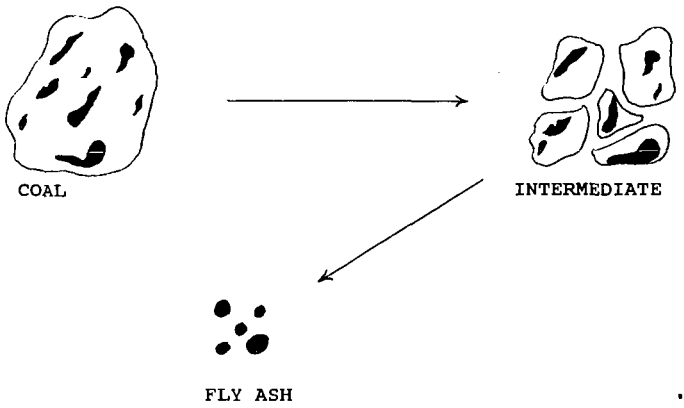

Figure 7 Diagram of the Formation of Fly Ash Particles Through Fragmentation.

Figure 8 High Magnification Photo of 900°C Fly Ash Particle Surface.

EFFECTS OF RESIDUAL CARBON ON DEPOSITION IN COAL-FIRED GAS TURBINES

Ronald G. Logan and Matthew J. Scanlon

Morgantown Energy Technology Center
United States Department of Energy
P.O. Box 880
Morgantown, WV 26505

and

Richard A. Wenglarz

Allison Gas Turbines
General Motors Corporation
P.O. Box 420
Indianapolis, IN 46206

ABSTRACT

The influence of residual carbon in coal ash on ash deposition at coal-fired gas turbine conditions has been investigated. Measurements of sticking coefficients (fraction of impacting ash particles that adhere) and ash deposit adhesion strength in a laminar-flow drop tube furnace indicate that high carbon levels in ash can decrease sticking fractions. However, high carbon levels also increased the adhesion strength of ash deposits, making them more difficult to remove. Possible mechanisms for the involvement of carbon in ash deposit formation are presented.

INTRODUCTION

The U.S. Department of Energy is currently sponsoring a program to develop direct coal-fired gas turbines. Direct coal-fired gas turbines are potentially attractive alternatives to conventional steam cycle electric power generation because of their higher efficiencies. However, the high mineral matter content of coal creates problems with deposition, erosion, and corrosion of turbine components. Ash deposits are formed in turbines by the adherence of ash particles to the surfaces of stators and blades. During combustion, components of the coal ash become molten and thus readily adhere to turbine components upon impaction. The tendency of various coals to form ash deposits during combustion is a complex function of many variables including the ash chemistry, gas temperature and pressure, gas velocity, and the temperature of the turbine components. Previous test results from this laboratory[1-2], from bench-scale combustor tests[3], and from tests on a gas turbine simulator[4-5] have indicated that unburned carbon in coal ash may affect the degree of deposit formation. The present study was initiated to further explore the effects of carbon on mechanisms of ash deposit formation.

Particulate in the products of combustion (POC) streams entering direct coal-fired gas turbines will probably contain much higher fractions of

unburned carbon than for past coal experience such as in boilers. The lower ash levels for potential turbine fuels compared to boiler fuels result in higher percentages of carbon in the POC for a given combustion efficiency. Figure 1 illustrates this effect for 99% carbon burnout of a solid fuel such as coal. This figure indicates that unburned carbon would constitute about 50% of the POC particulate for a 1% ash coal turbine fuel, but only about 15% of the POC particulate for a coal boiler plant using a 5% ash coal.

Past tests have indicated a significant effect of unburned carbon on deposition; however, data from different tests appear to be contradictory. Tests associated with an early coal-fired gas turbine program[4] showed that the presence of relatively coarse incandescent (burning) coal particles in the gas stream increased the rate and density of deposit buildup. On the other hand, more recent cascade tests at General Electric with low ash coal water fuels showed much lower deposition rates occurred when the combustion efficiency was reduced and unburned carbon levels were high[4-5]. Analyses of data from tests at General Motors Allison Division[3] resulted in the hypothesis that increased carbon levels could increase deposition at the highest temperature locations in the turbine flowpath. This was attributed to unburned carbon producing larger particle sizes and higher delivery rates, higher particle impact and surface temperatures, and locally reducing conditions with relatively low melting ash phases. For the lower temperature regions of the turbine flowpath, it was hypothesized that carbon could reduce deposition by eroding previously retained ash material on the surfaces.

The experiments described in this paper were designed to assess the effects on deposition of relatively high POC carbon-ash-ratios for conditions representative of direct coal-fired gas turbines. The data are expected to be useful in identifying parameters that need to be controlled to alleviate deposition in coal-fired gas turbines.

EXPERIMENTAL

Experiments were performed in an electrically heated, laboratory scale drop-tube combustor designed to operate at temperatures up to 1400°C. This combustor[7], the Combustion/Deposition Entrained Reactor (CDER), is shown in Figure 2. Approximately 3-10 grams per hour of -400 mesh pulverized coal was entrained in 5 standard liters per minute (lpm) of air from a circulating feeder. A water-cooled injection probe was used to introduce this particle-laden flow into the combustor where it mixed with 25 lpm of preheated primary air. The coal feed rates used in these experiments allowed long sampling times during deposition tests which resulted in excellent time resolution of the growth of the ash deposits. The residence time of coal particles in the combustor were controlled by changes in the total gas flow, or the position of the injection probe. In tests reported here, the residence time was varied over a range of 440 to 640 milliseconds by adjusting the position of the injection probe. This produced ash with a range of carbon levels from approximately 10 to 50%. The tests were conducted at gas temperatures of 1100 and 1200°C, which is representative of current and future industrial gas turbine inlet temperatures.

Experiments in the CDER were designed to simulate deposition on the leading edge of a gas turbine airfoil where the primary mode of particle delivery to the surface of the airfoil is inertial impaction. At the exit of

the combustion zone the products of combustion were accelerated through a 3.2 mm diameter nozzle, creating a jet which impinged on a flat, 12.7 mm diameter platinum disk. The resultant jet velocity of approximately 300 m/s is within the range expected in the first stage of a gas turbine. The platinum target was positioned 6 mm below the nozzle aperture (Figure 3). This nozzle/target configuration was developed according to procedures for inertial impactor design to insure that all particles larger than approximately 0.5 microns are forced by inertia to impact the target, as would occur on the leading edge of a gas turbine stator or blade. Platinum was used as an inert target material to eliminate surface reactions peculiar to a specific blade material which could affect the experimental results. The target could be cooled from the underside by an opposing jet of cooling air. Thus, a range of target temperatures were obtainable by varying the cooling air flow rate. The target temperature was measured throughout each test using a two-color optical pyrometer which monitored the temperature of the backside of the platinum target.

Sticking coefficients were measured by first passing the jet of exhaust through a filter to determine the total particle mass arrival rate. Gas flow through the filter (which was positioned in the same location as the target) was controlled via a vacuum pump and a mass flow controller. The rate of deposit buildup was determined by placing a target of known weight under the jet, and then withdrawing the target after a specified exposure period (usually ten minutes) to measure the weight gain. The sticking coefficient was calculated as the ratio of the weight gain of the target to the total mass arriving at the target (determined by the filter sample). The filter samples were quenched with cold air, resulting in unburned carbon in the samples. Since carbon was burned out of the deposits, filter samples were analyzed for carbon content to correct the ash arrival rate used to calculate the sticking coefficient.

Deposit adhesion strength (or shear strength) was measured using a device shown in Figure 4. The device consists of an alumina rod attached to a translation stage and linear actuator. A load cell is used to measure the force required to dislodge deposits from the targets using the blunt tip of the rod. The device is attached to the CDER, and the measurements are conducted at temperature. The measurements are in pounds of force, and are adjusted for the area of contact between the deposit and target to produce units of pounds per square inch.

DISCUSSION

The coal used in these tests was an Arkwright Pittsburgh bituminous containing approximately 7% ash and 2% sulfur. Ultimate and elemental analyses for the coal are shown in Table 1. Figure 5 shows measurements of sticking coefficients as a function of carbon levels in the ash at two gas temperatures. The data points are averages of a number of measurements collected on the same day at identical conditions. In Figure 6, the high and low data points are plotted along with the average to show the degree of scatter in the data. Figure 7 shows the trend in the sticking coefficient data compared to measurements of adhesion strength as a function of carbon.

The data show several significant effects of unburned carbon:

- Sticking fractions were highly sensitive to unburned carbon, decreasing by a factor of about seven when unburned carbon levels increased from 10 to 50%.
- Increased unburned carbon increased deposit adhesion strength.
- Carbon levels more significantly affected sticking fractions than changes in gas temperature from 1100 to 1200°C.

The following are proposed as possible mechanisms for the observed effects of unburned carbon. Unburned carbon may have a short term effect on sticking, and a long term effect on deposit strength. Some of the carbon may be captured by other molten material on the surface and oxidize under subsequent layers of deposits over longer periods of time (seconds or minutes) compared to the time frame of particle impacts (milliseconds). The increased temperatures and locally reducing conditions within the deposit could produce increased levels of molten phases and sintering to result in higher deposit strengths with increased carbon levels.

The sticking fraction of particles impacting at the outer deposit surfaces may be predominantly affected by the competition between capture of molten particles and erosion by harder particles. The ultimate sticking fraction may depend on factors affecting the balance of levels of molten phases versus hard materials (both the particles, and at the deposit outer surface). The levels of molten versus hard phases may be affected by the ash composition and local temperatures. The elevation in local temperature of both the impacting particles and the outer deposit surface due to oxidizing carbon may ultimately be limited by the local oxygen levels. In that case, additional carbon in the POC would not increase levels of molten ash phases, but would increase the amount of hard material to erode the deposit surface. This would cause a decrease in deposition with an increase in carbon levels as was observed in these experiments. And, since the local temperatures and levels of molten phases would be predominantly affected by local oxygen levels rather than gas temperature, the sticking fraction would not be strongly influenced by gas temperature as was observed in these experiments.

The increase in deposition with increased carbon levels mentioned previously for tests in an early direct coal-fired turbine program[1] may have involved changes in carbon fractions below levels where local oxygen concentrations limit the degree of melting. In that case, molten ash levels and sticking may be controlled by carbon fractions and would increase with increasing carbon levels.

SUMMARY AND CONCLUSIONS

Particulate in the POC streams entering direct coal-fired gas turbines will probably contain much higher fractions of unburned carbon than for past coal experience because of the use of beneficiated, low ash fuels. Measurements of ash sticking fractions and ash deposit adhesion strength in a

drop tube combustor indicate that high levels of carbon in ash can reduce sticking fractions significantly, while also increasing the deposit strength. It is suggested that increased carbon levels may increase the amount of hard material relative to molten phases in the particulate when carbon oxidation is limited by local oxygen concentrations. However, heat generation from the burning carbon in deposited particulate in a locally reducing environment may cause increased levels of molten species and sintering, creating deposits that are more difficult to remove.

REFERENCES

1. Logan, R. G., G. A. Richards, C. T. Meyer, and R. J. Anderson, "A Study of Techniques for Reducing Ash Deposition in Coal-Fired Gas Turbines," Accepted for publication in Progress in Energy and Combustion Science, 1990.

2. Richards, G. A., R. G. Logan, C. T. Meyer, and R. J. Anderson, "Ash Deposition at Coal-Fired Gas Turbine Conditions: Surface and Combustion Temperature Effects," Accepted for publication in Transactions of the ASME, 1990.

3. Wenglarz, R. A. and R. G. Fox, Jr., "Physical Aspects of Deposition from Coal Water Fuels Under Gas Turbine Conditions," Journal for Gas Turbines and Power, Vol. 112, January 1990.

4. Kimura, S. G., C. L. Spiro, and C. C. Chen, "Combustion and Deposition in Coal-Fired Turbines," Journal of Engineering for Gas Turbines and Power, Vol. 109, July 1987.

5. Staub, F. W., S. G. Kimura, C. L. Spiro, and M. W. Horner, "Coal-Water Slurry Combustion in Gas Turbines," Journal of Engineering for Gas Turbines and Power, Vol. 111, January 1989.

6. Morley, W. J. and J. C. Wisdom, "Brown Coal Ash Deposition in the Open-Cycle Gas Turbine," Journal of the Institute of Fuel, Vol. 37, No. 280, May 1964.

7. Anderson, R. J., R. G. Logan, C. T. Meyer, and R. A. Dennis, "A Combustion/Deposition Entrained Reactor for High Temperature/Pressure Studies of Coals and Coal Minerals," Accepted for publication in Review of Scientific Instruments, 1990.

Table 1. Coal Analyses

	Arkwright	Blue Gem
ULTIMATE ANALYSES		
% Ash	6.93	0.56
% Carbon	75.90	78.06
% Hydrogen	5.34	5.67
% Nitrogen	1.45	1.98
% Sulfur	2.03	0.99
ASH ANALYSES		
% SiO_2	48.09	16.86
% Al_2O_3	25.07	22.75
% Fe_2O_3	10.95	29.57
% TiO_2	1.27	1.95
% P_2O_5	0.18	0.48
% CaO	5.78	7.03
% MgO	1.25	2.46
% K_2O	1.16	0.53
% Na_2O	0.90	1.54
% SO_2	5.34	8.07
ASH FUSION TEMPERATURE (+/- 40°C)		
Initial Deformation	1,190	1,238
Softening	1,316	1,308
Hemispherical	1,356	1,371
Fluid	1,383	1,427

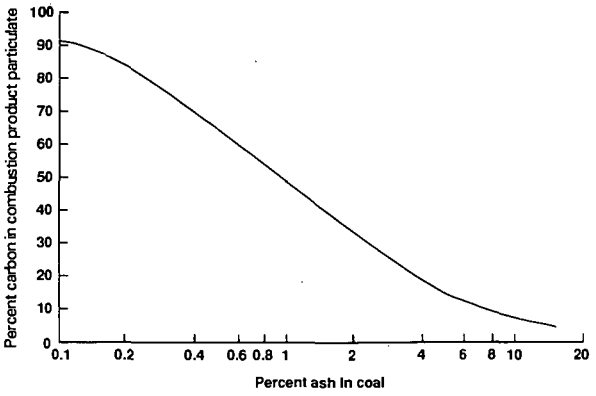

Figure 1: Percent of carbon in combustion particulate versus percent of ash in coal for 99% carbon burnout efficiency during combustion

Item	Test Section
PRESSURE, ABSOLUTE, atm	1-12
FLOW RATE, slpm	10-350
VESSEL LENGTH, cm	152
VESSEL OUTSIDE DIAMETER, cm	61
WALL THICKNESS, mm	9.5 (sch 40-304LSS)
PROCESS STREAM EXIT TEMPERATURE, °C	1,400
VESSEL SKIN TEMPERATURE, °C	< 150
ELEMENTAL TEMPERATURE (maximum), °C	1,650
HEATING ELEMENTS	KANTHAL SUPER 33 9/18
HEATER OUTPUT, watts	7,060
POWER SUPPLY, V/A	35/350
EXHAUST FLOW COMPOSITION	DILUTE COAL POC/ FILTERED
EXHAUST FLOW PRESSURE/TEMPERATURE	< 2 atm; < 200°C

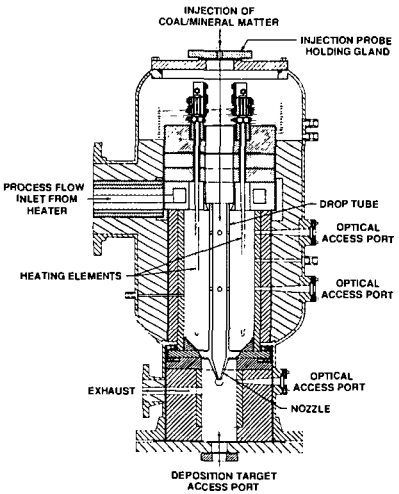

Figure 2: CDER System Design Specifications

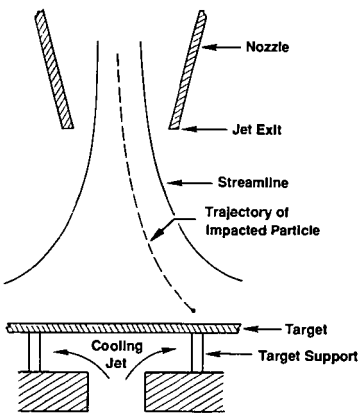

Figure 3: CDER Nozzle/Target Assembly

M90001853

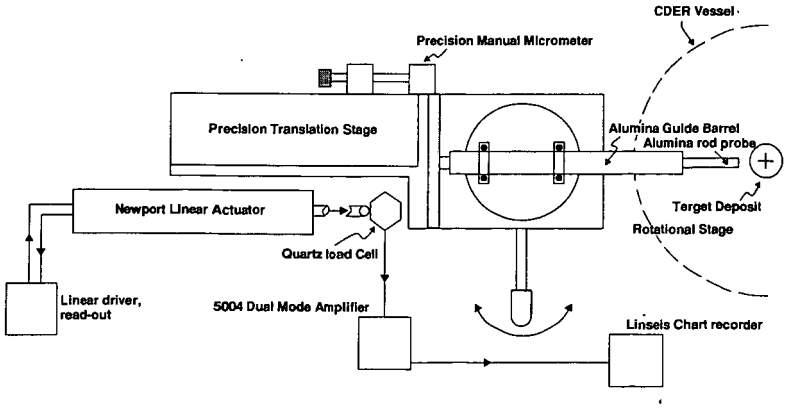

Figure 4: Adhesion Strength Meter

M90001854

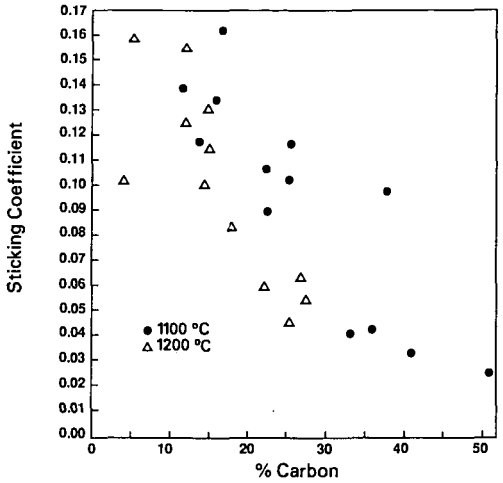

Figure 5: Sticking Coefficient vs % Carbon in Ash, Arkwright Bituminous Coal

M90001370

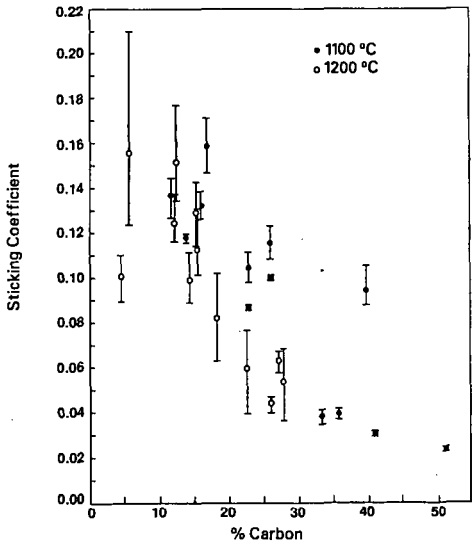

Figure 6: Sticking Coefficient vs % Carbon in Ash, Arkwright Bituminous Coal

M90001371

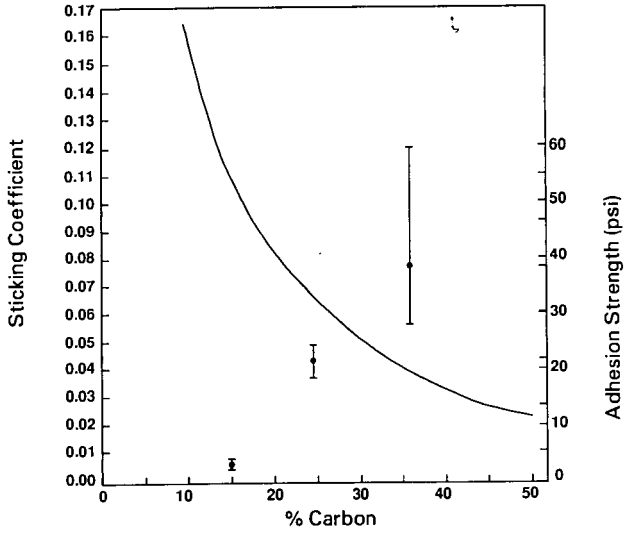

Figure 7: Adhesion Strength vs % Carbon in Ash Arkwright Bituminous Coal, T = 1100 °C

M90001376

EFFECTS OF INORGANIC CHANGES CAUSED BY NATURAL WEATHERING ON THE COMBUSTION BEHAVIOR OF BITUMINOUS COALS

SARMA V. PISUPATI and ALAN W. SCARONI
The Combustion Laboratory, 404 Academic Activities Bldg.
The Pennsylvania State University, University Park, PA 16802

Key words: Weathering; Mineral Matter; Combustion

INTRODUCTION

Weathering/oxidation is a process that can occur when coal is exposed to the atmosphere following mining and, in some instances, while it is still in the seam (outcropping). Weathering causes changes in the organic, inorganic and physical structure of coals. These structural changes can alter significantly the utilization behavior of the coals [1,2]. The most adverse effect of oxidation is probably experienced in the coking industry. Although attempts have been made to understand the mechanism of oxidation, and to elucidate the structural changes to the organic phase accompanying oxidation, [3,4,5] the reactions are still poorly understood and methods to suppress oxidation are often rather primitive [6]. Even though 70% of the coal mined in U.S is burnt in electric utility boilers, very little attention has been paid to the effects of weathering/oxidation/storage on combustion behavior. A few published studies[7,8] indicate that weathering/oxidation is detrimental to combustion in terms of carbon conversion. In addition, acid rain legislation is expected to increase the demand for low sulfur coals and therefore, electric utilities have begun to test blending strategies. As a result, coal suppliers have started blending fresh and naturally weathered/oxidized coals, because the latter generally have lower sulfur contents (for the reasons discussed later in the paper) than their fresh counterparts. Although desulfurization by weathering/oxidation may be desirable from an emissions point of view, the effects of the accompanying structural changes on combustion are not well established.

The structural differences between the organic phases and the relative combustion behavior of five outcrop coals and their fresh companions have been reported elsewhere[9]. The mineral matter is important from at least two aspects; its role in the combustion process itself and the operation and maintanence of combustion equipment (slagging, fouling and ash handling). It is known that inorganic species have a significant effect on the reactivity of coal chars to air depending on the amount, type and state of the species and rank of the coal. In this paper some of the changes in the inorganic species accompanying natural weathering, and their influence on the combustion process are discussed. A brief discussion on the likelihood of operational consequences due to these changes is also provided.

Unique Nature of Naturally Weathered Crop Coals

Inorganic matter in coals is basically present in two forms - as discrete mineral matter which are particles of micron size or larger and as inorganic metal cations bonded to organic matter. It is known that low rank coals contain as much as 30 - 40% of the inorganic matter bound to the organic structure. On the other hand high rank coals contain mostly discrete mineral matter. Compositionally, a decrease in oxygen content is accompanied by a change in the relative amounts of the various oxygen containing functional groups. Oxidation, a process by which oxygen is introduced into the coal structure, may therefore reinstate some coal properties and behavior which were eliminated by progressive coalification. A decrease in carbon content and heating value and an increase in volatile matter, oxygen content and oxygen functional groups, and loss of coking properties lead to a lower apparent rank of a weathered coal compared to its fresh companion. On the other hand an increase in the aromaticity and sometimes a small increase in reflectance give the appearance of increasing the rank of a coal upon oxidation.

The samples used in this study were obtained from two active mines in Pennsylvania (Fort Palmer and N.S.M #2) and their companion crop coals were taken from the same seams. The naturally weathered samples are termed " crop" coals in keeping with practical mining terminology. These samples were ground to utility grind specifications (80% through 200 mesh) and then sealed under a nitrogen atmosphere in polyethylene bags until used. The time - temperature history during weathering for these samples is not known. Two other samples were obtained from the Penn State/DOE Coal Data Bank . The fresh sample was PSOC 1448 (York Canyon seam, New Mexico) and the corresponding weathered sample was from a surface of the same seam partially mined and exposed to the atmosphere for about 20 years.

EXPERIMENTAL

Proximate analyses were performed on a Leco MAC 400 analyzer using the standard procedure. For carbon, hydrogen and nitrogen measurements, a Leco CHN 600 analyzer was used. Total sulfur was measured on a Leco Sulfur Analyzer.

Char Preparation and Measurement of Reactivity

Preparation of the chars and measurement of the reactivity were performed in a thermogravimetric analyzer (Perkin Elmer Series 7 Thermal Analyzer). The sample size used was 5 ± 0.5 mg. The experiments involved a multistep procedure. The furnace was purged with nitrogen for one hour and heated from room temperature to 110°C at the rate of 20°C/min and held at 110°C for 5 minutes. The temperature was then ramped to 930°C at the rate of 40°C/min and held at 930°C for 7 minutes in order for devolatilization to take place. The temperature of the furnace was reduced to 450°C at 50°C/min and allowed to thermally stabilize at 450°C for 10 minutes. The heating sequence above was conducted in a nitrogen atmosphere. The reactivity of the char thus produced was determined at 450°C (723 K) in one atmosphere of air. The change in the weight of the sample with time was recorded.

To determine the effect of mineral matter on the reactivity of the companion fresh and crop coal samples, about 10 grams of each coal were acid washed with 100 ml of 10% HCl for 24 hours at about 60°C. The samples were then filtered and washed thoroughly with distilled water until the filtrate was free of chloride ions (i.e. produced no precipitate with $AgNO_3$ solution). The residue was then dried overnight in a vacuum oven at 50°C and stored for subsequent reactivity measurements.

Chemical Analyses of the Inorganic Species

Chemical analyses were performed on the samples of ash produced by ashing coals in a Leco proximate analyzer (MAC 400) at 750°C. Determination of all the major elements was performed using the atomic absorption technique described by Meddlin et al.[10]. SO_3 was determined using a Leco Sulfur titrator. The acid wash extracts were analyzed for sodium, potassium, calcium, barium, magnesium and iron by spectrochemical - Lithium metaborate fusion into solution on a Spectrometrics Spectraspan III D.C. plasma Spectrometer with a CDAC 360 Data Acquisition System.

Qualitative mineralogical analysis was performed using a Rigaku X - ray Diffractometer with the low temperature ashes produced from the coals. Ash fusion temperatures were determined using a Leco - AF600 Ash Fusion Determinator.

RESULTS AND DISCUSSION

Proximate and elemental analyses of the samples are given in Table 1. The N.S.M.#2, Fort Palmer and New Mexico fresh coals have ranks of low volatile, medium volatile and high volatile bituminous (ASTM), respectively. Differences in chemical composition between the fresh and the crop coals have been discussed in detail elsewhere[9]. The most important difference pertaining to inorganics is the lower sulfur content of the crop coals relative to their fresh companions by about 20 - 80%. This is due mainly to the oxidation of pyrite in the coals. The difference in sulfur content between the N.S.M.#2 fresh and crop coals was about 80% (3.24 versus 0.68%), whereas it was only about 20% (0.51 versus 0.41%) for the New Mexico samples because of a very low pyritic sulfur content of this coal (0.05%). The sulfatic and organic sulfur contents were 0.01 and 0.45% respectively. Table 2 lists the qualitative mineralogical analysis of the fresh and the crop coals. The data confirmed the absence of pyrite in the Fort Palmer and New Mexico weathered samples. Similarly, a lower pyrite content was observed for N.S.M.#2 crop coal relative to its fresh companion. Desulfurization by oxidation of pyrite has been reported in the literature[11]. Chandra et al.[11] reported a 93% decrease in pyritic sulfur (from 0.89 to 0.06%) accounting for 92% of the total sulfur reduction due to weathering over a four year period. This desulfurization process is believed to take place as follows[12]

$$2FeS_2 + 7O_2 + 2H_2O \text{ --------> } 2FeSO_4 + 2H_2SO_4 + \text{Heat}$$

and

$$2\,Fe^{2+} + 3H_2O + 0.5\,O_2 \text{ -------> } Fe_2O_3.H_2O + 4H^+$$

$$2Fe^{2+} + SO_4^{2-} + x\,H_2O \text{ -------> } FeSO_4.x\,H_2O$$

(various hydrated ferrous sulfates)

Some of the ferrous sulfates, being soluble in water, and sulfuric acid are responsible for acid mine drainage. However, iron sulfates such as szolmolnokite are insoluble in water.

It can be seen from Table 1 that the ash contents of the weathered coals are lower and higher than their fresh companions, i.e. there is not a definite trend. This can be explained as follows. The weight of the oxidized minerals depends on the form of iron after oxidation (for example $FeSO_4$ or Fe_2O_3) and the extent of oxidation. The acidic water may also lead to leaching of some of the acid soluble components such as calcite and depending on the acidity, some of the clay minerals may also be leached. It can be seen from Table 2 that the New Mexico Fresh sample contained calcite but the oxidized companion did not and that the ash content of the crop coal was lower than that of fresh sample due to leaching. Table 3 gives the compositional analysis of the ash samples of the fresh, crop and acid washed samples. It is noted from Table 3 that the amount of iron per unit weight of coal in the Fort Palmer and N.S.M.#2 weathered samples is higher than in their fresh companions as is their ash contents (dry basis). This suggests that the iron sulfates formed by the oxidation of pyrite in these coals are insoluble (such as szolmolnokite) and therefore the iron was not leached out. The reduction in sulfur in the two Pennsylvania crop coals was due to sulfuric acid drainage. A reduced iron content in the New Mexico weathered sample is probably due to the formation of soluble iron sulfates.

Reactivity of the Fresh and the Crop Coals

The coal samples were pyrolyzed in a nitrogen atmosphere as described earlier. The resultant chars were stabilized thermally at 450° C for 10 minutes and were then reacted with air at 450°C until at least 50% burnoff (d.a.f. basis). The first derivative of the weight versus time curve was plotted as a function of time and a typical curve is shown in Fig.1 for the Fort Palmer fresh, crop and acid washed coals. Various parameters have been used in the literature to express the reactivity of coal chars[13,14,15]. Since the burnoff time of the particle is the ultimate indicator of its reactivity, the time for 50% burnoff (d.a.f. basis) of the char was used in this study as a measure of reactivity. The time required for 50% burnoff of the fresh, crop and acid washed fresh and crop coal chars is listed in Table 4. The times required for 50% burnoff were reproducible to within $\pm$ 3 min. In all cases, the time for 50% burnoff for the crop coal chars was found to be lower than that of the corresponding fresh sample. The higher reactivity of crop coals cannot be explained by the increase in the total and accessible surface areas as discussed elsewhere[9]. Therefore, an alternative explanation is provided here.

Possibility of Catalytic Activity in the Crop Coal Chars

It has been reported that mineral matter plays an important role in the reactivity of coal chars to various gases[14,16-18] depending on the rank of the coal precursor and the state and type of inorganic species present. Jenkins et al.[14] correlated reactivity with CaO and MgO contents although the state in which the elements were present was not reported. No correlation was obtained between the reactivity and the potassium, sodium and iron contents.

Depending on the local environment, oxygen partial pressure, moisture content, the chemical nature of the overburden, the concentration of ion - exchangeable cations and pH of the percolating water, there is a possibility of some cations being bound to the carboxylic functional groups produced during weathering. Since there was an indication of the presence of salts of carboxylic acids in the DRIFT spectra of the crop coals[9] and also a significantly higher CaO content in the Fort Palmer crop coal ash (16.5%) compared to that in its fresh companion coal ash (0.81%), and a substantially higher iron content in the N.S.M#2 crop coal ash (38.6%) compared to that in its fresh coal ash (23.9%), some catalytic activity due to these differences was suspected.

Figure 2 shows a plot of the time required for 50% char burnoff (d.a.f. basis) as a function of the calcium oxide content in the coal. It can be seen that there is a trend of increasing reactivity with increasing calcium oxide content in the coal for both the weathered and fresh coals. This is similar to the trend observed by Jenkins et al.[14].

A separate reactivity test was conducted to determine the influence of catalytic activity on the reactivity of the samples. Times required for 50% burnoff on d.a.f. basis ($T_{50\%}$) were obtained for the acid washed fresh and crop coal samples and are listed in Table 4. On examining the effect of acid washing on the reactivity of the fresh coals, in which no catalytic activity is expected, it was observed that there was an increase in the reactivity of N.S.M.#2 and Fort Palmer fresh coal chars upon acid washing. This shows that the reactivity of a char is a complex phenomenon which depends on the combined effects of the change in physical structure and the chemical nature of the coal. The ranks of these two coals are low and medium volatile bituminous, respectively. For such high rank coals with low porosity, the alteration of the pore system by acid washing increases the accessibility of oxygen into the pore structure. The effect of an increase

in the number of 'feeder pores' is significant compared to the reduction of the catalytic activity due to the removal of inorganic species upon acid washing, and hence, there is a net increase in the reactivity of the N.S.M.#2 and Fort Palmer fresh coals. Jenkins et al.[14] reported such a phenomenon for a low volatile bituminous coal (PSOC 127). Also, Mahajan and Walker[19]found an increase in the nitrogen and carbon dioxide surface areas for a low volatile bituminous coal char (from PSOC 127) by factors of 2 and 3, respectively upon removing the mineral matter from the coal. From Table 4 it is also noted that for the New Mexico coal the $T_{50\%}$ of fresh sample increased marginally upon acid washing. This is again in concurrence with the observations of Mahajan and Walker[19] of no significant difference in the surface areas of raw and acid washed, high volatile bituminous coal chars. The marginal decrease in the reactivity of the New Mexico fresh sample upon acid washing, could also be due to the removal of catalytically active inorganic species.

It was also observed that acid washing reduced the reactivity and thereby increased the $T_{50\%}$ for all the crop coals reported. The $T_{50\%}$ for the acid washed crop coal was almost twice that of the crop sample for the Fort Palmer coal (59 compared to 26 min) and the Mew Mexico coal (75 compared to 46 min), whereas the $T_{50\%}$ for N.S.M.#2 acid washed crop sample was only 13% higher (119 compared to 105 min) than that of the crop coal. In light of the above discussion, this significant decrease in the reactivity of the acid washed Fort Palmer crop char was a result of the removal of inorganic species, despite the likely attendant increase in the number of 'feeder pores'. This indicates a significant contribution by the inorganic species to the reactivity of the Fort Palmer crop sample. The reactivity of the New Mexico crop sample also decreased upon acid washing and this is attributed to the removal of catalytic species during acid washing since the surface area change was found to be negligible for the high volatile bituminous coal chars[19]. The reactivity decrease or the increase in the $T_{50\%}$, in the case of the N.S.M.#2 acid washed crop sample was not very high. This is attributed to the type of catalytic species present in the coal. Table 5 gives the spectrochemical analysis of the acid extracts. The species present in significant proportions relative to those in the fresh coal extracts were calcium, magnesium and iron in the case of the Fort Palmer coal. Although some minerals such as calcite and gypsum are acid soluble, such minerals are known to be catalytically inactive[20]. Hence, the catalytic activity in the Fort Palmer and New Mexico crop coals was attributed mainly to the presence of ion-exchangeable calcium since this cation is known to be highly catalytic towards gas - carbon reactions[17,21]. In the case of the N.S.M.#2 crop coal acid washing extract, a significant proportion of iron was found compared to that in the extract from the fresh coal and since some of the iron was present in sulfate form, the catalytic activity could be due to iron in ferrous form. However, during the carbon - oxygen reaction, iron is oxidized to ferric oxide and looses its catalytic activity quickly. The slope of the weight change curve for the N.S.M.#2 crop coal was initially high and then dropped off to a lower value as can be seen from Fig. 3. The slope of the curve for the N.S.M.#2 acid washed sample tended to be more linear. As previously noted, the catalytic activity of iron depends on the ratio of ferrous to ferric and how quickly ferrous is oxidized to ferric. This explains the smaller decrease in reactivity (only 13%) on acid washing the N.S.M. #2 crop sample.

Effect of Changes in Mineral Matter on Operational and Handling aspects

The nature and amount of inorganic matter in coal are important considerations in the design of a coal fired boiler. These influence fouling of convective heat transfer surfaces and affect heat transfer characteristics. The potential for slagging and fouling depends on the inorganic constituents and the temperature they attain during combustion. A reduction in acidic oxides (SiO_2, Al_2O_3 and TiO_2) and an enrichment in CaO (from 0.8 to 16.5%) was observed for Fort Palmer crop coal ash compared to the ash from the fresh sample. Other alkali oxides such as K_2O and Na_2O did not show any significant change. Similarly, a higher iron content was noted in the N.S.M.#2 weathered sample (23.9 to 38.6%). The New Mexico ash samples did not indicate any major differences that could affect the behavior of the ash in a boiler. An increase in the basic oxides in an ash usually indicates an increased potential for fouling and slagging. Many empirical indices have been proposed to predict slagging and fouling[22]. The ASTM fusion temperature determination, although purely empirical, was developed to measure the clinkering tendency of coal ash on a grate, but it is still widely used as a method for determining ash fusibility. The ash fusion temperatures for the fresh and crop coal samples are listed in Table 6. The initial deformation temperature (I.D.T.) of the Fort Palmer crop ash is about 430° F lower than for the corresponding fresh coal ash. Similarly, the Hemispherical Temperature (H.T.) is about 250° F lower than for the corresponding fresh coal ash. Although the I.D.T of the crop coal ash is relatively low it is still high enough for use in a dry bottom furnace. The fusion temperature for the New Mexico crop sample is also lower than that of its fresh companion ash by about 250° F. The difference in fusion temperatures for N.S.M.#2 crop and fresh samples is not significant. The slagging and fouling indices defined by Attig and Duzy[23] (base/acid ratio times coal sulfur and base/acid ratio times sodium content,

respectively) were also calculated and are listed in Table 7. They are within the values generally recommended for trouble free operation.

CONCLUSIONS

Weathering causes desulfurization of coals primarily through oxidation of pyrite and the reduction in sulfur has a direct impact on SO_x emissions from combustors. Some of the metal cations are incorporated into the organic structure as ion-exchangeable cations which catalyze the combustion reactions and thereby increase the heat release rate. The composition of the ash from weathered coals indicates a significant concentration of fluxing agents such as CaO and Fe_2O_3 which is reflected in the relatively low fusion temperatures. Although the empirical parameters used to predict slagging and fouling are within safe limits, caution should be exercised when burning these crop coals.

REFERENCES

1. Huggins, F. E., Huffman, G. P., Dunmyre, G. R., Nardozzi, M. J. and Lin, M. C., Fuel Processing Technology, 1987,vol. 15, pp. 233 - 244.
2. Gray, R. J., Rhoades, A. H. and King, D. T., Trans. Of Soc. of Min. Engrs., AIME, 1976, Vol. 260, pp. 334 - 341.
3. Wachowska, H. M., Nandi, B. N. and Montgomery, D. S., Fuel, 1974, Vol. 53, p. 212.
4. Liotta, R., Brons, G. and Isaacs, J., Fuel, 1983, Vol. 62, p. 781.
5. Rhoads, C. A., Senftle, J. T., Coleman, M. M., Davis, A. and Painter, P., Fuel, 1983, Vol. 62, p. 1387.
6. Gaines, A. F., in "New Trends in Coal Science", NATO Series, Kluwer Academic Publishers, The Netherlands, 1988, p. 206.
7. Nandi, B. N., Brown, T. D. and Lee, G. K., Fuel, 1977, Vol. 56, No. 4, pp. 125-130.
8. Lee, G. K. and Whaley, H., J. of Inst. of Energy, 1983, Vol. 12, pp. 191-197.
9. Pisupati, S. V., Scaroni, A. W. and Stoessner, R. W., " Combustion Characteristics of Naturally Weathered (Insitu) Bituminous Coals", submitted to Fuel Processing Technology
10. Meddlin, J. H., Suhr, N. H. and Bodkin, J. B. Atom. Abs. News, 1969, vol. 8, p. 25.
11. Chandra, D., Chakrabarti, J. N. amd Swamy, Y. V., Fuel, 1982, Vol. 61, pp. 204 - 205.
12. Berkowitz, N., in " Sample Selection, Aging and Reactivity of Coal", Klen, R. and Wellek, R (eds), John Wiley & Sons, N.Y., 1989, P. 226.
13. Walker, P. L., Jr., and Hippo, E. J., Div. of Fuel Chem., Am. Chem. Soc., 1977, Vol 20, pp. 45 - 51.
14. Jenkins, R. G., Nandi, S. P. and Walker, P. L., Jr., Fuel, 1973, Vol. 52, pp. 288 - 293.
15. Tomita, A., Mahajan, O. P. and Walker, P. L., Jr., Fuel, 1977, Vol.56, pp. 137 - 144.
16. Walker, P. L., Jr., Shelef, M. and Anderson, R. A., "Chem. and Phy. of Carbon", Walker, P.L., Jr., (Ed.), 1969, Vol. 4, Marcell Dekker Inc., N.Y., pp. 287 - 383.
17. Morgan, B. A. and Scaroni, A. W., "Pulverized Lignite Combustion", Int. Conf. on Coal Sci., Int Energy Agency, Sydney, Australia, 1985.
18. Radovic, L. R., Walker, P. L., Jr. and Jenkins, R. G., Fuel, 1983, Vol. 62, pp. 209 -212.
19. Mahajan, O. P. and Walker, P. L.,Jr., Fuel, 1979, Vol. 58, pp. 333 - 337.
20. Tomita, A., Mahajan, O. P. and Walker, P. L.,Jr., Div. of Fuel Chem., Am. Chem. Soc., 1977, Vol. 22, pp. 4 - 6.
21. Hippo, E. J., "The Effect of Cation Exchange on the Subsequent Reactivity of Lignite Chars to Steam", Ph.D Thesis, 1977, The Pennsylvania State University.
22. Sondreal, E. A., Tufte, P. H. and Beckering, W., Comb. Sci. and Tech., 1977, Vol. 16, pp. 95 - 110.
23. Attig, R. C. and Duzy, A. F., " Coal Ash Deposition Studies and Application to Boiler Design", Am. Power Conf., April 1969.

TABLE 1
Proximate Analysis (as determined) Wt%

Mine	Moisture	Ash	F.C. (d.m.m.f)	V.M. (d.m.m.f)	Rank (A.S.T.M)
N.S.M. #2 Fresh	0.54	8.70	79.06	20.94	l.v.bit.
N.S.M. #2 Crop	4.44	9.19	75.50	24.50	m.v.bit.
Fort Palmer Fresh	0.72	13.43	75.94	24.06	m.v.bit.
Fort Palmer Crop	8.34	15.91	67.19	32.81	sub.bit.A
New Mexico Fresh	1.48	11.27	60.17	39.82	h.v.A.b
New Mexico Crop	7.29	6.07	60.83	39.16	h.v.A.b

Elemental Analysis on dry, mineral matter free basis

Mine	Carbon	Hydrogen	Nitrogen	Sulfur	Oxygen(by diff.)
N.S.M. #2 Fresh	90.23	4.68	1.56	3.24	0.29
N.S.M. #2 Crop	86.11	4.04	1.47	0.68	7.70
Fort Palmer Fresh	89.61	5.04	1.83	2.09	1.43
Fort Palmer Crop	82.05	3.90	1.66	1.24	11.15
New Mexico Fresh	87.29	5.63	1.64	0.51	4.93
New Mexico Crop	78.66	4.24	1.70	0.41	14.99

TABLE 2
Qualitative Mineralogical Analysis

Mineral	N.S.M.#2 Fr	N.S.M.#2 Cr	F.P. Fr	F.P. Cr	N.M. Fr	N.M. Wea.
Kaolinite	X	X	X	X	X	X
Quartz	X	X	X	X	X	X
Pyrite	X	X	X	--	X	--
Illite			--	X		
m.l.c			X	--		
Calcite					X	--
Bassanite			--	X		
Fe sulfates	--	X	--	X		
Feldspars			X	--		

Fr = Fresh, Cr = Crop and Wea = Weathered

TABLE 3

Analyses of the Ashes (wt%)

Oxide	FPF	FPW	NSMF	NSMW	NMF	NMW	FPFAW	FPWAW	NMFAW	NMWAW
SiO_2	55.9	38.3	43.2	34.5	40.5	37.2	61.0	58.0	65.0	57.4
Al_2O_3	26.9	20.2	25.6	22.1	23.9	29.0	27.8	29.4	29.6	32.4
TiO_2	1.42	0.96	1.46	0.98	1.06	1.36	1.45	1.57	1.68	1.84
Fe_2O_3	10.3	9.31	23.9	38.6	7.00	9.02	6.89	5.99	1.88	2.55
MgO	0.59	1.33	1.12	0.48	2.11	2.97	0.48	0.7	0.49	0.96
CaO	0.81	16.5	2.71	1.24	15.7	11.0	0.26	1.53	0.48	2.17
MnO	0.02	0.03	0.03	0.02	0.01	0.02	0.01	0.01	0.01	0.01
Na_2O	0.57	0.45	0.22	0.22	1.09	2.13	0.61	0.85	0.74	1.41
K_2O	2.08	1.65	2.11	2.11	0.54	0.79	2.09	2.63	0.85	0.61
P_2O_5	0.38	0.41	0.3	0.18	1.39	1.67	#	#	#	#
SO_3	0.1	10.9	<0.05	<0.05	5.5	*	<0.05	<0.05	<0.05	<0.06
Total	99.1	100.0	100.7	99.4	98.8	95.2	100.6	100.7	100.7	100.0

FPF : Fort Palmer Fresh FPW: Fort Palmer Crop NSMF: N.S.M.#2 Fresh NSMW: N.S.M. # 2 Crop
NMF: New Mexico Fresh NMW: New Mexico Weathered FPF AW : Fort Palmer Fresh, Acid Washed FPW AW: Fort Palmer Crop, Acid Washed
NMF AW: New Mexico Fresh, Acid Washed NMW AW: New MexicoWeathered, Acid Washed

TABLE 4
Times for 50% Burnoff of Char (d.a.f. basis, min)

Sample	Original Coal Char	Acid Washed Coal Char
Fort Palmer Fresh	345	242
Fort Palmer Crop	26	59
N.S.M.#2 Fresh	668	572
N.S.M.#2 Crop	105	119
New Mexico Fresh	98	102
New Mexico Crop	46	75

TABLE 5
Spectrochemical Analysis of the Acid Extracts

Cation	Concentration (μ g / g of daf coal)					
	F.P. Fr.	F. P. Cr.	N.S.M.#2 Fr.	N.S.M.#2 Cr.	N.M. Fr.	N.M. Cr
Barium	82	181	47	144	555	580
Calcium	660	16634	608	1616	11786	4323
Iron	3690	9826	5891	13464	4853	3396
Potassium	260	470	140	287	372	438
Magnesium	140	1184	NA	NA	1450	988
Sodium	188	140	65	45	693	618

TABLE 6
Ash Fusion Temperatures (°F)

Sample	Initial Deformation	Softening	Hemispherical	Fluid
Fort Palmer Fresh	2775	2805	2830	2845
Fort Palmer Crop	2340	2375	2470	2590
N.S.M. # 2 Fresh	2540	2570	2595	2600
N.S.M. # 2 Crop	2540	2555	2560	2565
New Mexico Fresh	2435	2465	2480	2500
New Mexico Crop	2215	2405	2420	2425

TABLE 7
Slagging and Fouling Indices *

Sample	Slagging Index	Fouling Index
Fort Palmer Fresh	0.35	0.10
Fort Palmer Crop	0.61	0.22
N.S.M.#2 Fresh	1.39	0.10
N.S.M.#2 Crop	0.50	0.16
New Mexico Fresh	0.20	0.44
New Mexico Crop	0.16	0.94

* Attig and Duzy [23]

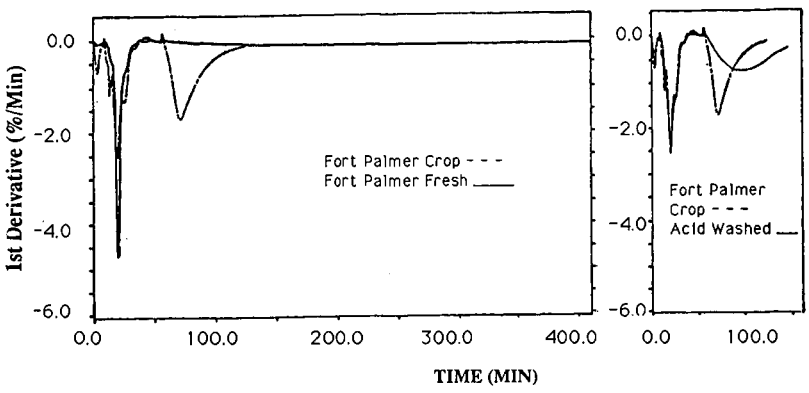

FIG.1. RATE OF WEIGHT LOSS (DERIVATIVE) AS A FUNCTION OF TIME FOR FORT PALMER FRESH, CROP AND ACID WASHED COALS

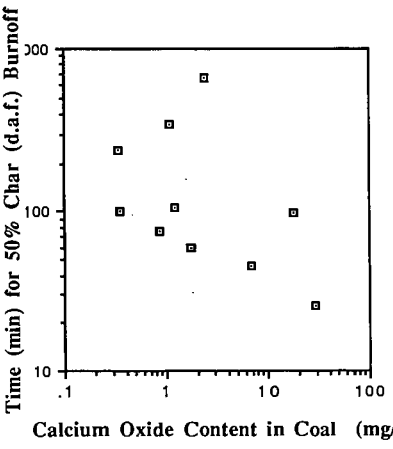

FIG.2. TIME FOR 50% BURNOFF (D.A.F.) AS A FUNCTION OF CALCIUM OXIDE CONTENT IN COAL

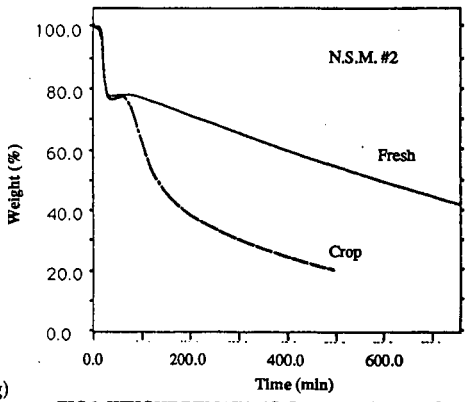

FIG.3. WEIGHT REMAINING CURVES AS A FUNCTION OF TIME FOR N.S.M. #2 FRESH AND CROP COALS

ENERGETIC DISTRIBUTIONS OF OXYGEN SURFACE COMPLEXES ON POROUS CARBONS AND CHARS

P.J. Hall and J.M. Calo
Chemical Engineering Program
Division of Engineering
Brown University
Providence, Rhode Island 02912

Keywords: Carbon-oxygen surface complex energetics; temperature programmed desorption; TPD spectra deconvolution.

INTRODUCTION

When an oxidized coal char is subjected to a program of increasing temperature, the surface oxides desorb primarily as the oxides of carbon, CO and CO_2 (e.g., [1]). This process produces TPD spectra which can be interpreted in terms of the energetic state of chemisorbed surface complexes and interaction phenomena occurring within the char structure during the TPD process. The latter have been shown to be [2]: (1) the desorption of rechemisorbed CO released at lower temperatures, appearing primarily as a feature centered typically *ca.* 1200K; and (2) secondary CO_2 evolution which appears as a reflection or satellite peak under primary CO desorption features. We have attributed the latter to:

$$CO(g) + C(O) \Leftrightarrow C_f + CO_2(g) \qquad [R.1]$$

where: CO(g) represents "free," gaseous CO resulting from the desorption of a surface oxygen complex; C(O) is a surface oxygen complex; and C_f is an unoccupied surface active site.

From the perspective of previous work, including our own, there appear to be two principal obstacles to the direct application of TPD to the understanding of the behavior of oxygen surface complexes: (1) a more quantitative interpretation of the data; (2) deconvolution of secondary interactions from TPD spectra in order to enable the analysis of such data in terms of the energetics of the surface complexes. These issues are addressed in the current communication.

EXPERIMENTAL

Chars were prepared from Pittsburgh #8 and Wyodak coals obtained from the Argonne Premium Coal Sample Bank *via* pyrolysis in ultrahigh purity helium at 1273K with a soak time of 1 hour.

The TPD apparatus and methods have been described elsewhere [2]. The most salient experimental details are as follows. Char oxidation/gasification was performed in a TGA

apparatus in 0.1 MPa O_2 at the temperatures noted. Following cooling to room temperature in the TGA apparatus, the samples were transferred to a TPD reactor. Tests involving comparisons of TPD spectra obtained using this procedure with those following *in situ* oxidation in the TPD reactor have shown that transfer of the sample does not affect the resultant spectra.

The TPD reactor was constructed from a high-purity silica tube, 1-cm inside diameter, within which a close-fitting, circular silica sinter is used to support the sample. Ultrahigh purity helium carrier gas is passed over the sample in downflow. Heating is accomplished electrically via nichrome wire wrapped around the outside of the silica tube, powered by a high current variable transformer. The heating regimen is controlled by a microcomputer. The resultant TPD reactor has a low thermal capacitance which allows linear heating rates of up to 500K/min.

Detection of desorbed species is accomplished with a quadrupole mass spectrometer (MS) which samples a small portion of the carrier flow. The MS output is fed to a microcomputer which also provides for multiple species detection via mass programming.

Typical sample sizes for the TPD measurements were ~10 mg. This size resulted in less than a monolayer coverage on the silica frit that was used as the sample holder in the TPD reactor. This, when combined with high helium carrier gas sweep rates, insured the absence of secondary interactions between the bulk gas species and the char samples.

Repeated experiments with char samples obtained from the same batch indicate that the reproducibility of gas desorption rates is approximately ±10%. This error is attributable to a combination of effects arising primarily from sample inhomogeneity, sample size and MS calibration. For this reason, the spectra reported are representative, rather than averages.

RESULTS AND DISCUSSION

Deconvolution of TPD Spectra.

Over the course of examining many TPD spectra from oxygen-oxidized chars, it was noted that the leading edge of the *total oxygen* (i.e., $CO+2CO_2$) desorption feature centered *ca.* 1000K always seems to be reasonably well approximated by a Gaussian distribution. For this reason, it was decided to investigate the deconvolution of the total oxygen production rate into two contributions - one as a Gaussian centered at the maximum rate of production, with the variance determined from the leading edge of the 1000K peak, and the other as a higher temperature residual difference peak. The results of such a deconvolution for spectra obtained from an oxidized Wyodak coal char are presented in Figure 1. As shown, the Gaussian approximation is quite reasonable for describing the leading edge of the total oxygen distribution, and the residual peak appears to be relatively smaller and non-Gaussian.

As it stands, such a deconvolution is nonunique, and thus we are faced with the question of whether the high temperature end of the 1000K oxygen peak remains near-Gaussian in the region

where it cannot be directly observed. There is some experimental evidence in support of this hypothesis.

One such piece of evidence is provided by a set of previously reported experiments with Wyodak coal char [3] in a slightly different context, and re-analyzed here. The coal char was gasified to 15.2% burn-off (in 0.1MPa oxygen at 623K) in the TGA apparatus. In the current analysis only the CO data are analyzed, although similar results were found for total oxygen spectra as well, due to the relatively minor contribution of the CO_2 in this case. A sample of the gasified char was *partially cleaned* by heating to 1100K at 100K/min, and was then quickly cooled (at a rate exceeding 200K/min) in ultrahigh purity helium. This was done not only to remove complexes stable below 1000K, but also as an attempt to effectively "titrate" the high temperature sites suspected of involvement in CO re-adsorption that give rise to the 1200K peak in TPD spectra. A second sample of the same coal char, oxidized under the same conditions, was subjected to TPD to 1100K and quick cooling in He to room temperature. Then, a TPD was carried out to 1400K. The result of this experiment is the "high temperature - clean" CO spectrum [HT] presented in Figure 2. The "partially cleaned" sample, with high temperature CO remaining on the surface, was then re-oxidized in the TPD apparatus under non-gasifying conditions in 0.1MPa of oxygen at 473K for 12 hours. We have shown that this treatment effectively reoxidizes practically all the surface sites created during the original gasification for the Wyodak coal char [3]. TPD was then carried out on this partially cleaned and reoxidized char, and this result is designated as the [PC] spectrum in Figure 2. The difference between the "high temperature - clean" TPD [HT] and the "partially cleaned/reoxidized" TPD [PC] then represents the surface oxygen added during reoxidation. This is designated as [HT-PC] in Figure 2. From the arguments presented above, this difference spectrum should be uncomplicated by CO re-chemisorption, and the resultant distribution should, therefore, be reflective of the original state of the oxygen chemisorbed during reoxidation. As shown in the figure, a Gaussian distribution seems to fit the difference spectrum reasonably well. This agreement suggests that the *intrinsic* 1000K peak for oxygen production may indeed be Gaussian over its entire range.

Energetic Distributions.

In view of the available evidence in support of a Gaussian distribution for the 1000K feature, the question naturally arises as to what the physical basis may be for this type of distribution. In considering this question, it is useful to transform the TPD spectra from a temperature to a desorption energy basis, using a procedure derived from the original work of Redhead [4]. A brief outline of the derivation follows.

For a *continuous* distribution of *i* species on a *heterogeneous* surface, each obeying a first order desorption rate law characterized by a single desorption activation energy, E_i, there must also be a *continuous* distribution of maximum desorption temperatures, $T_{p,i}$, one for each of the *i* species. These are related to the E_i *via* a familiar expression derived by Redhead [4]. Since the relationship between desorption activation energy and temperature is very nearly linear over

a large range of parameter values, this is closely approximated by the expression:

$$E_i/RT_{p,i} = \ln [\nu_o T_{p,i}/\beta] - 3.64, \quad [1]$$

which for $10^{13} > \nu_i/\beta > 10^8$ (K^{-1}), was shown to be accurate to within $\pm$ 1.5% [4].

If the $T_{p,i}$ are described by a continuous probability density function, then each instantaneous temperature, T, during a heating regimen must also correspond to some $T_{p,i}$. As a consequence, an expression like Eq. [1] provides a direct transformation between the observed experimental desorption temperature, T, and the desorption activation energy distribution, $S(E_i)$. Furthermore, since Eq.[1] is evaluated at the peak temperature, $T_{p,i}$, then the heating rate, β, is rigorously defined as the local *instantaneous* heating rate at $T_{p,i}$, or, more generally, at temperature T. Therefore, Eq. [1] applies to a first order desorption process for any monotonic heating regimen exhibiting a maximum in desorption rate.

An analysis of the continuity expression for surface oxygen complexes can be shown to yield the following expression for the total desorption rate of CO from the surface:In this expression,

$$d[CO]/dt = [C\text{-}O]_o \, S(E^*) \, dE^*/dt \quad [2]$$

where $[C\text{-}O]_o$ is the total amount of oxygen surface complex initially on the char surface, $S(E^*)$ is the probability density function of desorption activation energies, and dE^*/dt is the time derivative of the desorption activation energy during the heating regimen. In deriving this expression, the resultant integral over the distributed desorption rate constant was approximated as a step function occurring at a critical activation energy, E^* (*cf.* [5,6]), since it increases over a very narrow energy range from zero to unity. Since a TPD experiment yields the instantaneous d[CO]/dt directly, then knowledge of E^* and dE^*/dt defines the initial energetic distribution of surface complex, $[C\text{-}O]_o S(E^*)$, experimentally. Differentiating Eq. [1]:

$$dE^*/dt = R\beta \, [E^*/RT] = R\beta \, [\ln (\nu_o T/\beta) - 3.64]. \quad [3]$$

Combining Eqns. [2] and [3], then yields the energetic distribution of surface complexes as:

$$[C\text{-}O]_o S(E^*) = \{d[CO]/dt\}/\{R\beta \, [\ln (\nu_o T/\beta) - 3.64]\}. \quad [4]$$

From this expression, the energetic distribution of oxygen surface complexes can be determined experimentally from TPD spectra. Eq. [4] indicates that this transformation is practically linear for constant heating rate, β; i.e., the logarithmic term does not vary appreciably over the TPD temperature range. Thus, for *linear* TPD, if the distribution of the surface complex desorption in temperature is Gaussian, then the distribution of desorption activation energies will be close to

Gaussian as well.

One interpretation of a Gaussian energetic distribution is that the oxygen surface complexes exhibit a continuum, random distribution of binding energies. For many typical coal chars, most of the surface area and, consequently, most of the oxygen complexes, are present in micropores. In these small pores of molecular dimensions, the effective binding energies of the complexes would be strongly influenced by the local environment, the presence of neighboring complexes etc., and thus may be randomly distributed. For example, an oxygen atom could be bound to opposing walls of a micropore (e.g., an ether linkage). The binding energy of such a complex would vary according to the local width of the micropore, and, ultimately, in a very wide micropore, or a mesopore, the complex could be bound to only one wall, thereby assuming a semiquinone or carbonyl character. In other words, oxygen functional groups that may otherwise be chemically distinct on an "open" surface, may ultimately "blend" into one another in a multi-surface environment of molecular dimensions, as in micropores.

This *rationale* for a Gaussian distribution of desorption activation energies suggests that the resultant energetic distribution should be a characteristic property of the char and its porosity, and *not* a function of heating rate. In order words, once the distribution of desorption activation energies is known, it should enable the prediction of desorption spectra obtained under any heating regimen. In addition, the fact that it is the *total oxygen* distribution that appears to be Gaussian supports the hypothesis that the secondary interaction features arise primarily from the same source as the "1000K CO." These points are demonstrated below using TPD data obtained from Pittsburgh #8 coal char.

In Figure 3 is presented a 100K/min total oxygen TPD spectrum from a sample of Pittsburgh #8 coal char gasified to 10% burn-off at 723K in 0.1MPa of O_2, along with a Gaussian fit to the leading edge of the principal desorption feature. As discussed above, the high temperature peak/shoulder is believed to originate primarily from CO originally liberated during desorption of the 1000K oxygen complexes and re-chemisorbed to be liberated once again as "1200K CO." Therefore, in order to be consistent in reconstructing the original state of the oxygen complex distribution on the char surface, the additional oxygen represented by the difference between the integral over the total oxygen desorption and the Gaussian fit to the 1000K peak should be added to the latter to yield a "corrected" Gaussian, as shown in Figure 3. For example, for the Pittsburgh #8 coal char sample this amounted to an amplitude correction (increase) of 20%.

The "corrected" Gaussian distribution was then transformed into an energetic distribution using Eq. [4]. As indicated above, for a linear heating rate, the transformation between the TPD spectrum with respect to temperature and the energetic distribution is practically linear, so that the resultant S(E*) distribution is also quite close to Gaussian as well. The construction of this distribution requires the assumption of values for the pre-exponential frequency factor, ν_o. Originally we tried using ν_o=kT/h, the frequency factor predicted by transition state theory.

However, this did not result in the best fits to total oxygen TPD spectra obtained at different heating rates for the same char. In any case, these values are simply estimates. Therefore, it was decided to vary ν_o in such a manner as to obtain the best fit to TPD spectra obtained at the nominal heating rates of 20, 100, and 300K/min. The calculations were, therefore, iterative, and were performed using a spreadsheet program. Essentially, the procedure involved assuming a value of ν_o to obtain an energetic distribution from the 100K/min data. This distribution was then used to predict the 20 and 300K/min total oxygen TPD spectra, "corrected" for rechemisorbed oxygen as described above. The final energetic distribution, arrived at in this manner, was approximately Gaussian with a mean of 48.8 kcal/mol and a standard deviation of 6.9 kcal/mol. The total amount of surface oxygen was 2.4 mmol/g. A value of $\nu_o = 10^{11}$ min^{-1} yielded the best predictions, although reasonable results were also obtained over a range of ν_o of about an order of magnitude in either direction, so this value is not necessarily unique. A summary of the final TPD curves, predicted from the energetic distribution, for the three heating rates used, along with the corresponding "corrected" data, are presented in Figure 4.

CONCLUSIONS

Based on these results, it is concluded that Gaussian deconvolution of the 1000K peak from total oxygen TPD spectra seems to be a reasonable approximation. The amount of rechemisorbed CO may be estimated using this procedure. The resultant Gaussian spectra can be transformed to obtain the probability density distribution function of desorption activation energies which is related to the energetic state of oxygen complexes on coal char surfaces. This distribution is a characteristic property of the char and can be used for kinetic predictions involving the thermal desorption rates of such complexes, and/or as a diagnostic of the nature of the active sites.

The authors believe that the quantitative description of char surfaces *via* energetic distributions represents a new and more fundamental approach to all issues related to char reactivity. It is anticipated that techniques arising from such descriptions will eventually supplant more empirical methods.

Acknowledgement. This work was supported by the Morgantown Energy Technology Center of the Department of Energy under Contract No. DE-AC21-MC23284.

REFERENCES

1. Tremblay, G.; Vastola, F.J.; Walker, P.L., Jr., *Carbon* **1978,** *16,* 35.
2. Hall, P.J.; Calo, J.M., *Energy & Fuels* **1989,** *3,* 370.
3. Hall, P.J.; Calo, J.M.; and Otake *Proc. Nineteenth Biennial Conf. Carbon,* **1989,** p. 594.
4. Redhead, P.A. *Vacuum* **1962,** *12,* 203.
5. Suuberg, E.M. , *Comb. Flame* **1983,** *50,* 243.
6. Du, Z., Sarofim, A.F., and Longwell, J.P. *Energy & Fuels* **1990,** in press.

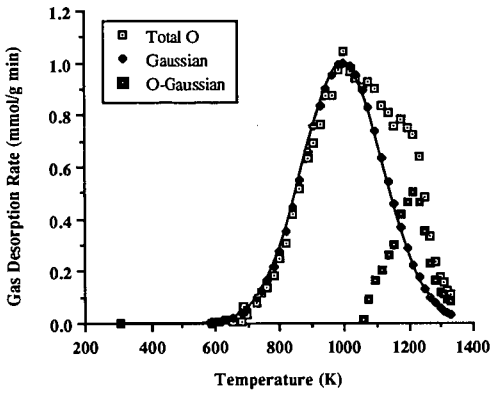

Figure 1. Deconvolution of 100K/min total oxygen TPD spectra from Wyodak coal char gasified to 15.2% burn-off in 0.1MPa of O_2 at 350°C into a Gaussian and a residual.

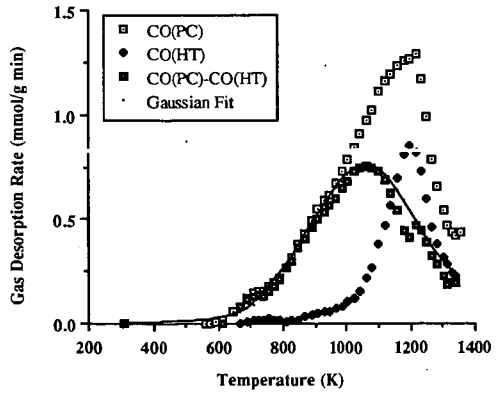

Figure 2. 100K/min CO TPD spectra from Wyodak coal char, originally burned-off to 15.2% in 0.1MPa O_2. CO(PC): after partial cleaning to 1100K and re-oxidation in 0.1MPa O_2 at 200°C for 12h; CO(HT): residual high temperature surface complexes after partial cleaning to 1100K; CO(PC)-CO(HT): difference spectrum.

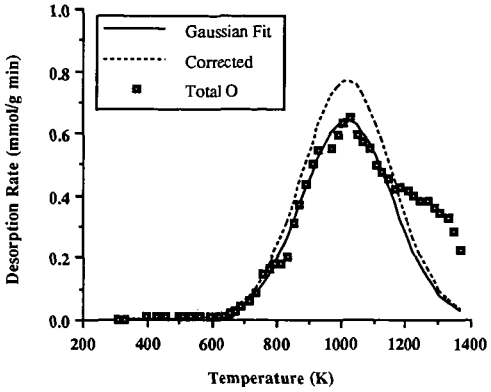

Figure 3. 100K/min total oxygen TPD spectrum from Pittsburgh #8 coal char gasified to 10% burn-off in 0.1MPa of O_2 at 723K, and Gaussian fits; both direct and "corrected."

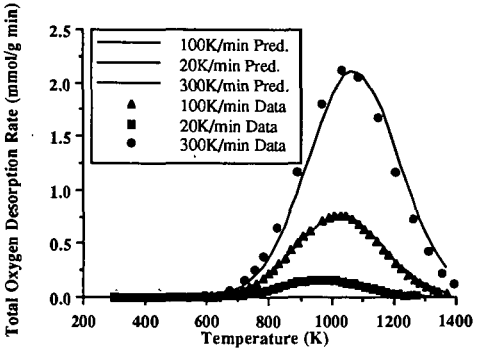

Figure 4. Total oxygen TPD spectra as a function of linear heating rate for Pittsburgh #8 coal char burned-off to 10% in 0.1MPa O_2 at 723K; both "corrected" data and predictions.

MASS SPECTROMETRIC STUDIES OF THE CHEMICAL COMPOSITION OF COAL TARS PRODUCED IN A LAMINAR FLOW REACTOR

Robert Lo, Ronald J. Pugmire*, Thomas H. Fletcher**,
and Henk L.C. Meuzelaar

Center for Micro Analysis and Reaction Chemistry
*Department of Fuels Engineering
University of Utah, Salt Lake City, UT 84112
**Sandia National Laboratories, Livermore, CA

ABSTRACT

Curie-point desorption in combination with Gas Chromatography/Mass Spectrometry (GC/MS) and, alternatively, with direct Low Voltage Mass Spectrometry (LV-MS) was used to investigate the chemical composition and structure of condensed tar vapors produced during rapid devolatilization (heating rate ~ 10,000 K/sec) of carefully sized coal particles representing the Beulah Zap, Big Blue, Illinois #6, Pittsburgh #8, and Pocahontas #3 seams, respectively, using the laminar flow reactor described by Fletcher et al [1]. at two gas temperatures (1050 K and 1250 K).

Tar samples were collected by means of a special probe [1] at different points downstream of and corresponding to residence times between 70 and 250 msec. GC/MS analyses of the corresponding tars indicate that the degree of aromaticity increased rapidly as a function of residence time at the 1250 K gas temperature condition. Moreover, at 1250 K devolatilization is complete within 70 msec and beginning secondary gas phase reactions of tar vapors (viz. marked increases in PNAH content and corresponding decreases in phenolic components) are observed within less than 100 msec. However, at 1050 K the coal devolatilization process appears to be barely complete after 250 msec and little or no evidence of secondary gas phase reactions is found.

INTRODUCTION

Recent devolatilization studies [1-5] have identified the rates and the temperature regimes of pulverized coal devolatilization as a function of heating rate, final temperature, and coal type. Careful particle temperature measurements during devolatilization at rapid heating conditions [1-2] have eliminated many uncertainties caused by estimations of particle temperatures in early studies.

Current devolatilization models have advanced beyond one-step Arrhenius kinetics to descriptions of the bonding structure in the coal, metaplast, and tar [6-9]. Other models include detailed empirical correlations to estimate yields of tar products from elemental compositions of the parent coal [10], as well as mechanism to describe the evolution of the physical structure of char particles [11]. Most of these models presume a mechanisms for generation of metaplast during pyrolysis, followed by release of lighter fractions of the metaplast as tar vapor, where tar is commonly defined as pyrolysis products that condense at room temperature and pressure. It is clear that quantitative experimental investigations of the evolution of the chemical structure of solid and condensible pyrolysis products (char and tar) are critical to the understanding of coal devolatilization mechanisms.

The present study addresses the characterization of condensible tar vapors, produced by rapid (~10^4 K/sec) heating of pulverized coals in a laminar flow reactor. Curie-point desorption GC/MS and

direct Low Voltage MS methods were used to characterize tar samples at the molecular level and to elucidate some of the underlying reaction mechanisms.

EXPERIMENTAL

Reactor and Sample Collection System:

Experimental details regarding the particle temperature measurements and sample collection system were previously published [1], and hence only a brief discussion will be given here. The pyrolysis studies were performed in 100% nitrogen in a laminar flow reactor [1]. Transparent (quartz flass) flow reactor walls allow radiant emission from the coal particles to be monitored at any axial location. Two gas temperature conditions were used in this study, with maximum centerline gas temperatures of 1050 and 1250 K.

An infrared sizing pyrometer system was used to measure size, temperature, and velocity of individual particles in the flow reactor at different axial locations. Typical standard deviations in measured particle temperatures are 5 K for pure carbon spheres (Spherocarb) and 30 K for coal particles. A water-cooled, helium-quench probe was used to collect solid samples iso-kinetically. A virtual impactor and three-stage Andersen cyclone system were used to aerodynamically separate char particles from condensed tar vapors and aerosols. Tars were collected on polycarbonate filters following the separation system [1].

Collected tars were shipped overnight to the analytical facility frozen in an ice chest and stored at -90 C. Five milligrams of the tar samples were suspended in 1 ml of Spectrograde methanol and the homogeneity of each suspension enhanced with a vibrating mixer.

Curie-Point GC/MS and Low Voltage MS Analyses:

GC/MS analyses of the tar samples were performed using a Hewlett-Packed 5890 chromatograph with a 15 m x 0.25 mm i.d. x 0.25 μm film thickness DB-5 column (J&W Scientific). The conditions used in GC/MS were as follows : electron energy 70 eV, Ion Trap Dector (ITD, Finnigan MAT) scanned from m/z 40-450 at 1 scan/sec, pyrolysis time 2 sec, 610 C Curie-point wires in an inlet set at 250 C. The column was temperature programmed from 40-300 C at 15 C/min.

LV-MS experiments were carried out using an Extranuclear Model 5000-1 Curie-point pyrolysis MS system. Twenty five microgram quantities of tar sample were coated on ferromagnetic wires from methanol suspensions. The wires were inserted into borosilicate glass reaction tubes and introduced into the vacuum system of the mass spectrometer. The ferromagnetic wires were inductively heated at approx. 100 C/s to an equilibrium temperature of 610 C. Total heating time was 10 s. LV-MS conditions were as follows : electron ionization at 12 eV (set value), scanning rate 1000 amu/s, total scanning time 20 s, mass range scanned m/z 40-260.

RESULTS AND DISCUSSION

Low Voltage mass spectra of tars obtained by Curie-point desorption directly in front of the ion source and representing two different coals are shown in Figure 1a-e. Comparison of the Beulah Zap tar sample produced at 1250 K and collected after 70 msec with the corresponding 250 msec sample shows major changes characterized by a marked decrease in hydroxyaromatic signals (e.g., alkylsubstituted phenols, dihydroxybenzenes and naphthalenes) accompanied by a strong increase in polycondensed aromatic hydrocarbons, e.g., phenanthrenes and pyrenes, in the 250 msec sample. Apparently, this marked change is due to secondary reactions. Especially the dominance of unsubstituted

pyrene among the various alkylsubstituted homologs is a telltale sign of high temperature gas phase reactions and may perhaps be seen as a first step in the direction of soot formation.

The Beulah Zap tar pattern at 70 msec, on the other hand, compares well with direct Curie-point pyrolysis mass spectra of North Dakota coal [12], indicating that at 70 msec primary pyrolysis products (e.g., dihydroxybenzenes) still dominate, although the yield of polycondensed aromatic hydrocarbons e.g., (alkyl) phenanthrenes, is already higher than would be observed under vacuum micropyrolysis conditions. The tar patterns of Pittsburgh #8 coal at 1250 K (Figures 1c and d) are in excellent agreement with these observations. Again the short residence time pattern (80 msec) corresponds quite well with the Curie-point pyrolysis mass spectrum, e.g. as reported by Chakravarty et al. [13], whereas the long residence time (250 msec) tar shows a pronounced shift towards polycondensed aromatic hydrocarbon. Due to the higher rank (hvAb) of the Pittsburgh #8 coal, however, the short residence time spectrum (Figure 1c) is clearly different from that of the Beulah Zap lignite, e.g., with regard to the lower (alkyl) dihydroxybenzene intensities and increased (alkyl) naphthalene series. This is in agreement with trends observed in earlier Py-MS studies of coals of different rank [14].

Finally, the effect of temperature is briefly illustrated in Figure 1e (Pittsburgh #8, 1050 K). In spite of the long residence time (250 msee) the MS pattern in Figure 1e is highly simlar to that in Figure 1c, indicating the absence of marked secondary reactions at this lower temperature.

The usefulness of Curie-point desorption GC/MS techniques for confirming and further elucidating the above discussed trends and effects is illustrated in Figures 2 and 3. Illinois #6 tars produced at 1250 K and collected after 70 msec (Figure 2) and 250 msec (Figure 3), respectively, show an approx. 100 X reduction in the relative abundance of (alkyl) phenols accompanied by a 10 X increase in selected polycondensed (4-6 ring) aromatic hydrocarbons.

Although in the current experimental set-up absolute tar yields cannot yet be established with sufficient certainty to enable precise quantitative studies, e.g., for determining the kinetics of the gas phase condensation reactions, changes in the relative composition as a function of residence time are illustrated for Big Blue tars at 1050 K in Figure 4 and for Beulah Zap, Illinois #6 and Pittsburgh #8 tars in Figures 5a, b and c, respectively. At 1050 K fragment ions of aliphatic hydrocarbons (e.g., at m/z 85, 57, 43, see Figure 4c) dominate the short residence time (120 msec) tar. Based on previous, time-resolved pyrolysis field ionization MS studies [15], early evolution of aliphatic hydrocarbon moieties during devolatilization of low rank coals is likely to represent the desorption of low MW biomarker type compounds, e.g., branched and/or alicyclic terpenoids. At 150 msec the relative intensities of the aliphatic hydrocarbon moieties are starting to decrease due to the strong increase in hydroxyaromatics. e.g., dihydroxybenzenes at m/z 110 and 124 (Figure 4b). Finally, at 250 msec, the relative abundance of compounds such as naphthols, are still increasing suggesting that the devolatilization process may not yet be fully completed. On the other hand, suspected secondary reaction products such as pyrenes and perylenes are starting to increase slightly. Nevertheless, the relative abundance of the highly reactive dihydroxybenzenes appears to be more or less stable. Altogether, our tentative conclusion is that at 1050 K the devolatilization process of Big Blue coal is close to being complete after 250 msec.

A drastically different picture is obtained at 1250 K, as illustrated for the three coals in Figure 5. Compounds such as pyrenes, perylenes and even picenes appear to be increasing right from the start, whereas the relative abundances of naphthols and even phenanthrenes are decreasing after approx. 100-150 msec., suggesting the occurrence of marked secondary gas phase reactions. Unfortunately, at the time of writing no tar samples had been produced at intermediate temperatures, e.g., 1150 K. If the above observations at 1050 and 1250 K are correctly interpreted, devolatilization at 1150 K should be completed within 100-200 msec and the onset of secondary gas phase reactions should become clearly visible at longer residence times.

CONCLUSIONS

Based on the Curie-point GC/MS and Low Voltage MS analyses of the tar formed during devolatilization of Beulah Zap, Big Blue, Illinois #6, Pittsburgh #8, and Pocahontas #3 coals, the following conclusions are reached:

1. The degree of aromaticity increases rapidly as a function of residence time at the 1250 K gas temperature.
2. However, little increase in aromaticity can be detected at the 1050 K gas temperature.
3. At a gas temperature of 1250 K devolatilization is complete within 70 msec and secondary gas phase reactions of tar vapors can be observed within 100 msec.
4. At 1050 K, the devolatilization process appears to be more or less complete after 250 msec.
5. In order to study complete devolatilization process and the possible onset of secondary reactions, further experiments should be conducted at an intermediate temperature, e.g., 1150 K.

ACKNOWLEDGEMENTS

This work was sponsored by the Advanced Combustion Engineering Research Center (funds for this Center are received from the National Science Foundation, the State of Utah, 23 industrial participants and the U.S. Department of Energy) and by the Consortium for Fossil Fuel Liquefaction Science (DOE grant no. UKRF-4-23576-90-10).

REFERENCES

1. Fletcher, T.H., Comb & FLame, 78, pp.223-226, 1989.
2. Solomon, P.R., Serio, M.A., Carangelo, R.M., and Markham, J.R., Fuel 65, pp.182, 1986.
3. Freihaut, J.D., and Proscia, W.M., Energy & Fuels, 3, pp. 625, 1989.
4. Gibbons-Matham, J., and Kandiyoti, R., Energy & Fuels, 2, pp. 505, 1988.
5. Serio, M.A., Hamblen, D.G., Markham, J.R., and Solomon, P.R., Energy & Fuels, 1, pp. 138, 1987.
6. Niksa, S., and Kerstein, A.R., Comb & Flame, 66, pp. 95, 1986.
7. Solomon, P.R., Hamblen, D.G., Carangelo, R.M., Serio, M.A., and Deshpande, G.V., Energy & Fuels, 2, pp. 405, 1988.
8. Grant, D.M., Pugmire, R.J., Fletcher, T.H., and Kerstein, A.R., Energy & Fuels, 3, pp. 175, 1989.
9. Fletcher, T.H., Kerstein, A.R., Pugmire, R. J., and Grant, D.M., accepted for publication, Energy & Fuels, 1989.
10. Ko, G.H., Sanchez, D.M., Peters, W.A., and Howard, J.A., Twenty-Second Synp. (Int.) on Comb., The Combustion Institute, pp. 115, 1988.
11. Oh, M.S., Peters, W.A., and Howard, J.B., AIChE Journal, 35:5, pp. 775, 1989.
12. Metcalf, G.S., Windig, W., Hill, G.R.,and Meuzelaar, H.L.C., Internatioanl Journal of Coal Geology, 7, pp. 245-268, 1987.
13. Chakravarty, T., Windig, W., Taghizadeh, K., and Meuzelaar, H.L.C., Energy & Fuels, 2, pp. 191-196, 1988.
14. Meuzelaar, H.L.C., Harper, A.M., Hill, G.R., and Given, P.H., Fuel, 63:5, pp. 640-652, 1984.
15. Yun, Y., Meuzelaar, H.L.C., Simmleit, N., and Schulten, H.-R., "The Mobile Phase in Coal Viewed from a Mass Spectrometric Perspective", ACS Symp. Series, 1990, in press.

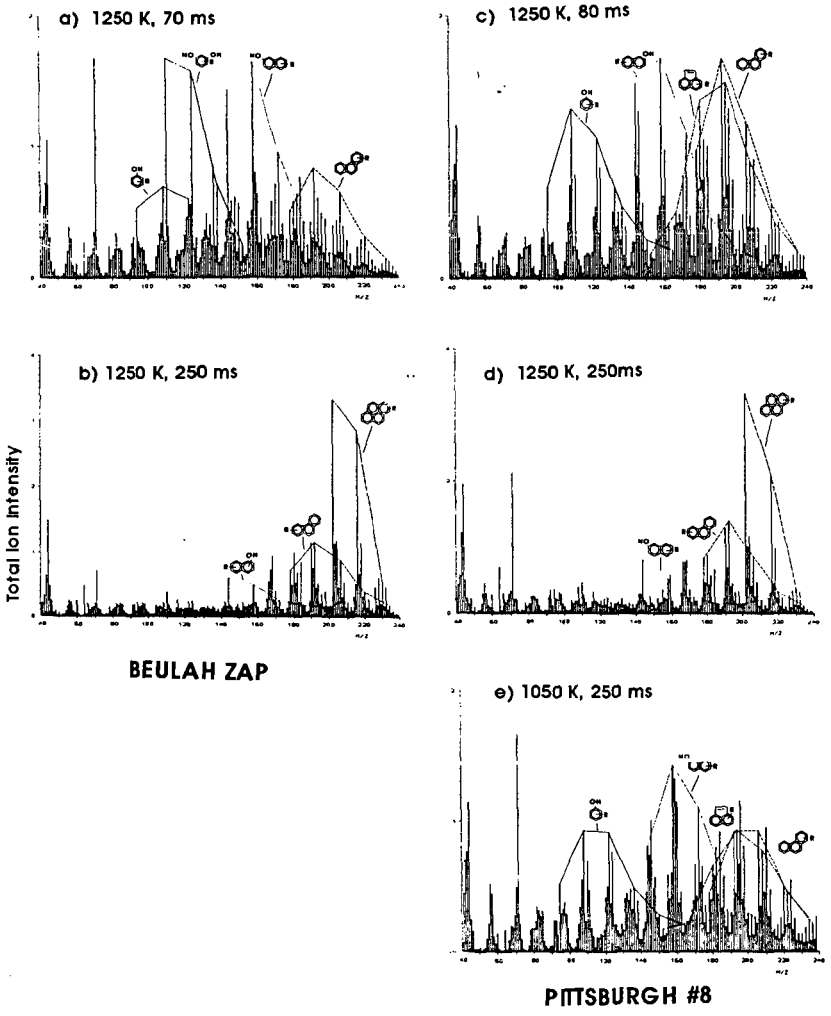

Figure 1. Curie-point desorption mass spectra of Beulah Zap and Pittsburgh #8 tars showing the effects of coal rank (a and b vs. c, d and e), residence time (a and c vs. b, d and e) and gas temperature (c vs. a, b, c and d).

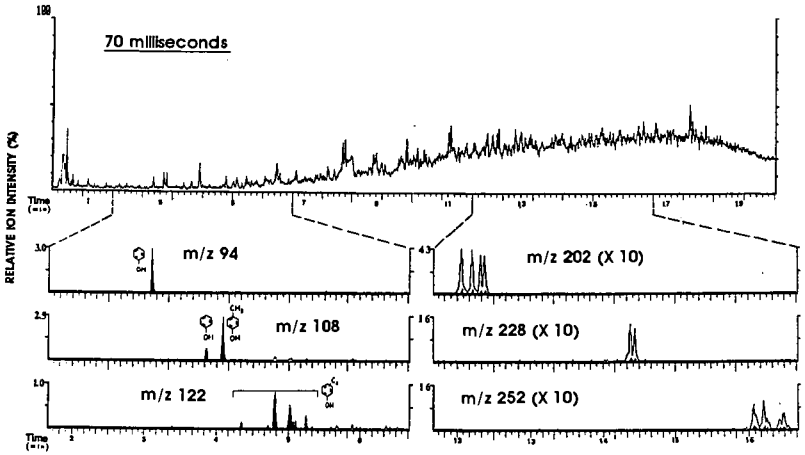

Figure 2. Curie-point desorption GC/MS profiles of Illinois #6 tar obtained at 1250 K after 70 msec. Total ion chromatogram (upper profile) and selected ion chromatograms (lower profiles) show relative abundance of (alkyl) phenols vs. pyrenes, perylenes and picenes.

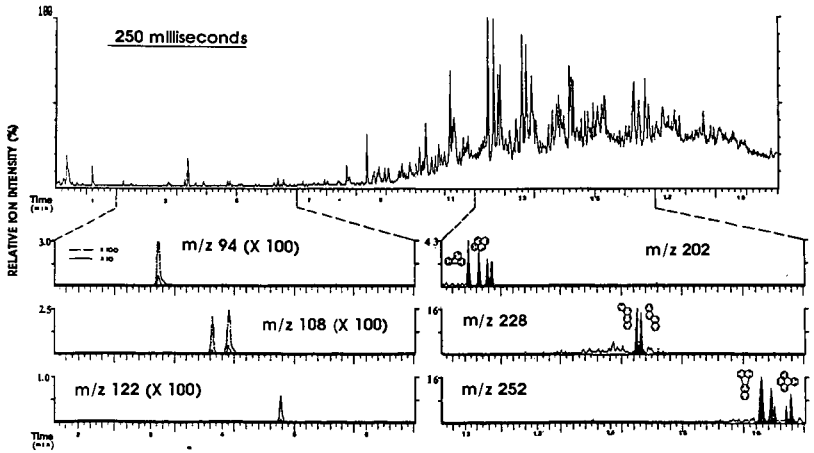

Figure 3. As Figure 2 but obtained after 250 msec. Note 100-fold decrease in (alkyl) phenol as opposed to 10-fold increase in polynuclear aromatic hydrocarbons.

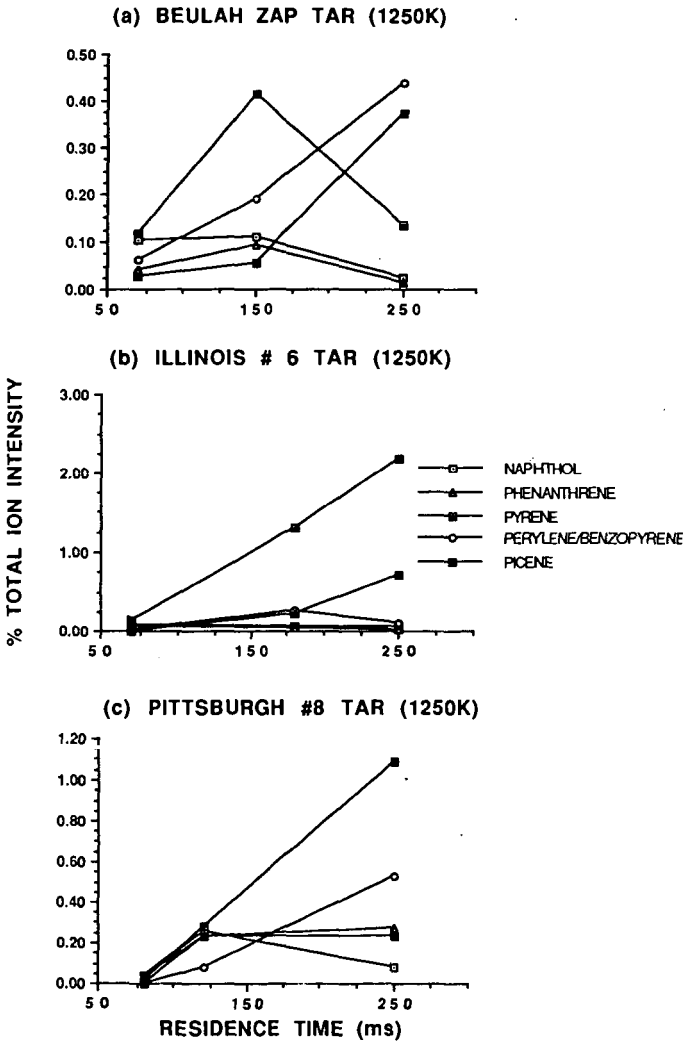

Figure 5. As Figure 4 but representing tars from 3 different coals obtained at 1250 K.

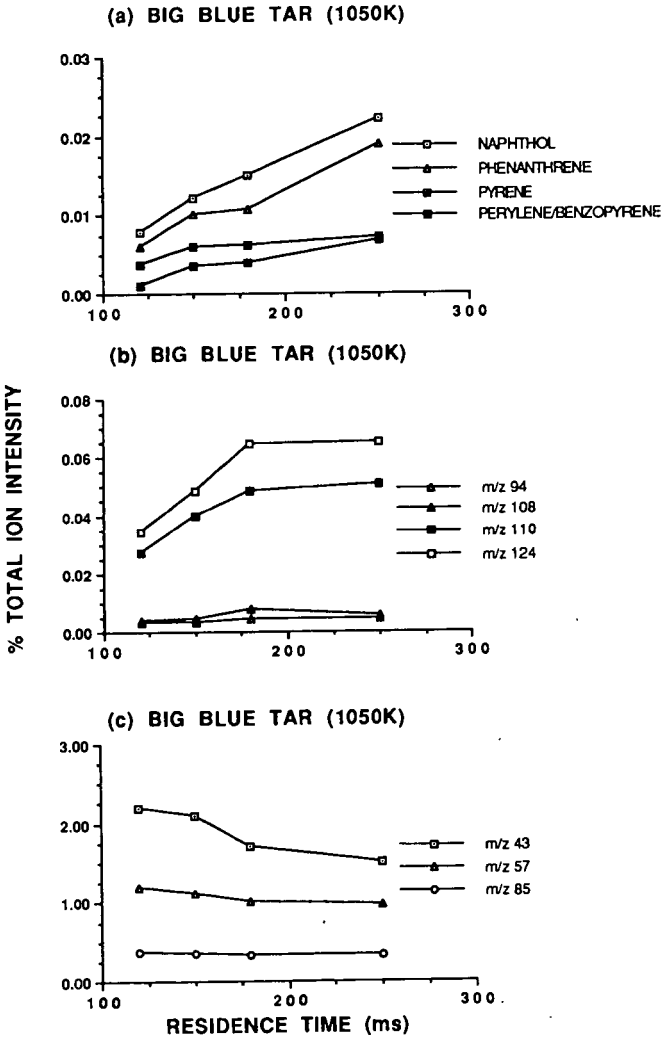

Figure 4. Relative abundance of selected ion profiles in Curie-point desorption GC/MS data on Big Blue tar samples obtained at 1050 K and at different residence times.

THE INTERPRETATION OF SECONDARY INTERACTIONS DURING TEMPERATURE PROGRAMMED DESORPTION OF OXYGEN COMPLEXES IN TERMS OF CHAR POROSITY MORPHOLOGY

P.J. Hall and J.M. Calo
Chemical Engineering Program
Division of Engineering
Brown University
Providence, RI 02912

Keywords: Coal char gasification; secondary interactions; coal char porosity development.

INTRODUCTION

Our recent work [1] concerning temperature programmed desorption (TPD) of oxygen complexes from oxidized coal char surfaces has demonstrated that secondary interactions during the thermal desorption process can convolute the resultant spectra. Their effects are generally enhanced by the presence of inorganic mineral matter impurities and seem to be influenced by the nature of the char porosity [2]. However, the relationship between pore morphology and the behavior of these secondary interactions was not systematically explored in our previous work performed on coal chars at constant burn-off [1]. In the current communication we investigate the variation of the extent of secondary interactions with char burn-off in oxygen. As shown, the results of this work suggest that the behavior of secondary interactions during TPD exhibit some potential as a diagnostic technique for monitoring the variation and development of char porosity; perhaps as a complement to other methods such as gas adsorption.

We have identified two different types of secondary interactions [1]. One involves the reaction of desorbed "free" CO in the process of out-transport to the bulk gas phase with other oxygen surface complexes to produce CO_2. This is primarily manifested as a reflection or satellite peak under primary CO desorption features, the largest of which is typically centered *ca.* 1000K. The other type of secondary interaction involves rechemisorption of "free" CO onto unoccupied active sites to form more stable complexes [1]. This is usually manifested as a high temperature peak or shoulder in TPD spectra, typically centered *ca.* 1200K. It will be demonstrated here that secondary CO_2 production appears to take place in the smaller pores of the char (i.e., the microporosity), while CO rechemisorption takes place primarily in the larger pores.

EXPERIMENTAL

Samples of two precursor coals -- Wyodak and Pittsburgh #8 -- were obtained from the Argonne Premium Coal Sample Bank. The coals were pyrolyzed in ultrahigh purity helium at 1273K with a soak time of one hour. Care was taken to insure that the coals did not come into contact with

oxygen during handling.

The chars from this treatment of the two coals exhibit distinct pore morphologies. During slow carbonization, and in the complete absence of oxygen, Pittsburgh #8 passes through a fluid state during which most of its original microporosity is lost [3]. The resultant char has a very low surface area and develops porosity during subsequent gasification. Conversely, Wyodak is a subbituminous coal which does not proceed through a fluid phase upon carbonization. Consequently, much of the original porosity present in the coal is preserved or enhanced during carbonization. A number of studies indicate that the original porosity consists of a random network of pores with extensive "ink-bottle"-type restrictions and a significant amount of "closed" porosity [3,4]. Our conclusions support these observations. Therefore, gasification of the Wyodak coal char not only develops new porosity, but also tends to enlarge restrictions and render previously closed pores accessible.

Details of the TPD apparatus and the experimental procedures are described elsewhere [1]. The typical sample size was ~10 mg, and ultrahigh purity helium was used as the carrier gas. A heating rate of 100K/min was used for the experiments reported here because this gave good peak resolution [2] and reasonable gas desorption rates. Also, our results [2] suggested that this heating rate tended to maximize the effects of secondary interactions for a number of different coal chars. Char gasification was performed in a TGA apparatus in 0.1 MPa of O_2 at the selected temperature. The 77K N_2 isotherms were measured in a Quantachrome Quantasorb gas adsorption apparatus. No significant differences were observed between N_2 isotherms and CO_2 isotherms obtained at higher temperatures for these chars.

RESULTS AND DISCUSSION

In a companion paper in this symposium [5], it is demonstrated that total oxygen TPD spectra from coal chars can be deconvoluted from secondary interactions by fitting the leading edge of the principal desorption feature to a Gaussian distribution. The residual spectrum, typically centered *ca.* 1200K, is believed to be primarily due to rechemisorbed CO. Typical total oxygen TPD spectra for Wyodak coal char gasified to varying extents are presented in Figure 1. The CO desorption spectra can also be fit to Gaussians in a similar fashion, since CO accounts for the majority of the total oxygen desorbed. For our purposes here, the resultant integral under the CO Gaussian will be termed "1000K CO," and that under the residual CO will be termed "1200K CO." Due to the relatively low amounts of primary CO_2 formed at the lower temperatures, all the CO_2 will be referred to as secondary CO_2.

Figures 2 and 3 show how the three contributions to total oxygen desorption -- "1000K CO," "1200K CO," and "secondary CO_2" -- vary as a function of burn-off for Wyodak and Pittsburgh #8 coal chars, respectively. These figures reveal some interesting behavior. Consider for example the analysis of these data presented in Figure 4. As shown, the "1200K CO/secondary CO_2"

ratio increases continuously with increasing burn-off for the Wyodak char, while it remains essentially constant for the Pittsburgh #8 coal char. This will be shown to be consistent with the expected porosity development for these chars with burn-off.

The available evidence suggests that the 1200K oxygen complexes arise primarily from "free" CO rechemisorbed during the TPD process, and not from just chemically different (i.e., from the 1000K complexes) oxygen complexes formed during steady-state gasification/oxidation. If these complexes did arise from the latter source, their population would tend to *increase* relative to the "low temperature" complexes with exposure under gasification conditions, rather than *decrease,* as generally observed. In fact, for both Wyodak and Pittsburgh #8, the 1200K CO shoulder actually decreases at high burn-off. Product CO formed during isothermal, steady-state gasification is not appreciably chemisorbed because CO chemisorption has been shown to be a highly activated process with a low sticking probability [6]. As a consequence, at the relatively low temperatures used for oxygen gasification, the rate of rechemisorption of product CO is too low to occupy the high energy sites available under gasification conditions. Moreover, any sites that may be accessible under these conditions would react preferentially with oxygen, which is present in considerably greater amounts and exhibits much greater reactivity towards the formation of stable complexes. During TPD, however, the high temperatures experienced during the nonisothermal heating process in the absence of oxygen serves provides the conditions necessary to "fix" a certain fraction of the desorbed CO.

The available evidence suggests that secondary CO_2 formation is a phenomenon associated with the smaller pores (e.g., the micropores) rather than the larger pores. For example, it has already been shown in Figure 4 that the "1200K CO-to-secondary CO_2" ratio is a minimum for zero burn-off Wyodak, which exhibits a "Type I" N_2 adsorption isotherm (as shown in Figure 5), characteristic of microporous materials. Further evidence derives from other oxidation studies where, for example, it has been reported that, due to the large size of the nitrate ion, nitric acid does not oxidize the surface within the microporosity, but rather only that accessible in the meso- and macroporosity, as well as the external surface [7]. TPD spectra on such nitric acid oxidized chars exhibit no secondary CO_2 in comparison to gas oxidized chars [7]. We obtained similar results from hydrogen peroxide-oxidized chars [8]. If secondary CO_2 production did take place appreciably in the larger pores, then significant amounts of secondary CO_2 would be expected from such chars. On the other hand, significant, discernible 1200K CO, which is believed to be due to CO rechemisorption, was evident upon TPD for both nitric acid and hydrogen peroxide-oxidized chars [8]. The reasons for this behavior are still a matter for speculation, but it may be that secondary CO_2 production takes place primarily in micropores for the same reason that a normal distribution of bond energies occurs [5]; that is, the low temperature, less stable complexes would also tend to be more reactive towards attack by "free" CO as they would be towards desorption. In a similar fashion, there is as yet no definitive evidence as to whether CO rechemisorption can occur in micropores to an appreciable extent. However, it is noted that the zero burn-off Wyodak which is known to have significant microporosity does not exhibit any

1200K CO. It may be that CO rechemisorption cannot compete with the more favorable secondary CO_2 production in the micropores. In any case, any CO that might be rechemisorbed in micropores may also participate in secondary CO_2 formation, and thus may not survive to desorb in the higher temperature peak *ca.* 1200K.

In summary then, it is hypothesized that secondary CO_2 formation takes place primarily in the more restrictive porosity, such as the microporosity, whereas CO re-chemisorption is favored in the larger pores. Therefore, the two secondary interactions are in a sense complementary and sensitive to different aspects of the char porosity. In this manner, the decrease in the relative magnitudes of both secondary interactions at high burn-off for Wyodak, as indicated in Figure 2, is consistent with a reduction in total porosity as a result of pore collapse at high burn-off.

It is of interest to compare these observations with information available from adsorption isotherms. 77K N_2 adsorption isotherms for gasified Wyodak and Pittsburgh #8 coal chars are presented in Figures 5 and 6, respectively. Examination of Figure 5 shows that at zero burn-off, the Wyodak char exhibits a classical "Type 1" isotherm [9], characteristic of a microporous material. Figure 2 shows that the secondary CO_2 is relatively high, and that there is virtually no 1200K CO for this char. Therefore the interpretations of both isotherm and TPD spectra are consistent for this char. At 15.2% burn-off, the isotherm appears to have evolved into something in between a "Type 1" and "Type 2". This suggests that at this stage micropores are still a significant part of the Wyodak porosity, but that larger porosity is also developing with burn-off [9]. Again, this is consistent with the increase in the relative amount of 1200K CO to secondary CO_2, as shown in Figure 4. At 48.6% and 61.8% burn-off, the isotherms appear to more closely approach "Type 2" behavior, indicative of larger porosity, and, consistently, secondary CO_2 decreases and 1200K CO increases significantly in this range. The corresponding N_2 surface area goes through a maximum between 15.2% and 48.6% burn-off. Following the maximum, the general tendency is for microporosity to be lost at the expense of larger pores.

For the Pittsburgh #8 char, the isotherms shown are similar for all degrees of burn-off, with some definite "Type 2" behavior characteristic of materials with significant mesoporosity. This is consistent with the even maintenance of the relative contributions of the two different types of oxygen over the entire burn-off range, as shown in Figure 4.

Proper interpretation of the TPD spectra may give additional insight into the nature of the porosity. For example, the isotherms for Wyodak burned-off to 61.8% at 623K and Pittsburgh #8 burned-off to 46% at 723K in Figures 5 and 6 are quite similar in shape, except that the Wyodak isotherm is about a factor of two greater in amplitude.. Therefore, if one were to draw conclusions on the pore morphology based upon this evidence alone the conclusion would be that they were chars of similar pore structure. However, Figure 4 reveals that for the 61.8% gasified Wyodak, the ratio of 1200K CO to secondary CO_2 is 1.47, compared to 0.36 for the 46% gasified Pittsburgh

#8. This suggests that a much higher proportion of the surface area is present in restrictive porosity for the Pittsburgh #8 coal char in this particular case.

At this point it should be noted that integral measures of the various contributions to desorbed oxygen may not be a good indicator of total surface area or pore volume. This is especially evident for the Pittsburgh #8 coal char for which the total oxygen coverage increases steadily with burn-off in Figure 3, whereas the N_2 surface area goes through a maximum between 25 and 46% burn-off (*cf.* Figure 6). It has been well established that total surface area, as measured by gas adsorption techniques, is generally not as good an indicator of char reactivity as is active surface area, as measured by oxygen chemisorption. The oxygen complexes that give rise to secondary interactions are obviously more related to active surface area and thus may behave in a similar fashion. However, it has also been shown that for some chars the amount of oxygen adsorbed under chemisorption conditions can be a fraction of that adsorbed under gasification conditions [10], and also that the amount of chemisorbed oxygen can yield larger apparent surface areas than the total surface area measured by gas adsorption [11]. Therefore, it is not clear at this stage exactly how the integrated amounts of the three contributions to desorbed oxygen are related to the absolute amount of macro-, meso-, and microporosity. In any case, the principal point to be made here is that the *relative* magnitudes of these contributions seem to be related to the char porosity morphology, and, moreover, seem to be quite sensitive to morphological changes during gasification.

CONCLUSIONS

The kinetics of secondary interactions during thermal desorption processes are not yet sufficiently well understood to allow a more quantitative treatment of pore morphology at this time. However, we have demonstrated that the *relative* magnitudes of secondary interactions appear to be sensitive to pore morphology. Although the total amount of surface complex may not be a good indicator of total surface area, the *relative* extents of secondary interactions can reveal information about the pore morphology that is difficult to derive from adsorption isotherm analysis. Thus, the two methods are complementary.

Acknowledgement. This work was supported by the Morgantown Energy Technology Center of the Department of Energy under Contract No. DE-AC21-MC23284.

REFERENCES

1. Hall, P.J.; J.M. Calo *Energy & Fuels* **1989,** *3,* 370.
2. Hall, P.J.; Calo J.M.; Lilly W.D. *Proc. Intl. Conf. Carbon, Carbon'88,* **1988,** McEnaney, B., Mays, T.J., eds.; IOP Publishing Company, Bristol, UK, p. 78.
3. Mahajan, O.P. in *Coal Structure* **1982,** Meyers, R.A., ed., Academic Press, NY, Ch. 3.
4. Larsen, J.W.; Wernett, P. *Energy & Fuels***1988,** *2,* 719.
5. Hall, P.J.; Calo, J.M. *ACS Div. Fuel Chem. Prepr.* **1990,** "Energetic distributions of oxygen

surface complexes on porous carbons and chars," this symposium.
6. Marchon, B., Carrazza, J., Heinemann, H. and Somorjai, G.A *J. Phys. Chem.* **1988,** *92,* 5447.
7. Otake, Y., Ph.D. Dissertation, **1986,** The Pennsylvania State University.
8. Hall, P.J., J.M. Calo, H. Teng, E.M. Suuberg, J.A. May, and W.D. Lilly, *ACS Div. Fuel Chem. Prepr.* **1989,** *34,* No. 1, 112.
9. Gregg, S.J.; Sing K.S.W. *Adsorption, Surface Area and Porosity* **1982,** 2nd ed., Academic Press London, UK.
10. Hall, P.J.; Calo, J.M.; and Otake *Proc. Nineteenth Biennial Conf. Carbon,* **1989,** p. 594.
11. Taylor, R.L., Ph.D. Dissertation, **1982,** The Pennsylvania State University.

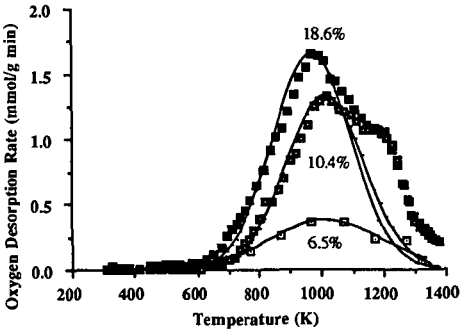

Figure 1. 100K/min TPD spectra total oxygen desorption spectra from Wyodak coal char gasified to varying extent in 0.1MPa oxygen at 573K and their Gaussian fits.

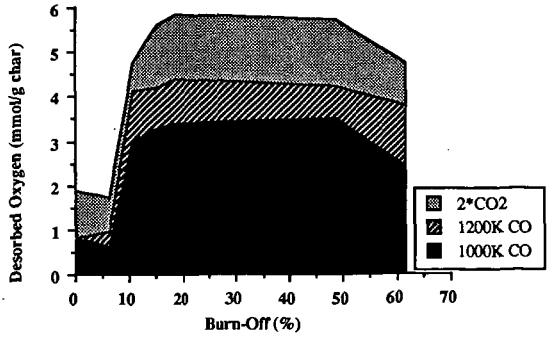

Figure 2. Desorbed oxygen distribution vs. burn-off for Wyodak coal char.

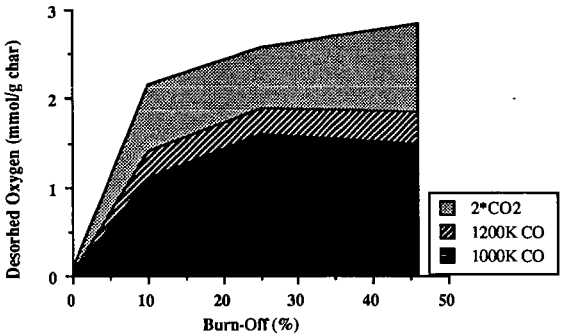

Figure 3. Desorbed oxygen distribution vs. burn-off for Pittsburgh #8 coal char.

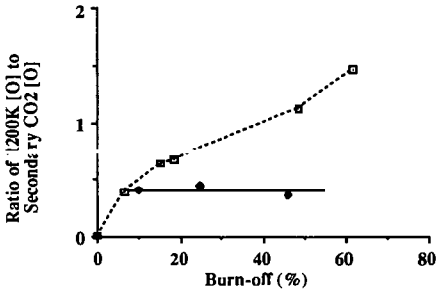

Figure 4. Variation of the ratio of [O] from 1200K CO to [O] from secondary CO_2 production as a function of char burn-off. --- Wyodak coal char; — Pitsburgh #8 coal char.

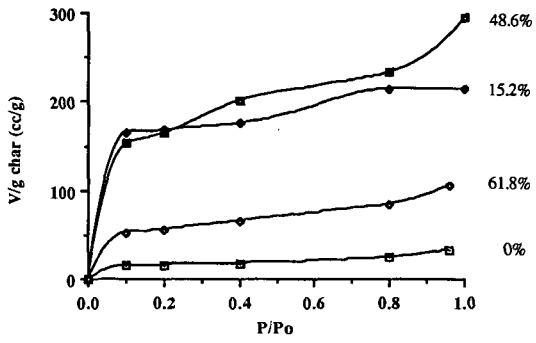

Figure 5. 77K nitrogen adsorption isotherms for Wyodak coal char gasified to varying extents in 0.1MPa O_2 at 623K.

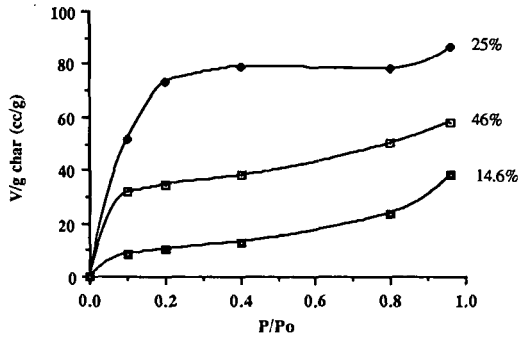

Figure 6. 77K nitrogen adsorption isotherms for Pittsburgh #8 coal char gasified to varying extents in 0.1MPa O_2 at 623K.

LASER PYROLYSIS-TRANSFER LINE CHROMATOGRAPHY/MASS SPECTROMETRY OF SINGLE, LEVITATED COAL PARTICLES

Waleed Maswadeh, Neil S. Arnold and Henk L.C. Meuzelaar
Center for Micro Analysis & Reaction Chemistry
University of Utah, Salt Lake City, UT 84112

Keywords: coal devolatilization, laser pyrolysis, mass spectrometry

INTRODUCTION

A laser pyrolysis transfer line gas chromatograph/mass spectrometry (laser Py-TLGC/MS) system based on the combination of an electronically pulsed CW CO_2 laser with an electrodynamic balance (EDB), a heated capillary ("transfer line") GC column and an ion trap mass spectrometer (ITMS) was constructed (Figure 1), as described previously [1].

The main purpose of the system is to study the devolatilization behavior of single, levitated coal particles at very high heating rates, e.g., 10^5-10^6 K/sec, while comparing the composition of the devolatilization products to those observed at much lower heating rates, e.g., 10^{-2}-10^2 K/sec. At the lower heating rates, several different time-resolved Py-MS techniques, including vacuum thermogravimetry/mass spectrometry (TG/MS) [2], Curie-point Py-MS [3] and pyrolysis Field Ionization mass speetrometry (Py-FIMS) [4] are available to provide kinetic information on coal devolatilization processes. Although kinetic parameters obtained at these lower heating rates may be directly applicable to fixed bed or even fluidized bed coal processes, the usefulness of these parameters for pulverized coal combustion processes at heating rates in the 10^4-10^5 K range remains to be determined. The laser Py-TLG/MS system shown in Figure 1, although not suitable for determining kinetic parameters at these high heating rates, enables us to verify the mechanistic aspects of coal devolatilization reactions. If the main coal devolatilization mechanisms remain unchanged at 10^5-10^6 K/sec, it may be argued that it should be possible to extrapolate the kinetic parameters obtained by the abovementioned TG/MS, CuPy-MS and Py-FIMS experiments.

CO_2 laser devolatilization experiments on single levitated coal particles using EDB type particle trapping devices have previously been described by several authors [5-7]. However, although successful in measuring particle temperatures and/or weight loss profiles as a function of time none of these prior studies addressed the characterization and identification of the complex mixture of devolatilization products generated during these experiments. To the best of our knowledge, the work reported here represents the first successful attempt to do so.

EXPERIMENTAL

The experimental set-up (Figure 1) consists of an EDB, a 50 w CW CO_2 laser and a Finnigan MAT ITMS system. The particle levitation cell was constructed in such a way as to provide line-of-sight access to the center of the cell for the CO_2 laser beam as well as for visual observation by means of a stereo microscope and for a two-color optical pyrometer (under development). Typical cell operating parameters for levitating a 120 μm dia. Spherocarb particle are: ring electrode 3000 V (60 Hz ac), upper end cap +100 V dc, lower end-cap -100 V dc.

The CO_2 laser (Apollo 3050 OEM) is capable of electronic pulsed beam operation. The 8 mm dia. beam is split equally into 2 opposing beams focussed at the center of the levitation cell (beam waist ca. 400 μm, power density ca. 4-10 MW/m^2). A co-linear parfocal HeNe laser beam permits positioning the levitated particle in the optical and electrical center of the cell. Two IR detectors measure the integrated pulse and time-resolved pulse energy.

A heated transfer line column (2m x .18 mm DB5) equipped with a special air sampling inlet [8] enables intermittent sampling of volatiles from the center of the levitation eell into the ITMS vacuum system.

Feasibility studies were performed on 120-150 μm Spherocarb particles impregnated with ng amounts of an alkylnaphthalenes mixture and other selected model compounds. Finally, a series of experiments was performed with actual coal particles in the 100-130 μm size range, prepared by careful sieving of coals from the Argonne National Laboratory Premium Coal Sample (ANL-PCSP) program.

RESULTS AND DISCUSSION

Before applying the laser Py-TLGC/MS technique to coals, we measured the shot-to-shot reproducibility of the electronically pulsed CW CO_2 laser system. As illustrated in Figure 2 overall linearity of the laser pulse energy in the 1-35 msec range is quite good. However, the cause of the unexpectedly large variation in pulse energy at 20 msec is being investigated further.

System performance was further tested with 120-130 μm sized Spherocarb particles loaded with known quantities of a well characterized mixture of alkylnaphthalenes and related aromatic compounds. Figure 3 shows the time-resolved TLGC/MS profiles obtained by using the 6 ft long heated transfer line between EDB and ITMS as a short capillary column. Various alkylnaphthalene homologs and isomers are readily separated and identified. Moreover, repeated laser pulse heating of the same Spherocarb particle shows that the devolatilization process is virtually complete within the duration of the first pulse (10 msec).

This encouraged us to perform laser Py-TLGC/MS analyses on real coal particles. The resulting TLGC/MS profiles shown in Figures 4 and 5 demonstrate a surprising level of chemical detail. Repeat analyses of Pittsburgh #8 coal shown in Figure 4 demonstrate an acceptable level of shot-to-shot reproducibility in spite of the unavoidably high heterogeneity of 100-150 μm dia. coal particles, Figure 4c illustrates the fact that, at these high heating rates oxygen does not markedly influence the devolatilization process. Apparently, the rapidly expanding and cooling cloud of devolatilization products surrounding the particle effectively protects the hot particle surface from severe oxidative changes.

As mentioned earlier, the main goal of the EDB-ITMS experiment is to verify the effect of high heating rates on devolatilization mechanisms. Assuming that any significant shift in mechanisms should be reflected in changes in the relative abundances of various structural isomers, e.g., alkylsubstituted phenols or naphthalenes, Figure 5 enables a side by side comparison of laser Py-MS profiles and more conventional Curie-point Py-GC/MS profiles obtained on samples of Pittsburgh #8 coal. Obviously, little if any changes in product distributions are observed, when

allowing for interparticle heterogeneity as well as for differences in chromatographic techniques. A high degree of correspondence between coal devolatilization products observed at 10^2 K/sec and at 10^5 K/sec was also found to exist for other ANL-PCSP coals (not shown here).

However, due to the inherently low tar yields of both the Beulah Zap lignite (see Figure 6) and the low volatile bituminous Pocahontas coal satisfactory laser pyrolysis mass spectra of single, levitated particles of these coals proved difficult to obtain. Therefore, it is too early to conclude that no significant mechanistic changes are observed at these high heating rates. Moreover, careful examination of the laser pyrolysis TLGC/MS profiles revealed the absence (or strongly reduced intensity) of dihydroxybenzenes and of long chain (e.g., C_{10}-C_{20}) n-alkane/alkene pairs. Whether these compounds are lost by secondary condensation reactions in the hot outer layers of the particle or by some other chemical or physical process is currently the focus of further investigations.

As noted earlier, a marked degree of interparticle heterogeneity is expected to exist in pulverized coals. Provided that a high level of shot-to-shot reproducibility can be achieved, the laser Py-TLGC/MS approach could become a powerful tool for studying interparticle heterogeneity. A preliminary indication of the effects of interparticle heterogeneity on successive laser Py-TLGC/MS profiles can be obtained from the bivariate plot in Figure 7. The clustering trends observed in the intensities of the peaks at m/z 94+108 and m/z 142+156 appear to be relatively independent of pulse length (except for very short laser pulse deviations which result in incomplete devolatilization reactions). At this point, differences in maceral and mineral composition between different particles are thought to be primarily responsible for the clustering behavior observed in Figure 7.

CONCLUSIONS

In conclusion, laser Py-TLGC/MS appears capable of producing a detailed chemical profile of the devolatilization products from single, levitated coal particles at very high heating rates (~10^5 K/sec), especially when using coals which produce relatively high tar yields. Most devolatilization products detected at these high heating rates appear to be identical to those observed at much lower heating rates, e.g., 10^{-2}-10^2 K/sec, indicating that coal devolatilization mechanisms remain essentially unchanged over some 7 orders of magnitude difference in heating rates!

A few compound classes found to be missing or strongly reduced, e.g., dihydroxybenzenes and long chain aliphatic hydrocarbons, are though to be lost by secondary condensation reactions. Another interesting observation is the absence of marked oxidative phenomena when performing laser pyrolysis TLGC/MS experiments in air rather than under inert atmospheric conditions. Apparently, the rapidly expanding and cooling vapor cloud protects the hot surface of the particle. Finally, it is concluded that interparticle heterogeneity has a marked effect on laser Py-TLGC/MS profiles and that this technique therefore offers a unique opportunity to study the effect of interparticle heterogeneity on coal devolatilization processes.

ACKNOWLEDGEMENTS

This work was sponsored by the Advanced Combustion Engineering Research Center. Funds for this Center are received from the National Science Foundation, the State of Utah, 23 industrial participants, and the U.S. Department of Energy.

REFERENCES

1. Maswadeh, W.M., Roberts, K.A., McClennen, W.H., Meuzelaar, H.L.C., "Laser Pyrolysis Mass Spectrometry of Single Levitated Coal Particles," Proc. 37th ASMS Conf. Mass Spectrom. All. Topics, Miami, FL, 1989.
2. Yun, Y., Meuzelaar, H.L.C., "Simultaneous Thermogravimetric and Mass Spectrometric Observations on Vacuum Pyrolysis of Argonne PCSP Coals," ACS Preprints, Div. of Fuel Chem., Vol. 33, #3, Sept. 1988, pp. 75-84.
3. Chakravarty, T., Windig, W., Hill, G.R., Meuzelara, H.L.C., "Time-resolved Pyrolysis Mass Spectrometry of Coal: A New Tool for Mechanistic and Kinetic Studies", Energy & Fuels, Vol. 2, 1988, pp. 400-405.
4. Yun, Y., Maswadeh, W., Meuzelaar, H.L.C., Simmleit, N., Schulten, H.-R., "Estimation of Coal Devolatilization Modeling Parameters from Thermogravimetric and Time-Resolved Soft Ionization Mass Spectrometric Data," ASMS, Miami, FL 1989
5. Phuoc, T.X., Maloney, D.J., "Laser Pyrolysis of Single Coal Particles in An Electrodynamic Balance," 22nd Symp. (Intl.) on Combustion (The Combustion Institute), 1988, pp. 125-134.
6. Smith, M.W., McMillen, D.F., Malhotra, R., Platz, R., "Laser Pyrolysis of an Entrained Stream of Coal Particles", ACS Preprints, Div. of Fuel Chem., Vol. 35, #2, April 1990, pp. 455-466.
7. Spjut, R.E., Sarofim, A.F., Longwell, J.P., "Laser Heating and Particle Temperature Measurement in an Electrodynamic Balance," Langmuir, Vol. 1, #3, 1985.
8. Arnold, N.S., Roberts, K.A., McClennen, W.H., Meuzelaar, H.L.C., "Direct On-line Vapor Mounting by Transfer Line GC/MS," 37th ASMS Conf. Mass Spectrom. All. Topics, Miami, FL, 1989.

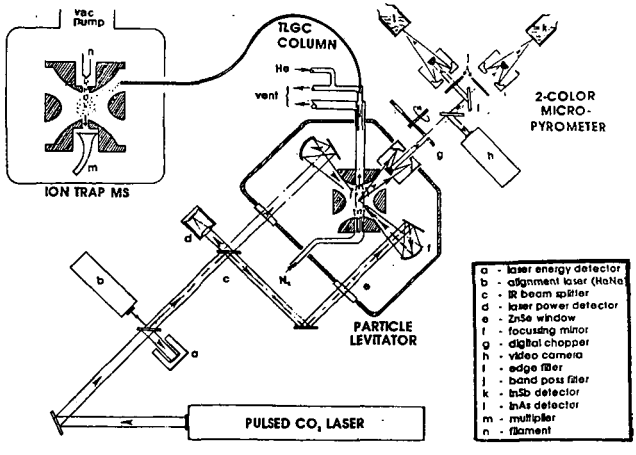

Figure 1. Schcmatic diagram of CO_2 laser pyrolysis TLGC/MS system consisting of a pulsed CO_2 laser, an electrodynamic balance ("particle levitator), a transfer line GC column and an ion trap mass spectrometer. The 2 color micropyrometer is currently under development.

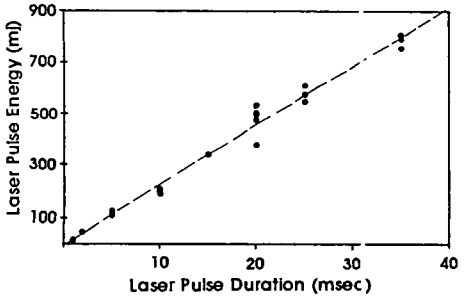

Figure 2. Variability in laser pulse energy at different pulse lengths.

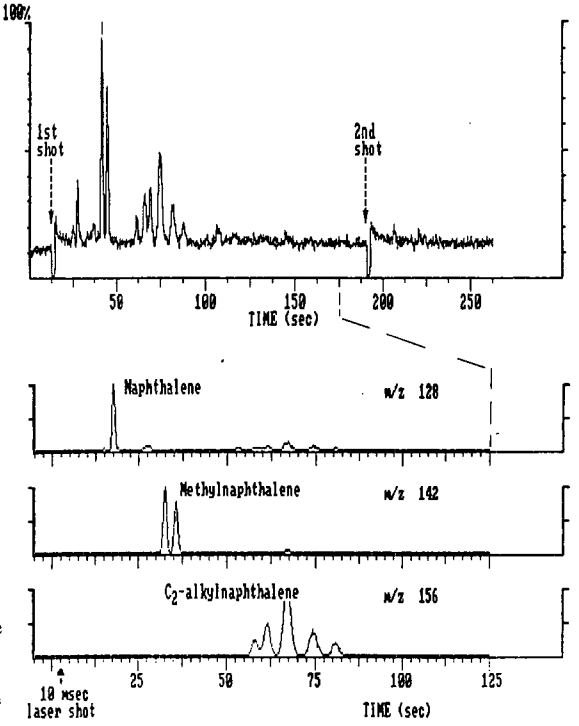

Figure 3. Total ion chromatogram (top) shows 2 consecutive laser shots at same Spherocarb particle (impregnated with alkylnaphthalenes mixture). Selected ion chromatograms illustrate TLGC separation of alkylnaphthalene homologs and isomers. Column temp: 50-200 C in 2 minutes.

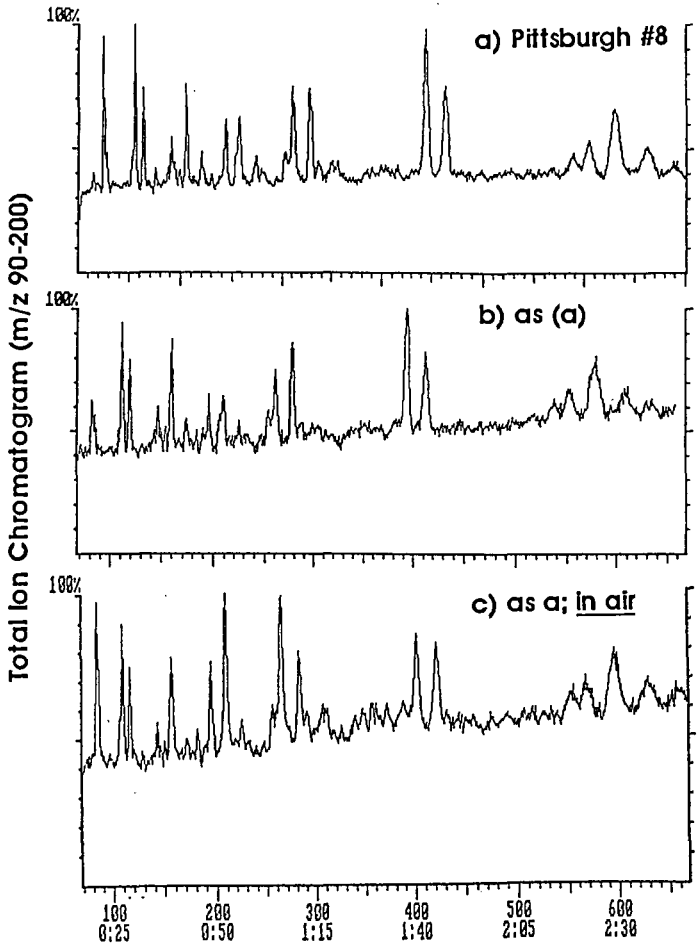

Figure 4. Repeatability of Laser Py-TLGC/MS profiles of single Pittsburgh #8 coal particles. Profile (c) falls within normal range of variation!

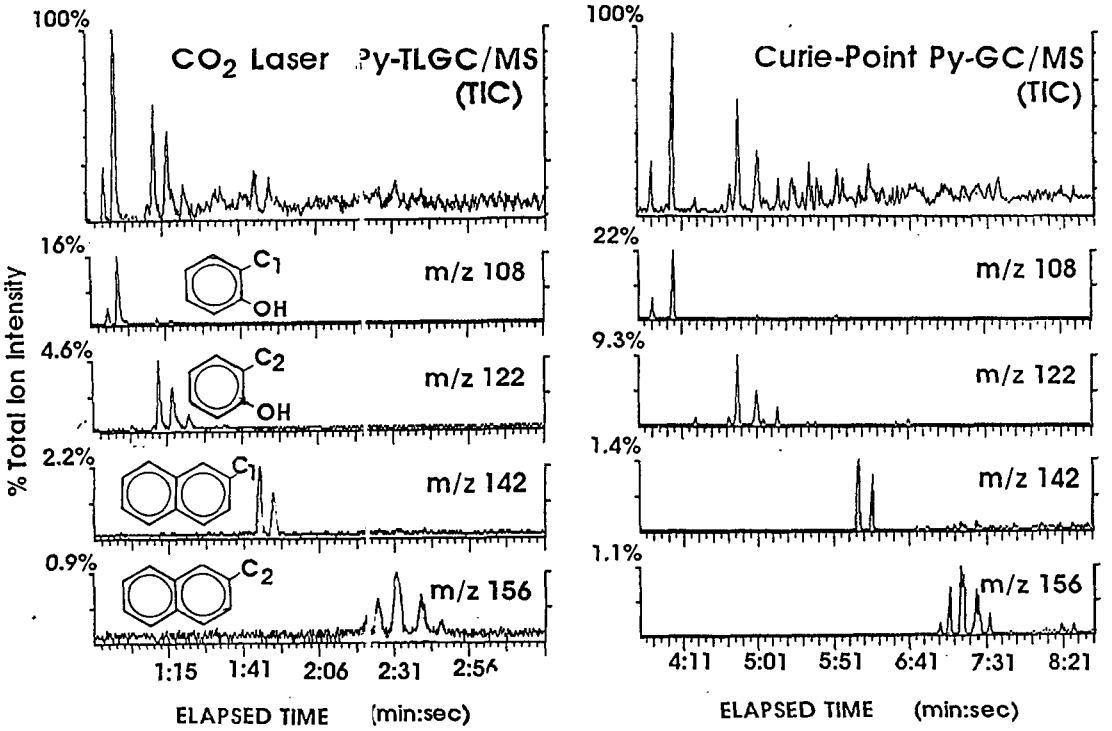

Figure 5. Comparison of CO_2 Laser Py-TLGC/MS profiles obtained at high heating rates (~10^5 K/sec) with Curie-point Py-GC/MS profiles obtained at lower heating rate (~10^3 K/sec). Note similar relative abundances of major tar components.

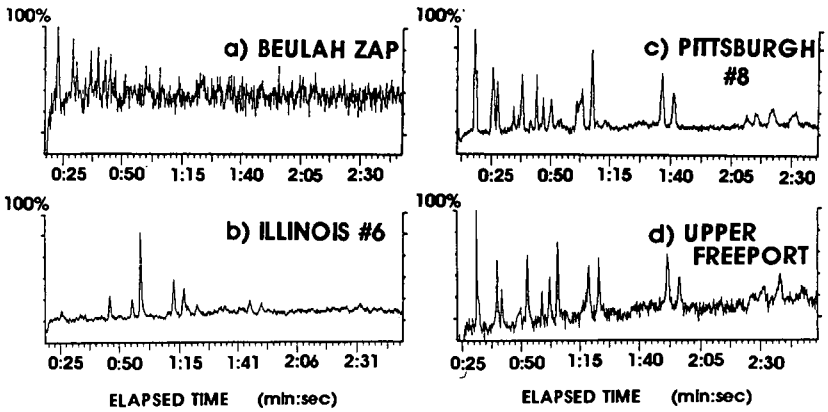

Figure 6. Comparison of laser Py-TLGC/MS profiles of 4 ANL-PCSP coals of different rank. Note lower signal-to noise ratio for Beulah Zap lignite and Upper Freeport, mvb coal compared to hvCb Illinois #6 and hvAb Pittsburgh #8 coals.

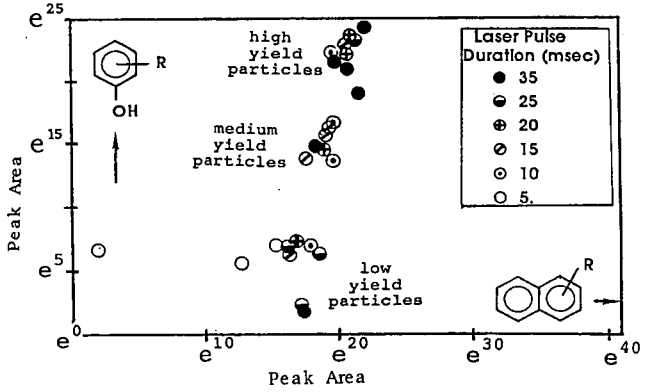

Figure 7. Scatter plot of peak areas at m/z 142 + m/z 156 (x-axis) vs. m/z 94 + m/ 108 (y-axis) from TLGC/MS profiles of 26 Illinois #6 coal particles analyzed at 6 different pulse lengths. Note variable naphthalene response at 5 msec (due to incomplete devolatilization) and presence of 3 phenol yield levels independent of pulse length (thought to be due to differences in maceral content).

TEMPERATURE MEASUREMENTS OF SINGLE COAL PARTICLES DURING THE EARLY STAGES OF HEATING AND DEVOLATILIZATION

Daniel J. Maloney, Esmail R. Monazam, Steven D. Woodruff and Larry O. Lawson
Morgantown Energy Technology Center
P. O. Box 880
Morgantown, West Virginia 26507-0880

Keywords: coal devolatilization, temperature measurement, combustion

ABSTRACT

Unique instrumentation was applied to measure changes in coal particle size and temperature during the early stages of heating and devolatilization. The system incorporated an electrodynamic balance and a pulsed radiation source with a high-speed photodiode array and single wavelength radiation pyrometer. Single coal and carbon particles were pulse heated to simulate the rapid heating rates experienced in high intensity combustion environments (10^5 K/s). Measured temperature histories for 135 μm diameter carbon spheres were in excellent agreement with theoretical predictions of the temperature response of radiatively heated spheres using heat capacity and thermal conductivity property correlations commonly applied in modeling coal devolatilization and combustion. Measured temperature histories of 115 μm coal particles, however, greatly exceeded (on the order of 50 percent) theoretical predictions of the temperature response using the same assumptions and property correlations. Potential causes for the high heating rates observed include uncertainty in assigning thermodynamic and heat transfer properties as well as failure to account for particle shape factors. It is concluded that heat transfer analyses employing spherical particle assumptions and commonly used coal property correlations can lead to significant underestimation of temperature histories and corresponding errors in associated devolatilization rates.

INTRODUCTION

The large discrepancies in observed temperature sensitivities for coal devolatilization are well documented.[1,2] with variations in reported rate constants at a given temperature of several orders of magnitude being common. These variations can in large part be attributed to the experimental techniques used to study rapid devolatilization because estimation and/or measurement of coal particle temperatures in these systems is difficult. Recent attempts to overcome these limitations have concentrated on in-situ temperature measurement or careful characterization of heat transfer fields. For example, Solomon and coworkers[3,4] developed and applied an FTIR emission/transmission technique to measure average temperatures for clouds of devolatilizing coal particles in an entrained flow reactor. Fletcher[5,6] recently reported using a two-color particle sizing pyrometer to characterize the temperature history of single devolatilizing particles in an entrained flow reactor. Friehaut and Proscia[7] performed a detailed characterization of the temperature rise in a screen heater system which was then applied to study rapid devolatilization. Results from these investigations suggest that coal devolatilization rates may be significantly faster and have a stronger temperature sensitivity than implied from many previous studies. The importance of accurate temperature measurements in future devolatilization studies is clear.

In the present paper a novel system is described for monitoring rapid changes in particle size and temperature during coal devolatilization at heating rates representative of high intensity combustion environments (on the order of 10^5 K/s).

The objective was to time and temperature resolve tar evolution and particle swelling that accompany devolatilization and thereby provide data needed to develop more accurate predictions of coal combustion behavior. Initial measurements are reported along with a discussion of the implications for predicting coal devolatilization in combustion systems.

EXPERIMENTAL

Single coal or carbon particles were statically charged and captured in an electrodynamic balance (EDB). Details of the design and operation of the EDB system are published elsewhere.[8,9] The captured particles were balanced at the EDB null position and then heated radiatively from opposite sides by well characterized pulsed Nd:YAG laser beams of equal intensity. Delivered energy fluxes were varied from 500 to 1200 W/cm^2 giving rise to heating rates on the order of 10^5 K/s. Heating pulse times were varied from 3 to 10 ms. The ambient gas was 1 atmosphere of air.

Photographic records of the volatile evolution and particle swelling that accompany devolatilization were obtained using a high-speed 16 mm movie camera which was operated at 5000 frames per second. Timing marks were recorded on the film to accurately determine the film speed and to mark the initiation of the heating pulse. As reported elsewhere,[10] these movies provided excellent time resolution of the particle response including rotation and swelling, and definition of distinct stages of the devolatilization process such as heavy (condensible) volatile evolution.

Changes in particle size and temperature that accompany rapid heating were measured using a novel imaging system and a single wavelength radiation pyrometer. The imaging system was developed around a 16 x 62 element silicon photodiode array. Particles were backlit with a HeNe laser and a magnified shadow image was projected onto the detector array. The full array was scanned at 6300 Hz yielding an analog output proportional to the particle cross-sectional area. A 7 percent reflecting beam splitter was placed in line between the focussing optic and the imaging system array to deflect part of the particle image onto a video camera detector. The video camera was employed to facilitate particle capture and positioning in the EDB.

The radiant power emitted from hot particles was measured using a single wavelength optical pyrometer which was filtered to provide a 100 nm bandpass centered at 1.5 μm wavelength. These measurements were made along the same line of sight as the particle size measurements by employing a set of dichroic beam splitters to separate the HeNe backlight laser from the near infra-red radiation required for the pyrometer. Particle temperatures were determined based on measurements of particle size and radiant emission intensity with application of the Wien approximation to Plank's law. Emissivities used in these calculations were estimated based on measurements' and on available literature.[11] Details of the temperature measurement system including pyrometer calibration, data analysis and associated measurement errors are published elsewhere.' A schematic of the measurement system is provided in Figure 1.

Analog outputs from the imaging system, the pyrometer and a heating beam synchronization pulse were acquired using a Data Translation DT2828 interface card in an AT compatible PC. Data acquisition was triggered from the movie camera, when a framing rate of 5000 per second was achieved, and continued at a rate of 10 kHz per channel for a period of 50 ms. Heating pulses were initiated 15.5 ms after initiation of data acquisition. Measurements were made on individual particles of Spherocarb (Foxboro, Analabs), a spherical, microporous molecular sieve carbon and PSOC 1451D a HVA Pittsburgh seam bituminous coal. Ultimate analysis for the carbon sample yielded 95.2 percent carbon, 0.4 percent hydrogen, and 0.7 percent nitrogen.

Ultimate analysis of the coal yielded 83.3 percent carbon, 5.4 percent hydrogen, and 1.6 percent nitrogen on a dry ash free basis.

ANALYSIS

Measured temperature histories were compared with theoretical estimates of the temperature response of radiatively heated particles. Temperature histories were modeled assuming that particles were spherical, heat flow was in the radial direction only, and the incident heating pulses were absorbed and distributed uniformly at the particle surface. Under these assumptions, the transient temperature distribution in the particles was obtained by solution of the Fourier equation for a sphere:

$$\rho_p C_p \frac{\partial T}{\partial t} = K \left(\frac{\partial^2 T}{\partial r^2} + \frac{2}{r} \frac{\partial T}{\partial r} \right) \qquad (1)$$

where ρ_p, C_p, T, K, and r represent particle density, heat capacity, temperature, thermal conductivity and radius, and t represents time. In solving equation 1, the following boundary conditions were applied:

(i) The initial condition at t = 0:

$$T(r,0) = T_0 \qquad 0 \leq r \leq R \qquad (2)$$

(ii) The symmetry condition at the center r = 0:

$$\frac{\partial T(0,t)}{\partial r} = 0 \qquad t \geq 0 \qquad (3)$$

(iii) The energy delivered at the surface r = R:

$$K \frac{\partial T}{\partial r} = \frac{\alpha I}{2} - [\, h(T_s - T_\infty) + \sigma\varepsilon(T_s^4 - T_\infty^4) \,] \qquad (4)$$

where α, I, h, σ and ε represent particle absorptivity, incident radiation flux, heat transfer coefficient, Stefan-Boltzman constant and particle emissivity respectively. The subscripts s and ∞ denote the particle surface and ambient environment.

Equation 1 was solved numerically using an implicit Crank-Nicholson scheme. Calculations were performed using the Merrick model[12] to estimate particle heat capacities. Thermal conductivities were estimated using the temperature data for coals and chars of Badzioch and coworkers.[13] The heat transfer coefficient at the particle surface was calculated assuming a Nusselt number of 2. Calculations were performed employing both a constant particle size assumption and using the measured particle size history as input to the model.

RESULTS

Experiments were conducted with carbon spheres to evaluate the capabilities of the measurement system and to test the validity of the heat transfer analysis. Previous experience with Spherocarb particles indicated sufficient temperature measurement accuracy and response to enable heat capacity measurements of individual particles in the EDB system.[9] Temperature traces for replicate experiments with three different Spherocarb particles are presented in Fig. 2. Heating pulse intensities

for the three experiments varied from 1100 to 1160 W/cm^2 with particle diameters ranging from 135 to 140 μm. The temperatures reported were determined using the pyrometer output and the measured particle size data assuming a particle emissivity of 0.85. The measured temperature histories for the three particles were all very similar with less than 50 K deviation at any given time during the particle heat up. The temperature histories showed a steady rise from 850 K (low temperature limit of pyrometer) up to a temperature around 1200 K and then exhibited a marked decrease in the rate of temperature rise at about 6.5 ms into the heating pulse. Analysis of the corresponding high speed movie records indicated that each of the particles passed through a plastic transition during heat up and showed clear signs of volatile evolution and fragmentation from the surface. The observed change in heating rate coincided with the initiation of volatile evolution and particle fragmentation.

The solid line in Fig. 2 represents the calculated temperature history at the surface of a 135 μm particle exposed to an incident flux of 1160 W/cm^2. Excellent agreement was obtained between temperature measurements and predictions with less than 50 K temperature difference being observed over the first 6.5 ms of particle heating. Beyond 6.5 ms the model predictions exceeded the measured temperature rise. Possible causes for the marked decline in the observed particle heating rate and the corresponding deviation from the predicted temperature rise include; a) thermochemical or thermophysical heat requirements which may be associated with volatile evolution and particle fragmentation, but were not accounted for in the calculations; b) attenuation of the particle emission due to the presence of the volatile aerosol cloud and/or small particle fragments; and, c) attenuation of the heating pulse due to the presence of the volatile cloud or particle fragments around the particle. Efforts are in progress to resolve this issue. The data shown in Fig. 2 are typical in terms of measurement reproducibility and agreement between model predictions and measurements for experiments conducted over a range of Spherocarb particle sizes (125 to 150 μm) and incident heat fluxes (500 to 1200 W/cm^2).

Measured temperature histories from six independent experiments with PSOC 1451D coal are presented in Fig. 3. Initial particle diameters for these experiments ranged from 110 to 127 μm , with heating pulse intensities and times varying from 1040 to 1100 W/cm^2 and 3 to 10 ms respectively. The temperatures reported represent data collected before the particles began to move out of the measurement focal volume. The six data sets, recorded at essentially identical heat input rates, but for different heating times, illustrate that the temperature rise was very similar in each case. The data indicate an initial heating rate on the order of 2.5 x 10^5 K/s to a temperature around 1400 K. For the particles that remained in the detection volume through the duration of the heating pulse, the temperature remained at a plateau value near 1400 K for the last several ms of heating. Analysis of the corresponding high speed movies showed rotation of particles beginning between 1.6 and 1.8 ms into the heating pulse at measured surface temperatures around 900 K. Similar observations of particle rotation were reported previously by Phuoc and Maloney[10] and are most likely associated with the inception of light (non-condensible) volatile evolution. Between 3 and 4 ms into the heating pulse, the first indications of a condensed volatile cloud were observed around the particles, afterwhich intense volatile evolution proceeded. Figure 4 illustrates particle size histories showing the swelling behavior of three particles. These data correspond with three of the temperature records shown in Fig. 3. Most of the observed particle swelling occurred between 3 and 5 ms with the maximum swelling values varying from 10 to 30 percent for the particles studied. During the last 5 or 6 ms of heating, in the longer pulse time experiments, the measured temperatures remained fairly constant at about 1400 K. At the present time it is not clear if this behavior is real or the result of interference from the volatile cloud that forms around the particle during the latter stages of devolatilization. This matter is

the subject of an ongoing investigation. The discussion below, therefore, is limited to the first 4 ms of the particle heat up until this issue can be resolved. It should be noted that intense volatile evolution continued during the last half and for several ms beyond the completion of the heating pulse in the 10 ms duration experiments.

Comparisons of one of the temperature records presented in Fig. 3 with temperature history predictions based on the heat transfer analysis described above are presented in Fig. 5. The base case for the analysis included an initial coal density of 1.2 g/cm^3, and particle emissivity and absorptivity of 0.8. The base case analysis gave poor agreement with the measured temperature histories using the same coal property correlations and initial assumptions that gave good agreement for the carbon spheres heating under similar incident heat flux conditions. A second comparison was made assuming an emissivity of one for the coal particles. As shown in Fig. 5 this modification did improve the agreement between the predicted temperature rise and the measurements, however, the agreement was still poor when compared with the results obtained for carbon spheres. The comparisons in Fig. 5 have significant implications because they suggest that the coal particles heated much faster than predicted based on commonly employed approaches to modeling heat transfer using assumptions routinely applied to coal. Fletcher[3] recently reported that the same coal studied here heated as much as 40 percent faster in an entrained flow reactor than predicted using a fairly comprehensive heat transfer analysis. He used a "corrected" characteristic heat transfer time to obtain good agreement between model predictions and particle temperature measurements. The results presented in Fig. 5 are similar to Fletchers observations and suggest significant errors in the assumed particle properties or model assumptions because, even when assuming all of the incident energy was absorbed by the particle, the measured temperature rise greatly exceeded the model predictions. This observation implies one or more of the following; a) significant temperature gradients existed in the particle, i.e. assumed thermal conductivities for the coal were too high; b) assumed particle thermal mass was too high, i.e. particle density and/or heat capacity were overestimated; and, c) the spherical particle assumption was inadequate to model heat transfer for coal particles, i.e. surface to mass ratios for coal particles significantly exceed that of a sphere.

Additional calculations were performed to evaluate the sensitivity of temperature history predictions to changing particle properties such as heat capacity and thermal conductivity. Some improvements were obtained in the model predictions relative to the measurements when lower heat capacity and thermal conductivities were employed in the analysis. However, there were still significant differences between measurement and prediction if coal property values were held within a range that is generally accepted. Additional improvements in the model predictions might be obtained if mass loss during particle heat up were accounted for in the particle energy balance. No attempt was made to do so, however, because there was no evidence of significant mass loss from the coal particles during the first 3 to 4 ms of particle heating. Attempts were made to estimate the relative contribution to the energy balance due to particle oxidation. Based on these calculations it was concluded that heat release due to oxidation during the initial 4 ms of particle heating was insignificant and should have little influence on the observed particle temperatures. This conclusion is supported by other evidence as well because, if the high heating rates observed resulted from oxidation the associated heat release would lead to particle ignition. No evidence of particle ignition was observed and following the heating pulse, the particles were observed to cool rapidly.

An alternative explanation for the high heating rates observed in the experiments arises from the irregular shape of the coal particles. As is typical when modeling coal behavior, the heat transfer analysis was based on an assumption of spherical particle shape. This analysis gave good agreement with experiments performed on

spherical particles. The mass per unit surface area is an important factor in the analysis and irregular shaped particles may not be dealt with adequately. For example, a cube has a mass per unit surface area approximately 40 percent less than a sphere of equivalent surface area. This may have a significant impact on the energy balance and could account for some of the errors in the predicted particle heating rate.

CONCLUSION

A novel imaging system was developed and applied to study changes in coal particle size and temperature during the early stages of devolatilization at heating rates representative of high intensity combustion processes. Based on these measurements, it is concluded that coal particles heat significantly (on the order of 50 percent) faster than is predicted using commonly employed approaches to model heat transfer. Potential causes for the differences between measured and predicted temperature histories include inadequate understanding of the temperature dependence of relevant coal thermodynamic and heat transfer properties and failure to account for particle shape factors. Regardless of the cause, heat transfer analyses employing spherical particle assumptions and widely accepted coal property correlations may yield significant errors in temperature histories and corresponding errors in the associated devolatilization time scales. Efforts are now in progress to address some of these issues.

ACKNOWLEDGEMENT

This work was funded through the U. S. Department of Energy Advanced Research and Technology Development Direct Utilization Program. E. R. Monazam would like to acknowledge Oak Ridge Associated Universities for their support in the form of a post-doctoral fellowship. The authors also wish to acknowledge the contributions of G. E. Fasching, K. Renner, J. D. Thornton and H. Lemley.

REFERENCES

1. Howard, J. B.: Chemistry of Coal Utilization (M. A. Elliot, Ed.) Second Supplementary Volume, p. 665, John Wiley, 1981.

2. Solomon, P. R. and Hamblen, D. G.: Chemistry of Coal Conversion (R. H. Schlosberg, Ed.) pp. 121-251, Plenum Press, 1985.

3. Solomon, P. R., Serio, M. A., Carangelo, R. M. and Markham, J. R.: Fuel **65**, 182 (1986).

4. Best, P. E., Carangelo, R. M., Markham, J. R. and Solomon, P. R.: Combustion and Flame **66**, 47 (1986).

5. Fletcher, T. H.: Combust. Sci. and Tech. **63**, 89 (1989).

6. Fletcher, T. H.: Combustion and Flame **78**, 223 (1989).

7. Freihaut, J. D. and Proscia, W. M.: Energy and Fuels **3**, 625 (1989).

8. Maloney, D. J., Fasching, G. E., Lawson, L. O. and Spann, J. F.: Rev. Sci. Instrum. **60**, 450 (1989).

9. Monazam, E. R., Maloney, D. J. and Lawson, L. O.: Rev. Sci. Instrum. **60**, 3460 (1989).

10. Phuoc, T. X. and Maloney, D. J.: Twenty-Second Symposium (International) on Combustion, p. 125, The Combustion Institute, 1988.

11. Baxter, L. L., Fletcher, T. H. and Ottesen, D. K.: Energy and Fuels **2**, 423 (1988).

12. Merrick, D.: Fuel **62**, 540 (1983).

13. Badzioch, S., Gregory, D. R. and Field, M. A.: Fuel **43**, 267 (1964).

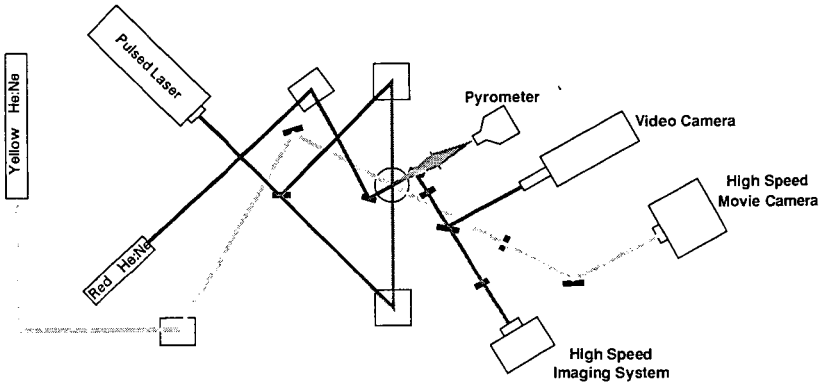

Figure 1. Diagram of EDB Measurement System

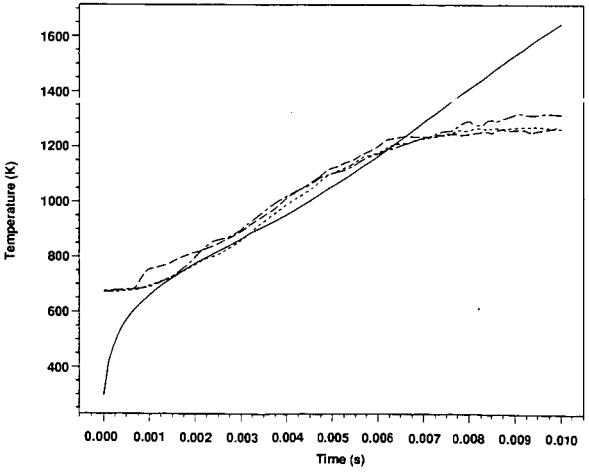

Figure 2. Comparison of Measured Temperature Histories and Model Predictions for Carbon Spheres

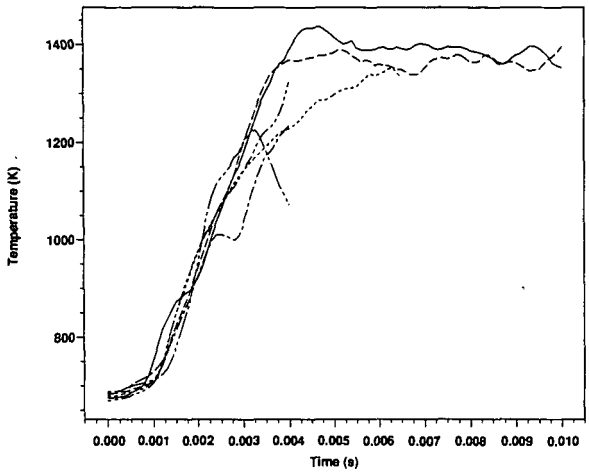

Figure 3. Measured Temperature Histories for Six Coal Particles at Similar Incident Heat Flux Conditions.

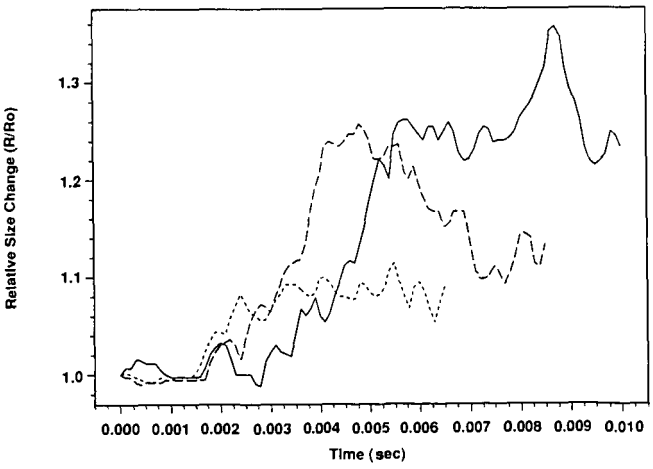

Figure 4. Measured Particle Size Histories for Three Coal Particles at Similar Incident Heat Flux Conditions.

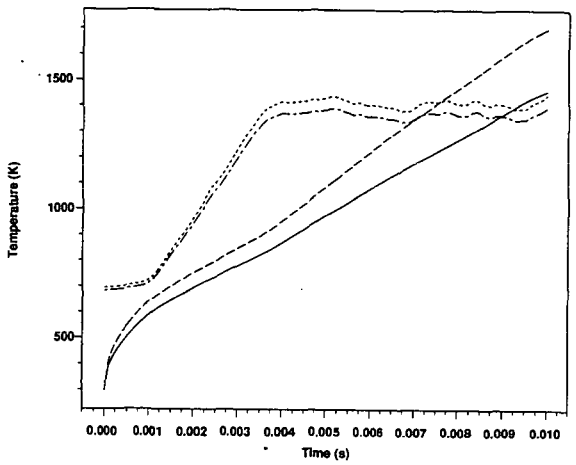

Figure 5. Comparisons of Measured and Predicted Temperature Histories for a Coal Particle as a Function of Assumed Particle Emissivity.
ε = 0.8: ------- Measured, ——— Predicted
ε = 1.0: — - — - — Measured, — — — Predicted

TRANSIENT HEATING OF COAL-WATER SLURRY DROPLETS

Phuoc X. Tran and Mahendra P. Mathur
Pittsburgh Energy Technology Center
Pittsburgh, PA. 15236

1. INTRODUCTION

Although many advantages can be derived from the use of CWF, the relatively large quantities of water in these fuels causes difficulties with ignition and flame stability. In addition, agglomeration of coal particles within the fuel droplets has been commonly observed to result in reduced combustion efficiency. Therefore, it is necessary to investigate the behavior of a CWF droplet undergoing heating and evaporation and the transient processes occurring in the interior of a CWF during this period so that processes such as disruptive burning, volatile release, combustion characteristics etc... are reliably predicted.

Theoretical model for the present analysis is illustrated in Fig. 1. For this droplet, the solid loading is initially large so that as the liquid component vaporizes, the evaporation front propagates into the interior of the droplet. In the wake of the evaporation front, coal particles support each other to form a porous shell keeping the droplet size constant during the evaporation history. The droplet now contains two different regions of consideration: the inner binary core whose surface is regressing with time and the porous shell which is thickening as the evaporation front moves. Thus the problem involves heating of the inner binary core, diffusion transport of the water vapor produced at the moving interface, and the diffusion transport of heat from an outer spherical boundary through the spherical porous shell of coal particle agglomerate. In addition to the complex phenomena, the inherent difficulties in the analysis are also due to the nonlinear nature of the moving interface and the transient behavior of the boundary conditions. Because of these difficulties any attempt to formulate any analytical solution must be accompanied with various model assumptions [1,2]. Such an attempt will obtain only relatively simple solutions in parametric forms and, therefore, many complicated phenomena associated with a slurry droplet during heating and evaporation will not be resolved. The main purpose of the present analysis is to develop numerical procedures to calculate the temperature distributions in both regions and the motion of the evaporation front under various conditions of heating rates, particle sizes.

2. FORMULATION OF THE PROBLEM

The present analysis is carried out under following assumptions: (i) spherical symmetry is valid, (ii) thermal properties are constant, (iii) internal mass transport is neglected, (vi) evaporation during the initial heat-up is neglected, (iv) surface absorption of the radiative heat flux is assumed and (v) the droplets behave like single phase with following properties:

$$\rho_d = (1-\phi)\,\rho_c + \phi\rho_w \quad ; \; m_d = \sum_i m_i \tag{1}$$

$$c_{p,d} = \sum_i Y_i \, c_{p,i} \quad ; \quad Y_i = \frac{m_i}{m_d} \tag{2}$$

where i is for coal and water; ϕ is the liquid volume fraction and it relates to m_c and m_w as:

$$m_c = (1-\phi)\, \rho_c V_d \quad ; \quad m_w = \phi\, \rho_w V_d \tag{3}$$

and the droplet thermal conductivity is calculated using Lee and Taylor analysis [3] as:

$$\frac{\lambda_d}{\lambda_w} = \frac{2\phi + (2-\phi)\, \lambda_c/\lambda_w}{3 - \phi\, (1-\lambda_c/\lambda_w)} \tag{4}$$

We define the following dimensionless groups for the present analysis:

$$\theta_i = \frac{T_i - T_o}{T_b - T_o} \quad ; \quad U_i = r\theta_i \quad ; \quad i = d,c \tag{6}$$

$$\tau = \alpha_d t / r_s^2 \quad ; \quad \xi = r/r_b \quad ; \quad \eta = (r-r_b)/(r_s-r_b) \tag{7}$$

$$\sigma = r_b/r_s \quad ; \quad \beta = \alpha_c/\alpha_d \quad ; \quad \kappa = \lambda_c/\lambda_d \tag{8}$$

$$\gamma = \varepsilon\, I_o r_s \,/\, \lambda_d\, (T_b - T_o) + \lambda_g\, (\theta_{g,e} - \theta_{d,s}) \,/\, \lambda_d \tag{9}$$

$$\nu = \rho_d\, c_{p,d}\, (T_b - T_o)/\rho_w\, \phi\, \Delta H \tag{10}$$

The process of the droplet heating and evaporation are described as:

At $0 \le \tau < \tau_p$

$$\frac{\partial U_d}{\partial \tau} = \frac{\partial^2 U_d}{\partial \xi^2} \tag{11}$$

At $\tau \ge \tau_p$

for the binary core

$$\frac{\partial U_d}{\partial \tau} = \frac{1}{\sigma^2} \frac{\partial^2 U_d}{\partial \xi^2} + \frac{\xi}{\sigma} \frac{\partial U_d}{\partial \xi} \frac{d\sigma}{d\tau} \tag{12}$$

for the porous shell

$$\frac{\partial U_c}{\partial \tau} = \frac{\beta}{(1-\sigma)^2} \frac{\partial^2 U_c}{\partial \eta^2} - \left(\frac{\eta-1}{1-\sigma}\right) \frac{\partial U_c}{\partial \eta} \frac{d\sigma}{d\tau} \tag{13}$$

and the droplet surface regression rate is calculated by:

$$\frac{d\sigma}{d\tau} = \frac{\nu}{\sigma} \left[\frac{1}{r_b} \left(\frac{\partial U_d}{\partial \xi}\right)_{\xi=1} - \frac{\kappa}{r_s - r_b} \left(\frac{\partial U_c}{\partial \eta}\right)_{\eta=0} + \kappa - 1\right] \tag{14}$$

These equations are subjected to the following conditions:

$$\text{At } \tau < 0 : \quad U_d = 0 \tag{15}$$

$$\text{At } 0 \leq \tau < \tau_p : \quad \sigma = 1 \; ; \quad U_d(0) = 0 \; ; \quad \left(\frac{\partial U_d}{\partial \xi}\right)_{\xi=1} = r_s \left(\gamma + \theta_{d,s}\right) \tag{16}$$

$$\text{At } \tau \geq \tau_p : U_d(0) = 0 \; ; \quad U_c(0) = U_d(1) = r_b \tag{17a}$$

$$\left(\frac{\partial U_c}{\partial \eta}\right)_{\eta=1} = (r_s - r_b) \left(\frac{\gamma}{\kappa} + \theta_{c,s}\right) \tag{17b}$$

3. NUMERICAL CALCULATIONS

Numerical procedures developed by Tran and Mathur [4] are used. The spatial coordinate of Eqs. (11), (12) and (13) are discretized employing the usual central difference approximation. These discretized equations are used to transform these equations into a system of ordinary differential equations in temporal coordinates as:

At $0 \leq \tau < \tau_p$

$$\left(\frac{\partial U_d}{\partial \tau}\right)^i = \frac{U_d^{i+1} - 2U_d^i + U_d^{i-1}}{\Delta \xi^2} \tag{18}$$

At $\tau \geq \tau_p$

for the binary core:

$$\left(\frac{\partial U_d}{\partial \tau}\right)^i = \frac{U_d^{i+1} - 2U_d^i + U_d^{i-1}}{\sigma^2 \Delta \xi^2} + \frac{\xi}{\sigma} \left(\frac{U_d^{i+1} - U_d^{i-1}}{2\Delta \xi}\right) \frac{d\sigma}{d\tau} \tag{19}$$

for the porous shell:

$$\left(\frac{\partial U_c}{\partial \tau}\right)^i = \frac{\beta\left(U_c^{i+1} - 2U_c^i + U_c^{i-1}\right)}{(1-\sigma)^2\,\Delta\eta^2} - \left(\frac{\eta-1}{1-\sigma}\right)\left(\frac{U_c^{i+1} - U_c^{i-1}}{2\Delta\eta}\right)\frac{d\sigma}{d\tau} \tag{20}$$

where i = 0 to k, k = $1/\Delta\xi$ for the binary core and $1/\Delta\eta$ for the porous shell.

The interface motion is now evaluated at i= k for the binary core and i = 0 for the porous shell as:

$$\frac{d\sigma}{d\tau} = \frac{\nu}{\sigma}\left[\frac{U_d^{k+1} - U_d^{k-1}}{2r_b\Delta\xi} - \frac{\kappa\left(U_c^1 - U_c^{-1}\right)}{2\Delta\xi\left(r_s - r_b\right)} + \kappa - 1\right] \tag{21}$$

To calculate the interface motion represented by Eq. (21), values of U_d^{k+1} and U_c^{-1} must be determined. Using conditions at the interface given by Eq. (17a), one can get:

$$\left(\frac{\partial U_d}{\partial \tau}\right)^k = \left(\frac{\partial U_c}{\partial \tau}\right)^0 = r_s\,\frac{d\sigma}{d\tau} \tag{22}$$

introducing Eq. (22) into Eq. (19) for i = k and into Eq. (20) for i = 0 to obtain U_d^{k+1} and U_c^{-1} as:

$$U_d^{k+1} = \frac{\left(r_s + \frac{U_d^{k-1}}{2\sigma\Delta\xi}\right)\frac{d\sigma}{d\tau} + \frac{2U_d^k - U_d^{k-1}}{\sigma^2\Delta\xi^2}}{\frac{1}{\sigma^2\Delta\xi^2} + \frac{d\sigma}{d\tau} \,/\, 2\sigma\Delta\xi} \tag{23}$$

$$U_c^{-1} = \frac{\left(r_s - \frac{U_c^1}{2(1-\sigma)\Delta\eta}\right)\frac{d\sigma}{d\tau} - \frac{\beta\left(U_c^1 - 2U_c^0\right)}{(1-\sigma)^2\,\Delta\eta^2}}{\frac{\beta}{(1-\sigma)^2\,\Delta\eta^2} - \frac{1}{2(1-\sigma)\Delta\eta}\,\frac{d\sigma}{d\tau}} \tag{24}$$

Hence value of $d\sigma/d\tau$ can be determined implicitly from Eqs. (21), (23) and (24) using method of halving of the interval. Using varying dimensionless time interval, and $\Delta\xi = \Delta\eta = 0.2$ these above equations are integrated using Adams-Moulton integration subroutine.

4. RESULTS AND DISCUSSION

The calculation was made for CWF droplet with 70 percent coal loading by weight heating and evaporation in an environment with $\lambda_g = 2.6\times10^{-4}$

cal/cm-s-K. Additional data for water are: ρ_w = 1.0 g/cm^3; $c_{p,w}$ = 1.0 cal/g-K; λ_w = 0.00146 cal/cm-s-K; ΔH = 540 cal/g and T_b = 373 K. For coal: ρ_c = 1.3 g/cm^3; $c_{p,c}$ = 0.35 cal/g-K and λ_c = 0.0003 cal/cm-s-K.

Shown in Fig. 2 are the typical temperature profiles in the interior of the CWF droplet i.e. the profiles of both the inner binary sphere and the porous coal agglomerate shell for I_o = 400 W/cm^2, r_s = 25 μm, ν = 1.326. In this figure the intersection of the temperature profiles and $\theta_d = \theta_c = 1$ gives the location of the evaporation front while the thickness of the developed porous shell is given by the width between these locations and σ = 1. For this CWF droplet, the temperature profile that exists when the droplet surface temperature increases to the boiling temperature of the water is far from uniform. As the surface temperature reaches the boiling temperature of the water, two regions of temperature distributions within the CWF droplet ensue: the inner binary core, whose surface is regressing with time and the porous shell which is thickening as the evaporation front moves.

The effects of radiation heat flux, I_o, droplet size, r_s, on the dimensionless temperature profiles of the binary core and of the porous shell are illustrated in Figs. 3a and 4a. To increase I_o and r_s leads to an increase in the heating rate, the surface temperature will rise rapidly and the droplet temperature deep inside will lag further behind the surface temperature. Eventually large temperature gradient is established and the intra-droplet temperature does not have enough time to keep pace with the motion of the evaporation front which depends strongly on the internal temperature gradient as describe by Eq. (14). As a result, the inner binary core is heated essentially by the thermal wave moving with the evaporation front. To decrease I_o and r_s results in lowering the heating rate, the surface temperature rises slowly and the internal temperature has enough time to keep pace with the surface temperature. In this instance, the internal temperature gradient is less significant leading to slow motion of the evaporation front. As a result, the heating of the binary core is due to thermal diffusion from the outer boundary.

The dimensionless temperature profiles of the porous shell of the coal particles agglomerate for various values of I_o and r_s were also illustrated in Figs . 3b and 4b. As shown, the temperature of the porous shell is distributed linearly across the porous shell for values of I_o and r_s used in the present analysis. Under opposite condition, such a linear distribution, however, was found only in the region closed to the droplet surface. As shown, the surface temperature is substantially higher than the boiling temperature of the liquid component and is also higher at higher radiant heat flux , I_o, large particle size, r_s.

5. CONCLUSION

A simple analysis has been made to investigate the transient processes occurring in the interior of a CWF droplet undergoing heating and evaporation. Two heating mechanisms have been obtained: at low heating rate the rate of heat diffusion is faster than the rate of the evaporation front motion, the transient heating of the inner binary core is controlled by diffusion and vanishes quickly after the evaporation begins. However, under opposite conditions, the rate of the motion of the evaporation is faster than the rate of the energy diffusion, the transient heating of the inner binary core occupies the entire period of evaporation and is controlled by the thermal wave moving with the evaporation front. The present numerical

technique is powerful for this kind of moving boundary and phase change problem.

NOMENCLATURE

c_p - specific heat
ΔH - heat of evaporation
I_o - radiant heat flux
r - r-coordinate
r_b - evaporation front location
r_s - droplet radius
T - temperature
T_b - temperature
T_o - initial particle temperature
t - time

Greek Symbols

α - thermal diffusivity
ε - emissivity
λ - thermal conductivity
ρ - density

Subscripts

b - evaporation front location
c - coal
d - droplet
e - ambient condition
g - gas phase
p - pyrolysis
s - surface
w - water

REFERENCES

1. P. Antaki, Transient Processes in a Rigid Slurry Droplet During Liquid Vaporization and Combustion, Combustion Science and Technology, 46, 113-135, (1986).

2. G. F. Carey and P. Murray, Perturbation Analysis of The Shrinking Core, Chem. Eng. Sci., 44, 979-983, (1989).

3. T. Y. R. Lee and R. E. Taylor, Thermal Diffusivity of Dispersed Material, J. of Heat Transfer, 400, 720-724, (1978).

4. P. X. Tran and M. P. Mathur, "Transient Heating of Coal Particles Undergoing Pyrolysis," 23rd Symposium (International) on Combustion, in press.

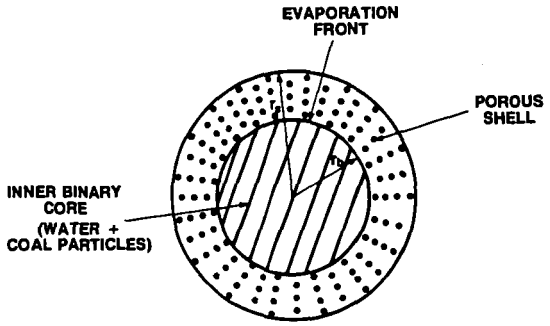

Figure 1. Theoretical Model.

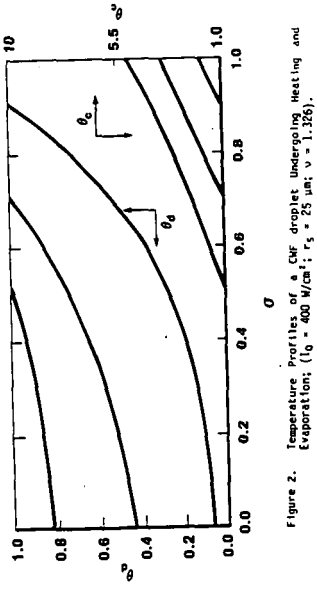

Figure 2. Temperature Profiles of a CWF droplet Undergoing Heating and Evaporation; (I_0 = 400 W/cm²; r_s = 25 μm; ν = 1.326).

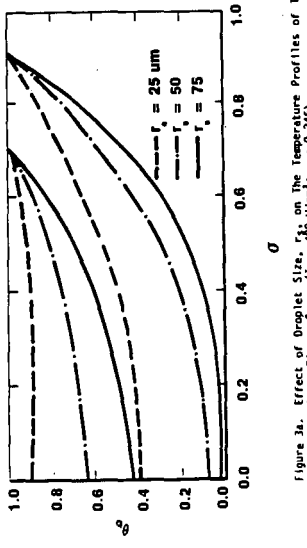

Figure 3a. Effect of Droplet Size, r_s; on The Temperature Profiles of The Inner Binary Core; (I_0 = 400 W/cm²; ν = 0.246).

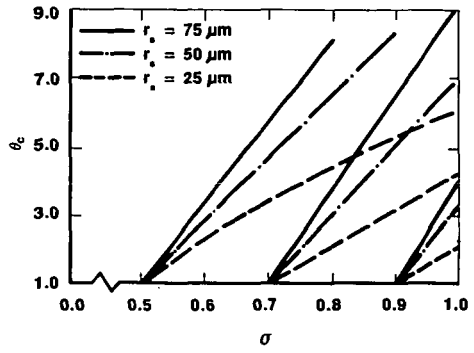

Figure 3b. Effect of Droplet Size, r_s, on The Temperature Profiles of The Porous Shell; (I_o = 400 W/cm²; ν_s = 0.246).

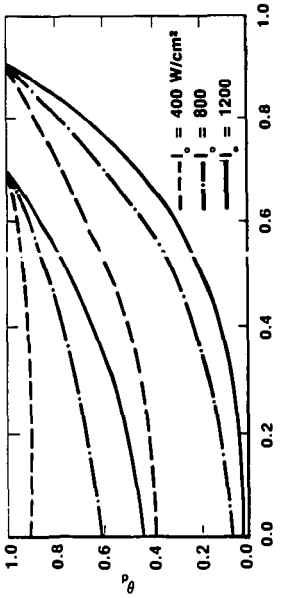

Figure 4a. Effect of Heat Flux, I_o, on The Temperature Profiles of The Inner Binary Core; (r_s = 25 μm; ν_s = 0.246).

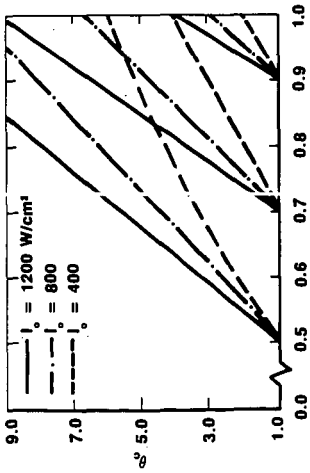

Figure 4b. Effect of Heat Flux, I_o, on The Temperature Profiles of The Porous Shell; (r_s = 25 μm; ν_s = 0.246).

Gas Stream Temperature Measurements Via Fourier Transform Infrared Spectroscopy

M. Shahnam*, S.D. Woodruff**, I. Celik* and R.G. Logan**

* Mechanical and Aerospace Engineering Department
West Virginia University, Morgantown, WV 26505

** U.S. Department of Energy, Morgantown Energy Technology Center
P.O. Box 880, Morgantown, WV 26507-0880

Abstract

A temperature measuring technique utilizing a Fourier Transform Infrared spectrometer (FT-IR) is reviewed and tested by applying it to a natural gas/air flame and to a hot gas (air) stream. The numerous problems encountered in using this technique are elucidated. Preliminary temperature measurement results based upon the intensity of the absorption spectrum of the ν_3 band of carbon dioxide is encouraging when compared to the standard thermocouple readings. Temperature measurements at different locations in a flame indicate that accurate temperature values can be obtained if there is sufficiently large amount of carbon dioxide present compared to the background carbon dioxide concentration.

Introduction

The problems in measuring the temperature and composition of hot, luminous, and particle-laden flows (i.e. inside coal combustors) have received increasing attention lately (Ottesen and Thorne, 1983). Particle temperature can often be measured by two color pyrometry. Gas phase information, however, is difficult to obtain in these dirty environments. FT-IR spectroscopy is a non-intrusive, in situ optical technique which can determine gas phase composition and temperature (Thorne and Ottesen, 1983). This technique does not perturb the chemical or flow characteristics of the combustion processes. Furthermore, the large spectral region sampled using FT-IR spectrometers permits quantitative determination of low molecular weight gases (CO, CO_2, H_2O, etc.) and hydrocarbons, as well as qualitative determination of heavier hydrocarbons. The temperature of the absorbing species can be determined if the individual vibration-rotation transitions of carbon dioxide, carbon monoxide, or low molecular weight hydrocarbons can be resolved. The aim of this study was to further the development of a procedure for measuring the temperature of hot combustion products based upon the individual vibration-rotation transitions of carbon dioxide. This paper reports on the preliminary results obtained from measurements in a natural gas/air laminar flame. Quantitative information such as temperature and concentration can be obtained from the observed absorption intensities. Ottesen and Thorne [1985] indicated that the characteristics of CO and CO_2 vibrational and rotational energy spectra are the most suitable for temperature measurements. They have mostly used CO spectra for this purpose. However for coal combustion, CO is usually an unstable reactive compound and may not be readily present for detection. Carbon dioxide will always be present in sufficient concentrations

in any coal combustion system. Therefore, a procedure has been developed to calculate the temperature of a natural gas/air diffusion flame based upon the υ_3 band of CO_2 absorption spectrum of the combustion products.

Theory

The flame temperature is obtained by resolving the vibrational-rotational transitions of CO_2 as pointed out by Herzberg [1939]

$$I = c_1 (J' + J'' + 1) \, EXP[-E(J'')/(kT)] \qquad (1)$$

where I = transition intensity, c_1 = a constant dependent on the vibrational transition, J', J'' = principal rotational quantum numbers for the upper and lower states respectively, $E(J'')$ = energy of the lower state, k = Boltzmann's constant and T = absolute temperature. Equation (1) can be rearranged as

$$\ln[I/(J' + J'' + 1)] = C - E(J'')/(kT) \qquad (2)$$

Assuming that the peak absorbance , H, of each transition is proportional to its transition intensity, a plot of $\ln[H/(J' + J'' + 1)]$ Vs. $E(J'')$ should give a straight line with a slope equal to $-1/(kT)$ according to (2). The rotational temperature, T, can then be obtained by calculating this slope. The energy levels of the lower state, E(J), of the υ_3 band of CO_2 (i.e. $00^0 1 - 00^0 0$) were tabulated by Air Force Geophysical Laboratory (AFGL) and are available upon request, Rothman [1989].

Experimental Setup and Procedure

The experimental apparatus consisted of four major components: the FT-IR spectrometer, transfer optics, the flame source, and an infrared detector. The FT-IR spectrometer was manufactured by Mattson Instruments, Inc. An Infrared beam was produced from the output of the interferometer and sent across the sample to an MCT infrared detector via transfer optics. Temperature measurements were taken in a flame and in a hot gas stream. The flame was created by burning natural gas with air in a bunsen burner, Figure 1. The hot gas stream was produced by heating the air inside a ceramic reactor, Figure 2. The high velocity jet emanating from the 1/8 inch ID nozzle fitted to the end of the reactor constituted the measuring section. The infrared beam traversing the flame or the hot jet measured the absorption spectra of carbon dioxide. Temperature measurements were based upon 100 scans at a resolution of 0.125 cm^{-1} of the background and the sample (i.e. flame). More details of the governing equations and procedure can be found in Celik et al. [1990].

Results and Discussion

Temperature measurements were taken at three different locations of (1) in the diffusion flame, Figure 1, (2) in the premixed flame, Figure 1, and (3) two inches away from the exit of a jet discharging hot air, Figure 2.

Location (1)

Figure 3 illustrates the absorption spectrum of the combustion gases in the outer cone of a natural gas/air flame, location (1). The various combustion species are evident based upon their absorption frequencies. Figure 4 shows the absorption spectrum of the υ_3 R-branch band of CO_2. The flame temperature is calculated based upon the intensity of each line, H, in this region. A plot of ln [H/(J + J + 1)] Vs. E(j) should yield a straight line whose slope is equal to -1/(kT) according to equation (2). This plot is shown in Figure 5. Since the slope of the straight line in Figure 5 is equal to -9.982E-04 , the flame temperature at the point of measurement should be 1441.37 K. A thermocouple reading of 1394.11 K was obtained at the same point in flame. The difference between the thermocouple reading and the FT-IR measured value can be attributed to the interference of the carbon dioxide absorption spectrum of flame by the amount of carbon dioxide already existing in the room (i.e. background). This is evident from comparison of Figures 6 and 7 which are the absorption spectrum of carbon dioxide at the point of measurement with and without the flame. The difference between these two distributions is the population distribution of carbon dioxide in the flame at the point of measurement. The larger this difference, the less interference exists. Since there is a significant population of the ν_3 vibration in the flame at this point compared to the population at room temperature, the temperature measured via FT-IR is close to the thermocouple measured value.

Location (2)

Temperature measurements based upon the υ_3 band of CO_2 absorption spectrum in the inner cone of the flame, approximately 10 mm above the surface of the burner Figure 8, resulted in erroneous values, location (2). The slope of the straight line in Figure 9 was -1.209E-03, that resulted in a temperature of 1190° K. A thermocouple reading of 589 K was obtained at the same point in the flame. This discrepancy is possibly due to the nonlinear distribution of carbon dioxide in the inner cone of the flame. Figures 10 and 11 illustrate the ν_3 population distribution of carbon dioxide at the point of measurement with and without the flame. A comparison of the difference between υ_3 band of CO_2 in Figures 10 and 11 with Figures 6 and 7, location (1), indicates a smaller distribution in location (2) compared to location (1); i.e. at the wavenumber of 2400.09, this difference is about 12.57 for location (1) and it is about 6.19 for location (2). This seems to indicate that for location (2) there was more interference from the existing amount of carbon dioxide in the room, causing much less accurate temperature readings.

Location (3)

Attempts were made to measure the temperature of hot gases in a heated air jet with an exit velocity of approximately 50 m/s, location (3). Figure 12 illustrates the absorption spectrum of carbon dioxide at 2 inches away from the exit of the jet. Carbon dioxide free air was purged through optical access holes on both sides of the jet in order to minimize the pollution of the jet by an external carbon dioxide source. The thermocouple reading was

560 F for this location. However the υ_3 band of carbon dioxide absorption spectrum was not sufficiently resolved to yield any temperature information. The background and the sample population distributions of the υ_3 band of carbon dioxide were virtually identical. This meant that there was a significant amount of interference from the carbon dioxide in the room, resulting in wrong temperature values.

Conclusions

A technique for measuring temperature using FT-IR spectroscopy based upon the ν_3 band of CO_2 absorption spectrum was evaluated in a flame and in a heated air jet. Since the intensity of the absorption spectrum of the υ_3 band of carbon dioxide was the basis for measuring the temperature, any interference of the infrared beam by an outside source (in this case background) seems to cause erroneous results. In the high temperature region of the diffusion flame, there was sufficient population distribution of CO_2 resulting in an accurate temperature measurement. However, since the population distribution of the ν_3 band of CO_2 in the premixed flame region and the hot air stream was comparable to that of the background, inaccurate results were obtained.

Acknowledgement

Support for this project was provided by Department of Energy, Morgantown Energy Technology Center under contract No. DE-FC21-87M24207, project A.2.

REFERENCES

Celik, I., Shahnam, M., Katragadda, S., and Usmen, R., "Deposition, Corrosion, Erosion and Sulfur Emission Studies Related to Coal Combustion", Final Report, No.: MAE/90/IC2, Mechanical and Aerospace Engineering Department, West Virginia University, February 1990.

Herzberg, G., "Molecular Spectra and Molecular Structure," V. I, Prentice-Hall. Inc.. 1939.

Herzberg, G., and Herzberg, L., "Rotation-Vibration Spectra of Diatomic and Simple Polyatomic Molecules with Long Absorbing Paths," Journal of Optical Society of America, Vol. 43, Number 11, November 1953, pp. 1037-1044.

Mavrodineanu, R., and Boiteux, H., "Flame Spectroscopy," Wiley, 1988.

Rothman, L., Private Communications, 1989.

Ottesen D.K. and Thorne L.R., International Conference on Coal Science, Pittsburgh, PA, p. 621 (August 15-19, 1983).

Ottesen, D.K. and Thorne, L.R., "In Situ Studies of Pulverized Coal Combustion by Fourier Transform Infrared Spectroscopy" International Conference on Coal Science, Sydney, NSW, Australia, p. 351 (Oct. 28-31, 1985).

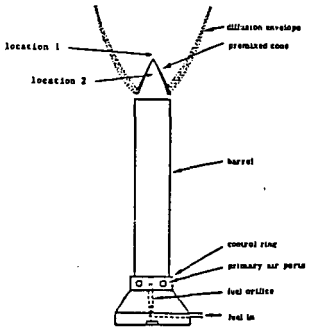

Figure 1 Schematic of a Bunsen Burner.

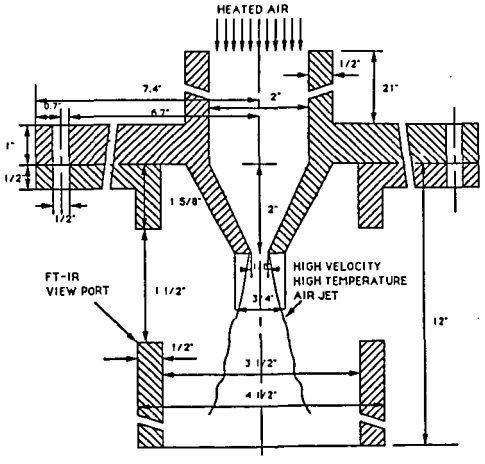

Figure 2 Side View of the Entrained Flow Reactor with the Nozzle.

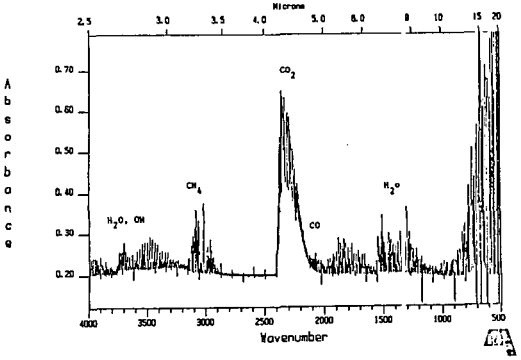

Figure 3 Absorption Spectra of Flame.

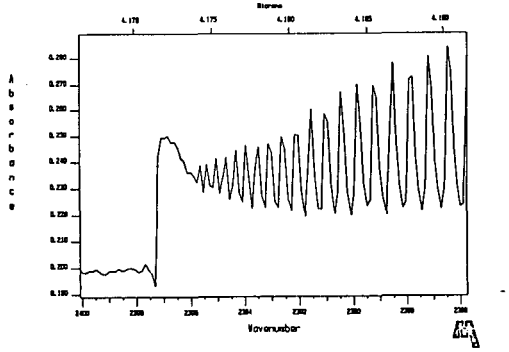

Figure 4 Absorption Spectra of the ν_3 Band of CO_2 (R-branch).

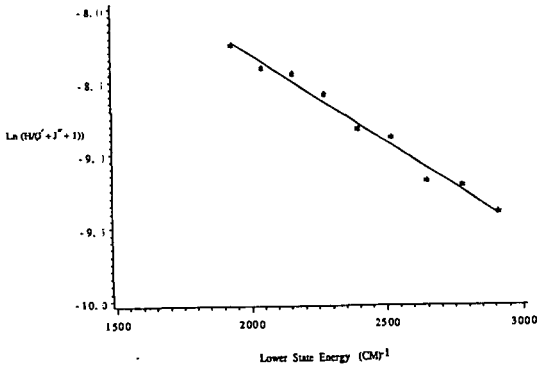

Figure 5 Rotational Temperature of Carbon Dioxide.

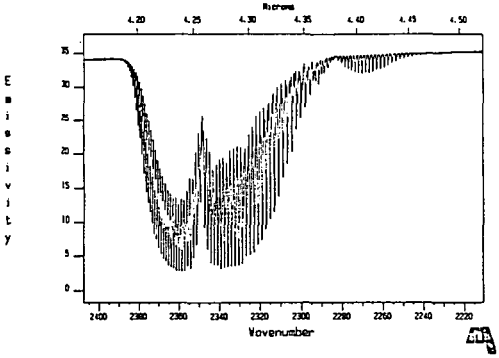

Figure 6 Background Single Beam.

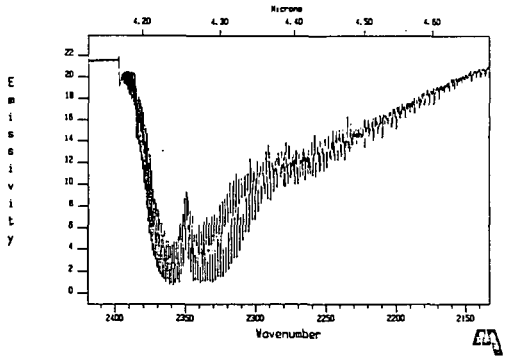

Figure 7 Sample Single Beam.

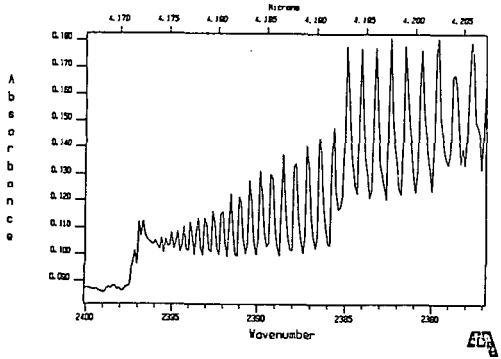

Figure 8 Absorption Spectra of the ν_3 Band of CO_2 (R-branch).

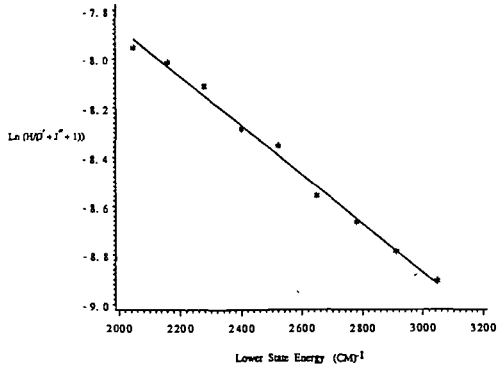

Figure 9 Rotational Temperature of Carbon Dioxide.

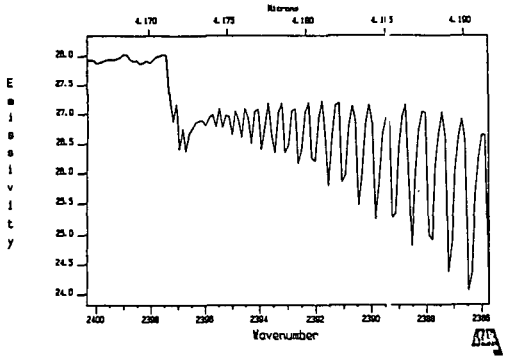

Figure 10 Sample Single Beam.

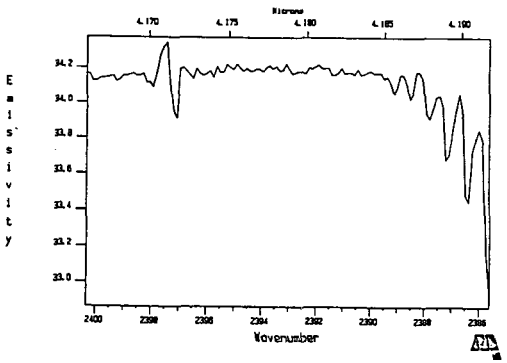

Figure 11 Background Single Beam.

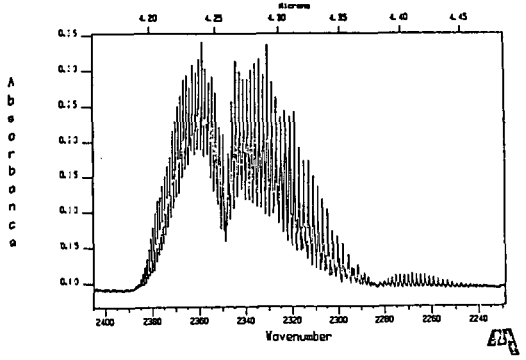

Figure 12 Absorption Spectra of CO_2 in a Hot Air Jet.

FT-IR EMISSION/TRANSMISSION TOMOGRAPHY OF COAL FLAMES

P.R. Solomon, J.R. Markham, Y.P. Zhang, and R.M. Carangelo
Advanced Fuel Research, Inc.
87 Church Street
East Hartford, CT 06108

INTRODUCTION

Fourier Transform Infrared (FT-IR) Emission/Transmission (E/T) spectroscopy has recently been shown to be a versatile technique for coal combustion diagnostics by allowing for measurements of particle concentrations and temperatures, and gas compositions, concentrations, and temperatures (1). These measurements are for the ensemble of particles and gases along a line-of-sight in the flame.

To correct the shortcoming of the line-of-sight measurements, tomography techniques have been applied to both the FT-IR emission and transmission spectra to obtain spatially resolved spectra from which local flame properties can be obtained. This method has been applied to a stable, well defined co-annular laminar ethylene diffusion flame (2,3). From the spatially resolved spectra, point values for species temperature and relative concentrations were determined for CO_2, H_2O, alkanes, alkenes, alkynes, and soot. Temperatures (for CO_2 and H_2O), and soot concentrations were found to be in good agreement with measurements performed on the same flame by coherent-anti-stokes Raman spectroscopy (CARS) (4) and laser scattering (5), respectively.

The technique was recently applied to a coal flame produced in a transparent wall reactor (TWR) using a Rosebud subbituminous coal (6). From these spectra, spatially resolved point values have been obtained for particle and CO_2 temperatures, relative particle, soot and CO_2 concentrations, the fraction of ignited particles, and the relative radiance intensity.

To study the effect of these conditions on coal type, two more flames have now been characterized. These are a second Rosebud subbituminous coal flame produced using a slower flow of preheated gas and a flame using Pittsburgh Seam coal produced under the same conditions. This paper compares the results from these three flames.

EXPERIMENTAL

Apparatus

The TWR facility has been described previously (1,6). The coal is injected upwards into the center of a 10 cm diameter upward flowing preheated air stream in the center of a 20 cm diameter x 70 cm tall glass enclosure. A flow of room temperature air along the perimeter of the reactor keeps the enclosure cool. Radial thermocouple measurements show that the preheated air stream provides a stable hot environment for the coal up to a height of about 30 cm. Our coal feeding system uses a carrier gas which exits the feeder through a tube as it is slowly lowered through a bed of coal particles. Mechanical vibration helps to displace and entrain particles into the tube. A steady feed results in a flame that is stable in shape and position except for the ignition point, where rapid verticle fluctuations of $\pm$ 5 mm are observed. The gas flows used for the high flow case were 2.9 l/sec in the preheated gas and 4.2×10^{-3} l/sec in the carrier gas. The gas flows used for the low flow case were 1.7 l/sec in the preheated gas and 3.6×10^{-3} l/sec in the carrier gas. The coal feed rate was 0.91 g/min for both cases.

The enclosure has movable KBr windows to allow access to the flame by the FT-IR spectrometer (a modified Nicolet 20SX). As discussed in Ref. 7, emission measurements are made by directing the radiation emitted by the hot sample stream through an interferometer to an "emission" detector. Transmission measurements are made by replacing this detector with a high intensity globar source which, after passing through the interferometer, is directed through the sample area to a "transmission" detector. The emission and transmission measurements are made along the same 1 mm wide by 4 mm high optical path defined with apertures. With this optical geometry, twenty-one parallel line-of-sight emission and transmission spectra were collected across the coal stream at 1 mm increments along the radius for each slice. Several slices were obtained for each flame.

The spatially resolved "point" values correspond to an average within 1 mm x 1 mm x 4 mm high volumes. In this work the data were smoothed by co-adding data from eight adjacent wavenumber bands. This results in degraded resolution from the 8 cm^{-1} used, although still sufficient to quantitatively measure the gas species.

Sample

The samples used in this experiment were sieved fractions (200 x 325 mesh) of dry Montana Rosebud subbituminous coal and dry Pittsburgh Seam coal. The characteristics of these coals have been published previously (1,8).

ANALYSIS

The analysis for the line-of-sight FT-IR E/T measurement pertaining to multi-phase reacting streams has been presented previously (1,6,7,9-11). The relative concentration and temperatures for individual components (gas, soot, and particles) are obtained from the transmission and normalized radiance spectra, respectively, as discussed in Refs. 1,6,7,9-11.

The reconstruction of spatially resolved FT-IR spectra from multiple line-of-sight spectra was first introduced elsewhere (2,3,6). We have employed the standard Fourier image reconstruction technique (12) which is capable of handling data from systems of arbitrary shape. Our flame, however, was cylindrically symmetric. The computer program published by Shepp and Logan was used for this work (12) by applying the reconstruction one wavelength at a time to determine spatially resolved spectra.

A straight-forward application of the reconstruction technique to radiance spectra is not possible, because of self-absorption in the sample. In the case of small absorbance encountered in this work (percent transmission > 80%), an emission measurement can be directly corrected by an absorption measurement made along the same path. A self-absorption correction corresponding to that used by Freeman and Katz was employed for the thin sample studied (13). The Fourier reconstruction program can be applied directly to the emission thus corrected, to obtain local radiances. These are then converted to normalized radiance and the analysis proceeds as for the line-of-sight spectra.

RESULTS

Flame Characteristics

The three flames are presented in Fig. 1. All three flames are characterized by a bright ignition zone followed by a region of lower intensity where burnout is occurring. Photographs show the high intensity zone to contain burning volatile clouds which are 3 to 5 times the diameter of the particles. The Pittsburgh Seam coal shows a region of distinct dimness after ignition which may occur after the initial oxygen is consumed by the volatiles.

Measurements were made of the particle velocities by measuring the length of tracks recorded with a video camera using a 1/250 shutter speed. The results are presented in Fig. 2. The particles accelerate as they leave the nozzle due to the heating of the carrier gas, the influence of the faster hot gas surrounding the carrier gas stream, and buoyancy effects. At ignition, the acceleration is increased as the center stream is rapidly heated. The data show the velocities increasing to above the hot gas velocity. The heating of the central stream appears to dominate the particle velocity as the two cases where the hot gas velocity is lowest (Fig. 2b and 2c) produces a higher particle velocity then in Fig. 2a where the hot gas velocity is higher. Based on these velocities, the particle residence times (given in Fig. 1) were computed.

The tomography data for these three flames are presented in Figs. 3 to 5. The seven parameters which were measured are: a) relative particle and soot concentration, b) the multiplier M which is the emissivity times the fraction of particles at the measured temperature, c) the spectral radiance at 4500 cm^{-1}, d) the particle and CO_2 temperatures, and e) the CO_2 concentration.
The tomography data for the Rosebud fast flow case are presented in Fig. 3. These data were presented previously (6) but are reproduced here for comparison. Figure 3a presents the height of

the continuum blockage determined from the transmittance spectra as percent blockage of the incident IR beam. The blockage is divided into particles and soot. Soot is observed to appear at ignition as inferred by the change in shape of the continuum as described below. Below the ignition (6 cm above the 4 mm diameter nozzle) there are particles only (no soot) confined to a radius of about 6 mm. This is in agreement with the boundaries as determined by scattering of a He-Ne laser beam. The multiplier, M (the product of emissivity times the fraction of ignited particles in Fig. 3b shows a few particles (up to 10%) have ignited at the edge of the coal stream. Such ignited particles can also be seen in Figs. 1b and 1c.

Just above ignition (10.5 cm above the nozzle), the particles appear to be forced inward into a more dense central stream at the same time that some particles are spread outward. The spreading of the stream is confirmed visually. This spreading is consistent with the location of the ignition zone centered at about 2 mm radius, indicated by the 0.35 M value in Fig. 3b (i.e., approximately one-third of the particles ignite). Considerably less material is ignited at the center and outer region of the ignition zone. The increase in gas volume in this zone acts to compress the stream inward and expand the stream outward. The total particle blockage (number in parentheses in Fig. 3a) determined by integrating the blockage times area indicates that the blockage is increased from 1.0 (by definition) at 6 cm to 1.7 at 10.5 cm to 1.5 at 12 cm. This suggests that the devolatilization which appears complete at this point may swell or fragment the particles to increase the blockage. Swelling is observed in SEM photographs of collected particles. Above 12 cm, the particle blockage is reduced as the material burns out (Fig. 3a).

The multiplier, M (Fig. 3b), indicates that the ignition zone quickly collapses to the center axis (compare 10.5, 12, and 14 cm). From 14 cm through 16 cm M again drops near the center region, but this may be caused by a build-up of ash in the center region, as evidenced by a corresponding drop in the relative amount of soot compared to particles at these positions. At 20 cm, an increase in blockage at radiuses above 4 mm is observed (ash dispersion) with a corresponding decrease in M above 4 mm and an increase in M at the center.

Figure 3c presents the local radiance determined at 4500 cm^{-1}. At 6 cm, high frequency radiance is detected from the previously mentioned few particles that are observed to ignite at the edge of the coal stream. Just above the ignition point (10.5 cm), the high values of radiance along the center result from the high density of particles blockage, even though M may be low. The radiance from 10.5 cm to 12 cm is observed to increase along the center, as was observed for M.

Figure 3d presents the temperature of CO_2 (dashed line) and total continuum, both particles and soot (solid line). Also presented are measurements with a Pt + PtRh thermocouple obtained in the flame at the 12, 16, and 20 cm positions. The particles have a relatively constant temperature between 1800 and 1900 K at 10.5 and 12 cm. The cooler center region at 10.5 cm (in agreement with M and radiance) is observed. Particle temperature increases from 1900 K to 2000 K at 14 cm, and to 2200 K to 2400 K through 16 to 20 cm. Above 20 cm the temperature falls.

The maximum CO_2 temperatures (2200 to 2600 K) occur in the regions of high particle radiance where the maximum combustion is occurring, although the center temperature at 12 and 16 cm are puzzling. In the beginning region of the flame, CO_2 is 400 to 700 K hotter than the particles in the same region suggesting that CO is burning to CO_2 away from the particles. CO_2 temperatures are generally closer to the particle temperatures above 14 cm. At the edge of the stream the CO_2 temperature is always lower due to rapid heat transfer to the surrounding air. At 20 cm the CO_2 and particle temperatures are within 100 K except along the axis where the CO_2 is hotter.

The CO_2 concentrations are presented in Fig. 3e. Below ignition the CO_2 concentration is very small. Above ignition the CO_2 level jumps drastically and spreads with increasing height. These data present a picture of the coal burning in a shrinking region which collapses to the center at the tip of the flame.

The results for the two other flames are presented in Figs. 4 and 5. The trends are qualitatively similar. There are, however, differences in the soot formation, swelling, ignition, particle temperatures, burnout, and CO_2 concentrations, and these will be discussed below.

Soot Formation - As described previously (1) the shape of the continuum spectra can be employed to separate the contributions from particles and soot. Two spectra for the Pittsburgh Seam coal are presented in Fig. 6. Figure 6a presents $1-\tau$, where τ is the transmittance, prior to ignition where no soot is present. The upward slope toward low wavenumbers (long wavelengths) is due to diffraction. Figure 6b presents a spectrum above ignition in the region of high soot. The spectrum now slopes in the opposite direction due to soot. To resolve the spectrum into particle and soot contributions, the frequency dependent extinction efficiency, F'_ν, for the particles (which is proportional to $(1-\tau)$) is assumed to have the same shape as prior to ignition, and the particle transmittance is assumed to be equal to the measured transmittance extrapolated to 0 cm^{-1} (where the attenuation from soot goes to zero). A straight line extrapolation is made below 3500 cm^{-1} excluding the region of the spectrum containing CO_2 and H_2O bands. The soot contributions is the difference between the particle attenuation and the total as shown in Fig. 6c.

The relative amounts of soot can be seen in Figs. 3a, 4a, and 5a. The soot concentration is highest just above ignition. The highest soot concentrations are observed for the Pittsburgh Seam coal followed by the Rosebud slow case and then the Rosebud fast case. For Pittsburgh Seam, the highest attenuation from soot is about three times that from the particles. For Rosebud (slow flow) the highest value is only 2.3 times and for Rosebud (fast flow) only a little over 1 times. The variation in soot concentration comes from two factors: 1) tar, which is the soot precursor (1) is higher for Pittsburgh Seam coal than for Rosebud, and 2) the better mixing in the fast flow increases the oxygen to the central core which reduces the soot.

Swelling and Fragmentation - The swelling or fragmentation of the particles is indicated by the integrated particle blockage values as a function of position. The 6 cm case of the Rosebud and the 4 cm case for the Pittsburgh provide the baseline before ignition. Both cases show a flat distribution over the center 2 mm and goes to zero between 4 and 5 mm. The integrated blockage is given in parenthesis on each of the figures.

If there was no swelling or fragmentation, the blockage would decrease due to the gas heating. For the Pittsburgh Seam coal, the integrated blockage more than triples. Photomicrographs of samples collected in the flame show both swelling of coal and the appearance of small ash particles. Both changes would increase the blockage. For the Rosebud coal, the increases are more modest. While swelling was observed for the fast flow case, the slow flow case does not indicate an obvious swelling or rounding.

Ignition - Ignition for all three cases occurs with the outside of the particle stream (which is in best contact with the hot gases) igniting first. This can be seen in the multiplier M, which is the fraction of ignited particles, in Figs. 3b, 4b, and 5b. At ignition, M is highest at the edge of the particle stream. A photograph in Fig. 7 looking at the ignition zone of the Rosebud slow case clearly shows the ring of ignition. The Pittsburgh which is also a slow flow case exhibits a similar ring while the faster flow case which appears to have better mixing shows the same effect but to a lesser degree. Ignition at the edges is consistent with the particle temperatures below ignition (Fig. 5d) which indicate that the particles at the edge of the stream have reached 800 K while those in the center are as low as 600 K.

Temperatures - The following observations can be made about particle temperatures. 1) Particle temperatures are highest at the edge of the flame where the concentration of oxygen is highest. 2) The lowest temperatures are observed for the Pittsburgh Seam coal, while the highest temperatures are observed for the fast flow Rosebud case. Particle temperatures are generally in the range 1400 to 2200 K.

CO_2 temperatures are always higher than the particle temperatures in the combustion region suggesting that most CO_2 is produced away from the particle surface (e.g., by CO oxidation). The highest CO_2 temperatures were observed in the fast flow case and approached 2600 K.

Burnout - The percent weight loss as a function of distance above the nozzle for the three flames is indicated in Fig. 1, and plotted in Fig. 8. Both slow flow cases display a transient plateau in their burnout profiles which begin within 5 cm past their respective ignition points. Rapid oxygen consumption and inadequate mixing of the surrounding air is believed to cause this effect, which is not displayed for the fast flow (better mixing) case. Both Rosebud flames exhibit essentially 100%

DAF burnout by 50 cm above the nozzle. The Pittsburgh flame, however, seems to contain - 10% char which displays a very low reactivity.

CO_2 Concentration - The concentration of CO_2 for all cases generally decreased with distance away from the centerline for each slice. The slow flow Rosebud case showed an overall larger amount of CO_2 in the combustion region than the fast flow Rosebud case, but this may be attributed to less mixing (and hence, less dilution) for the slow flow condition.

CONCLUSIONS

Tomographic reconstruction techniques have been applied to FT-IR E/T measurements to derive local values for species temperatures and concentrations within three laboratory scale coal flames. Values for particle temperature, relative particle density, relative soot concentration, the radiance intensity, the relative CO_2 concentration and the CO_2 temperature have been obtained as functions of distance from the flame axis and height above the coal injector nozzle. The spectroscopic data are in good agreement with visual observations and thermocouple measurements. These data present a picture of the coal burning in a shrinking region which collapses to the center at the tip of the flame. CO_2 temperatures are highest in the rapid burning zone (2200 to 2600 K). The highest particle temperatures in this zone are 1900 to 2000 K, with temperatures up to 2400 K outside the zone. The three flames showed both coal and flow dependent phenomena. The slow flow cases showed reduced mixing (more soot and more variations in flame properties with radius) compared to the fast flow case. The Pittsburgh Seam coal showed higher soot, higher swelling, lower particle temperatures, and lower char reactivity compared to the Rosebud coal.

ACKNOWLEDGEMENT

This work was supported under the U.S. Department of Energy, Morgantown Energy Technology Center Contract No. DE-AC21-86MC23075. Richard Johnson is the METC Project Manager.

REFERENCES

1. Solomon, P.R., Chien, P.L., Carangelo, R.M., Best, P.E., and Markham, J.R.: Twenty-Second Symposium (International) on Combustion, p. 211, The Combustion Institute, (1988).
2. Chien, P.L., Best, P.E., Carangelo, R.M., and Solomon, P.R., "Tomographic Reconstruction of Fourier Transformed Infrared (FT-IR) Spectra at Points within a Coannular Flame", poster session 22nd Symposium (Int) on Combustion, Seattle, Washington, DC, (Aug. 1988).
3. Best, P.E., Chien, P.L., Carangelo, R.M., Solomon, P.R., Danchak, M. and Ilovici, I.: "Tomographic Reconstruction of FT-IR Emission and Transmission Spectra in a Sooting Laminar Diffusion Flame: Species Concentrations and Temperatures", Combustion and Flame, submitted for publication (1989).
4. Boedeker, L.R., and Dobbs, G.M., Comb. Sci. Technol., **46**:301, (1986).
5. Santoro, R.J., Semerjian, H.G., and Dobbins, R.A., Combustion and Flame, **51**:203, (1983).
6. Markham, J.R., Zhang, Y.P., Carangelo, R.M., and Solomon, P.R., "FT-IR Emission/Transmission Tomography of a Coal Flame", 23rd Symposium (Int) on Combustion, France, (July 1990).
7. Best, P.E., Carangelo, R.M., and Solomon, P.R.: Combustion and Flame **66**, 47, (1986).
8. Serio, M.A., Hamblen, D.G., Markham, J.R., and Solomon, P.R.: Energy & Fuel, **1**, 138, (1987).
9. Solomon, P.R., Carangelo, R.M., Best, P.E., Markham, J.R., and Hamblen, D.G.: Twenty-first Symposium (International) on Combustion, p. 437, The Combustion Institute, (1987).
10. Solomon, P.R., Best, P.E., Carangelo, R.M., Markham, J.R., Chien, P.L., Santoro, R.J., and Semerjian, H.G.: Twenty-first Symposium (International) on Combustion, p. 1763, The Combustion Institute, (1987).
11. Solomon, P.R., Carangelo, R.M., Best, P.E., Markham, J.R., and Hamblen, D.G.: Fuel **66**, 897, (1987).
12. Shepp, L.A. and Logan, B.F.: IEEE Trans. Nucl. Science, NS-21, (1974).
13. Freeman, M.P. and Katz, S.J.: Optical Society of Am., 50, (8), 826, (1960).

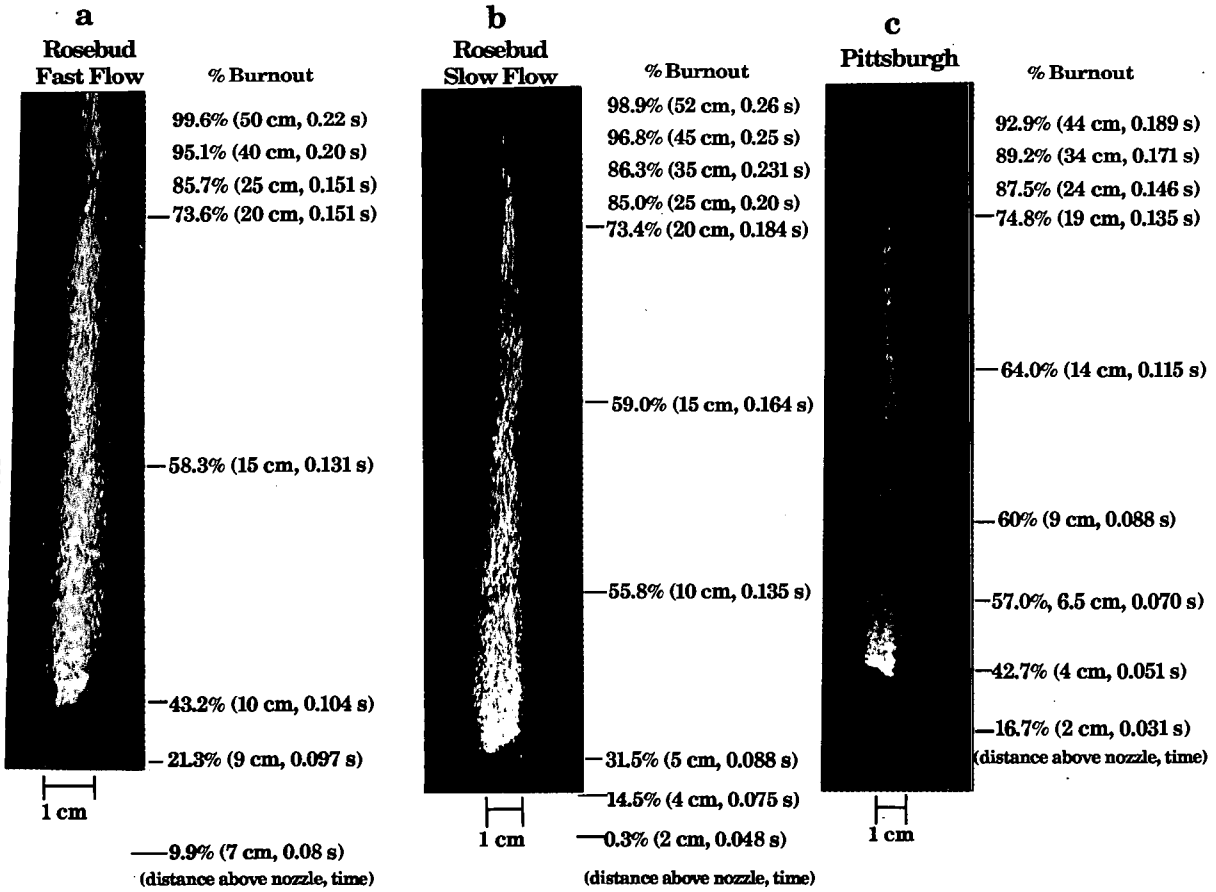

Figure 1. Photographs of Coal Flames in the TWR. a) Rosebud Subbituminous - Fast Flow, b) Rosebud Subbituminous Coal - Slow Flow, and c) Pittsburgh Seam Bituminous - Slow Flow. % Burnout as Determined from Particle Collections in each Flame is Indicated.

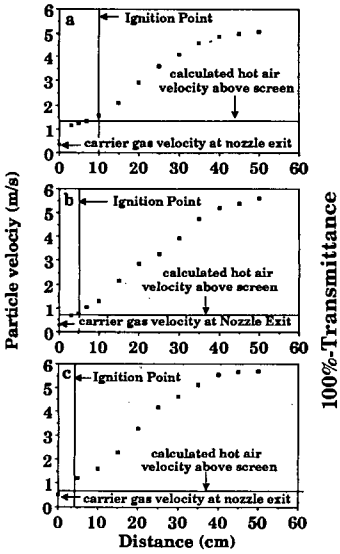

Figure 2. Particle Velocities as a Function of the Distance Above the Nozzle. a) Rosebud Subbituminous Coal - Fast Flow, b) Rosebud Subbituminous Coal - Slow Flow, and c) Pittsburgh Seam Bituminous Coal - Slow Flow.

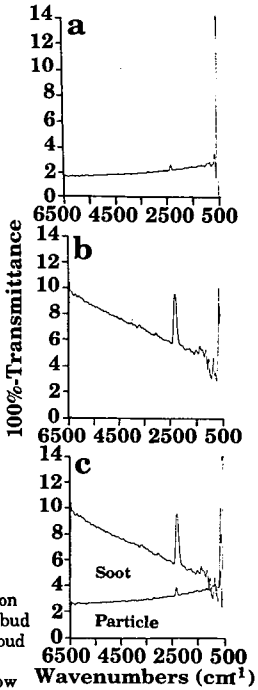

Figure 6. Analysis to Resolve Continuum Blockage Spectrum into Particle and Soot Contributions. a) Particle Blockage Below Ignition, b) Total Particle and Soot Blockage above Ignition, and c) Contribution of Each Component to Total Blockage.

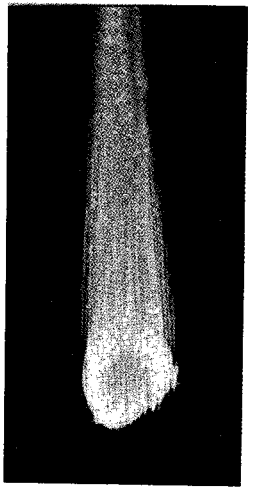

Figure 7. Photograph of Rosebud Subbituminous Coal - Slow Flow Flame Taken from Above the Ignition Region.

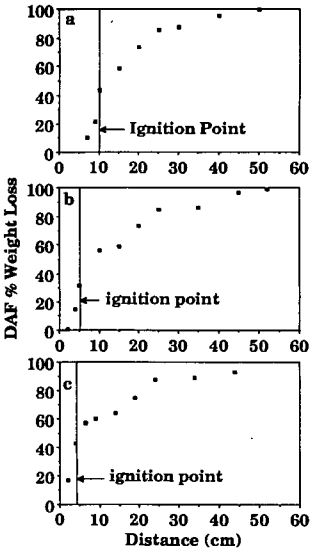

Figure 8. DAF % Weight Loss (burnout) as a Function of Distance Above the Nozzle for a) Rosebud Coal - Fast Flow, b) Rosebud Coal - Slow Flow and c) Pittsburgh Coal - Slow Flow.

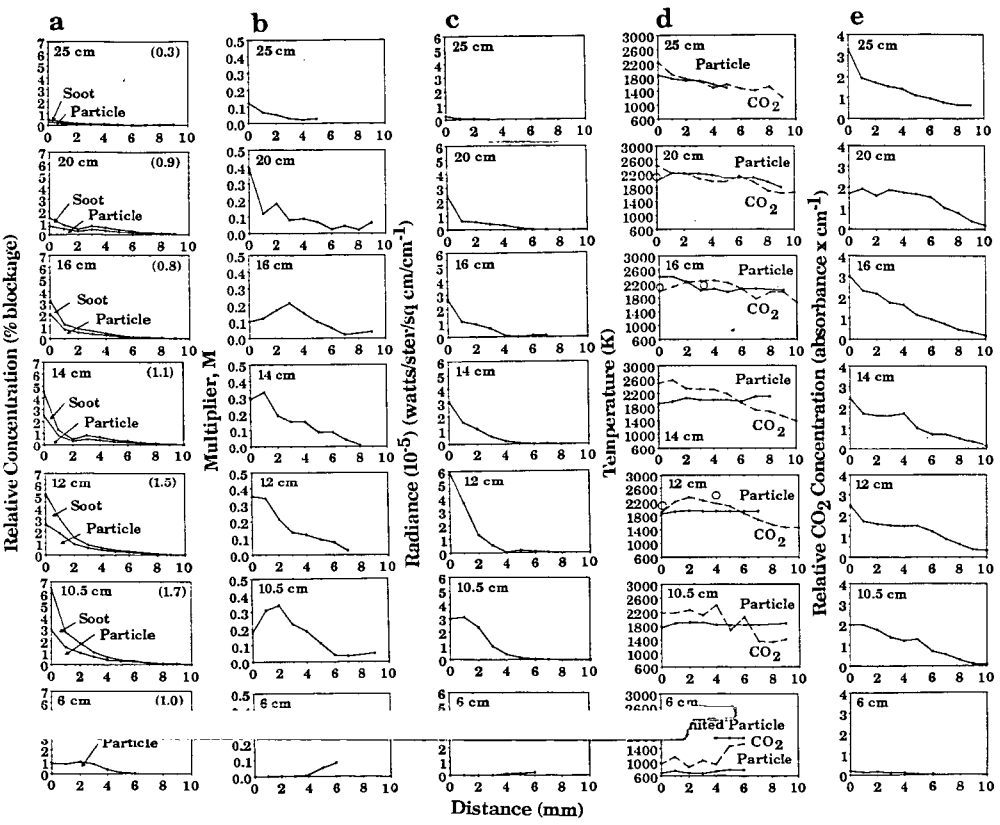

Figure 3. Data for Rosebud Subbituminous Coal - Fast Flow Flame. Radial Distributions of a) Particle and Total (particle + soot) Concentration. Integrated Particle Blockage is Indicated in Parenthesis; b) Multiplier for IgnitedParticles (Black-body intensity); c) Spectral Radiance at 4500 cm^{-1}; d) Particle (solid) and CO_2 (dashed) Temperature; e) CO_2 Concentration at Indicated Distances above the Nozzle for a Rosebud Coal Flame in the TWR.

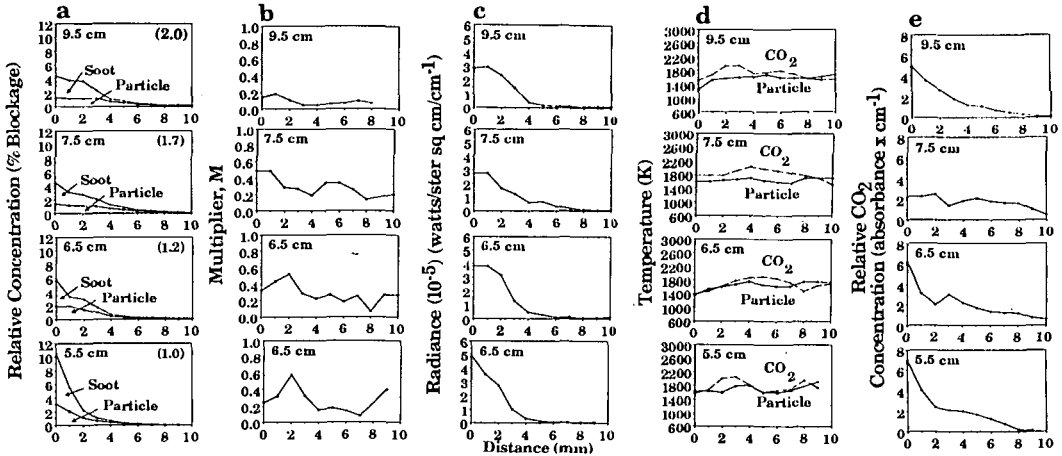

Figure 4. Data for Rosebud Subbituminous Coal - Slow Flow Flame. Radial Distributions of a) Particle and Total (particle + soot) Concentration. Integrated Particle Blockage is Indicated in Parenthesis; b) Multiplier for *IgnitedParticles (Black-body intensity)*; c) *Spectral Radiance at 4500* cm^{-1}; d) Particle (solid) and CO_2 (dashed) Temperature; e) CO_2 Concentration at Indicated Distances above the Nozzle for a Rosebud Coal Flame in the TWR.

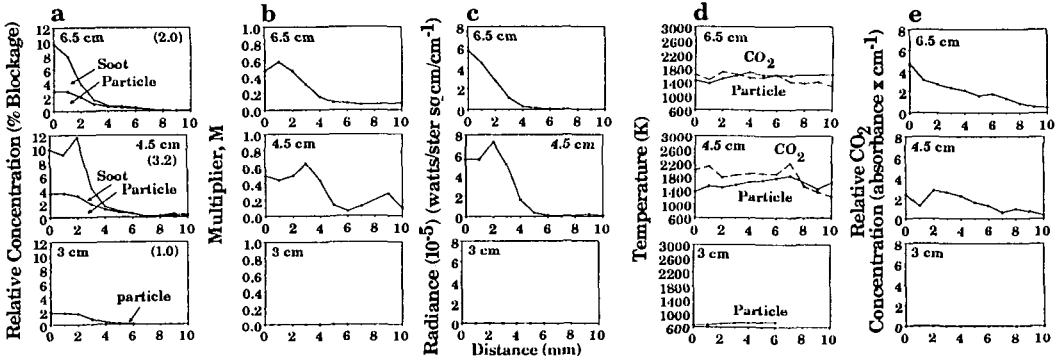

Figure 5. Data for Pittsburgh Seam Bituminous Coal - Slow Flow Flame. Radial Distributions of a) Particle and Total (particle + soot) Concentration. Integrated Particle Blockage is Indicated in Parenthesis; b) Multiplier for Ignited Particles (Black-body intensity); c) Spectral Radiance at 4500 cm^{-1}; d) Particle (solid) and CO_2 (dashed) Temperature; e) CO_2 Concentration at Indicated Distances above the Nozzle for a Rosebud Coal Flame in the TWR.

DEVELOPMENT OF NOVEL, MASS SPECTROMETRIC COMBUSTION MONITORING TECHNIQUES

William H. McClennen, Neil S. Arnold, Sue Anne N. Sheya, JoAnn S. Lighty* and Henk L.C. Meuzelaar

Center for Micro Analysis and Reaction Chemistry
University of Utah
Salt Lake City, UT 84112

*Chemical Engineering Department, University of Utah
Salt Lake City, UT 84112

KEYWORDS: combustion monitoring, gas chromatography, mass spectrometry

ABSTRACT

An on-line gas and vapor analysis method has been developed to monitor combustion products by short column ("transfer line") Gas Chromatography/Mass Spectrometry. An automated vapor sampling inlet with only inert materials (quartz and fused silica) in the sample path is utilized to introduce flue gases into a 1 m long "transfer line" capillary GC column for rapid, repetitive chromatographic separation of products. The column effluent is introduced directly into the source of an ion trap type mass spectrometer. Combustion products from a gas fired rotary kiln were monitored by this method using a standard Ion Trap Detector (ITD). Detection limits of 20 to 50 ppb were obtained for various substituted benzenes. Monitoring of polycyclic aromatic hydrocarbons (PAHs) from the thermal desorption of contaminated soils in a fixed bed reactor utilized a modified Ion Trap Mass Spectrometer (ITMS). Varying isothermal column temperature allowed analysis of PAHs from naphthalene through 6 ring PAHs. The ITMS system provides higher sensitivity (~4 ppb for benzene) in addition to tandem MS and chemical ionization capabilities for unambiguous identification of combustion products incompletely resolved by the transfer line GC approach.

INTRODUCTION

With the decreasing availability of hazardous waste disposal landfills, new technologies must be utilized for the permanent and proper elimination of these wastes. Of the approximately 265 million metric tons (MMT) of hazardous wastes generated yearly in the United States, at least 47 MMT per year could be incinerated [1]. In addition to the yearly generation of hazardous waste, the cleanup of uncontrolled hazardous waste sites must also be considered. The National Priority List (NPL) contains nearly 1000 sites which have been identified as hazards to public health and the environment and must be remediated. In addition there are estimated to be 10,000 sites which are presently uncontrolled [2]. Among the as yet uncontrolled sites are the widespread contaminated soils of former coal gas plant sites [3]. At these sites one may expect to encounter a broad range of polynuclear aromatic hydrocarbons (PAH's).

The importance of incineration technology for primary treatment of various types of industrial, medical, urban and agricultural waste as well as for remedial treatment of toxic waste dumps, landfills, chemical stockpiles, or accidental spill sites is widely recognized. Thermal treatment

is presently an effective way of removing organic contaminants from soil [4]. Generally, a two stage process is used in which the first stage is represented by a fixed bed or rotary kiln reactor [5] in which the organic contaminants are desorbed and/or pyrolyzed followed by a second stage, high temperature "afterburner" in which the volatile products of the first stage are effectively destroyed. Especially, the heaviest PAH components are likely to desorb very slowly from the soil matrix.

Continuous monitoring is needed to ensure that the incineration or thermal desorption system is operating properly at any given time [6]. Currently, unwanted emissions due to faulty equipment or operational procedures are generally detected (if at all) weeks or even months after the fact, when laboratory test data become available. Modern, on-line chromatographic and spectroscopic monitoring techniques offer the potential of near instantaneous feedback, thereby enabling immediate detection and correction of problems before significant levels of unwanted emissions have occurred. In view of their high sensitivity, specificity and speed, mass spectrometric methods play an important role among candidate monitoring techniques.

As shown by McClennen et al. [7,8] and Arnold et al. [9,10] a transfer line gas chromatography/mass spectrometry (TLGC/MS) technique, using the heated 1 m long coated fused silica capillary transfer line of a Finnigan-MAT Ion Trap Detector (ITD) as a short GC column, constitutes a powerful detection and characterization method for volatiles evolving from combustion reactors. In combination with a specially developed direct vapor sampling inlet [10] vapor detection levels in the low ppb range, corresponding to subpicogram quantities, can be achieved on an array of volatiles.

EXPERIMENTAL

The transfer line chromatography is performed using a 1 m fused silica capillary column which is contained and heated in the ITD transfer line. The inlet of the column is at ambient pressure, while the exit is evacuated in the ion trap. Using a .18 mm ID column, the carrier gas (helium) velocity is 2.7 m sec^{-1} (at 4400 ft elevation), which is close to optimum for the column length and pressure drop.

For both the fixed bed and kiln experiments a direct vapor sampling transfer line GC/MS method was used. The direct atmospheric vapor sampling inlet, shown in Figure 1, consists of three concentric tubes with appropriate flow control plumbing and electronics. The inlet system is made from deactivated fused silica, quartz and glass, or glass lined metal tubing. The sample path contains no moving parts. When sampling, the gas is exposed to the column inlet for a controlled period of time (0.5 to 2 s) while 30 to 200 μL of sample is admitted to the column. Helium carrier gas flow is then restored for the rest of the sampling cycle and GC separation of the sample takes place.

This inlet is coupled to fixed a pressure column drop transfer line chromatography. The 1 m long transfer line fused silica capillary GC column, provides both a nominal GC separation of components and a pressure drop to the ion source of the mass spectrometer. With the fixed pressure drop, the chromatographic conditions are controlled primarily by the column length, radius and temperature [11].

This transfer line inlet system was used with both a regular Finnigan MAT ITD and a modified ITMS system (termed MINITMASS) with axial modulation and Selective Mass Storage to allow for tandem mass spectrometry [12]. In addition to tandem capabilities, this second system permitted higher flow rates by using the axial modulation feature. The combination of increased resolution and increased flow rates resulted in higher sensitivity.

Rotary Kiln - The (GC/MS) system was used to monitor the evolution of trace amounts of hydrocarbons evolving from a material combusted in a rotary-kiln simulator. The rotary-kiln simulator is a useful tool for determining the transient emission of hydrocarbons from a control volume of waste. The simulator replaces the variable of kiln distance in a full-scale incinerator for that of time in the simulator; hence, the gas-phase concentrations of hydrocarbons are given as a function of combustion time for various combustion parameters. Approximately 11 g samples of a polymeric material were loaded into the kiln and incinerated at two different temperatures, 600 C and 760 C.

Rapid on-line analysis of rotary kiln combustion was obtained using the ITD based system. A sample flow of 25-50 ml/min of kiln gases were sampled from the transition area to the afterburner (see Figure 2). Samples were taken at 10 sec intervals to follow the concentration fluctuations following sample introduction into the kiln. The transfer line column was a 1 m long, .15 mm ID methyl silcone (DB-1) coated capillary column. The film thickness was 1.2 μm thick and for the present results the column was operated at ambient and 82 C. Carrier gas flow conditions were 250 cm/s or 1.7 ml/min. For these analyses the mass spectrometer was scanned at 4 scans/second from m/z 35 to 120 for the ambient column temperature runs and from m/z 50 to 148 for the 82 C runs.

Bed Characterization Reactor - The bed characterization reactor (BCR, see Figure 3) is used to study the thermal desorption of compounds from contaminated soils and is described in detail elsewhere [13]. Contaminated and uncontaminated clay soil samples were obtained from several undisclosed sites. The contaminated samples were air dried and designated simply as "soil A" and "soil B." Approximately 200 grams of soil were placed beneath the BCR radiant heaters with a 3 cm/sec gas stream flowing across the bed, and were monitored for temperature change and weight loss. The exhaust gas was monitored 25 cm beyond the bed by a quartz tube drawing ~25 ml/min of gas past the vapor inlet. Samples of these gases were taken at 60 sec intervals to monitor the release of volatiles from the soil. The transfer line separation was performed using a 1 m long, .18 mm ID methyl-phenyl silicone (DB-5) coated capillary column. A .4 μm thick stationary phase provided the separation of compounds in vapor phase. The larger column ID had carrier gas flows of 360 cm/sec or 3.5 ml/min. The modified ITMS (MINITMASS) system accommodated these higher flows with axial modulation. The spectra were scanned from m/z 50 to 200 or m/z 60 to 300 depending on the compounds of interest. Various boiling point ranges of compounds from naphthalene to 6 ring PAHs were monitored by isothermal operation of the transfer line at 125 or 230 C.

RESULTS AND DISCUSSION

Figure 4 shows the chromatograms for repetitive GC/MS sampling of the kiln exhaust gases at 10 s intervals as indicated; the column temperature was 82°C and the kiln temperature was 600°C. The top trace represents the total ion chromatogram while selected chromatograms of ions with mass to charge ratios (m/z) 78 and 92 show the individual peaks for benzene and toluene, respectively. Note that the chromatogram of Figure 4 consist of a series of short chromatograms with peak areas of the separate compounds being proportional to the exhaust gas concentrations at each sampling time. Higher boiling compounds which do not elute within the 10 s sampling interval overlap with subsequent sampling, but can still be resolved by separate ion chromatograms and related back to the correct sample time.

Concentration profiles for separate compounds, determined by the GC/MS data illustrated in Figure 4, are shown in Figure 5 for a kiln temperature of 600 C. The data show the concentrations (ppb) of benzene, toluene, C_2-benzenes, phenol, and styrene as a function of time, with peaks at 30 s (20 s into combustion) and 85 s (75 s into combustion). The polymeric material would initially melt and pyrolyze, releasing high concentrations of organic compounds which then ignited and burned to form water and carbon dioxide. The two peaks in organic products came prior to the flame totally engulfing the samples, and after the local flame began to burn out. During higher temperature kiln tests, at 760 °C, only the most stable products such as benzene were observed above the 20-40 ppb detection limits as the organics were more quickly and completely oxidized.

Figure 6 shows the total ion chromatograms and several selected ion chromatograms for a single vapor analysis during BCR thermal treatment in N_2 of soil B. C_1, C_2 and C_3 alkylnaphthalene peaks are indicated by selected ion traces of m/z 142, 156, 170, respectively. For these vapor analyses, data were not acquired for the first 2 s after sampling to allow elution of the major gas and vapor components which were essentially non-retained on the GC column. With the short column operated isothermally at 125 C, naphthalene was completely separated from the N_2 and other light gases while the combined phenanthrene/anthracene eluted less than 45 sec later.

By integrating the areas of specific molecular ion peaks within each 1 min segment, composite evolution curves were produced such as those shown for soil B in the BCR in Figure 7. Figure 7a compares the time evolution profiles for naphthalene at m/z 128, the combined phenanthrene/anthracene peaks at m/z 178, and their methyl homologs at m/z 142 and 192 respectively. In all cases a major evolution maximum is observed at approximately 10 minutes followed by a second minor peak at approximately 45 minutes into the run. The second evolution peak is larger relative to the first peak for the unsubstituted compounds than for the methyl homologs. In other words, a larger proportion of methyl homologs desorbed within the first 30 minutes or so when water is being desorbed from the soil bed.

The desorption of tar components from the BCR soil bed is further represented in Figure 7b where the heteroatomic compounds dibenzofuran at m/z 168, and dibenzothiophene at m/z 184, are compared to the PAH fluorene at m/z 166. As expected, the higher boiling dibenzothiophene (b.p. 332-333) has a slightly broader and later second peak than the dibenzofuran (b.p. 287). However, both of these have much larger second evolution peaks than the fluorene, similar to unsubstituted PAHs relative to their methyl homologs as in Figure 7a. One interpretation is that the four planar, fully aromatic compounds, namely naphthalene, phenanthrene/anthracene, dibenzofuran and dibenzothiophene, might be more strongly bound to the soil and less completely released in the first thermal desorption or "steam stripping" process than the alkyl substituted or non-planar (fluorene) compounds. A second possibility is that a larger fraction of the fluorene and methyl-aromatics might have reacted to form other products due to their greater ease of oxidation. This latter explanation is supported by the observation of aldehyde and ketone oxidation products such as 9-fluorenone in extracts from incompletely desorbed soils run at lower temperatures or shorter times.

CONCLUSIONS

The broad range of boiling points and polarities of the organic vapors produced during incineration or the thermal treatment of contaminated wastes and soils mandates the use of sophisticated instrumentation for monitoring their production, evolution, and destruction, especially during the design of new facilities. The results of this work have demonstrated that the on-line, short-column GC/MS approach is capable of reliably obtaining qualitative and quantitative data on the products evolving from two types of incinerators.

The on-line short column GC/MS systems are shown to be powerful instruments for measurement of transient concentrations (30-60 sec interval) of a broad range of aromatic compounds. Short column gas chromatography separates the organic vapors away from the major ambient atmospheric constituents and also provides some separation of isomers indistinguishable by MS. The mass spectrometer provides a rapid and sensitive method of compound identification and specific quantitation. A standard Ion Trap Detector is an economical MS system with 20-40 ppb detection limits for aromatics while the MINITMASS system offers improved sensitivity and the added selectivity of MS^n capability.

ACKNOWLEDGEMENTS

This work was sponsored by the Advanced Combustion Engineering Research Center. Funds for this Center are received from the National Science Foundation, the State of Utah, 23 industrial participants, and the U.S. Department of Energy.

REFERENCES

1. Oppelt, E.T., *J. Air Pollut. Control Assoc.*, **37**, 558 (1987).
2. Wentz, C.A., *Hazardous Waste Management*, McGraw-Hill, New York, 1989, p. 84.
3. de Leer, E.W.B., Bass, M., Erkelens, C., Hoogwater, D.A., de Leeuw, J.W., Schutl, P.J.W., de Leer, L.C. and Graat, J.W., *Proc. of Conf. on New Frontiers for Hazardous Waste Management, USEPA*, Cinn, OH, EPA/600/9-85025, (1985).
4. Troxler, W.L., Alperin, E.S. and Fox, R.D., *Proc. 8th Intl. Conf. on Thermal Destruction of Hazardous, Radioactive, Infectious and Mixed Wastes*, Knoxville, TN (1989).
5. Oppelt, E.T., *J. Air Pollut. Control Assoc.*, **37**, 558 (1987).
6. Lee, K.-C., *J. Air Pollut. Control Assoc.*, **38**, 1542 (1988).
7. McClennen, W.H., Arnold, N.S., Lighty, J.S., Eddings, E.G., Lindgren, E.R., Roberts, K.A. and Meuzelaar, H.L.C., *Proc. ACS, Div. of Fuel Chem.*, Miami, FL, **34**:3, p. 1028 (1989).
8. McClennen, W.H., Arnold, N.S., Roberts, K.A., Meuzelaar, H.L.C., Lighty, J.S., Lindgren, E.R., Fast, Repetitive GC/MS Analysis of Thermally Desorbed Polycyclic Aromatic Hydrocarbons (PAHs) from Contaminated Soils, *Combustion Science & Technology*, in press, 1990.
9. Arnold, N.S., McClennen, W.H., and Meuzelaar, H.L.C., *Proc. ACS, Div. of Environmental Chem.*, Miami, FL, Vol. 29, No. 2, p. 426. (1989).
10. Arnold, N.S., Roberts, K.A., McClennen, W.H., Meuzelaar, H.L.C., *Proc. of the 37th Annual Conf. on Mass Spec. and All. Topics*, Miami, FL, 1425 (1989).
11. Arnold, N.S., McClennen, W.H., Meuzelaar, H.L.C., Development of an On-line Transfer Line GC/MSn Sampling Method for Direct Atmospheric Vapor Analyses at Low PPB Levels, submitted to *Analytical Chemistry*, 1990.
12. Meuzelaar, H.L.C., McClennen, W.H., Arnold, N.S., Reynolds, T.K., Maswadeh, W., Jones, P.R., Urban, D.T., *Proc. 1st Intl. Symp. Field Screening Methods for Hazardous Waste Site Investigations*, Las Vegas, NV, 195 (1988).
13. Lighty, J.S., Silcox, G.D., Pershing, D.W., Cundy, V.A. and Linz, D.G., *Environ. Progress*, **8**, 57 (1989).

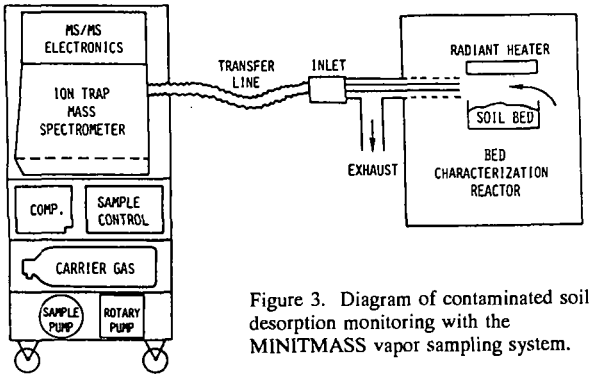

Figure 3. Diagram of contaminated soil desorption monitoring with the MINITMASS vapor sampling system.

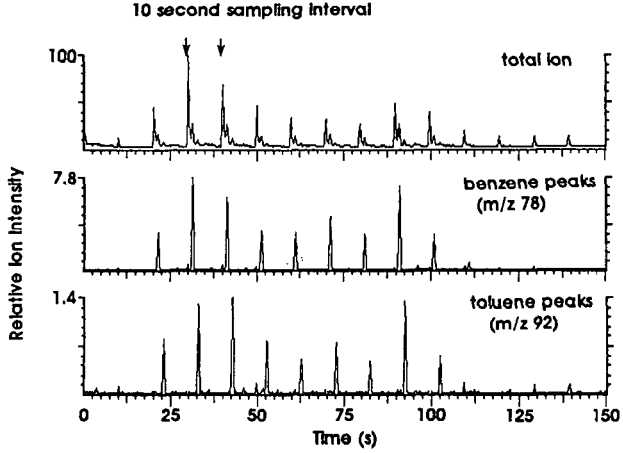

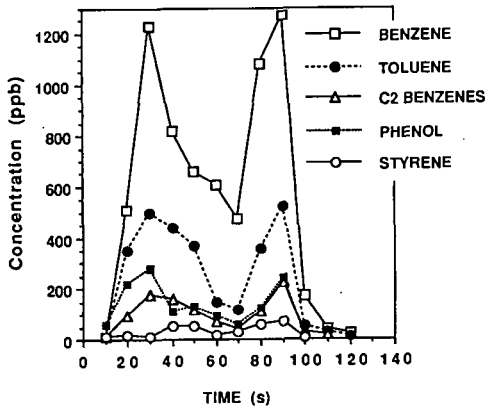

Figure 5. Time evolution of organic compounds during incineration of medical supplies at 600 C in a rotary kiln simulator.

Figure 4. Total and selected ion chromatograms from 16 repetitive GC/MS vapor samples during incineration of disposable medical supplies in the rotary kiln simulator.

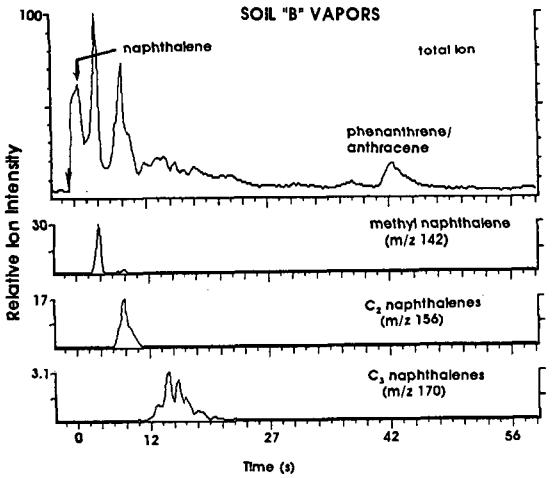

Figure 6. Total and selected ion chromatograms for a single on-line vapor sample GC/MS analysis during a 400 C BCR run on soil B.

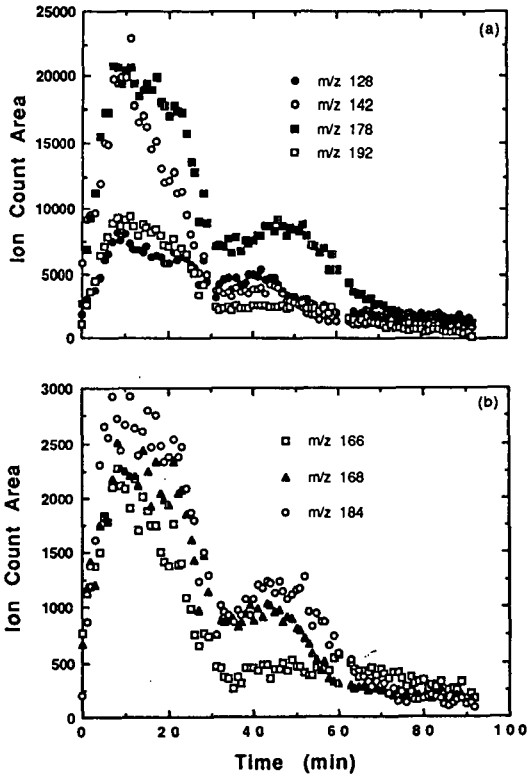

Figure 7. Time evolution profiles for several compounds from vapor sampling of the thermal treatment of soil B in the BCR at 400 C. Each point is from the integrated area of a specific peak in the molecular ion chromatogram for the 90 vapor samples. The ions represented are: in a) m/z 128, naphthalenes; m/z 142 methylnaphthalenes; m/z 178, phenanthrene/anthracene; m/z 192, methyl-phenanthrenes and anthracenes; in b) m/z 166, fluorene; m/z 168, dibenzofuran; and m/z 184, dibenzo thiophene.

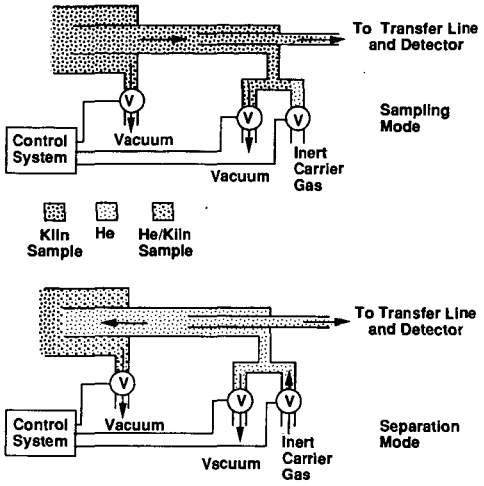

Figure 1. Schematic diagram of vapor sampling inlet operation.

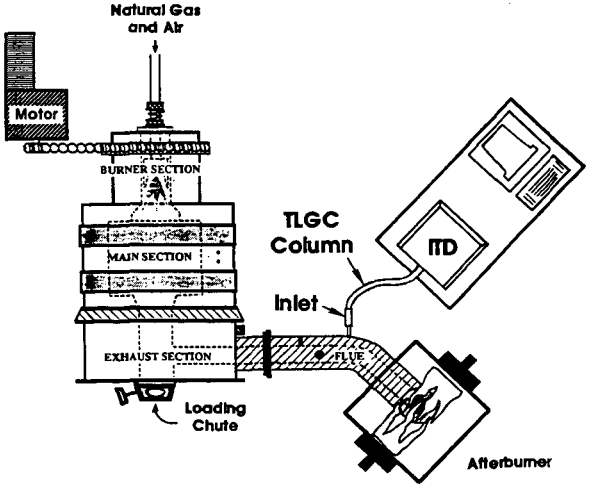

Figure 2. Top view of rotary kiln simulator with on-line GC/MS system using an Ion Trap Detector (ITD).

TRANSIENT EMISSIONS ASSOCIATED WITH VARIOUS FURNACE CYCLIC PATTERNS IN RESIDENTIAL OIL COMBUSTION - A LABORATORY STUDY

S. Win Lee

Energy Research Laboratories, CANMET
Energy, Mines and Resources Canada
555 Booth St. Ottawa. Canada. K1A 0G1

INTRODUCTION

Environmental considerations dictate that combustion processes increase energy efficiency, reduce pollutant emissions from fossil fuels and utilises alternate fuels that generate fewer particulates and volatile organics. These considerations will receive greater attention than the operational costs as the environmental awareness of a concerned public increases. All combustion processes are potential air pollution sources and most of the major fuel consuming units are covered by government regulations, the residential heating appliance being one of the few exceptions. In Canada, with its cold winter climate, energy in the form of electricity and heating fuel for domestic requirement makes up for about one-fifth of the total national energy consumption. Energy conservation in the residential sector is encouraged nationally and an average homeowner sees its direct effects as immediate dollar savings. However, there is a need to increase the public awareness on the environmental impact of reduced energy consumption since it is not as evident as in cost reduction.

The Combustion and Carbonization Laboratory, a federal research facility long associated with research programs to promote efficient use of energy, provides technical information including publications on conservation strategies and pollution emissions in residential oil heating (1, 2). Data from field studies revealed that the most effective strategies for both fuel saving and emission reduction are the use of a high efficiency low excess air burner, lowering the overnight thermostat setting significantly, and by reducing the burner firing rate. As for reduction of seasonal emissions of carbon monoxide and particulates, a combined strategy of reduced fuel consumption and reduced cycling frequency was suggested. The authors observed that these emissions were contributed equally by cyclic emissions and steady-state emissions at combustion air levels giving steady-state smoke numbers close to one.

Keywords: cyclic combustion, emissions, residential heating

A similar study by other researchers reported that particulates, carbon monoxide, and hydrocarbons decrease in concentration as the excess air level increases and that hydrocarbons tend to increase once excess air level reaches a certain level and beyond (3). An apparent linear correlation between particulate emissions and final boiling point of the fuel at low excess air conditions was also suggested. The present study focuses on laboratory measurements of startup transient emission levels at different burner on/off cyclic operations. The purpose is to determine the effect of burner cyclic pattern, especially "off" period on emission concentrations. This work is part of the ongoing research program on fuel quality and combustion characteristics of middle distillates at the Combustion and Carbonization Research Laboratory.

MATERIALS AND METHODS

Fuel Types and Properties

Eight specific fuels with different characteristics (Table 1) were selected for this work. Fuels N, Q, HH, and FF are commercial No. 2 heating fuels purchased locally. Three other fuels (OO, CC, PP, EE) were contributed by various Canadian oil companies. The origin of crudes and the refinery processes utilized to produce the fuels vary depending on the company and location. They were specially blended to obtain a wide range of properties especially varying aromatic concentrations. Fuel FF was used in combustion tests with variable cyclic pattern and the rest were used in simulation tests for reduced overnight thermostat cut-back (lowering of setting) situations.

Combustion Experiments

All combustion experiments were carried out using the procedure and facilities developed at the Combustion and Carbonization Research Laboratory (4). The schematic of the experimental facilities is shown in Figure 1. The experimental procedure can simulate the actual usage pattern of residential oil heating in Canadian homes. A typical experimental run starts with an initial burner startup (cold start) lasting one hour (steady state), immediately followed by five consecutive cyclic operations with selected on/off time pattern. Flue gas emissions and temperatures at specified locations of the test rig are continuously monitored over the entire run. The following experimental equipment and operating conditions were used.

Fuel temperature:	15 $\pm$ 2 °C
Nozzle oil temperature:	17 - 20 °C for cold start
Fuel pump pressure:	100 psi
Oil nozzle:	0.65 US gph, 80° spray angle
Combustion air:	Set to obtain a No 2 smoke at steady-state with Bacharach tester for each fuel

Cold air return temp:	15 ± 1 °C
Burner:	Beckett domestic gun type burner with Areo AFC-2 flame retention head
Furnace:	Forced air type. Brock model LO-1M, 74,000-120,000 Btu/h, with concentric tube type heat exchanger.
Furnace draft:	1 mm (0.04 in) of water column

Equipment for Emission Monitoring

The oxygen analyzer was a paramagnetic type instrument while the carbon dioxide and carbon monoxide analyzers used the infrared detection principle. Nitrogen oxides in the flue gas were measured by a chemiluminescent type instrument. Particulates were measured manually with a Bacharach smoke tester and continuously with a Celesco model 107 in-line smoke opacity meter. Temperature of the oil in the nozzle line was measured continuously using a "K" type thermocouple inserted through a hole in the nozzle adaptor located as close as possible to the nozzle.

The burner cold-start operation was simulated in the laboratory by cooling the appliance, especially burner and combustion chamber by a blast of chilled air until they attained temperatures comparable to those of a residential basement environment. Based on the actual readings from homes, oil temperature in the nozzle line was lowered to 17-20 °C.

RESULTS AND DISCUSSION

No two homes will have the same appliance on/off cyclic operation pattern since it varies depending on numerous factors. The appliance type and condition, level of home insulation, climate, location, user comfort level and life style, thermostat anticipator setting, and overnight temperature setting all determine the operation mode of a residential burner. The cyclic pattern strategy described in Table 1 attempts to simulate some of the possible situations but by no means represents the numerous real life conditions in homes. These patterns are selected to reflect the usage pattern of most Canadian homes where lowering the thermostat setting before retiring at night is the accepted practice for energy conservation.

The degree of severity in overnight thermostat cut-back, however, controls the length of the burner cycles and consequently the burner performance at the cold-temperature conditions. The performance may be adversely affected in the case of fuels with slightly lower grade specifications and of high aromatics as have been predicted for marketing, before the fall of oil prices in 86. Four special blends were selected to represent this senerio.

Transient emissions from cyclic combustion of a No. 2 fuel at variable on/off cyclic patterns

As reported in the literature, gaseous and particulate emissions of a residential burner are higher at transient startups and shutdowns than steady-state conditions. The peaking of emissions at startup is due to the cold temperature conditions, mainly low fuel volatility leading to a poor fuel/air mixing, before the combustion zone temperature rises. Immediately upon shutdown, incomplete combustion products result due to an excess fuel condition created by the high pressure oil pump and lack of combustion air supply. These emission peaks are difficult to reproduce by a burner and concentrations between five consecutive cycles show variations with a relative standard deviation of 5% to 20%. The reproducibility of emission data from controlled cyclic operations is much better for typical commercial fuels than those of lower grade fuels.

Data in Table 3 show particulate and gaseous emissions at different transient startup conditions. Each value represents the average of data from a minimum of three experimental runs, each run having five consecutive cycles. Opacity % reported in Table 3 represents the average maximum opacity reading at the peak of transient particulate emissions as recorded by the smoke opacity meter. The reproducibility of opacity, calculated as relative standard deviation, between each run ranges from 7% to 26%. Despite this moderate error margin, there appears to be a gradual trend to increasing particulate levels with the increase in burner cooling-down time. A noticeable increase in particulate emissions was noted after a 7 to 10 hours burner "off" period (simulation of an extreme overnight thermostat cut-back condition). A gradual decrease in the oil temperature in the nozzle line was noted as the burner off period increased. This cooling- down process is dependent of the combustion chamber design among other variables. Similar variable cyclic tests in a different appliance may or may not find the same observations. Data indicate that severe thermostat cut-back could increase pollution emissions from a residential oil burning unit. However, this emission increase is compensated, by several magnitudes, by the total emission reduction resulted from the long burner "off" period.

These combustion tests were carried out using Fuel FF under identical steady-state particulate concentrations of Bacharach smoke number 2. This condition provided an steady-state efficiency of 84% and an excess air of 36% (equivalence ratio of about 1.4). During a one hour steady-state run before cycling, the CO emissions were between approximately 30 ppm and no detectable hydrocarbons were recorded. CO and hydrocarbon emissions at transient startups are significantly higher than steady-state levels. They appear to be similar in magnitude for all variable cyclic operations. Nitrogen oxides concentrations are consistent in all steady-state and transient emissions.

Transient emissions from cold-start and cyclic combustion of different distillate oils

The difference in transient particulate emissions from cold-start and cyclic combustion experiments using different fuels is seen in Table 4. Data indicate that cold-start particulates are higher than cyclic emissions for all fuels. This could be mainly due to the combustion temperature differential between the two operations. The actual thermocouple reading recorded during an experimental run showed that the oil temperature in the nozzle line was between 17-21 °C at cold-start and between 35-65 °C during cyclic operations following a one hour steady-state run. The significant effect of oil temperature at ignition on particulate emissions of residential burners was reported elsewhere (5). Favourable warm temperatures of the oil and combustion zone allows efficient burner ignition and reduced incomplete combustion products.

Data in Table 4 also indicate that, using the same burner, higher cold-start smoke emissions resulted from fuels with higher aromatics. Cyclic transients of the fuels are comparable (Fig.2). Smoke opacity, resulting mainly from soot in the flue gas, is an indicative combustion parameter since other incomplete combustion products exhibit similar emission trends. Although the fuel aromatics are not included in current specifications, volumetric concentrations of aromatics of No. 2 heating fuels fall within 20 to 40%. Special blends have aromatics concentrations higher than 40 %. 90% boiling point of the fuels appear to be proportioal to aromatics. Data suggests that cold-start emissions may be of concern if the fuel aromatics reaches about a 60 % level. The strong influence of fuel viscosity and aromatics on burner performance have been reported previously by the author (6). It was shown that off-spec, low quality fuels generate higher emissions of incomplete combustion products such as particulates, carbon monoxides and hydrocarbons than normal fuels. A complex relationship among fuel properties such as aromatics, viscosity, boiling point range, carbon residue, and gravity influences combustion emissions. This paper is limited to the scope of burner performance at various cyclic patterns.

The following conclusions can be drawn from this study;

1. Transient emissions from varying burner on/off cyclic patterns show a slight increasing trend of particulate emissions as the burner cooling-down period increases.
2. Cold-start ignition after a burner cooling-down period of more than 7 hours, simulating a severe thermostat cut back situation generates higher emissions than cyclic operation.
3. Cold-start transient emissions increase with increasing fuel aromatics and final boiling point but cyclic emissions are less affected by fuel properties.

ACKNOWLEDGEMENT

The author thanks D.E. Barker and N. Rioux for combustion experiments and Canadian oil companies for contribution of fuels.

REFERENCES

1. Hayden, A.C.S, Braaten, R.W., and Brown, T.D. ASME Transactions. 1976. Paper No.76-WA/Fu-8.
2. Hayden, A.C.S, Braaten, R.W., and Brown, T.D. JPCCA. 1978. 28(7), 653-758.
3. Kraus, B.J. and Coburn, J.F. Prep. Am. Chem. Soc. 1974. 19(5), 49-58.
4. Lee, S.W. and Hayden, A.C.S. ASHRAE Transactions. 1986. 92. Part 1B, 667-682.
5. Lee, S.W. and Hayden, A.C.S. 1989. Prep. Am. Chem. Soc. Div. Fuel. Chem. 1989. 34(3), 1000-1007.
6. Lee, S.W. and Hayden, A.C.S. 1986. ASHRAE Transactions. 92. Part 2B, 223-238.

Table 1. Basic Properties of Fuels

Fuel	Density Kg/L @ 15°C	Viscosity c St @ 38°C	Aromatics Vol %	90% BP °C	Calorific Value MJ/kg
N	0.845	2.09	30.3	322	44.3
Q	0.846	2.59	30.6	325	45.5
FF	0.855	2.52	31.4	311	44.5
HH	0.861	2.82	39.2	308	45.1
CC	0.902	2.70	54.2	315	43.9
OO	0.914	2.56	55.2	304	43.7
PP	0.916	2.61	60.0	327	43.2
EE	0.912	2.90	68.0	368	43.2

Table 2. Laboratory Furnace Cyclic Operation Pattern to Simulate Various Periods of a Heating Season

ON time (m)	OFF time (m)	ON/OFF ratio	Approximate period
5	15	0.33	Fall and spring months
5	10	0.5	Fall and spring months
5	5	1.0	Most of winter days
10	10	1.0	Most of winter days
3.8	13.3	0.29	ASHRAE 103 standard average
10	30	0.33	At lower thermostat settings
10	overnight		Under extreme thermostat cut-back conditions

ASHRAE is American Society of Heating, Refregeration & Air-Conditioning Engineers

Table 3. Maximum Transient Emissions Resulting from Different Cyclic Combustion Processes of Fuel FF

on/off time (m)	Opacity (%) & BSN[a]	Carbon monoxides (ppm)	Hydrocarbons (ppmc)	Nitrogen oxides (ppm)
10/5	1.1 (6)	235	14	75
10/10	1.2 (6)	250	20	73
5/5	1.2 (6)	260	15	73
5/10	2.2 (7)	265	30	75
5/15	2.6 (8)	190	20	76
3.8/13.5	2.1 (8)	330	25	72
10/60	2.9 (8)	325	23	75
overnight	3.1 (9)	360	32	72

[a] BSN represents Bacharach smoke number

Table 4. Startup Transient Particulate Emissions from Different Fuels

Fuel	Maximum Cold-start Opacity %	Maximum Cyclic startup Opacity %
N	1.7	0.2
Q	1.6	0.4
FF	3.1	1.2
HH	1.4	0.9
CC	4.7	2.3
OO	2.8	1.3
PP	3.9	1.8
EE	26	2.9

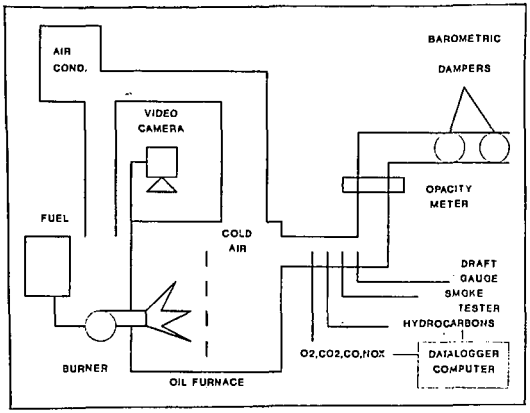

Figure 1. Schematic of equipment for combustion experiments.

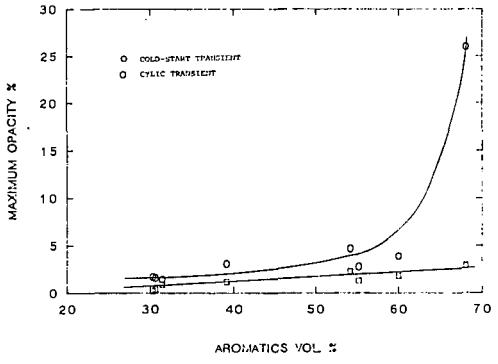

Figure 2. Startup transient particulate emissions from different fuels.

A CONTINUUM THEORY FOR THE FLOW OF PULVERIZED COAL IN A GASIFIER

M. Massoudi and P.X. Tran
U.S. Department of Energy
Pittsburgh Energy Technology Center
P.O. Box 10940
Pittsburgh, PA 15236

ABSTRACT

Multiphase flows have increasingly become the subject of considerable attention because of their importance in many industrial applications, such as fluidized beds, pneumatic transport of solids, coal combustion, etc. For example, coal conversion in an entrained flow reactor has received much attention as an important process for transforming coal into fuel gas [cf. Phuoc and Durbetaki (1987)]. In this work the behavior of coal particles in a down flow reactor is modeled using the theory of interacting continua (or mixture theory). The mixture is considered to be made up of saturated granular materials (coal particles) infused with a linearly viscous fluid (gas). Appropriate constitutive relations for stresses and interactive forces are motivated and proposed [Massoudi (1988)]. The conversion of coal particles is studied in terms of chemical kinetics, fluid dynamics flow of volatiles and the heat transfer mechanism at the interface.

INTRODUCTION

The flows of a mixture of solid particles and a fluid have relevance to several important technologies. Pneumatic transport of solid particles, fluidized bed combustors, and flow in a hydrocyclone are but a few examples. In many processes, such as coal conversion in an entrained flow reactor, coal is transformed into clean fuel gas. A fundamental understanding of the behavior of dense flow of coal particles and the interaction between the gas and the coal particles is extremely important.

In general, developing models capable of describing various multiphase flow regimes has attracted considerable attention due to their significant applications in many chemical and transport processes. These mathematical models or theories may be roughly classified into two categories. In one class, the basic conservation laws are postulated and the ideas in continuum mechanics are used to arrive at appropriate constitutive relations with proper restrictions. In the other class, averaging techniques are used to derive the fundamental balance laws. Whichever approach is used, constitutive relations are needed which would supply connections among kinematic, mechanical, and thermal fields which are compatible with the balance laws and which, in conjunction with them, provide a theory which can be solved for properly posed problems.

In this work the behavior of coal particles in a down flow reactor is modeled using the theory of interacting continua (or mixture theory). This theory is a means for the mathematical modeling of multicomponent systems by generalizing the equations and principles of the mechanics of a single continuum. This theory, which traces its origins to the work of Fick (1855), was first put into a rigorous mathematical format by Truesdell (1957). The theory is, in a sense, a homogenization approach in which each component is regarded as a single continuum and at each instant of time, every point in space is considered to be occupied by a particle belonging to each component of the mixture. That is, each component of the mixture is homogenized over the whole space occupied by the mixture. A historical development of the theory can be found in the review articles by Atkin and Craine (1976), Bowen (1976), and the book by Truesdell (1984). We assume the mixture is made up of saturated granular materials (coal particles) infused with a linearly viscous fluid (gas). Appropriate constitutive relations for stresses and interactive forces are

motivated and proposed. The conversion of coal particles is studied in terms of chemical kinetics, fluid dynamics flow of volatiles and the heat transfer mechanism at the interface. The specific assumptions in the theory of interacting continua, and the constitutive models are presented in the next section.

MODELING

In almost all the modeling of solid particles and a fluid, the solid particles are assumed to behave like a linearly viscous fluid [for a review of this, see Rajagopal, et al. (1990)] with a viscosity μ_s and an associated pressure field p_s. A fundamental shortcoming of assuming a fluid-like behavior for the solid phase is that, theoretically, in one limit, as the volume fraction of solids becomes zero, the mixture of fluid and solid particles should behave as a fluid; in the other limit, as the volume fraction of fluid becomes small, the mixture should behave as a granular material. This second limiting case is not described if the particles are assumed to behave like a Newtonian fluid. Indeed, rheological behavior of granular materials is quite different from that of Newtonian fluids. For example, phenomena such as normal stress effects which are observed experimentally, in the shearing motion of dense flow of granular materials, cannot be predicted using a Newtonian model [Massoudi and Boyle (1987)]. Recently, Massoudi (1988) advocated the modeling of the stress in the solid constituent of the mixture by a constitutive expression appropriate to flowing granular solids, and the stress in the fluid constituent of the mixture by a linearly viscous fluid. Therefore, we assume that the stress tensors ${}^{s}\underline{T}$ and ${}^{f}\underline{T}$ of a granular material and a fluid are, respectively [cf. Rajagopal and Massoudi (1990)].

$$ {}^{s}\underline{T} = [\beta_0(\rho_1) + \beta_1(\rho_1)\, \nabla\rho_1 \cdot \nabla\rho_1 + \beta_2(\rho_1)\, \mathrm{tr}\, {}^{s}\underline{D}]\, \underline{1} + \beta_3(\rho_1)\, \nabla\rho_1 \otimes \nabla\rho_1 + \beta_4(\rho_1)\, {}^{s}\underline{D} \,, \tag{1} $$

$$ {}^{f}\underline{T} = (1-\nu)\, \{[-p_f + \lambda_f(\rho_2)\, \mathrm{tr}\, {}^{f}\underline{D}]\, \underline{1} + 2\mu_f(\rho_2)\, {}^{f}\underline{D}\} \,, \tag{2} $$

where β_i's are material properties of the granular solid*, ν is the volume fraction of solid particles defined through

$$ \nu \equiv \rho_1/\rho_s \,, \tag{3} $$

in which ρ_s denotes the reference density for the granular solid. Notice that if the total stress tensor of the mixture is defined as the sum of the two stresses, ${}^{s}\underline{T}$ and ${}^{f}\underline{T}$, then indeed the two limiting cases (i.e., $\nu \to 0$ and $\nu \to 1$), mentioned earlier, are recovered with the present forumlation. In Equations (1) and (2) ${}^{s}\underline{D}$ and ${}^{f}\underline{D}$ denote the stretching tensor for the solid and fluid phases, respectively; λ_f and μ_f are coefficients of the viscosity of the fluid; p_f the pressure; ρ_2 the density of fluid; ∇ designates the gradient operator; $\otimes$ denotes the outer product; and $\underline{1}$ is the identity tensor.

CONSERVATION EQUATIONS

A detailed description of the conservation laws for mixtures is given in the review articles by Bowen (1976), Atkin and Craine (1976), and the book by Truesdell (1984). Associated with each constituent is its mass supply $\hat{c}_a$, momentum supply $\hat{m}_a$, and an energy supply $\hat{e}_a$, where all these quantities are assumed to be continuous functions. The balance laws are then expressed as

---

*For the meaning of material properties β_0 through β_4 and especially how they can be measured experimentally, we refer the reader to Rajagopal and Massoudi (1990).

$$\partial \rho_a / \partial t + \text{div}\,(\rho_a \underline{v}_a) = \hat{c}_a \tag{4}$$

$$\rho_a \underline{v}'_a = \text{div}\,\underline{T}_a + \rho_a \underline{b}_a + \hat{\underline{m}}_a - \hat{c}_a \underline{v}_a \tag{5}$$

$$\rho_a e'_a = \underline{T}_a \cdot \text{grad}\,\underline{v}_a + \text{div}\,\underline{q}_a + \rho_a r_a - \hat{\underline{m}}_a \underline{v}_a - \hat{c}_a (e_a - 1/2\, v_a^2) + \hat{e}_a \ , \tag{6}$$

$$a = 1, 2$$

where prime denotes material time derivative following the motion of the constituent a, $\underline{v}_a$ is the velocity of the constituent a, $\underline{T}_a$ the stress tensor, $\underline{q}_a$ the heat flux vector, r_a external heat sources, and e_a is the specific internal energy. Equation (4) is a statement of conservation of mass, Equation (5) conservation of linear momentum, and Equation (6) conservation of energy.

The modeling of $\underline{T}_a$ (a=1,2), was explained in the previous section. In addition, constitutive relations for $\hat{c}_a$, $\hat{\underline{m}}_a$, and $\hat{e}_a$, would also have to be provided so that the system of Equations (4) - (6) can be used to study this problem.

In this problem, we will study the downflow of coal-gas mixtures in a gasifier. Specific models for $\hat{c}_a$, $\hat{\underline{m}}_a$, and $\hat{e}_a$ will be proposed and motivated. Appropriate boundary conditions will be provided. The basic numerical scheme is that of Phuoc and Durbetaki (1987). Restrictions and assumptions concerning the material properties appearing in the constitutive relations will also be discussed. Quantities and fields of interest which will be calculated and plotted are velocity, temperature, density fields, and pressure distribution.

REFERENCES

Atkin, R.J., and R.E. Craine, Q. J. Mech. Appl. Math., 29, 290 (1976).

Bowen, R.M., in Continuum Physics, III, Academic Press (1976).

Fick, A., Ann-der Physik, 94, 56 (1855).

Massoudi, M., Int. J. Engng. Sci., 26, 765 (1988).

Massoudi, M., and E. Boyle, Technical Note DOE/METC-88/4077, U.S. Department of Energy (1987).

Phuoc, T.X., and P. Durbetaki, Int. J. Numerical Methods Engng., 24, 203 (1987).

Rajagopal, K.R., and M. Massoudi, Topical Report, DOE/PETC/TR-90/3, U.S. Department of Energy.

Rajagopal, K.R., M. Massoudi, and J.M. Ekmann, in Recent Developments in Structured Continua II, Longman Scientific (1990).

Truesdell, C., Lincei-Rend. Sc. Fis. Mat. E. Nat., Series 8, 22, 33 (1957).

Truesdell, C., Rational Thermodynamics, 2nd Ed., Springer-Verlag (1984).

GROWTH AND STATUS OF THE ARGONNE PREMIUM COAL SAMPLE PROGRAM

Karl S. Vorres
Chemistry Division, Building 211
Argonne, IL 60439

Keywords: samples, premium, information

ABSTRACT:

The Argonne Premium Coal Sample Program (APCSP) was established to provide samples to the basic coal research scientific community. The quality of these samples is intended to be the best that can be devised and implemented. Samples of eight U. S. coals have been selected, collected, processed and packaged, analyzed and distributed. Information has been disseminated through Symposia, Quarterly Newsletters, and a Users Handbook. The number of publications is now about 1 for each two shipments of coal samples, and is approaching 200.

INTRODUCTION:

There has been a need for a set of coal samples that can be compared and provide a basis for meaningful correlations, and that will also be stable over long periods of time. This set of samples must also be available over a long period of time to permit as extensive a set of studies to be done with this set of samples as the research community would need.

In response to the need and with the support of the U. S. Department of Energy, Office of Basic Energy Sciences, Chemical Sciences Division, the Argonne Premium Coal Sample Program (APCSP) was initiated. A set of eight U. S. coals was selected to represent a range of chemical parameters of importance (carbon, hydrogen, sulfur and oxygen content) as well as maceral concentrations, and paleobtanic origins. These coals were carefully collected with the help of personnel from the U. S. Geological Survey and the Pittsburgh Testing Laboratory.

The eight coals are indicated in Table I, below.

Table I. Argonne Premium Coal Samples and Some Characteristics

#	Seam	State	Rank	C	H	O	S	Ash
1	Upper Freeport	PA	Med. Vol. Bit.	86	4.7	8	2.3	13
2	Wyodak-Anderson	WY	Subbituminous	75	5.4	18	0.6	9
3	Illinois #6	IL	High Vol. Bit.	78	5.0	14	4.8	15
4	Pittsburgh (#8)	PA	High Vol. Bit.	83	5.3	9	2.2	9
5	Pocahontas #3	VA	Low Vol. Bit.	91	4.4	2	0.7	5
6	Blind Canyon	UT	High Vol. Bit.	81	5.8	12	0.6	5
7	Lewiston-Stockton	WV	High Vol. Bit.	83	5.3	10	0.7	20
8	Beulah-Zap	ND	Lignite	73	4.8	20	0.8	10

The coals are listed in the order collected. The weight % C, H and O values are given on the moisture and ash-free basis, while S and ash are on the dry basis.

The premium quality requires maximal effort to achieve each of several objectives with regard to the handling of the coal. These objectives included minimal oxygen exposure, humidity control, thorough mixing, extensive analysis and long term supplies. Minimal oxygen exposure involved the use of a freshly exposed coal face for the sample, and rapid removal of the sample. The samples were placed in stainless steel drums, sealed and purged with 99.999% argon at the mine site, typically starting within three hours of collection. The samples were sealed in the drums and slightly pressurized for transport to Argonne National Laboratory (ANL) for processing in a unique nitrogen-filled enclosure. This large glove box is about 5-6' wide, 13' tall and would be 40' long if it were built in a straight line. This glove box is operated with 100 ppm of oxygen or less during the processing to protect the samples from atmospheric oxygen. The samples are sealed in glass with this atmosphere. The humidity control is exercised to minimize any moisture loss during the processing. The lack of moisture loss is expected to avoid any damaging effect on the coal pores and retain the properties of the pristine coal as much as possible. The samples are thoroughly mixed in one ton batches in a mixer-blender to provide uniform properties throughout the entire batch. The samples have been extensively analyzed by the Commercial Testing and Engineering Company through a series of more than 50 different laboratories for the proximate and ultimate analyses. About 20% of the ton-sized batch was packaged into sealed glass ampoules containing either 5 grams of -100 mesh or 10 grams of -20 mesh material. This supply seems sufficient to meet current demand levels for about 30 years for the more popular samples and longer for those which are less frequently requested.

CURRENT STATUS AND USAGE

Requests for samples come at an irregular but frequent basis. The shipments to date exceed 12,000 ampoules to more than 256 users distributed over the world. The total number of ampoules which were shipped since January 1986 is shown in Figure 1. The most-requested samples can be seen from Figure 2, which shows the number of ampoules shipped for each of the samples in the order collected.

The inventory of ampoules is such that shipments can continue at the current rate for about 30 years. This would require the filling of additional ampoules to replenish the inventory from 5 gallon carboys which have been prepared for this purpose. The capacity exists to provide about 50,000 of the ampoules of 5 grams of -100 mesh material and 25,000 of the 10 grams of -20 mesh size.

USERS HANDBOOK

The Users Handbook for the Argonne Premium Coal Sample Program (1) has served as the primary document which provides information about the program. This Handbook was initially issued in March 1989 as a 37 page document. It contained a description of the program including the selection, collection, processing and packaging of the samples as well as the analysis and distribution methods. Later sections included analytical information and bib-

liography of references to the work published referring to the samples. Indices by author, subject and journal were included. Finally some safety and ordering information were included.

The popularity of the document and the increasing amount of available information led to the publication of the second edition in October 1989. The amount of analytical information was increased, the bibliography grew to 111 references, a coal index was added and a new literature summary was started. This document had grown to 64 pages. The material appeared also in the form of an Argonne National Laboratory report with the number ANL/PCSP-89/1 which is available through the National Technical Information Service as a referenceable document. Free copies may be obtained on request to the author.

The document is continually growing as the literature references increase in number. At the time of the writing of this paper, (May 1990) there were 178 references in the draft. The authors knows of enough additional papers in various stages of review to realize that the number should surpass 200 near the time of presentation of this paper. The analytical information grows as it is reported in the literature and individual investigators supply it to the author. There are over 30 pages of it in the draft. A new paper describing the APCSP has been prepared and is intended to appear in the literature (2) as well as in the future version of the Handbook. This reference can be used by all future authors of papers on research with these samples to facilitate future literature searches, and aid in providing complete bibliographies. A number of papers have already appeared which describe the program and related activities (3,4,5,6,7).

The number of publications and shipments continues to increase. The current ratio of shipments to papers is about two shipments per paper.

QUARTERLY NEWSLETTER

In addition to the Users Handbook a Newsletter is mailed without charge to the recipients of the samples and some individuals who have asked to be on the mailing list. This Newsletter provides information of value to the users and aids in keeping them current on additions to the bibliography which appears in the Handbook.

SYMPOSIA

This paper will be part of a Symposium on Research with Argonne Premium Coal Samples. The Symposium is the fourth in an annual series which have been organized to provide a forum for current work with the samples. The combination of Symposia, Newsletters and Handbooks is intended to provide an efficient and effective means of dissemination of information about the samples.

FUTURE PLANS

The APCSP plans included the development of the capability to offer separated macerals to the coal research community. Limitations on funding brought about by the U. S. budget deficit and

restrictions on support by the Gramm-Rudman bill have led to a postponement of new projects for an indefinite period. This activity will wait until funding is available. It is hoped that separated maceral concentrates from the Lewiston-Stockton sample will be available as a liptinite concentrate, a vitrinite concentrate, and an inertinite concentrate. The large amount of vitrinite in the Illinois #6 sample will lead to an effort to offer not just the three concentrates but also three vitrinite concentrates as low, medium and high density vitrinite.

The Users Handbook will continue to grow as the number of references continues to grow. These will be incorporated in the bibliography. The literature summary cannot be continued as originally envisaged due to limitations on the support for the program and the expertise of the author. Instead efforts are underway to recruit a number of volunteers to participate in the review of the literature and contribute to the Literature Summary section. Recognition of the authors will be included, and the reviews will be reviewed by other individuals for balance and completeness. As the number of pages grows this document will approach the size of a preprint of the Fuel Chemistry Division. The cost of printing and distribution will probably limit publication to an annual basis.

ACKNOWLEDGMENTS:

The author gratefully acknowledges the support of the U. S. Department of Energy, Office of Basic Energy Sciences, Chemical Sciences Division under contract W-31-109-ENG-38.

REFERENCES:

1. Users Handbook for the Argonne Premium coal Sample Program, Karl S. Vorres, ANL/PCSP-89/1, Argonne National Lab.

2. Karl S. Vorres, Energy & Fuels, in press

3. Directions of Research from the Argonne Premium Coal Sample Program, Vorres, Karl S., Coal Science & Technol. 11, 1987 Intl. Conf. on Coal Science, 937-940 (1987)

4. The Eight Coals in the Argonne Premium Coal Sample Program. Vorres, Karl S. and Janikowski, Stuart K., Preprints, Fuel Chem. Div., Am. Chem. Soc. 32 (1) 492-499 (1987)

5. The Preparation and Distribution of Argonne Premium Coal Samples. Vorres, Karl S., Preprints, Fuel Chem. Div., Am. Chem. Soc. 32 (4) 221-226 (1987)

6. Illinois Basin Coal Sample Program and Access to Information on Illinois Basin Coals. Kruse, Carl W.; Harvey, Richard D.; Rapp, David M., Preprints, Fuel Chem. Div., Am. Chem. Soc. 32 (4) 359-365 (1987)

7. Sample Preparation for, and Current Status of the Argonne Premium Coal Sample Program. Vorres, Karl S., Preprints, Fuel Chem. Div., Am. Chem. Soc. 33 (3) 1-6 (1988)

Fig. 1 Total Ampoule Shipments Through April 1990

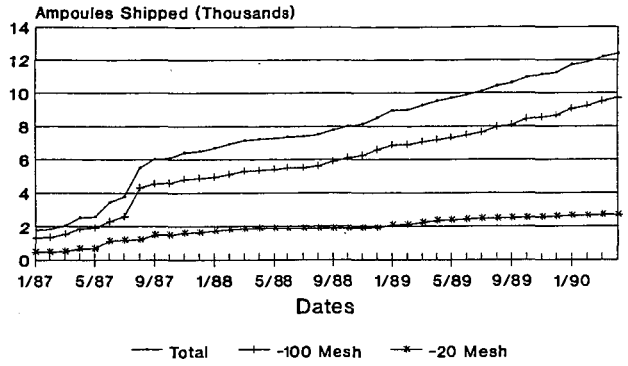

Fig. 2 Number of Ampoules Shipped Through April. 1990

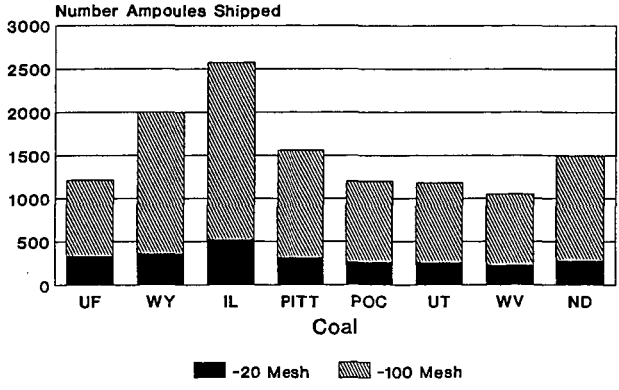

DIRECT DETERMINATION AND QUANTIFICATION OF SULFUR FORMS IN COALS FROM THE ARGONNE PREMIUM SAMPLE BANK

Martin L. Gorbaty, Graham N. George, Simon R. Kelemen and Michael Sansone
Exxon Research and Engineering Company
Annandale, NJ 08801

Keywords: Organic Sulfur, XANES, XPS, Rank

Sulfur K Edge X-ray Absorption Near Edge Structure Spectroscopy (XANES) and X-ray Photoelectron Spectroscopy (XPS) have been developed for the direct determination and quantification of the forms of organically bound sulfur in nonvolatile petroleum and coal samples. XANES and XPS spectra were taken of a number of model compounds, mixtures of model compounds, heavy petroleum and coal samples. A third derivative analysis of the XANES spectra and curve resolution of the XPS spectra allowed approximate quantification of the sulfidic and thiophenic components of the model mixtures and heavy hydrocarbon resources. Both techniques were used to characterize organically bound sulfur forms in coals from the Argonne Premium Coal Sample Bank and both show a monotonic increase of thiophenic sulfur with increasing rank.

Introduction

X-ray Absorption Near Edge Structure (XANES) Spectroscopy and X-ray Photoelectron Spectroscopy (XPS) are two techniques which have been applied recently for the direct speciation and approximate quantification of organically bound forms of sulfide and thiophenic sulfur in nonvolatile liquid and solid carbonaceous materials (1-5). Both techniques have been used to characterize the levels of sulfide and thiophenic sulfur forms in coals from the Argonne Premium Coal Sample Program and to develop a correlation of sulfur forms with rank.

It is known that organic sulfides can be converted to thiophenes on heating. For example, it has been shown that when benzylsulfide is heated to 290°C, tetraphenylthiophene, hydrogen sulfide and stilbene are produced (6). Extending this to organically bound sulfur forms in coals, it would be expected that the ratio of thiophenic sulfur to sulfide sulfur would increase with increasing rank, as the coal precursor materials experience more and more severe geological temperatures and pressures during metamorphism. Recent data on a number of coals of different rank, obtained by flash pyrolysis experiments (7) which measure and correlate H_2S evolution with level of sulfide sulfur present indicate this trend. However, these experiments leave open the question as to whether sulfur forms are interconverting during the pyrolysis. H_2S evolution may not correlate directly with sulfide sulfur and coupled with heat and mass transport limitation considerations, particularly for solids, it is not unreasonable to question whether at least some of the thiophenic forms observed by pyrolysis techniques are produced during heating. Therefore, the forms of organically bound sulfur in coals of different rank obtained from the Argonne Premium coal sample program were determined by direct measurement using XPS and XANES.

Experimental

The procedures for obtaining XANES and XPS spectra have been discussed elsewhere (1-4). The XANES spectra were recorded at the National Synchrotron Light Source at Brookhaven National Laboratory on line X-10C. To avoid ambient temperature oxidation, sample preparations were done in a glove bag filled

with nitrogen. Coal samples, which were all <100 mesh as-received, were dusted onto mylar tape and the sample holders transported to the beamline in nitrogen filled bottle. Similarly, preparation of samples for XPS were done in a nitrogen filled dry box, and the samples inserted into a fast entry air lock. Fluorescence XANES spectra were recorded using a Stern-Heald-Lytle detector (8). Pyrite interferences in the XANES spectra were removed by subtracting the third derivative spectrum of iron pyrite from the third derivative spectrum of the coals until the lowest energy pyrite "peak" was removed. Pyrite interferences in the XPS data from Illinois #6 coal were removed by subtraction during the curve resolution analysis by the method described previously (3). The accuracy of both the XANES and XPS methods for determining organically bound sulfide and thiophenic sulfur forms is estimated to be ± 10%.

Results

XANES spectra and their third derivative traces for the 8 Argonne Premium samples are shown in Figure 1. The feature at about 2468.5 eV is associated with pyritic sulfur, that at 2469.8 eV with sulfide sulfur and 2470.4 eV with thiophenic sulfur. After subtracting pyrite interferences, measurement of peak heights from the baselines provided the approximate quantifications of sulfide and thiophenic sulfur forms found in these samples. These data are listed in Table 1 and plotted in Figure 2 against carbon content of the coals. Except for the Illinois #6 data, there is a clear increase in thiophenic sulfur with increasing carbon content of the coals.

XPS data on the same samples are also shown in Table 1 and are plotted in Figure 2. With the exception of Illinois #6 coal, it was possible to curve resolve the organic sulfur 2p spectrum using sulfur species components fixed at 163.3 eV and 164.1 eV for sulfide and thiophenic sulfur respectively. The sulfur signals representative of these single species under the experimental conditions of this and previous studies (4,5) were determined from the instrumental response to pure sulfur model compounds. The signal of a single sulfur species is composed of two peaks representing 2p3-2 and 2p1-2 components having a 2:1 relative intensity and separated in energy by 1.2 eV. Each component is composed of equally mixed Gaussian and Lorentzian line shapes and a full width-half maximum of 1.4 eV. These conditions were used for all curve resolving procedures. The XPS data confirm the trend of increasing thiophenic sulfur content with increasing rank.

Pyritic sulfur was observed only in the Illinois #6 spectrum. The XPS spectra in the unoxidized region of all other Argonne Premium samples were found not to contain contributions from pyritic sulfur. A weak iron 2p signal was detected in the spectra of Upper Freeport, Pittsburgh #8, Lewiston-Stockton and Beulah-Zap. The levels, when normalized to the carbon 1s signal were lower than expected from bulk elemental analyses. This behavior has been noted before with other coals (3,9). In every case, a broad peak was centered well below 711 eV, indicative of iron oxides or sulfate in poor electrical contact with the organic matrix. No evidence was found for a pyritic iron signal in this study, and on this basis the XPS sulfur 2p spectra were judged to be free of interference effects due to pyritic sulfur.

Discussion and Conclusions

Both XPS and XANES data confirm the trend of increasing thiophenic sulfur content with rank for the coals studied. This is the first such evidence obtained by direct measurement. Figure 3 shows both sets of data plotted

against each other, the solid line being the parity situation. It is seen that the surface and bulk measurements are in good agreement and fall within the established limits of accuracy for both methods. The implication of this is that sulfur distributions at the surface and in the bulk are similar.

The outlying point in Figures 2 and 3 arises from the XANES data of Illinois #6 coal. If there are errors in the pyrite subtraction procedure, or if absorptions of the thiophenic species actually present are shifted due to substituent effects, the values reported herein for thiophenic sulfur in this coal would be low. These possibilities are under study at this writing.

Acknowledgments

X-ray absorption spectra were recorded at the National Synchrotron Light Source (Brookhaven National Laboratory), which is funded by the Division of Material Sciences, U. S. Department of Energy under contract DE-AC02-76CH-00016. The writers wish to thank Dr. K. S. Vorres (Argonne) for providing the samples used in this study, and Mr. P. Kwiatek for carrying out the XPS measurements.

References Cited

1) George, G. N.; Gorbaty, M. L. *J. Amer. Chem. Soc., 1989, 111*, 3182.

2) George, G.N.; Gorbaty, M.L.; Kelemen, S.R. In Geochemistry of Sulfur in Fossil Fuels; Orr, W.L., White, C.M., Eds.; ACS Symposium Series; American Chemical Society; Washington DC, In press.

3) Kelemen, S. R.; George, G. N.; and Gorbaty, M. L. *ACS Div. Fuel Chem. Preprints*, 1989, *34*, 729.; *FUEL*, 1990, *69*, in press.

4) Gorbaty, M. L.; George, G. N.; Kelemen, S. R. *ACS Div. Fuel Chem. Preprints*, 1989, *34*, 738; *FUEL*, 1990, *69*, in press.

5) Kelemen, S. R.; George, G. N.; Gorbaty, M. L. *Fuel Process. Technol.* 1990, *24*, 425.

6) Fromm, E. and Achert, O. *Ber.*, 1903, *36*, 545.

7) Calkins, W. H., *Energy Fuels*, 1987, *1*, 59; Torres-Ordonez, R. J.; Calkins, W. H.; Klein, M. T. In Geochemistry of Sulfur in Fossil Fuels; Orr, W.L., White, C.M., Eds.; ACS Symposium Series; American Chemical Society; Washington DC, In press.

8) Stern, E; Heald, S. *Rev. Sci Instrum.*, 1979, *50*, 1579.

9) Perry, D. L.; Grint, A. *Fuel*, 1983, *62*, 1029.

Table 1

THIOPHENIC SULFUR INCREASES WITH RANK
(ARGONNE PREMIUM COAL SAMPLES)

COAL	% CARBON (daf Basis)	MOLE % (± 10) BY XANES	BY XPS
BEULAH-ZAP	74.05	46	55
WYODAK-ANDERSON	76.04	58	83
ILLINOIS #6	80.73	47	89
BLIND CANYON	81.32	75	65
PITTSBURGH #8	84.95	77	75
LEWISTON-STOCKTON	85.7	74	88
UPPER FREEPORT	88.08	89	81
POCAHONTAS	91.81	98	100

Figure 1

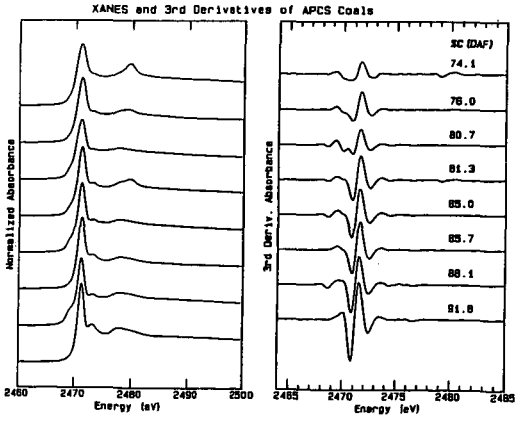

Figure 2

THIOPHENIC SULFUR INCREASES WITH RANK
ARGONNE PREMIUM COAL SAMPLES

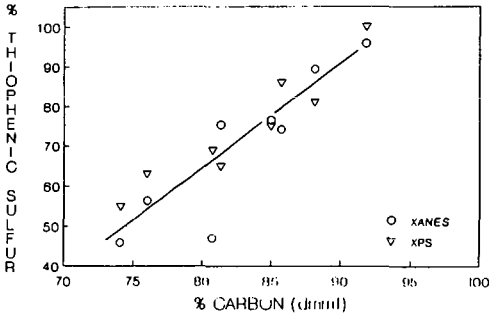

Figure 3

XPS/XANES DATA COMPARISON
(ARGONNE PREMIUM COAL SAMPLES)

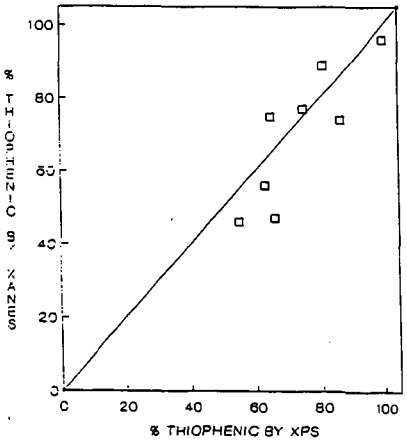

COAL MINERALOGY, FORMS-OF-SULFUR AND IRON, AND COAL LIQUEFACTION PROPERTIES FOR THE ARGONNE PREMIUM COALS AND NINE KENTUCKY COALS.

Naresh Shah, Robert A. Keogh, Frank E. Huggins, Gerald P. Huffman, Anup Shah, Bhaswati Ganguly, and Sudipa Mitra, 233 Mining and Mineral Resources Bldg., University of Kentucky, Lexington, KY 40506.

Keywords: Sulfur XAFS spectroscopy, ^{57}Fe Mössbauer Spectroscopy, Computer Controlled Scanning Electron Microscopy (CCSEM)

The eight Argonne Premium coal samples, augmented by nine Kentucky coals, were selected for this study of the relationship of mineral parameters and liquefaction behavior. Kentucky coals were screened from many coals as they exhibited high, low and intermediate values of rank, sulfur content and liquefaction yields. Table 1 lists the selected Kentucky coals and their carbon and sulfur analyses.

Liquefaction

Liquefaction experiments were carried out on all coals at 385 C with tetralin as solvent (1:1.5 coal/solvent ratio) and without any catalyst [1]. Microautoclaves (tubing bombs) were cold pressurized to 800 psi with hydrogen before heating to reaction conditions. Products of liquefaction were classified as: oils - pentane soluble; asphaltenes - pentane insoluble, benzene soluble; preasphaltenes - benzene insoluble, pyridine soluble; insoluble organic matter (IOM) - pyridine insoluble. Total conversion is defined as 100-IOM. Figure 1 is the bar chart showing the results of liquefaction reactions for all coals.

CCSEM

The mineral and inorganic species can act as catalysts or poisons during liquefaction depending on reaction conditions. It is, therefore, important to know the types of minerals present and how they are distributed in coal. Computer controlled scanning electron microscopy (CCSEM) is an excellent tool to rapidly characterize mineralogical information of coals [2]. Tables 2 and 3 list the mineralogical data obtained to date by CCSEM examination of Argonne and Kentucky coals. Two of the Argonne coals remain to be analyzed. With CCSEM, we can also determine average sizes and size distributions of the various minerals present in the coal. We are currently trying to correlate the pyrite surface area to the liquefaction conversion percentages.

It may be noted that "mixed silicates" account for a fairly large percentage of the mineral matter in these raw coal samples. This phase primarily includes clay minerals and quartz in juxtaposition to each other, perhaps in partings. This is illustrated by the ternary diagram in Figure 2. Here, each point represents a mineral feature identified in the CCSEM analysis that contains ≥90% of (K + Fe) + Al + S on the basis of its energy dispersive X-ray (EDX) spectrum. The composition is normalized to these four elements and plotted in a ternary representation, as shown. It is evident that there is a range of compositions extending between the quartz, kaolinite, and illite composition areas. It is these intermediate compositions that the coal mineral analysis (CMA) program identifies as mixed silicates.

Mössbauer Spectroscopy

Mössbauer spectroscopy is used to identify and quantify iron bearing phases present in the coals. [3,4]. Iron predominantly exists as pyrite, siderite or Fe-containing clay in coals. Mössbauer spectroscopy is the most accurate tool to quantify pyrite in coal and by using simple stoichiometric formula we can obtain the pyritic sulfur content of the coal. Table 4 lists the Mössbauer spectroscopy results for all coals. As it is clearly evident, the Argonne coals were in pristine condition and do not exhibit any pyrite oxidation.

However, some of the Kentucky coals, mainly those with high pyrite contents have undergone some minor oxidation that converts pyrite to sulfate form.

In order to examine the transformations of Fe-bearing minerals in coals as they undergo liquefaction and thereby assess the role of the inherent iron minerals as catalysts, the insoluble organic matter (IOM) of the Argonne Premium Sample coals were also investigated using Mössbauer spectroscopy. Figure 3 shows room temperature Mössbauer spectra of Illinois #6 coal before and after liquefaction treatment. In Illinois #6 coal, almost all Fe is present in the form of pyrite; after the liquefaction test, about 60% of the pyrite converts to pyrrhotite, while the remaining pyrite is unconverted. Under more severe conditions and/or longer periods of time, all of the pyrite would convert to pyrrhotite. In the Pocahontas #3 coal, iron is distributed among clays, siderite, and pyrite; however, in the Pocahontas #3 IOM, Fe in clays and carbonate remains unchanged whereas pyrite has been converted to pyrrhotite. As summarized in the Table 5 for the Argonne Premium Samples, this observation appears quite general: the Fe-bearing minerals, other than pyrite, do not appear to undergo significant transformation during liquefaction, whereas, some or all of the pyrite converts to pyrrhotite. It is likely that only Fe in the form of pyrrhotite is the primary catalytic species. Fe in the coal present in the form of clays is likely to be inactive.

Sulfur XAFS

It can be expected that different sulfur forms will behave differently under the same process conditions during liquefaction conditions and so it is important to identify the presence and reactions of each sulfur form under different conditions. The combination of Mössbauer and XAFS spectroscopy provides a unique approach to focus on both the different organic and inorganic forms of sulfur [5]. Figure 4 shows the sulfur K-edge XANES of three Argonne coals with pyrite removed. All three spectra are quite similar to each other indicating that the forms of sulfur present after pyrite removal are essentially the same in the three different coals. From our previous studies, we can assign various peaks in sulfur XANES to various forms of sulfur present in coals as follows: sulfidic sulfur (peak at 1.6 eV), thiophenic sulfur (peak at 2.6-2.8 eV), sulfoxide (peak at 4.5 eV), sulfone (peak at 9 eV) and sulfate (peak at 11 eV). We are currently trying to quantify the forms of sulfur present in these coals by curve fitting various features of the spectra and comparing the results to the data from standards.

REFERENCES

1. R.A. Keogh, B.H. Davis, J. Coal Quality, 7(1), (1988), 27.
2. F.E. Huggins, G.P. Huffman, Analytical methods for coal and coal products, Vol. III, Chapter 50, Ed. K.Vorres, (1981), 371.
3. F.E. Huggins, G.P. Huffman, R.J. Lee, ACS Symposium Series, 205, (1982), 239.
4. G.P. Huffman, F.E. Huggins, Fuel, 57, (1978), 592.
5. G.P. Huffman, F.E. Huggins, S. Mitra, N. Shah, R.J. Pugmire, B. Davis, F.W. Lytle, R.B. Greegor, Energy and Fuels, 3, (1989), 200.

Table 1. Rank and total sulfur content of selected Kentucky coals

UKCAER Coal #	Seam	County	%C DAF	%S DAF
91864	WKY #9	Union	82.15	3.93
6398	Horton	Horton	85.33	0.86
2145	Peach Orchard #3	Magaffin	83.66	0.63
71302	WKY #6	Caldwell	82.50	3.37
3913	Stockton	Martin	82.34	0.75
2167	Cannel City	Magaffin	80.97	1.62
5416	Beaver Creek	Pulaski	74.45	13.92
71464	WKY #9	Henderson	79.44	3.84
71468	WKY #9	Muhlenberg	80.27	4.15

Table 2. Mineral Composition of Six Argonne Coals

	Wt% of Mineral Matter					
Mineral Species	Up. Fr.	Ill #6	Pitt #8	Poca #3	Bl. Cany	Lew Stoc
Quartz	5	9	12	4	4	10
Kaolinite	9	3	8	10	9	15
Illite	35	18	19	8	36	48
K-feldspar		<1		<1		
Chlorite	1			4		
Montmorillonite		<1	<1	<1	1	
Misc. Silicates	17	23	26	34	41	25
Pyrite	25	27	25	4	3	1
FeSO4					<1	
Gypsum	<1					
Chalcopyrite	<1			1		
Misc. Sulf.	1	1	1	<1	<1	<1
Halite (NaCl)				<1		
Apatite			<1			
Misc. Phosphates				<1		<1
Fe-rich		<1		<1	<1	<1
Calcite		8	1	7	2	
Ankerite				<1		
Mixed Carbonates	1	1	<1	5	1	<1
Ti rich		1	1	<1		1
Trace-rich	<1					
Qtz-Sulfur		1	<1			
Qtz-Pyrite	<1	<1		<1		
Sil-Sulfur	<1	3	2		<1	
Sil-Pyrite	<1	1	<1			
Al-rich				3		
Misc. Mixed	2	3	4	15	3	<1

Table 3. Mineral Composition of Kentucky Coals

Mineral Species	Wt% of Mineral Matter								
	6398	71468	2145	71302	3913	91864	2167	5416	71464
Quartz	3	8	11	7	10	13	6	1	8
Kaolinite	12	4	7	3	8	3	2		7
Illite	5	17	43	21	27	16	21	1	12
K-feldspar		<1		1	<1	1	1		
Chlorite	<1		<1	<1			1		
Montmorillonite	1		<1		<1	<1	<1		<1
Misc. Silicates	57	20	36	27	50	22	30	6	27
Pyrite	2	31		26		26	6	55	27
FeSO4		<1		<1		<1	<1	1	<1
Jerosite								1	
Gypsum									
Chalcopyrite									
Misc. Sulf.	<1	1		4	1	5	1	13	3
Halite (NaCl)									
Apatite							<1		
Misc. Phosphates									
Fe-rich	1						14	<1	
Calcite	1	11				<1			4
Ankerite									
Mixed Carbonates	1	1	<1			<1	11	<1	<1
Ti rich	3	<1	<1		<1	<1		<1	<1
Trace-rich			<1						
Qtz-Sulfur		<1		<1		1		1	1
Qtz-Pyrite		<1		3		1	<1	6	<1
Sil-Sulfur	5	3		2	2	5		2	5
Sil-Pyrite	<1	1	<1	2		1	<1	7	1
Al-rich						<1			
Misc. Mixed	10	3	1	5	2	5	7	6	5

Table 4. Mössbauer Data for Argonne Premium and Selected Kentucky Coals

Argonne Premium or Kentucky coals	Wt% pyritic sulfur	%Fe in			
		Clay	Siderite	Pyrite	Sulfate
Upp. Freeport	1.60	6	0	94	
Wyodak	0.13	0	26	74	
Illinois #6	2.14	3	0	97	
Pittsburgh #8	1.26	1	0	99	
Pocahontas #3	0.11	33	46	20	
Blind Canyon	0.25	0	28	72	
Lewis-Stockton	0.20	32	15	53	
Beulah-Zap	0.22	0	0	100	
91864	2.04			95	5
6398	0.03	61	16	22	
2145	0.15	57		43	
71302	1.86	5		88	7
3913	0.17	34		66	
2167	0.93	9	72	19	
5416	11.50			92	8
71464	1.87			96	4
71468	2.14			95	5

Table 5. Mössbauer Data for Argonne Coal IOMs

Argonne Premium Coal	%Fe in			
	Clay	Siderite	Pyrite	Pyrrhotite
Upper Freeport				100
Wyodak		21	42	37
Illionis #6			40	60
Pittsburgh #8			33	67
Pocahontas #3	38	50		12
Blind Canyon		31		69
Lewis-Stockton	32		31	37
Beulah-Zap			31	69

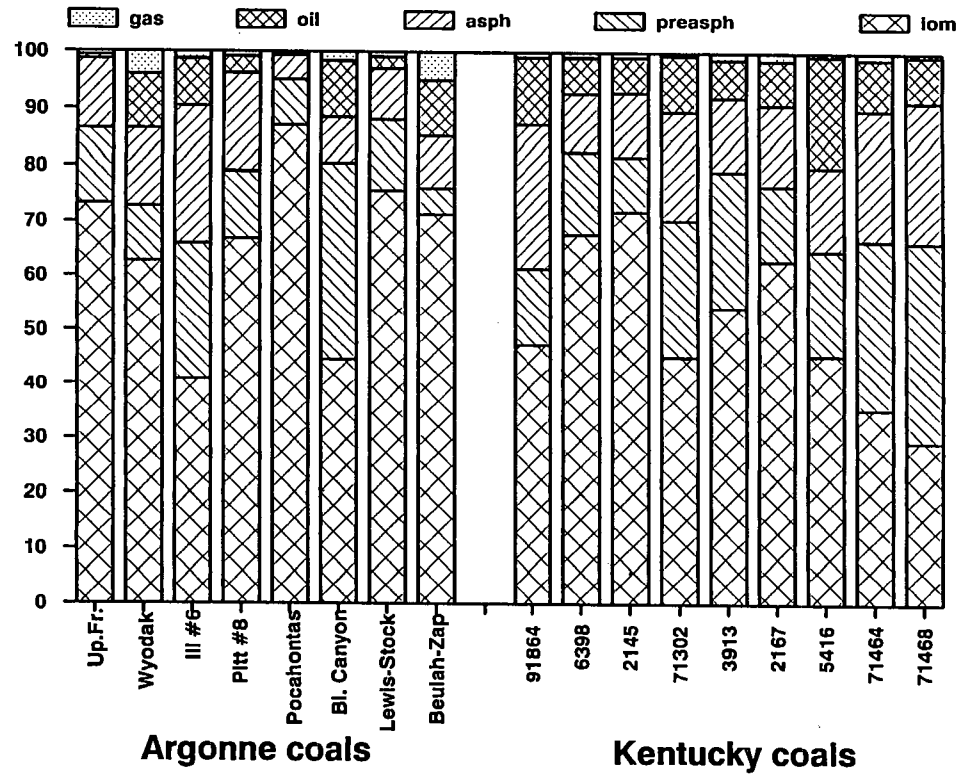

Figure 1. Liquefaction conversion percentages for Argonne Premium Coals and Kentucky Coals.

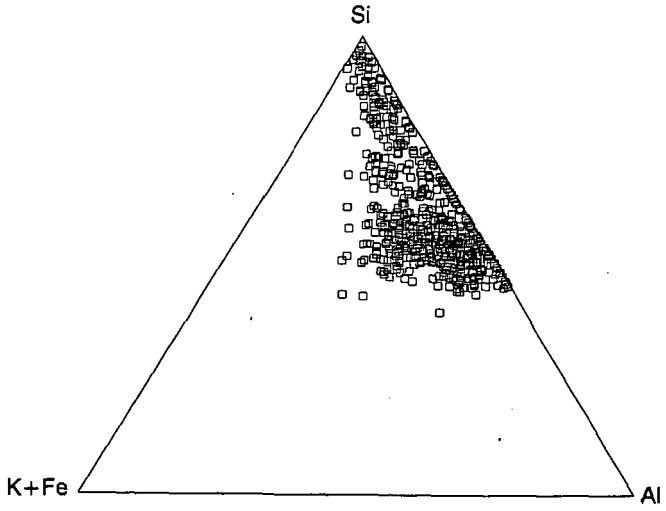

Figure 2. Ternary presentation of compositional data for quartz and clay minerals in Kentucky coal #3913.

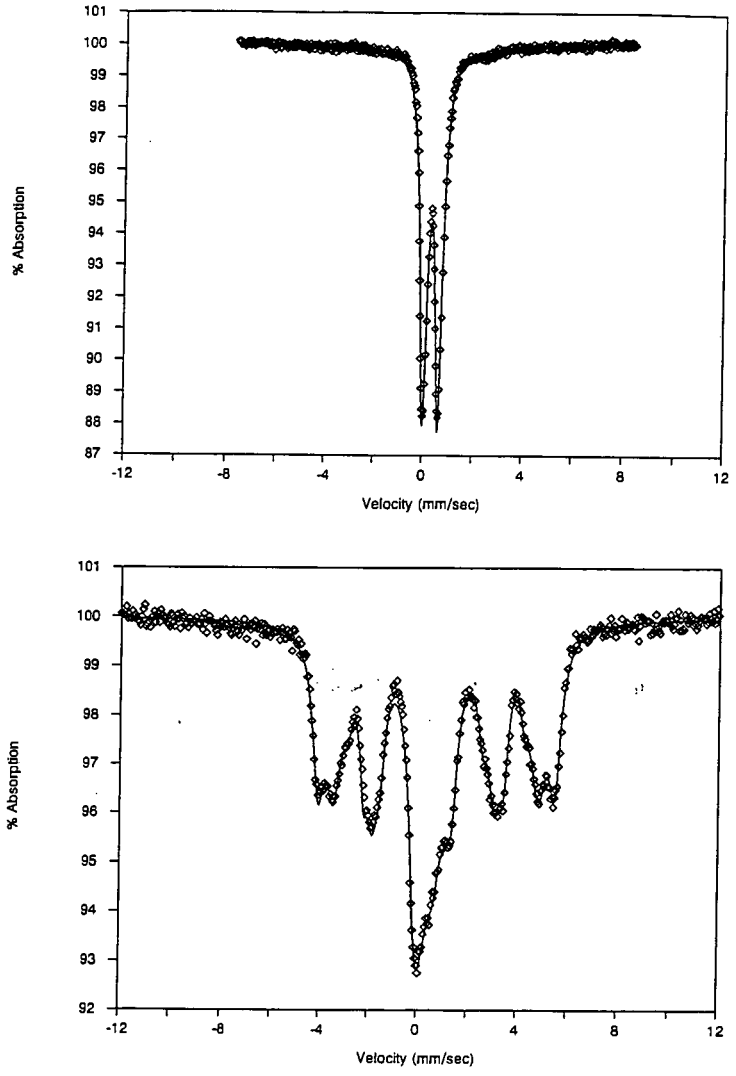

Figure 3. Mössbauer spectra of Illinois #6 raw coal (Top) and IOM (Bottom)

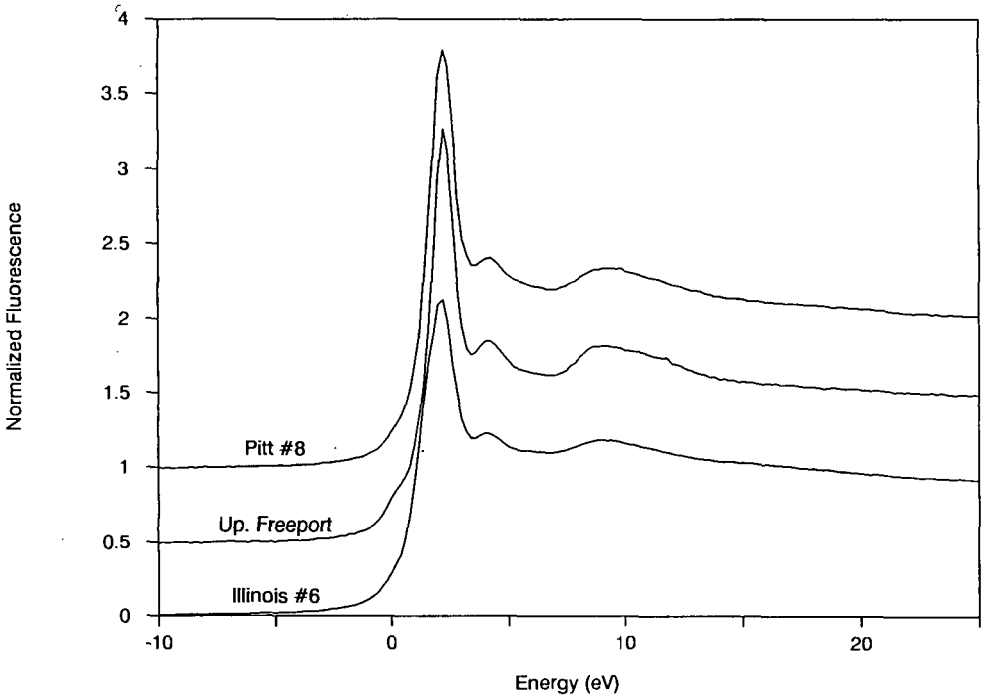

Figure 4. Sulfur K-edge XANES of three Argonne coals with pyrite removed.

SULFUR-PROMOTED METAL OXIDES AS COAL LIQUEFACTION CATALYSTS

Vivek Pradhan, J. W. Tierney and Irving Wender

Department of Chemical and Petroleum Engineering
University of Pittsburgh
Pittsburgh, PA 15261

Keywords: Catalysis, Sulfated Iron and Tin Oxides, Coal Liquefaction

ABSTRACT

This paper reports an investigation of the activities of iron and tin oxides treated with varying amounts of sulfate for the direct liquefaction of a bituminous coal (Illinois No. 6 from the Argonne Premium Coal Sample Bank). The work described here also attempts to correlate the physico-chemical properties of the sulfate-promoted oxides before the reaction and the types of active phases formed under liquefaction conditions with their apparent activities for hydrocracking of coal. $Fe_2O_3.SO_4^{2-}$ was found to be an effective catalyst for coal liquefaction even when used in small concentrations (<0.7 wt % iron). It resulted in an 86 wt % (maf basis) conversion of Illinois No. 6 coal at 400°C and 1000 psig hydrogen (initial); more than 50 wt % of the products consisted of oils (n-pentane solubles). Addition of elemental sulfur to the same catalyst (at 0.35 wt % Fe) enhanced the overall conversion to 90.3 wt % with more than 60 % of products consisting of oils. Similar results for coal conversion were obtained for a solid superacid made from tin, $SnO_2.SO_4^{2-}$. These conversions were much higher than those obtained in a thermal run under the same reaction conditions (% conversion = 52 % , wt % oils = 16). For both iron and tin oxides, sulfated forms containing between 1.5 wt % to 6 wt % of SO_4^{2-} group on the surface were more active than their respective unsulfated forms. Promotional effects of sulfate group are believed to be due to an increase in "catalyst-dispersion" and surface acidity.

INTRODUCTION

Catalysts in highly dispersed form are believed to be very active for conversion of coal to liquids via direct coal liquefaction.[1,2,3] Understanding the effects of catalyst dispersion (catalyst surface area per mass) and composition on catalyst performance is still far from complete. In direct coal liquefaction, the supported metal catalysts such as Co-Mo/Al_2O_3 may suffer from poor contact with the feed and rapid deactivation.[4] Unsupported dispersed catalysts derived from finely divided solid precursors offer efficient contact of coal-solvent slurries with catalyst surfaces. Addition of a low surface area solids requires high catalyst concentrations.[5] Particulate pyrite (FeS_2) with average particle size of several microns is not very effective at low catalyst concentrations. A catalyst with a high specific surface area and fine particulate size can be utilized even at very small concentrations[6]for achieving better performance in terms of overall coal conversion and selectivity to lighter products (oils) in direct coal liquefaction. A cheap disposable catalyst such as iron is highly desirable.

High dispersions of catalysts have been obtained by different methods such as the impregnation technique[5], use of water-soluble[7] or oil-soluble precursor[8], and use of finely divided powders.[9] All these methods allow the formation of finely dispersed active inorganic phases under reaction conditions. Maximum interaction of coal, vehicle, and H_2 can occur on the catalyst surface with a highly dispersed catalyst. One method of increasing dispersion of a catalyst is to introduce it as a very finely divided solid

(average particulate size of a few nanometers) to the coal-solvent reaction mixture. Such finely divided powdered precursors are believed to achieve good distribution throughout the coal-solvent slurry and are converted to active inorganic sulfide phases. The high dispersions of active phases thus achieved is believed to allow the use of catalyst concentrations below 1.0 wt % with good performance.[10]

We chose to study the catalytic activity of sulfate-treated iron and tin oxides and its relation to catalyst properties. These oxides have been claimed to be "superacidic"[11,12] as have the oxides of other transition metals such as Ti, Zr, Hf. These oxides have a Hammett acidity function, $H_0 < -12.0$ and catalyze a variety of hydrocarbon transformations at low temperatures.[12] It is believed that the bidentate sulfate group on the oxide surface increases its acidity. It is also known[13] that the sulfate anion prevents sintering of ceramic oxide powders during calcination, thereby reducing the degree of crystallinity and lowering the average crystallite size of these oxides. It was reported first by Tanabe et al.[14,15] that a sulfate- promoted iron oxide ($Fe_2O_3.SO_4^{2-}$), claimed to be a solid superacid, was active for promoting C-C bond cleavage in coals and therefore for the hydrocracking of a bituminous Akabira coal (% C = 83.0) at 400°C and under 1000 kg/cm^2 of H_2. A sulfated iron oxide with about 2 wt % sulfate group (SO_4^{2-}) on its surface was found as active as a well known hydroprocessing catalyst $CoO-MoO_3-Al_2O_3$. The iron oxide in its sulfated form gave about 75 wt % coal conversion (with 31 % "oils") as compared to unsulfated iron oxide which resulted in only 60 wt % coal conversion with 20 % of "oils". Later work reported by Kotanigawa et al.[16] mentions tha use of sulfate-treated iron oxide for some model compound reactions and for direct coal liquefaction reactions. They attributed higher activity of the sulfate- promoted iron oxide to the possible synergism between sulfate (S^{6+}) and sulfide (S^{2-}) phases of iron formed under coal liquefaction conditions. Mariadassou et al.[17,18] have reported the use of finely divided iron oxides/oxyhydroxides (avg. particle size = 50 nm) such as FeOOH, $FeOOH-Al_2O_3$ sulfided *in situ* by addition of CS_2 for the hydroliquefaction of a high volatile bituminous coal. They observed an increase in the activity of iron sulfide with decrease in the particle size of iron oxide added as precursor. They also reported that sintering of the oxide particles at high temperatures of coal liquefaction was inhibited by the textural promoter effects of coal. The same group recently reported the activity of finely divided tin oxide-sulfur systems for coal liquefaction.

EXPERIMENTAL

Chemicals: Illinois No. 6 hvB bituminous coal ground to below 100 mesh (<120 μm) was obtained in ampules and under N_2 storage from the Argonne Sample Bank and used as received. Tetralin (99+% pure) was obtained from the Fisher Scientific Co. Illinois No. 6 coal contained 4.8 % sulfur of which 46 % was organic and 54 % was pyritic. It had a composition of 77.7 % C, 5.0 % H, 13.5 % O, 4.8 % S, and 15.5 % ash. The starting materials used for the catalyst preparation were iron alum, urea, 28 % ammonia water which were purchased from the Aldrich Chemical Co. and tin(IV)chloride and iron(III)nitrate were purchased from the Strem Chemical Co.

Catalyst Preparation and Characterization: The sulfate treated oxides of iron and tin were prepared starting from their respective sulfate or chloride salts precipitated with either ammonia water or urea. Both homogeneous as well as heterogeneous coprecipitation routes were followed to prepare the intermediate oxyhydroxides of iron and tin. These oxyhydroxides were then treated with sulfuric acid in varying concentrations. The resultant powders were then dried and calcined at appropriate temperatures. The preparation conditions of these catalysts are indicated in Table 1. The catalysts thus prepared were characterized by various techniques such as BET-surface area analysis, sulfur analysis, thermogravimetry (TGA), X-ray diffraction, and electron microscopy. A Phillips X-ray Diffractometer using Cu-Kα radiation at 30 kV and 25 mA was used to obtain the powder diffraction patterns of the catalysts.

Table 1. Summary of Preparation Conditions of Sulfate Treated Metal Oxides

Cat.Code	Catalyst	Starting Salts	Norm. H_2SO_4	Calcination, T°C
FeCat1	Fe_2O_3	$Fe(NO_3)_3$	–	500
FeCat4	$Fe_2O_3SO_4^{2-}$	$Fe(NO_3)_3$	1.0	500
FeCat7	$Fe_2O_3SO_4^{2-}$	Fe Alum*	–	500
FeCat8	$Fe_2O_3SO_4^{2-}$	Fe Sulfate	–	700
SnCat1	SnO_2	$SnCl_4.5H_2O$	–	600
SnCat3	$SnO_2SO_4^{2-}$	$SnCl_4.5H_2O$	1.0	600
SnCat5	$SnO_2SO_4^{2-}$	$SnCl_4.5H_2O$	6.0	600

* Urea was used as a precipitating agent in this preparation.

Average crystallite sizes were calculated from line broadening of the peaks, corrected for instrumental broadening. A Cahn electrobalance was used for thermogravimetric analyses and acidity measurements of catalysts. Transmission electron microscopy(TEM) and scanning electron microscopy (SEM) were carried out for structural investigation of the catalysts using JEOL 35 CX SEM and JEOL 200 CX TEM models. The residues of coal liquefaction experiments were also analyzed using X-ray diffraction and a JEOL 2000 FX STEM (100 kV beam) with an energy dispersive X-ray spectrometer. for the composition and dispersion information about the catalytic phases formed under liquefaction conditions.

Reaction Studies: Direct coal liquefaction experiments were carried out in a 300 ml stainless steel autoclave (Autoclave Engineers) agitated by a turbine impeller and heated by a tube furnace. Illinois No. 6 coal (10 g), tetralin (40 g), and 0.35 or 0.7 wt % Fe or Sn (added as their respective sulfate-treated oxides) were mixed first manually in a beaker and then placed into the reactor, which was flushed with helium and pressurized with 1000 psig hydrogen at room temperature. Stirring was started at room temperature to allow for hydrogen dissolution in the coal-solvent slurry and proper mixing of the reactants. After about 30 minutes, the reactor was heated with furnace heater to 400°C in approximately 35-40 minutes, and held at that temperature for 60 minutes while stirring about 1400 rpm. The reactor was then cooled to below 300°C in about five minutes. Soxhlet extraction with CH_2Cl_2 was used to determine the coal conversion. Soluble products were recovered by rotary evaporation at 45°C under vacuum. Pentane solubles (oils) were determined by adding 40 volumes of n-pentane to CH_2Cl_2 solubles and using Soxhlet extraction with n-pentane. Pentane-insoluble but CH_2Cl_2 soluble material was referred to as asphaltenes. Methylene chloride insolubles (residues) were recovered and stored for further characterization.

RESULTS AND DISCUSSION

Catalyst Characterization: The iron and tin oxides treated with different amounts of sulfate were characterized by the different techniques mentioned above. Interestingly, the average crystallite size of the oxide particles was found to decrease upon treatment with 2 to 6 wt % sulfate anion. A distinct broadening of the X-ray diffraction peaks was observed for these oxides with the increasing sulfate group loadings. At the same time a corresponding increase in the specific surface areas of these oxides was observed when liquid nitrogen physisorption was carried out on the catalysts for determining the surface areas using the BET equation. A linear relationship was observed between the concentration of sulfuric acid used for sulfate treatment and the final amount of SO_4^{2-} group that remained on the surface. The decrease in the crystallite size can be explained if we hypothesize that a bulky sulfate group on the surface of the intermediate oxyhydroxide particles prevents the agglomeration or sintering of the oxide particles

at high temperature. It also probably delays crystallization. Evidence for acidity enhancement of these oxides upon the sulfate-treatment was also observed from pyridine adsorption experiments carried out using a Cahn electrobalance. From X-ray diffraction studies for iron oxides, α- and γ-Fe_2O_3 were found out to be the most abundant crystalline phases, while for tin oxides, the most abundant phase was crystalline SnO_2. Catalyst characterization results are listed in Table 2. The values of onset liquefaction temperatures of Illinois No.6 coal using different sulfate-treated oxides as catalysts have also been listed in this table. These temperatures were determined using a high pressure, high temperature polarizing light microscope with flowing hydrogen at 300 psig pressure.

Table 2. Effect of Sulfate Loading on Surface Area [S_g] and Crystallite Size [$D_{average}$]

Cat.Code	Wt % SO_4^{2-}	S_g, m^2/g	XRD: $D_{avg.}$	TEM :$D_{avg.}$	Onset*L.T, °C
FeCat1	0.0	26.82	46 nm	60-70 nm	415
FeCat7	3.4	81.72	16 nm	20-25 nm	410
FeCat4	6.1	79.50	12 nm	20-30 nm	400
SnCat1	0.0	60.50	19 nm	–	410
SnCat3	1.8	97.48	9 nm	15-20 nm	395
SnCat5	3.9	146.23	5 nm	10-15 nm	385

* Onset liquefaction temperature for a thermal run was about 450°C.

As seen from this table, the average crystallite sizes determined for both the sulfated and unsulfated iron and tin oxides based on the X-ray line broadening agree fairly well with those determined with transmission electron microscopy (TEM) using the bright field. Scanning electron micrographs of these catalysts samples were also taken to determine their particle size distribution and surface structure morphology. It was found from both the TEM and SEM images that sulfate-treated iron oxide consists of a bimodal-type distribution of crystallites, with some crystals being rod-like while other are plate-like. The average crystallite size was about 20 nm. Sulfate-treated tin oxides have a porous structure with a sausage-like surface morphology. Their average crystallite size was found to be 15 nm.

Reaction Studies: The coal liquefaction reactions were carried out in a 300 ml stainless steel autoclave. Initially a thermal run was carried out to determine the catalytic activities of the mineral matter (especially pyrite) inherent to coal, i.e., without addition of any external catalyst. This resulted in 52 wt % (maf) total conversion of Illinois No.6 coal, with about 16 wt % n-pentane solubles (oils). The total coal conversion values are calculated based on the weight of the final residue. The sulfate-treated iron and tin oxides were then used in very small concentrations for the liquefaction reactions. One of the iron oxides, Fe Cat 4 (wt % sulfate = 6.1) resulted in a substantially high coal conversion of 86 wt % with 39 wt % conversion to n-pentane solubles. A comparitive experiment with Fe Cat 1, which did not contain any sulfate group gave 74 wt % total conversion and 23 wt % conversion to oils. Less than 0.7 wt % Fe was used with respect to coal in these experiments. Similar experiments were run with tin oxides treated with sulfate to determine their efficacy for direct coal liquefaction reactions and to determine the promotional effect of the sulfate group on the activity of the oxides. About 0.8 to 0.9 wt % of tin was used in these runs with respect to coal. Two bar-charts demonstrating conversions and product-distributions for different oxide catalysts based on iron and tin are shown in Figure 3.

As can be seen from the bar-charts in Figure 1, addition of 0.7 wt % Fe in the form of oxide to the reaction mixture enhances total coal conversion as well as conversion to lighter oils. Both sulfate-treated oxides of iron, Fe Cat 4 and Fe Cat 7, were found to increase the total conversions to 86 % and 79 % respectively as compared to 74 % obtained with Fe_2O_3 alone (unsulfated form). Importantly, the amounts

of oils increased from about 23 % for Fe_2O_3 alone to about 38 to 40 % for $Fe_2O_3.SO_4^{2-}$ catalysts. Promotional effects of sulfate groups on catalytic activities of oxides for coal liquefaction were seen for sulfate-treated tin oxides as well. As seen in Figure 1, Sn Cat 5 (wt % sulfate=3.9) resulted in about 85 % total coal conversion with more than 40 % of the products consisting of oils. These values were again higher than those obtained for the unsulfated SnO_2, which gave 72 % total coal conversion with 32 % oils. A run was also made using iron oxide prepared directly from ferric sulfate by calcination at 700°C (Fe Cat 8). It resulted in about 80 % total coal conversion with 32 % conversion to oils. Some reactions were made at much reduced wt % of Fe and Sn but in the presence of an elemental sulfur added to the reaction mixture. The amount of sulfur added was enough(about 1.1 times the quantity that is required for complete sulfidation of added Fe as $Fe_2O_3.SO_4^{2-}$) to bring about complete *in situ* conversion of oxides to sulfides.[19] Fe Cat 1 and Fe Cat 7 were used separately with the added sulfur. The amount of catalyst was 0.35 wt % with respect to coal. As shown in the Figure 1, total conversions as high as 90+ % were obtained with both the sulfated (Fe Cat 7) and the unsulfated (Fe Cat 1) forms of iron oxides, but the former catalyst resulted in higher conversion to oils (47 %) than the latter one (28 % oils). This suggests that the non-stoichiometric iron sulfides (detected later by XRD) formed from sulfate-treated iron oxide were more active for the conversion of asphaltenes to lighter oils than those formed from unsulfated oxide (Fe_2O_3). Comparison of two runs, one with Fe Cat 7 (0.7 % Fe) and other with Fe Cat 7 + S (0.35 % Fe), shows an enhancement in conversion levels (Figure 3). Elemental sulfur was used with one of the sulfated tin oxide for coal liquefaction (wt % Sn=0.4), but no significant effect on conversion was observed. The enhancements in total conversions as well as conversions to oils obtained with sulfate-treated oxides over the unsulfated ones might be attributed mainly to the enhanced "dispersions" (surface area/gm) of the oxides upon the sulfate treatment. Due to increase in the specific surface area and decrease in the average particle size of the oxides upon the addition of small amounts of the sulfate group, the conversion of oxides to active catalytic sulfide phases, especially non-stoichiometric sulfides for iron, is facilitated.[19] (Pyrrhotite, a non-stoichiometric sulfide of iron, is a semiconductor. One wonders whether this property of pyrrhotite has any bearing upon its catalytic activity for coal liquefaction.) More of the active catalyst surface of these sulfides probably becomes available for reaction.

Product Characterization: The CH_2Cl_2 insolubles (residues) recovered from the coal liquefaction reactions were analyzed to determine the composition of metal-sulfide phases formed under coal liquefaction conditions. X-ray diffraction was carried out on these residues to determine their composition and the particle sizes of the inorganic phases formed. Residues recovered from the reactions which employed sulfate-treated iron oxides invariably showed the presence of non-stoichiometric iron sulfides (pyrrhotites) as the major constituent along with traces of FeOOH and Fe_3O_4. The average crystallite size of the pyrrhotite formed was found to be about 25 to 30 nm. Autoclave runs with sulfate-treated tin oxides resulted in residues rich in SnS with a small amount of pyrrhotite formed by the decomposition of pyrite in coal. These tin sulfides were found to have an average crystalline diameter of about 30 nm. A run was also made with one of the iron oxides (Fe Cat 7) in the presence of activated carbon instead of coal to characterize the dispersions using scanning and transmission electron microscopy (STEM). Some of the liquefaction residues were also characterized using STEM and energy dispersive microanalysis (EDX) and found to contain well dispersed iron-containing particles with particle sizes ranging between 10 to 100 nm. A typical TEM-mode image of iron-containing particles on activated carbon and the X-ray microanalysis are shown in Figure 2. This TEM-image shows a distribution of fine iron-containing particles over the activated carbon support. The EDX spectrum of one of the liquefaction residues indicates the presence of both Fe and S in these fine particles. Further detailed investigation of these liquefaction residues by Mossbauer spectroscopy and EXAFS is in progress.

The composition of CH_2Cl_2 solubles was determined by elemental analysis which was performed by Galbraith Laboratories Inc. (Table 3). Methylene chloride solubles consisted of a mixture of recovered tetralin (GC-analysis) (about 50 wt %, H/C=1.2), naphthalene (about 35 wt %, H/C=0.8) and soluble products from coal (about 15 wt %).

Table 3. Elemental Analysis of CH_2Cl_2 Solubles Obtained from Liquefaction Reactions Employing Different Catalysts

Analysis by Wt % as Received						
Catalyst	% C	% H	% N	% S	% O	{H/C}atom
Thermal	83.97	6.37	1.85	1.23	6.76	0.91
FeCat4	84.69	7.68	<0.50	0.084	0.74	1.09
FeCat1	88.98	8.94	1.30	0.21	1.09	1.20
FeCat7	86.25	8.47	<0.50	0.28	1.25	1.18
SnCat3	87.94	8.80	<0.50	0.24	1.32	1.20
SnCat5	87.44	9.10	<0.50	0.25	1.07	1.25

All the iron and tin oxides used as catalysts for the reaction under the same conditions yielded CH_2Cl_2 solubles with an enhancement in H/C ratios (about 1.2) along with a significant heteroatom removal. This could be due to the increased acidic character of these oxides. A very small amount of both nitrogen (Wt %<0.5) and sulfur (Wt%<0.28) was obtained in the solubles from almost all the catalytic runs. From these results, both iron and tin oxides (after transformation into their respective active sulfide phases) seem to function as good hydrogenation and hydrogenolysis catalysts.

CONCLUSIONS

Our experimental work on sulfate-treated metal oxides has shown that the sulfate group immobilized on the surface of these oxides helps increase its surface acidity and promotes the catalytic activity of these oxides for direct coal liquefaction reactions, probably by causing reduction in their average particle diameter and subsequent increase in the specific surface area available for catalysis. The sulfate-treated iron and tin oxides resulted in better coal conversions and product slates than the unsulfated oxides. It appears that finely divided sulfate-treated oxides are effective for overall coal conversion as well as the conversion of the asphaltenes to lighter oils. The oxides seem to convert themselves in to their respctive metal-sulfides with nano-size particles (10 to 100 nm), which is an indication of good catalyst-distribution during coal liquefaction reaction. These sulfate-treated oxides of iron and tin also seem to function as better hydrogenolysis catalysts for hydrodesulfurization and hydrodenitrogenation reactions.

ACKNOWLEDGEMENTS

The authors gratefully acknowledge the contributions of Cole van Ormer and Dr. W. Soffa for the TEM work and George McNaumus and Dr. J. R. Blachere for the SEM and STEM work. Funding support from the U.S. Department of Energy under grant number DE-FG22-87PC79928 is gratefully acknowledged.

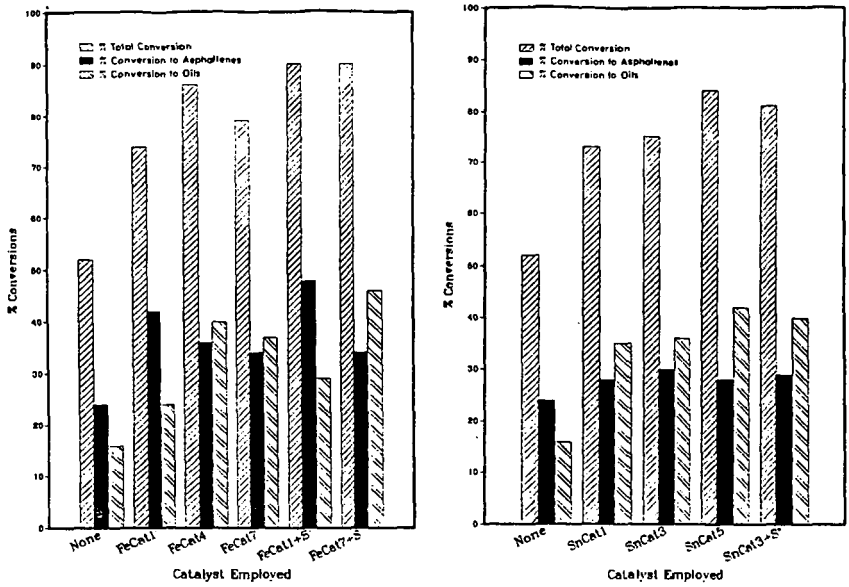

Figure 1. Activities of The Sulfate-Treated Iron and Tin Oxides for Liquefaction of Argonne Illinois No.6 Coal at 400°C, 1000 psig H_2, 1 hr run time

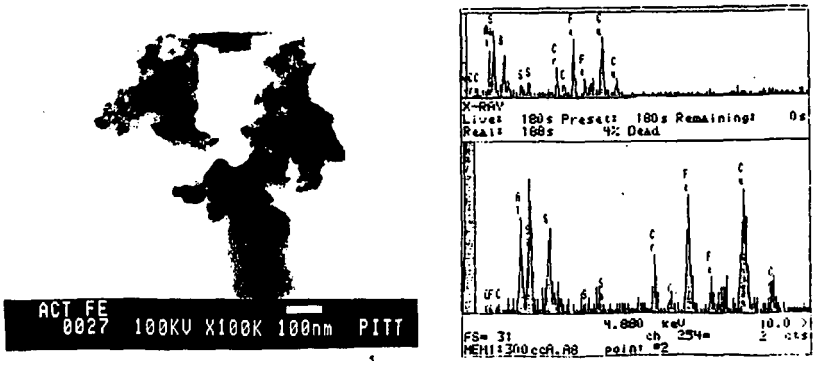

Figure 2. TEM-mode image of iron-containing particles on activated carbon and EDX Spectrum of Coal Liquefaction Residue using sulfated Iron Oxide Catalyst

References

1. Derbyshire, F. J., Catalysis in Coal Liquefaction: New Directions for Research, (IEA CR-08, London. U.K., IEA Coal Research, Jan. 1988).
2. Cugini, A. V., Lett, R. G., Energy and Fuels, (1989), Vol. 3, pp. 120-126
3. Weller, S., Pelipetz, M. G., Industrial and Engineering Chemistry, (1951), Vol. 43, No. 5, pp. 1243-1246
4. Derbyshire, F. J., Energy and Fuel, (1989), Vol. 3, No. 3, pp. 273-277.
5. Garg, D., Givens, E., Ind. Eng. Chem. Proc. Des. Dev., (1982), Vol. 21, pp. 113-117
6. Suzuki, T., Yamada, H., Sears, P., Watanabe, Y., Energy and Fuels, (1989), Vol. 3, pp. 707-713
7. Cugini, A. V., Utz, B. R., Fromell, E. A., Preprints, Div. of Fuel Chemistry, Am. Chem. Soc., Sept. 1989
8. Herrick, D. E., Ph.D. Thesis, University of Pittsburgh, 1990
9. Marriadassou, D., G., Charcosset, H., Andres, M., Chiche, P., Fuel, (1983), Vol. 62, pp. 69-72
10. Mukharjee, D. K., Mitra, J. R., Fuel, (1984), Vol. 63, pp. 722-723
11. Olah, G. A., Prakash, G. K. S., Sommer, J., Superacids, (New York: John Wiley and Sons, 1985), pp. 15-42.
12. Tanabe, K. in Heterogeneous Catalysis, (Texas A & M Univ., College Station, Texas, 1984), pp. 71-94.
13. Nakatani, Y., Sakai, M., Matsuoka, M., J. of Appl. Physics, Vol. 21, (1982), pp. L758
14. Tanabe, K., Yamaguchi, T., Hattori, H., Sanada, Y., Yokoyama, S., Fuel Processing Technology, (1984), Vol. 8, pp. 117-122
15. Tanabe, K., Yamaguchi, T., Hattori, H., Matsuhashi, H., Kimura, A., Fuel Processing Technology, (1986), Vol. 14, pp. 247-260
16. Kotanigawa, T., Yokoyama, S., Mitsuyoshi, Y., Maekawa, Y., Fuel, Vol. 68, (1989), pp. 531-533
17. Besson, M., Bacaud, R., Charcosset, H., Varloud, J., Fuel Processing Technology, (1986), Vol. 14, pp. 213-220
18. Besson, M., Bacaud, R., Charcosset, H., Sharma, B. K., Fuel, (1989), Vol. 69, pp. 213-220
19. Montano, P.A., Bommannavar, A. S., Shah, V., Fuel, (1981), Vol. 60, P. 703

PYRIDINE SORPTION BY PYRIDINE-EXTRACT OF ILLINOIS NO. 6 COAL

Thomas K. Green and James E. Ball
Department of Chemistry
Center for Coal Science
Western Kentucky University
Bowling Green, KY 42101

KEYWORDS: Coal swelling, Extracts, Pyridine

INTRODUCTION

The principal goal of this research is to develop an understanding of the thermodynamics of the swelling of coals in various solvents. The approach is unique in the sense that the uncrosslinked portion of the coal is being swollen, as opposed to the crosslinked portion. This approach avoids complications due to the crosslinked nature of coals, and allows the experimental data to be interpreted in terms of modern theories developed for polymer solutions.[1]

The uncrosslinked portion of the coal is obtained by pyridine-extraction of the coal. The extract is then swollen with the solvent at several relative pressures until equilibrium is established. In principle, free energies, enthalpies, and entropies of swelling can be determined from such an approach.

We are currently working with the pyridine-extract of an Argonne premium Illinois No. 6 coal. This coal is about 27% (wt) Soxhlet extractable in pyridine. The carbon, hydrogen and nitrogen contents of the extract are very similar to those of the original coal. The extract was exposed to pyridine at several relative pressures and the equilibrium weight of pyridine was measured. Studies were conducted at both 50°C and 70°C. We also studied the O-methylated extract under the same conditions.

EXPERIMENTAL

Sample preparation. Argonne Premium Illinois No. 6 coal was obtained from Argonne National Laboratory in ampoules of five grams of -100 mesh coal. The coal was first dried under vacuum at 105°C to constant weight and then analyzed for carbon, hydrogen, and nitrogen. Analysis found: C, 65.57; H, 4.66; N, 1.24 (duplicate).

Approximately 4.5 g of the sample was Soxhlet-extracted with dry pyridine under argon for several days until the siphon liquid was clear. The pyridine solution was then filtered through a 0.4 um nylon membrane filter to insure removal of particulates and colloidal material. The filter did not plug. Most of the pyridine was removed by rotovaporization under reduced pressure at 70-80°C. Approximately 200 mL of a methanol/water (80/20 vol.) mixture and 2 mL of conc. HCl were added to the flask and the mixture was stirred under nitrogen for two days. The solid extract was then filtered and dried under vacuum at 105°C for 24 hours. The extractability was 27.2% (wt.). This value agrees well with that found by Buchanan et al.[2] Analysis found: C, 78.32; H, 5.62; N, 1.65 (duplicate).

The pyridine-insoluble residue obtained from the extraction was first dried under vacuum to remove most of the pyridine, treated with the methanol/water/HCl mixture, and then dried under vacuum. Analysis found: C, 60.47; H, 4.39; N, 1.30 (duplicate).

The extract was O-methylated according to the procedure of Liotta.[3] FT-IR analysis and carbon and hydrogen analysis confirmed that reaction had occurred. Analysis found: C, 76.7; H, 6.04; N, 1.24.

Sorption Experiments. Sorption experiments using pyridine as solvent were carried out using a quartz spring balance shown in Figure 1. The balance consists of a quartz spring, a large 5 liter flask, vacuum inlet system, and MKS pressure transducer (0-1000 torr, 0.5% accuracy). The entire balance chamber, including transducer, is housed in a Precision Scientific circulating (forced air) drying oven, which is maintained at a constant temperature by a I^2R thermowatch temperature regulator which activates a light bulb.

The sample is suspended from the quartz spring and, as the sample sorbs solvent, the spring extends until equilibrium is reached. The extension of the spring is measured through a window on the door of the oven using a sensitive Eberbach cathetometer (travelling telescope). The spring is calibrated at the appropriate temperature using standard weights before the experiment is conducted. The experiment thus allows determination of the mass of solvent sorbed by the sample at a given partial pressure and temperature. The purpose of the 5 liter flask to minimize pressure changes caused by sorption of solvent by the sample. Quartz springs of the type used here have a linear-extension versus suspended-weight relationship and exhibit no hysteresis within the range of weights for which the spring is designed.

For the particular spring used in these experiments, the calibration factor was determined to be 0.48 mm/mg. The uncertainty of the cathetometer is ± 0.1 mm. Since two measurements must be made to obtain the weight of solvent, the uncertainty in the solvent weight is ± 0.2 mm x 1 mg/0.48 mm = ± 0.4 mg. In a typical experiment, 50 mg of extract was used, so the uncertainty per gram of extract is ± 0.4 mg/0.050 g = ± 8 mg/g extract.

The experimental procedure was as follows. Approximately 50 mg of extract was placed in the quartz bucket and weighed on an electronic balance. The bucket and sample were then suspended on the spring. The hangdown tube was replaced and the system was evacuated to less than 0.1 torr and brought to the appropriate temperature. The system was allowed to evacuate overnight. Purified pyridine was placed in the round bottom flask shown in Figure 1 and frozen with dry ice/isopropanol. Stopcock B was closed, and stopcock C was opened to evacuate air from the flask. Then stopcock C was closed, and the pyridine was thawed and refrozen. Stopcock C was again reopened for evacuation. This procedure insures removal of last traces of air. Stopcock A was closed and stopcocks B and C were then opened until the appropriate pressure of pyridine was reached. After equilibrium was achieved, the pressure of pyridine was again raised. This procedure was repeated until the entire pressure range was covered.

RESULTS

Characterization of Pyridine Extract. Residual pyridine was removed from the pyridine-extract of the Argonne Illinois No. 6 coal by stirring with a methanol/water/HCl mixture for two days. Elemental analyses of the pyridine-extract revealed 1.65% N compared to 1.47% N (daf) in the original coal. The possibility exists that a small amount of pyridine remains bound to the extract. If one assumes that the additional N content of 0.18% is attributed to residual pyridine, then 10 mg pyridine/g extract was not removed from the extract by the methanol/water/HCl washing. FT-IR analysis failed to detect any residual pyridine, however.

The O-methylated extract was analyzed for carbon and hydrogen to establish the number of methyl groups added. The H/C ratio of the original extract is 0.86 and

the ratio of the O-methylated extract is 0.94. This increase in H/C ratio corresponds to the addition of 7.5 methyl groups per 100 carbon atoms of original extract. Liotta determined that there were approximately 5 acidic hydroxyl groups in an Illinois No. 6 coal,[3] which is considerably lower than that determined here. However, our value is for the extract, not the whole coal, and it does not seem unreasonable. The O-methylated extract exhibited a reduced hydroxyl group absorption compared to the original extract, consistent with the conversion of phenolic hydroxyl groups to methyl ethers. In addition, a significant absorption at 1700 cm^{-1} appears in the spectrum of the O-methylated extract, consistent with the conversion of carboxylic acids to methyl esters.

Sorption Experiments. The pyridine-extract and O-methylated extract of the Argonne Illinois No. 6 coal were exposed to pyridine at various vapor pressures at 50°C and 70°C. Several incremental sorption experiments were conducted in that, once equilibrium was attained at a particular pressure, the pressure was raised, and the system was again allowed to attain equilibrium. Typical sorption curves for the extract and O-methylated extracts are shown in Figures 2 and 3, respectively. Note that a wide range of pressures was covered, ranging from 0.20 to 0.99. For the extract, several hours are required to reach equilibrium at each pressure and, in general, equilibrium was achieved more rapidly at the higher pressures. Equilibrium was achieved more rapidly for the O-methylated extract in comparison, particularly at the lower pressures.

The equilibrium amounts of pyridine determined from each sorption experiment are plotted against relative pressure of pyridine in Figure 4. Note that there is a good straight-line correlation between the sorption values and pressure for each extract and each temperature. The curves drawn are least-squares fits. The slope of the curve decreases upon O-methylation, i.e. the O-methylated extract sorbs less pyridine at equivalent relative pressures. Both extracts sorb less pyridine at the higher temperature.

DISCUSSION

The results in Figure 4 demonstrate that sorption of pyridine by the extract of the Illinois No. 6 coal obeys Henry's Law, i.e, the solubility of pyridine in the extract increases linearly with pressure. However, the curves do not pass through the origin. This result is similar to those of Michaels et al, who observed that the solubilities of several gases in polyethylene terephthalate obeyed Henry's law.[4] For two of the gases, carbon dioxide and ethane, the sorption isotherms were curved at low pressures but linear at higher pressures. They interpreted their results by proposing that sorption took place by two concurrent mechanisms at the lower pressures; ordinary dissolution and "hole-filling". At higher pressures, the holes or microvoids were saturated with only dissolution occurring. The intercept was interpreted as the total amount of sorption due to filling of the microvoids. Thus, a quantitative separation of the two processes was possible.

Following the work of Michaels et al., we suggest that the intercepts observed in Figure 4 represent the total amount of pyridine that fills holes in the extracts. Using a density of 0.98 g/mL for pyridine, the total microvoid volume occupied by pyridine is determined to be 0.079 mL per g of extract (average of two values). Using a density of 1.3 g/mL for the extract (determined with helium), this corresponds to 9% microvoid volume for the extract. The same calculation for the O-methylated extract yields a value of 7% microvoid volume. Although caution is warranted at this time, we feel the magnitude of these values is reasonable.

Finally, we have corrected the sorption curves shown in Figure 4 for hole-filling according to the above model. The results are shown in Figure 5. These curves represent dissolution of pyridine into the extracts if our interpretation is

correct. We can calculate the differential heats of dilution for both the extract and the O-methylated extract from the data using Equation 1. The differential heat of dilution is defined as the heat change when one mole of pyridine is added to an infinite amount of the mixed phase at the specified concentration, and is given by

$$\Delta H_{dil} = \frac{-RT^2 \, d(\ln p/p_o)}{dT} \qquad (1)$$

For the case in which solubility follows Henry's law, the heat of dilution is constant as a function of concentration, as long as the curves have the same intercept. Using a average temperature of 333 K, we calculate a ΔH_{dil} of -2.3 kcal/mole for the extract-pyridine system and a value of -4.5 kcal/mole for the O-methylated extract-pyridine system.

We feel the sign and magnitude of ΔH_{dil} calculated for the extract-pyridine system is reasonable, since pyridine is expected to hydrogen bond to phenolic groups in the extract, a process which is expected to be exothermic. Although the strength of hydrogen bonds between pyridine and phenols are typically on the order of 7 kcal/mole,[5] it must be considered that coal-coal hydrogen bonds probably have to broken in the extract in order to form a pyridine-coal hydrogen bond. (It is obvious in the IR spectrum of the extract that the hydroxyl groups in the extract must be hydrogen bonded). This process obviously costs energy, so the magnitude of ΔH_{dil} for this system is not unreasonable.

The more negative ΔH_{dil} for the O-methylated extract is surprising, particularly since hydrogen bonding is expected to be absent in this system. We currently have no explanation for this result. We simply suggest that perhaps there is a small population of sites in the O-methylated extract which interact strongly with pyridine. The nature of these sites is unknown, but they may be hydroxyl groups that were left unreacted by O-methylation. Clearly, more studies need to be done before conclusions can be drawn.

Finally, we note that the curves in Figure 4 indicate that there should be only limited swelling of the extracts at a relative pressure of 1.0. However, we have noted that both extracts can be substantially redissolved in liquid pyridine (p/p_o=1.0). Thus, it seems that the curves must rise very steeply as a relative pressure of 1.0 is approached. The data shown in Figure 4, however, do not support this idea. We presently have no explanation for this result.

CONCLUSIONS

Equilibrium sorption of pyridine by the pyridine-extract and the O-methylated extract of the Illinois No. 6 coal increases linearly with pressure. We tentatively interpret the intercept as the total amount of pyridine that fills microvoids in the extract. Equilibrium sorption of pyridine decreases with increasing temperature at equivalent relative pressures for both extracts, consistant with exothermic processes. We are currently conducting experiments on the whole coal to see if it might behave similarly. The results will be presented in the talk.

ACKNOWLEDGEMENTS

We gratefully acknowledge the Department of Energy, Grant No. DE-FG22-88PC88924, and the Research Corporation for support of this work.

REFERENCES

1. Treloar, L.R.G., "The Physics of Rubber Elasticity," Clarendon Press, Oxford, 1975, 128-129.

2. Buchannan, D.H.; Warfel, L.C.; Bailey, S.; Lucas, D., Energy Fuels, 1988, 2(1), 32-36.

3. Liotta, R.; Rose, K.; Hippo, E., J. Org. Chem., 1981, 50 277-283.

4. Michaels, A.S.; Vieth, W.V.; Barrie, J.A., J. Appl. Phys., 1963, 34, 1-12.

5. Arnett, E.M.; Joris, L.; Mitchell, Murty, T.S.S.R.; Gorric, T.M.; Schleyer, P.v.R., J. Am. Chem. Soc., 1970, 92, 2365.

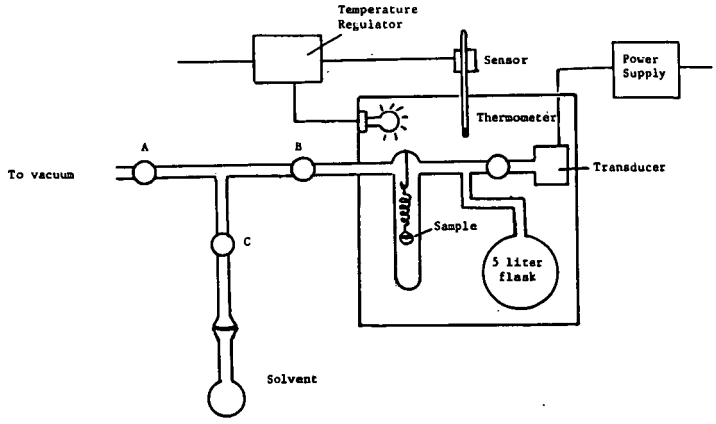

Figure 1. Sorption Apparatus

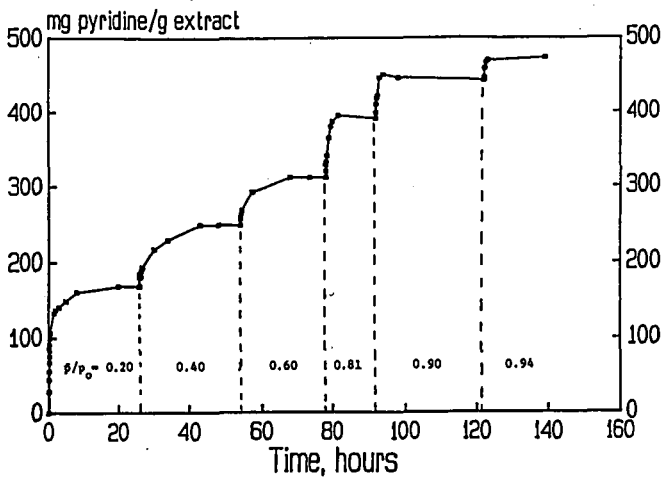

Figure 2. Sorption of Pyridine by Pyridine-extract of Illinois No. 6 Coal at 50°C.

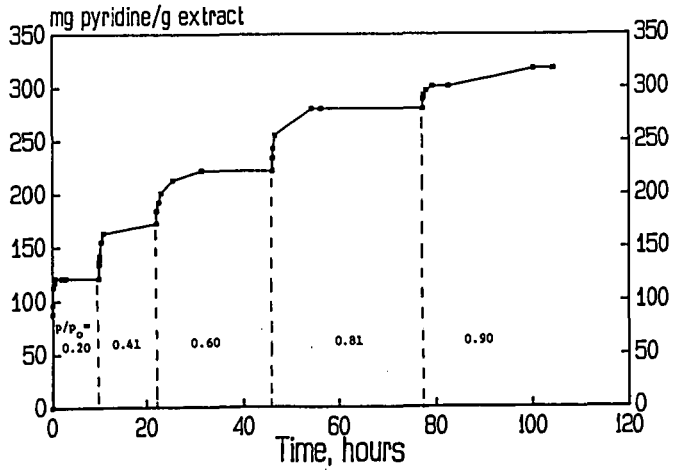

Figure 3. Sorption of Pyridine by O-methylated Pyridine-extract of Illinois No. 6 Coal at 50°C.

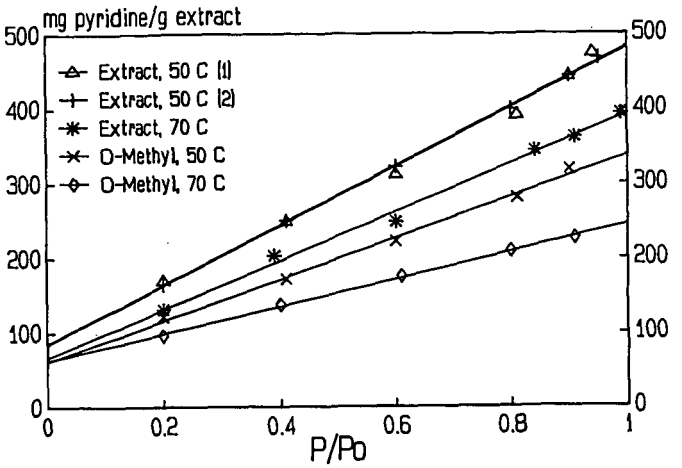

Figure 4. Sorption Isotherms of Pyridine-extracts of Illinois No. 6 Coal.

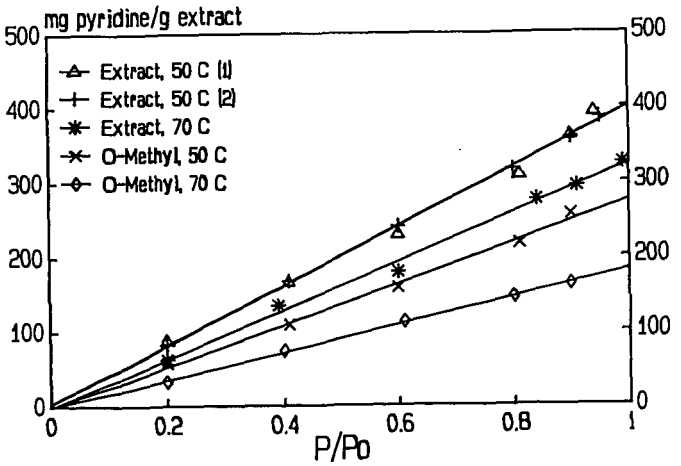

Figure 5. Corrected Sorption Isotherms of Pyridine-extracts of Illinois No. 6 Coal.

KINETICS OF VOLATILE PRODUCT EVOLUTION FROM THE ARGONNE PREMIUM COALS

Michael A. Serio, Peter R. Solomon, Sylvie Charpenay, Zhen-Zhong Yu,
and Rosemary Bassilakis

Advanced Fuel Research, Inc., 87 Church Street, East Hartford, CT 06108

Keywords: Coal Pyrolysis, Kinetics, Argonne Premium Coals

ABSTRACT

This paper describes the development of a set of rank dependent kinetic parameters for the evolution of the major volatile species from pyrolysis of the eight Argonne Premium coals. Programmed pyrolysis experiments are done over a range of heating rates (3, 30, 50, 100°C/min) in an instrument which combines Thermogravimetric Analysis (TG) with evolved product analysis using Fourier Transform Infrared Spectroscopy (FT-IR) (the Bomem TG/Plus). An analysis of the data on the temperature for the peak evolution rate (T_{max}) for tar, CH_4, and CO_2 as a function of heating rate is used for obtaining a preliminary estimate of the mean kinetic parameters. The parameters are further refined by using the FG-DVC model for coal pyrolysis to best fit the complete evolution profiles at each of the four heating rates. A final test is done by use of the parameters to predict pyrolysis data obtained under high heating rate conditions. The kinetics are found to vary systematically with rank and are faster for lower rank coals. The variations with rank are most significant for high rank coals with greater than ~ 86% daf carbon (< 8% daf oxygen). These differences can be important in accurately predicting coal fluidity and ignition phenomena.

INTRODUCTION

This paper is a continuation of work reported previously, related to the measurement and modeling of the pyrolysis kinetics for the Argonne Premium coals (1-3). In the first paper (1), the results for pyrolysis of the Argonne Premium coals at 30°C/min in the TG-FTIR and 3°C/min in a Field Ionization Mass Spectrometer (FIMS) apparatus were reported. Comparisons were made of the T_{max} values for the evolution of major volatile products and the molecular weight distributions (MWD) of the tars from pyrolysis-FIMS experiments. In the next paper (2), the FG-DVC coal pyrolysis model was used to simultaneously fit the pyrolysis data from the 30°C/min TG-FTIR experiments, the 3°C/min (vacuum) FIMS experiments and the ~ 5000 K/s entrained flow reactor (EFR) experiments.

The third paper (3) was a preliminary evaluation of the rank dependence of the pyrolysis kinetic rates for tar, CH_4, and weight loss for the Argonne coals based on TG-FTIR experiments at four different heating rates with all eight coals and from entrained flow reactor experiments in a Transparent Wall Reactor (TWR) with two of the coals (Zap lignite, Pittsburgh Seam bituminous) at ~ 5000 K/s. In the current paper, the rank dependent kinetic parameters have been further refined and developed for additional species (CO_2). For the Illinois coal, an extrapolation has been made to high heating rate conditions for the case of tar evolution.

EXPERIMENTAL

Coal Properties

The elemental and ultimate analysis data for the Argonne Premium coals are given in Refs. 4 and 5.

Reactor System

Pyrolysis experiments were done with the Argonne premium coals at heating rates of 3, 30, 50, and 100°C/min up to 900°C in a TGA with FT-IR analysis of evolved products (TG-FTIR). The TG-FTIR apparatus consists of a sample suspended from a balance in a gas stream within a furnace. As the sample is heated, the evolving tars and gases are carried out of the furnace directly into a 5 cm diameter gas cell (heated to 150°C) for analysis by FT-IR. With this geometry under low heating rate conditions, the temperature of the sample is assumed to be the same as that of a thermocouple which is next to the sample. The TG-FTIR system used in the current work is the TG/Plus from Bomem, Inc.

The TG/Plus couples a Dupont 951 TGA with a Bomem Michelson 100 FT-IR spectrometer (6,7).

High heating (~ 20,000 K/s) pyrolysis rate measurements were previously made in a heated tube reactor (HTR) with an Illinois No. 6 coal, as described in Ref. 8. These experiments included in-situ FT-IR diagnostics for measurement of the coal particle temperature. A heat transfer model was developed which provided a good fit to the measured temperature profile (8,9). The predictions of the heat transfer model were subsequently input into the FG-DVC pyrolysis model.

RESULTS

The TG-FTIR results for the Pittsburgh Seam coal at three heating rates are given in Fig. 1. The dashed lines are the prediction of the FG-DVC model (9-11) while the experimental data are plotted as asterisks connected by solid lines. The left hand set of curves is for the cumulative weight loss from the balance. Superimposed on each of these plots is the time-temperature profile. Except for very low heating rates, the coal is heated first to 150°C for drying before heating at the designated rate to 900°C.

The agreement between the experimental and predicted weight predictions is quite good at each of the three heating rates. The predicted weight loss is the sum of the tar evolution and the major gases (CO, CO_2, H_2, H_2O, CH_4, paraffins, olefins) which are included in the FG-DVC model.

The middle set of curves in Fig. 1 is for the tar evolution while the right hand set is for CH_4 evolution. The prediction of tar evolution is based on the breaking of weak linkages between an assumed polymeric structure for coal followed by transport of the molecule out of the coal if it meets the volatility criteria (10). The position and shape of the main tar peak is predicted very well for the Pittsburgh Seam coal and for several other coals that have been tested. The early part of the tar evolution is not as well predicted. This part of the tar evolution arises primarily from "guest" molecules which are physically bound in the coal. We are working on a new version of the FG-DVC model which includes the quest molecules (11).

The evolution of CH_4, shown on the far right hand side of Fig. 1 is also well predicted. The CH_4 evolution is modeled using two sources which evolve in a manner such that the peaks are usually merged into a single peak (9,10).

Both the tar and CH_4 evolution profiles show a systematic shift with increasing heating rate. The change in the temperature for the maximum evolution rate (T_{max}) with temperature can be used in preliminary analysis to derive kinetic parameters (12,13). We have used this approach to obtain a preliminary estimate of the mean values of the distributed activation energy parameters. The parameters are further refined by using the FG-DVC model to best fit the complete evolution profiles at each of four heating rates.

Similar comparisons are made in Figs. 2-5 for other coals in the Argonne series. In this case, the data are shown for a single heating rate (30°C/min) but one additional species (CO_2). Again, good agreement is obtained for the actual weight loss and the predicted values from all four coals. In the case of the Utah Blind Canyon coal and the Zap lignite, the predicted curves have been horizontally displaced to match the weight loss after moisture evolution since the model predictions are all done on a dry basis.

The prediction of the tar evolution profile is also good except for the very early tar as discussed above for the Pittsburgh Seam coal. The methane evolution profile is very well predicted in each case. The CO_2 evolution profiles are not as well predicted as the evolution of hydrocarbon species. The CO_2 evolution is predicted based on three assumed sources (extra loose, loose, and tight) (9,10). At 30°C/min, the peaks are centered at approximately 16, 22, and 28 minutes, respectively. However, because the mineral sources are not included in the model, the quality of the fits is not the same as for hydrocarbon species where there are no mineral contributions.

DISCUSSION

The use of the TG-FTIR method over a range of heating rates has allowed the development of a set of rank dependent kinetic parameters for tar, CH_4, and CO_2 (and indirectly the weight loss). The

parameters for the tar evolution were obtained by adjusting the value of the pre-exponential and activation energy for the bridge breaking rate in the FG-DVC model in order to match the evolution profiles at the four heating rates. In general, these rates increase monotonically with decreasing rank (increasing oxygen content). For very low rank coals, the contribution of polymethylenes is sufficiently large that it partly obscures the tar evolution from bridge breaking. In this case, the TG-FTIR results from demineralized coals are used to obtain a more reliable estimate of the bridge breaking rate. The lower amount of crosslinking in the demineralized coals reduces the relative contribution of the polymethylene tar.

In the case of the CH_4 and the CO_2, good results were obtained by adjusting only the pre-exponential factors. The values of the activation energies used were the same as those reported previously (10).

The importance of the rank dependence of the pyrolysis kinetics for tar and CH_4 evolution was evident in the modeling of coal fluidity behavior (14). When modeling fluidity, it was found that relatively small differences in the methane evolution rate (which is related in our model to the moderate temperature crosslinking which shuts down the fluidity) and the tar evolution rate (which is based on the bridge breaking rate as discussed above) have a large effect on the fluidity predictions. In Fig. 6 are shown comparisons of the measured fluidity with the predicted fluidity (based on the rank dependent rates) for five of the eight coals. With the possible exception of the Pocahontas coal, the agreement between the measured and predicted fluidity is quite good.

A good test of the validity of using the TG-FTIR method over a range of low heating rates to obtain kinetic parameters is the ability to use the kinetic parameters to extrapolate to high heating rate conditions. An example of this is shown in Fig. 7, where the parameters obtained for the Illinois No. 6 coal using the TG-FTIR method were used to simulate previously obtained high heating rate (~ 20,000 K/s) data for tar evolution (9). Again, the agreement between the theory and data is quite good.

Finally, a comparison can be made for results obtained for T_{max} for tar evolution at 3°C/min for the eight Argonne premium coals using the TG-FTIR method with results obtained by Burnham et al. (15) using a Rock-Eval experiment at 4°C/min. This comparison is shown in Fig. 8. The agreement between the two experiments is generally very good.

CONCLUSIONS

The conclusions of this work are as follows:

- The TG-FTIR method has been used to provide a set of rank dependent kinetic parameters for tar, CH_4, CO_2, and weight loss for the eight Argonne coals.
- These rank dependent kinetic parameters will be important in predicting fluidity and ignition behavior.
- The parameters obtained by this method extrapolate well to high heating rate conditions.
- Good agreement was found with low heating rate kinetic data obtained elsewhere with a different technique.

ACKNOWLEDGEMENTS

This work was supported under DOE Contract DE-AC21086MC23075. Richard Johnson is the Project Manager.

REFERENCES

1. Serio, M.A., Solomon, P.R., and Carangelo, R.M., ACS Div. of Fuel Chem. Preprints **33**, (2), 295, (1988).
2. Serio, M.A., Solomon, P.R., Yu, Z.Z., Desphande, G.V., and Hamblen, D.G., ACS Div. of Fuel Chem. Preprints, **33**, (3), 91, (1988).

3. Serio, M.A., Solomon, P.R., Yu, Z.Z., Bassilakis, R., ACS Div. of Fuel Chem. Preprints, **34**, (4), 1324, (1989).
4. Vorres, K.S., ACS Fuel Chem. Div. Preprints, **33**, (3), 1, (1988).
5. Vorres, K.S., Users Handbook for the Argonne Premium Coal Sample Program, Argonne National Lab., (September 1989).
6. Carangelo, R.M., Solomon, P.R., and D.G., Gerson, Fuel, **66**, 960, (1987).
7. Whelan, J.K., Solomon, P.R., Deshpande, G.V., and Carangelo, R.M., Energy & Fuels, **2**, 65, (1988).
8. Solomon, P.R., Serio, M.A., Carangelo, R.M., and Markham, J.R., Fuel, **65**, 182, (1986).
9. Serio, M.A., Hamblen, D.G., Markham, J.R., Solomon, P.R., Energy & Fuel, **1**, 138, (1987).
10. Solomon, P.R., Hamblen, D.G., Carangelo, R.M., Serio, M.A., and Deshpande, G.V., Energy & Fuel, **2**, 405, (1988).
11. Solomon, P.R., Serio, M.A., Hamblen, D.G., Yu, Z.Z., and Charpenay, S., ACS Div. of Fuel Chem. Preprints, **35**, (2), 479, (1990).
12. Jüntgen, H. and Van Heek, K.H., Fuel, **47**, 103 (1968) and "Progress Made in the Research of Bituminous Coal," paper given at the annual meeting of the DGMK, Salzburg, (1968), Translated by Belov and Associates, Denver, CO, APTIC-TR-0779 (1970).
13. Braun, R.L. and Burnham, A.K., Energy & Fuels, **1**, 153, (1987).
14. Solomon, P.R., Best, P.E., Yu, Z.Z., and Deshpande, G.V., ACS Div. of Fuel Chem. Preprints, **34**, (3), 895, (1989).
15. Burnham, A.K., Oh, M.S., Crawford, R.W., and Samoun, A.M., Energy & Fuel, **3**, 42, (1989).

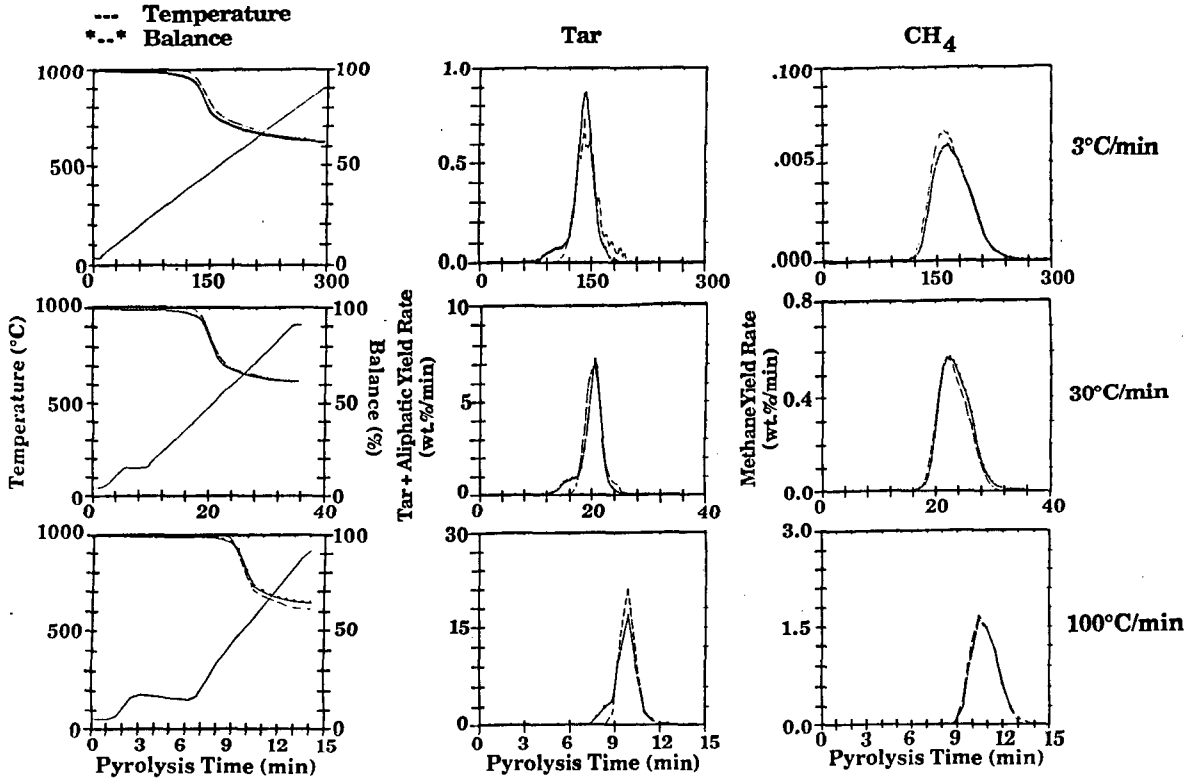

Figure 1. Kinetic Analysis at Three Heating Rates for Pittsburgh Seam Coal. Comparison of Theory (---) and Data (*-*).

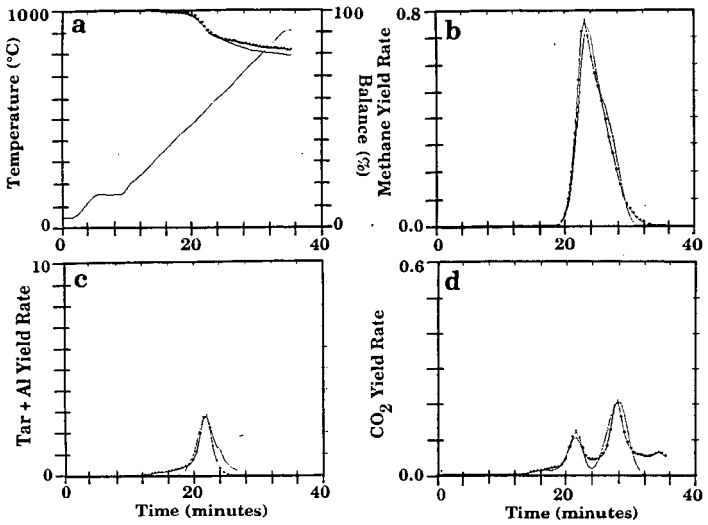

Figure 2. Kinetic Analysis at 30°C/min for Major Volatile Products. Comparison of Theory (—) and Data (*-*) for Pocahontas Coal.

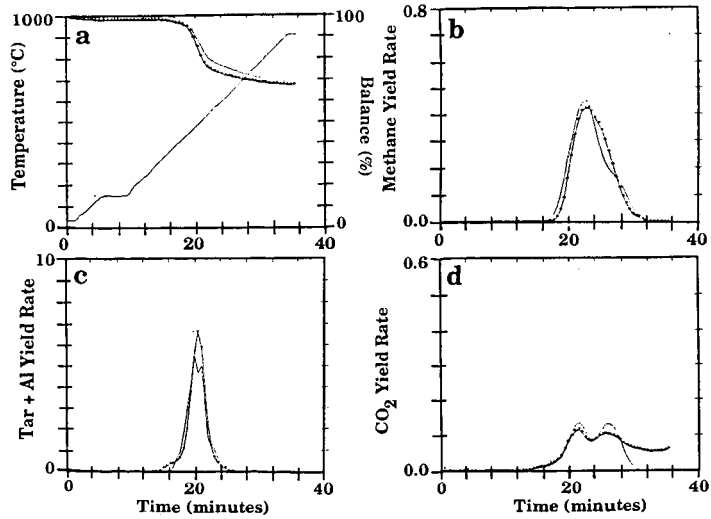

Figure 3. Kinetic Analysis at 30°C/min for Major Volatile Products. Comparison of Theory (—) and Data (*-*) for Lewis-Stockton Coal.

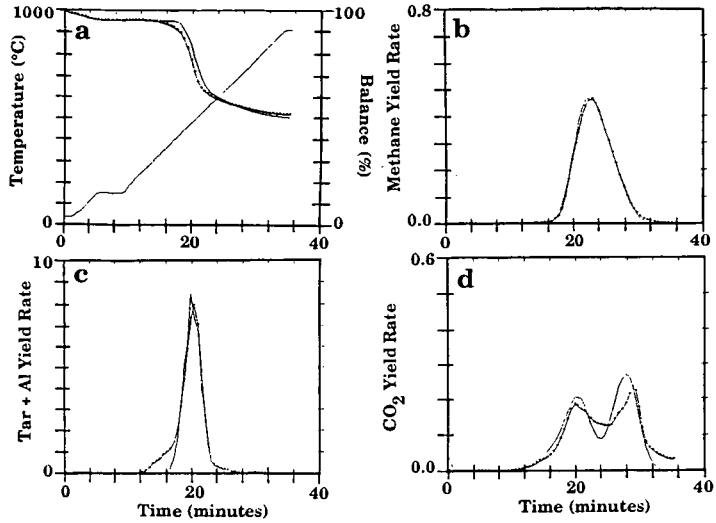

Figure 4. Kinetic Analysis at 30°C/min for Major Volatile Products. Comparison of Theory (—) and Data (*-*) for Utah Blind Canyon Coal.

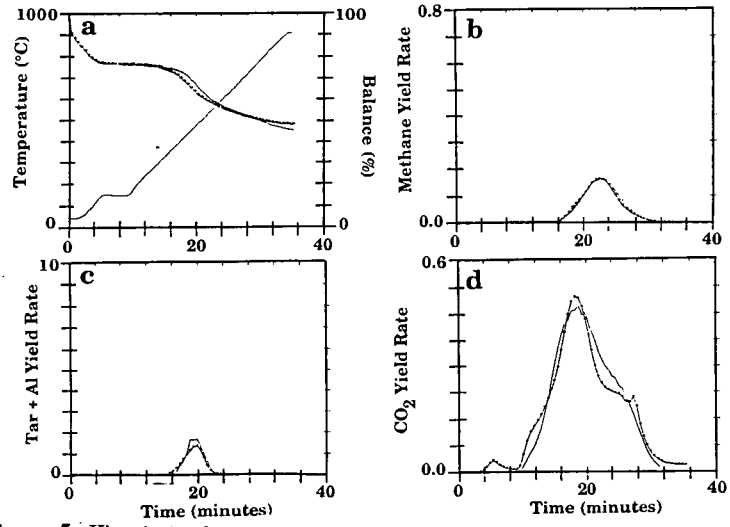

Figure 5. Kinetic Analysis at 30°C/min for Major Volatile Products. Comparison of Theory (—) and Data (*-*) for Zap Lignite

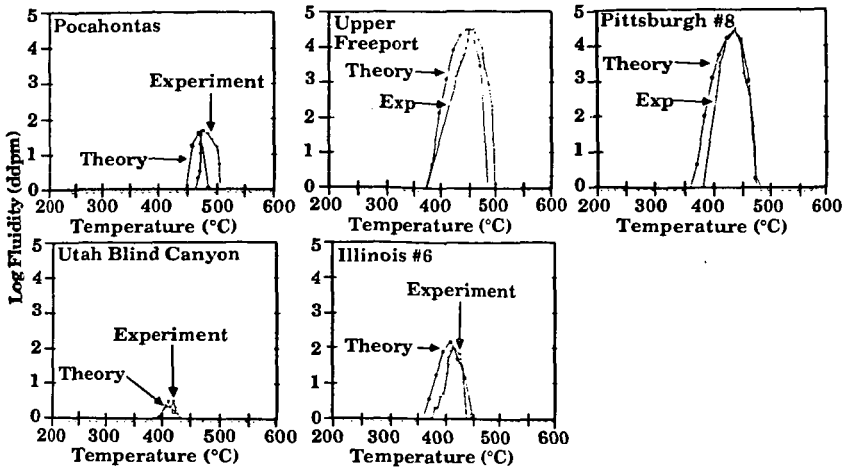

Figure 6. Comparison of Measured (*-*) and Predicted (o-o) Fluidity for Five Argonne Coals.

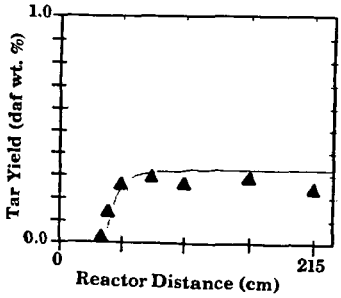

Figure 7. Pyrolysis Tar Yield Results for Illinois No.6 Coal, 200 x 325 mesh, in the HTR at an Equilibrium Tube Temperature of 800°C. The Solid Lines are Predictions of the FG-DVC Model.

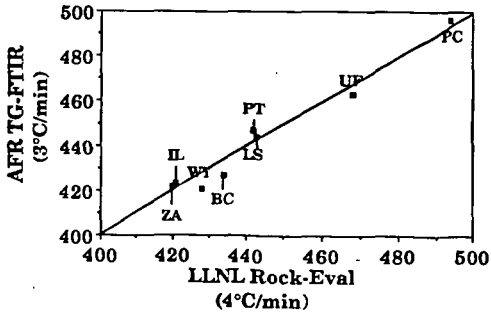

Figure 8. Comparison of AFR Data for T_{max} from TG-FTIR Analysis at 3°C/min with Rock-Eval Data from LLNL at 4°C/min.

A COMPARATIVE STUDY OF 8 US COALS BY SEVERAL DIFFERENT PYROLYSIS MASS SPECTROMETRY TECHNIQUES

Huaying Huai, Robert Lo, Yongseung Yun and Henk L.C. Meuzelaar
Center for Micro Analysis and Reaction Chemistry
EMRL 214 Building 61, University of Utah, Salt lake City, UT 84112

KEYWORDS: pyrolysis mass spectrometry, coal structure

ABSTRACT

Eight US coals of different rank and/or composition, obtained through the Argonne National Laboratory Premium Coal Sample Program, were analyzed by means of several different pyrolysis-MS (Py-MS) techniques, namely: direct Curie-Point Py-MS, Curie-point Py-GC/MS (including GC/EIMS, GC/CIMS and "short column" GC/CIMS), and vacuum thermogravimetry/MS (TG/MS). The data obtained were compared to Pyrolysis-Field Ionization MS (Py-FIMS) data.

The results show a very good agreement between all techniques used in spite of the marked differences in pyrolysis techniques (Curie-point, furnace, direct probe), "soft" ionization methods (low voltage EI, CI, FI) and mass spectrometer types (quadrupole, ion trap, magnetic sector) used. As might be expected, the most pronounced variations between techniques appear to be due to mass dependent differences in ion transmissivity and detector response, with the type of soft ionization method taking second place and the type of pyrolysis technique showing least effect on the results. Whereas Py-FIMS provides the most complete and detailed overview of the coal pyrolysis tars, Curie-point Py-MS and TG/MS methods provide more reliable information on relatively light gaseous products, and Curie-point Py-GC/MS shows the detail composition of the 2/3 of the total pyrolysis tars.

INTRODUCTION

The extremely complex nature of coal samples necessitates application of a wide range of sophisticated as well as conventional analytical techniques.

Pyrolysis mass spectrometry (Py-MS) is a relatively novel, advanced technique used for studying coals [1-5]. From an instrumental perspective, different Py-MS systems can be distinguished by: (1) pyrolysis technique, such as Curie-point pyrolysis, furnace pyrolysis and direct probe; (2) ionization method, such as electron ionization (EI), low voltage electron ionization (LVEI), Chemical ionization (CI), field ionization (FI), plasma desorption (PD), and fast atom bombardment (FAB); and (3) mass spectrometer type, such as quadrupole, ion trap, electric sector, magnetic sector, time-of-flight, and Fourier transform ion cyclotron resonance.

In this paper, several different Py-MS techniques, namely: direct Curie-point Py-MS, Curie-point Py-GC/MS (including GC/EIMS, GC/CIMS, "short column" GC/CIMS), and vacuum thermogravimetry/MS (TG/MS) were used for studying the 8 US coals from the Argonne National Laboratory Premium Coal Sample Program (ANL-PCSP). The results of a comparison between these methods as well as Py-FIMS will be discussed.

EXPERIMENTAL

Sample Collection and Preparation for Py-MS and Py-GC/MS

All 8 ANL-PSCP coals were obtained as 5 g, -100 mesh aliquots in dark tinted glass ampules closed under argon. The closed ampules were stored at -30 C until used. A 5-10 mg coal sample was suspended in 1-2 ml of Spectrograde methanol (5 mg/ml) and carefully hand-ground to a fine, uniform suspension. Then, a 5 µl drop of the coal suspension was coated on the pyrolysis wire and air-dried. Next, the coated wire was inserted into a borosilicate glass reaction tube. Details of the sample preparation technique have been described by Meuzelaar et al. [1,6].

Curie-point Py-MS

Curie-point Py-MS was performed with an Extranuclear 5000-1 quadrupole Py-MS system as described previously [3]. The Py-MS conditions are listed in Table 1.

Curie-point Py-GC/MS

The Curie-point pyrolysis reactor [7] was controlled by a Fischer Labortechnik, 1.1 MHz, 1.5 kW high frequency power supply. A HP 5890a gas chromatograph using both regular (15 m) and short (4 m) fused silica capillary GC columns, and coupled directly to a Finnigan MAT 700 ITD mass spectrometer operating in EI or CI (isobutane) mode was used. Experimental conditions are shown in Table 1.

Vacuum Thermogravimetry/MS

Experiments were conducted on a Mettler TA1 thermoanalyzer coupled directly to a Finnigan MAT 3200 quadrupole MS system [5]. Table 1 shows details of the experimental conditions.

Py-FIMS

A Finnigan MAT 731 double-focussing magnetic sector mass spectrometer, a combined EI/FI/FD/FAB ion source and an AMD Intectra direct probe introduction system [8] was used for this experiment. Experimental conditions are given in Table 1.

RESULTS AND DISCUSSION

Figure 1 shows the mass spectra of three coals, Beulah Zap (lignite), Pittsburgh #8 (hvb) and Pocahontas #3 (lvb), obtained by Curie-point Py-MS at ambient inlet temperatures.

The spectra reflect the well-known fact that the pyrolysis products are coal rank dependent. The most prominent products from lignite (Beulah Zap) are oxygen-containing compounds, including (alkyl) phenols, (alkyl) dihydroxybenzenes and (alkyl) methoxyphenols. With increasing rank, the relative abundance of these oxygen-containing compounds decreases. The (alkyl) dihydroxybenzenes and (alkyl) methoxyphenols have nearly disappeared in the Pittsburgh #8 spectrum whereas (alkyl) naphthalene abundances have markedly increased. The most prominent pyrolysis products from Pocahontas #3 coal are aromatic and aliphatic hydrocarbons whereas oxygen-containing compounds are hardly detectable.

All other five Py-MS techniques show a similar rank dependence. With increasing rank aliphatic and aromatic oxygen-containing compounds decrease while aliphatic and aromatic hydrocarbon intensities increase. Rank effects on pyrolysis patterns observed by Curie-point Py-GC/MS, Py-FIMS and TG/MS have been discussed in more detail elsewhere [5,9].

Effect of Pyrolysis Method

Figures 1b, 2 and 3 illustrate the Py-MS patterns of Pittsburgh #8 coal as obtained by Curie-point, furnace and direct probe pyrolysis, respectively. As listed in Table 1, the detailed experimental conditions are quite different from one another, e.g., with regard to sample amount (25 μg to 5 mg) and heating rate (1,000 C/sec to 25 C/min). However, as seen from Figures 1b, 2 and 3, the three techniques produce rather similar mass spectral patterns in the overlapping mass ranges, viz m/z 50-200. This may imply that the pyrolysis mechanisms are similar under the experimental conditions used.

Effect of Ionization Method

As expected, regular (70 eV) voltage electron ionization methods tend to break molecular ions into smaller fragment ions. Figure 4 shows that the dominant peaks are found at odd mass numbers in the low mass range. The spectra in Figures 1 and 2, however were produced by low voltage EI (12 eV and 14 eV, respectively). Consequently, molecular ions, seen primarily at even mass numbers because of the relatively low fragmentation of compounds as well as a low abundance of nitrogen compounds, dominate. However, as expected the CI spectra in Figures 5 and 6 are dominated by odd mass numbers due to the fact that most molecular ions are protonated $[M+H]^+$ forms. As shown in Figure 3, the FI technique produces largely even numbered molecular ions.

Variations between Methods

Notwithstanding the apparent similarities between the different techniques, as demonstrated in Figures 1-6, there are several other sources of variance that have not yet been discussed.

Except for the differences in pyrolysis techniques and type of quadrupole mass spectrometer used, distances between pyrolysis zone and ion source as well as transfer zone and ion source temperatures are comparable in Curie-point Py-MS and TG/MS techniques. Since, as shown above, differences in pyrolysis techniques appear to have minimal effect on pyrolysis mechanisms, the results from both techniques are quite similar (Figures 1 and 2).

Figure 3 shows the Py-FIMS results. Compared to Curie-point Py-MS and TG/MS, the distance between pyrolysis zone and ionization region is approx. 50% shorter. More importantly, ion source temperatures are higher and we are dealing with a different type of mass spectrometer (magnetic sector vs. quadrupole). Consequently, Py-FIMS detects far more high molecular weight components (Figure 3). Components below m/z 240 constitute only about 10-40% of the total signal intensity, depending on rank. Comparison of Figures 1 and 2, with Figure 3 indicates that Curie-point Py-MS and TG/MS detect only 10-40% of the total pyrolysis products, which agrees with previously published results [1]. The main reasons appear to be: (1) low transmissivity of quadrupole mass spectrometers in the higher mass ranges, and (2) unheated transfer zones and ion sources in the standard Curie-point Py-MS and TG/MS configurations causing condensation losses of large molecules (heating inlet system and ion source markedly increases signal intensities in the higher mass range [10] but also tends to lead to more rapid contamination of the ion source).

Figures 5 and 6 shows the effect of column length on Curie-point Py-GC/MS results. As expected, the use of short capillary GC columns at high linear carrier gas flow velocities enhances the detection of large molecules. The molecular weight averages (Table 2) shift some 15 to 60 mass units towards the high mass range. Compared to Py-FIMS, however, average Py-GC/CIMS molecular weight values are still considerably lower. Currently, efforts are underway to correct the molecular weight profiles obtained by short column Py-GC/CIMS for known differences in ion transmissivity between quadrupole, ion trap and magnetic sector MS systems.

CONCLUSIONS

1. The known rank dependence of coal pyrolysis produets is readily detected by all six Py/MS techniques used.
2. Within the range covered by these six techniques, differences in heating rate and sample size do not have a strong effect on the distribution of coal pyrolysis products.
3. All three soft ionization methods used (CI, FI, low voltage EI) appear useful for studying molecular weight distributions.
4. Although the type of pyrolysis method used has little effect on the composition of the pyrolysis products, the choice of the product analytical method has a major influence.
5. Magnetic sector instruments, e.g., as used in FIMS appears to provide the most complete and detailed overview of the coal pyrolysis tars.
6. Py-GC/MS (EI and CI) is capable of providing detailed information on compounds in the molecular weight range up to m/z 400, representing about 2/3 of the total tar.
7. Finally, the information obtained by Curie-point Py-MS and TG/MS methods for high molecular tar products is strongly dependent on inlet and ion source temperatures.

ACKNOWLEDGEMENT

The authors wish to thank Drs. Hans-Rolf Schulten and Norbert Simmleit for performing the Py-FIMS analyses. This work was supported by DOE grant #UKRF-4-23576-90-10 (Consortium for Fossil Fuel Liquefaction Scienee).

REFERENCES

1. Harper, A.M., Meuzelaar, H.L.C., and Given, P.H., Fuel, 63, 793-802 (1984).
2. Marzec, A., J. Anal. Pyrolysis, 8, 241-254 (1985).
3. Metcalf, C.S., Windig, W., Hill, G.R., and Meuzelaar, Int. J. Coal Geol. 7, 245-268 (1987).
4. Tromp, P.J.J., Ph.D. Thesis, University of Amsterdam, (1987).
5. Yun, Y., Maswadeh, W., Meuzelaar, H.L.C., Simmleit, N., and Schulten, H.-R., ACS Preprints, Div. Fuel Chem., 34(4), 1308-1316 (1989).
6. Meuzelaar, H.L.C., Haverkamp, J., and Hileman, F.D., "Curie-point Pyrolysis-Mass Spectrometry of Recent and Fossil Biomaterials; Compendium and Altas", (Eds. H.L.C. Meuzelaar et al.), Elsevier, Amsterdam (1982).
7. Meuzelaar, H.L.C., McClennen, W.H., and Yun, Y., 35th ASMS Conf. on Mass Spec., All Topics, Denver, CO., May 24-29, 1142-1143 (1987).
8. Schulten, H.-R., Simmleit, N., Muller, R., Anal. Chem., 59, 2903-2908 (1987).
9. Huai, H., Lo, R., and Meuzelaar, H.L.C., in preparation (1990).
10. Taghizadeh, K., Hardy, R.R., Davis, B.H., Meuzelaar, H.L.C., "Comparison of Low Voltage and Field Ionization Mass Spectra of Coal-derived Liquids from the Wilsonville Pilot Plant", submitted to Fuels Processing Technology (1990).

Table 1. Experimental Conditions

	Py-MS	TG/MS	Py-GC/MS			FIMS
			15m EI	15m CI	4m CI	
Sample Size (g)	2.5×10^{-5}	5.0×10^{-3}	2.5×10^{-5}	2.5×10^{-5}	2.5×10^{-5}	1.0×10^{-4}
Pyrolysis Method	Curie-point	Furnace	Curie-point	Curie-point	Curie-point	direct probe
Final Temp. (C)	610	700	610	610	610	750
Heating Rate (K/sec)	1×10^{2}	4×10^{-1}	1×10^{3}	1×10^{3}	1×10^{3}	1×10^{0}
Inlet Temp. (C)	~ 100	~ 100	290	290	290	~ 200
Pressure in Pyrolysis Zone	high vacuum ($<10^{-4}$ torr)	high vacuum ($<10^{-5}$ torr)	30 p.s.i. (abs)	30 p.s.i. (abs)	25 p.s.i. (abs)	high vacuum (~ 10^{-5} torr)
Distance (from Pyrolysis Zone to Ion Source)	5 cm	5 cm	15 m	15 m	4 m	2 cm
MS Type	quadrupole	quadrupole	Ion Trap	Ion Trap	Ion Trap	magentic sector
Ionization Method	EI (12 eV)	EI (14 eV)	EI (70 eV)	CI (isobutane)	CI (isobutane)	FI
Ion Source Temp (C)	~ 100	~ 100	230	230	230	200
Mass Range Scanned	20-240	33-200	50-450	90-500	100-600	50-900

Table 2. Molecular Weight Averages ($\overline{Mn}$)
Obtained by Different Techniques

Coal	Curie-point Py-GC/MS		FIMS
	15 m CI	4 m CI	
Beulah Zap	172	185	792
Wyodak-Anderson	184	203	338
Illinois #6	222	270	367
Blind Canyon	226	269	366
Pittsburgh #8	222	264	324
Lewiston-Stockton	218	263	327
Upper Freeport	223	277	386
Pocahontas #3	195	251	359

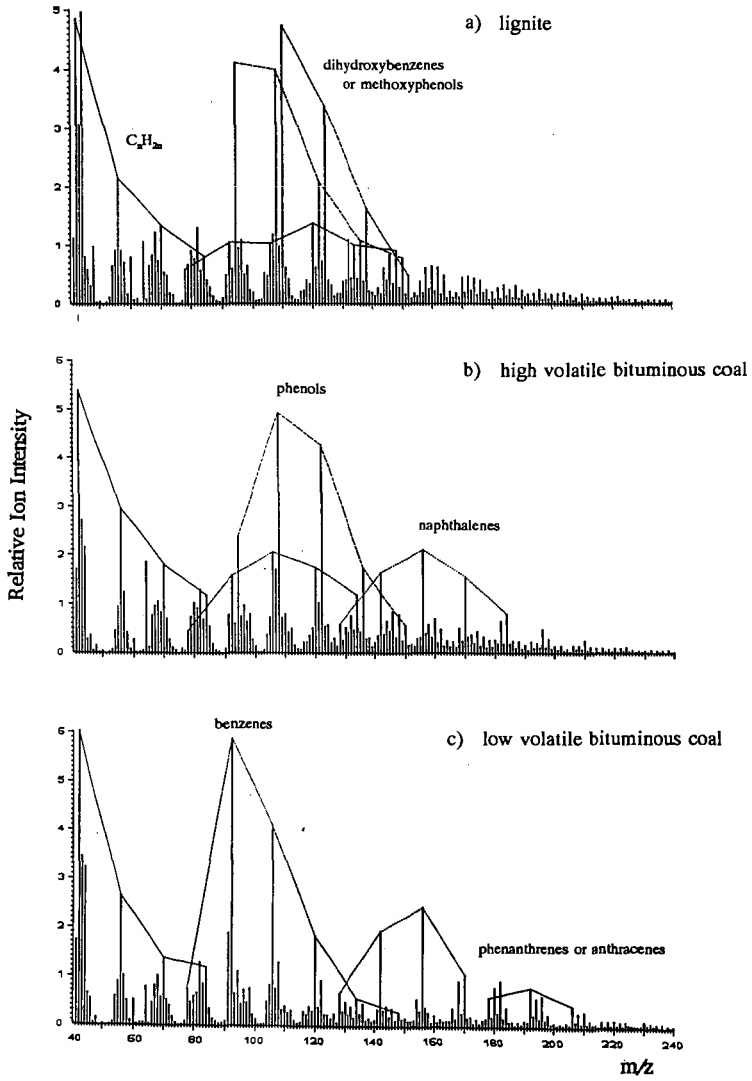

Figure 1. Curie-point pyrolysis low voltage EIMS spectra of a) Beulah Zap lignite, b) Pittsburgh #8, c) Pocahontas #3 coals.

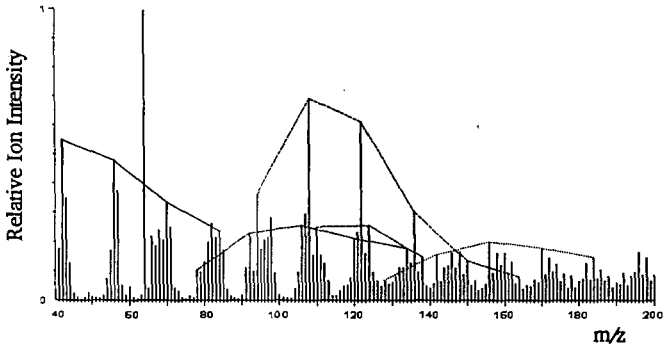

Figure 2. Mass spectrum of Pittsburgh #8 coal by TG/MS.

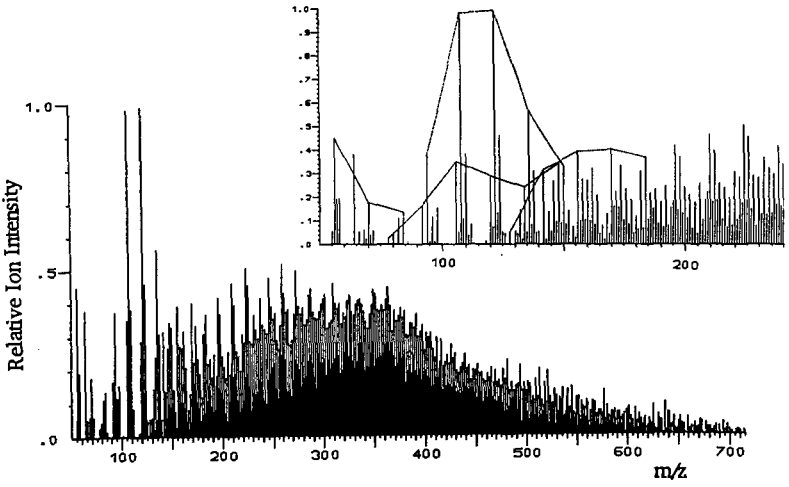

Figure 3. Mass spectrum of Pittsburgh #8 coal by Py-FIMS.

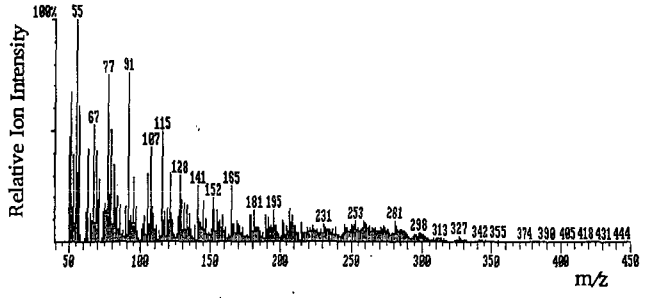

Figure 4. 70 Mass spectrum of Pittsburgh #8 coal obtained by Curie-point Py-GC/EIMS (70 eV).

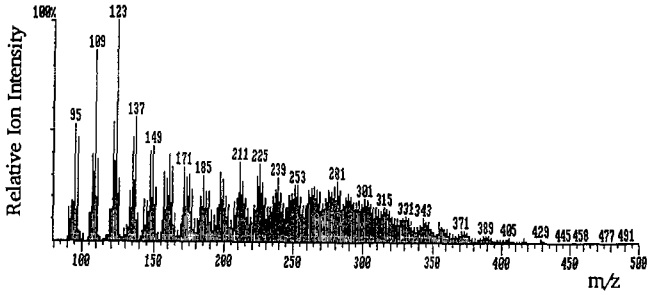

Figure 5. As Figure 4, obtained by Curie-point Py-GC/CIMS.

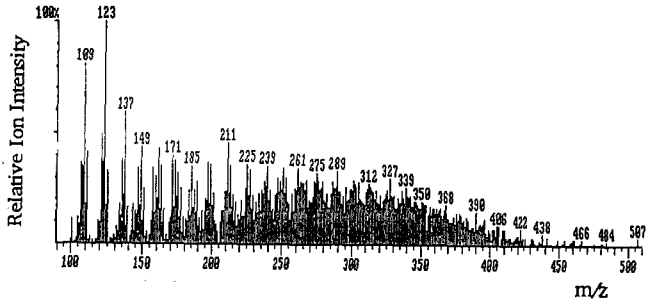

Figure 6. As Figure 4, but obtained by "short column" by Curie-point Py-GC/CIMS.

Ronald R. Martin, Jinjiang Li
Department of Chemistry, University of Western Ontario
London, Ontario, Canada, N6A 5B7
J. Anthony MacPhee
CANMET/ERL, 555 Booth Street
Ottawa, Ontario, Canada, K1A 0G1

Keywords: colorimetry, Fe^{3+}, coal

ABSTRACT

Solutions of $FeCl_3/K_3Fe(CN)_6$ have been used to stain coal macerals. In this paper the development of a blue color in coal slurries in contact with $Fe^{3+}/Fe(CN)_6^{3-}$ resulting from oxidation of the coal by Fe^{3+} is used as a measure of the reactivity of the coal surface.

INTRODUCTION

Salehi and Hamilton[1] have used iron salts to stain coal surfaces as an aid in optical and electron microscopy. The authors did not speculate on the chemistry involved in the staining process. We suggest that the development of blue colors on the coal surfaces following exposure to $Fe^{3+}/Fe(CN)_6^{3-}$ solutions results from oxidation of the coal surface by Fe^{3+} with the subsequent formation of a charge-transfer complex (prussian blue) between $Fe^{2+}/Fe(CN)_6^{3-}$. Since this complex absorbs strongly in the visible region the reaction can be followed by colorimetry of appropriate coal slurries. The kinetics of the Fe^{3+} reduction are a direct measure of the reactivity of individual coals and may provide a means of predicting coal quality in specific industrial useage.

EXPERIMENTAL

Five of the coals used were obtained from the Argonne Premium Coal Sample Program while an additional two coals, P851 and P832 were mid volatile bituminous coals from Western Canada, supplied by CANMET, Ottawa, Canada. All samples were 100 mesh.

Coal slurries were maintained at 30°C and stirred with a magnetic stir bar for periods ranging from five to twenty minutes. The slurries were then filtered to remove all solid matter. The resulting solutions were subjected to colorimetric analysis at 700 nm. Coal slurries were prepared in two different ways: a) 0.30 g of coal were added to a solution prepared by mixing 20 ml of 0.60 M $FeCl_3$ with 10 ml of 0.30 M K_3FeCN_6 - this method did not yield satisfactory results and was used only for one sample; b) 0.30 g of coal were added to 20 ml of 0.60 M $FeCl_3$. This slurry was filtered after reaction with the coal and 10 ml of 0.30 M $K_3Fe(CN)_6$, which served as an indicator of the Fe^{3+}/coal interaction, was added after filtration was complete.

RESULTS AND DISCUSSION

The coal P851 was used to test the two procedures used in preparing the coal slurries. Figure 1 shows the results obtained by procedure a) while Figure 2 shows the results from procedure b). The first procedure leads to little measurable reaction while the second yields a well defined increase in the concentration of Fe^{2+} with time. These results suggest that K^+, $Fe(CN)_6^{3-}$ and/or the $Fe^{2+}/Fe(CN)_6^{3-}$ complex are strongly adsorbed on the coal surface and prevent further reaction of Fe^{3+} with the coal surface. The $Fe^{2+}/Fe(CN)_6^{3-}$ seems to be the most likely explanation since Salehi and Hamilton observed a blue stain on coal surfaces after rinsing and drying coal surfaces identical to those used in preparing the coal slurries in procedure a). Accordingly procedure b) was used throughout the remainder of this study.

Figures 3-7 show the increase with Fe^{2+} concentration with time as well as the reaction rate obtained from the slope of this plot. In the case of the North Dakota coal only the first two points were used since the graph shows an initial fast reaction followed by a plateau with little further reaction. Figure 8 shows a plot of reaction rate vs O/C ratio for each of the Argonne coals.

It is clear that each coal yields a reaction rate which is strongly correlated with O/C ratio. The North Dakota coal shows an initial fast reaction while the other coals have an apparent non-zero intercept for Fe^{2+} in the Fe^{2+} vs time plot. This result may be due to an initial rapid reaction or to Fe^{2+} present in the coal prior to reaction.

CONCLUSIONS

Fe^{3+}, from $FeCl_3$, in solution oxidizes coal surfaces and the resulting Fe^{2+}/Fe^{3+} charge transfer complex may be used as an indicator of the extent of reaction when Fe^{3+} is introduced as $Fe(CN)_6^{3-}$.

The $Fe^{2+}/Fe(CN)_6^{3-}$ is strongly adsorbed on the coal surface and inhibits further reaction. The kinetics of the Fe^{3+} reduction can be followed colorimetrically if $K_3Fe(CN)_6$ is added to solutions obtained from coal slurries in contact with $FeCl_3$.

The kinetics of Fe^{3+} reduction can be correlated with the O/C ratio in the coal.

REFERENCE

1. MORTAZA R. SALEHI and LLOYD H. HAMILTON. Surface-reaction of Australian coal macerals and coke by iron salts: an aid in microscopy. Fuel, 1988, 67, 296-297.

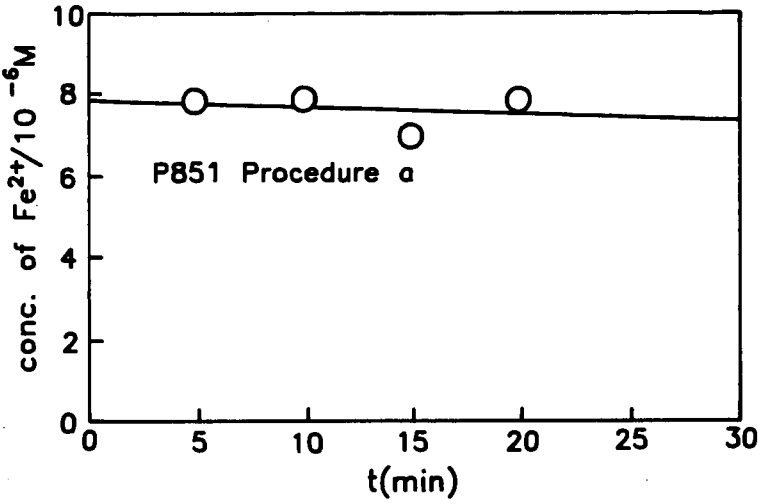

Figure 1

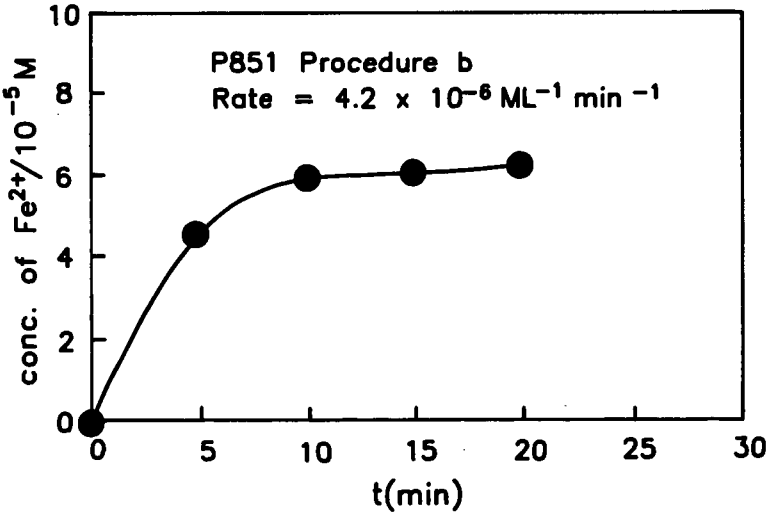

Figure 2

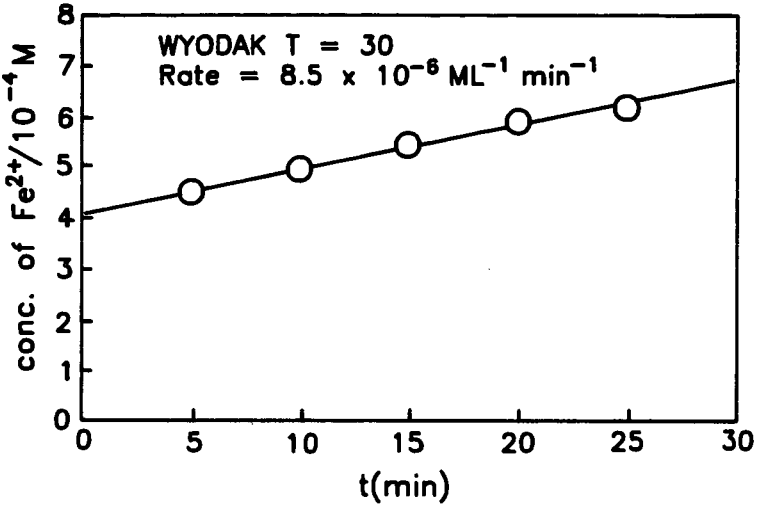

Figure 3

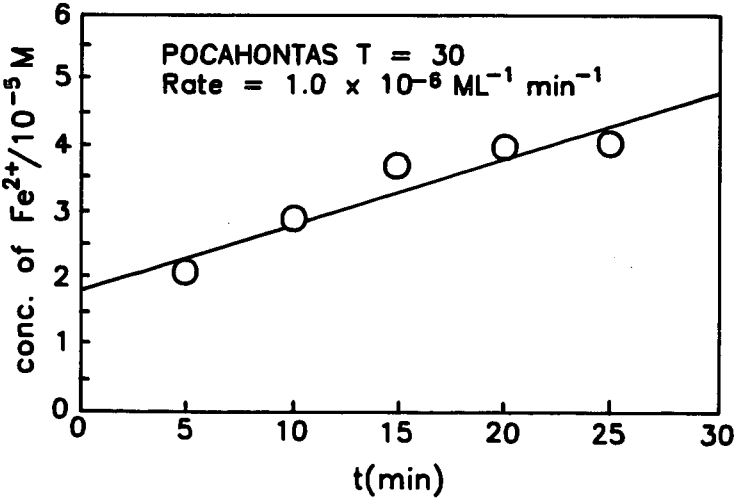

Figure 4

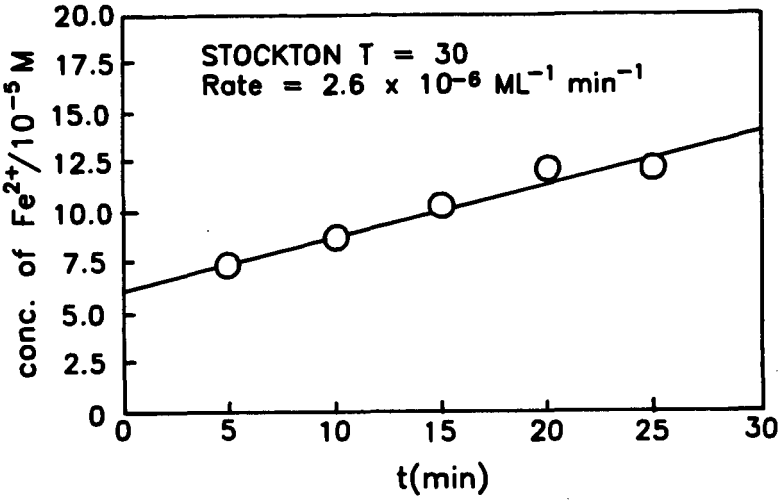

Figure 5

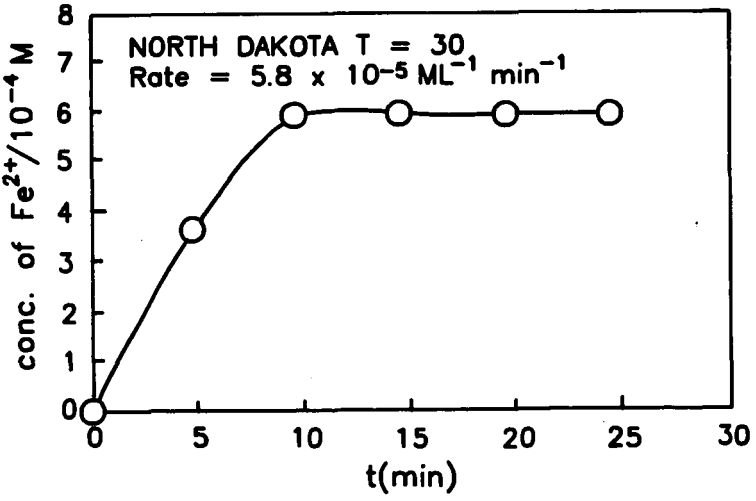

Figure 6

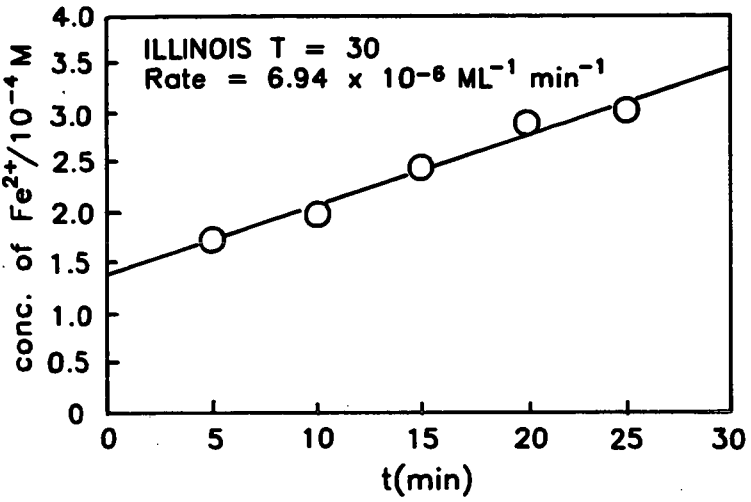

Figure 7

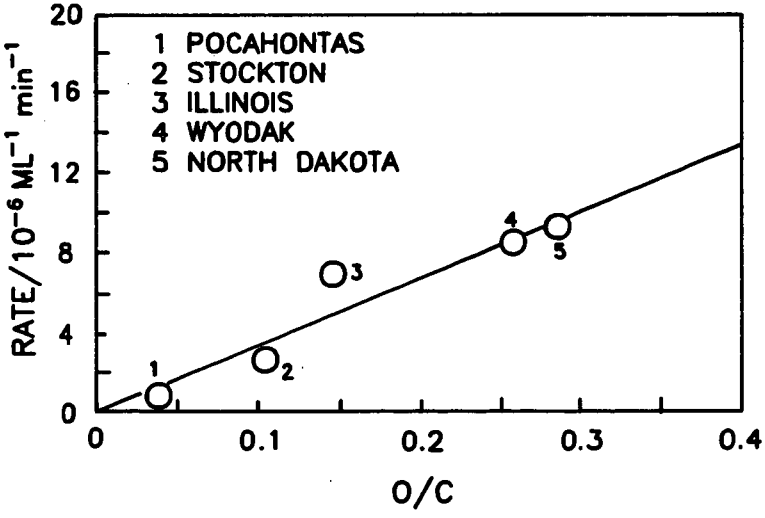

Figure 8

ANAEROBIC BIOPROCESSING OF SUBBITUMINOUS COAL

Mahendra K. Jain*, Deborah Burgdorf, and Ramani Narayan
Michigan Biotechnology Institute, P.O. Box 27609, Lansing, MI 48909

Keywords: Anaerobic bioprocessing, coal decarboxylation, biocoal product

ABSTRACT

Subbituminous and lignite coals contain high levels of oxygen. Extensive structure reactivity studies of Wyodak coal done by us revealed that carboxy groups, along with ether linkages, are the predominant oxygen functionalities of this coal. Chemical decarboxylation to remove oxygen and upgrade the coal can be achieved at high temperatures and under such conditions the low rank coals undergo retrogressive reactions. We are developing a anaerobic microbial process to decarboxylate coal that would operate at ambient conditions. The anaerobic microbial consortia developed has resulted in decarboxylation of coal and anaerobically bioprocessed coal has exhibited an increase in H/C ratio in comparison to unprocessed coal. In this paper, we show our new results and their implications in microbial processing of coal in relation to the current bioprocessing schemes.

INTRODUCTION

The most common biological processes applied to coal conversion have been focussed on oxidative biosolubilization. The mechanism of such coal solubilization under aerobic conditions is probably dependent on the aromatic ring hydroxylations followed by ring scission. Such reaction results in oxygenated coal product which, in turn, makes the coal poorer fuel than the starting material. In addition, requirement of aeration makes the process highly energy intensive and less practical.

Anaerobic bioconversion of coal provides alternative technology for biological processing of coal. The major advantages of this approach is that it can: 1) remove oxygen from coal by decarboxylation; 2) cleave ether linkages of coal; and 3) reduce the contaminants such as sulfur from the coal. Moreover, the process is less energy intensive and requires simple engineering design. The approach to use anaerobic bacteria/enzyme promises to be most rewarding and exciting, since this involves depolymerization/solubilization of coal reductively, that is, the reduction of aromatic rings and promotion of reductive cleavages to produce hydrogenated products (Fig. 1). In other words, hydrogenation of coal via an anaerobic microbial process results in a more desirable fuel; oxidation via an aerobic microbial process results in a less desirable fuel form. Indeed, coal scientists throughout the ages have been trying to achieve this objective, that is, to find an inexpensive approach to producing a deoxygenated, hydrogen-rich coal fuel. In work done by us (Narayan, 1985; 1986 a,b; 1987; 1988; 1989) on the structure of Wyodak subbituminous coal (Figure 2) we have shown that carboxyl groups are a major oxygen functionality. They exist predominantly as carboxylate anions strongly chelating metal cations like Ca^{2+} and forming strong macromolecular crosslinks which contribute in large measure to the network polymer structure. Furthermore, the coal oligomer chains are not very long i.e. molecular weights of the coal clusters comprising the coal macromolecule have M_n = 800-1000 and M_w - 2500-3500.

Unfortunately, chemical or thermal decarboxylation can be performed only at elevated temperatures. This results in retrogressive crosslinking reactions. Indeed, Suuberg et al., (1985, 1987) have documented that low temperature crosslinking associated with low rank coal correlates well with evolution of CO_2. This correlation has been confirmed in recent work done by Solomon and co-workers (Deshpande et al., 1988; Solomon et al., 1988, 1990). In a structural sense, what these results imply is that at temperatures needed to remove the carboxyl group, the chains are still in close proximity, and the carboxylate and hydrogen bonded crosslinks are replaced by much stronger carbon-carbon covalent crosslinks. This results in a much more intractable coal macromolecule.

In principle then, removal of the carboxyl groups at room temperature (reductive decarboxylation) would unravel the macromolecular network, resulting in a very low molecular weight coal macromolecule with increased H/C ratio. With a increased hydrophobic character, this coal could be easily cleaned and serve directly as a solid fuel source. Since the coal macromolecular network has been dismantled, this coal could be easily processed in a subsequent liquefaction step. In summary, decarboxylation of coal at ambient temperatures has the potential for developing a coal product which has better fuel value and better processing prospects.

EXPERIMENTAL

All the experiments were carried out in anaerobic pressure tubes (27 mL, Bellco Glass, Inc., Vineland, NJ) and the manipulations were performed anaerobically using sterile syringes and needles. All chemicals and gases were of analytical grade. Chemicals were obtained from Sigma Chemical Co. (St. Louis, MO). Gases (N_2, H_2) and gas mixture N_2-CO_2 (95:5) and H_2-CO_2 (80:20) were obtained from Union Carbide Corp., Linde Division (Warren, MI) and passed over heated copper fillings to remove traces of O_2.

Liquid media and solutions were prepared and sterilized under a stricly anaerobic N_2 atmosphere by methods previously described (Zeikus, et al., 1980). The phosphate buffered basal (PBB) medium (Kenealy and Zeikus, 1981) was used for all the experiments. This medium was supplemented with (per 100 mL): 1.0 mL phosphate buffer, 1.0 mL vitamin solution (Wolin et al., 1963), 0.05 g yeast extract, and 2.5 mL of 2.5% $Na_2S.9H_2O$ as well as, where added, 0.25 g supplemental carbon and energy source. Coal (Subbituminous, Wyodak) was added @ 0.15 g/10 mL media. The pH of the medium was about 7.0. Inoculum used in the present studies was obtained from a waste treatment site in Michigan and was collected and stored anaerobically at 4°C.

Initially, appropriate tubes were inoculated with mixed microbial consortia of anaerobic bacteria @ 5% and the tubes were then incubated at 37°C. Periodically the gas phase of the tubes was analyzed for CO_2 and CH_4. Gas samples were withdrawn from the tubes with a 1.0 mL glass syringe (Container Corp., Sioux City, Iowa) equipped with a gas tight mininert syringe valve (Alltech Associates, Inc., Deerfield, MI) and a 23 gauge needle. Coal was separated from medium by centrifugation at 4,500 rpm for 10 minutes, suspended in 3 N HCl and washed with distilled water until free of acid. The coal was then vacuum dried at 70°C for 24 hours before used for elemental analysis and subjected to FT-IR analyses. Carbon dioxide and methane gas was analyzed using a Gow-Mac series 580 gas chromatograph (GOW-MAC Instrument Co., Bridgewater, NJ) equipped with a thermal conductivity detector (TCD) and cabosttpere SS column with helium as carrier gas.

RESULTS AND DISCUSSION

Microbial Non-oxidative Decarboxylation of Coal:

Subbituminous Wyodak coal was used in the present studies since this coal contains much higher levels of oxygen than bituminous coals. It has been reported that the carboxyl groups account for an estimated two thirds of this oxygen (Sandreal and Wiltsee, 1984). Microorganisms capable of reductive decarboxylation of organic compounds may have the potential of removing carboxyl oxygen from coal. We, therefore, developed appropriate enrichments for developing anaerobic mixed cultures capable of decarboxylating coal under batch conditions. Various supplemental carbon and energy sources were used to support the growth of bacteria. The tubes containing coal and an additional carbon source were inoculated with a mixed microbial consortia and incubated at 37°C. The gas phase of these tubes was analyzed for CO_2. The coal was also analyzed for carbon and hydrogen and the change in H/C ratio was calculated.

The preliminary results presented in Table 1 indicate that CO_2 was produced in all the tubes and that level of CO_2 increased over the period of incubation. The increase in H/C ratio can be attributed to loss of carbon along with oxygen. Lactate, succinate and malonate supplemented tubes showed higher levels of CO_2 from coal than those supplemented with vanillate and glutamate. It seems that these substrates supported better growth of the microbial population that has decarboxylating enzymes. Crawford and Olson (1978) used vanillate as a model compound to examine microbial decarboxylation of complex aromatic compounds. They reported non-oxidative decarboxylation of vanillate by a single enzymatic transformation and also showed, using FT-IR, removal of carboxyl groups of coal when it was incubated with *Bacillus megaterium*. Decarboxylation of succinate to propionate under anaerobic conditions has also been observed using *Selenomonas ruminantium* (Scheifinger and Wolin, 1973), *Propionibacterium pentosaceum, Veillonella alcalescens* (Yousten and Delwiche, 1961; Samuelov et al., 1990) and *Propionigenium modestum* (Schink and Pfenning, 1982). Decarboxylation reaction also occurs when L-glutamate is anaerobically metabolized by *Acidaminococcus fermentans, Peptostreptococcus asaccharolyticus*, and *Clostridium symbosium* (Dimroth, 1987). Thus, the supplemental carbon sources used in the present study have been shown by other groups to support growth of anaerobic cultures having decarboxylases.

Based on the preliminary experiment, succinate and lactate were selected to be used as supplemental carbon sources in conducting further experiments on coal decarboxylation. From the previous experiment it was not possible to conclude whether all or any CO_2 was produced from coal. Therefore, another experiment was designed to include controls without coal to determine CO_2 production from supplemental carbon sources as well. Also, since the tubes were inoculated from an anaerobic mixed microbial consortia that contained methanogenic population, it was likely that some of CO_2 will have converted to methane especially under the long-term incubation conditions. No attempts were made to inhibit methanogenesis since the adverse effects of inhibitors of methanogens on the organisms responsible for coal decarboxylation is not known. Therefore, gas phase of these tubes were analyzed for both CO_2 and CH_4. The results obtained are summarized in Table 2 and Figures 3 and 4.

The data presented in Table 2 show that CO_2 was produced from succinate as well as lactate. However, it is important to note that levels of CO_2 produced from succinate

supplemented coal and lactate supplemented coal were higher than succinate or lactate alone indicating that additional CO_2 was produced as a result of coal decarboxylation. In addition, methane was also produced and the increased levels of methane were observed in tubes containing coal and supplemental carbon source than in tubes that contained no coal. Figures 3 and 4 show decrease in CO_2 and increase in CH_4 levels after day 9. Also the levels of CO_2 and CH_4 produced from succinate or lactate were always lower than those obtained from coal supplemented with succinate or lactate. Acetate, methanol, methylamines, formate, H_2-CO_2, and CO are known to serve as methanogenic substrates to different methanogenic bacteria (Jain et al., 1988). Neither succinate nor lactate is a substrate for methanogens; however, under these experimental conditions methane is expected to be produced from acetate as well as CO_2. Succinate upon decarboxylation would be converted to propionate which in turn will be degraded to acetate by syntrohpic propionate degraders. Acetate and CO_2 so produced will then be converted to methane by methanogenic bacteria. Syntrophic propionate degraders are very slow growing organisms and as a result propionate onversion to acetate is a slow reaction. It is likely that sudden increase in methane at 4 weeks time in coal supplemented with succinate may be the result of establishment of such a consortia (Figure 3). These results, however, clearly show decarboxylation of coal under anaerobic conditions. Since these experiments were carried out with mixed microbial consortia, it is not possible to hypothesize the number or type of organisms responsible for coal decarboxylation.

Energetics and Process Considerations:

One of the major problems plaguing coal bioprocesses is the consumption of coal carbon for microbial growth and maintenance. In the present decarboxylation scheme, the decarboxylation reaction is coupled to generation of an electrochemical gradient of sodium ions. This gradient can be transformed into a pH gradient that can be taken advantage of by the ATP synthase. The decarboxylation of oxaloacetate, for example, is associated with a free energy change of Δ Go' = -30 kJ (-7.2 kcal) mol^{-1} and one could expect synthesis of 1/3 ATP per 1 CO_2 formed (Gottschalk, 1986). The uptake of $3H^+$ per ATP synthesized would be in agreement with this assumption. Based on this assumption, a hypothetical model showing sodium dependent coal decarboxylation is proposed (Figure 5).

Another problem confronting coal bioprocesses particularly anaerobic is the reaction rate. In work done by us on succinate decarboxylation to propionate we used *Veillonella alcalescens* (Samuelov et al., 1990). Kinetic analysis of our results indicate that under steady-state conditions ($D=0.02\ h^{-1}$) the optimal specific rate of propionate formation from succinate was 0.252 g propionate/g cells/h. The non-growth related production coefficient was 0.246 g propionate/g cells/h. The high ratio between these two kinetic parameters indicates that the decarboxylation energy was used mainly for culture maintenance. From the steady-state rate of propionate formation the apparent in-vivo specific activity of decarboxylation was calculated to be 90-100 m moles/mg protein/min (Samuelov, et al., 1990).

In conclusion, preliminary work reported in this paper demonstrates that decarboxylation of coal can be achieved at ambient temperature and pressure using anaerobic microbial catalyst. The ability to eliminate carboxyl groups and thereby break up of the macromolecular cross-links without the thermal retrogressive cross-linking reactions has major implications for processing of this low-rank subbituminous Wyodak coal and understanding its reactivity.

ACKNOWLEDGEMENTS

We thank Amit Lathia for assistance in elemental and FT-IR analyses of coal samples. This work was supported by funds from the Michigan Strategic Fund and the Kellogg Foundation to Michigan Biotechnology Institute.

REFERENCES

1. Crawford, R.L. and P.P. Olson, Appl. Environ. Microbiol. 36:539, (1978).
2. Dimroth, P., Microbiol. Rev. 51:320-340, (1987).
3. Deshpande, G.V., P.R. Solomon and M.A. Serio, ACS Fuel Chem. Preprints 33(2):310 1988).
4. Gottschalk, G., Bacterial Metabolism, pp. 359, Springer-Verlag, New York, (1986).
5. Jain, M.K., L. Bhatnagar and J.G. Zeikus, Indian J. Microbiol., 28:143-177 (1988).
6. Kenealy, W. and J.G. Zeikus, J. Bacteriol. 146:133-140 (1981).
7. Narayan, R., Abstracts of Papers, 189th National Meeting of the Amer. Chem. Soc., Miami, FL, INDE, 24, (1985).
8. Narayan, R., EPRI AP-4441, Final Report, Feb. 1986a.
9. Narayan, R., Proc. 10th Annual EPRI Contractors Conf., EPRI AP-4253-SR, p. 7, 1986b.
10. Narayan, R., Proc. 11th Annual Conf. on Clean Liquids and Solid Fuels, EPRI AP-5043-SR, 5-53, April, (1987).
11. Narayan, R., Proc. First Annual Workshop on Biological Processing of Coal, EPRI, EPRI ER-5709-SR, March, (1988).
12. Narayan, R., Proc. 1987 Workshop on Coal Structure, EPRI ER-6099-SR, November (1988).
13. Narayan, R., Final Report, EPRI GS-6473 Research Project 8003-1, July, (1989).
14. Samuelov, N., R. Datta, M.K. Jain, and J.G. Zeikus, Ann. NY Acad. Biochem. Engg. (in press) (1990).
15. Sandreal, E.A. and G.A. Wiltsee, Ann. Rev. Energy, 9:473 (1984).
16. Scheifinger, C.C. and M.J. Wolin, Appl. Microbiol. 26:789-795, (1973).
17. Schink, B. and N. Pfenning, Arch. Microbiol. 133:209-216, (1982b).
18. Solomon, P.R., D.G. Hamblen, R.M. Carangelo, M.A. Serio and G.V. Deshpande, Energy and Fuels, 2:405 (1988).
19. Solomon, P.R., M.A. Serio, G.V. Deshpande, and E. Kroo, Energy and Fuels (in press), (1990).
20. Suuberg, E.M., D. Lee and J.W. Larsen, Fuel 64:1668, (1985).
21. Suuberg, E.M., P.E. Unger and J.W. Larsen, Energy and Fuels, 1:305, (1987).
22. Wolin, E.A., M.R.J. Wolin and R.S. Wolfe, J. Biol. Chem., 238:2882-2886 (1963).
23. Yousten, A.A., and E.A. Delwiche, Bacteriol. Proc. 61:175 (1961).
24. Zeikus, J.G., A. Ben-Bassat and P.W. Hegge, J. Bacteriol., 143:432-440 (1980).

Table 1. Coal Decarboxylation by an Anaerobic Microbial Consortium in Presence of Other Carbon Sources.

	% CO_2 in Gas Phase After		*H/C Ratio in decarboxylated coal at 100 days
	15 days	100 days	
Coal + Succinate	9.86	16.17	1.10
Coal + Lactate	5.98	19.04	1.37
Coal + Malonate	12.72	14.65	1.22
Coal + Vanillate	1.58	9.47	1.08
Coal + Glutamate	5.38	9.69	1.14

*H/C ratio of original control = 0.92

Table 2. Decarboxylation of coal in presence of succinate or lactate as supplemental carbon source.

Substrate	Gases after 9 days	
	CO_2 (%)	CH_4 (mM)
Succinate	8.74	1.04
Coal + Succinate	14.63	1.99
Lactate	8.47	1.83
Coal + Lactate	16.34	6.09

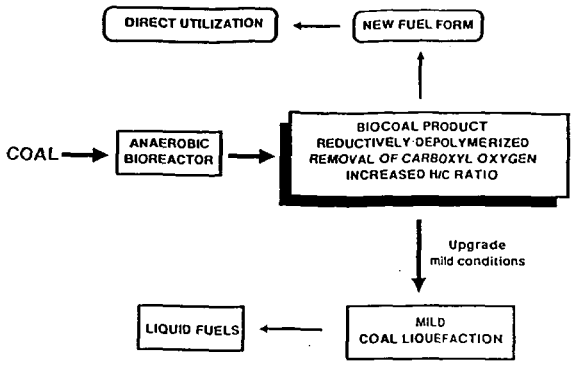

Figure 1. Schematic anaerobic bioprocess technology for conversion of coal to biocoal product and its further use.

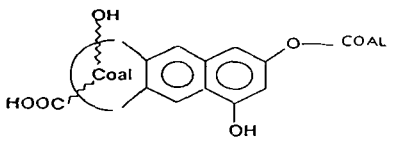

Carboxy and dioxy groups are major oxygen functionalities

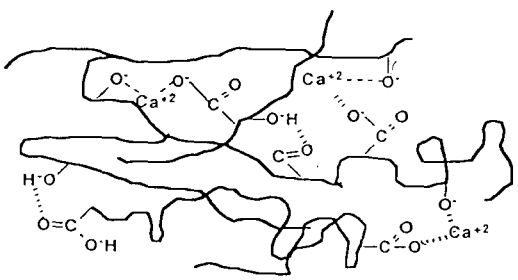

Network polymer structure due to secondary forces - hydrogen bonding and chelate crosslinks

Figure 2. Salient structural features of Wyodak subbituminous coal (Narayan, 1989).

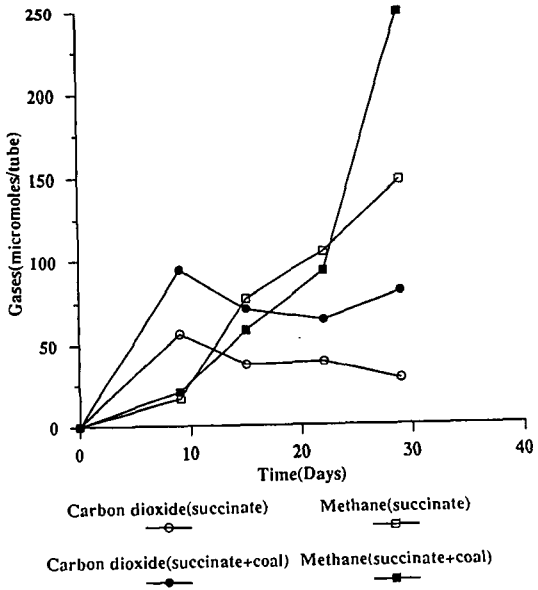

Fig.3. Production of carbon dioxide and methane from Succinate, and Coal + Succinate using anaerobic microbial consortium

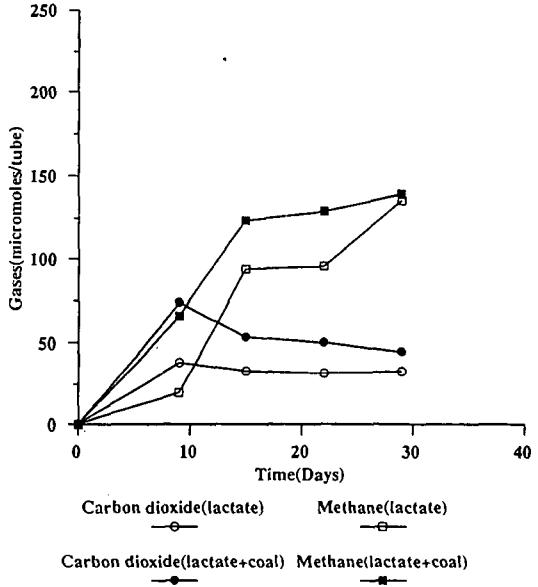

Fig.4. Production of carbon dioxide and methane from Lactate, and Coal + Lactate using anaerobic microbial consortium

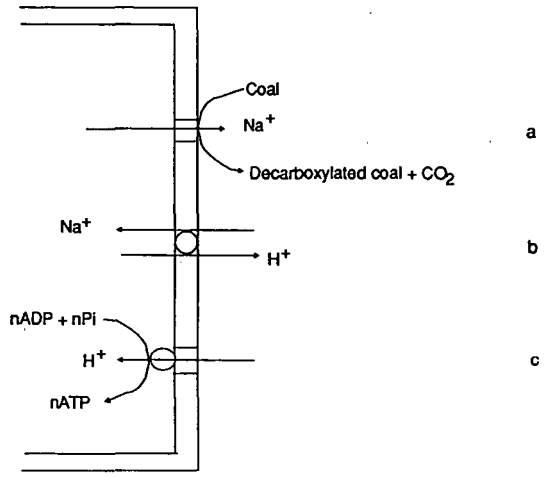

Figure 5. Hypothetical model showing sodium-dependent coal decarboxylation a: sodium translocation as coupled to the decarboxylation reaction. b: Na^+ - H^+ antiporter. c. Proton-translocating ATP synthase; n may be in the order of 1/3.

HYDROGEN PEROXIDE, PEROXIDASES AND LOW RANK COAL

D. R. Quigley, C. R. Breckenridge, J. K. Polman and P. R. Dugan
Biotechnology Unit and Center for Bioprocessing Technology
Idaho National Engineering Laboratory
Idaho Falls, ID 83415-2203

Keywords: peroxidases, biosolubilization, hydrogen peroxide

ABSTRACT

Horseradish peroxidase was tested to determine if it catalyzed any reaction between coal and hydrogen peroxide. Experiments were performed in aqueous buffers of either pH 5.0, 6.5 or 8.0 and used either particulate Wyodak, Beulah Zap, Texas lignite, Mississippi Wilcox lignite or solubilized Mississippi Wilcox lignite. Reactions were monitored by determining amounts of hydrogen peroxide consumed at various points in time. All coals reacted rapidly with hydrogen peroxide in the absence of peroxidase and these reaction rates increased as pH increased. Horseradish peroxidase did not measurably increase these reaction rates even when present in large concentrations. These data suggest that coal is not a substrate for horseradish peroxidase.

INTRODUCTION

Reports in the early 1980's that microorganisms were able to transform low rank coals into a liquid or water soluble form (1,2) generated interest in using bioprocessing as a possible route to convert coal into liquid fuels. Many organisms and enzyme systems have been examined since then for their ability to solubilize and/or depolymerize coal. Those enzyme systems that have received the most attention are those that catalyze the oxidative cleavage of carbon-carbon bonds in model compounds. These enzymes include laccases and peroxidases.

Laccase from Trametes versacolor (a.k.a. Coriolus versacolor and Polyporus versacolor) has been extensively studied (3,4). This enzyme utilizes molecular oxygen to cleave carbon-carbon bonds adjacent to aromatic nuclei (5) and has been implicated as the agent produced by T. versacolor responsible for the organism's coal solubilizing ability (1,3,4). Subsequent work indicated that the majority of coal solubilizing activity present in culture fluids was low in molecular weight (<1,000) and did not appear to be a laccase. A higher molecular weight material that had some coal solubilizing activity was found, but this was later identified as an esterase (6,7,8). It now appears that laccases are not significantly involved in coal biosolubilization.

Peroxidases are enzymes that utilize hydrogen peroxide and include horseradish peroxidase (HRP) and lignin peroxidases. When these enzymes are incubated with hydrogen peroxide (HP) and coal in either aqueous or nonaqueous solutions, coal biosolubilities increase (9,10). These increases have been attributed to the action of the peroxidases, but, since HP is quite reactive with coal, it is not known whether the rate of the enzyme catalyzed reaction is significant as compared to the nonenzymatic chemical reaction. In this manuscript we report on the relative rates of HRP catalyzed reactions as compared to the nonenzyme catalyzed chemical reaction.

EXPERIMENTAL

Mississippi Wilcox, Texas lignites were obtained as described and ground to -100 mesh (11). Beulah Zap (-100 mesh) and Wyodak (-100 mesh) were obtained from the Argonne Premium Coal Bank, Argonne, IL. Horseradish peroxidase type II (HRP) was obtained from Sigma Chemical Company, St. Louis, MO.

Solubilized Wilcox was obtained by placing 5g of coal in 1l of 50mM Tris buffer, pH 8.0. After mixing for several days, the suspension was centrifuged at 10,000xg for 20 minutes and the supernatant obtained. Solubilized coal was precipitated by acidifying the supernatant to pH 2 with HCl and allowing the suspension to stand for several hours. Precipitated coal was collected by centrifugation, washed several times with 1mM HCl and redissolved in 50mM Tris buffer. This solution was then filtered (Gelman type GA, 0.2µm pore dia.) to remove any insoluble material. The final concentration was approximately 2g coal/liter. Iron concentrations present in the solubilized coal was determined using an ARL Model 3520 atomic absorption spectrophotometer in the ICP mode.

Assays to determine relative rates of enzyme and nonenzyme catalyzed reactions were performed at 30°C and used either 1g of particulate coal or 5ml of solubilized coal. Reactions were initiated by the addition of 50ml of the appropriate buffer containing approximately 1mM HP. Actual concentrations of HP present were determined iodometrically (12). Buffers used were 500mM acetate, pH 5.0, 500mM phosphate, pH 6.5 and 500mM Tris, pH 8.0. At indicated time points, 50µl aliquots were removed from the reaction mixture and concentrations of HP present determined using the leucocrystal violet assay (13). Controls included HP with no additions, HP with 5mM resorcinol (positive control) and HRP, resorcinol with no other additions and HP with coal, resorcinol and HRP (positive control).

RESULTS AND DISCUSSION

Hydrogen peroxide, in the absence of HRP, reacted rapidly with all coals at each pH tested (Figure 1). Reactions profiles were similar in every case. Initial reactions were rapid and slowed as the reaction proceeded. This reaction appeared to be second order with respect to peroxide since a plot of 1/peroxide vs. time was linear (Figure 2). Assuming that this reaction was second order, values for the reaction constants could be obtained by determining slopes of lines generated by these plots (Table 1). Typically, these plots yielded lines with correlation coefficients 0.975 or better. As a general rule reactions were slowest at lower pH values and increased as pH increased. This is consistent with the literature indicating that hydrogen peroxide becomes a more powerful oxidizing agent as pH increases (14).

The reaction of HP with resorcinol as catalyzed by HRP was used as a positive control. This reaction not only demonstrated that HRP was active, but also gave an indication as to the activity of the enzyme with a preferred substrate and yielded some insight into the peroxidase reaction. Once again, a plot of 1/peroxide vs time yielded a straight line indicating that this reaction was second order with respect to HP (Figure 2). This result was obtained every time the experiment was performed and is consistent with earlier reports in the literature (15,16).

Because rates were determined by measuring HP disappearance, it was not known if the disappearance of HP was due to coal oxidation. Coals were not analyzed to determine if the coal itself was being oxidized because the amount of oxidation occurring would have been too small to measure using ultimate analyses. Other possible causes that could have accounted for the disappearance of HP were, therefore, investigated. An alternate material that might have been oxidized at the expense of HP would have been pyrite (17). The ability of HP to oxidize pyrite using the above conditions indicated that no significant rates of pyrite oxidation occurred at pH values of 5.0 and 6.5. At pH 8.0, significant amounts of HP were consumed in short periods of time indicating that pyrite was being oxidized (data not shown). Another possibility was that iron ions present in the coal could catalytically decompose HP (18). Solubilized Wilcox coal was analyzed and found to contain 1mM iron. Addition of 0.5mM and 1mM Fe^{+++} to solubilized Wilcox did not increase rates of HP consumption and the addition of 2mM Fe^{+++} resulted in only a slight increase in HP consumption (data not shown). These data suggest that the carbon present in the coal was being oxidized.

The addition of HRP to reaction mixtures containing both coal and HP generally had very little effect upon rates of HP consumption (e.g., Figure 1) and in most cases decreased rates of HP disappearance (Table 1). The lack of change in rates of HP consumption in the presence of coal was not due to the coal rendering the HRP inactive since HRP was able to oxidize resorcinol in the presence of coal. Also, the amount of enzyme in reaction mixtures containing coal was 10-fold greater than that present in positive controls containing resorcinol. Since no significant increases in rates of HP consumption were observed when large quantities of HRP were present in coal mixtures, then at least one of two possibilities must have existed. The first possibility was that HRP was unable to use coal as a substrate. A second possibility was that HRP was able to use coal as a substrate, but the number of sites where this could be done was extremely small which would have limited increases in HP consumption to below detection limits. Also, if there were such a small number of sites present, then increasing the amount of peroxidase present in reaction mixtures would not result in an increase in HP consumption.

Results from this study indicate that HRP is able to catalyze little or no reaction between coal and HP. Since peroxide reacts readily with coal and since HRP is an expensive enzyme, it would appear that continued use of HP in the presence of HRP would be of little value. This work does not preclude the possibility that other more powerful peroxidases (e.g., lignin peroxidases) might be able to catalyze the oxidative depolymerization of coal. A study involving the ability of lignin peroxidases to oxidatively depolymerize coal will be the subject of a subsequent manuscript.

ACKNOWLEDGEMENTS

This work was supported under contract no. DE-AC07-76ID01570 from the U.S. Department of Energy, Office of Advance Research and Technology Development, Office of Fossil Energy to the Idaho National Engineering Laboratory/ EG&G Idaho, Inc.

REFERENCES

1. Cohen, M. S. and P. D. Gabriele. 1982. Appl. Environ. Microbiol. 44:23.

2. Fakoussa, R. M. 1981. Ph.D. Thesis, Freidrich-Wilhelms University, Bonn, Federal Republic of Germany.

3. Cohen, M. S., W. C. Bowers, H. Aronson and E. T. Gray, Jr. 1987. Appl. Environ. Microbiol. 53:2840.

4. Pyne, J. W., D. L. Stewart, J. Fredrickson and B. W. Wilson. 1987. Appl. Environ. Microbiol. 53:2844.

5. Dodson, P. J., C. S. Evans, P. J. Harvey and J. M. Palmer. 1987. FEMS Microbiol. Lett. 42:17.

6. Campbell, J. A., D. L. Stewart, M. McCulloch, R. B. Lucke and R. M. Bean. 1988. Prep. Pap.-Am. Chem. Soc., Div. Fuel Chem. 33(4):515.

7. Pyne, J. W., D. L. Stewart, J. C. Linehan, R. M. Bean, M. A. Powell, R. B. Lucke, B. L. Thomas, J. A. Campbell and B. W. Wilson. 1987. Proceedings of the Biological Treatment of Coals Workshop, U.S. Department of Energy, pp. 174-194.

8. Bean, R. M., J. K. Fredrickson, J. A. Campbell, D. L. Stewart, J. A. Franz, B. L. Thomas, M. McCulloch, J. C. Linehan and B. W. Wilson. 1989. Proceedings: 1989 symposium on Biological Processing of Coal and Coal-Derived Substances, Electric Power Research Institute, pp. 3-1 - 3-25.

9. Scott, C. D. and S. N. Lewis. 1988. Appl Biochem. Biotech. 18:403.

10. Scott, C. D., C. A. Woodward, J. E. Thompson and S. L. Blankinship. 1990. Appl. Biochem. Biotech. In Press.

11. Quigley, D. R., C. R. Breckenridge, P. R. Dugan and B. Ward. 1989. Energy Fuel. 3:371.

12. Allen, A. O., C. J. Hochanadel, J. A. Gormley and T. W. Davis. 1952. J. Phys. Chem. 56:575.

13. Mottola, H. A., B. E. Simpson and G. Gorin. 1970. Anal. Chem. 42:410.

14. Sidgwick, N. V. 1950. Chemical Elements and Their Compounds, Vol II. Oxford University Press. pp. 868-874.

15. Chance, B. 1951. Advances in Enzymology. 12:153.

16. Chance, B. 1949. Arch. Biochem. 22:224.

17. Boron, D. J., A. G. Dietz and S. R. Taylor. 1981. Fuel. 60:991.

18. Walling, C. 1975. Acc. Chem. Res. 8:125.

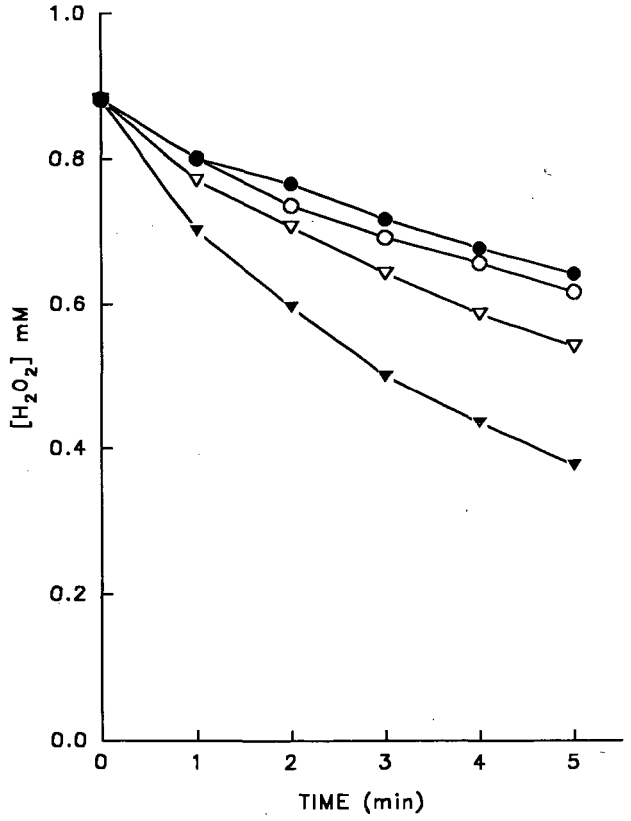

Figure 1. Disappearance of Hydrogen Peroxide in the Presence of Texas Lignite and Resorcinol at pH 8.0. Reaction mixtures are as described. Texas lignite = open circles; Texas lignite with HRP = closed circles; Resorcinol with HRP = open triangles; Texas lignite with Resorcinol and HRP = closed triangles.

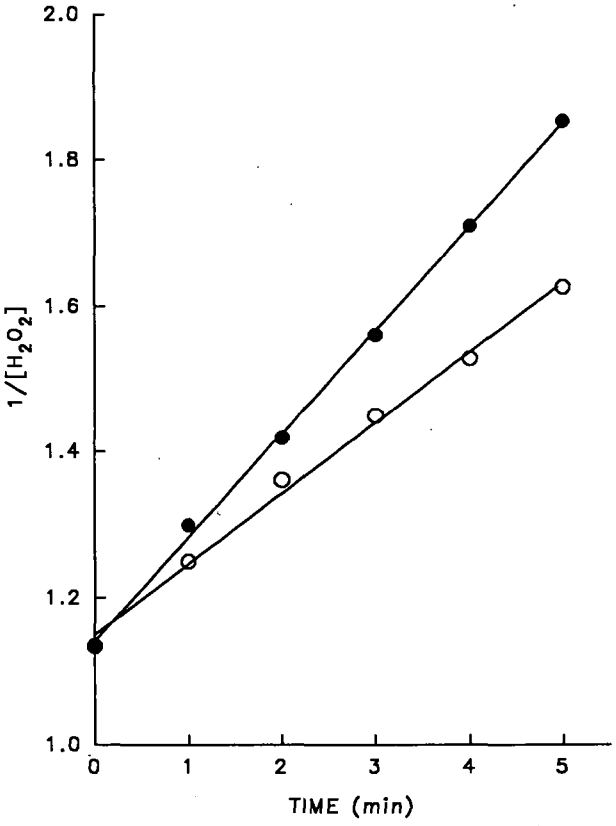

Figure 2. Plot of Inverse Hydrogen Peroxide Concentration vs. Time. Data taken from Figure 2. Correlation coefficients are 0.998 and 0.999 respectively for Texas lignite reacting with HP in the absence of HRP (open circles) and resorcinol reacting with HP in the presence of HRP (closed circles.

Coal		pH 5.0	6.5	8.0
Wilcox lignite	-HRP	0.078	0.146	0.269
	+HRP	0.053	0.112	0.319
Beulah Zap	-HRP	N.M.	0.029	0.064
	+HRP	N.M.	0.025	0.051
Texas lignite	-HRP	0.017	0.119	0.097
	+HRP	0.015	0.080	0.084
Wyodak	-HRP	0.073	0.058	0.109
	+HRP	0.045	0.039	0.099
Soluble Wilcox	-HRP	0.037	0.044	0.029
	+HRP	0.031	0.043	0.036

Table 1. Rate Constants for the Reaction of Various Coals and Hydrogen Peroxide in the Presence and Absence of Horseradish Peroxidase. -HRP indicates the absence of horseradish peroxidase; N.M. indicates not measured. Values are given as $(\text{mmoles/liter/min})^{-1}$.

CHARACTERIZATION OF EXTRACELLULAR BACTERIAL ENZYMES WHICH DEPOLYMERIZE A SOLUBLE LIGNITE COAL POLYMER

Don L. Crawford
Rajinder K. Gupta

Deppartment of Bacteriology and Biochemistry
Institute for Molecular and Agricultural
Genetic Engineering (IMAGE)
University of Idaho
Moscow, Idaho 84843

KEYWORDS: Streptomy cetes
Depolymerization

ABSTRACT

Several Gram negative and positive soil bacteria, isolated by enrichment technique in a liquid minimal medium containing water soluble lignite coal polymer as a sole source of carbon and energy, were screened for their abilities to depolymerize coal when growing in peptone broth containing soluble coal. One Gram positive and 3 Gram negative strains significantly depolymerized the coal within 3-6 days. These strains were screened for the production of extracellular coal depolymerizing enzymes. Each bacterium, including Gram negative strains DLC-BB2, DLC-62 and DLC-63/9, and Gram positive strain DLC-21, produced lignite depolymerizing enzymes. Extracellular filtrates from 3-day cultures grown in peptone medium supplemented with an inducing level of soluble coal polymer, contained an enzymatic activity which caused significant depolymerization of the coal polymer after 4 hr of incubation of enzyme with coal ($30^{o}C$), as shown by High Performance Liquid Chromatography. Each bacterium produced similarly acting enzymes which progressively converted the principal broad coal polymer peak of about 174,000 MW into a much sharper peak of about 113,000 MW. In some cases, even lower molecular weight products appeared upon prolonged incubation of the reaction mixtures. The activities were inactivated by boiling of culture supernatants. While chemical analyses of enzymatically depolymerized coal products indicated that the depolymerization was non-oxidative, the specific type(s) of enzymes involved in the depolymerization remain to be identified. The results show that nonoxidative, enzymatic depolymerization of coal is possible.

INTRODUCTION

Selected biotransformations of coal may aid in its conversion to liquid and/or gaseous fuels. Such transformations include depolymerizations (1), reductions (2), and/or solubilization (3-6). Both fungi and bacteria have been shown to solubilize coal. Some appear to excrete

enzymes that oxidize coal into water soluble polymeric products (7-9). However, coal solubilization more typically involves the excretion of basic, low molecular weight coal-solubilizing metabolites by the microbes, and coal solubilization is nonenzymatic (3-5, 10-12). Few papers have reported the microbiological depolymerization of coal. One paper (13) reported that lignin peroxidase from the white-rot fungus Phanerochaete chrysosporium oxidized water soluble coal polymers, converting them into smaller molecular weight polymers. Pseudomonas cepacia Strain DLC-07, when growing in liquid media at pH 5.5 depolymerized a water soluble Vermont lignite coal polymer (1). Deploymerization was found to be optimal when the bacterium was grown on coal in a mineral salts-peptone-soluble coal polymer medium (14). Here, we report on characterizations of 3 Gram negative and 1 Gram positive aerobic bacterial strains which metabolize lignite coals. These strains significantly depolymerize base-solubilized lignite when growing on the coal in liquid media and excrete enzymes which catalyze lignite depolymerization via a non-oxidative mechanism. This is the first report of such enzymes from both Gram negative and positive bacteria. Our results are indicative of the positive potential for using bacteria to biotransform coal into useful liquid fuels.

MATERIALS AND METHODS

Isolation of Aerobic Bacteria. The bacteria were isolated from soil associated with coal seams (1) and from other soils rich in decomposing plant residues. The enrichment medium (pH 5.5) was a mineral salts solution supplemented with 0.01% (w/v) of yeast extract (Difco, Detroit, MI) and 0.2% (w/v) of soluble, nitric acid pre-treated Alabama lignite coal polymer (1). The enrichment-isolation procedure was carried out at 30°C as described previously (1). Stock cultures of each bacterium were maintained on Sabouraud Dextrose Agar (SDA) slants at 4°C. Strains DLC-62, DLC-63/9, and DLC-BB2 are as yet unidentified aerobic Gram negative rods, while strain DLC-21 is a spore-forming, Gram positive Bacillus species.

Assay for Extracellular Coal Depolymerizing Enzyme Activity. Each bacterium was grown in shake flasks for three days (30°C) in 250 ml of mineral salts-peptone broth (14) also containing 2mg of water soluble coal polymer. Cultures were then harvested, and the cells removed by centrifugation. The supernatant was used as the source of enzyme. If desired, the supernatants can be concentrated 10-fold by ultrafiltration prior to use. For the assay, 100 ul of soluble coal polymer solution was added to 10 ml of crude or concentrated supernatant. After 0 and 4 hr incubation (30°C; pH 5.5) the reaction was stopped by acidifying 1.0 ml of the solution to pH 2.0. The precipitated coal was collected by centrifugation, washed, redissolved in 1.0 ml

of HPLC solvent, and analyzed by HPLC. Controls contained reaction mixtures treated similarly, but heat-inactivated supenatant was substituted for active enzyme. Coal depolymerization was monitored by observing the appearance of lower molecular weight HPLC peaks.

Coal Substrate Used and Growth of Bacteria on Coal. The coals used was a weathered Vermont lignite (1,2). A coal substrate water soluble at pH 5.5 or higher was prepared from the Vermont lignite as described by Gupta et al.(1). One hundred grams of powdered coal were soaked in water for 8 hr and then dissolved in 1 liter of 1N NaOH. The solution was centrifuged to remove undissolved coal, and the pH of the supernatant was adjusted to pH 7.0 with HCl. Coal that precipitated was collected, washed, dried, and powdered (yield: 40 g). The supernatant from the precipitation was acidified to pH 5.5, and the resulting precipitate was collected, washed (pH 5.5 water), dried, and powdered (yield: 15 g). The remaining coal in solution was precipitated at pH 1.5, collected, washed (pH 1.5), and powdered (yield: 10 g). This final coal polymer precipitate, which was soluble at pH's of 5.5 or higher, was used as the substrate in both growth and enzyme studies.

Molecular Weight Distribution of the Coal Polymers. Bacterial depolymerization of the soluble coal polymer was monitored by HPLC, as described previously (1), using a Hewlett Packard 1090A instrument equipped with an HP-1040 diode array detector and a Synchropak GPC-300 column (1000-500,000 MW separation capability) (Synchrom Inc., Lafayette, IN). The mobile phase consisted of phosphate buffer (0.02M KH_2PO_4) containing 0.5% (w/v) Tween 80, pH 7.1, set at a flow rate of 0.25 ml min^{-1}. The column was equilibrated with high and low molecular weight protein standards (1). Coal containing culture medium samples (0.5 ml) were centrifuged, the supernatants acidified to pH 2, and the precipitated coal recovered by centrifugation. The wet precipitate was redissolved in 0.5 ml of HPLC solvent and injected into the HPLC. Elution of the coal polymer was then monitored at 254 nm.

Elemental Anaylsis of the Coal Polymers. Elemental analysis of 1-3 mg samples of control and depolymerized coal polymers were performed by Desert Analytics, Inc. (Tuscon, AZ) according to the procedure described by Gupta et al. (5).

RESULTS

Coal Depolymerization During Growth of the Bacteria. From among numerous bacteria isolated from the liquid enrichments, 4 were selected for their ability to depolymerize the soluble Vermont lignite coal in liquid mineral salts-peptone broth. Micrographs of each organism, including Gram negative strains DLC-62, DLC-63/9, and DLC-

BB2 and Gram positive strain DLC-21 are shown in Figure 1. DLC-21, the only Gram positive bacterium in the group, is a nonmotile, spore-forming rod (Fig 1,A). We have classified it as a Bacillus species. All of the Gram negative bacteria are strictly aerobic. DLC-62 ane DLC-BB2 are both highly motile, short rods (Fig 1,B and D), while DLC-63/9 is a very long and thin nonmotile rod (Fig 1,C).

As shown in Figures 2 and 3, each bacterium significantly depolymerized soluble Vermont lignite coal polymer within 3 days when growing in mineral salts-peptone-coal polymer broth. Over the same period, the molecular weight of the coal polymer (130,000) remained unchanged in incubated, uninoculated, controls (Figs. 2A, 2B). In contrast, depolymerization resulting from bactrial metabolism (Figs. 3A-D) was significant, and greater than that previously seen with Pseudomonas cepacia DLC-07 after growth for 2 weeks on coal in the same medium (1).

Detection of Extracellular Coal Depolymerizing Enzymes. Preliminary assays for the presence of extracellular enzymes catalyzing coal depolymerization were carried out by incubating cell free culture filtrates from 3-day cultures grown in mineral salts-peptone broth supplemented with an inducing level of coal polymer (2mg/250ml). Each bacterium produced lignite depolymerases. Cell free culture filtrates from each of the cultures enzymatically transformed the coal polymer within a period of 1-4 hr. (data not shown). HPLC elution profiles shifted to lower moleceular weight peaks in a pattern like that observed when the bacteria were grown on the coal polymer in peptone broth. In contrast, elution profiles of reaction mixtures incubated with heat-inactivated (boiled; 5 min) culture filtrates replacing untreated filtrate (=inactivated controls) did not change over the incubation period. In active filtrates HPLC elution profiles of the coal polymer shifted from a single major peak with a retention time corresponding 167,000-174,000 MW to a sharper peak averaging about 113,000 MW, and having a higher molecular weight shoulder of 144,000-170,000 MW. With several of the reaction mixtures, a shoulder peak corresponding to about 87,000 MW also appeared after extended incubation. All of the bacteria produced similarly acting enzymes. The time of harvesting of the filtrates was critical to their activity. If harvested too early or too late, activities were low.

Elemental Composition of the Coal Polymers. Elemental analyses of the depolymerized coal polymers showed no major changes in C, H, O, N, or S content relative to the starting coal (Table 1). The ash contents increased slightly. These data show that the depolymerizations were non-oxidative, although additional data will be needed to refine this conclusion.

DISCUSSION

This is the first report of coal depolymerizing enzymes in Gram postive and negative bacteria. Previously, Wondrack et al. (13) reported that the lignin peroxidase of the fungus Phanerochaete chrysosporium would depolymerize soluble base-solubilized coal polymers. The enzyme was oxidative, utilizing H_2O_2 to oxidize the coal. The enzymes produced by our bacterial isolates, in contrast, act non-oxidatively, perhaps hydrolytically.

We have found that careful timing of culture harvest is critical to obtaining optimally active enzyme preparations. Thus, we need to carry out a study that relates coal depolymerizing enzyme production to the growth curves of each of these bacteria. Then, we can establish the optimal incubation times for production of the enzymes by each strain. The rapid rate of depolymerization we observe (1-4 hr), and the appearance of a sharp product peak in HPLC chromatograms lead to some intriguing hypotheses concerning the nature of these enzymes. The enzymes may act to cleave structurally important internal linkages such as ether or ester bonds within the lignite macromolecule, thereby significantly depolymerizing the polymer. The remaining undepolymerized polymer, accumulating as the 113,000 MW peak in HPLC chromatograms, may represent a macromolecular structure more resistant to the enzymes and/or not containing susceptible linkages. Additional research will hopefully determine if this is the case. Regardless, the overall data show clearly that bacterial enzymes may be useful in breaking down the macromolecular structure of coal to produce lower molecular weight products potentially useful in the microbiological production of liquid or gaseous fuels.

ACKNOWLEDGMENTS

This research was supported by grant DE-FG22-88PC88919 from the U.S. Department of Energy, Pittsburgh Energy Technology Center, by a subcontract from EG&G Idaho, Inc. funded by the U.S. Department of Energy under contract DE-AC07076ID01570, and by the Idaho Agricultural Experiment Station.

REFERENCES

1) Gupta, R.K., L.A. Deobald, and D.L. Crawford. 1990. Depolymerization and Chemical Modification of Lignite Coal by Pseudomonas cepacia Strain DLC-07. Appl. Biochem. Biotechnol., **24/25**: In press.

2) Deobald, L.A. and D.L. Crawford. "Isolation of Microorganisms Able to Reductively Transform Aromatic Compounds and Their Relevance to Coal Liquefaction. In Proceedings of the Second International, Institute of Gas Technology Symposium on Gas, Oil, and Coal Biotechnology. December 11-13, 1989. New Orleans, LA.

3) Scott, C.D., G.W. Standberg, and S.N. Lewis. "Microbial Solubilization of Coal," Biotech. Progress, **2**: 131-139 (1986).

4) Quigley, D.R., B. Ward, D.L. Crawford, H.J. Hatcher, and P.R. Dugan. "Evidence that Microbially Produced Alkaline Materials are Involved in Coal Biosolubilization." Appl. Biochem. Biotechnol., **20/21**: 753-763 (1989).

5) Gupta, R.K., J.K. Spiker, and D.L. Crawford. "Biotransformation of Coal by Ligninolytic Streptomyces," Can. J. Microbiol., **34**: 667-674 (1988).

6) Cohen, M.S. and P.D. Gabriele. "Degradation of Coal by the fungi Polyporus versicolor and Poria monticoloa," Appl. Environ. Microbiol., **44**: 23-27 (1982).

7) Cohen, M.S., W.C. Bowers, H. Aronson, and E.T. Gray, Jr. "Cell-free Solubilization of Coal by Polyporus versicolor. Appl. Environ. Microbiol., **53**: 2840-2843 (1987)/

8) Pyne, J.W., D.L. Stewert, J. Fredrickson, and B.W. Wilson. "Solubilization of Leonardite by an Extracellular fraction from Coriolus versicolor," Appl. Environ. Microbiol., **53**: 2844-2848 (1987).

9) Moolik, R.T., J.C. Linden, and M.N. Karim. "Biosolubilization of Lignite," Appl. Biochem. Biotechnol., **20/21**: 731-742 (1989).

10) Maka, A., V.J. Srivastava, J.J. Kilbane II, and C. Akin. "Biolgocial Solubilization of Untreated North Dakota Lignite by a Mixed Bacterial and a Mixed Bacterial-Fungal Culture," Appl. Biochem. Biotechnol., **20/21**: 715-729 (1989).

11) Strandberg, G.W. and S.N. Lewis. "The Solubilization of Coal by an Extracellular Product of Streptomyces setonii," J. Ind. Microbiol., 1: 371-375 (1987).

12) Faison, B.D. and S.N. Lewis. "Production of Coal-Solubilizing Activity by Paecilomyces sp. During Submerged Growth in Defined Liquid Media," Appl. Biochem. Biotechnol., 20/21: 743-752 (1989).

13) Wondrack, L., M. Szanto, and W.A. Wood. "Depolymerization of Water Soluble Coal Polymer from Subbituminous Coal and Lignite by Lignin Peroxidase," Appl. Biochem. Biotechnol., 20/21: 765-780 (1989).

14) Crawford, D.L. and R.K. Gupta. "Influence of Cultural Parameters on the Depolymerization of a Soluble Lignite Coal Polymer by Pseudomonas cepacia DLC-07," Resources, Conservation, and Recycling, In Press.

Table 1. Elemental Analyses of Control and Bacterially Depolymerized Coal Polymer Samples after Incubation in the Peptone-Coal Polymer Broth for ? days.

SAMPLE	%C	%H	%N	%O	%S	ASH
Control	49.1	4.1	3.3	35.6	1.0	3.8
DLC-21	49.9	4.0	3.1	33.8	1.5	4.8
DLC-62	50.7	4.0	3.1	35.0	1.2	4.2
DLC-63/9	51.0	4.0	3.1	35.4	1.3	5.1
DLC-BB2	50.6	4.0	3.2	35.5	1.2	5.1

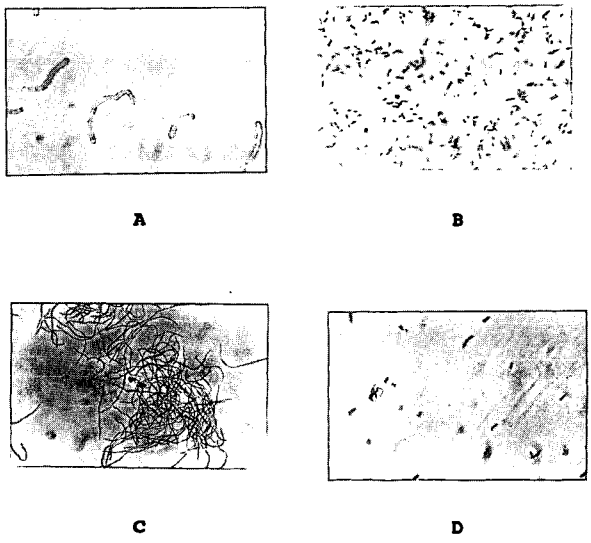

Figure 1. Light micrographs of aerobic bacterial strains **a)** DLC-21, **b)** DLC-62, **c)** DLC-63/9, and **d)** DLC-BB2. All micrographs are from wet mounts photographed at 1000X magnification.

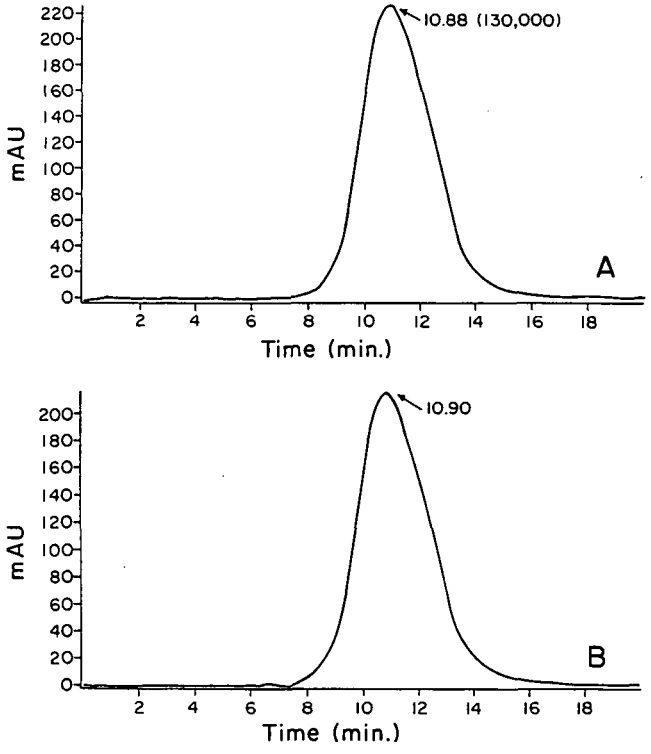

Figure 2. HPLC chromatograms showing the molecular weight distributions of the soluble lignite coal polymer in uninoculated controls at time 0 and after 3 days incubation in the mineral salts-peptone-coal broth at 30°C. A) Uninoculated control, time 0; B) Uninoculated control, 3 day. The retention time for the principal peak (10.9 min) represents an averager molecular weight of 130,000 daltons.

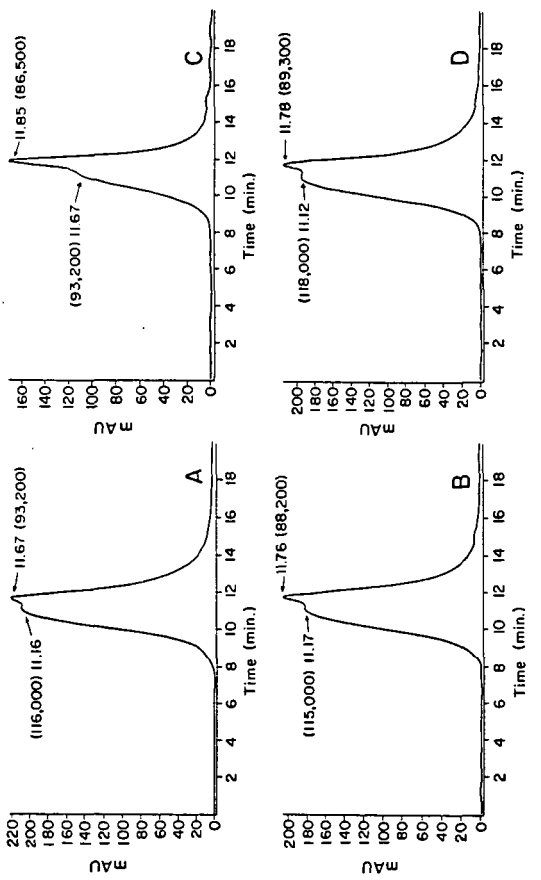

Figure 3. HPLC chromatograms showing the molecular weight distributions of the soluble lignite coal polymer in bacterially inoculated cultures after 3 days incubation in the mineral salts-peptone-coal polymer broth at 30°C. **A)** DLC-21; **B)** DLC-62; **C)** DLC-63/9; **D)** DLC-BB2. The retention times for the principal peaks are given in minutes, and the average molecular weights for each are presented beside the retention times in parentheses.

MASS AND ENERGY BALANCE CONSTRAINTS ON THE BIOLOGICAL PRODUCTION OF CHEMICALS FROM COAL

Graham Andrews
Biochemical Engineering Unit
Idaho National Engineering Laboratory
P.O. Box 1625
Idaho Falls, ID 83415-2203

Keywords: Coal, Bioprocessing, Chemicals

INTRODUCTION

Several proposals have been made for the bioprocessing of coal to produce useful liquid or gaseous chemicals. (1) They have included direct microbial production of methane, microbial production of chemicals from solubilized coal, (2) and a chemical gasification followed by a microbial product synthesis. (3) New microorganisms, biochemical pathways and potential products are reported at regular intervals. It is timely to ask where attention should be focused and which products and processes, if any, hold promise of commercial success. This is a complex economic balance, involving questions of market size, process rates, product separation costs, etc. An important factor in this overall equation is the yield of the process, that is the amount of product that can be obtained from unit mass of coal. The objective of this paper is to apply the standard theory of bioprocess yields to the particular problem of predicting the possible yields from coal bioprocesses.

The standard theory (4,5) is essentially a set of mass and energy balances applied to the particular conditions of a bioprocess. It provides insight into the main factors governing the yield of a product, fixes definite upper limits on the yield, and thus allows a preliminary economic analysis that will eliminate some products from consideration and allow a more rational choice between those that remain. The theory contains little information about metabolic pathways or the internal workings of microorganisms, and it can even be applied to hypothetical bioprocesses for which no microorganisms have yet been isolated. Experience seems to indicate that if a reaction involving naturally-occurring substances is stoichiometrically possible and thermodynamically advantageous in dilute aqueous solution then there exists a microorganism somewhere that will catalyze it.

THE MASS BALANCE

The simplest way to keep track of the substrates and products in a fuel bioprocessing operation is to write it as a pseudo chemical reaction. This reaction is best written in terms of carbon equivalents, that is the amount of organic matter that contains 1 mole of carbon. Nitrogen and sulfur will be included in the formulae because they are often important in fuel bioprocessing, and are significant microbial nutrients.

Coal — Auxiliary Nutrient

$$CH_aO_bN_cS_d + Y_o\,O_2 + Y_n\,NH_3 + Y_a\,CH_eO_fN_gS_h \text{ (+ other nutrients)} \longrightarrow$$

$$Y_b\,CH_iO_jN_kS_l + Y_p\,CH_mO_nN_pS_q + Y_c\,CO_2 + Y_H\,H_2O + Y_s\,H_2SO_4 \text{ (+ other products)} \quad (1)$$

Biomass — Product

The Y values are yields expressed as carbon equivalents or moles of a compound produced or consumed per carbon equivalent of fuel. Converting these to a dry/mass basis requires correction for the inorganic (ash) constituents of the compound. For example

$$\text{Biomass yield from Fuel (wt/wt)} = \frac{Y_b M_b}{M_f} \frac{1 - r_f}{1 - r_b} \quad (2)$$

M is the mass of a carbon equivalent and r is the mass fraction of mineral matter ("ash") in the dry compound (r~0.08 for biomass).

Note that reaction (1) shows ammonia as a nutrient and water as a product. This is not necessarily so; the metabolism of coal and the auxiliary nutrients may involve more hydrolysis than dehydration steps and more deamination than amination. Water would then be a nutrient, ammonia a product and both Y_n and Y_H, as calculated here, would be negative.

If the possible other nutrients and products are ignored, Equation (1) contains eight unknown yields, and five element balances (C, H, N, O, S) can be written for it. Using these element balance equations to eliminate Y_N, Y_c, Y_H and Y_s gives the result

$$\gamma_p Y_p + \gamma_b Y_b + 4Y_o = \gamma_f + \gamma_a Y_a \quad (3)$$

This equation is essentially an oxidation/reduction balance over reaction (1). The γ coefficients represent the oxidation/reduction state of a compound, specifically the number of available electrons per carbon equivalent of each compound. Thus the definition for the fuel is:

$$\gamma_f = 4 + a - 2b - 3c + 6d \quad (4)$$

Typical values of γ for different ranks of coal, different types of (dried) biomass and several chemicals that could be produced by bioprocessing are shown in Table 1. Several points should be noted from this table.

First, this type of analysis is useful only because the γ values for biomass are surprisingly constant between species. This is confirmed by larger compilations of data on the elemental compositions of living material. (6) The data for the yeast Candida utilis shows that the carbon source used to grow a microorganism also makes little difference to it's elemental composition. A rapidly growing microbe does have a lower value of γ (mainly due to increased RNA production) but the difference is not of major significance.

Table 1 also shows that the γ values for coal are not only fairly consistent between ranks, but also very close to the values for biomass. This may seem surprising in view of the very different elemental composition of the coal, yet it reflects the fact that coal is made from living matter. The coalification process consists mainly of natural reactions (dehydration, deamination) that do not alter the oxidation/reduction state of the starting material.

Most of the chemicals that we want to produce by liquefaction or gasification of coal are fuels which are, by definition, reduced compounds such as methane ($\gamma = 8$), methanol ($\gamma = 6$) and others shown in Table 1. The oxidation/reduction state of the biomass (and coal) is seen to be more comparable to that of carbohydrate ($\gamma = 4$).

Among bulk chemicals that could be produced from coal only acetic acid has a comparable γ value.

THE GENERAL PRODUCT YIELD

Equation (3) can easily be generalized for the common situation where several products are made. Each product adds an additional term to the left hand side of the equation. The auxiliary nutrients may be specific product precursors (e.g., phenyl-acetic acid in penicillin production) or less well defined compounds like yeast extract that provide a mixture of precursors for biomass growth. It is assumed that each additional nutrient is associated with the formation of a specific product, and that the ratio of nutrient consumed to product (or biomass) produced is a constant (e.g., for biomass $Y_{ab} = Y_a/Y_b$). Equation (3) becomes

$$\sum_{\text{cells and products}} Y_p(\gamma_p - \gamma_a Y_{ap}) = \gamma_f - 4Y_o \qquad (5)$$

Note that, for the purposes of this yield analysis, biomass can be treated as just another product. In coal bioprocessing it is unlikely (on economic grounds) that chemical precursors would be added to direct the formation of specific products, so the biomass term will be the only one in the summation which involves an auxiliary nutrient. The effect of this nutrient is to reduce the amount of fuel required to make biomass, and thus to decrease the "cells" term in the summation. In the limit where the auxiliary nutrient (yeast extract ?) has the same composition as the biomass ($\gamma_a = \gamma_b$) and provides all the precursors for cell growth ($Y_{ab} = 1$) the "cells" term is zero. This situation produces the highest possible, or "theoretical," product yields but, since yeast extract costs 5 \$/lb and coal 0.01 \$/lb it is unlikely to be a commercial strategy.

The most obvious consequence of equation (5) is that the more oxygen is consumed by a process (higher Y_o) the lower the total yield of products. The same applies to most other, externally supplied, terminal electron acceptors (NO_3^-, SO_4^{--}) but not to CO_2, which can be reduced to CH_4, a useful product, by methanogenic bacteria metabolizing hydrogen. A consortium of fermentative and methanogenic organisms similar to that used in anaerobic digestion would not only produce the highest yields, but also avoid the costs and problems associated with aerating a coal slurry. (7)

THE SINGLE PRODUCT

The above discussion outlines an optimum commercial process. It would be based on anaerobic metabolism and make a single product, since the cost of separating multiple products can be prohibitive. The bioreactor would be continuous and contain a high concentration of biomass to offset the low specific rates of anaerobic metabolism. The biomass must be immobilized and slow-growing to maximize product yields and minimize the cost of providing auxiliary growth nutrients. The question is what product should be produced?

The first constraint is that an anaerobic process cannot produce a single product that is more oxidized than the substrate. However the values in Table 1 show that most products of interest are fuels or chemicals with $\gamma_p > \gamma_f$, so this is not a serious restriction. The maximum possible, or "theoretical," yield of the product is $Y'_p = \gamma_f/\gamma_p$ (equation (5) with $Y_b = Y_o = 0$) so it makes sense to look for a product with γ_p only slightly larger than γ_f. Some potential candidates are listed

in Table 2. They are all known end-products of fermentative metabolism, although microorganisms capable of producing them from coal have not necessarily been isolated. Also shown in Table 2 are their approximate current prices. Multiplying these prices by the theoretical yields gives the maximum possible financial return per pound of coal processed. This must be considerably larger than the price of coal (approximately 1 c/lb) to make a feasible process. On this basis ethanol and propionic acid appear very promising and methane less so. However it must not be forgotten that the manufacture of methane, a gas, does not involve the considerable costs involved in separating the other two products from the fermentation media.

TWO PRODUCTS

Most fermentative metabolic pathways produce not a single product but a mixture of two or more. (5) For two products, the "theoretical yield" situation (equation (5) with $Y_o = Y_b = 0$) must be represented not by a single value but by a graph such as Figure 1 (for CH_4 and H_2 over the entire range of γ_f values for coal) or Figure 2 (for ethanol and acetic acid from a coal with $\gamma_f = 4.5$). These graphs are useful in several ways. They show clearly what combinations of yields are feasible (anything below the constant γ_f line) and what are ruled out by stoichiometry (anything above the line). They therefore provide a useful check on experimental data. For example the yields of methane and hydrogen from a Texas lignite ($\gamma_f = 4.52$) reported by Barik et al (2) are shown in Figure 1. They fall comfortably within the feasible region, and it is immediately apparent from the graph how much the yields could be improved either by improving the microbial culture or by using a more reduced lignite. Note however that a yield of 511 cm^3 CH_4 per gram of coal ($Y_{p2} = 0.73$) claimed in the same report would be outside the feasible region, suggesting perhaps that some methane was generated from the auxiliary nutrient.

The "feasible" region on these graphs may be further constrained by biochemical hypotheses. For example there is no known mechanism by which non-photosynthetic anaerobic bacteria can produce molecular hydrogen from water. The dashed line in Figure 1 shows the maximum yield of H_2 that could be produced from the hydrogen in the lignite ($CH_{0.89}\ N_{0.016}\ S_{0.12}\ O_{0.20}$) and the data is seen to fall within this more constrained area.

When there are two products one of them can be more oxidized than the coal without violating the requirements of stoichiometry. This situation is illustrated for acetic acid ($\gamma_{p1} = 4$) and ethanol ($\gamma_{p2} = 6$) from a typical coal ($\gamma_f = 4.5$) in Figure 2. It creates the possibility of a truly optimal situation in which all the coal carbon is converted into products, with no net production of CO_2. This happens along the section of the $(Y_{p1} + Y_{p2}) = 1$ line that is in the feasible region. Compare this with the methane/hydrogen situation (Figure 1) where $0.55 \geq Y_{p2} \geq 0$, implying that anywhere from 45% to 100% of the coal carbon must be converted to CO_2.

In the area above the $(Y_{p1} + Y_{p2}) = 1$ line inside the feasible region in Figure 2, carbon dioxide is not a product but a reactant. This may seem unlikely, but is not excluded either by stoichiometry or by the energy balance which will be shown in the next section, to a first approximation, to be identical to the mass balance (greater precision requires knowledge of the free energy of formation of the coal's organic matter). Furthermore, if the reduced product is methane, there is no biochemical barrier to a net fixation of CO_2. Besides the methanogenic bacteria that produce methane from CO_2 and hydrogen, there are several examples of exergonic carboxylation reactions catalyzed by the acetogenic bacteria. For example one step in the digestion of glucose to methane is the carboxylation of butyrate (8)

$$2C_3H_7COO^- + OH^- + HCO_3^- \text{-----> } 4CH_3COO^- + CH_4 \qquad \Delta G_r = -12.5 \text{ kcal}$$

Long chain organic acids are known to be a major component of solubilized coal, and it is conceivable that a carefully controlled coal bioprocess continuously provided with CO_2 could result in a series of such reactions with a net fixation of carbon and production of acetate and methane with a total carbon yield greater than unity.

THE ENERGY BALANCE

The other main constraint on the formation of products is that they do not violate the conservation of energy. The energy balance for a bioprocess can be written in several different ways. For example an energy balance over the entire process can be written in terms of the heats of combustion (ΔH = heat of combustion per C equivalent of the substrates and products).

$$\sum_{\substack{\text{cells and}\\ \text{products}}} Y_p(\Delta H_p + Y_{ap}\,\Delta H_a) = \Delta H_f - Q \qquad (7)$$

Here Q is the heat generated per C- equivalent of fuel consumed. It is a common observation that the heat of combustion of a compound is approximately proportional to its degree of reduction; i.e., $\Delta H = K\gamma$. Substituting this into equation (7) and subtracting equation (5) gives a standard result for metabolic heat production.

$$Q = 4KY_o \qquad (8)$$

Note that for a fermentative process ($Y_o = 0$) the approximation $\Delta H = K\gamma$ makes equations (5) and (7) identical, and thus the energy balance would produce no extra information. The implication that no metabolic heat would be generated ($Q = 0$) in this case is not correct but results from inexactitudes in the assumption that $\Delta H = K\gamma$ (K is in the range 26-31 kcal/mol electrons depending on the compound). Heat is generated during fermentative processes, although far less than in aerobic processes.

An alternative way of writing the conservation of energy for a bioprocess is to balance the production and consumption of ATP, the cell's main energy carrier, inside the cell. The general equation is (4)

$$\sum_{\substack{\text{cells and}\\ \text{products}}} \alpha_p Y_p = \alpha_f - m \qquad (9)$$

$\alpha_f = N + \gamma_f(P/O)/2$ is the amount of ATP that would be generated by substrate-level (1st term) and oxidative (2nd term) phophoylation during the complete catabolism of one C-equivalent of fuel.

$\alpha_p = (1/Y_{ATP}) + (N - N_p)/Y_c + (\gamma_p - \gamma_a Y_{ap})(P/O)/2$ is the total ATP cost to the cell of making one C-equivalent of product. The first term gives the actual consumption of ATP in the anabolic pathways. This extension of the Y_{ATP} concept from biomass to any product has been discussed by Andrews. (4) For a catabolic product Y_{ATP} is infinite by definition. The second and third terms account for the ATP and reducing power (in the form of NADH etc.) that the cell can not produce due to the diversion of intermediates from the catabolic pathway to the anabolic reactions that form the product. The contribution of substrate-level phosphorylation (second term) is usually small enough to be ignored in respiratory processes. Adding an auxiliary

nutrient that provides better precursors reduces the oxidative phosphorylation contribution (third term) by reducing the amount of catabolic intermediates that must be diverted to product formation. When the auxiliary nutrient provides all the precursors and electrons needed for product formation (or growth in the case of biomass) then this term is zero. Note that the auxiliary nutrient may also increase the value of Y_{ATP}. In the case of biomass growth for example, it is obviously easier (less energy consuming) for the cell to make new biomass from pre-formed nucleotides and amino-acids than if it must synthesize these compounds from intermediates in the catabolic pathway. (9)

Equation (9) is general and it can usually be greatly simplified, for example in aerobic processes (substrate-level phosphorylation negligible), fermentative processes (P/O = 0) or in cases where no metabolic products are produced. It can be very useful for processes involving well-studied metabolic pathways giving, for example, quite accurate predictions for aerobic cell yield on carbohydrates ($\gamma_f = 4$) using the Embden-Meyerhof pathway (N = 1/3), the common cytochrome chain (P/O ~ 2.5) and the usual estimate of $Y_{ATP} \sim 10$ gm/mol. Unfortunately, in coal bioprocessing neither the substrate or the metabolic pathways leading to the products of interest are well characterized. Values of the energy parameters N, (P/O) etc. are not known, so application of equation (9) would be premature. Research in this direction should be encouraged.

CONCLUSIONS

The amounts and types of products that can be produced by any type of coal bioprocessing are constrained by the requirements of stoichiometry and energy conservation. The critical parameter is the number of available electrons per carbon equivalent in the organic fraction of the coal. This value shows no systematic variation with coal rank, but is always close to the value for carbohydrate and biomass ($\gamma \sim 4$). This reflects it's origin as living matter and implies that, in this respect at least, coal is a reasonable substrate for biological activity.

Anaerobic (fermentative) processes will give higher product yields than processes based on respiratory metabolic pathways where an external electron acceptor is provided. The only possible exception is methanogenic metabolism in which CO_2 acts as the electron acceptor, being reduced to CH_4. With certain combinations of products from coal, it may be possible to use these organisms to "fix" externally supplied CO_2. For fermentative metabolism, the maximum "theoretical" yields of various combinations of products can be calculated directly from the mass balances. These provide an excellent yardstick with which to judge experimental data.

In order to obtain useful extra information from the energy balance equation several metabolic parameters, including the production of ATP by substrate-level and oxidative phosphorylation, must be known. This requires further study of coal bioprocessing organisms.

ACKNOWLEDGMENTS

This work was supported under Contract No. DE-AC07-76ID01570 from the U.S. Department of Energy, Office of Advanced Research and Technology Development, Office of Fossil Energy to the Idaho National Engineering Laboratory/EG&G Idaho, Inc.

NOMENCLATURE

ΔH	Heat of combustion per C-equivalent
M	Weight of a C equivalent

m	Maintenance requirement for ATP
N	Moles ATP produced by substrate level phosphonylertion per C-equivalent of compound
(P/O)	Oxidative phosphorylation ratio
Q	Metabolic heat release per C-equivalent of fuel
r	Mass fraction of mineral matter
Y	Yield; moles of C-equiv of compound per C equivalent of fuel
α	Total moles ATP involved in breakdown or production of a C-equivalent of compound
γ	Available electrons per C-equivalent of compound

Subscripts

a	Auxiliary nutrient
b	Biomass
f	Fuel
o	Oxygen
p	Product

LITERATURE CITED

(1) Srivastava R. D., Campbell I. M., and Blaustein B. D. Coal Bioprocessing: A Research Needs Assessment, Chemical Engrg. Progress, 85, #12, 45 (1989).

(2) Barik S., Wyza R., Isbister J. D. Biological Conversions of Low Rank Coals, Proceedings: Symposium on the Biological Processing of Coal and Coal-derived Substances, EPRI #ER6572, (1989).

(3) Vega J. L., Elmore B. B., Ackerson M. D., Clausen E. C., Gaddy J. L. Biological Production of Liquid Fuels from Coal, Proceedings: Symposium on the Biological Processing of Coal and Coal Derived Substances, EPRI #ER6572, p. 3-69 (1989).

(4) Andrews G. F. Estimating Cell and Product Yields, Biotechnology Bioengineering, 33, 256 (1988).

(5) Papoutsakis E. T., Meyer C. L. The Fermentation Equation. Biotechnology Bioengineering, 27, 67 (1985).

(6) Atkinson B., Mavituna F. Biotechnology and Biochemical Engineering Handbook, Nature Press (1983).

(7) Andrews G. F., Quintana J. Mixing and Mass Transfer in the Aerated Trough Bioreactor, 1st International Symposium on the Biological Processing of Coal. Orlando, FL. May (1990).

(8) McCarty P. L. The Energetics of Organic Matter Degradation, In, Water Pollution Microbiology, Mitchell R. (ed) p. 91, Wiley (1972).

(9) Forrest W. W., Walker D. J. The Generation and Utilization of Energy During Growth, Advances in Microbial Physiology, 5, 213 (1971).

TABLE 1. VALUES OF THE γ PARAMETER

Substance	Composition of Organic Fraction	γ
Coals (Typical)		
Anthracite	$CH_{0.5}O_{0.03}N_{0.02}S_{0.01}$	4.44
Bituminous	$CH_{0.7}O_{0.06}N_{0.02}S_{0.01}$	4.58
Sub-bituminous	$CH_{0.8}O_{0.15}N_{0.02}S_{0.01}$	4.50
Lignite	$CH_{0.8}O_{0.22}N_{0.02}S_{0.01}$	4.36
Biomass (Dried)		
Yeast (C utilis)		
Glucose $\mu = 0.08\ hr^{-1}$	$CH_{1.82}O_{0.47}N_{0.19}$	4.32
$\mu = 0.45\ hr^{-1}$	$CH_{1.84}O_{0.56}N_{0.20}$	4.12
Ethanol $\mu = 0.06\ hr^{-1}$	$CH_{1.82}O_{0.46}N_{0.19}$	4.33
$\mu = 0.43\ hr^{-1}$	$CH_{1.84}O_{0.55}N_{0.20}$	4.13
Bacteria (A aerogenes)	$CH_{1.78}O_{0.33}N_{0.24}$	4.40
Possible Products		
Activated sludge	$CH_{1.4}O_{0.4}N_{0.2}$	3.99
Carbohydrate	CH_2O	4.0
Acetic acid	CH_2O	4.0
Ethanol	$CH_3O_{0.5}$	6.0
Octane	$CH_{2.25}$	6.25
Methane	CH_4	8.0

TABLE 2. POSSIBLE PRODUCTS FROM SUB-BITUMINOUS COAL

Product	γ_p Electrons/Equiv	Y'_p Equiv/Equiv	Price c/lb	Possible Return c/lb coal
Propionic acid	4.67	0.96	34	43
Butanediol	5.5	0.82	16	16
Ethanol	6.0	0.75	30	28
Methane	8.0	0.56	7.3	3.5

FIG 1 ; THEORETICAL YIELDS OF METHANE AND HYDROGEN

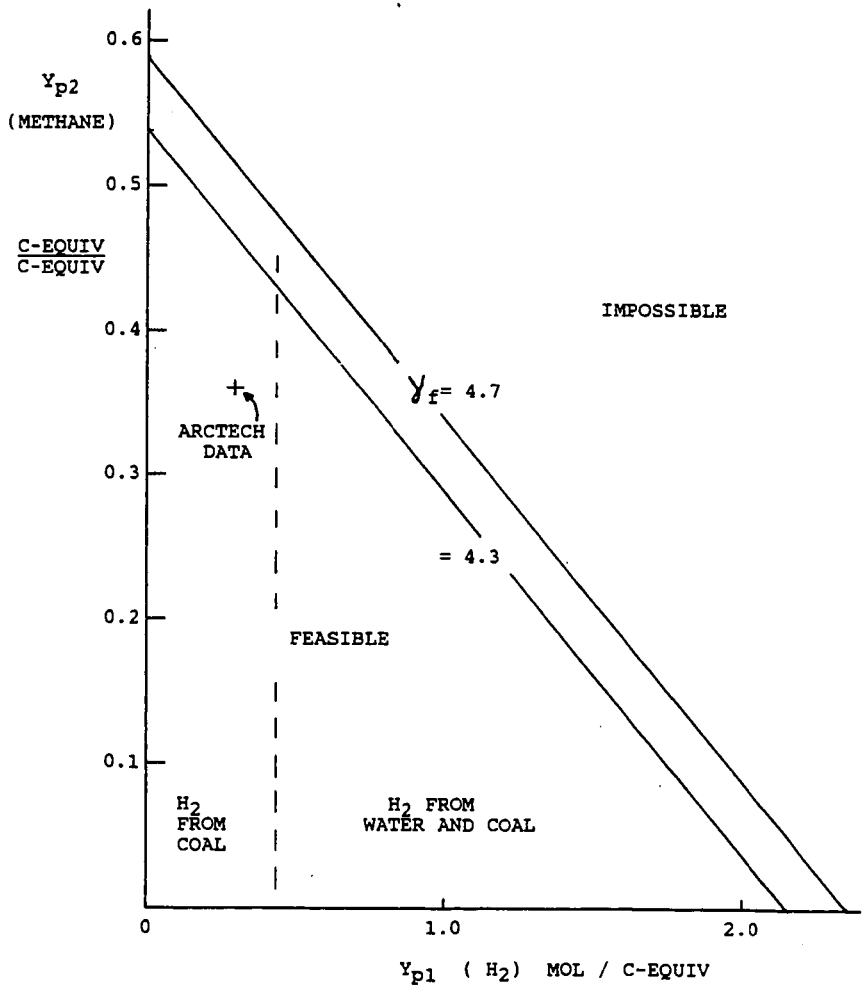

FIG 2 : THEORETICAL YIELDS OF ETHANOL AND ACAETIC ACID FROM A TYPICAL COAL ($\gamma_f = 4.5$)

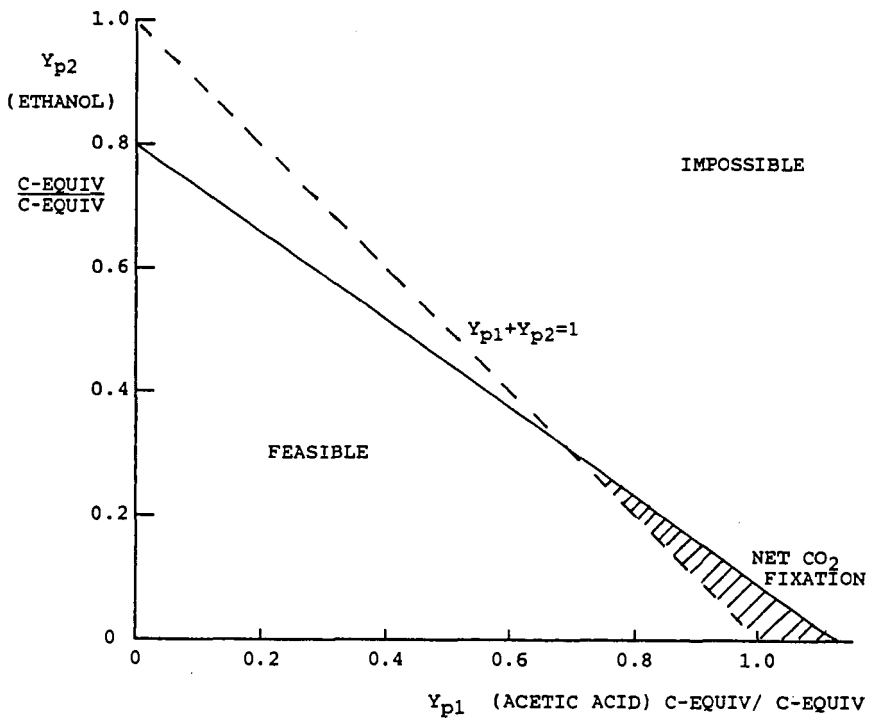

GENETIC MANIPULATION OF ACIDOPHILIC BACTERIA WHICH ARE POTENTIALLY APPLICABLE IN COAL BENEFICIATION

F.F. Roberto, A.W. Glenn, D. Bulmer, D.F. Bruhn and T.E. Ward
Biotechnology, Mailstop 2203
Idaho National Engineering Laboratory
Idaho Falls, ID 83415

Keywords: acidophilic bacteria; conjugation; coal desulfurization

INTRODUCTION

The economic and practical aspects of a biological coal desulfurization process are the subject of increasing study (1-6). Depyritization of coal by the bacterium, *Thiobacillus ferrooxidans* has been known for some time (7-9), and pilot scale experiments are underway (3,6). A number of limitations have already been recognized for this process, foremost of which is the speed with which the microorganisms grow and attack the pyritic sulfur. Metal toxicity and mass transfer dynamics also present formidable hurdles.

Removal of organic sulfur substituents poses even more difficult problems at this time, not least of which is the lack of efficient candidate organisms. Potential candidates at this time resemble members of the *Pseudomonadaceae*, common environmental bacteria. These organisms enjoy moderate temperatures (28-37 °C) and neutral pH, while the organisms investigated for depyritization processes are typically acidophiles, some of which also happen to be thermophiles (*Sulfolobus*, for example).

These various limitations in the microorganisms being examined for a viable desulfurization process have led us to initiate studies on the extension of molecular genetic techniques to acidophilic bacteria, with an ultimate goal of introducing desirable characteristics for desulfurization (enhanced growth rate, metal resistance, biochemical capacity to degrade organic sulfur) either directly into *T. ferrooxidans*, or, alternatively, into a heterotrophic acidophile which can coexist in the same environment as *T. ferrooxidans*. We are focusing on members of the genus *Acidiphilium*, one such acidophilic heterotroph.

EXPERIMENTAL

Bacterial strains and plasmids. Strains and plasmids used in this study are described in Table 1. *Acidiphilium* strains were grown in Modified Acidophile Salts (MAS) media, which is a modification of that used by Wichlacz and Unz (10). MAS medium contained 1 mM $(NH_4)_2SO_4$, 2 mM KCl, 0.86 mM K_2HPO_4, 10 mM $MgSO_4$, 6.6 mM $CaCl_2$, 2.6 mM $FeSO_4$, 0.01% yeast extract and 0.1% glycerol, pH 3.5. Solidified media were prepared with the addition of 0.4 % GelRite gellan gum (Kelco). Where indicated, tetracycline (Tc) was added to the media at 40 µg/ml.

Electroporation. Cells were electroporated as described previously (14-16). A BTX Transfector 100 electroporation device was used. Late log phase cells were washed and concentrated to cell densities of between 10^9-10^{11} cells/ml in 1 mM HEPES, pH 7.0. After electroporation, cells were diluted 20-fold into MAS medium to allow expression of the antibiotic resistance phenotype. Cells were

plated on 40 μg/ml Tc in MAS medium, and transformed colonies were clearly visible after three days. The experiments were performed at 32 °C unless otherwise indicated.

Conjugation. Spot matings were performed essentially as described by Miller (11). One milliliter exponential cultures of donor and recipient cells were centrifuged, washed twice and resuspended in 1 ml of 1 mM HEPES, pH 7.0. Donor cells were diluted 50-fold and a 25 μl aliquot was spotted onto a dry nutrient agar (Difco) plate. The liquid was allowed to absorb into the agar, at which time a 25 μl aliquot of the undiluted recipient cells was spotted directly onto the dried donor cells. Approximately 1 x 10^8 recipient cells were used. Matings were allowed to proceed for three hours, after which the cells were recovered and resuspended in 200 μl MAS medium. The cells were then plated on solid MAS medium containing 40 μg/ml Tc. Transconjugants usually appeared within 3-4 days.

Selection of rifampicin-resistant acidophiles. Mutants resistant to rifampicin were selected by plating cells on MAS plates on which a sterile filter disk (1/2" diameter) impregnated with 200 μg/ml rifampicin was placed. Colonies growing up to the filter disk, within the zone of inhibition were picked and checked for stable resistance by repeated subculturing on liquid and solid media. Mutants were typically resistant to 50-200 μg/ml rifampicin.

Conjugal transfer between acidophiles. Spot matings between acidophiles were performed as described above, with the exception that matings were allowed to proceed overnight, and all recipients used were resistant to rifampicin. All selective plates contained 50 μg/ml each of tetracycline and rifampicin.

Plasmid isolation, restriction digestion gel electrophoresis and ligation. Plasmids were isolated using the alkaline lysis method of Birnboim and Doly (12), as described for small scale isolations in Maniatis (13).

Restriction enzymes and T4 DNA ligase were purchased from Boehringer Mannheim and Promega, and digestions and ligations were carried out in appropriate buffers according to the manufacturers' instructions. Agarose gel electrophoresis was typically performed using 0.4% agarose (FMC, LE grade) gels prepared in 0.5X TBE and run in the same buffer (13). After running, gels were stained in a 2μg/ml ethidium bromide solution for 30 minutes and DNA was visualized with a UV transilluminator (Spectroline) at 310 nm.

RESULTS AND DISCUSSION

RP4-based plasmids have previously been introduced into *Acidiphilium facilis* by conjugation and electroporation (14-16). Plasmids based on RP4 belong to the incompatibility group, IncP1. In order to determine whether plasmids from other incompatibility groups were stably maintained in *A. facilis*, we obtained the plasmids pSUP104 (IncQ) and pUCD615 (IncW). These plasmids were introduced into the mobilizing *Escherichia coli* strain, S17.1 (17). When compared with the mobilization of pRK415 (ca. 1 x 10^{-5} transfers/recipient), transfer of pSUP104 and pUCD615 are much less efficient, with frequencies of transfer on the order of 10^{-9} and 10^{-8} per recipient, respectively.

Acidiphilium spp. contain numerous plasmids of varying sizes, whose functions are unknown (14-16). Conjugation functions could be readily assayed for by monitoring the ability of these strains to mobilize broad-host range plasmids to other acidophiles. The identification of such plasmid(s) would be of great interest, since it would be expected that such transfer could occur at acid pH,

allowing the horizontal transfer of genetic information, not only between acidiphilia, but between other acidophiles as well, including *Thiobacillus ferrooxidans*, which has been demonstrated to possess mobilizable, broad-host range plasmids (18, 19). The discovery of such a genetic transfer mechanism in acidophilic bacteria might allow the exploitation of such a process for genetic manipulation of these bacteria.

Acidiphilium strains PW2, CM9, and CM9A harboring the mobilizable plasmid, pRK415 (20, 14-16) were mated with rifampicin-resistant mutants PW1, PW2 and AWB. Very low frequencies of plasmid mobilization were observed, although PW2(pRK415) and CM9A(pRK415) donors gave rise to some 50 colonies in two instances (Table 2). Owing to the number of spontaneous Rf/Tc double mutants arising from CM9A (data not shown), there is some question as to whether these are legitimate transconjugants. However, in the case of the PW2 donor, no spontaneous Rf/Tc mutants were observed, and subsequent analysis of the putative transconjugants revealed the presence of the mobilized plasmid. Genomic fingerprinting experiments are underway to further verify that the transconjugants are derived from the recipient strains used, and not some other class of donor mutant.

As part of our goal to establish techniques for genetic manipulation of *T. ferrooxidans* and *Acidiphilium*, we are constructing vector plasmids using native plasmids. A 2.1 kilobase (kb) plasmid was isolated from *T. ferrooxidans* strain A6. This plasmid, designated pTfA6, was originally cloned in pBR322, and subsequently, subcloned into pUC128, taking advantage of a unique Hind III site. The orientation of restriction sites in this plasmid on a circular map is shown in Figure 1. The Hind III fragment containing the A6 plasmid DNA was clone *in toto* into pLVC18, a mobilizable pBR322 derivative (G. Warren, unpublished results). This construct is being used to examine the ability of a *Thiobacillus* origin of replication to function in other acidophiles, namely, *Acidiphilium*. The chimeric plasmid, pIRC4, was introduced into *E. coli* strain S17.1 and subsequently mobilized into *A. facilis* PW2. 19 putative transconjugants arose from this mating. Since pLVC18 does not possess a broad-host range origin of replication, we must assume that the origin of replication resident on the A6 plasmid is functioning in *Acidiphilium*. It should be noted that several *T. ferrooxidans* plasmids have previously been shown to replicate in *E. coli*, *Pseudomonas aeruginosa* and *T. novellus* (18, 19).

CONCLUSIONS

In our continuing efforts to develop genetic methodologies for manipulating acidophilic bacteria which are useful in the biological desulfurization of coal, we have discovered evidence for conjugative plasmids in *Acidiphilium*. The presence of such plasmids in acidophiles suggests that horizontal transfer of genetic information occurs naturally, and these plasmids may provide a suitable vehicle for the introduction of desirable traits into these bacteria.

In addition, an examination of the relative transfer frequencies of various plasmids of different incompatibility groups appears to indicate that IncP1-based vectors are the vehicles of choice when introducing exogenous genetic material into *Acidiphilium*.

ACKNOWLEDGEMENTS

This work was supported under contract No. DE-AC07-76IDO1570 from the U.S. Department of Energy to the Idaho National Engineering Laboratory/EG&G Idaho, Inc.

REFERENCES

1. Dugan, P. 1986. *Proceedings, Biological Treatment of Coal,* Herndon, VA, pp65-82, U.S. Department of Energy

2. Dugan, P. 1985. *Processing and Utilization of High Sulfur Coals,* Y.A. Attia, ed., pp717-726, Elsevier, New York, NY

3. Bos, P., T.F. Huber, C.H. Kos, C. Ras and J.G. Kuenen. 1986. *Fundamental and Applied Biohydrometallurgy,* R.W. Lawrence, R.M.R. Branion and H.G. Hubner, eds. Vancouver, BC, Canada, pp129-150, Elsevier, Amersterdam

4. Uhl, W., H.-J. Hone, M. Beyer and J. Klein. 1989. *Biotechnol. Bioengineer.* **34**, 1341-1356

5. Detz, C.M. and G. Barvinchak. 1979. *Mining Congr. J.* **65**, 75-86

6. Orsi, N., G. Rossi, P. Trois, P.D. Valenti and A. Zecchin. 1989. *Bioprocessing of Fossil Fuels Workshop,* Tyson's Corner, VA, CONF-890884, P.E. Bayer, ed., pp182-207, U.S. Department of Energy

7. Zarubina, A.M., N.N. Lyalikova and E.I. Shmuk. 1959. *Izvest. Akad. Nauk. SSSR Oteld. Tekh. Nauk. Me i Toplivo* 1, 117-119

8. Silverman, M.P., M.H. Rogoff and I. Wender. 1963. *Fuel* **42**, 113-124

9. Beier, E. 1985. *First International Conference on Processing and Utilization of High Sulfur Coals,* Columbus, OH, pp653-672, Elsevier, Amsterdam

10. Wichlacz, P.L. and R.F. Unz. 1981. *Appl. Environ. Microbiol.* **41**, 1254-1261

11. Miller, J. H. 1972. *Experiments in Molecular Genetics,* pp82-83, Cold Spring Harbor Laboratory, Cold Spring Harbor, NY

12. Birnboim, H.C. and J. Doly. 1979. *Nucl. Acids. Res.* **1**, 1513-1523

13. Maniatis, T., E.F. Fritsch and J. Sambrook. 1982. *Molecular Cloning: A Laboratory Manual,* Cold Spring Harbor Laboratory, Cold Spring Harbor, NY.

14. Roberto, F.F., A.W. Glenn, M.L. Rowland, C.S. Watkins, D.F. Bruhn, D. Bulmer and T.E. Ward. 1989. *Bioprocessing of fossil fuels workshop,* Tyson's Corner, VA, CONF-890884, pp267-287, U.S. Department of Energy

15. Roberto, F.F. , A.W. Glenn and T.E. Ward. 1989. *Biohydrometallurgy '89*, EMR CanMet, U.S. Bureau of Mines, U.S. Department of Energy, Jackson, WY *Submitted for publication*

16. Ward, T.E. , A.W. Glenn, M.L. Rowland , C.S. Watkins, D.F. Bruhn, D. Bulmer and F.F. Roberto. 1989. Pittsburg Coal Conference, Pittsburgh, PA *Submitted for publication*

17. Simon, R., U. Priefer and A. Puhler. 1983. *Biotechnol.* **1**, 784-791

18. Rawlings, D.E. and D.R. Woods. 1988. *Recombinant DNA and Bacterial Fermentation*, J.A. Thomson, ed., pp.277-296, CRC Press, New York, NY

19. Woods, D.R., D.E. Rawlings, M E. Barros, I.M. Pretorius and R. Ramesar. 1986. *Biotechnol. Appl. Biochem.* **8**, 231-241

20. Keen, N.T., S. Tamaki, D. Kobayashi and D. Trollinger. 1988. *Gene* **70**, 191-197

21. Priefer, U.B., R. Simon and A. Puhler. 1985. *J. Bacteriol.* **163(1)**, 324-330

22. Rogowsky, P.M., T.J. Close, J.A. Chimera, J.J. Shaw and C.I. Kado. 1987. *J. Bacteriol.* **169(11)**, 5101-5112

TABLE 1. Bacterial strains and plasmids used in this study

Strain or plasmid	Genotype	Source or reference
Acidiphilium strains		
PW2		10
PW2-Rf	Rf	This study
CM9		D. Thompson
CM9A		D. Thompson
AWB-Rf	Rf	10, This study
PW1-Rf	Rf	10, This study
E. coli strains		
S17.1	*pro res*$^-$ *mod*$^+$ *rec*A RP4-2-Tc::Mu-Km::Tn7	17
Plasmids		
pRK415	*ori*RK2 Tc^r 10.5 kb	20
pLVC18	*ori*pBR322 RSF1010 *mob bom* Tc^r Ap^r 5.9 kb	G. Warren
pSUP104	*ori*p15A *ori*RSF1010 Tc^r Cm^r 9.5 kb	21
pUCD615	*lux* promoter probe, *ori*pSa *ori*pBR322 Ap^r Km^r 17.55 kb	22
pTfA6	Cryptic *T. ferrooxidans* plasmid, 2.1 kb	This study

TABLE 2. Transfer frequency of pRK415 between acidophilic heterotrophs (per recipient)

Donor (pRK415)	Recipient (Rf-resistant)		
	AWB	PW1	PW2
CM9	0	8.55×10^{-9}	1.57×10^{-8}
CM9A	3.65×10^{-7}	0	5.51×10^{-8}
PW2	6.41×10^{-9}	4.27×10^{-7}	1.57×10^{-8}

Figure 1. Restriction map of *T. ferrooxidans* plasmid TfA6

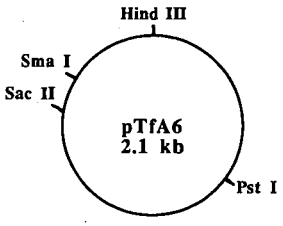

PRODUCTION OF BUTANOL AND ETHANOL FROM SYNTHESIS GAS VIA FERMENTATION

R. M. Worden[1,2], A. J. Grethlein[1,2], M. K. Jain[1], and R. Datta[1]

[1]Michigan Biotechnology Institute
P.O. Box 27609
3900 Collins Road
Lansing, MI 48909

[2]Department of Chemical Engineering
Michigan State University
East Lansing, MI 48824

Keywords: Carbon monoxide, Fermentation, Butyribacterium methylotrophicum

INTRODUCTION

Development of alternative liquid fuels based on raw materials other than petroleum would benefit the U.S. both economically, by reducing the trade deficit, and strategically, by reducing U.S. dependence on politically unstable oil exporters. The 1987 D.O.E. report entitled "Energy Security--a Report to the President" concluded that if present trends continue, the U.S. is likely to become far more dependent on the Persian Gulf for oil and that "The most promising technological opportunities for further reductions in oil consumption rest in the development of alternative fuel systems." Indirect coal liquefaction could provide such alternative fuels. In this process coal is first thermally converted to synthesis gas, consisting primarily of carbon monoxide (CO) and hydrogen (H_2). The gas is then catalytically reacted to form liquid fuels, such as mixed alcohols.

The catalytic gas-conversion step is subject to several processing problems. First, sulfur contaminants found in the synthesis gas, primarily hydrogen sulfide (H_2S) and carbonyl sulfide (COS), are potent catalyst poisons. The sulfur-gas content of coal-derived gases varies considerably, but is typically in the range of a few percent (TRW, 1980). These gases must be removed in energy-intensive purification steps that add significantly to the product costs, particularly for coals having a high sulfur content (Wilson et al., 1988). Second, catalytic processing of synthesis gas often requires strict CO/H_2 ratios to maintain a particular product mix, necessitating gas recompression and shift reaction conversion operations. Third, the gas-phase reactors operate at high temperatures and pressures. Operation under extreme conditions increases reactor costs and presents potential safety issues. Fourth, the product specificity of the catalysts is often poor, resulting in a broad product spectrum, decreased product yield, and increased separations difficulties. In some cases, hazardous or environmentally unacceptable by-products may also be produced.

Biological conversion of synthesis gas offers some key advantages over catalytic routes. Sulfur-gas removal will not be required. With sulfur-tolerant microorganisms, the H_2S and COS gases will pass through the process as inert components. Thus, the capital and operating costs associated with conventional gas separation and upgrading equipment could be avoided. Because the CO/H_2 ratio is not a key factor in biological conversion, gas-shift operations would be unnecessary. Also, biological reactions have evolved to operate efficiently at relatively low temperatures and pressures--at least an order of magnitude less than in conventional gas-phase catalysis. The milder processing conditions may reduce both operating and capital costs. Finally, biological catalysts are typically more specific than their inorganic counterparts. Consequently, few by-products result from synthesis gas fermentations, and no hazardous or xenobiotic fermentation by-products are expected.

The recent discovery of microbial pathways to directly convert CO to useful products such as butanol, ethanol, butyric acid and acetic acid provides significant new capabilities for biological processing of synthesis gas. The purpose of this paper is to summarize the novel pathways and fermentation patterns we have discovered in the anaerobe Butyribacterium methylotrophicum and to discuss their impact on the feasibility of producing butanol and ethanol by fermentation of synthesis gas.

ANAEROBIC BIOCONVERSION OF 1-CARBON COMPOUNDS

Numerous microorganisms are capable of metabolizing 1-carbon compounds such as CO, methanol, and CO_2. Those able to grow on 1-carbon compounds as the sole carbon and energy source are referred to as unicarbonotrophs. This trait is desirable for commercial synthesis gas bioconversions, because no additional organic feedstock would be required as a co-substrate. Anaerobic bioconversion is also preferable to aerobic, because in anaerobic fermentation no electrons are lost to molecular oxygen. Thus, the chemical energy content of the gas is efficiently conserved in the products. Two groups of unicarbonotrophic, anaerobic bacteria, acidogens and methanogens, can use 1-carbon compounds or acetate as energy sources. Acidogens convert 1-carbon compounds to fatty acids such as acetate and butyrate, while the methanogens produce methane (Zeikus, 1983).

The metabolism of homo-acetogens is characterized by synthesis of the intermediate acetyl-CoA from either heterotrophic or unicarbonotrophic modes of growth (Zeikus, 1983). Clostridium thermoaceticum generally ferments hexose or pentose to acetate (Fontaine, et al., 1942), but C. thermoaceticum type strain Fontaine can also grow readily on H_2/CO_2. It can also be adapted to grow on CO as an energy source. However, this organism is not able to utilize methanol (Kerby and Zeikus, 1983). Peptostreptococcus productus strain U-1 is also capable of growth and production of acetate on either CO or H_2/CO_2 (Lorowitz and Bryant, 1984). Similarly, Acetobacterium woodii ferments H_2/CO_2, glucose, lactate, formate (Balch, et al., 1977) and can grow on CO after adaptation (Kerby et al., 1983). This species also ferments methanol or cleaves and ferments the methoxyl moieties from a variety of aromatic acids (Balch, et al., 1977). Clostridium ljungdahli is able to co-metabolize CO and H_2 to form acetate and ethanol (Clausen and Gaddy, 1988).

Butyribacterium methylotrophicum is a unique microorganism capable of growing on multicarbon compounds (glucose, lactate, or pyruvate) as well as 1-carbon compounds (H_2/CO_2, formate or methanol) (Zeikus, et al., 1980; Lynd and Zeikus, 1983). A strain of B. methylotrophicum (designated the CO strain) was adapted to grow with a 12 h doubling time on 100% CO, producing acetate and minor amounts of butyrate (Datta, 1982; Lynd et al., 1982). Eubacterium limosum appears to be similar to B. methylotrophicum in general fermentation properties, including the ability to ferment methanol or CO (Sharak-Genthner and Bryant, 1982; Sharak-Genthner, et al., 1981). However, E. limosum requires adaptation and utilization of methanol and needs rumen fluid, yeast extract or acetate in the medium (Sharak-Genthner and Bryant, 1987). Moreover, it produces copious amounts of slime (Sharak-Genthner et al., 1981).

Recently, we have discovered unique metabolic properties of the CO strain of B. methylotrophicum that greatly enhance the prospect of commercially feasible synthesis gas fermentations. In extended batch fermentations, where 100% CO was continuously sparged as the sole carbon and energy source, pH was found to strongly influence the relative amounts of acetate and butyrate produced from CO. By decreasing the pH from 6.8 to 6.0, the fraction of electrons from CO going into butyrate was increased from 6% to 70% at the expense of acetate production (Worden et al., 1989). This finding was significant in that it demonstrated the synthesis of a 4-carbon organic acid from a 1-carbon, inorganic substrate. High levels of butyrate are desirable for the production of butanol in a two-stage

synthesis gas fermentation, as discussed below. In continuous-culture experiments using a 100% CO gas sparge, small quantities of butanol and ethanol were produced in addition to butyrate and acetate (Grethlein et al., in press). This discovery represented the first evidence of a direct microbial pathway for butanol production from CO.

In both batch and continuous-culture experiments with B. methylotrophicum, we have consistently observed a trend toward production of more reduced products (acids with longer chain lengths and alcohols) as the fermentation pH is reduced. This trend is evident in the steady-state fermentation carbon balances shown in Table 1 (Grethlein et al., in press). This pH effect provides a potential mechanism by which the product spectrum of CO fermentations may be manipulated to give either high acid or alcohol yields, depending on the fermentation objectives.

Although the pathways and stoichiometries obtained from the batch and continuous CO fermentations were promising, both the volumetric reactor productivities and the product concentrations were low. To increase these parameters, additional continuous-culture experiments were conducted using a microfiltration-based, cell recycle system. Details of the experimental system have been described elsewhere (Grethlein et al., manuscript submitted). Results to date have been encouraging. Five- to 20-fold increases in cell and product concentrations have been observed relative to continuous culture without cell recycle, and the system has been operated for more than 5 weeks at a time without significant membrane fouling.

SOLVENT PRODUCTION BY CLOSTRIDIUM ACETOBUTYLICUM

Acetone, butanol, and ethanol (ABE) were produced commercially via fermentation of glucose by Clostridium acetobutylicum from World War I until the 1950's. This batch fermentation follows a biphasic pattern (Weizmann, 1918). During the initial, acidogenic phase, growth is exponential, and organic acids (acetic and butyric) and H_2 are the primary products. After accumulation of a certain concentration of acids, the pH decreases to approximately 4.5, and the fermentation switches to the solventogenic phase, where the organic acids are reduced to solvents, the rate of H_2 gas production decreases, and cell growth ceases. Early attempts to induce C. acetobutylicum to take up acids for alcohol production indicated that a concentration of butyric acid higher than 2 g/L inhibited the solvent production (Soni et al., 1982). More recently, it has been shown that acids concentration in the first stage is a determinant factor for solvent production in the second stage of a two-stage continuous fermentation (Godin and Engasser, 1989).

Continuous cultures of C. acetobutylicum may be maintained in either the acidogenic or the solventogenic phase by manipulating the fermentation conditions. A generally observed trend is that higher pH values are associated with acid production, and lower pH values favor solvent production (Kim and Zeikus, 1985). Meyer et al. (1986) found that CO gasing led to continuous butyrate uptake and solvent production without the production of acetone. Extremely high specific butyrate uptake rates and butanol production rates were measured during this CO challenge. These trends were attributed to altered electron flow arising from CO inhibition of production hydrogenase activity. During acidogenesis, excess electrons are typically eliminated by H_2 formation. Because this reaction was inhibited by CO, electron flow to other products had to be increased. Acetone formation does not consume electrons, so the cellular control mechanisms shut off carbon flow to acetone, and increased carbon flow to electron-consuming alcohol production.

ENERGETICS OF ACID AND ALCOHOL PRODUCTION FROM CO

The $\Delta G^{0\prime}$ values for production of acids and alcohols from CO, shown in Table 2, were calculated using published free energy of combustion data (Roels, 1983).

The values for butyrate and acetate production are approximately the same, and only slightly higher than those for butanol and ethanol production. All four reactions are sufficiently exergonic to drive ATP synthesis. However, it is not currently known whether metabolic mechanisms exist in B. methylotrophicum for net ATP synthesis during direct conversion of CO to alcohols. Acetyl CoA and butyryl CoA are thought to be intermediate branch points from which either acids or alcohols may be produced. Acid production generates ATP but consumes no electrons, whereas alcohol production consumes electrons but produces no ATP. Consequently, the cells can replenish energy reserves via acid production and eliminate excess electrons via alcohol production. If no net ATP is generated via alcohol formation, then alcohols must be produced either in the absence of growth or concurrently with acid formation. Further research is needed to elucidate the mechanisms for energy flow within B. methylotrophicum under these fermentation conditions.

PROPOSED PROCESSES FOR SYNTHESIS GAS BIOCONVERSION TO BUTANOL AND ETHANOL

Single-stage Fermentation Process

A proposed single-stage fermentation process is shown in Figure 1. In this process, CO and H_2 would be fed to a bioreactor containing B. methylotrophicum, in which the fermentation conditions were optimized for solventogenesis. Our previous results indicate that growth and alcohol production are metabolically uncoupled, and that a reduction in pH may be used to trigger solventogenesis. Thus, the fermenter could be operated batchwise, with a pH shift at the onset of the stationary phase (Worden et al., 1989). Alternatively, the fermenter could be operated continuously, using pH oscillations to allow alternate periods of alcohol production and cell regeneration. In either case, the product stream would be sent to a separation unit for selective removal of the alcohols, and the acids would be recycled to the reactor for further conversion. Either cell recycle or cell immobilization would be used to maintain high reactor cell densities.

This single-stage process appears to be technologically feasible, based on preliminary fermentations using 100% CO as the gaseous feedstock. At a pH of 5.5, transient butanol concentrations as high as 2.7 g/L have been achieved in continuous culture using cell recycle (Grethlein et al., manuscript submitted). By comparison, butanol concentrations from commercial ABE fermentations were approximately 16 g/L. Thus, even before process and strain optimization, CO fermentation yields are within an order of magnitude of the maximum butanol concentration produced by C. acetobutylicum from glucose.

Ideally, the reducing equivalents needed to convert acetic and butyric acids to the respective alcohols would come from H_2 in the synthesis gas. B. methylotrophicum is known to take up and metabolize H_2 and CO_2 to form primarily acetate (Lynd and Zeikus, 1983). However, the effects of factors such as the presence of CO and fermentation pH on this reaction are unknown. Carbon monoxide is a potent inhibitor of production hydrogenase in C. acetobutylicum (Kim et al, 1984), but its effect on the uptake hydrogenase of B. methylotrophicum is not known. Fermentation experiments using a mixture of H_2 and CO are currently underway in our laboratory to determine these effects. Even if hydrogen uptake is inhibited by CO, it may be possible to substitute other metabolizable electron donors, such as glucose. This substitution should not greatly affect the process economics, because only a small amount of the electron donor would be required. On a combustion energy basis, 83% of the butanol energy content would come from CO, and only 17% would come from the secondary electron donor.

Two-Stage Fermentation Process

The flowsheet of a proposed 2-stage fermentation process is shown in Figure 2. In the first, acidogenic stage, CO would be converted to primarily butyric

and acetic acids using an acidogenic culture of B. methylotrophicum. Results to date suggest that B. methylotrophicum is quite well suited for this application. Using fermentation conditions appropriate for acidogenesis, butyrate and acetate concentrations of 4 g/L and 8 g/L, respectively, have been achieved in steady-state, continuous operation with cell-recycle (Grethlein et al., manuscript submitted). Future strain development efforts should increase these values even further. The acids produced in the first stage would then be combined with H_2 from the synthesis gas (or some other electron donor) in the second stage to yield butanol and ethanol. Two alternative biocatalysts are currently under investigation for use in the second stage: C. acetobutylicum and B. methylotrophicum. C. acetobutylicum has been studied much more extensively and thus has better characterized enzymes and metabolic-regulation mechanisms. It is capable of producing high concentrations of mixed solvents when grown on glucose, and can also take up externally added acids and H_2 for solvent production. When grown in a glucose-limited chemostat in the presence of CO, H_2 and acetone formation are inhibited, while butyrate uptake and butanol production are increased to extremely high levels (Meyer et al., 1986). These effects are beneficial, since production of H_2 and acetone reduces alcohol yields. Thus, it may be possible to use residual CO from the first stage to improve alcohol yields in the second stage.

The solventogenic capability of B. methylotrophicum was discovered in our laboratory only recently (Grethlein et al., in press), and it has not yet been well characterized. Results to date have included transient butanol concentrations as high as 2.7 g/L in continuous operation using cell recycle. Ongoing investigations include characterization of enzyme-regulation mechanisms, and capacity for H_2 and acid assimilation.

As indicated in Figure 2, bioreactors for both stages will utilize either cell recycle or immobilization to maintain high cell concentrations. The product stream from the solventogenic bioreactor will be stripped of alcohols in a separation unit and then recycled to the first stage.

FUTURE PROSPECTS FOR BIOCONVERSION OF SYNTHESIS GAS TO BUTANOL AND ETHANOL

Two basic problems with the classic ABE fermentation using C. acetobutylicum were identified in a report to the Office of Technology Assessment entitled "Biological Production of Liquid Fuels and Chemical Feedstocks" (Humphrey and Nolan, 1979): the formation of multiple products, requiring additional recovery steps, and the low solvent yields (34 g/100 g fermentable sugar). Our results to date indicate that these problems may not be as severe for the unique synthesis gas fermentation processes proposed here, as described below.

Acetone production by B. methylotrophicum has never been observed. It is currently unknown whether the enzymes necessary for acetone production from acetoacetyl CoA (e.g., phosphate acetoacetyltransferase, acetoacetate kinase and acetoacetate decarboxylase) are lacking in B. methylotrophicum, or whether one or more of these enzymes may be under strong regulation by CO. In the proposed two-stage process, where C. acetobutylicum is used in the solventogenic stage, the presence of CO has been shown to block acetone production while enhancing butanol production to the highest levels ever reported (Meyer et al., 1986). Thus, it appears possible to avoid undesirable acetone formation.

Despite extensive strain-development and optimization efforts, ABE fermentations using C. acetobutylicum are presently unable to achieve high electron recovery in butanol and ethanol. An improved process for ABE production from corn starch using an efficient, asporogenous mutant and stillage recycle was recently described by Marlatt and Datta (1986). In this process, only 63% of the electrons from the glucose ends up in the alcohols, and 31% ends up in H_2 and acetone. For our proposed process using C. acetobutylicum in the solventogenic bioreactor, the presence of CO may block or reduce unwanted production of H_2 and

acetone, maximizing electron capture in alcohols. Less is known about the electron-capture efficiency of B. methylotrophicum. Using carbon and electron balances (Erickson and Oner, 1983), we have estimated that in recent continuous fermentation experiments using cell recycle, as much as 44% of the electrons from CO has been transferred to butanol (Grethlein et al., manuscript submitted). The butanol concentration measured during this time was 2.7 g/L. However, because these data were not measured at steady-state, they should only be taken as suggestive that high electron capture efficiency in alcohols appears possible with B. methylotrophicum.

The unique metabolic capabilities for CO conversion found in B. methylotrophicum indicate its potential for production of butanol and ethanol from synthesis gas in either a 1- or 2-stage fermentation system. In addition, the CO-induced enhancement of acid uptake and butanol production in C. acetobutylicum make this species well-suited for assimilation of H_2 and acids in the second, solventogenic stage. Research to better understand the complex metabolic regulation patterns of these two species is continuing in our laboratory. Successful manipulation of carbon and electron flow in these cultures could make bioconversion of synthesis gas to butanol and ethanol a commercial reality.

ACKNOWLEDGMENT

This research was supported by the U.S. Department of Energy, under Contract No. 22-88PC79815.000. Fellowship support for A. J. Grethlein was provided by the Michigan Biotechnology Institute.

REFERENCES

Balch, W. E., S. Schoberth, R. S. Tanner and R. S. Wolfe. (1977) Int. J. of Syst. Bacteriol. 27:355.

Clausen, E. C. and J. L. Gaddy (1988) Proc. of Indirect Liquefaction Contractors Review Meeting for U.S. D.O.E., Pittsburgh Energy Technology Center, 639-670.

Datta, R. (1982) Biotech. and Bioeng. Symp. 11:521-532.

Erickson, L. E. and M. D. Oner. (1983) Ann. N.Y. Acad. Sci. 413:99.

Fontaine, F. E., W. H. Peterson, E. McCoy, E. Johnson and M. T. Titter. (1942) J. Bacteriol. 43:704.

Godin, C. and J. M. Engasser. (1989) Biotechnol. Lett. 12:903-906.

Grethlein, A J. (1989) M. S. Thesis, Dept. of Chemical Engineering, Michigan State University, East Lansing, Michigan.

Grethlein, A. J., R. M. Worden, M. K. Jain and R. Datta. 1990. Appl. Biochem. Biotechnol. 24/25 (in press).

Humphrey, A. E. and E. J. Nolan (1979) Biological Production of Liquid Fuels and Chemical Feedstocks, Report to U.S. Office of Technology Assessment, 5-7.

Kerby, R., W. Niemczura and J. G. Zeikus. (1983) J. Bacteriol. 155:1208-1218.

Kerby, R. and J. G. Zeikus. (1983) Curr. Microbiol. 8:27-30.

Kim, B. H., P. Bellows, R. Datta and J. G. Zeikus. (1984) Appl. Environ. Microbiol. 48, 4,764-770.

Kim, B. H. and J. G. Zeikus. (1985) Dev. Ind. Microbiol. 26:549-556.

Lorowitz, W. H. and M. P. Bryant. (1984) Appl. Environ. Microbiol. 47:961-964.

Lynd, L. H., R. Kerby and J. G. Zeikus. (1982) J. Bacteriol. 149:255-263.

Lynd, L. H. and J. G. Zeikus. (1983) J. Bacteriol. 153:1415-1423.

Marlatt, J. A. and R. Datta. (1986) Biotechnol. Progress, 2,1, 23-28.

Meyer, C. L., J. W. Roos and E. T. Papoutsakis. (1986) Appl. Microbiol. Biotechnol. 24:159-167.

Roels, J.A. (1983) Energetics and Kinetics in Biotechnology, Elsevier, New York, 40.

Sharak-Genthner, B. R., C. L. Davis and M. P. Bryant. (1981) Appl. Environ. Microbiol. 42:12-19.

Sharak-Genthner, B. R. and M. P. Bryant. (1982). Appl. Environ. Microbiol., 43:70-74.

Sharak-Genthner, B. R. and M. P. Bryant. (1987) Appl. Environ. Microbiol., 53:471.

Soni, B. K., K. Das and T. K. Ghose. 1982. Biotechnol. Lett. 4:19-22.

TRW (1980) Development Status of Key Emerging Gasification Systems, TRW Report, Sept., 1980.

Weizmann, C. (1918) U. S. Patent #1,315,585.

Wilson, J. S., J. Halow and M. R. Ghate. (1988) Chemtech. Feb. 1988, 123-128.

Worden, R. M., A. J. Grethlein, J. G. Zeikus and R. Datta. (1989) Appl. Biochem. Biotech. 20/21:687-698.

Zeikus, G. Z. (1983) Adv. Microb. Physiol. 24:215-297.

Zeikus, J. G. (1980) Ann. Rev. Microbiol. 34:423-464.

Zeikus, J. G., L. H. Lynd, T. E. Thompson, J. A. Krzycki, P. J. Weimer and P. Hegge. 1980. Curr. Microbiol. 3:381-386.

Table 1. Influence of pH on Steady-State Fermentation Stoichiometry of Butyribacterium methylotrophicum (Source: Grethlein et al., in press)

pH	Fermentation Stoichiometry*
6.8	$4CO \longrightarrow 2.09\ CO_2 + 0.63\ Ac + 0.043\ Bu + 0.027\ EtOH + 0.43\ Cells$
6.5	$4CO \longrightarrow 2.13\ CO_2 + 0.56\ Ac + 0.082\ Bu + 0.026\ EtOH + 0.37\ Cells$
6.0	$4CO \longrightarrow 2.27\ CO_2 + 0.30\ Ac + 0.161\ Bu + 0.032\ EtOH + 0.029\ BuOH + 0.31\ Cells$

Table 2. Standard Free Energies of Reaction for CO Bioconversion

Reaction Stoichiometry*	$\Delta G^{0'}$ (kcal/gmole CO)
$10\ CO + 4\ H_2O \longrightarrow Bu + 6\ CO_2$	- 9.7
$4\ CO + 2\ H_2O \longrightarrow Ac + 2\ CO_2$	- 9.8
$12\ CO + 5\ H_2O \longrightarrow BuOH + 8\ CO_2$	- 9.0
$6\ CO + 3\ H_2O \longrightarrow EtOH + 4\ CO_2$	- 8.1

*Ac, Bu, EtOH, and BuOH stand for acetic acid, butyric acid, ethanol, and butanol, respectively. The coefficient on cells represents the number of moles of carbon contained in the cells mass.

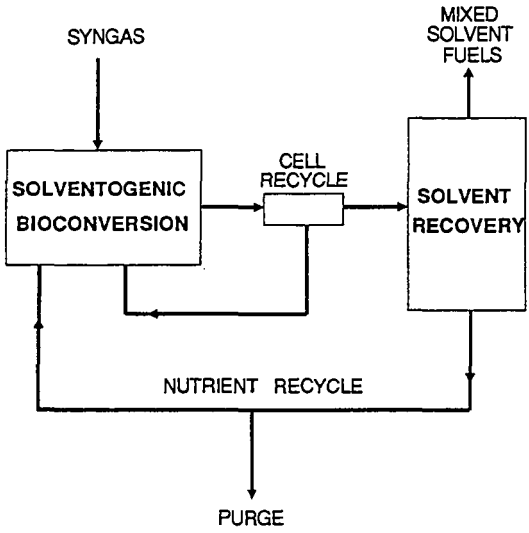

Figure 1. One-Stage Fermentation Process for Synthesis-Gas Bioconversion

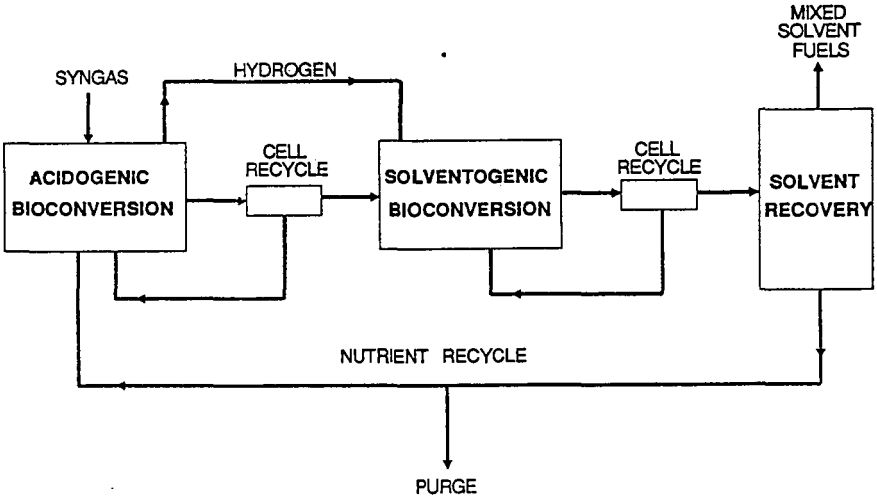

Figure 2. Two-Stage Fermentation Process for Synthesis-Gas Bioconversion

BIOREACTOR DESIGN FOR SYNTHESIS GAS FERMENTATIONS

K. T. Klasson, M. D. Ackerson, E. C. Clausen, and J. L. Gaddy
Department of Chemical Engineering
University of Arkansas
Fayetteville, AR 72701

ABSTRACT

Fermentation of slightly soluble gaseous substrates, such as CO and H_2, requires the transport of the substrate from the gas phase, through the liquid phase, and into the solid phase for conversion. These reactions are generally mass transport limited, and bioreactor designs must achieve high mass transfer coefficients, as well as high cell concentrations, to minimize reactor volume. Immobilized cell systems are ideal for these fermentations, and operation at high pressure facilitates gas solubility and faster mass transfer. This paper compares the performance of a continuous stirred tank reactor, a bubble column reactor, and a trickle-bed reactor for the conversion of CO, CO_2, and H_2 in coal synthesis gas into methane using a tri-culture of Rhodospirillum rubrum, Methanobacterium formicicum, and Methanosarcina barkeri. R. rubrum is a photosynthetic bacterium, and special provisions for supplying light for growth of this organism are necessary. Mass transfer coefficients are compared and intrinsic kinetics presented. Gas retention times of a few minutes have been achieved for complete conversion of the gaseous substrate.

INTRODUCTION

Synthesis gas, a mixture of primarily CO, H_2 and CO_2, is a major building block in the production of fuels and chemicals. The gas may be produced from several sources, including coal, oil shale, tar sands, heavy residues, biomass or natural gas. Most synthesis gas is produced today by catalytic reforming of natural gas, although the partial oxidation of heavy liquids is also practiced (Graboski, 1984). Only a small percentage of the synthesis gas currently produced is by gasification of solid fuel. However, because of the large reserves of coal in the United States (300 year supply at the current consumption rate (Specks and Klussman, 1982)), synthesis gas production from coal will become an important technology in the future.

Coal gasification, which is a combination of pyrolysis and combustion reactions, (Simbeck *et al.* 1982), produces a gas consisting of more than 50 percent H_2 and CO, the balance being a mixture of CO_2, CH_4, H_2S, COS and nitrogen compounds. The actual composition depends upon process conditions and the coal that is employed. The raw gas has a low to medium Btu content, with a heating value of 160-450 Btu/SCF, depending on whether air or oxygen is used during gasification (Coffin, 1984). Following quenching and purification, the synthesis gas contains 25-35 percent H_2, 40-65 percent CO, 1-20 percent CO_2, 0-7 percent CH_4 and other compounds in small quantities.

Catalytic processes may be used to convert syngas into a variety of fuels and chemicals, such as, methane, methanol, formaldehyde, acetic acid, etc. (Courty and Chaumette, 1978). Microorganisms may also be used to convert synthesis gas components into fuels and chemicals. Biological processes, although generally slower than chemical reactions, have several advantages over catalytic processes, such as higher specificity, higher yields, lower energy costs and generally greater resistance to poisoning. Furthermore, the irreversible character of biological reactions allows complete conversion and avoids thermodynamic equilibrium relationships.

The purpose of this paper is to present data for the development of optimal bioreactor concepts for syngas fermentations. Laboratory data for continuous culture experiments for the conversion of synthesis gas components into methane and ethanol are presented. Various bioreactor schemes for synthesis gas fermentations have been investigated and mathematical models that define intrinsic kinetics and mass transfer relationships are developed. Methods to predict reactor performance and gas retention times for the CSTR and immobilized cell reactor are presented.

SYNTHESIS GAS FERMENTATIONS

Methane Production

Methane may be produced by methanogenic bacteria from either acetate or H_2 and CO_2, both of which may be produced from syngas components. Acetate may be produced by several anaerobic bacteria, including Peptostreptococcus productus, (Barik *et al.* 1987; Lorowitz and Bryant, 1984), Acetobacterium woodii (Kerby *et al.* 1983) Clostridium thermoaceticum (Wood *et al.* 1982; and Kerby and Zeikus, 1982) and Eubacterium woodii (Genthner and Bryant, 1982), which produce acetate by the reaction:

$$4\ CO + 2\ H_2O \rightarrow CH_3COOH + 2\ CO_2 \qquad (1)$$

Among these bacterial species, P. productus utilizes CO very rapidly with a doubling time of less than two hours, and can grow with as much as 90 percent CO in the gas phase (Barik *et al.* 1987).

Many anaerobic bacteria, including P. productus, are known to produce acetate from H_2 and CO_2, (Mayer *et al.* 1977; Sleat *et al.* 1985; and Balch *et al.* 1977), which produces a homoacetic fermentation by anaerobically oxidizing hydrogen and reducing CO_2 according to the equation:

$$4\ H_2 + 2\ CO_2 \rightarrow CH_3COOH + 2\ H_2O \qquad (2)$$

Two species of purple non-sulfur bacteria, Rhodopseudomonas gelatinosa (Uffen, 1976; and Dashkevic and Uffen, 1979) and Rhodospirillum rubrum (Breed *et al.* 1977) are known to perform the water gas shift reaction to produce H_2 as follows:

$$CO + H_2O \rightarrow H_2 + CO_2 \qquad (3)$$

R.gelatinosa grows under strict anaerobic conditions on the dark with CO as the only carbon and energy source, although growth is stimulated by the addition of trypticase. R. rubrum requires tungsten light and the presence of a carbon source other than CO (sugars, acetate, yeast extract etc.) for growth. In comparing these two species, R. rubrum grows faster and reaches higher cell concentrations that uptake CO more rapidly. R. rubrum has also been found to tolerate small amounts of oxygen and sulfur compounds often present in synthesis gas.

Almost all methanogenic bacteria, including Methanospirillum hungatii, Methanobacterium formicicum, Methanobrevibacter smithii, Methanosarcina barkeri, utilize CO_2 and H_2 to produce CH_4 according to (Thauer *et al.* 1977; Balch *et al.* 1979; and Zehnder *et al.* 1981:

$$4\ H_2 + CO_2 \rightarrow CH_4 + H_2O \qquad \Delta G' = -31.3\ \text{Kcal/reaction} \qquad (4)$$

Methane may also be produced from acetate by Methanosarcinaceae sp., such as Methanosarcina barkeri, as well as Methanothrix soehngenii (Jones *et al.* 1987). While Methanosarcine barkeri will utilize acetate only in the absence of other preferred substrates (such as H_2 and CO_2), Methanothrix sp. does not utilize H_2 and CO_2 and growth and methane formation is observed exclusively in the presence of acetate (Huser *et al.* 1982. Both microorganisms show comparable specific growth rates at low acetate concentrations (< 3mM). However, from the Monod saturation constants (K_s = 0.7 mmol/l for Methanothrix and 5 mmol/l for M. barkeri, it is expected that at low acetate concentrations Methanothrix will give faster rates and predominate.

From the above, it can be seen that the production of methane from syngas is a two-step process; formation of the methane precursors (acetate or hydrogen) and the biomethanation of the precursor. These reactions may be carried out in separate stages or as a CO culture in the same reactor. Compatibility of the cultures with substrates and products is essential for an efficient process.

Methane Production from Acetate. In order to product methane from synthesis gas through acetate, CO (and possibly CO_2 and H_2) is first converted to acetate using the bacterium P. productus. The acetate is then reacted to methane using either Methanothrix sp. or M. barkeri.

In order to develop a successful co-culture, both the acetogenic and methanogenic bacteria must have resistance to CO toxicity. Studies of the CO uptake rate with time for P. productus using various initial CO partial pressures showed an increase in the rate of reaction with increasing partial pressure up to a partial pressure of 1.6 atm. At a partial pressure of 2.5 atm, however, the culture failed to utilize the gas after a short initial period of uptake. At 2.5 atm, the dissolved CO concentration reached toxic levels due to insufficient cell mass to keep the reaction mass transfer-limited. Studies have shown that both growth and CO uptake by P. productus are inhibited at dissolved CO tensions above 016-0.8 atm (Vega *et al.* 1989). Higher gas phase CO partial pressures may be employed as long as a sufficient number of cells are present to keep the dissolved CO tension low.

Figure 1 illustrates a gradual stepwise procedure where CO partial pressures as high as 10 atm are successfully employed. The pressure was gradually increased in this study only after the cell concentration increased in order to keep the process mass transfer-limited. The effects of CO on methanogens may be illustrated using the bacterium M. barkeri. The consumption of H_2 with time for M. barkeri at various initial CO partial pressures is shown in Figure 2. As noted, the time for consumption essentially doubled when increasing the CO partial pressure from 0 to 0.59 atm. This result is expected due to the well-known inhibitory effect of CO on hydrogenases. Similar results were obtained for Methanothrix sp. It is thus essential for hydrogen-utilizing organisms such as methanogenic bacteria that a low dissolved CO concentration be maintained.

A second factor in evaluating methane production from synthesis gas through acetate is the potential inhibitory effects of acetate on both P. productus by product inhibition and methanogens by substrate inhibition. It has been found that acetate concentrations of 20-25 g/L may be successfully employed with P. productus without appreciable product inhibition. Figure 3 shows the effect of acetate concentration on methane production by M. barkeri in batch culture. As noted, the methane production increased with increasing acetate concentration up to 6 g/L acetate, with some inhibition noted at the 6 g/L level. At acetate concentrations above 6 g/L, however, methane production was severely inhibited. Similar inhibitory effects were seen with Methanothris sp. where methane production was slowed at 9 g/L acetate and stopped at 12 g/L.

Figure 4 shows the methane productivity in an immobilized cell reactor (ICR) employing Methanothrix sp. at various feed acetate concentrations. The column was operated over a period of nearly 250 days by gradually increasing the inlet acetate concentration and flow rate as cell growth allowed. As noted in the figure, a maximum inlet acetate concentration of 10 g/L was successfully employed at a methane productivity of 5 VVD. Further increases in the acetate concentration were not possible, even with the simultaneous addition of high concentrations of yeast extract. Thus, comparitively low productivities, even in an ICR, result for methane production from acetate.

Co-culturing of P. productus and methanogens utilizing acetate was not found feasible due to the slow rate of growth and low acetate tolerance of methanogens. P. productus totally dominated the co-cultures, producing acetate much faster and in higher concentrations than the methanogens were capable of utilizing. The methanogens were thus inhibited by acetate and the co-culture could not be sustained. The production of methane through acetate will, therefore, require separate reaction vessels.

Methane Production from H_2 and CO_2. An alternative route involves the conversion of CO and H_2 by R. rubrum, followed by conversion of all the H_2 and CO_2 to methane using either M. formicicum or M. barkeri. It has been found that H_2 production by R. rubrum is essentially unaffected by CO partial pressures up to 2.0 atm. Therefore, as with P. productus, the limiting factor in CO utilization by R. rubrum is the ability to maintain a high cell concentration and, consequently, a low dissolved CO tension in the liquid phase. M. formicicum has been shown to be able to uptake H_2 and CO_2 to produce methane much faster than M. barkeri. However, in order to form a successful co-culture, M. formicicum must be able to tolerate low levels of dissolved CO. The utilization of H_2 by M. formicicum in the presence of various CO partial pressures is shown in Figure 5. As noted, nearly complete inhibition of H_2 uptake was found at a CO partial pressure of only 0.76 atm. the inhibition of CO on M. barkeri might enable a rapid rate of uptake of H_2.

R. rubrum is a photosynthetic bacteria requiring tungsten light for growth, but not for CO uptake. Figure 6 shows the growth and consumption of CO with time at various light intensities for R. rubrum. As shown, the cell growth rate increased with light intensity up to 1490 lux, however, no further enhancement was found at higher intensities. CO consumption was essentially

unaffected by the presence of light. Methanogens have been found to be unaffected by the presence of light.

An experiment was performed in a continuous stirred-tank reactor to study the simultaneous conversion of CO_2 and H_2 directly to CH_4 employing a co-culture of R. rubrum and M. formicicum. Since the organisms have different optimum temperatures, the lower temperature, 30°C, was chosen for study. Figure 7 shows the CH_4 and CO production with time since since start-up in the CSTR. Following a significant period of methanogen acclimation, almost complete conversion of both CO and H_2 occurred after 300 hours of operation. The methane production rate shown in Figure 7 reached a steady-state level after 350 hours of operation of about 1.6 mmole CH_4/hr, which represents a methane yield from CO, and H_2 and CO_2 of about 96 percent of theoretical. The system was operated with a retention time of one hour and stable operation was monitored for several weeks.

Ethanol Production

While many anaerobic, facultatively anaerobic and even some strictly aerobic microorganisms form various amounts of ethanol from glucose (Wiegel, 1980), no organisms were known to form ethanol autotrophically from synthesis gas components. In 1987, a strict anaerobic mesophilic bacterium was isolated that was capable of converting CO, H_2 and cO_2 to a mixture of acetate and ethanol (Barik *et al.* 1987). Identification and characterization studies have shown that the bacterium is a new clostridial species, named Clostridium ljungdahlii, Strain PETC, in honor of Dr. Lars G. Ljungdahl for his work on clostridia and acetogens (Clausen and Gaddy, 1988). C. lungdahlii is a gram-positive, motile, rod-shaped anaerobic bacterium which sporulates infrequently. In addition to synthesis gas components, it is capable of growing on xylose, arabinose and fructose. As with other class I clostridia, it is expected that ethanol and acetate are formed through acetyl-CoA as the central intermediate (Rogers, 1986).

The overall stoichiometry for the formation of ethanol and acetate from CO and H_2/CO_2 has been established as (Vega *et al.* 1989):

$$6\ CO + 3\ H_2O \rightarrow CH_3CH_2OH + 4\ CO_2 \qquad (1)$$
$$\Delta G^\circ = -59.9\ \text{Kcal/reac.}$$

$$2\ CO_2 + 6\ H_2 \rightarrow CH_3CH_2OH + 3\ H_2O \qquad (2)$$
$$\Delta G^\circ = -23.2\ \text{Kcal/reac.}$$

$$4\ CO + 2\ H_2O \rightarrow CH_3COOH + 2\ CO_2 \qquad (3)$$
$$\Delta G^\circ = -37.8\ \text{Kcal/reac.}$$

$$2\ CO_2 + 4\ H_2 \rightarrow CH_3COOH + 2\ H_2O \qquad (4)$$
$$\Delta G^\circ = -18.7\ \text{Kcal/reac.}$$

Under usual laboratory conditions, C. ljungdahlii produces acetate as the major product, with only small quantities of ethanol present in the product stream. Figures 8 and 9 show the acetate and ethanol production profiles as a function of yeast extract concentration. The data show an ethanol/acetate

ratio of only 0.5. It is also noted that yeast extract has an influence on the product ratio, which leads to the hypothesis that high ethanol production is non-growth related. An examination of the acetyl-CoA pathway shows that production of acetate is balanced in ATP, while ethanol production results in a net consumption of ATP which would not support growth of the bacteria. Therefore, studies to minimize acetate production have concentrated upon factors which would not support growth of the bacteria. Therefore, studies to minimize acetate production have concentrated upon factors which regulate the growth of the organism.

Control of Growth Rate Parameters. C. ljungdahlii grows well and produces ethanol and acetate within a pH range of 4-6 with typical anaerobic media. Figure 10 shows the product distribution for Clostridium sp. with various initial yeast extract concentrations in batch culture. As noted, a molar ethanol to acetate ratio of 1:0 was obtained for yeast extract concentrations between 0.005 and 0.05 percent. The normal ratio of 1:22 results under more favorable growth conditions when employing 0.1 and 0.2 percent yeast extract. Studies with a defined medium of only vitamins, minerals and salts showed similar results in increasing the product ratio to about .1.

Recent research has shown that the presence of reducing agents in the liquid media of Clostridium fermentations has brought about an increase in solvent formation (Rao and Muetharsan, 1987; 1988). Reducing agents apparently cause altered electron flow, which direct carbon flow and acid to alcohol production. Reducing equivalents are directed to the formation of NADH which, in turn, resulted in increased alcohol production. Batch experiments were carried out with C. ljungdahlii by adding small quantities of reducing agents (30,50 and 100 ppm) to assess the feasibility of increasing the ethanol to acetate ratio. The experiment carried out with 100 ppm of reducing agents resulted in very limited growth in all cases. On the other hand, 50 ppm and 30 ppm concentrations were successful in improving the ethanol to acetate ratio in some cases, as is shown in Table 1. The experiment with benzyl-viologen at a concentration of 30 ppm produced 3.7 mmol of ethanol with a ratio of 1.1, the highest ratio observed in batch experiments. It is interesting to mention that those reducing agents that improved the product ratio always resulted in slower growth rates of the bacteria, as could be expected from decreased ATP formation.

Table 1. Peak Levels for Ethanol Production and the Molar Ratio (ETOH/ACH at 30 and 50 ppm Reducing Agent Concentrations

	(50 ppm)		(30 ppm)	
Reducing agent	Etoh(mmol)	ETOH/ACH	ETOH(mmol)	ETOH/ACH
Control	0.60	0.12	1.40	0.24
Sodium thioglycolate	1.30	0.20	1.30	0.25
Ascorbic acid	1.50	0.24	1.50	0.25
Menthyl Viologen	1.90	0.20	2.50	0.40
Benzyl Viologen	1.25	0.21	3.70	1.10

Recently, the connection between sporulation and increased solventogenesis has been identified (Jones *et al.*1982; Long *et al.* 1984; Gattschal and Morris, 1981). Under certain conditions, which are strain-dependent, a shift of the bacteria into a sporulation phase is accompanied by morphological changes (elongation of the cells) and the production of solvents rather than acids. A batch experiment with C. ljungdahlii was conducted on the premise that by forcing the culture to grow at a reduced rate, sporulation could be induced with an accompanying improvement in ethanol production. Synthesis gas was used as the primary carbon substrate. However, the complex nutrient yeast extract was replaced by various sugars and starches which, in previous studies, promoted sporulation of Clostridium thermosaccharolyticum (Pheil and Ordal, 1967). Table 2 summarizes the results obtained for each of the nutrients studies, along with the maximum values obtained for cell concentration, ethanol concentration and molar product ratios. As noted, the highest product ratios were obtained for cellobiose and rhamnose, with product ratios over 3 times the ratio obtained in the presence of yeast extract. Ethanol and cell concentrations were highest in the presence of cellobiose and galactose, where the ethanol concentrations were over 4 times the value obtained in the presence of yeast extract and the cell concentrations were 20 percent greater. Thus, cellobiose as a nutrient produces not only higher ratios of ethanol to acetate, but also higher concentrations of ethanol and cells.

Table 2. Summary of Results with Nutrient Sources Bringing About Sporulation

Nutrient	Maximum Cell Conc (mg/L)	Maximum ETOH (mmol)	ETOH/ACH molar ratio
Yeast Extract	140	0.13	0.13
Cellobiose	170	0.56	0.45
Rhamnose	135	0.31	0.44
Galactose	168	0.53	0.36
Starch	130	0.27	0.36

Continuous Stirred-Tank Reactor Performance. An obvious method to produce high ethanol ratios is to operate two continuous reactors in series, with the first used to promote cell growth, while the second reactor is used for increased ethanol production. A pH shift between the reactors from 4.5 to 4.0, as well as a dilution rate shift, are used to cause the onset of ethanol production while, at the same time, causing growth to cease. Media constitutents to promote growth can be added to the first reactor, and constitutents to promote ethanol production at the expense of acetate can be added to the second reactor.

Figure 11 shows the molar product ratios for both stirred-tank reactors. yeast extract (0.02 percent) was added to the liquid medium of Reactor A (first in the series initially and cellobiose later). Ethanol concentrations in Reactor B increased to nearly 3 g/L and seemed to be stimulated somewhat by the use of cellobiose as the nutrient for cell growth. Substrate CO and H_2 conversions were essentially 100 percent in Reactor A, and fluctuated somewhat in Reactor B. The product ratio increased with time in both reactors, reaching a value of about 1.0 in Reactor A and a value of about 1.5 in Reactor B. The addition of cellobiose seemed to improve the product ratio over yeast extract. By subtracting the product concentrations produced in Reactor A, an ethanol ratio of 4 moles is obtained in Reactor B.

The specific productivity steadily improved to levels of 250-300 mmole ethanol/gcell·day throughout the experiment, which is a 30-fold improvement over specific productivities in a single CSTR.

BIOREACTOR DESIGN

The choice of a suitable bioreactor for synthesis gas fermentations will be a matter of matching reaction kinetics with the capabilities of the various reactors. It has been found that for these slightly soluble gases, the rate of mass transfer usually controls the reactor size (Vega *et al.* 1989a, 1989b). Mass transfer capabilities of the reactor must be balanced with the cell

density achieved. The proper reactors for these systems will likely be ones that achieve high mass transfer rates and high cell densities. These concepts will be expanded in this and the following section.

Gas-Liquid Mass Transfer Concepts

The transfer of gas phase substrates in fermentation systems involves three heterogeneous phases: the bulk gas phase, the culture medium (liquid) and microbial cells (solid) suspended in the medium. The reactants, present in the gas phase, must be transported across the gas-liquid interface and diffuse through the culture medium to the cell surface to be consumed by the microbes. In general, a combination of the following resistances can be expected (Bailey and Ollis, 1986)

1. Diffusion through the bulk gas to the gas-liquid interface.

2. Movement across the gas-liquid interface.

3. Diffusion of the solute through the relatively unmixed liquid region (film) adjacent to the bubble and into the well-mixed bulk liquid.

4. Transport of the solute through the bulk liquid to the stagnant film surrounding the microbial species.

5. Transport through the second unmixed liquid film associated with the microbes.

6. Diffusive transport across the liquid/solid boundary and into the microbial floc, mycelia, o r particle, if appropriate. When the microbes take the form of individual cells, this resistance disappears.

7. Transport across the cell envelope to the intracellular reaction site.

As with the conventional chemical engineering analysis of absorption processes, mass transfer through the bulk gas phase is assumed to be instantaneous. Also, when individual cells are suspended in a medium, the liquid film resistance around the cells is usually neglected with respect to other resistances, because of the minute size and the enormous total surface of the cells (Finn, 1954). Thus, for the transfer of sparingly soluble gases, such as CO, the primary resistance to transport may be assumed to be in the liquid film at the gas-liquid interface.

It can be shown that the substrate rate per unit of reactor volume, $\frac{dN_S^G}{V_L dE}$, is given in terms of the gas phase partial pressures as:

$$\frac{d N_S^G}{V_L dt} = \frac{K_L a}{H} (P_S^G - P_S^L) \qquad (1)$$

where N_S^G = moles substrate transferred from the gas phase, V_L is the volume of the liquid phase, t is time, K_L is the overall mass transfer coefficient, a is the gas-liquid interfacial area per unit volume, H is Henry's law constant, P_S^G is the partial pressure of the substrate in the bulk gas phase, and P_S^L is the partial paressure (dissolved tension) of the substrate in the liquid phase ($P_S^G = HC_L$). The rate of transport from the gas phase must be equal to the rate of consumption in the liquid phase, given by a Monod relationship:

$$\frac{d N_S^G}{V_L dt} = \frac{X q_m P_S^L}{K_p' + P_S^L + (P_S^L)^2/W'} = \frac{K_L a}{H} (P_S^G - P_S^L) \qquad (2)$$

where X is cell concentration and q_m, K_p', and W' are Monod constants.

Equation (2) shows that a bioreactor for these gaseous systems must operate in either of two regimes. In one case, sufficient cells are present to react more solute, but the mass-transfer rate cannot keep pace. Therefore, the liquid phase concentration goes to zero and the reactor is mass transport limited. The cell concentration and rate of consumption are limited by the ability of that particular reactor to transfer substrate. In the other case, sufficient substrate can be supplied, but the cell concentration does not allow consumption at an equal rate. Then the liquid phase concentration is not zero (with possible inhibitory effects) and the rate is limited by the cell concentrations in that particular bioreactor. Obviously, the best bioreactor is one that will achieve high cell concentrations and high mass transfer rates.

Bioreactors for Synthesis Gas Fermentations

Since large volumes of syngas must be processed, continuous reactors are dictated. Stirred-tank reactors achieve high mass transfer rates, but require substantial energy input for agitation. Immobilized cell reactors achieve high cell concentrations, without agitation, and are promising for these applications. Trickle-bed columns, where the gas is the continuous phase and the liquid flows over packed internals, is a unique means of increasing the mass transfer for these systems.

Stirred-Tank Reactor. The traditional CSTR assumes complete mixing and uniform concentrations throughout the bulk liquid phase. For syngas fermentations, the gas must be sparaged into the liquid phase, be consumed, with any excess and product gases leaving the top of the liquid and eventually the reactor. High gas flow rates are required and near complete conversion of substrate is necessary. Conversely, only small liquid flow rates, essential to supply nutrients and remove liquid products, are necessary. Consequently, high cell concentrations should be possible. In most cases, the reactor volume will be controlled by the necessary gas retention time to achieve the desired conversion of substrate. Relatively high agitation rates will be required to promote transfer of the slightly soluble gas substrate.

Mass transfer coefficients, necessary for prediction of CSTR performance and scale-up, may be obtained from an analysis of the operation under mass-transfer limited conditions. A material balance around the CSTR with perfect mixing gives the relationship defining concentrations:

$$\frac{1}{Y_o} = \frac{1}{Y_i} + \frac{V_L}{Y_i} \quad \frac{K_L a}{H} \quad \frac{P_I^G}{n_I} \qquad (3)$$

Equation (3) is expressed in terms of an inert component, whose quantity and partial pressure does not change through the system. Therefore, to simplify the model, concentrations are in the ratio of substrate to inert (Y), with Y_o at the outlet and Y_i at the inlet. P_I^G is the partial pressure of inert in the gas stream and n_I is the molar flow rate of inert. The agreement of this model with experimental data for P. productus is shown in Figure 12. Good agreement is achieved with a linear relationship. The slope of this line gives the mass transfer coefficient, $K_L a/H = 30$. A model including Equation (3), as well as material balances for the gases flowing into the reactor and equilibrium relationships for the gas phase CO_2 with the bicarbonate and the pH level in the liquid, has been developed (Vega *et al.* 1989b). Solutions of the model for various volumetric mass transfer coefficients and various total operating pressures are shown in Figures 13 and 14, respectively. Experimental data at 1 atm and a mass transfer coefficient of 30 are also included in the figures. As observed, increases in the mass transfer coefficient or in total operating pressure leads to higher reactor productivities. Due to the perfect mixing in a CSTR, complete conversion is only possible when the gas flow rate is very low.

Figure 13 shows that with a mass transfer coefficient of 100, a pseudo retention time of one hour would result in a conversion of 80 percent. From Figure 14, the retention time could be reduced to 6 minutes at 10 atm for the same amount of CO converted. The use of the model allows the extrapolation of performance of the CSTR system and will permit preliminary economic evaluation of an industrial scale process when coupled with suitable equations for scale-up of properties such as the mass transfer coefficient.

Immobilized Cell Column (ICR). Column fermenters, with immobilized or suspended cells, offer the advantages of high cell densities and plug flow operation. These systems do not require mechanical agitation, with mixing provided by counter flow of gas and liquid. Energy for mixing is supplied by gas pressure drop and such systems are potentially more economical than the CSTR. Packed columns also offer the advantages of high surface to volume ratios and high mass transfer rates with reduced back-mixing.

Whole cell immobilization techniques can be classified into two major groups, entrapment and carrier binding (Vega *et al.* 1988). Entrapment includes both enclosure of a catalyst being a membrane or within a gel structure. Carrier binding includes all methods where there is a direct binding of cells to water-soluble carriers by physical adsorption or by ionic

and/or covalent bonds. Potential mass transfer limitations are always present with entrapment systems, either across the gel matrix or gel occlusion, or across the system membrane. On the other hand, the carrier-binding methods allow direct contact between the fermentation broth and the biocatalyst, with potentially enhanced mass transfer rates.

Microorganisms can be immobilized to insoluble biosupport materials by two methods: crosslinking and adsorption. Crosslinking, or covalent bonding, involves the use of a chemical agent, like glutaraldehyde or cyanuric chloride, to link the cells to the support. The chemical reaction is between the hydroxyl or lipid groups in the cell wall and a durable coating, like gelatin or agar, applied to the packing. Adsorption is the physical (occasionally ionic) attachment of the cell to the support. This method has been found to be effective for some small bacteria that can adhere to crevices in a support like wood chips.

In these reactors, the microorganisms are in direct contact with the substrate, minimizing diffusional resistance. These packed columns operate close to plug flow and, thereby, offer kinetic advantages for these reactions. Cells attached to the support grow and multiply into a film, which may be several layers of cells in thickness. In fact, cell overgrowth can result in completely filling the interstitial spaces, such that channeling may be a problem. Therefore, high cell densities and low retention times are possible.

By combining a material balance along the column with the rate expression for gas transport into the liquid phase, the following expression for the ratio of partial pressures of gaseous reactant entering and leaving the reactor is obtained:

$$\ln \frac{P_S^o}{P_S^i} = \frac{K_L a}{H} \frac{\epsilon_L \, h \, RTS}{G} \qquad (4)$$

where ϵ_L is the fraction of liquid in the column, h is the height of the column, S is the cross-sectional area of the column, R is the ideal gas constant, T is the absolute temperature, and G is the gas flow rate. A plot of ln Y_i/Y_o vs ShRT/G yields a straight line with slope $K_L a \epsilon_L/H$. The numerical solution (Runge-Kutts) of the differential equations that describe the system were solved for other operating conditions and are shown in Figure 15. Experimental data are given for $K_L a \epsilon_L/H$ of 13.5.

The immobilized cell column achieves higher rates of specific CO conversion than the stirred tank reactor without the need for more expensive mechanical agitation. More importantly, at the same mass transfer coefficients as in the CSTR, conversions are substantially higher. For example, at $K_L a/H = 100$, the conversion at a one hour retention time is 95 percent, compared to 80 percent for the CSTR. Alaternatively, 80 percent conversion could be achieved in a retention time only 3 min in the ICR. The major disadvantage of the ICR is the lack of flexibility in operating conditions since the contacting capabilities are mainly fixed with the design of the column dimensions and packing.

CONCLUSIONS

The fermentation of coal synthesis gas has been demonstrated to methane and ethanol. Two pathways for the indirect production of methane from synthesis gas have been evaluated. Production through acetate as an intermediate is limited by acetate inhibition of methanogens. Production through H_2 with a co-culture of R. rubrum with methanogens gives faster rates without inhibition.

Ethanol can be produced from synthesis gas with a new species of Clostridium isolated from animal waste. The ratio of ethanol to acetate in the product stream is affected by many variables including pH, nutrient composition and the introduction of reducing agents to alter electron flow. High ethanol ratios are favored by non-growth conditions. Product ratios of 4:1 (ethanol to acetate) are achieved in a two-stage continuous culture with pH and dilution rate shift.

Bioreactors that achieve high mass transfer rates and high cell concentrations are desirable for synthesis gas fermentations. Methods to determine mass transfer coefficients for CSTR and ICR reactors have been developed. High pressure has been found to increase the reaction rate proportionately. Models for these bioreactors show high conversion of gaseous substrate can be achieved in a retention time of a few minutes.

LIST OF REFERENCES

Bailey, J. E. and D. F. Ollis, Biochemical Engineering Fundamentals, McGraw-Hill, New York (1986).

Balch, W. E., S. Schoberth, R. S. Tanner, and R. S. Wolfe, "Acetobacterium, New Genus of Hydrogen-Oxidizing, Carbon-Dioxide-Reducing Anaerobic Bacteria," Int'l. J. Syst. Bacteriology. 27, 355-361 (1977).

Barik, S., E. R. Johnson, E. C. Clausen, and J. L. Gaddy, "Conversion of Coal Synthesis Gas to Methane," Energy Progress, 7, 157 (1987).

Barik, S., J. L. Vega, E. R. Johnson, E. C. Clausen, and J. L. Gaddy, "Methanation of Synthesis Gas Using Biological Processes," CRC Series, (1987).

Breed, R. S., E. G. D. Murray, and N. R. Smith, Bergey's Manual of Determinative Bacteriology, The Williams and Wilkins Company, Baltimore, MD (8th ed.) (1987).

Clausen, E. C. and J. L. Gaddy, "Advanced Studies of the Biological Conversion of Synthesis Gas to Methane," Topical Report 1: Reactor Optimization, Performed on METC Contract DE-AC21-86MC23281, U. S. Department of Energy, March 1988.

Coffin, J. M., "Industrial Coal Gasification: Applications and Economy," Energy Progress, 4, 131-137 (1984).

Courty, Ph. and P. Chaummette, "Syngas: A Promising Feedstock in the Near Future," Energy Progress, 7, 23-30 (1987).

Dashekvicz, M. P. and R. L. Uffen, "Identification of a Carbon Monoxide-Metabolizing Bacterium as a Strain of Rhodopseudomonas gelatinosa," International Journal of Systematic Bacteriology, 29, 145-148 (1979).

Finn, R. K., "Agitation-Aeration in the Laboratory and in Industry," Bacteriol. Rev. 18, 154-274 (1954).

Genthner, B. R. S. and M. P. Bryant, "Growth of Eubacterium limosum with Carbon Monoxide as the Energy Source," Appl. Environ. Microbiol. 43, 70-74 (1982).

Gottschal, J. C. and J. G. Morris, Biotechnology Letters, 3, 525-530 (1981).

Graboski, M. S.,"The Production of Synthesis Gas from Methane, Coal, and Biomass. In Catalytic Conversion of Synthesis Gas and Alcohols to Chemicals, R. G. Herman (ed.) PLenum Press, New York, pp. 37-50 (1984).

Huser, B. A., K. Wuhrmann, and A. J. B. Zehnder, "Methanothrix soehgenii gen. nov. sp. nov., a New Acetotrophic Non-hydrogen-oxidizing Methane Bacterium," Arch. Microbiol. 132, 1-9 (1982).

Jones, D. T. *et al.* "Solvent Production and Morphological Changes in Clostridium acetobutylicum Induced by Viologen Dyes," Applied and Environmental Microbiology, 53, No. 6, 1232-1235 (June 1987).

Jones, W. J. D. P. Nagle, Jr., and W. B. Whitman, "Methanogens and the Diversity of Archaebscteria," Microbiol. Rev. 51, 135-177 (1978).

Kerby, R., W. Niemczura, and J. G. Ziekus, "Single Carbon Catabolism in Acetobacterium woodii and Butyribacterium methylotrophicum by Fermentation and 13C Nuclear Magnetic Resonance Measurement," J. Bacteriol. 155, 1208-1218 (1983).

Kerby, R. and J. G. Zeikus, "Growth of Clostridium thermoaceticum on H_2/CO_2 or CP as Energy Source," Curr. Microbiol. 132, 1-9 (1982).

Long, S *et al.* "Isolation of Solvent Production, Clostridial Stage and Endospore Formation in Clostridium acetobutylicum." Applied Microbiology and Biotechnology, 20, 256-261 (1984).

Lorowitz, W. H. and M. P. Bryant, "Peptostreptococcus productus Strain that Grows Rapidly with CO as the Energy Source," Appl. Environ. Microbiol. 47, 961-964 (1984).

Mayer, F., R.Lurz, and S. Schoberth, "Electron Microscopic Investigation of the Hydrogen-Oxidizing Acetate-Forming Anaerobic Bacterium Acetobacterium woodii," Arch Microbiol. 115, 207-214 (1977).

Pheil, C. G. and Z. G. Ordal, "Sporulation of the Thermophilic Anaerobes," Applied Microbiology, 51, No. 4, 893-898 (1967).

Rao, G. and R. Murtharasan, "Altered Electron Flow in a Reducing Environment in Clostridium acetobutylicum," Biotechnology Letters, 10, No. 2, 129-132 (1988).

Rao, G. and R. Mutharasan, "Altered Electron Flow in Continuous Cultures of Clostridium acetobutylicum Induced by Viologen Dyes," Applied and Environmental Microbiology, 53, No. 6, 1232-1235 (June 1987).

Rogers, P., "Genetics and Biochemistry of Clostridium Relevant to Development of Fermentation Processes." Advances in Applied Microbiology, 31, 1-60 (1986).

Simbeck, D. R., R. L. Dickenson, A. J. Moll, "Coal Gasification, An Overview, Energy Progress, 2, 42-46 (1982).

Sleat, R., A. Mah, and R. Robinson, "Acetoanaerobium noterae: New Genus, New Species, An Anaerobic Bacterium that Forms Acetate from Hydrogen and Carbon Dioxide," Intl. J. Syst. Bacteriol. 35, 10-15 (1985).

Specks, R. and A.Klussmann, "German Hard Coal Conversion Projects, Energy Progress, 2, 60-65 (1982).

Thauer, R. K., K. Jungnermann, and K. Decker, "Energy Conservation in Chemotrophic Anaerobic Bacteria," Bacteriol. Rev. 41, 100-180 (1977).

Uffen, R. L., "Anaerobic Growth of a Rhodopseudomonas Species in the Dark with Carbon Monoxide as Sole Carbon and Energy Substrate," Proc. Natl. Acad. Sci. U.S.A. 73, 3298-3302 (1976).

Vega, J. L., S. Prieto, B. B. Elmore, E. C. Clausen, and J. L. Gaddy, "The Biological Production of Ethanol from Synthesis Gas," Appl. Biochem and Biotech. 20, 781 (1989).

Vega, J. L., E. C. Clausen, and J. L. Gaddy, "Biofilm Reactors for Ethanol Production," Enzyme Microb. Technol. 10, 403 (1988).

Vega, J. L., E. C. Clausen, and J. L. Gaddy, "Study of Gaseous Substrate Fermentations: Carbon Monoxide to Acetate. 1. Batch Culture," Biotechnol. Bioeng. (accepted for publication) (1989a).

Vega, J. L., G. M. Antorrena, E. C. Clausen, and J. L. Gaddy, "Study of Gaseous Substrate Fermentations: Carbon Monoxide to Acetate. 2. Continuous Culture," Biotechnol. Bioeng. (accepted for publication) (1989b).

Wiegel, J., "Formation of Ethanol by Bacteria. A Pledge for the Use of Extreme Thermophilic Anaerobic Bacteria in Industrial Ethanol Fermentation Processes." Experientia, 36, 1434-1446 (1980).

Wood, H. G., H. L. Drake, and S. Hu, "Studies with Clostridium thermoaceticum and the Resolution of the Pathway Used by Acetogenic Bacteria that Grow on Carbon Monoxide or Carbon Dioxide and Hydrogen." Proc. Biochem. Sym. 29-56 (1982).

BIODESULFURIZATION SYSTEMS FOR REMOVAL OF ORGANIC SULFUR FROM COAL: A CRITICAL REVIEW

Abdel El Sawy and David Gray
The MITRE Corporation
7525 Colshire Dr.
McLean, VA 22102

KEYWORDS: Biodesulfurization

ABSTRACT

This study evaluates approaches for the biological removal of organic sulfur from coal. In this area, Atlantic Research Corporation's (ARCTECH's) biodesulfurization system is the only one that has been demonstrated on coal with mixed success on a continuous bench-scale unit of 10 lb/day capacity. Other biocatalytic systems developed by the Institute of Gas Technology (IGT) or Southern Illinois University (SIU) are still in the laboratory-scale microbial selection and screening stage. Yet, the successful use by IGT of a sulfur-limited, continuous chemostat for the selection of bacterial strains with appropriate desulfurization activities has provided a convenient and powerful strain selection technique. The IGT work has also established the possibility of changing the metabolic pathway by proper modification of the bacterial growth medium and introduced the sulfur bioassay technique to help compare the effectiveness of different microorganisms grown with different substrates under different conditions on a comparable basis. SIU was successful in mapping the desulfurization genes in a mutant *E. coli*.

There is still a need for faster growing, stable, and more active biodesulfurization microorganisms than those which have been developed so far. This calls for a program of strain selection and improvements through molecular genetics, a thorough understanding of coal biodesulfurization metabolism and its associated metabolic pathways, investigation of extracellular enzymatic removal of organic sulfur from coal, and identification of new acidophillic heterotrophs that have broad organic sulfur removal capabilities and that can coexist with other bacterial strains currently used for inorganic sulfur removal.

BACKGROUND

Historically, most of the research on the biological processing of coal was directed to pyrite removal; very few studies have been explicitly devoted to organic sulfur removal although there are three studies that are particularly interesting. One study conducted in 1979 by Chandra et al.[1] indicated that a heterotrophic bacterium, enriched on dibenzothiophene (DBT), can remove up to 20 percent of the organic sulfur present in Indian coal after 10 days of incubation in a laboratory rotary shaker at 30°C. Another study conducted by Gokcay and Yurteri[2] in 1983 on Turkish lignite showed that 50 to 57 percent of the organic sulfur and 90 to 95 percent of the pyritic sulfur were removed over a 25-day incubation period. The third study was conducted by Kargi and Robinson[3] at Lehigh University using bituminous coal suspended in a growth medium inoculated with *Sulfolobus acidocaldarius* organism. After 28 days of incubation with the DBT-adapted culture at 70°C, nearly 19 percent of the initial organic sulfur in the pretreated coal was removed. Further studies on the ability of the *Solfolobus* species to desulfurize coal continued at Lehigh University in 1983 under the sponsorship of the U.S. Department of Energy's (DOE) Pittsburgh Energy Technology Center (PETC).

CURRENT STATE OF THE ART

Since 1983, DOE has continued to sponsor the investigation of various biological approaches for organic sulfur removal from coal at various U.S. institutions. Thus, ARCTECH Inc. (formerly Atlantic Research Corporation) was funded to continue their work on the development of *Pseudomonas* and other "Coal Bugs" that were able to release organically-bound sulfur from DBT and from selected coals. The Institute of Gas Technology (IGT) was funded to investigate the general feasibility of the microbial removal of organic sulfur from coal. Southern Illinois University (SIU) was also funded under DOE's University Coal Research Program in support of the overall coal biodesulfurization mission. All these DOE-supported research efforts are critically reviewed in this report.

ARCTECH Inc. has isolated a mutant *Pseudomonas* microorganism designated CB1 ("coal bug 1") that has shown the ability to remove sulfur, both from model sulfur compounds and from various coals.[4] Studies using dibenzothiophene (DBT) indicate that CB1 appears to be most effective in removing thiophenic sulfur. In laboratory-scale studies of coal desulfurization, CB1 reduced the percent organic sulfur by 18 and 47 percent at residence times of 9 - 18 hours depending on the coal, particle size, initial organic sulfur content and other, as yet unidentified, parameters. Various coals have also been treated with CB1 in a continuous bench-scale unit that can process 10 pounds/day of coal. Percent organic sulfur reductions varied from 10 to 29 weight percent, depending apparently on the coal and other unidentified parameters.

ARCTECH Inc. has also isolated another microorganism designated CB2 that has shown the ability to oxidize aryl sulfide model compounds like diphenyl sulfide (DPS) and benzyl phenyl sulfide (BPS). This microorganism was also tested on various coals with mixed success. Between 14 and 34 weight percent organic sulfur reduction was achieved for three coals. Again, the variation in effectiveness seemed to be coal dependent, but other factors were obviously present. Like CB1, CB2 has a negligible effect on the pyritic sulfur.[4]

Since experimental evidence from model compound studies indicated that CB1 and CB2 were metabolizing different sulfur functionalities, coal desulfurization experiments were performed by ARCTECH using a mixed culture of CB1 and CB2 in an attempt to improve the overall sulfur removal. The results indicated that coal desulfurization using mixed cultures was generally less effective than that achieved using the pure culture.[4] Furthermore, it appears that a metabolic by-product of CB2 inhibits the growth of CB1, thus allowing CB2 to become predominant in the total biomass.[4] This indicates that sequential desulfurization using the two cultures independently may be the preferred and only solution.

The Institute of Gas Technology has developed a sulfur bioavailability assay to identify microorganisms capable of degrading model sulfur compounds.[5] Recently (1989) efforts in this area have resulted in the successful adaptation of the IGT Sulfur Bioavailability Assay to microtiter plates.[6] This allows large numbers of mutagenized colonies to be conveniently screened to detect desulfurization-deficient mutations. Using this bioassay, IGT has identified a strain of microorganism designated IGTS7 that, when grown on several carbon substrates, is capable of degrading a wide variety of model sulfur compounds, including DBT. Using a sulfur-limited continuous chemostat, IGT further tested this microorganism on Illinois #6 coal. The chemostat effluent was monitored for the presence of metabolizable sulfur, and two peaks were found corresponding to 30 and 70 days of operation. It was surmised that the second peak represented the metabolism of organic sulfur in the coal by the IGTS7 strain that had survived the continuous operation of the chemostat during the sulfur-free period following the decline of the first peak. To test this, samples of coal were analyzed initially, at day 53 and at day 91. The last sample indicated a decrease in organic sulfur content for the coal of about 24 weight percent. Subsequent to this work, IGT has reported an organic sulfur removal of 90 percent using this microorganism after 212 days of chemostat operations. The coal apparently experienced a carbon loss of 39 percent during this procedure. Such an extraordinarily high sulfur removal needs to be replicated in further experiments at considerably shorter residence times before general scientific acceptance is forthcoming. The major thrust of current experimental efforts at IGT is the isolation of pure cultures out of the IGTS7 mixed culture.[7] A pure culture capable of desulfurization would greatly aid future research in genetics. Two pure cultures of bacteria

that are each capable of utilizing dibenzothiophene (DBT) as their sole source of sulfur were isolated from the mixed IGTS7. These cultures have been identified as *Rhodococcus rodochroas* and *Bacillus sphaericus* species, and have been designated IGTS8 and IGTS9, respectively.[7] None of these cultures alone was found capable of sulfur-specific metabolism. However, the pairwise combinations of any of these cultures with *Enterobacter* species can reproducibly perform well in the Sulfur Bioavailability Assay. At this point, it is believed that the *Enterobacter* species is only a nutritional component needed for the growth of the *Rhodococcus* and *Bacillus* species, with no contribution to desulfurization.[8]

Research at SIU at Carbondale has utilized two approaches for isolating and developing bacteria capable of removing organic sulfur from coal: enrichment culture and genetic manipulation. In the enrichment culture approach, which incidentally is the approach used by ARCTECH, the organism is isolated from naturally-occurring bacteria and adapted for growth on model sulfur compounds. The adapted organism is then subjected to a repetitive selection and mutation cycle to provide the enriched culture with the desired traits. The desulfurization potential of the isolated strains was determined by measuring sulfate and/or hydrogen sulfide released during bacterial degradation of model sulfur compounds. Several isolates were selected that could degrade dibenzothiophene sulfane (DBTS), dibenzothiophene (DBT), benzene sulfonic acid (BSA) and cystine (CYI).[9] The isolates that degraded the latter compound were particularly active in their growth and were selected as potential candidates for future coal desulfurization studies.

The genetic manipulation approach of SIU involves mutation of *E. coli*, a genetically well-understood organism for metabolizing sulfur containing amino acids. *E. coli* NAR3 is a bacterial strain produced after successive cycles of mutation and selection. This strain can degrade thiophenes, furans, and other sulfur-containing aromatic compounds.[10] Genetic analysis of NAR3 has been undertaken at SIU, and since then other mutants showing improved degradation of thiophene and other sulfur containing aromatic substrates have been isolated. One of these, designated NAR41, has shown increased affinity for thiophene rings and decreased affinity for other non-sulfur containing rings.[10] This is clearly in the right direction since the goal is to remove sulfur with as little loss of coal carbon as possible.

CRITICAL REVIEW

The basic goal of all biodesulfurization processes is to remove the organically-bound sulfur from coal while retaining the fuel value of the coal. This means that biodesulfurization should follow a metabolic pathway that eliminates sulfur with little destruction of the coal carbon. Investigations to date have focused on the metabolic pathway analysis for DBT and not for coal. In the desirable pathway, the so-called 4-S, the DBT is successively oxidized to sulfate and 2,2'-dihydroxybiphenyl.[11,12] The other pathway results in destruction of the aromatic ring structure of DBT with no liberation of sulfur. CB1 apparently releases sulfur from DBT as sulfate, and 2,2'-dihydroxybiphenol has been identified as the organic product. Thus, CB1 seems to operate via the 4-S pathway. IGT finds monohydroxybiphenyl as a product, so it is likely that IGTS7 metabolizes DBT using a variant of the 4-S pathway. The other microorganisms under development appear to involve some participation of carbon-destructive metabolic pathways.

All coal desulfurization organisms developed so far have been recovered from microbial populations isolated from soil near coal mines or petroleum refineries. These microorganisms are single cell (procaryotes), rod-like aerobic bacteria that remain active only in neutral or alkaline medium at temperatures between 25 and 35°C. Because of this, they are unable to coexist with those acidophillic heterotrophs currently used for inorganic sulfur removal. Furthermore, the metabolism of most of these organisms is poorly understood at present, and therefore, their growth media have generally not been optimized.

Despite its attractive potential, the biodesulfurization of coal has its problems and limitations. One major problem is the heterogeneity of coal, which means that the same microorganism may not be effectively used with all types of coal. In other words, the biological removal of organic sulfur from coal may have to be tailored to each coal separately. Possible instability of genetically-engineered microbial cultures is another problem. Over

extended periods of usage, an originally effective desulfurization organism may give rise to spontaneous derivatives that lack desulfurization ability. The long residence time required for bioprocessing is also a major obstacle to the usefulness of this technology. Low biodesulfurization rate, slow bacterial growth, and low process yield may all contribute to limit future application of biodesulfurization. The other potential limiter is the surface availability of the organic sulfur for microbial attack.

For any desulfurization process to be viable from a utility boiler aspect, it should be capable of reducing the sulfur content of coal to produce compliance fuels. For typical U.S. coals with 3 percent total sulfur and assuming 90 percent physical removal of inorganic sulfur, the removal of 50 percent of the organic sulfur is required. Thus, about 60 percent of the total coal sulfur must be accessible for microbial metabolism at the coal surface. This can be achieved theoretically with finely-ground coal having an average particle size of 38 microns (200-400 mesh), assuming that the thickness of the outer coal surface layer accessible for microbial action is 5 microns. Fine grinding of coal can be both an economic and a technical penalty since dewatering of coal slimes is a difficult problem. Whether microbial action can penetrate below the coal surface for non-extracellular enzymatic processes remains to be investigated.

An important economic criterion is the growth rate of the microorganism. This determines the capacity of the fermenters and therefore impacts capital cost. Economically attractive growth rates of 0.66 $hour^{-1}$ have been quoted in the literature,[13] and this corresponds to a bacterial generation time of 1.05 hours, compared to 3.8 hours for CB1 and 4.0 hours for CB2. Other microorganisms isolated so far in the biodesulfurization program have much longer generation times of two days or more. Another consideration is the biomass yield. This determines the necessary growth media, oxygen demand, productivity, plant size and thus operating and capital costs. The typical economic biomass yield for *Pseudomona* grown on benzoic acid is 0.60 grams of dry cell biomass per gram of benzoic acid consumed. This is 15 percent higher than that achieved by CB1 under current growth conditions on benzoic acid. The kinetics of the process also determine economic viability. Assuming first-order biodesulfurization kinetics and removal of 50 percent organic sulfur at the best currently achieved residence time of 9 hours, the rate constant is 0.08 $hour^{-1}$. The desulfurization rate constant for CB1 currently ranges between 0.01 and 0.05, depending on conditions and the coal type.

CONCLUSIONS AND RECOMMENDATIONS

This analysis of the various techniques being investigated for the chemical cleaning of coals has not been able to positively identify the most promising approaches to this problem. One reason is lack of overall process data in much of the current research effort. Emphasis has been on overall sulfur removal efficiency. The relative proportion of organic vs inorganic sulfur has often not been identified. The issues of carbon losses and product characteristics have essentially been neglected. Other aspects generally not addressed in current research are the potential costs and process energy requirements.

If, as conventional wisdom suggests, the organic sulfur in coal is an integral part of the coal matrix, then disruption of the coal matrix must occur before organic sulfur can be removed. This disruption implies that the product may have properties and characteristics different from the parent coal, this difference being a function of the severity of the desulfurization process.

These considerations point to major recommendations for research priorities in the area of coal desulfurization. Of prime importance is to attempt to develop analytical techniques for identifying organic sulfur speciation. Potential techniques are already in existence, and very likely several of them will have to be used in combination to unequivocally assign sulfur functionalities in the coal matrix. Once we know what compounds we are dealing with and have a reliable way to measure them, we stand a better chance of developing chemistry and biochemistry that will remove them.

In addition, research in coal desulfurization must constantly be concerned not only with desulfurization efficiency, but also with the characteristics and potential uses of the desulfurized product. Superclean coals may well be superclean from the standpoint of low sulfur and mineral matter content, but they may also have limited utility as a fuel form.

The use of biological means for the removal of organic sulfur from coal must be looked upon as a potential long-term development. Assuming that stable microorganisms can be developed that degrade organic coal sulfur, there are still many uncertainties yet to be resolved before biodesulfurization of coal becomes a realistic commercial option. These uncertainties include (1) a realistic estimate of the accessible organic sulfur available for microbial metabolism at the coal particle surface, (2) reliable determination of the various sulfur species in coal, (3) scale-up considerations for bioreactors, and (4) reasons for the variable response of different coal types to bioprocessing.

The ARCTECH biodesulfurization system is currently the only one that has been demonstrated on coal, although with mixed success, using a continuous bench-scale unit of 10 lb/day capacity. Other biocatalytic systems developed by IGT or SIU are still in the laboratory-scale microbial selection and screening stage. The research work of IGT and SIU has, nevertheless, contributed significantly to the coal biodesulfurization mission. IGT's successful use of a sulfur-limited, continuous chemostat for the selection of bacterial strains with appropriate desulfurization activities has provided a convenient and powerful strain selection technique. The IGT work has also established the possibility of changing the metabolic pathway by proper modification of the bacterial growth medium, and has introduced the sulfur bioassay technique to help compare on a common basis the effectiveness of different microorganisms grown with different substrates under different conditions. SIU was successful in mapping the desulfurization genes in a mutant *E. coli*. This is an important step towards the application of molecular genetics for the development of improved bacterial strains with enhanced desulfurization capabilities.

The conclusion is that there is a need for faster growing, stable, and more active biodesulfurization microorganisms than those that have been developed so far. To this end, there are several major research needs that can be identified. There is a need for a structured and systematic program of strain selection and improvements through molecular genetics, and a need for a thorough understanding of coal biodesulfurization metabolism and its associated metabolic pathways. A similar approach was successfully applied in penicillin production and resulted in a thousandfold increase in yields. There are also needs to investigate extracellular enzymatic removal of organic sulfur from coal, and to identify new acidophillic heterotrophs that have broad organic sulfur removal capabilities and that can coexist with other bacterial strains currently used for inorganic sulfur removal.

ACKNOWLEDGEMENT

This work was supported at the MITRE Corporation by Sandia National Laboratories under contract to the U.S. Department of Energy (DE-AC04-76DP00789).

REFERENCES

1. Chandra, D., P. Roy, A. K. Mishra, J. N. Chakrabarti, and B. Sengupta. "Microbial Removal of Organic Sulfur From Coal". *Fuel*, 58, 549, 1979.

2. Gokcay, C. F. and R. N. Yurteri. "Microbial Desulfurization of Lignites by a Thermophillic Bacterium". *Fuel*, 62, 1223, 1983.

3. Kargi, F. and J. M. Robinson. "Removal of Organic Sulfur from Bituminous Coal". *Fuel*, 65, 397, 1986.

4. *Microbially Mediated Removal of Organic Sulfur from Coal.* A report prepared by Atlantic Research Corporation under DOE/PETC Contract No. DE-AC22-85PC81207, November 6, 1987.

5. Kilbane II, J. and Andrea Maka. *Microbial Removal of Organic Sulfur from Coal.* Tenth Quarter Report, prepared for DOE/PETC, DOE Contract No. DE-AC22-85PC81201, IGT Project No. 61078, March 1988.

6. Bielage, Barbara and John J. Kilbane. *Molecular Biological Enhancement of Coal Biodesulfurization: Third Quarter Report.* Prepared for DOE/PETC under DOE Contract No. DE-AC22-88PC8891, IGT Project #61095, July 1989.

7. Bielaga, Barbara and John J. Kilbane. *Molecular Biological Enhancement of Coal Biodesulfurization: Second Quarter Report.* Prepared for DOE/PETC under DOE Contract No. DE-AC22-88PC91, IGT Project #61095, April 1989.

8. Bielaga, Barbara and John J. Kilbane. *Molecular Biological Enhancement of Coal Biodesulfurization: First Quarter Report.* Prepared for DOE/PETC under DOE Contract No. DE-AC22-88PC91, IGT Project #61095, December 1988.

9. Klubek, B. and D. Clark. *Microbial Removal of Organic Sulfur from Coal (Bacterial Degradations of Sulfur-Containing Heterocyclic Compounds).* Final Report Submitted to the U. S. Department of Energy under Contract No. DE-FC22-86PC91272, 1987.

10. Abdulrashid, N. and D. Clark. "Isolation and Genetic Analysis of Mutations Allowing the Degradation of Furans and Thiophene by *E. Coli.*" *Journal of Bacteriology*, 169, 1267-1271, 1987.

11. Kadama, K. S. Nakatani, K. Umehara, K. Shimizu, Y. Minoda, and K. Yamada, "Microbial Conversion of Petrosulfur Compounds: Isolation and Identification of Products from Dibenzothiophene", *Agr. Biol. Chem.*, 34, 1320-1324, 1970.

12. Kilbane II, J. *Microbial Removal of Organic Sulfur from Coal: Current Status and Research Needs.* A preprint of a chapter to appear in *Biotechnology Applied to Fossil Fuels*, Donald L. Wise, Editor, Boca Raton, Florida: CRC Press, 1988.

13. Atkinson, B. and F. Mavituna. *Biochemical Engineering and Biotechnology Handbook*, New York: The Nature Press, 1983.

COAL SULFUR TRANSFORMATIONS MONITORED BY HYPERTHERMOPHILIC ARCHAEBACTERIA

T.L. Peeples, S. Hirosue, V. Muralidharan, R. M. Kelly

Department of Chemical Engineering
The Johns Hopkins University
Baltimore, MD 21218

Gregory J. Olson

Polymers Division
Nationl Institute of Standards and Technology
Gaithersburg, MD

Introduction

Microbial processes have been used as the basis for significant chemical transformations in several industries including but not limited to pharmaceuticals, foods processing and waste management. However, biotransformations are often limited by the metabolic rate of the organism and the stability of its constituent enzymes and other biomolecules. Industries which have successfully applied microoganisms for commercial purposes have developed processes that are consistent with whatever biological limitations prevail.

The spread of biotechnology has resulted in considerable attention to the use of biological systems in mineral and fossil fuel processing. For example, the acidophilic bacterium *Thiobacillus ferrooxidans* has been used in copper and uranium leaching as well as in small scale studies of pyrite removal from coal (1,2). Other potential uses for microbes in coal processing include desulfurization, denitrification, oxygen removal, solubilization and gasification of coals (3). The wide range of metabolic characteristics available in the global pool of microorganisms may enable researchers to discern more about the functionalities in coal structure as well as to build cultures in which the desired conversions can be engineered.

Hyperthermophiles

During the past decade, several bacteria have been isolated that thrive at temperatures at or above 100 °C (4) . These hyperthermophiles may have potential for a variety of significant biotransformations in the field of biotechnology. The high temperature optima of hyperthermophiles and their associated biomolecules may be useful in industrial processes by carrying out transformations at faster rates and with high levels of stability. Recently, we have been evaluating the potential for using hyperthermophilic archaebacteria in coal upgrading (5). In doing so, both the ecology and physiology of these organisms must be considered.

Hyperthermophiles are associated with geothermally heated areas, which often are sulfur- and metal-rich environments. Several sulfur-metabolizing species have been isolated from these areas. The ability of these organisms to transform sulfur compounds at high temperatures is the interesting metabolic trait that could be capitalized upon for sulfur removal from coal. However, the nature of the various sulfur metabolisms differ and are not completely understood (4).

In preliminary studies, *Pyrococcus furiosus*, an anaerobic heterotroph isolated from geothermally heated marine sediments off of the coast of Vulcano, Italy (6), has been used as a representative hyperthermophilic strain. In the absence of S^0, *P. furiosus*, produces H_2, which is inhibitory for growth, and CO_2 (7,8). In the presence of S^0, *P. furiosus* produces H_2S, either respiring sulfur or utilizing it to remove H_2 from the environment (8). *P. furiosus* grows to higher maximum cell densities (10^8 cells/ml) with faster doubling times (1 hour) than most of the hyperthermophilic

archaebacteria (6,9). Because of the easier cultivation of the organism, *P. furiosus* appears to be more suitable for coal upgrading. In addition to sulfur removal capabilty, thermophilic heterotrophy may make *P. furiosus* suitable for breaking down complex coal constituents.

Hyperthermophiles and coal-sulfur

Previously, we examined the feasibility of coal desulfurization with *P. furiosus* (5,10,11). Various coals and model compounds were screened for sulfur removal activity. Success in sulfur removal was measured by the production of H_2S. Only highly weathered gob coals showed the production of H_2S upon exposure to *P. furiosus* (5,11). Continuous culture of *P. furiosus* with coal containing elemental sulfur showed that *P. furiosus* can remove sulfur from coal at rates comparable and in most cases higher than mesophilic organisms studied for sulfur removal (10). The drawback is that the sulfur within coal must be in the form useful to the microorganism in order to be converted. Very few of the more pristine coals tested showed H_2S production upon exposure to *P. furiosus*, suggesting that sulfur metabolizable by *P. furiosus* is not present in these coals (5,11).

Model compound studies showed that P. furiosus metabolizes only those sulfur compounds which are polysulfidic or form polysulfides near culture temperatures (98 °C). Compounds with $-(S-S-S)-_x$ bonds are believed to be only a small fraction of coal sulfur. The specificity of *P. furiosus* for these compounds may be useful in settling a few disputes about polysulfidic compound generation in coal. (7)

Coal Weathering and Sulfur Speciation

Elemental sulfur in coal is believed to be a product of pyrite oxidation (12-14). During coal weathering under varying reaction conditions, oxidation products from FeS_2 have been reported to include S_n as well as FeO, FeS, Fe_2O_3, $FeSO_4$, $Fe_2(SO_4)_3$, SO_2 and SO_3. The weathering products of the organic sulfur components of coal have not yet been determined, because the organic sulfur species themselves are not known. Postulated organic sulfur compounds in coal are thiols, sulfides, disulfides, and thiophenic residues. Oxidation experiments both with model sulfur species and with coal have resulted in the production of sulfones, sulfonic acids and sulfates (12,13).

The formation of elemental sulfur from organic sulfur compounds under mild oxidation is thought to be unlikely primarily because the oxidation of the organic moieties would require gasification of the carbon skeleton of the coal (14). Mild oxidation of coals is a surface phenomenon involving the addition of oxygen molecules and small-scale rearrangement. Breakdown of the carbon backbone would require more extreme processing conditions (15).

By ASTM guidelines, sulfur speciation in coals requires experimental determination of sulfatic, pyritic, and total sulfur content. Organic sulfur is determined by difference. This calculational procedure tends to propagate experimental error of the analytical techniques and therefore leads to inaccuracy in organic sulfur values (12,13,16-18). In addition to technical error, the presence of elemental sulfur can lead to overestimation of organic sulfur content (19).

Artificial Weathering Experiments

Many mild oxidation experiments have been run on on both coal and mineral pyrite in attempts to discern the mechanisms of sulfur transformations during weathering. Although the reactivities differ between ore pyrite and coal pyrites and among pyrites from different coal sources (20-22), parameters that have been tested and shown to affect the distribution of sulfur oxidation products for all pyritic substrates include: temperature, humidity, oxygen content, acidity and the presence of chemical oxidants.

Water, both in vapor and liquid forms has been shown to have an accelerating effect on the weathering process (12,13,17,24). These results indicate the interaction of water with oxygen groups on the coal surface. The enhancement of oxygen uptake due to the presence of water agrees with the theory of peroxygen formation at the coal surface as the initiation step of weathering (25).

Results from several artificial weathering studies suggest that the mechanism of pyrite oxidation is strongly dependent upon temperature. Sulfate products have been found to prevail at low temperature conditions, while a complex range of oxidation products are generated at higher temperatures (13,17). Even within the range of 'realistic' weathering temperatures (25 to 80 °C), the products of coal pyrite oxidation vary considerably. (23)

In the pyrite crystal, iron is anchored in the lattice and sulfurs extend from the surface. Each of the two pyritic sulfurs is bound to another sulfur molecule yeilding an FeS_4^{-4} configuration of pyrite. The extended sulfurs become oxygenated as a result of weathering. Oxygenation can occur as the result of peroxygen or hydrated Fe^{3+} producing dissociation conditions on the pyrite surface. (26) The Fe-S bond weakens and breaks before the S-S bond in the disulfide groups. This is confirmed by the appearance of thiosulfate as a specific intermediate (26,27). The production of a polysulfide could be consistent with this theory. At pH lower than 5 thiosulfate decomposes to elemental sulfur and sulfate.

There have been several studies of pyrite oxidation in aqueous suspension. Most of the work at low temperature 30 °C and pH greater than 6 has shown little or no production of elemental sulfur. McKay and Halpern weathered mineral pyrite in aqueous suspension under varying levels of acidity (27). Through mass balance it was suggested that elemental sulfur was formed at low levels. These authors assumed that no thiosulfates and thionates were formed from the oxidation. All of the oxidized sulfur that was not accounted for in the form of sulfate was assumed to be elemental sulfur. It was found that 'elemental' sulfur was produced at low pH.

Moses et. al. used ion chromatography to analyze pyrite oxidation solutions for sulfoxy anions (26). At higher pH, oxidation of pyrite to sulfate was rapid with little production of sulfoxy intermediates. At low pH, 10 - 25% of sulfur in solution was determined to be thiosulfate and polythionate. No analysis for elemental sulfur was performed.

Like Moses, Goldhaber predicts the production of elemental sulfur at low pH. However, neither of these researchers performed low pH oxidations (28). McKibben and Barnes oxidized pyrite at low temperature under acidic conditions and did not note the production of elemental sulfur (29).

Despite agreement on the theory of the formation of sulfoxy intermediates, their is some confusion as to the products of pyrite oxidation. Luther suggests that in the presence of excess Fe^{3+}, thiosulfate is oxidized to sulfate (26). Meyer used Fe^{3+} to oxidize pyrite and produced elemental sulfur as an oxidation product (30). Which parameters can be manipulated to increase the selectivity of the thiosulfate oxidation for elemental sulfur has yet to be determined.

The microbial role in weathering

The deposition of elemental sulfur in coals is thought to be largely the result of microbial action (31). Although most of the microbial generation of elemntal sulfur is thought to be through sulfate reduction, several pyrite oxidizing organisms have been reported to produced S^0. Numerous studies on the feasibility of microbial coal desulfurization have focused on the use of such organisms for leaching pyrite from coals. Much of the work has centered around acidophilic aerobic systems including *Thiobacillus ferrooxidans, Sulfolobus*, and mixed cultrues of *T. ferrooxidans* and *T. thiooxidans* (1-3). These bacteria mediate the oxidation of FeS_2 to Fe^{3+} and $SO_4^{=}$. Elemental sulfur has frequently been observed as an intermediate or end product of these oxidations (32).

Due to the aerobic nature of microhial pyrite leaching systems, it is difficult to discern whether the distribution of oxidation products is a direct result of microbial metabolism or of simultaneous abiotic weathering. It has been suggested that the initial dissolution of FeS_2 to Fe^{2+} is a result of chemical weathering (33). Microhial action mediates the oxidation of Fe^{2+} to Fe^{3+} at rates higher than those in the absence of microhial catalysts (34) The accelerated accumulation of Fe^{3+} in the biological systems could account for the production of more elemental sulfur than in chemical weathering. In this scenario, elemental sulfur is not the result of direct microbial action, but of the precipitation of sulfur in the acidic culture media as affected by Fe^{3+} levels in solution. However, it is plausible that elemental sulfur is generated by the microbiological utilization of

pyritic sulfur.

Pyrite leaching experiments with a *Leptospirrilum*-like bacterium in pure culture produced higher levels of elemental sulfur than in abiotic weathering (34) . In mixed culture with *T. ferrooxidans* sulfur yields were comparable if not lower than abiotic controls. These results suggest that the *Leptospirrilum*-like organism "prefers" the presence of S^0 whereas S^0 is oxidized by *T. ferrooxidans*. The discussion becomes more confusing as the severity of the weathering conditions are considered. The *Leptospirrilum*-like bacterium carries out pyrite leaching reactions at pH values lower than *T. ferrooxidans*. The bigher acidity of the culture environment may be the determining factor in S^0 generation. Again, the interaction between biological and abiotic sulfur production is unclear and may vary from organism to organism.

Experimental

Currently, we are investigating the effects of varying conditions on the products of pyrite weathering. Motivations for this study are two-fold: 1.) to achieve a chemical/microbial mechanism that would enable us to capitalize on the high rates of S^0 or plysulfide utilization of *P. furiosus* 2.) to determine the involvement of both organic and inorgainic sulfur species in the deposition of polysulfidic compounds in coal.

Using approaches outlined in previous literature on artifical weathering, we are examining the activity of *P. furiosus* to sulfur species in coal exposed to various levels of temperature, acidity, ferric iron concentrations among other parameters. Weathering conditions have been chosen in attempt to optimize the selectivity for reducible sulfur generation rather than sulfate formation. In conjuntion with the *P. furiosus* bioassay, ASTM speciation of coal sulfur, as well as standard chemical analysis for sulfoxy intermediates in solution are being used to follow the transformation of sulfur species during weathering.

Figure 1 shows the results of a long-term coal weathering experiment in which *P. furiosus* is used to determine the levels of available reducible sulfur. The results illustrate the interrelationship between iron and sulfur species and show that the reducible sulfur availble to the bacteria varies through the process. The weathering conditions are relatively mild so that only inorganic sulfur in coal is likely to be affected. The bacteria in the bioassay are probably active towards elemental sulfur formed from pyrite. The sulfide generated at varous time points suggest that there is no accumulation of S^0 but that it is an intermediate in the weathering process as inorganic sulfur is converted to sulfate.

The exposure of coals to elevated levels of oxygen and temrprature under aqueous conditions has been considered as a means for both inorganic and organic sulfur removal from coal. Air/water oxydesulfurization of coal was evaluated by Warzinski et. al. (35) They showed that while inorganic sulfur could be converted to sulfate under conditions that minimized the loss in heating value of coals, organic sulfur removal lead to significant heating value losses. For example, for an Indiana No.5 coal, they showed that the percent heating value loss in the coal was approimately the same as the apparent sulfur removal. However it may be possible that more subtle changes in the coal matrizx related to certain sulur moietis cold lead to effective biological treatment.

Table 1 shows the results of a mild weathering experiment using two coals: a pristime Illinois No. 6 containing 0.7% (w/w) pyritc sulfur and 3.4% (w/w) organic sulfur; and an Australian brown coal containing 0.03% (w/w) pyritic sulfur and 3.7% (w/w) organic sulfur. After 21 days of exposure to the conditions listed, coal samples were incubated with *P. furiosus* at 98 °C to determine to what extent the coal sulfur had become available to theis bacterium. Only an end point sample of weathered coal was taken in this weathering experiment. Whether the distribution of sulfur endproducts is the result of one day of weathering versus 21 days of weathering cannot be ascertained. Note the unweathered coals yilded little if any sulfide when exposed to *P. furiosus*. In several of the experiments with the Australian coal, we detected significantly larger amounts of sulfide than in the experiments with the Illinois coal. Although only about 1% of the organic sulur in the Australian coal was apparently converted to sulfide, the fact that less sulfide was generted from the Illinois coal was surprising. The pyritic sulfur in the Illinois coal was expected to be converted to elemental sulfur and sulfate with the result that significant amounts of sulfide would be

generated from S^0 by *P. furiosus*. The differences between the sulfide generated form the two coals may or may not reflect differences in tbe forms of orgnaic sulfur in the two coals. As mentioned earlier, *P. fuiosus* metabolizes aliphatic sulfur compounds such as cystine (8) but not aromatic sulfur in compounds such as dibenzothiophene. Further work is need in the development of the bioassy, but it is clear tbat biological activity may prove to be a sensitive and illuminating probe for sulfur speciation in coals.

Summary

In developing biologically-based desulfurization process to determine not only the organic sulfur content of the coal, but how it occurs. For example, certain microbial systems will be more active to aliphatic sulfur than aromatic sulfur. While analytical techniques for determining the distribution of organic sulfur in coal are emerging, they are not readily available. Nonetheless, microbial treatment processes based on better chance of succeeding. Secondly, organic sulfur removal in coal may be best approached by a combination of biological and chemical steps. The chemical steps need not severely reduce the heating value of tbe coal but rather be directed at modifying the sulfur bound in the coal matrix to improve its biological availability. For the case of the weathering experiments described here, it would be interesting to see if microbially mediated weathering of coal would produce similar changes in sulfur availability to sulfur reducers such as *P. furiosus*. This would suggest that the microbial portion of a chemical/mirobial treatment system not be limeited to a particular species, but may encompass several microbial metabolisms. The weathering experiment described here is prelimenary, but closer examination to combining the oxydesulfurization process with subsequent biological treatment will be persued.

References

1. C. L. Brierly, "Microbilogical Mining" *Scientific American* **247** 44-53, 1982
2. D. J. Monticello and W. R. Finnerty "Microbial Desulfurization of Fossil Fuels" *Ann. Rev. of Microbiol.* 39 371-389 1985
3. R. Srivastava, l. M. Campbell and B. D. Blaustien "Coal Bioprocessing: A Research-Needs Assessment" *Chemical Engineering Progress* **85** 45-53 1989
4. K.O. Stetter. "Diversity of Extremely Thermophilic Archaebacteria." in **Thermophiles: General, Molecular, and Applied Microbiology**., T.D. Brock, ed., John Wiley and Sons, New York, 1986.
5. R. N. Schicho, S. H. Brown, G. J. Olson, E. J. Parks, and R. M. Kelly "Probing coals for non-pyritic sulfur using sulfur-metabolizing mesophilic and hyperthermophilic bacteria." *Fuel* **68** 1368-1375 1989
6. G. Fiala and K.O. Stetter. "*Pyrococcus furiosus* sp. nov. represents a novel genus of marine heterotrophic archaebacteria growing optimally at 100° C." *Arch. Microbiol.*, **145**, 56-61, 1986.
7. B. Malik, W-w. Su, H.L. Wald, I.I. Blumentals and R.M. Kelly. "Growth and Gas Production for the Hyperthermophilic Archaebacterium, *Pyrococcus furiosus.*" *Biotechnol. Bioeng.*, **34**, 1050-1057, 1989.
8. I.I. Blumentals, M. Itoh, G.J. Olson and R.M. Kelly. "Role of Polysulfides in the Reduction of Elemental Sulfur by the Hyperthermophilic Archaebacterium *Pyrococcus furiosus.*" *Appl. Environ. Microbiol.*, in press.
9. K.O. Stetter, H. Konig and E. Stackebrandt. "Pyrodictium gen. nov., a New Genus of Submarine Disc-Shaped Sulfur-Reducing Archaebacteria Growing Optimally at 105° C." *Sys. Appl. Microbiol.*, **4**, 535-551, 1983.
10. T. L. Peeples, R.N. Schicho, R. M. Kelly and G. J. Olson "Bioprocessing of Fossil Fuels Using Hperthermopbilic Archaebacteria" EPRI symposium paper *Biological Processing of Coal and Coal-Derived Substances* May, 1989
11. D. Wise. **Bioprocessing and Biotreatment of Coals.**, Marcel Dekker, New York, in press.
12. D. C. Frost, W. R. Leeder and R. L. Tapping. "X-ray photoelectron Spectroscopic investigation of coal." *Fuel* **53** 206-211, 1974
13. D. C. Frost, W. R. Leeder, R. L. Tapping and B. Wallbank. "An XPS study of the oxidation of pyrite and pyrites in coal." *Fuel* **56** 277-280, 1977
14. R. K. Sinha and P. L. Walker "Removal of sulphur form coal by air oxidation at 350-450° C" *Fuel* **51** 125-129 1972
15. H. H. Lowry, ed. **Chemistry of Coal Utilization** vol II John Wiley and Sons 1945 New York
16. American Society for Testing and Materials. Designation D 2492-84 "Standard Test Method for **Forms of Sulfur in coal**
17. V. Calemma, R. Rausa, R. Margarit and E. Girardi. "FT-i.r. Study of coal oxidation at low temperature." *Fuel* **67** 764-770, 1988
18. D. L. Perry and A. Grint, "Application of XPS to coal characterization" *Fuel* **62** 1024-1033 1983
19. R. Markuszewski, "Some thoughts on the difficulties in the analysis of sulfur forms in coal." **Journal of Coal Quality**, Jan. 1988, vol 7. no. 1 pp 1-4
20. F. G. Smith "Variation in the properties of pyrite" *The American Mineralogist* **27** 1-19

21. R. M. Garrels and M. E. Thompson "Oxidation of pyrite by iron sulfate solutions" *American Journal of Science* **258-A** 57-67 1960

22. M. C. Esposito, S. Chander and F. F. Aplan "Characterization of pyrite from coal sources" In: *Process Mineralogy VII* Vassilou ed. 475-493 The Metallurgical Soc., Warrendale, PA 1987

23. M. M. Wu, G. A. Robbins, R. A. Winschel and F. P. Burke "The effects of weathering on floatation and thermoplastic properties of coal" *Abstracts of Papers of the American Chemical Society Division of Fuel Chemistry*, **193** 73 1986

24. D. J. Maloney, R. G. Jenkins, and P. L. Walker Jr."Low-Temperature air oxidation of caking coals. 2. Effect on swelling and softening properties." *Fuel* **61** 175-181, 1982

25. G. R. Ingram and J. D. Rimstidt. "Natural weathering of coal." *Fuel* **63** 292-296, 1984

26. C. O. Moses, D. Nordstrom, J. S. Herman and A. L. Mills. "Aqueous pyrite oxidation by dissolved oxygen and by ferric iron " **Geochemica et Cosmochimica Acta.**, **51** 1561-1571, 1987

27. G. W. Luther. "Pyrite oxidation and reduction: Molecular orbital considerations " *Geochimica et Cosmochimica Acta* **51** 3193-3199, 1987

28. D. R. McKay and J. Halpern. "A kinetic study of the oxidation of pyrite in aqueous suspension." *Transactions of the Metallurgical Society of AIME* **210** 301-309, 1958

29. M. B. Goldhaber. "Experimental study of Metastabele sulfur oxyanion formation during pyrite oxidation at pH 6-9 and 30 °C" *American Journal of Science* **283** 193-217, 1983

30. M. A. McKibben and H. L. Barnes. "Oxidation of pyrite in low temperature acidic solutions: Rate laws and surface textures ", *Geochimica et Cosmochimica Acta* **50** 1509-1520, 1986

31. P. R. Dugan. "Microbial Conversions of Sulfur and their Potential for Bioprocessing of Fossil Fuels", Proceedings: Bioprocessing of Fossil Fuels Workshop, Tysons Corner, VA , August 1989

32. W. Hazeu, R. Steudel, W. H Batenburg-van de Vegete, P. Bos, and J. G. Kuenen, "Elemental sulfur as an intermediate in the oxidation of reduced sulphur compounds by *Thiobacillus ferrooxidans* Localization and characterization" Proceedings: Bioprocessing of Fossil Fuels Workshop, Tysons Corner, Va., August, 1989

33. W. Strumm and J. J. Morgan ed. **Aquatic Chemistry** 2nd ed. John Wiley and Sons, New York 1981, 469-471

34 U. Merrettig, P. Wlotzka and U. Onken, "The removal of Pyritic Sulfur from coal by *Leptospirillum*-like bacteria." *Applied Microbiology and Biotechnology* **31** *626-628, 1989*

35 R. P. Warzinski, S. Friedman, J. A. Ruether and R. B. LaCount. "Air/Water Oxydesulfurization of Coal - Laboratory investigation." Department of Energy Report DOE/PETC/TR-80-6, Pittsburgh Energy Technology Center, Pittsburgh, PA, August, 1980.

Table 1. Artificial Weathering Experiments with Illinois/Australian Coals

Sulfide Generation by *Pyrococcus furiosus*

Coal	*Temp (°C)*	*pH*	*Air* (atm)	*Sulfate* (ppm)	*Sulfide* (nmol/ml)	*Cell Density* (cells/ml)
AUS	80	1.6	1	953	21	9.8E6
	80	0.6	1	1480	16	1.5E7
	80	1.6	3	280	160	1.4E7
	80	0.6	3	275	263	1.1E7
	100	1.6	1	262	133	9.9E6
	100	0.6	1	967	158	1.3E7
	100	1.6	3	250	89	9.0E6
	100	0.6	3	358	152	1.0E7
ILL	80	1.6	1	738	22	8.8E6
	80	1.6	1	870	25	8.8E6
	80	1.6	1	798	20	9.4E6
				±54	±2	±0.2E6
	80	0.6	1	1015	63	1.5E7
	80	1.6	3	798	93	1.1E7
	80	0.6	3	1743	67	8.3E6
	100	1.6	1	228	74	1.5E7
	100	0.6	1	645	18	1.2E7
	100	1.6	3	905	45	1.0E7
	100	0.6	3	824	51	1.1E7
P. furiosus Growth on S°					>2000	2.4E8
AUS (Unweathered)					30	8.4E6
ILL (Unweathered)					12	9.6E6

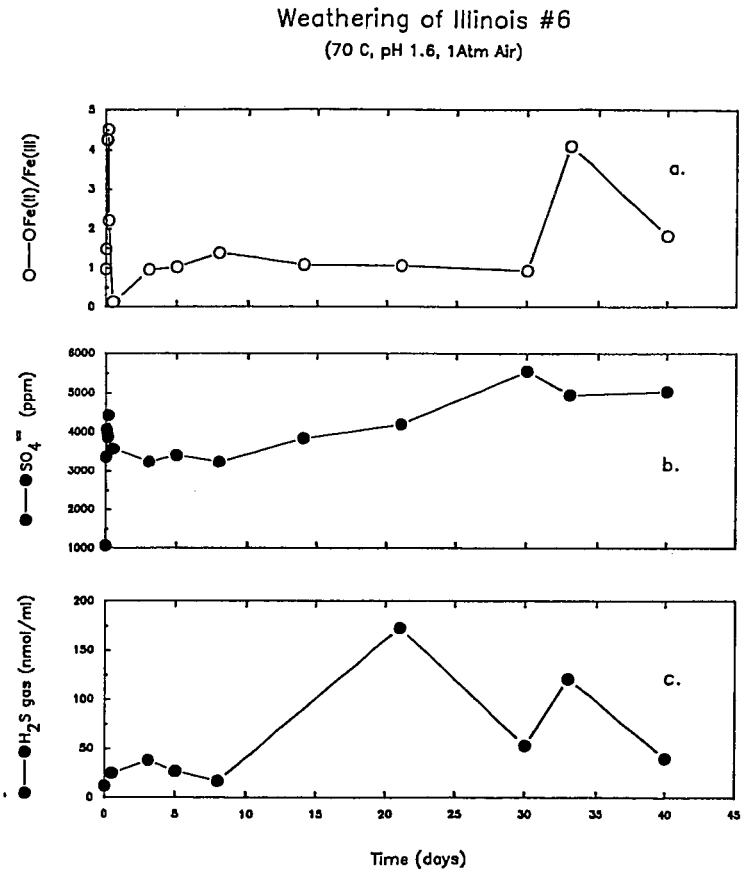

Figure 1. Illinois no. 6 coal (20 g) weathered in an acidic, aqueous suspension (1L, 0.04 M H_2SO_4) gave the above profiles for iron and sulfate concentrations in solution and H_2S generation upon bioassay. a) For the Fe(II)/Fe(III) ratio, total and ferrous iron concentrations were determined spectrophotometrically (1,10 phenanthroline reaction, absorbance 510nm). Ferric iron was determined by difference. b) Concentration of SO_4 was determined turbidimetrically ($BaSO_4$, absorbance 340nm). c) In the bioassay, gaseous H_2S was determined through gas chromatographic analysis of head gas from batch cultures of *P. furiosus* on timepoint samples of weathered coal (0.25g). Values of H_2S are normalized by gas injection volume.

Note: The amount of reducible sulfur available to the microorganisms changes during the course of weathering suggesting a change in the distribution of oxidation products.

Coal Desulfurization Studies: Inability of *Sulfolobus* spp. to oxidize sulfur compounds in coal

J. B. Risatti, Illinois State Geological Survey, 615 E. Peabody Dr., Champaign, IL 61820; K.W. Miller, Dept. Biological Sciences, Illinois State Univ., Normal, IL ; S. Broeren, Illinois State Geological Survey, 615 E. Peabody Dr., Champaign, IL 61820

Key Words: Sulfolobus, chemolithotrophy, desulfurization

Introduction

A major problem associated with direct combustion of high sulfur coal is the emission of sulfurous gases into the atmosphere. To address this problem, a number of pre- and post combustion processes, including bacterial leaching, have been proposed. Economically, microbial desulfurization requires low capital output and consequently, has the potential to be significantly less expensive than other methods.

A number of chemolithotrophic bacteria (eubacteria) readily obtain energy by oxidizing elemental sulfur and sulfide minerals. The sulfidic mineral, pyrite, is a major sulfur contaminant in many coals and the conditions governing rates of bacterial pyrite oxidation in coal have been extensively studied[1,2,3,]. Although iron and sulfur oxidizing microorganisms may remove up to 97% of the pyrite from coal in approximately 8 days[4] they are unable to remove the organic sulfur fraction[5].

Recently, several coal leaching studies using archaea[6] belonging to the genus *Sulfolobus* have reported the oxidation of both inorganic (pyritic)[7,8] and organic sulfur[9,10,11] in coal and also, the oxidation of dibenzothiophene [12] by *Sulfolobus acidocaldarius*. Because of these studies, we compared *Sulfolobus acidocaldarius* strains 98-3 and DSM 639 and *S. solfataricus* ATCC 35091 with *Thiobacillus ferrooxidans* to determine how effectively sulfolobus could remove organic and inorganic sulfur from a pyritic Illinois coal and a washed (low pyrite) Illinois coal. In addition, the oxidation of sulfur to sulfate by *Sufolobus* spp.was determined for elemental sulfur, thiosulfate and dibenzothiophene.

Experimental Methods

Sulfolobus acidocaldarius strains DSM 639 and 98-3, were provided by Carl Woese (University of Illinois, Urbana-Champaign). *S. solfataricus* ATCC 35091 was purchased from the American Type Culture Collection . Cultures were maintained at 70 °C in Allen's [13] mineral salts medium (SMS) as modified by Brock et al.[14] and amended with sucrose (0.2%) and yeast extract (0.1%). To adapt cells to chemolithotrophic growth, yeast extract was replaced with either pyrite at 5 g L^{-1} or with elemental sulfur at 10 g L^{-1}. Elemental sulfur was sterilized by tyndallisation and added separately to autoclaved medium. The type strain of *Thiobacillus ferrooxidans* was obtained from A. Harrison, University of Missouri, Columbia, MO, and maintained at 28°C on ATCC medium 64 with pyrite (0.5%) replacing $FeSO_4 \cdot 7H_2O$ as a growth substrate.

Coal sample IBC-104, obtained from the Illinois Basin Coal Bank Program, Champaign, IL, is a high-sulfur, run of mine Herrin coal which was deslimed to lower the ash yield to 15% and ground to -200 mesh. Coal sample FCC-103 was prepared from Illinois Bank Coal IBC-103 (a blend of 80% Springfield no.5 and 20% Herrin no.6) by froth flotation to sulfur contents of 1.76% total, 0.42% pyritic, and 1.26% organic. Forms of sulfur in coal were determined using ASTM standard methods [15]. Mineral pyrite (Sargent-Welch, Skokie, IL), approximately 85% pure, dibenzothiophene (DBT), elemental sulfur and sodium thiosulfate (analytical grade) were used as sulfur sources. Coal at 5%

pulp density, was added to 125 mL Erlenmeyer flasks containing 50 mL SMS medium without yeast extract for *Sulfolobus* spp. or to TMS medium without pyrite for *T. ferrooxidans*. Sulfate salts in the media were replaced with their chloride equivalents. The pH was adjusted to 2.5 with HCl and the flasks autoclaved at 121°C for 20 minutes. *T. ferrooxidans* inocula consisted of 0.5 ml of exponential phase culture. Sulfolobus inocula (10%) consisted of 48 h cultures washed with unammended SMS and with OD's adjusted to 0.5 at 620 nm. *T. ferroxidans* cultures were incubated at 28°C with shaking at 150 rpm; *Sulfolobus* spp. were incubated at 70°C in a waterbath shaker. Uninoculated controls containing the sterile media and target substrates were incubated with all experiments and all experiments were performed in duplicate. Periodically, 1.0 ml samples were withdrawn, centrifuged to remove particulates, and analyzed turbidometrically for sulfate [16]. At this time, flasks were weighed to determine evaporation, which was never more than 5% during the course of an experiment. At the conclusion of the experiments, coal was retrieved by vacuum filtration, rinsed with 0.1 N HCl, air dried, and analyzed for forms of sulfur.

Results

After 27 days of leaching by *T. ferrooxidans*, 90.9% of the inorganic sulfur in the IBC-104 coal was solublized to sulfate, decreasing the total sulfur content of the coal from 4.78% to 2.58%. Assuming that all of the original sulfate in the coal (0.12%) was leached into the supernatant, *T. ferrooxidans* removed at least 89.6% of the pyritic sulfur at a maximum rate of about 12% day^{-1}. In the concomitant controls, pyrite decreased by approximately 24%. Most probable number (MPN) estimates of viable cells increased from 1.9×10^6 to 2.4×10^9 cells ml^{-1} in the inoculated coal cultures; no cells were observed in the sterile controls.

After 22 days of leaching coal samples IBC-104 and FCC-103 with *S. acidocaldarius* 98.3 and DSM 639 and *S. solfataricus*, organic sulfur content (2.38% and 1.26% respectively) remained unchanged and pyrite decreased by approximately 80 to 83% in all cases (including controls) implying *Sulfolobus* spp. did not oxidize either the pyritic or the organic sulfur in these coals. The observed decreases in pyrite were not from microbial activity but are a result of the increased oxidation occuring at 70°C at a pH of 2 to 3. As determined from MPN estimates, viable cells on the order of 1.9×10^4 cells mL^{-1} were present after 22 days both in cultures with coal and in inoculated controls without coal. Sterilized, uninoculated controls showed no cell growth after 22 days. These results demonstrate that neither the pyrite nor the organic sulfur in the coal supported growth of *Sulfolobus* spp. and also that the coals had no deleterious effects on the organisms.

In experiments with pyrite (-150 mesh), sulfate was produced at the same rate in both the inoculated and the uninoculated flasks and there was no evidence that any of the three strains of *Sulfolobus* oxidized pyrite. Additional experiments in which pyrite was amended with sucrose or yeast extract, gave similar results. *Sulfolobus* spp. were also unable to utilize elemental sulfur or thiosulfate. After 15 days of incubation, 4.6 - 5.6% of the elemental sulfur in the cultures was oxidized to sulfate and in experiments with thiosulfate as the sole energy source, only 3.0 - 3.6% of the thiosulfate (1 mg mL^{-1}) was oxidized to sulfate.

Experiments with dibenzothiophene (DBT) as sole substrate indicated that *S. solfataricus* and both strains of *S. acidocaldarius* converted approximately 10-15% of the sulfur in DBT to sulfate. However, based on protein analyses[17] and cell counts by light microscopy, DBT did not appear to be utilized as a growth substrate.

From our data, we question the ability of *S. acidocaldarius* 98-3 and DSM 639 and *S. solfataricus* ATCC 35901 to oxidize pyritic minerals or organic sulfur in coals at a demonstrable rate or to grow lithotrophically using elemental sulfur, pyrite or thiosulfate.

Acknowledgement

Research sponsored by the Illinois Coal Development Board through the Center for Research on Sulfur in Coal (CRSC) under contracts to the Illinois State Geological Survey (JBR) through the University of Illinois at Urbana-Champaign.

References

(1) Silverman, M. P.and D. G. Lundgren, 1959 Jour. Bacteriology 78:326-331.
(2) Silverman, M. P., M. H. Rogoff and T. Winder, 1961 Applied. Microbiology. 9:491-496.
(3) Detz, C. M. and C. Barvinchak, 1979 Mining Congress Journal 66:75-86
(4) Dugan, P.R. and W. A. Apel, 1978 Microbial desulfurization of coal. pp.223-250. In Metalurgical applications of bacterial leaching and related microbiological phenomena. L. E. Murr, A. E. Torma and J. Breirley (eds.), Academic Press, New York.
(5) Bos, P., T. F. Huber, C. Kos, C. Ras and J. G. Kuenen, 1985 International Symposium on Biohydrometallurgy, Vancouver, British Columbia.
(6) Woese, C.,O. Kandler and M. Wheelis, 1990 Proceed. Nat. Acad. of Science (In Press).
(7) Kargi, F. and J. M. Robinson, 1982 Applied and Environmental Microbiology 44:878-883
(8) Kargi,F. and J. M. Robinson, 1982 Bioeng. and Biotechnology 24:2115-2121
(9) Murphy, J., E. Riestenberg, R. Mohler, D. Marek, B. Beck and D. Skidmore, 1985 Coal desulfurization by microbial processing. pp.643-652. In Processing and Utilization of High Sulfur Coals, Y. A. Attia (ed.), Elsevier.
(10) Kargi F. and J. M. Robinson, 1985 Bioeng. and Biotechnology 27:41-49
(11) Kargi, F. and J. M. Robinson, 1986 Fuel 65:397-399
(12) Kargi F. and J. M. Robinson, 1984 Bioeng. and Biotechnology 26:687-699
(13) Allen, M. B., 1959 Arch. Mikrobiol. 32:270-277
(14) Brock, T. D. ,K. M. Brock, R.T. Belly and R.L. Weiss, 1972 Arch. Mikrobiol. 84:54-68.
(15) Annual Book of American Society of Testing Materials Standards, 1979 American Society of Testing Materials, Philadelphia, PA, USA.
(16) Miller and Risatti, 1988, Biooxidation of pyrrhotites in coal chars. Fuel 67: 1150- 1154.
(17) Lowry, O. H., N. J. Rosrbrough, A. L. Furr and R. J. Randall, 1951 Jour. Biol. Chemistry 193:265-275.

BIOLEACHING OF MOLYBDENUM FROM A COAL LIQUEFACTION CATALYST RESIDUE

Bernard Blaustein, David Suhy and Eric Spana
U.S. Department of Energy
Pittsburgh Energy Technology Center
Pittsburgh, PA 15236

Keywords: bioleaching, molybdenum disulfide, catalyst residue

ABSTRACT

Molybdenum disulfide, MoS_2, is used as a catalyst in coal-oil coprocessing. For most processes using molybdenum catalysts to be economical, the molybdenum must be recovered and recycled. Chemical recovery schemes have been devised, but typically recover only a fraction of the molybdenum. There are reports in the literature that bacteria can oxidatively solubilize MoS_2 (molybdenite) ore. This paper reports the initial results of experiments where Thiobacillus ferrooxidans are shown to microbially solubilize MoS_2 present in coal liquefaction catalyst residues. Small-scale shake-flask experiments show that after leaching of the catalyst residue by T. ferrooxidans at pH ~2 for 6-7 weeks, as much as 66-71% of the Mo can be solubilized. Analyses of the microbially-leached products and mass-balance calculations can account for 78-103% of the Mo initially present in the coal liquefaction residue.

INTRODUCTION

Molybdenum disulfide is used as a catalyst in coal-oil coprocessing. It is effective at concentrations as low as 200 ppm Mo by weight, based on coal (ref. 1). Molybdenum is added to the coal in the form of aqueous solutions of ammonium heptamolybdate, $(NH_4)_6Mo_7O_{24}$, or ammonium tetrathiomolybdate $(NH_4)_2MoS_4$. The MoS_2 catalyst is then formed in situ at coal liquefaction conditions at about 350°C, in the presence of hydrogen.

Even though MoS_2 is used at low concentrations, it is necessary to recover the molybdenum so that it can be recycled. A chemical recovery scheme has been developed (ref. 2). The coal liquefaction residue is first roasted (calcined). Under these conditions, the mineral matter in the residue and the molybdenum from the MoS_2 form compounds that are only partially soluble in the aqueous NH_3 used to leach the roasted material. This results in only a partial recovery of the molybdenum from the MoS_2 present in the coal-oil coprocessing liquefaction residue.

There are reports in the literature (refs. 3-7) that bacteria can oxidatively solubilize MoS_2 (molybdenite) ore. This paper reports on the use of Thiobacillus ferrooxidans to aerobically solubilize MoS_2 present in a coal liquefaction (coprocessing) catalyst residue to facilitate recovery of the molybdenum.

EXPERIMENTAL

Catalyst Residue: Two gallons of liquids produced from reaction of Illinois No. 6 hvB bituminous coal and Maya atmospheric tower bottoms under coprocessing conditions (ref. 1) were processed as shown in Figure 1. Approximately 100 grams of catalyst residue that contained MoS_2, obtained as the tetrahydrofuran-insolubles, were dried in a vacuum oven at 100°C for 4 hours and then ground to

pass a 60-mesh screen. Analysis of the catalyst residue (done by Huffman Laboratories, Inc., Golden, Colorado) is given in Table 1.

Source of Microbes: Several strains of Thiobacillus ferrooxidans were obtained from the Center for Bioprocessing Technology of the Idaho National Engineering Laboratory (INEL). The original source of two of the strains (23270 and 13598P) was the American Type Culture Collection. Two other strains, A6 and PH, were obtained from Doris Thompson at INEL. The Bureau of Mines, Bruceton Research Center, provided a sample of acid mine drainage muck, which was designated as culture BOM and assumed to contain, inter alia, T. ferrooxidans.

In general, the several strains of T. ferrooxidans were maintained on 9K or INEL medium (see below). After the preliminary bioleaching experiments with catalyst residue were completed, inocula were taken from these finished experiments to start new bioleaching experiments. Thus, in some cases, the bacteria now being used have been exposed to catalyst residue and/or molybdate leachate solutions for as long as 6 months.

Preparation of Media: T. ferrooxidans grow optimally at pH 2.0-2.5. After some preliminary experiments, it was decided to use the 9K medium as described by Silverman and Lundgren (ref. 8). However, due to large amounts of ferric iron precipitates on the glassware with the use of 9K, most additional work was done with the INEL medium. The recipe (shown below) was obtained through Idaho National Engineering Laboratories, via Dr. Paul Wichlacz (ref. 9).

Recipe for INEL Salts

To 1 liter of distilled water adjusted to pH 2.0 with H_2SO_4, add:

$(NH_4)_2SO_4$	0.15 g
KCl	0.15 g
K_2HPO_4	0.15 g
$MgSO_4 \cdot 7H_2O$	3.36 g
$CaCl_2 \cdot 2H_2O$	1.28 g
$Al_2(SO_4)_3 \cdot 18H_2O$	2.25 g
$MnSO_4 \cdot H_2O$	0.12 g

200 mL of the solution is removed. Autoclave the remaining 800 mL portion in ten flasks (250 mL size) with 80 mL in each. Add 7.46 g of $FeSO_4 \cdot 7H_2O$ to the 200 mL portion while stirring. Filter sterilize the iron solution and add 20 mL aliquots to each 80 mL of sterile salts when cool.

Bioleaching experiments: The bioleaching experiments were carried out in 250 mL Erlenmeyer flasks on a shaker (125 rpm) in an incubator maintained at 29°C. Catalyst residue (0.5g) was added to 100 mL of medium (pH = 2). This mixture was then inoculated with 1 mL of the bacterial culture. After bacterial growth and leaching for 6-7 weeks, the microbially-treated sample was filtered and worked up as shown in Figure 2. The filtrates were analyzed for Mo by atomic absorption spectral analysis. The initial and final solid residues were analyzed for molybdenum as follows. First, the sample was ashed in a muffle furnace at 750°C. The ash was fluxed in lithium tetraborate and then dissolved in HCl. The HCl solution was analyzed by AA according to ASTM D3682-87.

RESULTS AND DISCUSSION

Results from small-scale shake-flask experiments are shown in Table 2. The dates that the experiments were run are given in parentheses above the column headings. In these shake-flask experiments, which demonstrate the feasibility of bioleaching MoS_2, as much as 71% of the Mo initially present in the catalyst

residue was solubilized. Results of the control experiments given in Table 2 show that the amounts of Mo solubilized in the controls are low compared to amounts of Mo solubilized in the microbial leaching experiments. In order to estimate the overall precision in these experiments, values calculated for the mass balance for molybdenum are also shown in the sixth row of the table. For the experiments described in Table 2, the amount of Mo found by analysis of solutions B and D and of residue E (see Figure 2) could account for 78 to 103% of the molybdenum present in the original catalyst residue A.

These initial experiments, which show that some strains of Thiobacillus ferrooxidans can solubilize MoS_2 when it is present in a residue from coal-oil coprocessing, also show that the other materials present in the residue do not stop the bioleaching of the molybdenum. It is interesting to note that molybdate concentrations in solution at the end of the experiments were as high as 51 ppm. Reports in the literature (refs. 4-7, 10-12) suggest that a concentration as low as 10 ppm molybdate is toxic to T. ferrooxidans. However, inocula taken from these high concentration molybdate flasks, and used in subsequent experiments, proved viable and capable of additional bioleaching. This would suggest that we have developed a strain of T. ferrooxidans that has adapted to high molybdate concentrations. But also, it is possible that the condition designated as "toxic" to the bacteria might be better described as "inhibitory."

Both media used (9K and INEL) contain ferrous iron, as does the liquefaction catalyst residue. After bio-oxidation, this results in relatively high concentrations of ferric iron in the leachate solutions. We hypothesize that the iron(III) species present in solution form insoluble iron(III)molybdate compounds, as depicted in Figure 2. After the microbially-leached solutions are filtered, the iron(III) molybdate present (mixed with the unreacted catalyst residue in mixtures) was dissolved in 3N HCl. After filtration, this HCl solution (acid extract D) contains most of the molybdate that was formed during the bioleaching. In the best result, solutions B and D together contain 71% of the Mo solubilized from the MoS_2 initially present in the catalyst residue.

ACKNOWLEDGEMENTS

David Suhy and Eric Spana held appointments as Professional Interns at the Pittsburgh Energy Technology Center. This intern program is administered for the U.S. Department of Energy by Oak Ridge Associated Universities, Oak Ridge, Tennessee.

DISCLAIMER

Reference in this paper to any specific commercial product, process, or service, is made to facilitate understanding and does not imply its endorsement or favoring by the U.S. Department of Energy.

REFERENCES

1. Lett, R.G., Cugini, A.V., Utz, B.R., Krastman, D., Cillo, D.L., and Jin, G.T. 1989. Dispersed-Phase Catalyst Approaches in Coal Liquefaction and Coprocessing. Sixth Joint U.S.-Korea Workshop on Coal Utilization Technology, October 16-18, 1989, Seoul, Korea.

2. Krastman, D., Utz, B.R., Cugini, A.V., and Lett, R.G. 1990. Dispersed Phase Molybdenum Catalyst Recovery in Coprocessing. Preprints, Div. Fuel Chem., Am. Chem. Soc., 35(2):570-576.

3. Bryner, L.C., and Anderson, R. 1957. Microorganisms in Leaching Sulfide Minerals. Ind. Eng. Chem. 49:1721-1724.

4. Bhappu, R.B., Reynolds, D.H., and Roman, R.J. 1965. Molybdenum Recovery from Sulfide and Oxide Ores. J. of Metals. 17:1199-1205.

5. Brierley, C.L. 1974. Molybdenite Leaching: Use of a High-Temperature Microbe. J. Less Com. Met. 36:237-247.

6. Lyalikova, N.N., and Lebedeva, E.V. 1984. Bacterial Oxidation of Molybdenum in Ore Deposits. Geomicrobiology Journal. 3:307-318.

7. Kelley, B.C. 1986. Biological Contributions to Mineral Cycling in Nature with Reference to Molybdenum. Polyhedron. 5:597-606.

8. Silverman, M.P., and Lundren, D.G. 1959. Studies of the Chemoautotrophic Iron Bacterium Ferrobacillus ferrooxidans I. An Improved Medium and Harvesting Procedure for Securing High Yields. Journal of Bacteriology. 77:642-647.

9. Wichlacz, P.L., and Unz, R.F. 1985. Appl. Environmental Microbiology. 50:460-467.

10. Tuovinen, O.H., Niemelä, S.I., and Gyllenberg, H.G. 1971. Tolerance of Thiobacillus ferrooxidans to Some Metals. Antonie Van Leeuwenhoek. 37:489-496.

11. Karavaikd, G.I., Dzhansugurova, R.S., and Pivovarova, T.A. 1989. Factors Increasing Resistance of Thiobacillus ferrooxidans to Molybdenum. Mikrobiologiya. 58:412-418.

12. Thompson, D.L., Wichlacz, P.L., and Bruhn, D.F. Heavy Metal Tolerance in Thiobacillus ferrooxidans and Genus Acidiphilium, In Press.

TABLE 1. Analysis of the THF-Insoluble MoS_2/Co-Processing Residue

Element	Percent
Carbon	24.5
Hydrogen	1.95
Oxygen (Direct)	7.2
Nitrogen	0.72
Sulfur	7.4
Iron	9.9
Molybdenum	2.80

TABLE 2. Results of Shake-Flask Bioleaching Experiments Using 0.5 Gram MoS_2 Catalyst Residue

	9K Experiments (7/26 - 9/8)				INEL Experiments (8/17 - 10/4)						Bioleaching Group #5	
Inoculum Medium	23270 + 9K	13598P + 9K	UNINOC 9K	23270 + Salts (9K)	13598P + INEL	23270 + INEL	PH + INEL	A6 + 9K	BOM + 9K	UNINOC + INEL	13598P + INEL	23270 + INEL
Mo Conc., Filtrate B (ppm)	40	43	0.3	47	51	39	0.5	0.1	33	2.3	34	31
Mo in Filtrate B (mg)	2.71	3.00	0.02	1.89	4.32	3.45	0.04	.01	2.28	0.15	2.46	2.25
Mo in Acid-Extract D (mg)	3.36	4.13	1.13	3.26	5.64	5.82	1.44	1.38	3.36	1.26	6.15	6.11
Mo in Acid-Extract Residue E (%)	1.65	1.70	3.16	2.19	1.40	1.22	2.80	2.65	2.25	3.06	1.20	1.31
Mo in Acid-Extract Residue E (mg)	5.91	5.98	11.22	6.24	4.58	3.84	9.38	8.93	7.43	9.85	3.92	4.20
Mo Recovery (%)	85	94	88	81	103	94	78	74	93	80	90	90
Mo Solubilized (%)	43	51	8	37	71	66	11	10	40	10	62	60

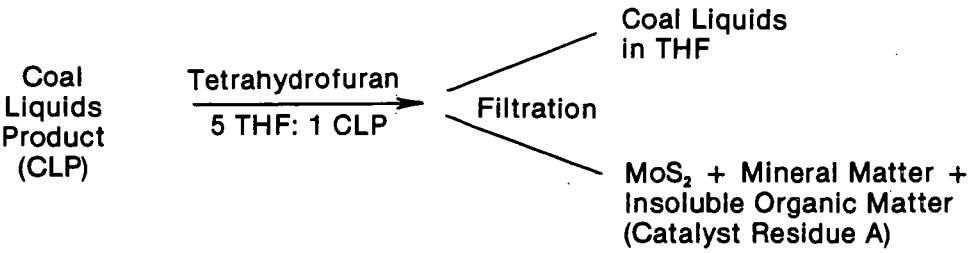

FIGURE 1. SEPARATION OF MoS_2 CATALYST RESIDUE FROM COAL-OIL CO-PROCESSING LIQUIDS.

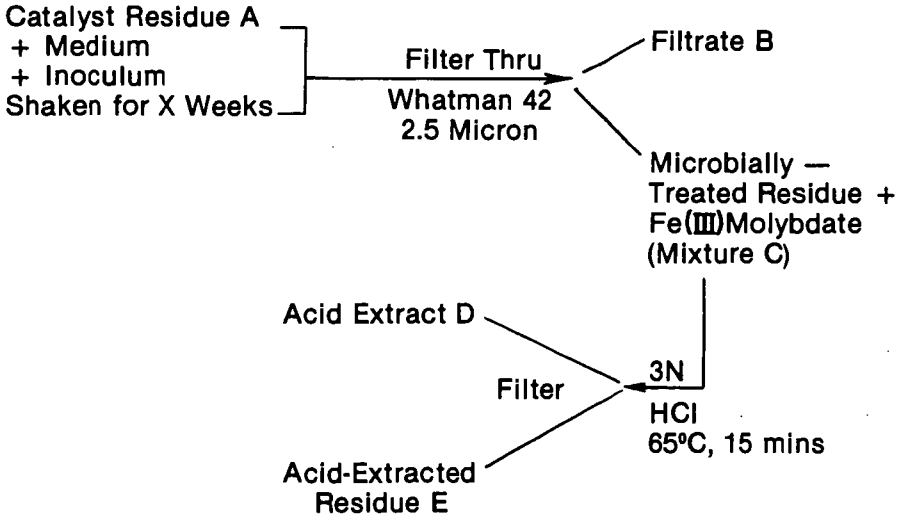

FIGURE 2. SHAKE-FLASK BIOLEACHING OF MoS_2 CATALYST RESIDUE: MASS BALANCE EXPERIMENTS.

BACTERIOELECTRIC DEASHING OF COALS

Norman Lazaroff
State University of New York, Binghamton, NY 13901

John E. Wey and Patrick R. Dugan
Idaho National Engineering Laboratory
EG&G Idaho, Inc.
Idaho Falls, ID 83415-2203

The premise that a combination of electric current and bacterial action would remove metals from coal more effectively than either of the factors acting alone, stemmed from earlier observations of enhanced pyritic ore leaching and iron corrosion by suspensions of *Thiobacillus ferrooxidans* in galvanic cells. Although sulfide minerals are oxidized more slowly than native metals under acid abiotic conditions, like metals their oxidation can be greatly accelerated by an imposed voltage in a galvanic cell. The consequent release of metal ions from pyritic substrates as the result of electrooxidations is analogous to the solubilization of minerals by the action of chemolithotrophic microorganisms which catalyze the transport of electrons from oxidizable cations or sulfide ligands to oxygen.

When metals are placed at the anode of a galvanic cell, the liberation of ionic species by electro-oxidation is dependent upon provision of a polarizing voltage and the presence of electron acceptors that promote current flow by cathode depolarization. While a metal in elementary form can be electrolytically oxidized to form a soluble cation, the insoluble metal in a sulfide mineral is already in cationic form complexed with a sulfur anion. If a sulfide mineral species conducts electricity, its cations can be released by electro-oxidation of the reduced sulfur ligands to produce elementary sulfur. The knowledge that pyritic minerals are good electrical conductors (Decker, R. F., 1986) as well as substrates for oxidation by thiobacilli, implied that the two phenomena could operate synergistically. It was visualized that the Fe(II) released electrolytically would be oxidized by chemolithotrophic iron oxidizing bacteria and that the soluble Fe(III) produced in an acid environment would oxidize pyritic sites insulated from electro-oxidation.

Conceptually, a suitable electrical potential, would liberate Fe(II) cations by oxidizing reduced sulfur anions of pyritic minerals. Electric current would flow from the source as the cathode is depolarized by hydrogen ions of the acid lixiviant and Fe(II) cations move into solution toward the cathode. In dilute sulfuric acid solution, as the Fe(II) is oxidized by iron oxidizing thiobacilli, the resultant Fe(III) sulfato complex would have the possibility of participating in several different reactions depending upon the conditions existing in the galvanic cell (Figure 1). These include: (1) aggregation (polymerization) to an insoluble amorphous hydrated Fe(III) sulfate; (2) reduction at the cathode forming additional substrate for bacterial iron oxidation in the bulk phase of solution; (3) reduction, after recirculation to non-anodic sites on pyritic surfaces, liberating oxidized sulfur species and Fe(II) from the pyrite; (4) alkaline precipitation; when proton consumption by cathode reactions occurs to the extent that the environment of the cathode becomes basic, the Fe(III) sulfato complex decomposes and iron is precipitated in the form of Fe(III) oxides and oxyhydroxides. The proton concentration in this system is also dependent upon the activities of thiobacilli which oxidize

sulfides, polythionates and elementary sulfur derived from the oxidation of pyritic minerals. Acidity produced from those activities counteracts proton consumption from cathode depolarization reactions and the reduction of O_2 by chemoolithotrophic oxidation of Fe(II). At low pH the iron sediments formed are those typical of chemolithotrophic iron oxidation, amorphous hydrated Fe(III) sulfate and jarosites. Consequently, cleaning coal by ordinary bacterial leaching may leave iron sediments remaining on the coal that contain sulfur in iron sulfato complexes. However, in a galvanic cell the iron and sulfur of the sulfato-complexes appear to be transported together to the cathode and remain undissociated under acid conditions. Therefore, this means of sulfatic sulfur removal represents further benefit to be gained from cleaning coal by a combined bacterial and electrolytic leaching process.

The following account describes an exploratory investigation of the feasibility of using the bacterioelectric phenomenon for metal removal and recovery from different coals.

Materials and Methods

Bulk leaching was carried out in magnetically stirred glass beakers equipped with glass cathode and anode chambers fitted with platinum electrodes as shown in Figure 2. Initially, approximately 0.4 g of a powdered coal sample was placed at the anode either wrapped in ashless filter paper, such as Whatman 41, or placed within a cellulose extraction thimble. The powdered coal was compressed around the platinum foil of the electrode by inserting the wrapped combination into the tightly fitting perforated glass tube that served as anode chamber. The leaching system was filled with a lixiviant of pH 2.5 sulfuric acid or some experimental modification thereof. The bacteria that were used, consisted of suspensions of the Leathen strain of *Thiobacillus ferrooxidans* prepared as previously described (Lazaroff, et al. 1982). The electric current and voltage were monitored by provision of individual integrated circuits for each bacterioelectric unit. These employed National Semiconductor LM117 voltage regulators as shown in Figure 2. In subsequent experiments powdered coal was rapidly circulated around an anode with a magnetic stirrer and the cathode was inserted in a medium porosity "alundum" extraction thimble. Usually the cathode chamber sediments were collected in centrifuge tubes, then washed by sedimentation and decantation; first in pH 2.5 H_2SO_4 then distilled water. Prior to analysis washed sediment or coal samples were dried overnight at 85°C in a forced draft oven. The pre-weighed coal samples were ashed in tared porcelain crucibles in an electric furnace kept at 850°C overnight.

Energy Dispersive X-Ray analysis were used to identify and measure relative amounts of the different metals in sediments collected from the cathode chamber, as coatings on the platinum cathodes and from drying the bulk lixiviant to recover solubilized metals. Conventional methods were used to examine the IR spectra of sediments prepared in KBr discs (Lazaroff et al. 1982).

A laboratory scale continuous bacterioelectric reactor was constructed that utilized a porous alundum cathode chamber contained in a horizontal air-lift device that impinges a rapidly stirred coal slurry on a platinum anode. The system shown in Figures 3 and 4 allows periodic recovery of processed coal and electrically separated metals, while adding the feedstock coal.

Results

The metals deposited on the cathode or in the cathode chamber following galvanic treatment of coal qualitatively reflect the metal composition of the heterogeneous starting material. While iron is most abundant in cathode sediments from pyritic coals, significant amounts of sodium, potassium, rubidium, magnesium, calcium, strontium, aluminum, titanium, copper, manganese, zinc, lead, nickel and chromium have also been recovered there, depending upon the coal sample studied. Although the univalent cations, sodium and potassium are found in the cathode sediments, often larger quantities are found in soluble form in the acid lixiviant along with much aluminum, calcium and magnesium as well as smaller amounts of heavier metals such as iron. In some coal samples, the rarer elements, lutecium, yterbium, lanthanum and neodymium were found usually by inspection of localized deposits on the platinum cathodes with scanning electron microscopy and ED x-ray analysis (Lazaroff and Dugan, 1989). The non-metallic elements found at the cathode, presumably complexed with cations, include sulfur, phosphorous, silicon and less frequently chorine. One coal sample yielded significant amounts of bromine. Not all of the metals leaching from coal samples deposited at the cathodes of the galvanic systems.

PSOC 667, a sub-bituminous Iowa coal containing approximately 6% pyrite, was found to be particularly suitable for studying bacterioelectric deashing. Earlier studies had shown that bacterial presence during galvanic treatment resulted in more complete removal of metals from the slurried coal compacted at a platinum anode (Lazaroff and Dugan, 1989). Table 1 compares the results of deashing in the presence of bacteria or by increasing the conductivity of the galvanic cell through addition of 10^{-3}M Li_2SO_4. The enhancement of conductivity alone, resulted in removal of as much as 75% of the ash from the PSOC 667 coal in 20 hrs treatment. It was found that comparable results could be obtained with dispersed stirred coal particles at the anode if the lithium solute was present or with slower rates of deashing in the presence of bacteria in the absence of lithium sulfate. With protracted bacterioelectric leaching of stirred PSOC 667 coal slurries, over 90% of ash has been removed (Table 2).

Examination of the leachability of other coals by the bacterioelectric system indicated that most pyritic bituminous and subbituminous coals were susceptible to galvanic deashing but with considerable variation in efficiency of metal removal. The lignites investigated were not enhanced in deashing by the presence of bacteria which was possibly correlated with the absence of Pyrite (Table 1).

Although pyritic coals show the effect of bacterial enhancement of metal removal, there is no clear indication that the only metals removed from the coal are associated with pyritic inclusions. A good example of this is observed with PSOC 1322, an Illinois #6 high volatile bituminous coal. The presence of bacteria significantly contribute to metal removal. The cathode chamber deposit is mainly iron when the iron oxidizing bacteria are present but copper, calcium, silicon, manganese and aluminum are present as well. Without the additional iron oxidizing thiobacilli, the smaller cathode accumulation is qualitatively similar in metal composition but is predominantly calcium with comparatively little iron. The calcium is removed from the coal in large amounts without the added bacteria but it is found in

soluble form in the lixiviant rather than precipitated at the cathode (Figure 5). Figures 6 and 7 are ED-X-ray spectra of additional pyritic bituminous coals presented in Table 1 (PSOC 1316 and IBCSP #2) that further illustrate the removal of metals by the bacterioelectric effect.

An interesting aspect of this fractionation of metals in different phases of the system undergoing deashing is shown in Figure 8. As with the PSOC 1322 coal, the cathode chamber sediment from bacterioelectric leaching is largely iron while the comparable sediment from galvanic leaching without bacteria is mainly calcium. However, the calcium can be collected as a solid phase separate from the main cathode sediment or the dissolved solutes of the lixiviant by placing a membrane filter over the cathode chamber port. The calcium then deposits almost exclusively on the filter along with iron, and very little calcium enters through the porous membrane to deposit in the cathode chamber. This does not occur in the absence of added iron oxidizing bacteria suggesting that the Fe(III) sulfato-complex produced by chemolithotrophic iron oxidation is in some way responsible for co-precipitation of iron and calcium on the membrane.

The encouraging results obtained from deashing subbmituminous coal galvanically in dispersed suspension, in the presence of bacteria or lithium sulfate led to construction of a system which allows re-use of the lixiviant and bacteria in a continuously fed laboratory scale reactor (Figures 3 and 4). In limited trails, so far, it appears possible to use the horizontal air-lift flowing system to remove 80 to 90% of ash from bacterially pre-treated Iowa subbituminous or Illinois #6 bituminous coal.

Summary

1. Metals can be removed from bituminous and sub-bituminous coals in galvanic cells at low voltages and currents. Originally this involved compressing powdered coal at an inert anode in a stirred dilute sulfuric lixiviant.

2. Pyritic coals may be simultaneously oxidized by acidic iron formed by iron oxidizing thiobacilli. This results in some coals yielding enhanced metal deposition at galvanic cathodes.

3. More complete deashing of a sub-bituminous coal was accomplished at high current densities in systems containing 10^{-3} -> 10^{-2} M Li_2SO_4 in the sulfuric lixivant. 74% of ash removal has been accomplished.

4. The galvanic deashing can be carried out with dispersed-suspended coal particles in the Li_2SO_4 lixiviants or in systems containing cells of *Thiobacillus ferrooxidans* or with coal slurries pre-treated with *Thiobacillus ferrooxidans*.

5. A continuous laboratory-scale system for bacterioelectric deashing of pyritic coals has been developed.

Acknowledgments

This work was supported under contract No. DE-AC07-76IOD1570 from the U.S. Department of Energy, to the Idaho National Engineering Laboratory/EG&G Idaho, Inc.

References

Decker, R. F. 1986. Metall. Trans A, 17:5-30.

Lazaroff, N., Sigal, W., and Wassenman, A. ,1982. Appl. and Env. Microbiol. 43:924-938.

Lazaroff, N. and Dugan, P. R. 1989. Proceedings, Bioprocessing of Fossil Fuels Workshop. Tyson's Corner, VA. pp. 79-104 (CONF-890884) available from NTIS U.S. Dept. Commerce, Springfield, VA 22161.

TABLE 1. ELECTROBACTERIAL DEASHING OF COAL SAMPLES

Coal Sample	Treatment	Ash (% by wt.)
HBV		
PSOC 1322	None	12.13
1.98% pyrite S	46 hrs 8V, 2mA + Bact.	9.92
	46 hrs 8V, 2mA - Bact.	10.92
	Bact. pre-treat 56 hrs. 10V, 5 mA	6.99
HBCB		
PSOC 1316	None	11.06
1.47% pyrite S	91 hrs 16V, 5mA + Bact.	10.86
	91 hrs 16V, 5mA - Bact.	11.16
PSOC 551	None	14.74
4.68% pyrite S	43 hrs 16V, 5mA + Bact.	11.10
	43 hrs 11V, 5mA - Bact.	4.24
IBCSP 2	None	5.70
2.34% pyrite S	90 hrs 15V, 5mA + Bact.	4.17
	90 hrs 15V, 5mA - Bact.	4.19
Sub-bit. A		
PSOC 667	None (as rec.)	18.73
6.0% pyrite S	Bact. pre-treat + 45 hrs 7V, 2mA ave	7.04
	None (dry basis)	21.23
	in thimble, 20 hrs 12V, 5mA	13.04
	in thimble, 20 hrs 12V, 35mA + Li_2SO_4	4.80
	dispersed, 14 hrs, 12V, 38mA	7.96
Sub-bit. C		
PSOC 637	None	10.41
0.64% pyrite S	Bact. Pre-treat + 67V, 3mA ave	4.79
Lignite		
PSOC 1489	None	6.90
0.02% pyrite S	41 hrs 17V, 5.0mA + Bact.	3.60
	41 hrs 15V, 5.0mA - Bact.	3.20
Spanish Lignite	None	12.48
	66 hrs 10V, 2mA - Bact.	9.46
Lignite A		
PSOC 245	None	8.89
0.22% pyrite S	90 hrs 10V, 2.5mA + Bact.	7.14
	90 hrs 13V, 2.5mA - Bact.	6.69

TABLE 2. BACTERIOELECTRIC DEASHING	
	Ash %
Iowa 667 Subbituminous Coal H_2SO_4 pH 2.5	
	10 volts, 8.75 ma
Untreated control	21.23%
72 hrs	4.72%
140 hrs	1.22%
	10 volts, 21.82 ma
24 hrs	12.72%
96 hrs	7.74%
	5 volts, 7.70 ma
24 hrs	15.92%
96 hrs	5.53%
Illinios #6 Coal Argonne ID 301	
	10 volts, 12.5 ma
Untreated control	25.5%
72 hrs	15.5%
96 hrs	10.68%
168 hrs	10.70%
With 1 x 10^{-3}M Li_2SO_4	
168 hrs	8.50%

SOLUBILIZATION OF PYRITE AND FORMATION OF OXIDIZED IRON SEDIMENTS IN A GALVANIC CELL WITH AN IMPOSED E.M.F., IRON OXIDIZING THIOBACILLI AND H_2SO_4 pH 2.5

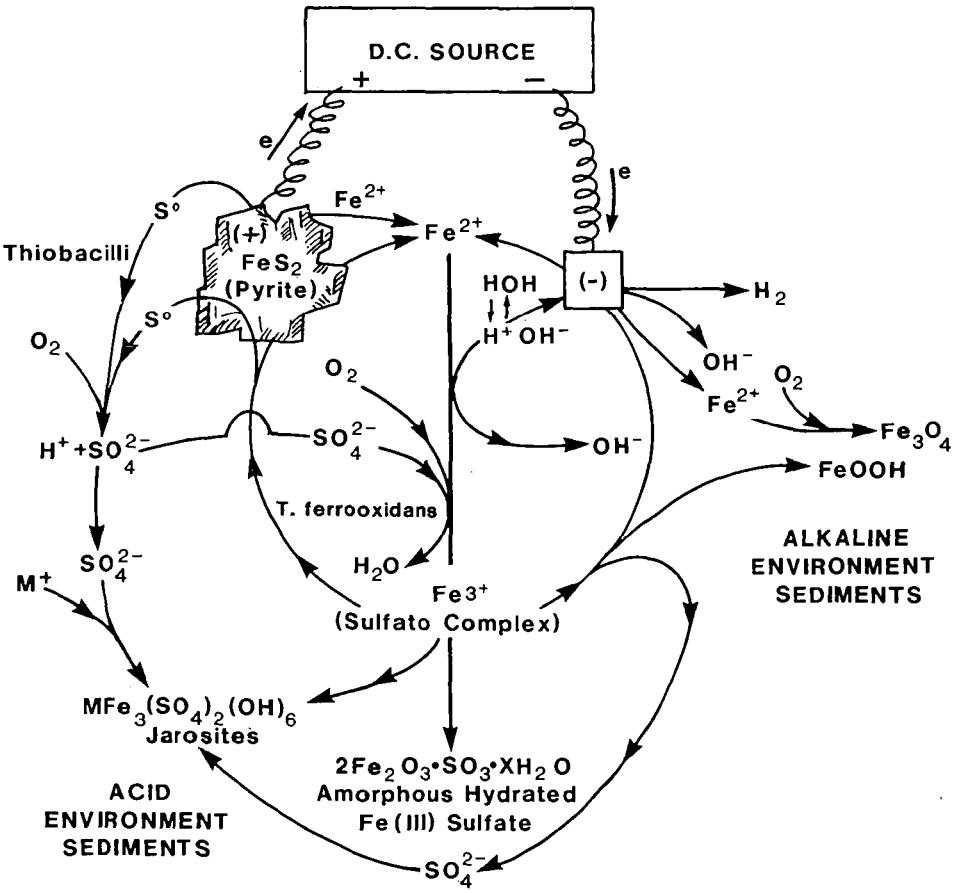

FIG. 1

LAB SET-UP of D.C. POWER SUPPLY WITH VOLTAGE REGULATOR and VOLTAGE, CURRENT MEASUREMENT

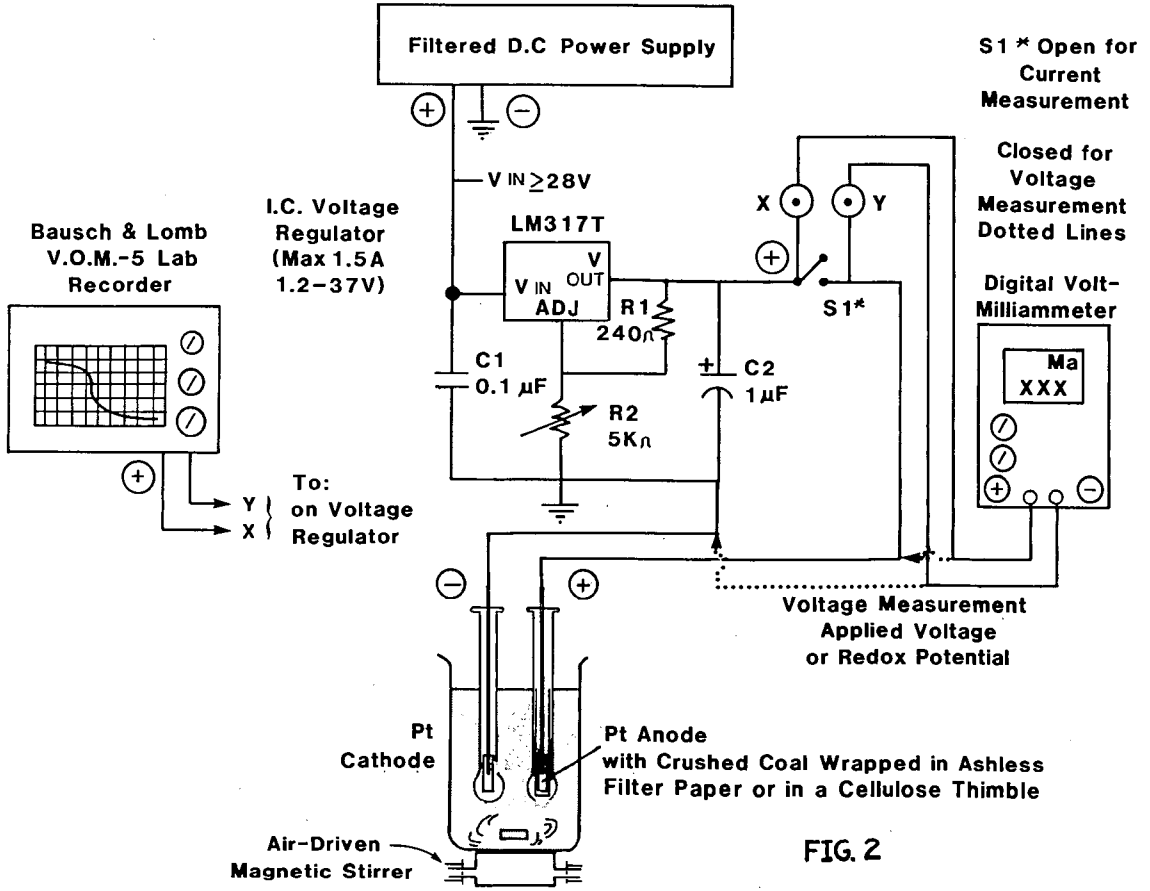

FIG. 2

LABORATORY SYSTEM for CONTINUOUS
BACTERIO-ELECTRIC REMOVAL of METALS FROM COAL

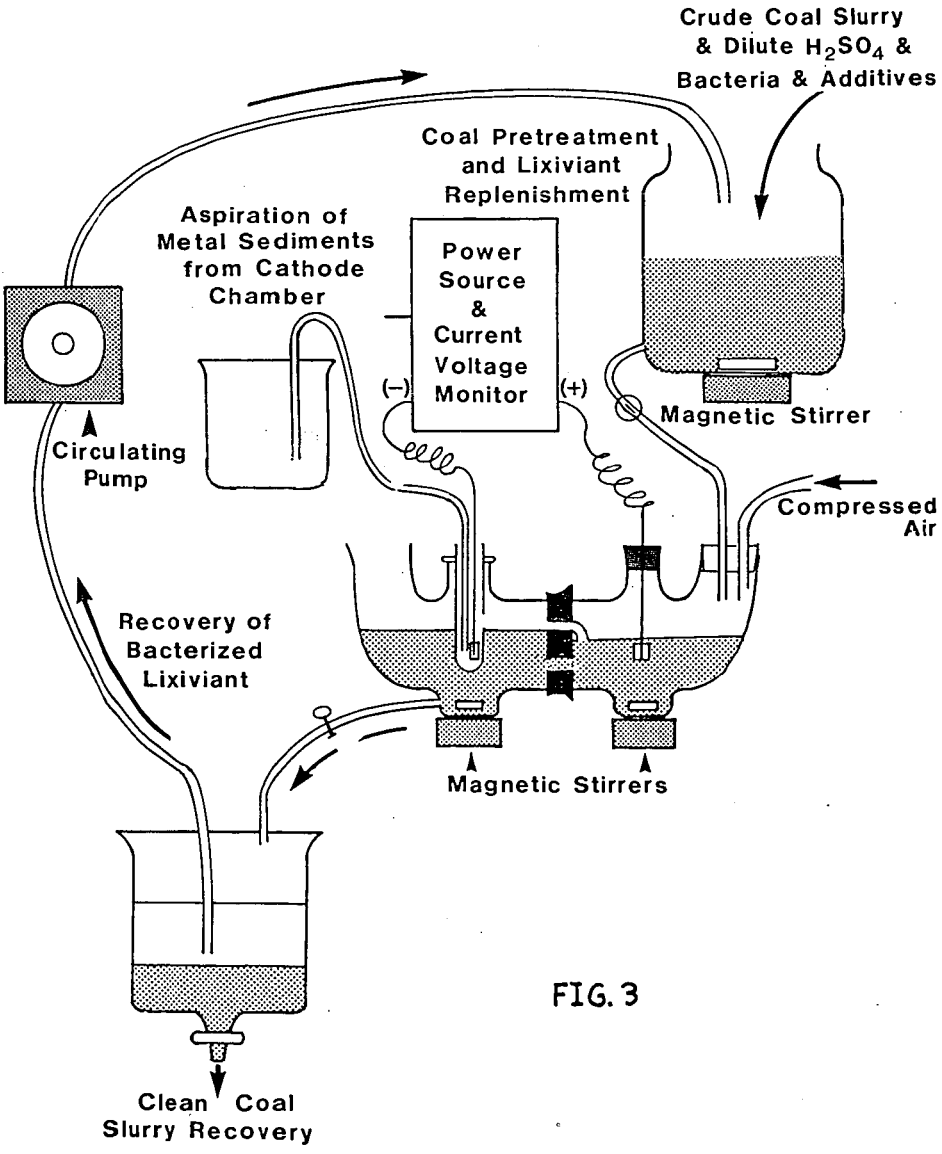

FIG. 3

HORIZONTAL AIRLIFT BACTERIO-ELECTRIC LEACHING CHAMBER

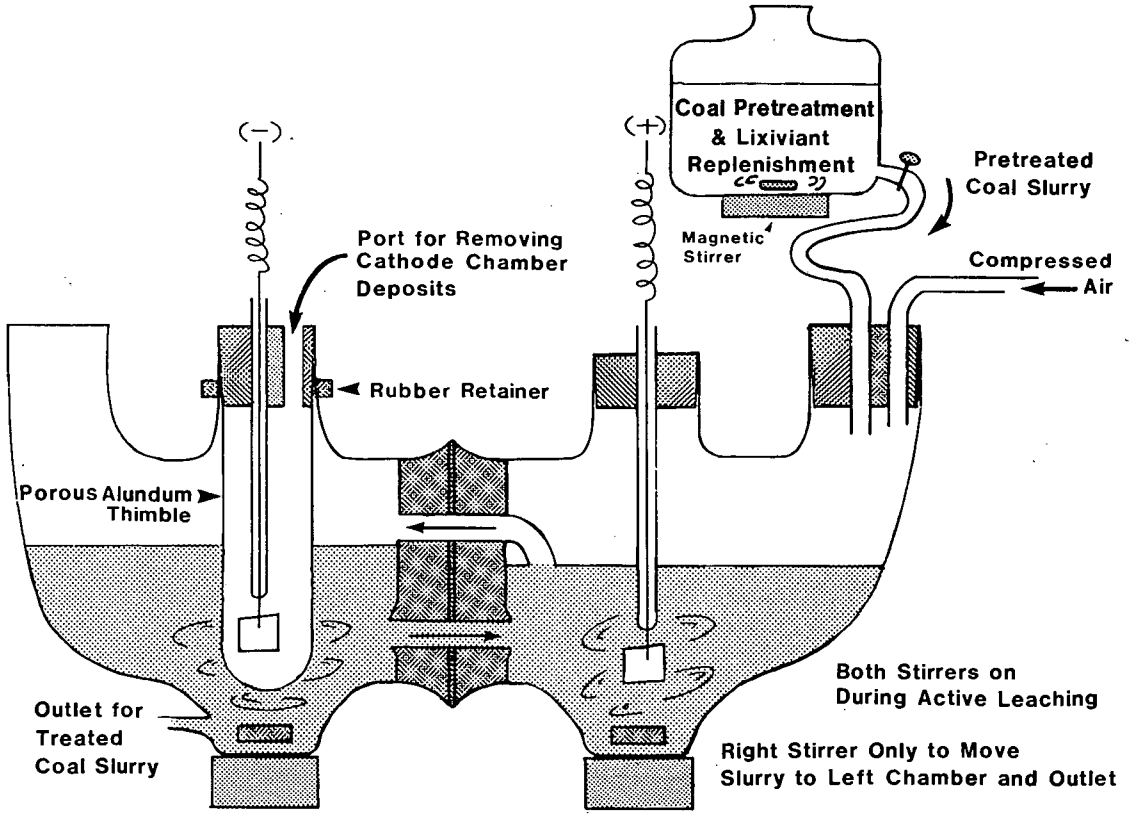

FIG. 4

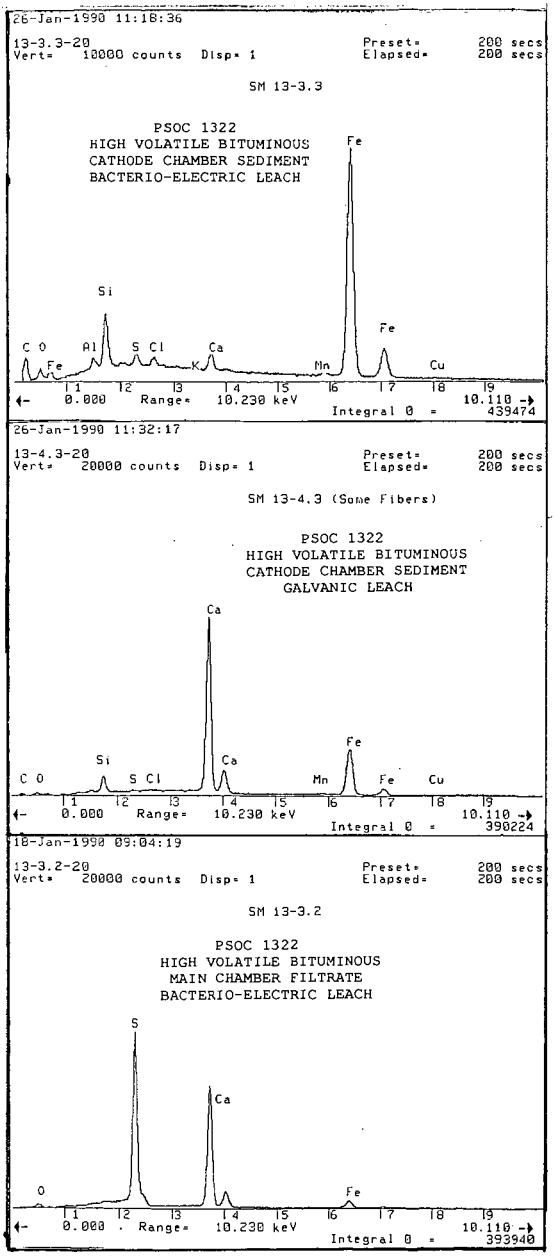
26-Jan-1990 11:18:36
13-3.3-20
Vert= 10000 counts Disp= 1
Preset= 200 secs
Elapsed= 200 secs
SM 13-3.3
PSOC 1322
HIGH VOLATILE BITUMINOUS
CATHODE CHAMBER SEDIMENT
BACTERIO-ELECTRIC LEACH
Fe
Si
Fe
C O
Al
S Cl
Ca
Fe
K
Mn
Cu
0.000
Range= 10.230 keV
10.110
Integral 0 = 439474
26-Jan-1990 11:32:17
13-4.3-20
Vert= 20000 counts Disp= 1
Preset= 200 secs
Elapsed= 200 secs
SM 13-4.3 (Some Fibers)
PSOC 1322
HIGH VOLATILE BITUMINOUS
CATHODE CHAMBER SEDIMENT
GALVANIC LEACH
Ca
Fe
Si
Ca
C O
S Cl
Mn
Fe
Cu
0.000
Range= 10.230 keV
10.110
Integral 0 = 390224
18-Jan-1990 09:04:19
13-3.2-20
Vert= 20000 counts Disp= 1
Preset= 200 secs
Elapsed= 200 secs
SM 13-3.2
PSOC 1322
HIGH VOLATILE BITUMINOUS
MAIN CHAMBER FILTRATE
BACTERIO-ELECTRIC LEACH
S
Ca
O
Fe
0.000
Range= 10.230 keV
10.110
Integral 0 = 393940

FIG. 5

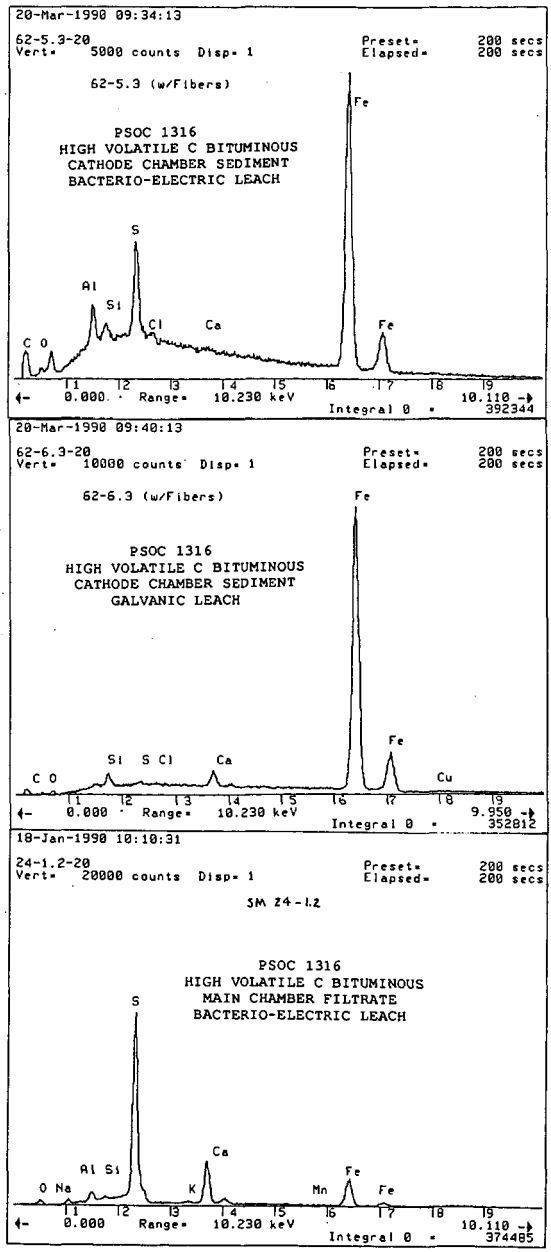
20-Mar-1990 09:34:13
62-5.3-20
Vert= 5000 counts Disp= 1
Preset= 200 secs
Elapsed= 200 secs
62-5.3 (w/Fibers)
PSOC 1316
HIGH VOLATILE C BITUMINOUS
CATHODE CHAMBER SEDIMENT
BACTERIO-ELECTRIC LEACH
C O Al Si S Cl Ca Fe Fe
0.000 Range= 10.230 keV 10.110
Integral 0 = 392344
20-Mar-1990 09:40:13
62-6.3-20
Vert= 10000 counts Disp= 1
Preset= 200 secs
Elapsed= 200 secs
62-6.3 (w/Fibers)
PSOC 1316
HIGH VOLATILE C BITUMINOUS
CATHODE CHAMBER SEDIMENT
GALVANIC LEACH
C O Si S Cl Ca Fe Fe Cu
0.000 Range= 10.230 keV 9.950
Integral 0 = 352812
18-Jan-1990 10:10:31
24-1.2-20
Vert= 20000 counts Disp= 1
Preset= 200 secs
Elapsed= 200 secs
SM 24-1.2
PSOC 1316
HIGH VOLATILE C BITUMINOUS
MAIN CHAMBER FILTRATE
BACTERIO-ELECTRIC LEACH
O Na Al Si S K Ca Mn Fe Fe
0.000 Range= 10.230 keV 10.110
Integral 0 = 374485

FIG. 6

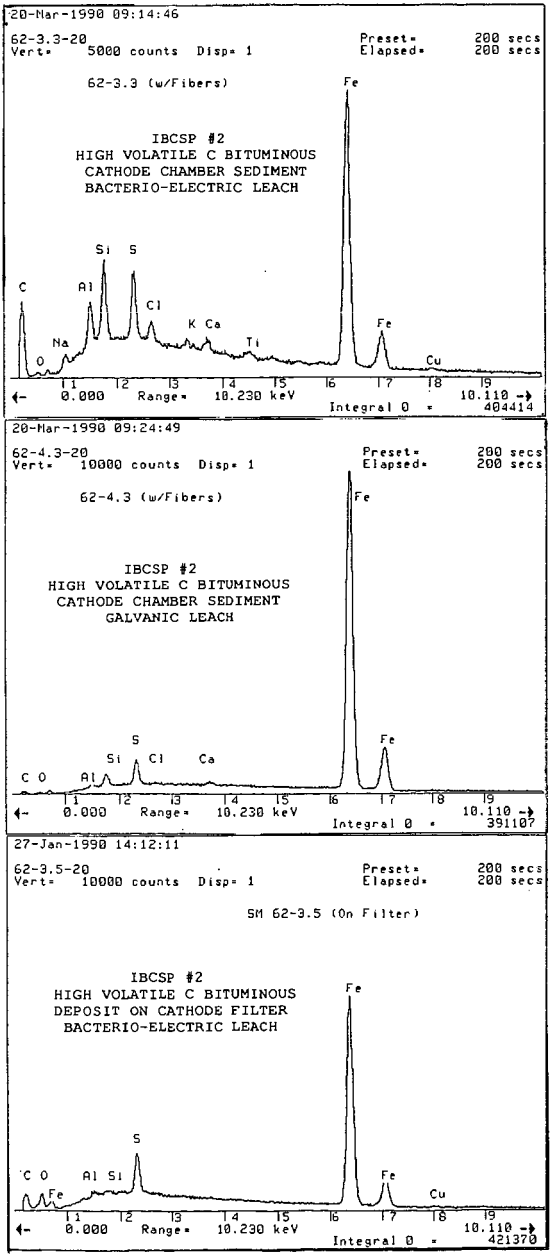
20-Mar-1990 09:14:46
62-3.3-20
Vert= 5000 counts Disp= 1
Preset= 200 secs
Elapsed= 200 secs
62-3.3 (w/Fibers)
IBCSP #2
HIGH VOLATILE C BITUMINOUS
CATHODE CHAMBER SEDIMENT
BACTERIO-ELECTRIC LEACH
C
O
Na
Al
Si
S
Cl
K
Ca
Ti
Fe
Fe
Cu
0.000
Range= 10.230 keV
10.110
Integral 0 = 404414
20-Mar-1990 09:24:49
62-4.3-20
Vert= 10000 counts Disp= 1
Preset= 200 secs
Elapsed= 200 secs
62-4.3 (w/Fibers)
IBCSP #2
HIGH VOLATILE C BITUMINOUS
CATHODE CHAMBER SEDIMENT
GALVANIC LEACH
C O
Al
Si
S
Cl
Ca
Fe
Fe
0.000
Range= 10.230 keV
10.110
Integral 0 = 391107
27-Jan-1990 14:12:11
62-3.5-20
Vert= 10000 counts Disp= 1
Preset= 200 secs
Elapsed= 200 secs
SM 62-3.5 (On Filter)
IBCSP #2
HIGH VOLATILE C BITUMINOUS
DEPOSIT ON CATHODE FILTER
BACTERIO-ELECTRIC LEACH
C O
Fe
Al Si
S
Fe
Fe
Cu
0.000
Range= 10.230 keV
10.110
Integral 0 = 421370

FIG. 7

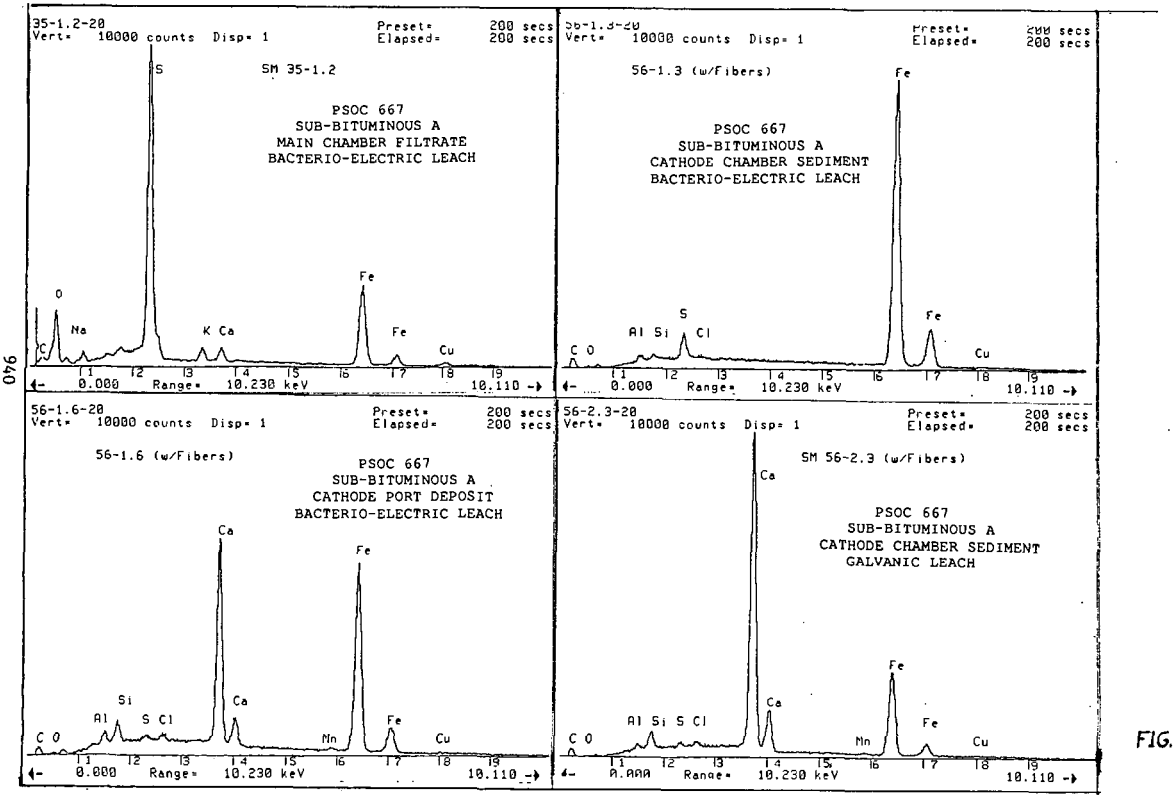
35-1.2-20
Vert= 10000 counts Disp= 1
Preset= 200 secs
Elapsed= 200 secs
SM 35-1.2
PSOC 667
SUB-BITUMINOUS A
MAIN CHAMBER FILTRATE
BACTERIO-ELECTRIC LEACH
S
O
Na
K Ca
Fe
Fe
Cu
C
0.000
Range= 10.230 keV
10.110
56-1.3 (w/Fibers)
PSOC 667
SUB-BITUMINOUS A
CATHODE CHAMBER SEDIMENT
BACTERIO-ELECTRIC LEACH
Fe
S
Al Si
Cl
Fe
Cu
C O
56-1.6-20
Vert= 10000 counts Disp= 1
Preset= 200 secs
Elapsed= 200 secs
56-1.6 (w/Fibers)
PSOC 667
SUB-BITUMINOUS A
CATHODE PORT DEPOSIT
BACTERIO-ELECTRIC LEACH
Ca
Fe
Si
Al
S Cl
Ca
Mn
Fe
Cu
C O
56-2.3-20
Vert= 10000 counts Disp= 1
Preset= 200 secs
Elapsed= 200 secs
SM 56-2.3 (w/Fibers)
PSOC 667
SUB-BITUMINOUS A
CATHODE CHAMBER SEDIMENT
GALVANIC LEACH
Ca
Fe
Al Si S Cl
Ca
Mn
Fe
Cu
C O
940

FIG. 8

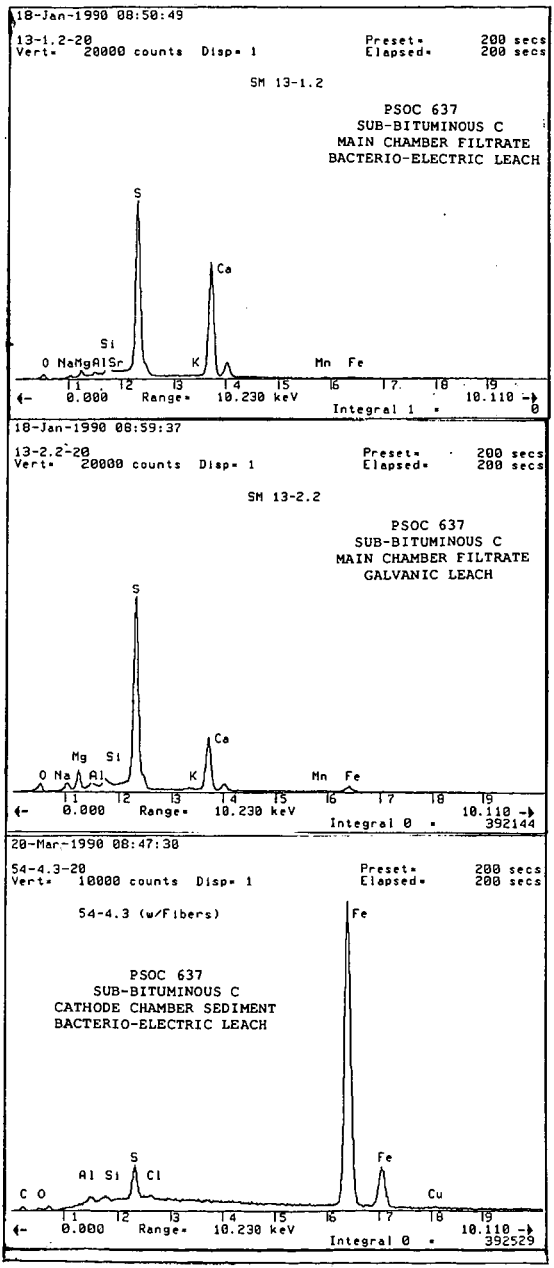
18-Jan-1990 08:50:49
13-1.2-20
Vert= 20000 counts Disp= 1
Preset= 200 secs
Elapsed= 200 secs
SM 13-1.2
PSOC 637
SUB-BITUMINOUS C
MAIN CHAMBER FILTRATE
BACTERIO-ELECTRIC LEACH
S
Ca
Si
O Na Mg Al Sr
K
Mn Fe
0.000 Range= 10.230 keV 10.110
Integral 1 = 0
18-Jan-1990 08:59:37
13-2.2-20
Vert= 20000 counts Disp= 1
Preset= 200 secs
Elapsed= 200 secs
SM 13-2.2
PSOC 637
SUB-BITUMINOUS C
MAIN CHAMBER FILTRATE
GALVANIC LEACH
S
Ca
Mg Si
O Na Al
K
Mn Fe
0.000 Range= 10.230 keV 10.110
Integral 0 = 392144
20-Mar-1990 08:47:30
54-4.3-20
Vert= 10000 counts Disp= 1
Preset= 200 secs
Elapsed= 200 secs
54-4.3 (w/Fibers)
Fe
PSOC 637
SUB-BITUMINOUS C
CATHODE CHAMBER SEDIMENT
BACTERIO-ELECTRIC LEACH
S
Fe
Al Si Cl
C O
Cu
0.000 Range= 10.230 keV 10.110
Integral 0 = 392529

FIG. 9

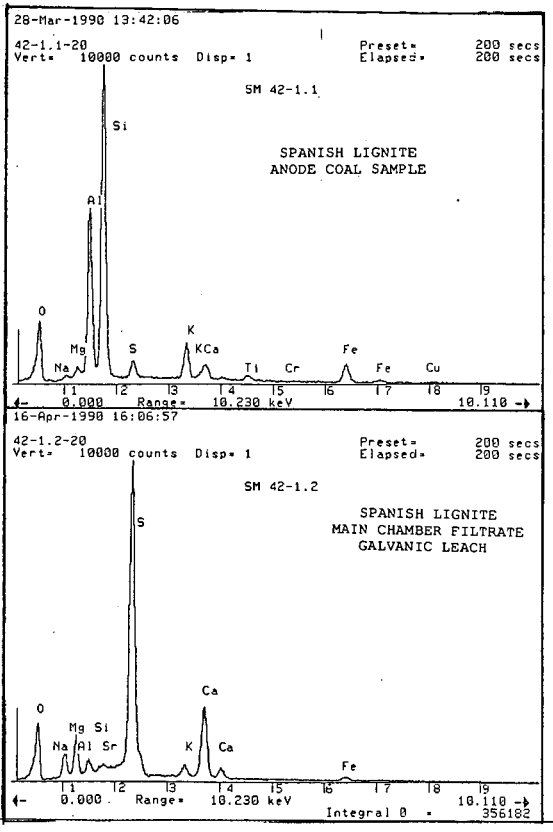
28-Mar-1990 13:42:06
42-1.1-20
Vert= 10000 counts Disp= 1
Preset= 200 secs
Elapsed= 200 secs
SM 42-1.1
SPANISH LIGNITE
ANODE COAL SAMPLE
Si
Al
O
Mg
Na
S
K
KCa
Ti
Cr
Fe
Fe
Cu
0.000 Range= 10.230 keV 10.110
16-Apr-1990 16:06:57
42-1.2-20
Vert= 10000 counts Disp= 1
Preset= 200 secs
Elapsed= 200 secs
SM 42-1.2
SPANISH LIGNITE
MAIN CHAMBER FILTRATE
GALVANIC LEACH
S
Ca
O
Mg Si
Na Al Sr
K
Ca
Fe
0.000 Range= 10.230 keV 10.110
Integral 0 = 356182

FIG. 10

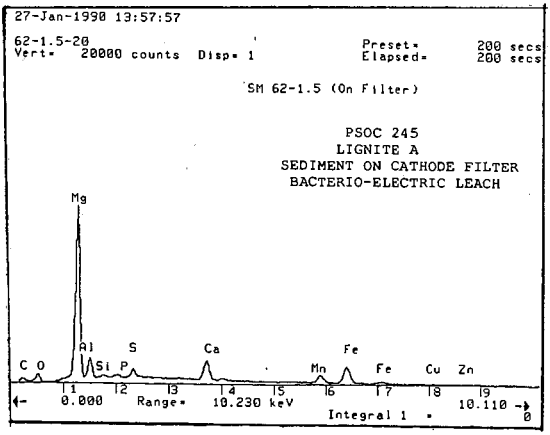
27-Jan-1990 13:57:57
62-1.5-20
Vert= 20000 counts Disp= 1
Preset= 200 secs
Elapsed= 200 secs
SM 62-1.5 (On Filter)
PSOC 245
LIGNITE A
SEDIMENT ON CATHODE FILTER
BACTERIO-ELECTRIC LEACH
Mg
Al
S
Ca
Fe
C O
Si P
Mn
Fe
Cu Zn
0.000 Range= 10.230 keV 10.110
Integral 1 = 0

FIG. 11

USE OF METHANOTROPHIC BACTERIA IN GAS PHASE BIOREACTORS TO ABATE METHANE IN COAL MINE ATMOSPHERES

William A. Apel, Patrick R. Dugan, and Michelle R. Wiebe

The Idaho National Engineering Laboratory
EG&G Idaho, Inc.
P.O. Box 1625
Idaho Falls, Idaho 83415-2203

Keywords: Methanotrophic Bacteria, Methane Removal From Mine Atmospheres, Gas Phase Bioreactors

Introduction

Coal mining activities often lead to the release of methane into the mine atmosphere from subterranean pockets that are disturbed during the normal course of mining. This methane can pose a distinct explosion hazard in the mine environment when combined with oxygen from air. It has been reported that the explosive range for methane in air is 5.53% to 14% with methane concentrations above 14% burning without explosion (10). In reality, many mine operations have safety requirements dictating evacuation if mine methane levels exceed 1-2%, since the accidental ignition of methane at concentrations below 5.53% may initiate coal dust explosions (3). Thus, the presence of methane in mines can result in economic loss. This is due to the need to either install ventilation systems and sustain air flow for maintaining methane at safe levels, or terminate operations and evacuate the mine if methane concentrations exceed those deemed safe.

Certain types of bacteria collectively known as methanotrophs are capable of utilizing methane as their sole source of cellular carbon and energy (9). The methanotrophs are nonpathogenic and taxonomically are assigned to several different genera. These bacteria are designated as type I or type II depending on the intracytoplasmic membrane arrangement displayed when grown on methane (1). Methanotrophic bacteria aerobically oxidize methane via a sequential pathway with biomass, carbon dioxide and water being the primary end products of the process (2). Some isolates under certain conditions also have the capability to grow on alternate carbon and energy sources such as alcohols, propane, short chained organic acids, hexadecane, etc. (4).

The methanotrophs are ubiquitous in nature and actively grow in environments where both methane and oxygen or alternate growth substrates are available. This type of environment is most typically found in rich soils, water, and upper layers of

sediments from lakes, harbors, estuaries, ponds, ditches, marshes, and other sites of active methanogenesis (5,8). As a result of their metabolic activities in these environments, methanotrophic bacteria are believed to play a key role in eutrophication by capturing and locking into their ecosystem the carbon from methane (6).

Due to their unique ability to utilize methane as a sole carbon and energy source, methanotrophic bacteria appear to be ideally suited for growth in gas phase bioreactors. In these reactors methane is readily available for cellular metabolism. As such, gas phase bioreactors offer an advantage over liquid phase bioreactors where under certain conditions methane can become limiting due to its relatively low solubility in water.

This paper reports the results from preliminary studies on the growth of a particular type I methanotrophic bacterium, Methylomonas methanica, in gas phase bioreactors. The ability of these bacteria to strip methane from methane-containing atmospheres such as those sometimes found in mine environments was also examined.

Experimental

Culture Maintenance

Methylomonas methanica isolate number O.S.U. 739 was obtained courtesy of the Ohio State University Department of Microbiology culture collection. The culture was maintained in 50 ml aliquots of CM mineral salts medium (7) contained in 125 ml serum bottles sealed with teflon coated rubber stoppers. The bottles were gassed with approximately 30% methane in air and incubated at 37° C on a rotary shaker. Gas levels in the culture vials were monitored using gas chromatographic analysis as described below. Culture bottles were regassed when either the methane or oxygen levels were depleted. Cultures were transferred to fresh medium at least every two weeks to maintain viability.

Gas Phase Bioreactor Design and Maintenance

The bioreactors were constructed from a 3 X 30 inch i.d. glass column sealed at the open end with a rubber stopper (Figure 1). Flexible 5/32 inch o.d. teflon tubing connected the upper end of the column to a stoppered 1 L Erlenmeyer flask that served as a gas volume reservoir. The flask in turn was connected via tubing to the lower end of the column so that a closed recirculation loop was formed. A peristaltic pump which allowed recirculation of gas through the closed system was situated in line between the gas reservoir flask and the lower end of the column. The column interior was filled with polypropylene bio-rings which acted as supports for the growth of the methanotrophs in the gas phase.

The bioreactors were prepared for growth of M. methanica by removing the stopper from the top of the column and pouring

approximately 50 ml of CM mineral salts medium into the upper end of the column. The medium was allowed to trickle over the bio-rings and collect in the bottom of the column. A 50 ml culture of stationary phase M. methanica grown in serum bottles as described above was then poured into the column in a manner similar to that described for the medium. Both the CM minerals salts medium and the inoculum were allowed to remain as a heel in the base of the column to help humidify the bioreactor. Following this, the stopper was tightly reinserted into the upper end of the column and further secured into place by wrapping with parafilm.

The inoculated bioreactor was incubated at 20±2° C for a period of 3 weeks. During this period, methane levels were targeted to approximately 30% methane in air. The gas mixture was constantly recirculated through the column at a rate of 200 ml per minute and gas levels were monitored via gas chromatography. The bioreactors were regassed to the above target levels whenever the methane or oxygen levels fell below 5.0%. Growth of M. methanica was monitored visually via the appearance of the pink pigmented organism on the bio-rings.

Rates of gas depletion were determined by first flushing the bioreactors with air and then gassing the bioreactors with a known mixture of methane in air. The gas mixture was recirculated through the bioreactor at a rate of 200 ml per minute. Gas levels were monitored via gas chromatography.

Analytical Methods

Gas levels (methane, oxygen, and carbon dioxide) in the serum bottle cultures and the bioreactor were analyzed using a Gow-Mac Series 550P gas chromatograph equipped with a thermal conductivity detector and an Alltech CTRI column. The gas chromatograph was connected to a Hewlett Packard model 3390A integrator. Samples consisted of 600 µl gas volumes manually injected into the gas chromatograph which was operated with helium as the carrier gas at a flow rate of 60 ml per minute under isocratic conditions at 30° C.

Results and Discussion

M. methanica was capable of growing to relatively high densities on the polypropylene bio-ring supports contained in the gas phase bioreactors. This growth was apparent visually in the form of highly pigmented pink biomass which adhered to the supports. The ability to directly visualize the growth of M. methanica throughout the bioreactor due to the organism's distinct pink pigmentation was of significant aid in easy, direct, nondestructive evaluation of growth patterns. Visual observation showed the growth to be distributed relatively evenly over the supports throughout the bioreactor with the exception of somewhat

heavier growth on the supports near the gas/liquid interface in the very bottom portion of the bioreactor.

The biomass in the bioreactor was quantitated by simple weighings which showed the average amount of biomass per support to be approximately 0.2 g (wet weight), with the total amount of biomass in the bioreactor being calculated to be 133.4 g (wet weight).

The M. methanica biomass in the bioreactors was assessed relative to its capability to strip methane from air. Figure 2 illustrates the results of experiments to strip a variety of methane levels from air over a 24 hour period. In these experiments the methane/air mixture inside the bioreactor was allowed to continuously recirculate. As can be seen in Figure 2, 35% methane in a total gas volume of 4.5 L was depleted by 90.4% in 24 hours. As would be anticipated, lower methane levels, e.g. 10.6%, were depleted to below the analytical detection limit in less than 24 hours.

In an effort to better simulate the methane levels likely to be encountered in mine environments, the same experiments were repeated using significantly lower starting methane levels measured at more frequent intervals. The results from these experiments are shown in Figure 3 using computed best fit curves. The data indicate that at levels up to 10% methane in air, the removal of methane by M. methanica is linear with the same rates of removal over the entire range under consideration. This is supported by the similar slopes on all three curves.

Under the conditions employed in the experiments illustrated by Figure 3, (i.e. methane < 12%), rates of methane removal for the 133.4 g (wet weight) of biomass contained in the bioreactor were calculated to be 22.9 mg of methane per hour. At higher methane levels such as 30%-45% methane in air, rates of removal were approximately 60% higher averaging 37.7 mg of methane removed per hour.

Further experimentation is necessary to ascertain the reason(s) for this difference in methane removal rates. One possible explanation could be increased transport of the higher concentrations of methane through the biofilm growing on the bio-rings. This increased transport could thus be making methane more available to cells deep within the biofilm and, as a result, greater rates of overall methane degradation could be observed.

Figure 4 illustrates the change in oxygen and carbon dioxide levels in the column during methane removal by the methanotrophic bacteria. Since oxygen serves as a terminal electron acceptor for the methane oxidation pathway, oxygen levels decrease as methane decreases. Similarly as methane is oxidized, the carbon from methane is either incorporated into bacterial biomass or released from the oxidation process as carbon dioxide, thus

explaining the gradual observed increase in carbon dioxide as methane is removed. In the specific example illustrated, with methane levels starting near 11%, a 50% decrease in methane led to an 11% decrease in oxygen. Concurrently, carbon dioxide increased from below the lower limit of detection to approximately 0.8%. These data indicate that methanotrophic bacterial bioreactors would also lower oxygen levels in coal mines. However, the amount of oxygen removed would be modest relative to the amount of methane eliminated, i.e. methane in a mine environment would usually be below 2% whereas oxygen would be approximately 20%.

Conclusions

Conclusions from these preliminary studies are as follows:

- Methanotrophic bacteria such as M. methanica are capable of growing to significant densities in gas phase bioreactors of the types used in this work.
- These organisms remove significant amounts of methane at significant rates from air/methane mixes, and as such may be of practical use in stripping methane from mine atmospheres.
- Additional work needs to be done to optimize reaction rates. This would include a more refined gas phase bioreactor design to (1) increase overall bacterial cell numbers, and (2) maximize bacteria/gas contact. Concurrently, methanotrophic culture optimization needs to be performed. Experiments already being initiated indicate the methane removal rate can be ultimately increased to at least 10 times those reported in this paper.

Acknowledgement

This work was supported under contract no. DE-AC07-76IDO1570 from the U.S. Department of Energy, to the Idaho National Engineering Laboratory/EG&G Idaho, Inc.

References

(1) Davies, S. L., and R. Whittenbury. 1970. Fine Structure of Methane- and Other Hydrocarbon Utilizing Bacteria. J. Gen. Microbiol. 61: 227-232.

(2) Haber, C. L. , L. N. Allen, S. Zhao, and R. S. Hanson. 1983. Methylotrophic Bacteria: Biochemical Diversity and Genetics. Science 221: 1147-1153.

(3) Lambecki, K. T. 1988. Methane Explosions at High Volume and Low Concentration. Fourth International Mine Ventilation Congress, Brisbane, Queensland, Australia

(4) Reed, W. M., and P. R. Dugan. 1987. Isolation and Characterization of the Facultative Methylotroph Mycobacterium ID-Y. J. Gen. Microbiol. 133: 1389-1395.

(5) Reed, W. M., and P. R. Dugan. 1978. Distribution of Methylomonas methanica and Methylosinus trichosporium in Cleveland Harbor as Determined by an Indirect Fluorescent Antibody-Membrane Filter Technique. Appl. Environ. Microbiol. 35:(2) 422-430.

(6) Weaver, T. L., and P. R. Dugan. 1972. The Eutrophication Implications of Interactions Between Naturally Occurring Particulates and Methane Oxidizing Bacteria. Water Res. 6: 817-828.

(7) Weaver, T. L., and P. R. Dugan. 1975. Ultrastructure of Methylosinus trichosporium as revealed by freeze etching. J. Bacteriol. 121:704-710.

(8) Whittenbury, R. and H. Dalton. 1981. The Methylotrophic Bacteria. In: The Prokaryotes. A Handbook on the Habitats, Isolation, and Identification of Bacteria, Starr, H. P., H. Stulp, H. G. Trupper, A. Balows, and H. G. Schlegel (eds). Springer-Verlag, Berlin.

(9) Whittenbury, R., K. C. Phillips, and J. F. Wilkinson. 1970. Enrichment, Isolation, and Some Properties of Methane-Utilizing Bacteria. Gen. Microbiol. 61:205-218.

(10) Windholz, M., S. Budavari, R. F. Blumetti, and E. S. Otterbein. 1983. The Merck Index, 10th Edition, pp. 852-853, Merck and Co., Inc., Rahway, N.J.

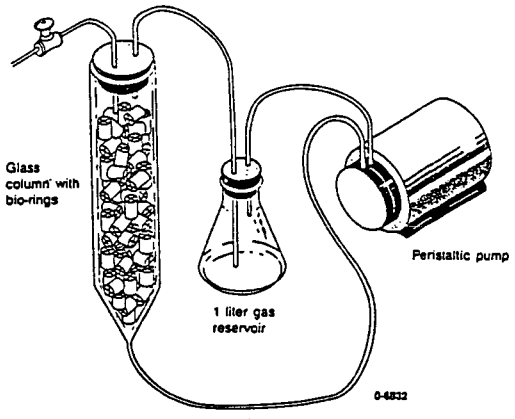

Figure 1
Schematic Diagram of Gas Phase Bioreactor

FIGURE 2
PER CENT METHANE REMOVED IN 24 HOURS
(4.5 L gas volume; 133.4 g (wet weight) M. methanica)

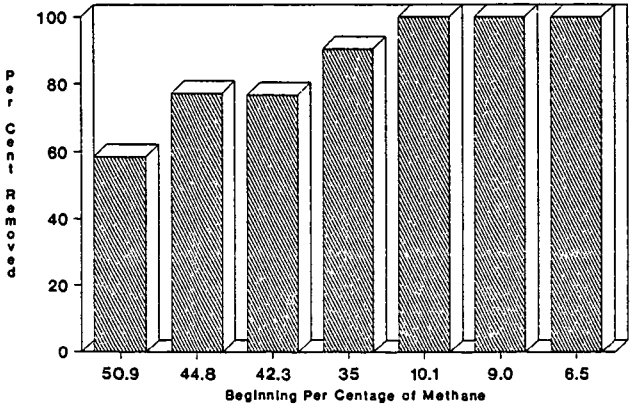

FIGURE 3
METHANE REMOVAL FROM AIR BY M. METHANICA

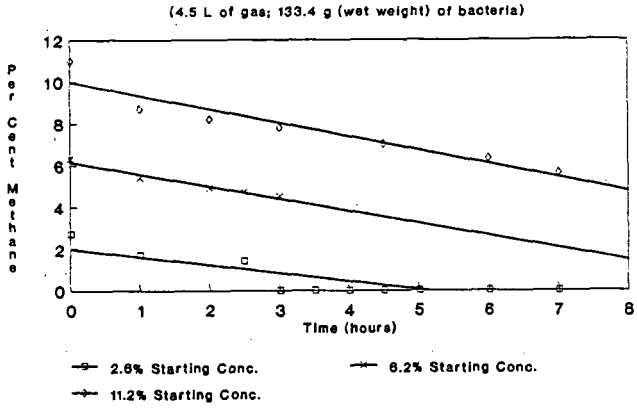

FIGURE 4
CH4 REMOVAL RELATIVE TO O2 AND C02

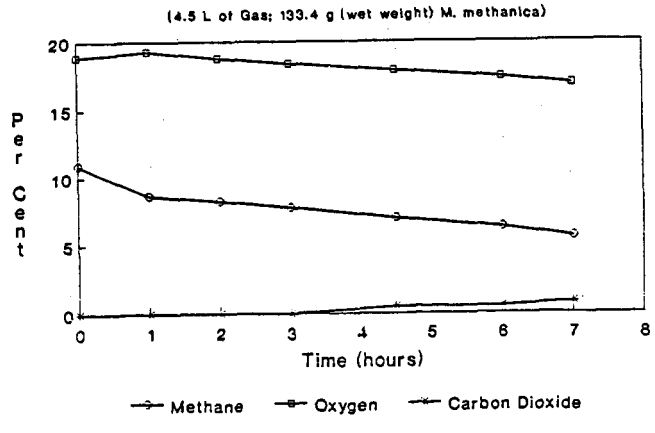

CELLS ON ROTATING FIBERS FOR CLEAN FUELS

Robert A. Clyde
P.O. Box 740644
New Orleans, LA 70174

Keywords: Zymomonas, yeast, coal, methane

INTRODUCTION

Rotary biological contactors have been made 10 feet in diameter but the discs are plastic. Fibers have more surface area. Half a pound of celite trapped in the fibers has the area of a football field so more cells can be immobilized. This concept is covered by a Clyde patent (1). Another patent (2) describes photo production of hydrogen and a third (3) cane fibers from the discs. Sulfur can be removed from coal and methane converted to methanol. In a recent 28 page booklet (4), several observations were made:

pg. 6. At current rates, there will be 13,000 to 23,000 deaths in California from cancer.

pg.18. About one billion gallons of gasoline would be displaced by clean fuel in 1997, increasing to about 11 billion by 2006.

pg.21. The year 2000 marks the first year in which all vehicles for sale in California would either be LEVs (low emission vehicles) or ULEVs (ultra low emission vehicles).

ALCOHOL FROM SUGAR

Parekh and Wayman (5) describe fermentation of glucose to ethanol in 15 minutes as "remarkable", using Zymomonas in a 4 inch diameter unit of rotating fibers (Fig. 1). In a letter they say the CO_2 came off so fast it's like an "explosion". They did not use Celite entrapped in the fibers. Celite is not expensive and neither is polyester fiber. Eight inch diameter units have been run by Clyde using Reemay polyester (6) type 2033 which is only 70 cents per sq. yard. Typar style 3301 from the same company is only 42 cents per sq. yard. Larger units are now being constructed. To provide stiffness, the fiber can be stapled to a screen.

ALCOHOL FROM WOOD

Wyman et. al. (7) say that SSF (simultaneous saccharification and fermentation) has great potential for production of ethanol at competitive prices. The key to this process is the ability to rapidly convert the sugars because they inhibit the conversion. They do it in 7-12 days, but Chen and Wayman (ref. 8 and Fig. 1) do it in 2 days using rotating fiberglass discs.

HYDROGEN

Several investigators have described hydrogen production from algae. Laws (9) describes the advantages of a flashing light which can be done in a rotary biological contactor. Weetal (10) also has a method. Greenbaum (11) also has a method and Mitsui at the University of Miami has written several articles. Veziroglu, also at the University of Miami, is the

editor in chief of a hydrogen journal. Nelson (12) at Argonne Lab. said one problem was availability of CO_2 but large amounts of that are produced in an alcohol plant.

COAL

Thiobacillus ferrooxidans grows on fibers as in patent 4,530,763 and it removes pyrite from coal. Pseudomonas and Phanerochaete chrysosporium solubilize coal and the former removes organic sulfur (13). Loganback from Morgantown (14) describes biotreatment of syngas.

METHANE

Large amounts of methane are flared (wasted) from oil refineries, since it cannot be economically transported. Lipscomb from the University of Minnesota (15) has a bacterium which converts methane to methanol, but burning methanol an a car or turbine produces formaldehyde. Methanol can be converted to clean burning hydrogen and CO with a 30% increase in energy (because waste heat is utilized) as in patent 4,420,462 where the catalyst can easily be removed out the bottom (Fig. 2). In other designs, catalyst is inside the tubes, but when the tubes expand with heat, the pellets pack in, and when the tubes cool they crush the catalyst.

REFERENCES

1. 4,407,954
2. 4,446,236
3. 4,600,694
4. Low Emission Vehicles/Clean Fuels and New Gasoline Specifications, by Air Resources Board, 9528 Telstar Ave., El Monte, Cal.
5. Parekh, S., Parekh, R., and Wayman, M. Ethanolic Fermentation of Wood-derived Cellulose Hydrosylates by Zymomonas mobilis in a Continuous Dynamic Immobilized Biocatalyst Bioreactor. Process. Biochem. June '89 p. 88-91.
6. Reemay Co. Industrial Road. P.O.Box 511, Old Hickory, TN 37138
7. Wyman, C. et.al. The Impact of Glucosidase in the Simultaneous Saccharification and Fermentation Process. Paper given at the AIChE 1990 meeting in Orlando in March.
8. Chen, S. and Wayman, M. Continuous Production of Ethanol from Aspen Cellulose by Co-immobilized Yeast and Enzymes. Process Biochem. Dec. '89 p. 204-207.
9. Laws. Biotech and Bioeng. 25, 2319-2335
10. Weetal. Biotech and Bioeng. 23, 605-614
11. Greenbaum, E. Photochem. and Photobiol. Oct. '89 p. 571-576
12. Nelson. Availability of CO_2 in the Southwest
13. Srivastava, R. et.al. Coal Bioprocessing: A Research-Needs Assessment. Chem. Eng. Progress Dec. '89 p.45-53
14. Talk 100A, Amer. Inst. Chem. Eng. Orlando, Mar. 1990
15. Talk given at Midwest Biotech. Symp. May 1990, St. Paul

SEPARATION OF PHENOLIC COMPOUNDS FROM COAL LIQUIDS

Yoichi Kodera, Koji Ukegawa, and Tetsuo Nakayama
National Research Institute for Pollution and Resources
16-3 Onogawa, Tsukuba, Ibaraki 305, Japan

Keywords: solvent extraction, phenolic compound, coal liquid

INTRODUCTION

Coal liquids contain considerable amounts of phenolic compounds which are industrially important chemicals. Upgrading of coal liquids have been performed by catalytic hydrogenation to produce fuel oils of good quality. Because of the existence of phenolic compounds, the upgrading requires hydrogen in quantity. Thus, an economical and effective method for separation of these compounds from coal liquids has been expected to develop. Here we report that a solvent extraction of phenolic compounds from naphtha distillates of coal liquids using methanol and water as solvents (1). The present presentation discusses the experimental conditions for the effective separation and the composition of the products.

EXPERIMENTAL

Materials. Feed oils, naphtha distillates of Battle River and Wandoan coal liquids, were supplied by a 1 t/d plant of Sumitomo Metal Ind. Ltd. The boiling range of each sample is IBP-185 °C. The distribution of acidic compounds in the feed oils is summarized in Table 1. Methanol (99.6 % pure) and dichloromethane (99.0 % pure) were from Wako Pure Chemical Ind. Ltd. and used without purification.

Procedure for solvent extraction. Scheme 1 shows the procedure of the present separation. To a mixture of a feed oil (5.0 mL) and methanol (5-20 mL) was added water (5-40 mL) at 30 °C. The resulting mixture immediately separated into two layers of a methanol-water layer and an oil layer. Phenolic compounds in a feed oil were extracted into the methanol-water layer. After 10 min, the methanol-water layer was taken out and evaporated to remove methanol. The aqueous phase was extracted with dichloromethane (30 mL x 3). The extracts were dried over sodium sulfate. Filtration and removal of the solvent gave a mixture of phenolic compounds as a brown oil. The compound distribution and selectivities of phenolic compounds in the products were determined with a gas chromatograph using a Shimadzu 50-m HR-101 (corresponding to OV-101) capilary column and a Shimadzu FAP-S 3.1-m x 3 mm packed column.

RESULTS AND DISCUSSION

Effect of solvents on the percent extraction

Methanol. When the feed oil was treated with water, only 20 % of phenolic compounds were extracted. However, extraction of a mixture of the feed oil (5 mL of a Battle River naphtha) and methanol (5-20 mL) with water (5 mL) gave better results in the extraction percents as shown in Fig. 1. The percent extraction was determined by the comparison of phenolic compounds separated

as a mixture with those contained in the feed oil. The yields increased significantly with the amount of methanol. There must be an appreciable interaction between phenolic compounds and methanol in the mixture of the feed oil and methanol. Addition of water caused phase separation to give an oil layer and a methanol-water layer rich in phenolic compounds. The methanol-water layer contained larger amounts of phenolic compounds with the increase of methanol. Removal of methanol and subsequent extraction with dichloromethane of the resulting aqueous solution gave a mixture of phenolic compounds as a brown oily product. It is noteworthy that the extraction of phenolic compounds from an aqueous solution with dichloromethane gave these compounds in 90 % or above under the present conditions.

Water. Fig. 2 shows the results of the extraction using the feed oil (5 mL), methanol (5 mL), and water in the range of 5 to 40 mL. The percent extraction of phenolic compounds increased with the amount of water. However, the yield was reached to the limmiting value of about 40 %. Thus, methanol gave a stronger effect than water on the yields of the phenolic compounds.

Effect of solvents on the compound distribution

The effects of the amounts of the solvents on the distribution of the phenolic compounds in the separated products was examined. The results of the distribution of the representative compounds, phenol and o-cresol were shown in Fig. 3 and 4. These results indicate that the changes of the amounts of methanol and water gave little influence on the distribution. These values of the distribution (about 36 % for phenol and about 10 % for o-cresol) correspond with those of the distribution of acidic components in the feed oil. Similarly, other compounds, m, p-cresol, o, m, and p-ethylphenol were extracted efficiently, corresponding with the distribution of the acidic components as shown in Table 2.

Application

The present method can be applied to the separation of nitrogen compounds in middle distillates of coal liquids (2) and in coal tar (3). Nitrogen compounds such as quinoline and indole can be extracted efficiently.

In summary, the solvent extraction using methanol and water is easy to perform. All solvents can be recovered. The present method provides a new effective method for the industrial separation of phenolic compounds from coal liquids.

References

1) Y. Kodera, K. Ukegawa, A. Matsumura, T. Kondo, and T. Nakayama, Japanese Patent, Serial No. Toku-gan hei-1-225967 (1989).
2) Y. Kodera, K. Ukegawa, and T. Takahashi, 1989 International Conference on Coal Science, Tokyo, Oct. 24, 1989.
3) K. Ukegawa, A. Matsura, K. Yazu, and T. Kondo, 1989 International Conference on Coal Science, Tokyo, Oct. 24, 1989.

Table 1 Characteristics of naphtha distillates

	Battle River	Wandoan
Acidic components, wt%	22.5	13.8
Compounds distributuion of acidic components, wt% a)		
phenol	39.4	36.6
o-cresol	12.5	13.3
m-cresol	19.8	14.2
p-cresol	17.3	15.6
o-ethylphenol	1.2	1.5
m-ethylphenol	3.5	6.0
p-ethylphenol	1.7	3.7
others	4.6	4.1

a) The distribution was determined by GC.

Scheme 1 Procedure for the solvent extraction

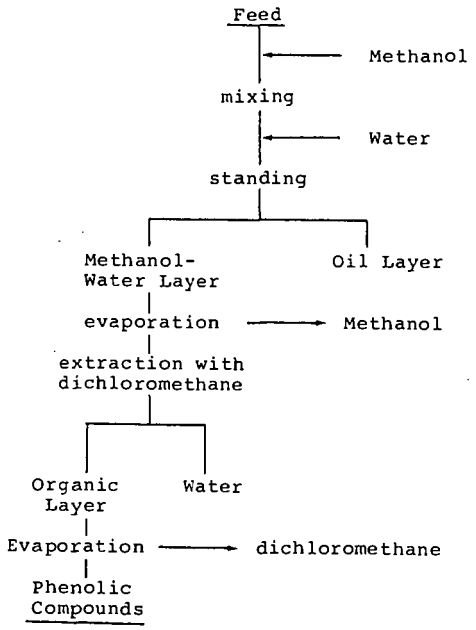

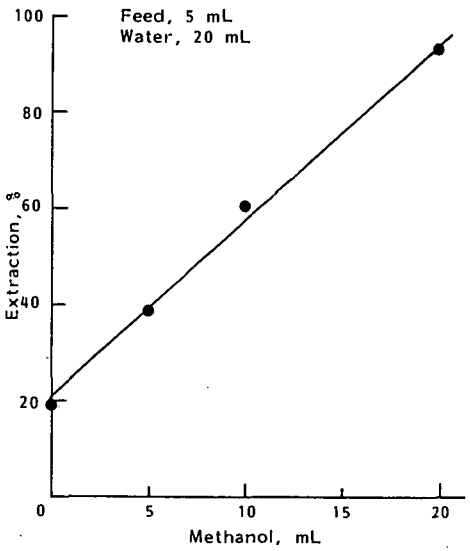

Figure 1 Effect of methanol on the percent extraction

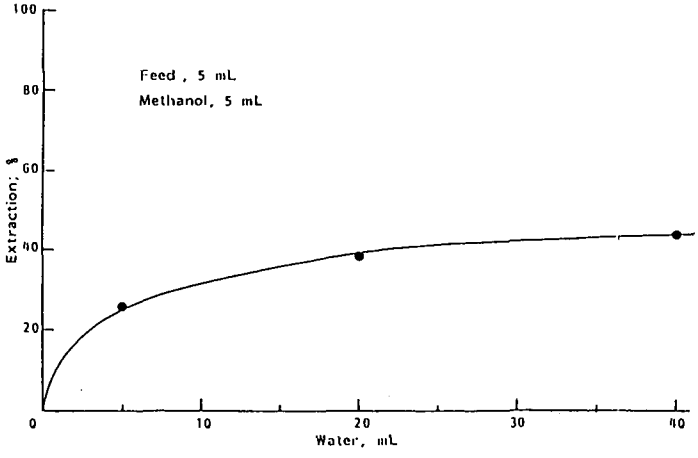

Figure 2 Effect of water on the percent extraction

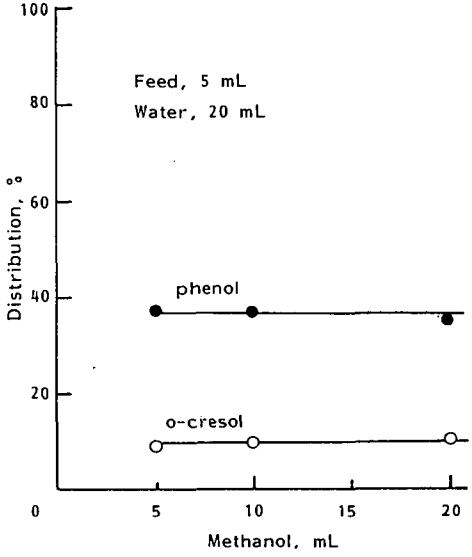

Figure 3 Effect of methanol on the compound distribution

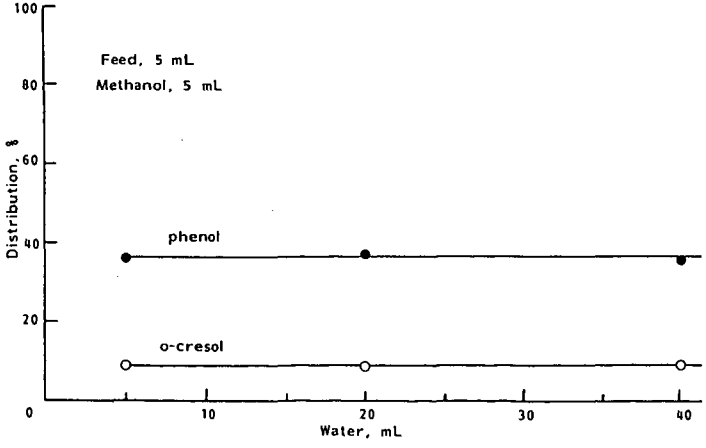

Figure 4 Effect of water on the compound distribution

Table 2 Compound distribution in the separated products

Entry	Methanol mL	Water mL	Distribution, % cresol(m,p)/ethylphenol(o,m,p)
1	5	5	16.9, 12.1 / - , 2.9, 1.7
2	5	20	15.9, 11.4 / - , 2.2, 1.2
3	5	40	16.8, 11.8 / 1.0, 2.3, 1.5
4	10	20	17.5, 12.7 / 1.4, 2.9, 1.4
5	20	20	18.3, 12.7 / 1.5, 3.2, 1.2

CORRELATION OF THE pH OF A COAL-METHANOL/WATER SOAK WITH COKE STRENGTH AFTER REACTION WITH CO_2 (CSR)

David H. Buchanan and Kenneth J. Coombs

Chemistry Department
Eastern Illinois University
Charleston, IL 61920

Hardarshan S. Valia

Inland Steel Flat Products Co., Research Laboratories,
East Chicago, IN 46312

Keywords: Coke Strength After Reaction (CSR), Weathering Index, pH Coal Slurry

ABSTRACT

Weathering of coals during storage at coke plants leads to a decrease in coke quality and an increase in operating costs for iron making. Coke Strength After Reaction with CO_2 (CSR) is an important measure of coke quality for blast furnace operation. This study was undertaken to predict changes in CSR values of coke caused by weathering of coals during storage. CSR values of coke were compared with a variety of feed coal properties, including pH of a methanol/water soak. The results indicated that an increase in coal oxidation resulted in a drop in pH of methanol/water soak. CSR generally dropped with a drop in pH for all the coals. However, good correlation existed between CSR and pH for lower rank (high volatile) coals.

INTRODUCTION

At Inland Steel Flat Products Company, the improvement in CSR had a major stabilizing influence on blast furnace operation.(1) The CSR is primarily dependent on the plastic properties of coal which are known to deteriorate with oxidation of coal.(2-4) Hence, a research program was initiated to decipher how coal oxidation affects coke quality, especially CSR, and cokemaking operations. The primary objectives were to develop means for measuring coal oxidation and to learn how to interpret these measurements in ways useful to the coke plant operators.

Although documentation exists detailing the relationship of coal oxidation to coke properties, little information has been published regarding the effect of coal oxidation on hot strength properties of coke. Crelling, et al. (5) correlated coke reactivity to the amount of weathered coal in the mix. The reactivity increased with an increase of weathered coal in the mix; however, the reactivity was measured through the Bethlehem method. Huffman, et al. (6) reported loss in coke reactivity for the most highly weathered Pittsburgh seam (VM = 36.2%, db) coal; the coke reactivity was measured as percent of coke reacted after 2 hours at 1000 °C in CO_2. Pis, et al. (7) reported an increase in coke reactivity with increase in coal oxidation under accelerated oxidation conditions; the reactivity was measured through the ECE

method. Price, et al. (8) indicated a decrease in CSR for a western Canadian coal after storage in barrels for 20 weeks.

Because an appreciable portion of coal used in the coking industry is stored in large piles for various periods of time, it was appropriate to study the deterioration in coal properties due to natural weathering and assess its effect on coke properties, especially CSR, and cokemaking. In this paper, only the statistically significant correlations between CSR and pH of methanol/water soak are discussed. The effect of weathering on other properties of coke and cokemaking operations are discussed more fully elsewhere.(9)

EXPERIMENTAL

Six piles, 3 tons each, of each of the coals that were in use at Inland, were made in the open yard at the Research pilot facility. The coals were Coal A (High Volatile), Coal B (High Volatile), Coal C (High Volatile), and Coal D (Medium Volatile). The analytical data for the fresh coals are given in Table I. Pile No. 1 was the base fresh coal and was subjected to carbonization in Inland's 565 kg movable-wall pilot oven with interior dimensions of 1,143 mm high x 1,219 mm long x 457 mm wide.(10) The operational data summary for the carbonization tests is given elsewhere.(2) Also, a wet charge of 30% Coal A, 30% Coal B, and 40% Coal D was carbonized in the pilot oven for coals from the respective piles. CSR and other coke quality parameters were measured. The CSR was determined through the NSC method. Coke quality data, from the pilot oven carbonization of fresh coals, are also included in Table I. Pile Nos. 2 to 6 were carbonized after 35 days, 70 days, 105 days, 180 days, and 420 days of natural oxidation, respectively. The coals from each pile were subjected to the following analyses: rheological, proximate, ultimate, alkali solubility, petrography, pH (methanol/water soak), FTIR-PAS, and sole-heated oven (SHO) analysis. For the pH measurements, HPLC grade methanol and Milli-Q™ purified water (resistance > 16 MΩ) were used. A 25 mL aliquot of 20% (v/v) methanol/water was pipetted into a 50 mL Erlenmeyer flask containing 2.000g coal. The flask was closed with a rubber septum cap fitted with gas inlet and outlet needles and nitrogen gas bubbled through the slurry for 20 minutes. Placing the flask in an ultrasonic bath maintained at 25 Deg.C improved coal wetting. A septum cap with an all-glass pH electrode inserted through a hole was placed on the flask and the pH measured after equilibrating the electrode for 10 minutes in the slurry. The Orion Research Model 710 pH meter was calibrated with buffers prepared in 20% methanol/water at pH 4 and 7.

RESULTS AND DISCUSSION

1) Change in pH with Time

Figure 1 shows plots of pH measurement of methanol/water soak for individual coals; measurements were not made for the blend. For all coals, there is a rapid drop in pH for the first 2-3 months. Beyond this time, the drop is generally insignificant. A drop in pH with oxidation has been reported in literature.(11-13) It is also apparent that the pH of methanol/water soak from fresh Coal A is distinctly acidic (possibly due to the combination of lower rank, higher microporosity, and higher sulfur content) and with oxidation, it becomes more acidic due to the release of sulfur and acids produced from coal oxidation reactions. It is known that lower

rank coals produce more acidic products during weathering.(13) The pH of methanol/water soak from the fresh Coal D, Coal C, and Coal B is distinctly basic, and the pH value drops with an increase in oxidation. Thus, both the absolute value and the change in pH are coal dependent.

The reproducibility of the pH measurements on triplicate samples was = 0.07 units. Because particle size has an significant effect on the pH of the slurry it is important to standardize the grinding of coal samples for these measurements for sample to sample consistency. Data in Table 2 are for a -8 mesh, weathered Illinois No. 6 coal (River King Mine) which was ground in a nitrogen-flushed ball mill and separated into size fractions by sieving. The pH of the larger particles is lower than that of the smaller particles. A sample of the same River King coal which had been ground to -100 mesh prior to weathering had a pH of 5.02 compared to the pH of 5.36 found for the -100 mesh fraction of the coal weathered as larger particles. These results indicate that the surfaces exposed in grinding had been protected from oxidation and had developed fewer acidic groups than surfaces on the un-ground larger particles. The observed differences in pH values of the unweathered coals may be a function of the mineral matter composition of each coal.

2) Change in CSR with Time

Figure 2 shows variation in CSR with weathering time for all individual coals and blends.(9) CSR in all cases decreases with an increase in weathering time. The drop in CSR was most dramatic during the first few months of summer exposure; thereafter, the CSR generally decreased with time or there was little change in CSR.

Using the highest and lowest CSR values, and not the trend lines, it can be deduced that the magnitude of CSR drop is highest for the lowest rank Coal A, followed by the blend, Coal B, Coal D, and Coal C. The CSR dropped by about 24 points for Coal A, 19 points for the blend, 13 points for Coal B and D, and 8 points for Coal C. The large drop in CSR for the blend may be due to a combination of higher amount of Coal A and higher amount of oxyvitrinite from Coal A, Coal C, and Coal D. It is interesting to note that Coal D, a medium volatile rank, undergoes oxidation-induced loss in CSR by the same amount as the high volatile Coal B. The Coal C is least susceptible to weathering-induced CSR loss.

3) Correlation of Change in pH to CSR

The changes observed in this study were for a small 3-ton pile. Different natural conditions exist in large coal piles, hence, the time period may not be applicable when the results are applied to the large commercial piles. Hence, it is important to come up with a coal oxidation monitoring device that directly relates to coke properties and can be monitored constantly in the pile. With this premise, the changes in coal quality were correlated to coke quality. The increase in coal weathering resulted in deterioration in CSR and was accompanied by a drop in pH of methanol/water soak.

Figure 3 shows the correlation between the pH of coal-methanol/water soak and the CSR for all the coals. CSR generally drops with a drop in pH for all the coals. However, good correlation exists between CSR and pH for Coal A and Coal B (the lower rank high volatile coals). It was reported elsewhere that for Coal C and Coal

D (the borderline high volatile/medium volatile coal, and medium volatile coal) the fluid temperature range, (as determined through Gieseler plastometer) correlated well with CSR.(9) This relationship can be used to predict CSR of lower rank (high volatile) coals by monitoring pH.

APPLICATION

On the basis of results from this study, a coal oxidation monitoring plan for the lower rank (high volatile) coal has been devised as follows:

1) Obtain the pH of the incoming coals from the respective mines.

2) Identify the placement of incoming coals in the coke plant yard.

3) Monitor the drop in the pH of coal in the coal piles.

4) Estimate the loss in CSR by using a set of graphs that depict a drop in pH versus a drop in CSR. Figures 4 shows one such example.

5) Once the coal oxidation has affected CSR in such a way that the target CSR is not met, as indicated through the drop in pH, then the usage of oxidized coal in the blend should be redefined.

6) If new high volatile coals are brought in, the graphs of a drop in pH versus CSR could be developed while monitoring the new coal pile and verifying the results through pilot oven carbonization.

CONCLUSIONS

On the basis of this study, the following conclusions can be made:

1) An increase in coal weathering resulted in a drop in pH of methanol/water soak.

2) An increase in coal weathering resulted in a drop in CSR and the drop in CSR can be correlated to a drop in pH of coal methanol/water soak.

3) pH measurement can be used as a quality control tool for monitoring weathering of low rank (high volatile) coals that are characterized by low fluid properties.

ACKNOWLEDGEMENT

Partial support of this work by the Council on Faculty Research at Eastern Illinois University is gratefully acknowledged. H.S.V. would also like to acknowledge the assistance of several colleagues at the Inland Steel Research Laboratory for their assistance with various aspects of this work.

REFERENCES

1) Valia, H.S., et al., "Production and Use of High CSR Coke at Inland Steel Company," ISS-AIME Proc., Vol 48, 1989, pp. 133-146.

2) Valia, H.S., "Prediction of Coke Strength After Reaction with CO_2," Iron and Steelmaker, May 1989, pp. 77-87; also to be published in Iron & Steel Soc. Trans., Vol 11, 1990.

3) Schmidt, L.D., "Changes in Coal During Storage," in "Chemistry of Coal Utilization," Lowery, H.H., (Ed), Vol. I, 1945, John Wiley & Sons, N.Y., pp. 627-676.

4) Gray, R.J. and Lowenhaupt, D.E., "Aging and Weathering," in "Sample, Selection, Aging, and Reactivity of Coal," Klein, R. and Wellek, R. (ED.), 1989, John Wiley & Sons, N.Y., pp. 255-334.

5) Crelling, J.C., et al., "Effects of Weathered Coal on Coking Properties and Coke Quality," Fuel, Vol. 58, 1979, pp. 542-546.

6) Huffman, G.P., et al., "Comparative Sensitivity of Various Analytical Techniques to the Low Temperature Oxidation of Coal," Fuel, 1985, Vol. 64, pp. 849-856.

7) Pis, J.J., et al., "Effect of Aerial Oxidation of Coking Coals on the Technological Properties of the Resulting Cokes," Fuel Processing Technology, 1988, Vol. 20, pp. 307-316.

8) Price, J.T., et al., "Effect of the Properties of Western Canadian Coals on Their Coking Behavior," ISS-AIME Proc., 1988, Vol. 47, pp. 39-55.

9) Valia, H.S., "Effects of Coal Oxidation on Cokemaking," ISS-AIME Proc., 1990, Vol. 49.

10) Kaegi, D.D. and Osterman, C.A., "The Use of Illinois Coal for the Production of High Quality Coke," ISS-AIME Proc., 1980, Vol. 39, pp. 239-248.

11) Gray, R.J., et al., "Detection of Oxidized Coal and the Effect of Oxidation on the Technological Properties," SME-AIME Trans., Vol. 260, 1976, pp. 334-341.

12) Mikula, R.J. and Mikhail, M.W., "A Delta P Technique for the Prediction and Monitoring of Coal Oxidation," Coal Preparation, 1987, Vol. 5, pp. 57-69.

13) Yun, Y., et al., "Attempted Development of a 'Weathering Index' for Argonne PCSP Coals," Am. Chem. Soc. Div. Fuel Chem. Preprints, 1987, Vol. 32, No. 4, pp. 301-308.

Table I. Analyses of coals and their cokes

	Coal A	Coal B	Coal C	Coal D	Blend 30%A 30%C 40%D
Petrographic Analysis					
Total Inerts (%)	7.61	16.76	20.62	20.29	14.55
Oxyvitrinite (%)	0.0	0.0	0.60	0.20	0.20
Pseudovitrinite (%)	0.60	0.40	0.20	0.60	0.40
Mean Max. Vitrinite Reflectance (%)	0.67	0.90	1.07	1.35	1.04
Alkali Extraction (%, Transm.)	97.0	96.0	99.0	97.0	98.0
Proximate Analysis (%, db)					
Volatile Matter	35.7	31.2	27.1	23.2	27.7
Fixed Carbon	58.7	62.3	67.0	71.7	66.9
Ash	5.6	6.5	5.9	5.1	5.4
Sulfur	1.11	0.56	0.82	0.8	0.87
Alkali Index	1.98	0.81	1.82	1.89	1.56
Free Swelling Index	3.0	7.5	8.0	7.5	5.0
Ultimate Analysis (%,db)					
Carbon	76.64	79.07	81.90	83.94	81.46
Hydrogen	5.09	4.96	5.01	4.86	5.03
Nitrogen	1.74	1.52	1.67	1.55	1.64
Oxygen (by difference)	9.83	6.88	5.00	3.73	5.43
Gieseler Max Fluidity (log ddpm)	1.25	2.78	4.43	3.50	3.03
Gieseler Fluid Range (Deg.C)	66.0	71.0	116.0	106.0	106
pH (methanol/water)	4.12	8.50	8.99	7.57	NA
Area under the absorbance peak, carbonyl band (1850-1636 cm-1), arbitrary unit	20.7	21.93	17.74	16.83	NA
Sole-Heated Oven Analysis (at normalized conditions 52 pcf, 2% moisture)	+1.0	-9.0	-5.4	+0.3	NA
Heating Value (cal/gm)	7618	7874	8140	8084	8084
Pilot Oven Carbonization Test					
Coal Moisture (%, db)	8.5	2.9	1.7	1.9	3.7
Coal Grind (%, -3.35 mm)	82.2	86.5	89.1	91.5	85.6
Dry Oven Bulk Density (kg/m³)	801.0	885.0	884.0	866.0	906.0
Max. Oven Wall Pressure (kPa)	3.7	6.7	12.9	16.3	5.9
Coking Time (h)18.4	18.4	17.3	16.2	17.1	17.0
ASTM Stability	23.0	50.0	55.0	65.0	63.0
NSC Coke CSR	36.0	62.0	69.0	66.0	60.0
NSC Coke CRI	57.0	24.0	22.0	27.0	31.0
Coke Hardness	71.0	67.0	68.0	71.0	72.0
Coke Size (mm)	50.7	61.5	72.7	69.6	66.8
Coke Yield (%)	67.9	69.2	76.2	79.3	72.4
Coke Volatile Matter (%)	2.2	0.9	0.9	0.9	0.6

TABLE 2 pH of Size Fractions of Ground +8 mesh Illinois No.6 Coal

Mesh size	-8 + 24	-24 + 100	-100
Wt% of total	47.6	35.4	17.0
pH	2.88	3.00	5.36

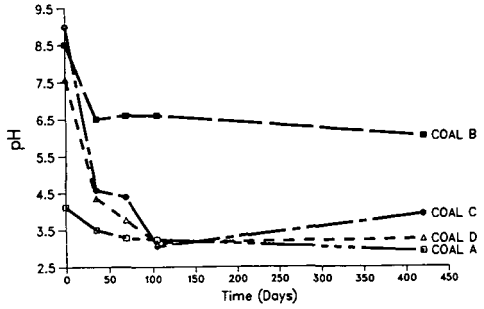

Fig. 1 pH (methanol/water) as a function of coal oxidation time

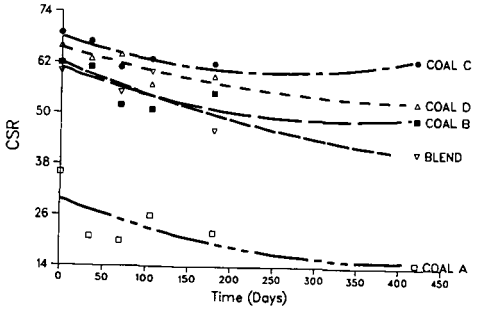

Fig. 2 Effect of coal oxidation time on CSR

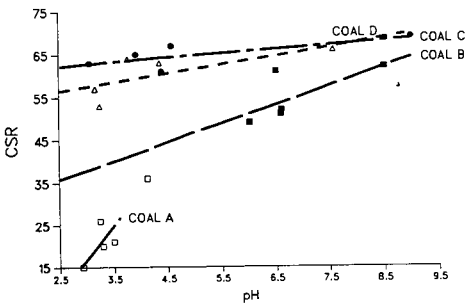

Fig. 3 Oxidation effects indicated through pH (methanol/water) and CSR

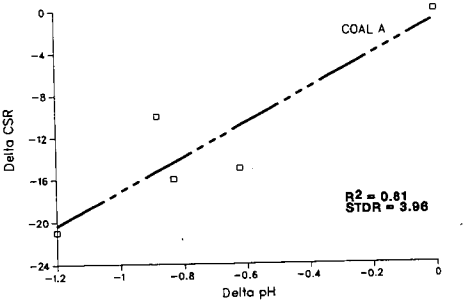

Fig. 4 Use of pH (methanol/water) for assessing CSR loss

EFFECT OF ELECTROREDUCTION PRETREATMENT IN AQUEOUS MEDIA ON HYDROPYROLYSIS OF A BITUMINOUS COAL

Li Baoqing

Service de Chimie Générale et Carbochimie, Université Libre de Bruxelles, Av. F.D. Roosevelt, 50(CP 165), B-1050, Bruxelles, Belgium

Keywords: electrochemical reduction, hydropyrolysis, pretreatment

Abstract

Electroreduction of coal (ER) is studied in aqueous tetrabutylammonium hydroxide (TBAOH) solution and tetrabutylammonium tetrafluoroborate ($TBABF_4$)-THF-H_2O solution by using platinum as anode and Hg pool as cathode. The electrolysis in aqueous TBAOH solution seems to have little effect on the following hydropyrolysis (HyPy) although the pyridine extractable yield of the reduced coal increases. In an undivided cell the re-oxidation of the reduced coal occurs. Cathodic reduction in $TBABF_4$-THF-H_2O solution gives a pronounced effect on HyPy. Higher conversion (60.9%) and total oil yield (50.6%)(THF soluble + oil formed in HyPy) are obtained in a divided cell as compared with 42.1% and 28.4% for untreated coal, respectively. The electroreduction pretreatment of coal enhances the rate of oil formation and oil yield in HyPy, indicating that the reduced coal can be depolymerized more easily due to the solvolysis and hydrogenation.

Introduction

The conversion of coal to oil needs undoubtedly to increase the H/C ratio in coal. Therefore, gaseous hydrogen is always used in coal liquefaction, HyPy and other hydrogenation processes. Considering the high activation energy for the dissociation of gaseous hydrogen, the addition of hydrogen to coal using gaseous hydrogen is so difficult that the elevated pressure has to be used. As a result, the high cost makes these processes hardly competitive with those using petroleum as raw materials. To reduce the hydrogen consumption and even to avoid the use of gaseous hydrogen and/or elevated pressure are very interesting in coal hydrogenation processes.

Previous studies[1-3] showed the posibility to improve the quantity and quality of oil and the efficiency of hydrogen utilization in HyPy by pretreatment of coal using catalyst and various gases. Although these pretreatments are effective, the improvements are still not optimistic even the use of impregnated sulphided Mo catalyst because of the cost of catalyst and an increasing sulphur content in char.

Earlier studies[4,5] indicated that hydrogen can be added to coal by electroreduction using LiCl as electrolyte in an organic solvent. Recently, It is reported[6] that hydrogenation of coal can be carried out by electroreduction in an aqueous solution. They used a mediator ($CrCl_3$)/Ni powder/LiCl/aqueous THF solution/ultrasonic irradiation system, which is too complicated to be performed practically. It is known[7-9] that the effective electroreduction of benzene and related compounds can be performed in tetraakylammonium aqueous solution. Reduction in water is economically attractive because of the cost and of the high conductivi-ty of the medium. Kariv-Miller[7] has mentioned that a practical applica-tion of this method could be in hydrogenation processes which are important for coal conversion. However, the studies are still limited to the model compounds.

This research is aimed to investigate the cathodic reduction of coal in aqueous solution using TBAOH and $TBABF_4$ as electrolyte. The effects of various parameters on electroreduction of coal are studied in TBAOH solution system, while the cathodic reduction in $TBABF_4$-THF-H_2O solution is investigated as comparison.

Experimental

A cylindrical cell, 15 cm high, with a hot water jacket and a 44,18 cm^2 mercury pool cathode at the bottom is used as a electrolysis cell. With a fritted glass-cup dipped in the solution as an anode compartment it is a divided cell. A coiled platinum wire is used as anode (7,85 cm^2). The reference electrode is a calomel electrode. The cell is fitted a thermometer, a gas exit with a reflux condenser and a gas inlet for a nitrogen flow during the electrolysis. The cell is filled with 45 ml Hg, 150 ml electrolyte solution and 7,5 g coal(as received). The stirring is carried out during electrolysis by means of a magnetic bar placed on the mercury surface.

Mecury is purified before use. All the electrolyses are performed by using constant current. During electrolysis the cathode potential and the cell voltage are recorded. Gas formed during electrolysis is totally collected in a tyre. Hydrogen in gas is analysed by G.C. and oxygen in gas is determined by paramagnetic Magnos 3 analyser.

After electrolysis mercury is separated and the treated coal is filtered out. When TBAOH is used as electrolyte, the treated coal is washed with water, 10% HCl and again with water to neutral state. In the case of as electrolyte, the treated coal is washed by THF, dried and then extracted with THF in a Soxhlet for 6 hr. The washed coal is dried at reduced pressure for one night. Although more or less grey 'TBA-Hg' compound which is difficult to be separated from the reduced coal, it can be evaporated and/or decomposed before 600 K, i.e. before coal thermal decomposision occurs. Thus, the content of 'TBA-Hg' in the reduced coal can be estimated by thermogravimetric study.

The effect of electroreduction pretreatment on HyPy is studied in a thermobalance under 3 MPa and heating rate of 5 K/min upto 1073 K. The oil yield is determined by carbon balance. Pyridine extraction is carried out in a Soxhlet with a sample of 1 g under nitrogen for 24 hr. The risidue is dried at 60 °C and reduced pressure for 6 hr.

A bituminous Beringen Belgian coal with a granulometry of 45-90 μm is used in this study. Its characteristics are: proximate analysis (wt%, as received): moisture, 1.5; ash, 4.7; volatile matter, 34.5; ultimate analysis (wt%, daf): C, 84.7; H, 4.9; N, 1.7; S, 0.9; O (by difference), 7.8.

Results and Discussion

1. Electroreduction in TBAOH Aqueous Solution

The effects of various parameters on pyridine extractable yield, current efficiency for H_2 production and oil yield in HyPy of the reduced coal are listed in Table 1.

The electrolyte concentration remarkably influences the electrochemical reactions. When TBAOH concentration decreases from 40% to 30%,

pyridine extractable yield is reduced from 17.0% to 7.6%. With increasing concentration, the current efficiency for hydrogen production decreases from 68.7% with 30% TBAOH solution to 46.6% with 55% TBAOH solution.

The influence of current density ranging from 1 to 8 A/dm^2 is shown in Table 1. The higher pyridine extractable yield is given with a current density of 4 A/dm^2 in a 40% TBAOH solution. Similar results were obtained by other authors in the study on effect of current density on current efficiency in electroreduction of benzene in TBAOH solution[7].

It is suggested that the first step for the electroreduction in TBAOH solution is the formation of TBA-metal which could transfer an electron to the aromatic hydrocarbon to initiate the reduction[7,11]. The formation of colloidal Hg on the cathode surface is visually apparent during electrolysis. The slow formation of the colloidal Hg might be related to the current density and time.

It is also found that CO_2 yield obtained in HyPy enhances with increasing current densities. Re-oxidation of the reduced coal appears to occur, which will be discussed later.

Figures 1 and 2 show the influence of current density on conversion and oil yield formed in HyPy of the electroreduced coal. About 4% higher conversion and 3% more oil yield are obtained from the coal reduced in a 55% TBAOH solution than from the unreduced coal.

With increasing charge the current efficiency for H_2 production increases, while the pyridine extractables decreases at 0.088 F/g(daf) of charge transfered.

Table 2 shows the comparison of elemental analysis between raw coal and reduced coal. After electrolysis the H/C atomic ratio slightly increases from 0.69 to 0.70, while the O/C ratio enhances from 0.07 to 0.10. 1 hydrogen and 3 oxygen atoms per 100 carbon atoms are added to coal after electrolysis in these conditions, indicating the re-oxidation of cathodic reduced coal in an undivided cell.

Table 1 also compares the results obtained by electrolysis of coal at 60 °C and 80 °C using a 55 % TBAOH solution in an undivided cell. An increase in temperature decreases the current efficiency for the production of hydrogen. The little higher pyridine extractable yield and less current efficiency for hydrogen production obtained in a 40% TBAOH solution at 80°C also demonstrates the positive effect of the temperature on the reduction. However, the oil yields formed in HyPy of the coal reduced at 60 °C and 80 °C are the same.

The comparison of electrolysis in divided and undivided cell shows that lower pyridine extractable yield and higher current efficiency for hydrogen production are obtained in electrolysis with the divided cell. These might result from the re-oxidation in undivided cell as described before.

The comparison of elemental analysis of reduced coal in divided and undivided cells are also given in Table 2. The O/C ratio of the reduced coal in the divided cell is unchanged as compared to the raw coal, while it increases in the undivided cell. This further indicates the re-oxidation of the reduced coal in the undivided cell. The comparison of CO_2 yield (Figure 3) formed in HyPy of coal reduced in the same

conditions gives another prove. The higher CO_2 yield is produced in HyPy of the coal pretreated in the undivided cell.

The oil yield obtained in HyPy of the reduced coal in various conditions is 2-4% higher than that of the raw coal. The electrolysis in aqueous TBAOH solution seems to have little effect on the following HyPy although the pyridine extractable yield increase. Kariv-Miller et al.[8] concluded that the solubilization of the reactant in water by TBAOH could be an important factor. Coal can be easily dispersed but is hardly dissolved in a TBAOH solution (See Table 1). The less efficiency in improving the oil yield may be related to the low solubility of coal and its reduction products in TBAOH solution[8]. Therefore, the electro-reduction of coal in a TBAOH solution is not sensible to the various parameters and little or not effecient for subsequent HyPy.

2. Electroreduction in a $TBABF_4$-THF-H_2O Solution

Electroreduction of coal in 0.5 M $TBABF_4$-THF-H_2O(5 M) solution is performed at 33 °C, a current density of 0.6 A/dm^2 and a charge amount of 0.16 F in divided and undivided cells. The results are shown in Table 3. As a comparison, the results obtained in 55% TBAOH solution and catalytic HyPy using impregnated sulphided Mo catalyst are also listed.

The THF soluble yield for raw coal is 4.5%, indicating the solubility of coal in THF. After electrolysis in the divided cell the THF solubles markedly increase to 21.7%, showing the notable depolymerization of coal during electrolysis. The less THF solubles obtained in electrolysis in the undivided cell (12.4%) demonstrates that electro-reduction in the divided cell is much more effective than in the undivided cell. This may be due to the re-oxidation of reduced coal in the undivided cell as described in electrolysis in TBAOH solution.

The dramatic increase in THF solubles also indicates that the electron and proton produced in electrolysis can attack to not only the weak bonds but also macromolecular structure in coal, leading to the depolymerization of coal. The products thus formed can be disolved in THF and be further reduced in solution. Due to the remove of the products by disolvation, more surface are exposed to electron and proton and thus, more THF solubles are produced. This may explain the importance of solubility of products.

The conversion and oil yield produced in HyPy of reduced coal are shown in Table 3 and Figures 4 and 5. Cathodic reduction in $TBABF_4$-THF-H_2O solution gives a pronounced effect on HyPy. Higher conversion (60.9%) and total oil yield (50.6%) are obtained in a divided cell as compared with 42.1% and 28.4% for unreduced coal respectively. The cathodic reduction of coal is found to be a better method for coal pretreatment even compared to catalytic HyPy using impregnated sulphided Mo catalyst (conversion: 47.7%; oil yield: 38.4%). That the coversion and oil yield for reduced coal in divided cell are much higher than in undivided cell also proves the extensive hydrogenation during electroreduction in divided cell. The conversion and oil yield in HyPy of the solvated coal are less than raw coal because some soluble substances which will be converted to oil are already removed during solution.

The elemental analysis of reduced coal is also shown in Table 2. Although the H/C ratio in the reduced coal is lower than that in raw coal, it is higher than in the solvated coal. The low value of H/C in

solvated coal indicates the THF solubles with high H/C value. Considered the THF solubles is much higher in electroreduced coal than in solvated coal, a considerable of hydrogen does add to electroreduced coal.

Figure 6 gives the rate of oil formation in HyPy. The reduced coal increases the rate of oil formation in HyPy. The enhances for the reduced coal in divided cell are higher than that in undivided cell. Like catalytic HyPy using impregnated sulphided Mo catalyst[3], the remarkable increase in the rate of oil formation appears in the pyrolytic and hydrogenation stages (< 800 K), while the second peak (> 800 K) formed by hydrocracking reactions is dissappeared. This indicates that the added hydrogen to coal in electroreduction enhances the amount of the intrinsic hydrogen which can saturate the free radicals at low temperature. When more free radicals are stabilized by hydrogenation, less polycondensation reactions take place and therby less hydrocracking reactions occur at high temperatures, leading to the dissappearance of the second peak in the rate of oil formation. The similar behaviours between catalyst-impregnated coal and electroreduced coal in HyPy show that hydrogenation reactions can be accelerated by using either catalyst or electrolysis. However, the functions of both processes are different. Electroreduction adds hydrogen into coal, while the promotion of hydrogenation by catalyst is related to the ability of adsorption and dissociation of gaseous hydrogen.

The problems for electrochemical reduction of coal in $TBABF_4$-THF-H_2O are the use of Hg and divided cell and the seperation of TBABF4 from THF solubles and reduced coal. However, electrochemical reduction of coal is an attractive method for pretreament in hydrogenation processes of coal because of high conversion and oil yield and is worth investigating further for practical use.

References

1. Cyprès, R. and Li Baoqing, Fuel Proc. Technol., 20, 337 (1988).
2. Li Baoqing, ACS Div. Fuel Cham., preprint, 34(4), 1085 (1989).
3. Li Baoqing, Braekman-Danheux, C. and Cyprès, R., submitted to present in 'Coal Structure and Reactivity Conference', Cambridge, UK, Sep. 1990.
4. Given, P. H. and Peover, M. E., Fuel, 39, 463 (1960).
5. Sternberg, P. H., Delle Donne, C. L., Markby, R. E. and Wender, I., Fuel, 45, 469 (1966).
6. Miyaka, M., Hamaguchi, M. and Nomura, M., Energy Fuel, 3("), 362 (1989).
7. Coleman, J. P. and Wagenknecht, J. H., Electrochem. Sci. Technol., 128(2), 322 (1981).
8. Kariv-Miller, E., Swenson, K. E. and Zenmach, D., J. Org. Chem., 48, 4210 (1983).
9. Kariv-Miller, E., Swenson, K. E., Lehman, G. K. and Andruzzi, R., J. Org. Chem., 50, 556 (1985).
10. Kariv-Miller, E. and Pacut, R. I., Tetrahedron, 42(8), 2185 (1986).
11. Svetlicic, V. and Kariv-Miller, E., J. Electroanal. Cham., 209, 91 (1986).

TABLE 1 EFFECT OF SOME PARAMETERS IN ELECTROREDUCTION OF COAL USING TBAOH SOLUTION ON PYRIDINE EXTRACTABLES, CURRENT EFFICIENCY FOR HYDROGEN AND OIL YIELD IN HyPy UNDER 3 MPa, 5 K/min, 913 K

Type	T °C	I A/dm²	Q F/g(daf)	TBAOH C. wt%	Ex.Yield wt%,daf	Effi.for H_2 %	Oil Yield wt%,daf
--	--	--	--	--	11,8	--	28.4
--	60	--	--	40	11,8	--	/
Undiv.	60	2	0.022	40	13,7	52,5	/
	60	4	0.022	40	17,0	52,9	29.3
	60	6	0.022	40	14,0	31,9	/
	60	4	0.022	30	7,6	68,7	/
	60	4	0.044	40	16,4	58,4	/
	60	4	0.088	40	4,2	69,9	/
	80	8	0.022	40	18,4	41,5	/
	60	4	0.022	55	N.D.*	46,6	31.2
	60	2	0.022	55	N.D.	27,8	32.6
	60	1	0.022	55	N.D.	27,3	33.8
	80	4	0.022	55	N.D.	27,2	32.3
Divided	60	4	0.022	40	14,9	52,9	29,9
	60	4	0.022	55	N.D.	68,4	31,3
	60	2	0.022	40	9,7	85,9	/

* Not Determined. After electrolysis coal seems to be a mixture with TBAOH and mercury.

TABLE 2 ELEMENTAL ANALYSIS OF ELECTROREDUCED COAL

wt%, daf	Raw Coal	TBAOH#		$TBABF_4$^	
		Undiv. Cell	Divided Cell	Solcated Coal	ER-Coal
C	84.7	81.9	84.6	84.0	85.8
H	4.9	4.8	4.9	4.1	4.4
N	1.7	1.7	2.0	1.7	1.9
S	0.9	0.9	0.9	N.D.°	N.D.
O(by difference)	7.8	10.7	7.5	10.2*	7.9*
H/C	0.69	0.70	0.70	0.59	0.62
O/C	0.07	0.10	0.07	0.08¨	0.06¨

Electrolysis in 40% TBAOH, 60 °C, 4 A/dm², 0.022 F/g(daf)
^ Electrolysis in $TBABF_4$ -THF-H_2O, 0.6 A/dm², 33°C, 0.022 F/g(daf), Divided Cell
° Not Determined
* O+S: by difference
¨ Assume 0.9% of sulphur content

TABLE 3 COMPARISON OF ELECTROREDUCTION PRETREATMENT AND CATALYTIC HyPy
HyPy: 3 MPa, 5 K/min, 913 K

Type	THF Soluble (wt% daf)	Oil Yield in HyPy (wt% daf)		Total Oil Yield (wt% daf)	Conversion (wt% daf)	
		as Treated	as Raw Coal		as Treated Coal	as Raw Coal
Raw Coal		/	28.4	28.4	/	42.1
Electrolysis						
$TBABF_4$						
Solvated	4.5	27.9	26.6	31.1	41.6	44.2
Undiv. Cell*	12.4	30.3	26.5	38.9	44.2	51.1
Divided Cell*	21.7	36.9	28.9	50.6	50.0	60.9
TBAOH^						
Undiv. Cell		/	31.2	30.1	/	43.3
Divided Cell		/	31.3	31.3	/	43.8
Catalytic HyPy*		/	38.4	38.4	/	47.7

* 0.5 M $TBABF_4$ -THF-H_2O (5 M), 0.6 A/dm^2, 0.022 F/g(daf), 33 °C
^ 55% TBAOH in H_2O, 4 A/dm^2, 0.022 F/g(daf), 60 °C
# Impregnated MoS_2 (0.5% Mo), 3 MPa, 5 K/min, 873 K

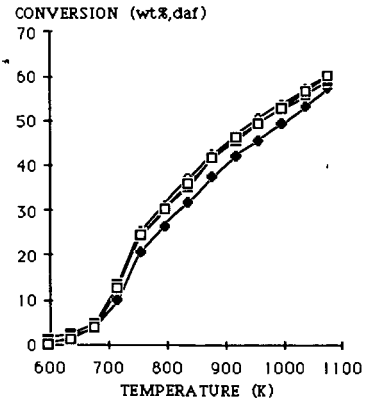

Fig. 1 Effect of Current Density in ER Pretreatment on Conversion in HyPy under 3 MPa, 5 K/min. ER: 40% TBAOH, 60 °C, 0.022 F/g(daf), Undiv. Cell. ● Raw Coal; ◇ 1 A/dm^2; ■ 2 A/dm^2; □ 4 A/dm^2

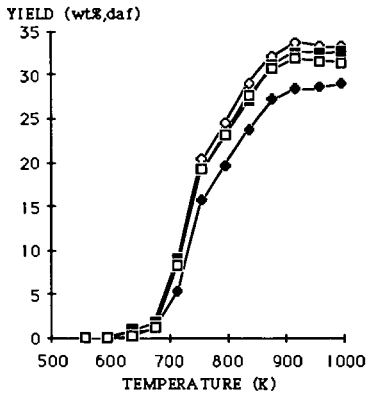

Fig. 2 Effect of Current Density in ER Pretreatment on Oil Yield in HyPy under 3 MPa, 5 K/min. ER: 40% TBAOH, 60 °C, 0.022 F/g(daf), Undiv. Cell. ● Raw Coal; ◇ 1 A/dm^2; ■ 2 A/dm^2; □ 4 A/dm^2

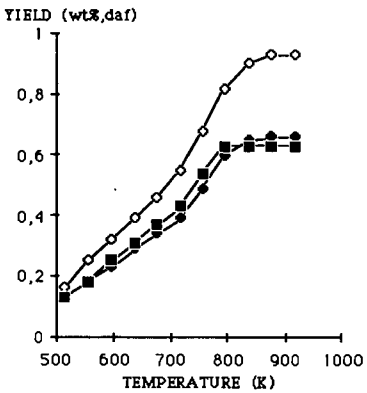

Fig. 3 Effect of Cell Type in ER Pretreatment on CO2 yield in HyPy under 3 MPa, 5 K/min. ER: 40% TBAOH, 4 A/dm^2, 60 °C, 0.022 F/g(daf). ● Raw Coal; ◇ ER-Undiv. Cell; ■ ER-Divided Cell.

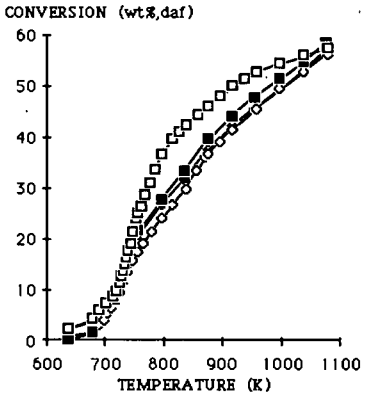

Fig. 4 Effect of ER Pretreatment on Conversion under 3 MPa, 5 K/min. ER: TBABF$_4$-THF-H$_2$O, 33 °C, 0.6 A/dm^2, 0.022 F/g(daf). ● Raw Coal; ◇ Solvated; ■ ER-Undiv. Cell; □ ER-Divided Cell.

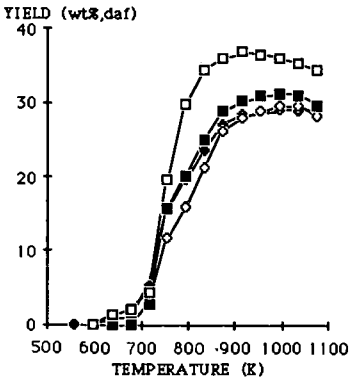

Fig. 5 Effect of ER Pretreatment on Oil Yield in HyPy under 3 MPa, 5 K/min. ER: 0.6 A/dm^2, TBABF$_4$-THF-H$_2$O, 33 °C, 0.022 F/g(daf). ● Raw Coal; ◇ Solvated; ■ ER-Undiv. Cell; □ ER-Divided Cell.

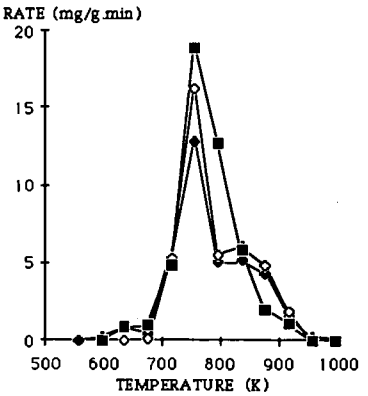

Fig. 6 Effect of ER Pretreatment on Rate of Oil Formation in HyPy under 3 MPa, 5 K/min. ER: TBABF$_4$-THF-H$_2$O, 0.6 A/dm^2, 33 °C, 0.022 F/g(daf). ● Raw Coal; ◇ ER-Undiv. Cell; ■ ER-Divided Cell.